



Universiteit
Leiden
The Netherlands

Multimodality imaging to guide cardiac interventional procedures

Tops, L.F.

Citation

Tops, L. F. (2010, April 15). *Multimodality imaging to guide cardiac interventional procedures*. Retrieved from <https://hdl.handle.net/1887/15228>

Version: Corrected Publisher's Version

License: [Licence agreement concerning inclusion of doctoral thesis in the Institutional Repository of the University of Leiden](#)

Downloaded from: <https://hdl.handle.net/1887/15228>

Note: To cite this publication please use the final published version (if applicable).

Multimodality imaging to guide cardiac interventional procedures

Laurens F. Tops

The studies described in this thesis were performed at the Department of Cardiology of the Leiden University Medical Center, Leiden, the Netherlands, and the Division of Cardiology, Department of Medicine of Johns Hopkins University, Baltimore, USA.

Cover: Optima Grafische Communicatie, Rotterdam, The Netherlands

Lay-out and print: Optima Grafische Communicatie, Rotterdam, The Netherlands

ISBN: 978-90-8559-949-4

Copyright © Laurens F. Tops, Leiden, the Netherlands. All rights reserved. No part of this book may be reproduced or transmitted, in any form or by any means, without prior permission of the author.

Financial support to the costs associated with the publication of this thesis from Biosense Webster, Biotronik Nederland BV, Boston Scientific BV, Edwards Lifesciences BV, 3mensio Medical Imaging BV, Bracco Imaging Europe BV, Daiichi Sankyo Nederland BV, HagaZiekenhuis, Siemens Nederland NV, Sorin Group Nederland NV, St. Jude Medical Nederland BV, Stichting Imago, Stichting J.E. Jurriaanse, Vital Images BV, Toshiba Medical Systems Nederland, AstraZeneca BV, Boehringer Ingelheim BV, Eli Lilly Nederland BV, Merck Sharp & Dohme BV, Schering-Plough BV, Brahms Nederland, Guerbet Nederland BV, Servier Nederland Farma BV, and Sanofi-Aventis BV is gratefully acknowledged.

Multimodality imaging to guide cardiac interventional procedures

Proefschrift

ter verkrijging van
de graad van Doctor aan de Universiteit Leiden,
op gezag van Rector Magnificus prof. mr. P.F. van der Heijden,
volgens besluit van het College voor Promoties
te verdedigen op donderdag 15 april 2010
klokke 16.15 uur

door

Laurens Franciscus Tops

geboren te Oss
op 17 april 1979

PROMOTIECOMMISSIE

Promotores: Prof. dr. J.J. Bax
Prof. dr. M.J. Schalij

Overige leden: Prof. dr. D. Poldermans (Erasmus MC, Rotterdam)
Prof. dr. A. de Roos
Prof. dr. E.E. van der Wall
Dr. E.R. Holman
Dr. J.D. Schuijf
Dr. K. Zeppenfeld

Financial support by the Netherlands Heart Foundation for the publication of this thesis is gratefully acknowledged.

Great minds have purposes,
others have wishes
Washington Irving

CONTENTS

Chapter 1	General introduction and outline of the thesis	9
PART I	Catheter ablation for atrial fibrillation	
Chapter 2	Multi-modality imaging to assess left atrial size, anatomy and function <i>Heart 2007;93:1461-70</i>	29
Chapter 3	Imaging and atrial fibrillation: the role of multimodality imaging in patient evaluation and management of atrial fibrillation <i>Eur Heart J 2010, in press</i>	51
Chapter 4	Fusion of multislice computed tomography imaging with three-dimensional electroanatomic mapping to guide radiofrequency catheter ablation procedures <i>Heart Rhythm 2005;2:1076-81</i>	73
Chapter 5	Real-time integration of intracardiac echocardiography and multislice computed tomography to guide radiofrequency catheter ablation for atrial fibrillation <i>Heart Rhythm 2008;5:1403-10</i>	85
Chapter 6	Impact of pulmonary vein anatomy and left atrial dimensions on the outcome of circumferential radiofrequency catheter ablation for atrial fibrillation <i>Submitted</i>	101
Chapter 7	Effect of radiofrequency catheter ablation for atrial fibrillation on left atrial cavity size <i>Am J Cardiol 2006;97:1220-2</i>	113
Chapter 8	Comparison of left atrial volumes and function by real-time three-dimensional echocardiography in patients having catheter ablation for atrial fibrillation with persistence of sinus rhythm versus recurrent atrial fibrillation three months later <i>Am J Cardiol 2008;102:847-53</i>	121
Chapter 9	Left atrial strain predicts reverse remodeling after catheter ablation for atrial fibrillation <i>Submitted</i>	135
Chapter 10	Long-term improvement in left ventricular strain after successful catheter ablation for atrial fibrillation in patients with preserved left ventricular systolic function <i>Circ Arrhythmia Electrophysiol 2009;2:249-57</i>	151

PART II Ventricular pacing and dyssynchrony

- Chapter 11 The effects of right ventricular apical pacing on ventricular function and dyssynchrony: implications for therapy 171
J Am Coll Cardiol 2009;54:764-76
- Chapter 12 Right ventricular pacing can induce ventricular dyssynchrony in patients with atrial fibrillation after atrioventricular node ablation 195
J Am Coll Cardiol 2006;48:1642-8
- Chapter 13 Acute effects of right ventricular apical pacing on left ventricular synchrony and mechanics 209
Circ Arrhythmia Electrophysiol 2009;2:135-45
- Chapter 14 Speckle-tracking radial strain reveals left ventricular dyssynchrony in patients with permanent right ventricular pacing 227
J Am Coll Cardiol 2007;50:1180-8
- Chapter 15 The effect of right ventricular pacing on myocardial oxidative metabolism and efficiency: relation with left ventricular dyssynchrony 245
Eur J Nucl Med Mol Imaging 2009;36:2042-8
- Chapter 16 Prevalence and pathophysiologic attributes of ventricular dyssynchrony in arrhythmogenic right ventricular dysplasia/cardiomyopathy 257
J Am Coll Cardiol 2009;54:445-51

PART III Percutaneous valve procedures

- Chapter 17 Percutaneous valve procedures: an update 275
Curr Probl Cardiol 2008;33:417-57
- Chapter 18 Noninvasive evaluation of coronary sinus anatomy and its relation to the mitral valve annulus: implications for percutaneous mitral annuloplasty 307
Circulation 2007;115:1426-32
- Chapter 19 Assessment of mitral valve anatomy and geometry with multislice computed tomography 321
J Am Coll Cardiol Img 2009;2:556-65
- Chapter 20 Percutaneous aortic valve therapy: clinical experience and the role of multimodality imaging 339
Heart 2009;95:1538-46
- Chapter 21 Noninvasive evaluation of the aortic root with multislice computed tomography: implications for transcatheter aortic valve replacement 359
J Am Coll Cardiol Img 2008;1:321-30
- Chapter 22 Role of multislice computed tomography in transcatheter aortic valve replacement 377
Am J Cardiol 2009;103:1295-301

Summary, conclusions and future perspectives	389
Samenvatting, conclusies en toekomstperspectieven	401
List of publications	415
Acknowledgements	423
Curriculum Vitae	427



General introduction and outline of the thesis

In the past decades, tremendous advances have been made in both the imaging and interventional field of clinical cardiology. Dedicated imaging techniques such as multi-slice computed tomography have been introduced and enable detailed non-invasive evaluation of cardiac anatomy. Furthermore, conventional techniques such as echocardiography have been improved and nowadays allow a more comprehensive assessment of cardiac morphology and function. At the same time, percutaneous interventional procedures for arrhythmias and valvular heart disease have been further explored. While conventional invasive treatment of these conditions requires open-heart surgery, nowadays it has become feasible to perform these procedures with minimal-invasive techniques.

These advances allow a more integrative approach to cardiac imaging and interventions. The combination and integration of different imaging modalities and subsequent use of these techniques during interventional procedures will further enhance the evaluation and treatment of cardiac arrhythmias and valvular heart disease. In this thesis, the role of multimodality imaging to guide cardiac interventional procedures is investigated. In particular, catheter ablation for atrial fibrillation (AF), cardiac pacing and resynchronization therapy, and percutaneous valve procedures are explored.

CATHETER ABLATION FOR ATRIAL FIBRILLATION

Atrial fibrillation is the most commonly encountered cardiac arrhythmia. It is characterized by rapid, irregular activity of the atria. In the general population, the prevalence of AF is approximately 1% (1). Since the prevalence of AF increases with age, it may become 'epidemic' in the coming decades, with an estimated 3.3 million patients in the United States in 2020 (Figure 1). Importantly, AF is associated with an increased risk of both cardiac morbidity and mortality (2).

The most important goals in the treatment of AF are: reduction of the risk of thromboembolism and control of AF-related symptoms (3). To reduce the risk of thromboembolism, a tailored anti-thrombotic regimen (e.g. anticoagulation or aspirin) should be chosen depending on clinical characteristics (4). To control symptoms of AF, both 'rate control' and 'rhythm control' strategies can be chosen. Again, an individualized approach is preferred, since the superiority of one strategy has not been proven. Large randomized trials have not demonstrated differences in mortality or quality of life between the two strategies (5,6).

If a 'rhythm control' strategy is chosen, anti-arrhythmic drugs and/or electrical cardioversion are used to restore sinus rhythm. Unfortunately, anti-arrhythmic drugs may have side-effects and often fail to maintain sinus rhythm. In the past decade, catheter ablation procedures have been introduced as a new therapeutic option in the treatment of patients with AF.

Haissaguerre et al. demonstrated that the pulmonary veins (PVs) are the main source of ectopic beats that initiate AF (7). Subsequently, it was shown that electrical isolation of these PVs with the use of (radiofrequency) catheter ablation is effective for the restoration and

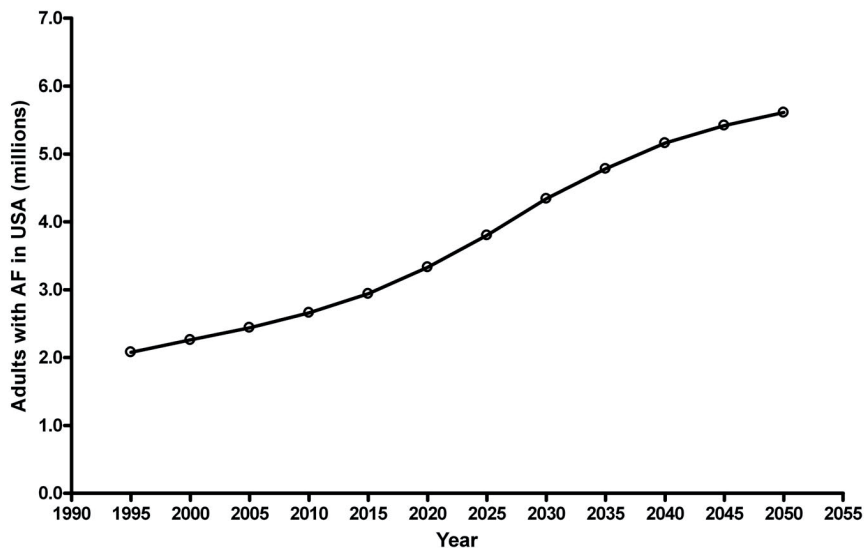


Figure 1. Estimated number of patients with atrial fibrillation (AF) in the United States of America (USA). The total number of patients may increase up to 2.5-fold in the coming 4 decades. Adapted with permission from Go AS et al., reference (1).

maintenance of sinus rhythm. During the catheter ablation procedure, the PVs are isolated from the left atrial (LA) wall by applying radiofrequency current around the PV ostia (Figure 2). Several randomized controlled trials have compared anti-arrhythmic drugs and catheter ablation procedures regarding the efficacy to maintain sinus rhythm during long-term follow-up (8-11). From these studies, it has become apparent that catheter ablation may be more effective than anti-arrhythmic drugs (Table 1). It should be noted however, that serious complications may occur in up to 5% of patients undergoing catheter ablation for AF (12). Therefore, at present catheter ablation still is considered a second-line therapy, but an excellent treatment option

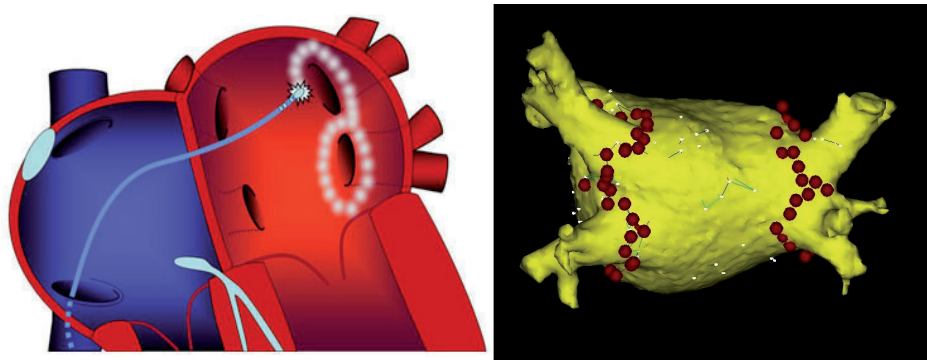


Figure 2. The left panel shows a schematic representation of a catheter ablation procedure. The ablation catheter is introduced into the left atrium (LA) through the foramen ovale. Subsequently, radiofrequency current is applied around the ostia of the pulmonary veins (PVs) (indicated with the white dots). The right panel shows a volume-rendered reconstruction of multi-slice computed tomography images of the LA and PVs that is used to guide the ablation procedure. The red dots indicate the ablation lesions.

Table 1. Randomized studies comparing catheter ablation and anti-arrhythmic drugs

Study (reference)	Number of patients	Type of AF	Follow-up	Primary endpoint: Freedom from AF (Ablation vs. AAR)	Secondary endpoints	Complications ablation
Oral et al. (9)	146	146 persistent (100%)	12 months	74% vs. 58%, p=0.05	- Decrease in LA diameter in successful ablation patients - Increase in LVEF in successful ablation patients - Improvement in symptoms in all ablation patients	None reported
Pappone et al. (10)	198	198 paroxysmal (100%)	12 months	86% vs. 22%, p<0.001	N/A	- TIA: 1 - Pericardial effusion: 1
Stabile et al. (11)	137	92 paroxysmal (67%) 45 persistent (33%)	12 months	66% vs. 9%, p<0.001	N/A	- Stroke: 1 - Transient phrenic nerve paralysis: 1 - Pericardial effusion: 1
Jais et al. (8)	112	112 paroxysmal (100%)	12 months	89% vs. 23%, p<0.001	- No differences in LA diameter and LVEF at follow-up - Greater reduction in AF burden in ablation patients - Improvement in quality of life and exercise capacity in ablation patients	- Cardiac tamponade: 2 - Hematoma: 2 - PV stenosis: 1

AF = atrial fibrillation; AAR = anti-arrhythmic drugs; LA = left atrial; LVEF = left ventricular ejection fraction; PV = pulmonary vein; TIA = transient ischemic attack

after at least one anti-arrhythmic drug has failed (3). Interestingly, an increasing number of AF patients worldwide are treated with catheter ablation (Figure 3).

The cornerstone of AF ablation procedures is electrical isolation of the PVs. However, anatomical studies have demonstrated that PV anatomy is highly variable (13). In particular, the exact number and location of the PVs has large inter-individual variation. Therefore, careful identification of the PVs is important both before and during the catheter ablation procedure. Several imaging modalities are available to evaluate the anatomy of the LA and the PVs. Multi-slice computed tomography and magnetic resonance imaging provide excellent images of the PVs. However, they do not provide real-time information since the images are acquired before the actual ablation procedure. On the other hand, intracardiac echocardiography and electroanatomic mapping enable online visualization of the PVs in relation with the ablation catheters. However, these techniques are limited by the two-dimensional character and the use of reconstructed anatomy, respectively. Ideally, the information of the different imaging

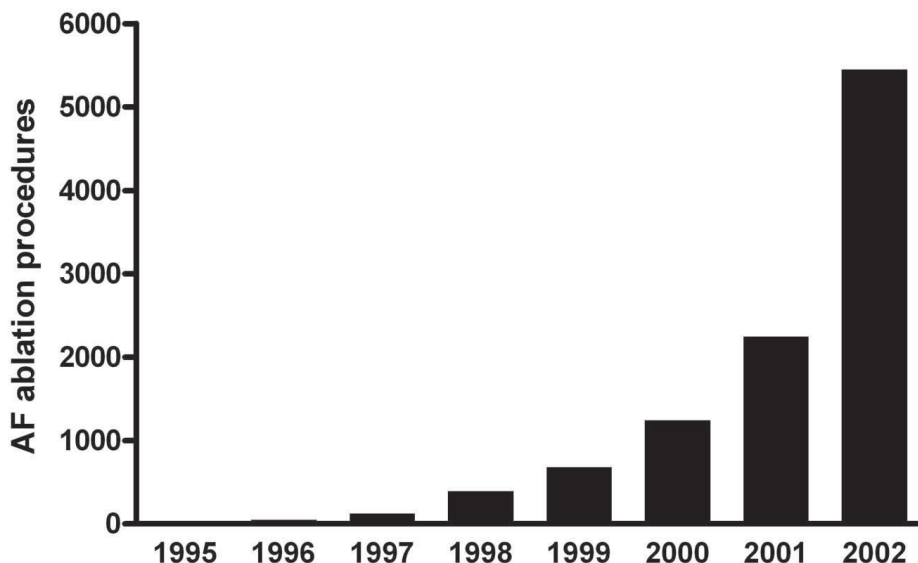


Figure 3. World-wide number of catheter ablation procedures for AF between 1995 and 2002. A clear increase in the annual number of procedures is noted. Adapted with permission from Cappato R et al. Worldwide survey on the methods, efficacy, and safety of catheter ablation for human atrial fibrillation. *Circulation* 2005;111:1100-5.

techniques is integrated, providing highly detailed on-line anatomical information during the catheter ablation procedure.

Another important issue is the effect of catheter ablation procedures for AF on cardiac size and function. It has been well recognized that there is a close relation between AF and LA size (14). After catheter ablation, the ablation lesions may result in scarring of the LA wall. This may negatively affect LA size and contractile function. On the other hand, a reduction in LA size may result in lower susceptibility to AF (15). In addition, the restoration of sinus rhythm may ultimately result in an improved LA function. Furthermore, normalization of heart rhythm may result in more efficient left ventricular (LV) function. It has been demonstrated that catheter ablation results in significant improvement in LV ejection fraction in patients with AF and systolic heart failure (16). However, the effect of catheter ablation on LV function in patients with preserved LV ejection fraction is unclear.

Multimodality imaging and image integration may enhance AF ablation procedures by improved visualization of cardiac structures, and may result in better understanding of the effects of catheter ablation on cardiac function. Accordingly, the aims of the studies described in this thesis are to test the feasibility of image integration to guide catheter ablation procedures and to assess the effects of catheter ablation procedures on LA and LV function.

VENTRICULAR PACING AND DYSSYNCHRONY

In 1958, the first pacemaker implantation was performed in a patient with high degree atrio-ventricular block. Since then, cardiac pacing has been an effective treatment in the management of patients with symptomatic brady- and tachy-arrhythmias. The annual number of new pacemaker implantations in the Netherlands is about 6000, and is steadily increasing (17). High degree atrioventricular block and sick sinus syndrome are the most important indications for implantation of a conventional pacemaker (Figure 4).

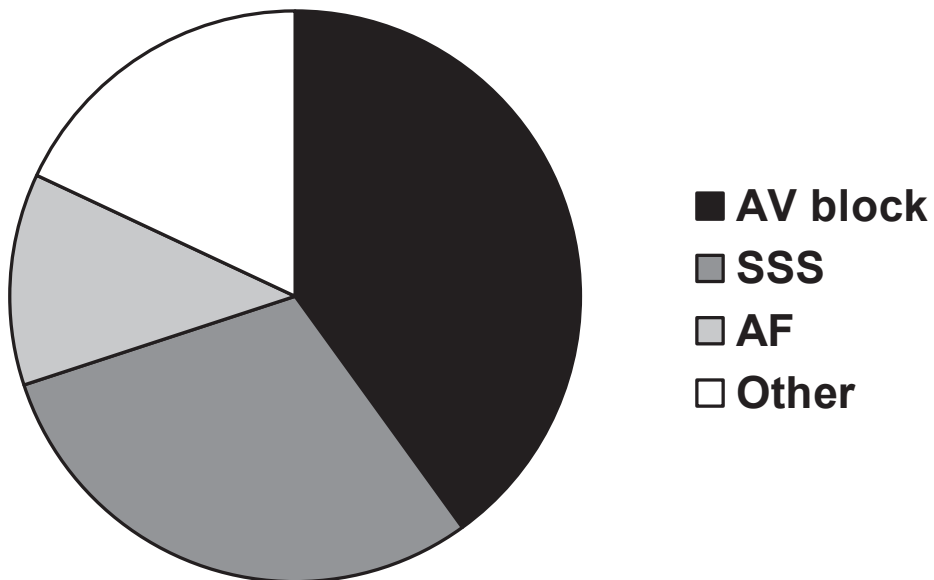


Figure 4. Indications for new pacemaker implantations in the World Survey of Cardiac Pacing and Cardioverter Defibrillators 2001. High degree atrio-ventricular (AV) block (40%) and sick sinus syndrome (SSS, 30%) remain the most important indications for pacemaker implantation. Less frequently, atrial fibrillation (AF, 12%) and other indications (e.g. bundle-branch block, cardiomyopathy) result in implantation of a pacemaker. Adapted from Mond HG et al., reference (17).

Typically, the endocardial ventricular pacing lead is positioned at the right ventricular (RV) apex. However, large randomized trials have revealed a possible association between RV apical pacing and deterioration of cardiac function (18,19). In the Mode Selection Trial (MOST), it was demonstrated that a high percentage of ventricular pacing is associated with an increased risk of heart failure hospitalization (Figure 5). Furthermore, other studies have shown that RV apical pacing results in changes in myocardial perfusion (20) and ventricular remodeling (21). At the same time, minimizing RV apical pacing with dedicated algorithms can prevent harmful effects of cardiac pacing (22).

The deleterious effects of conventional RV apical pacing may be associated with the abnormal electrical and mechanical activation pattern of the cardiac chambers. During RV apical

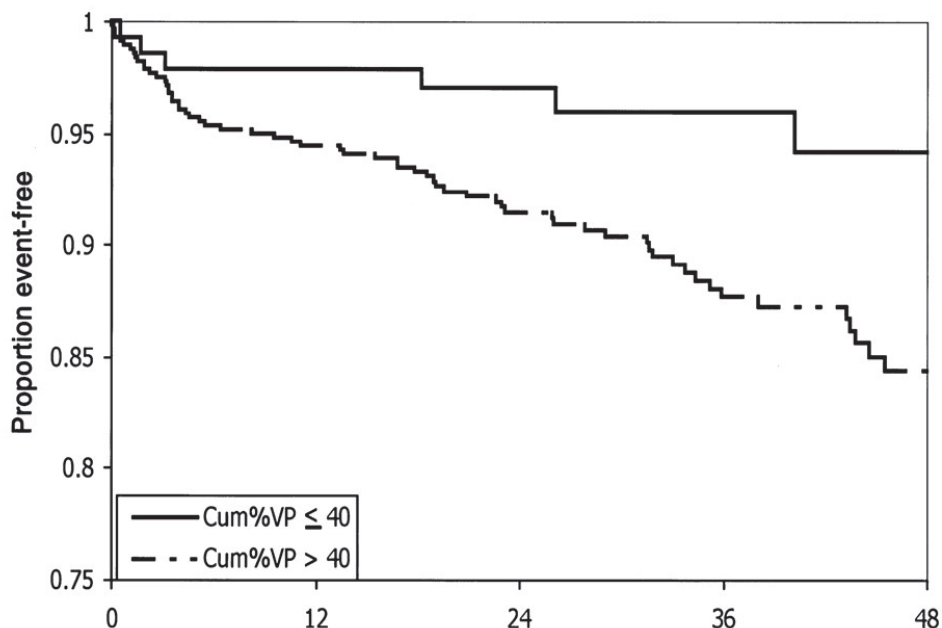


Figure 5. In the MOST trial, >40% cumulative percentage of ventricular pacing (Cum%VP) in the DDDR pacing group (n=707) significantly increased the risk of heart failure hospitalization compared with <40% pacing (hazard ratio 2.60; 95% CI 1.05 - 6.47; p<0.05). This figure demonstrates the Kaplan-Meier plots relating time to first heart failure hospitalization (event) by cumulative percentage of ventricular pacing. Reprinted with permission from Sweeney MO et al., reference (18).

pacing, the electrical wave front propagates through the myocardium, rather than through the His-Purkinje conduction system. Due to the differences in conduction velocity, heterogeneity in electrical activation of the cardiac chambers occurs (23). Simultaneously, changes in the mechanical activation pattern are noted. In particular, the onset and magnitude of mechanical contraction of various LV walls change (24). The temporal occurrence of peak strain of different ventricular segments exhibits an asynchronous pattern during RV apical pacing. This is referred to as 'ventricular mechanical dyssynchrony' (Figure 6).

Mechanical dyssynchrony can be assessed with various non-invasive imaging modalities. Already in 1977, Gomes et al. noticed the asynchronous contraction pattern of the LV during RV apical pacing with the use of transthoracic echocardiography (25). A significant delay between the (early) posterior motion of the interventricular septum and the (delayed) contraction of the posterior wall was observed immediately after onset of pacing. Nowadays, additional echocardiographic techniques are available for assessment of ventricular dyssynchrony (26). With the use of tissue Doppler imaging, myocardial velocities of different ventricular segments can be assessed throughout the cardiac cycle (Figure 6). Off-line analysis of the regional time-to-peak systolic velocity enables quantification of ventricular mechanical dyssynchrony (27). Speckle-tracking strain analysis is another echocardiographic technique that allows assessment of regional timing of peak strain (28). The assessment of myocardial strain permits differentiation

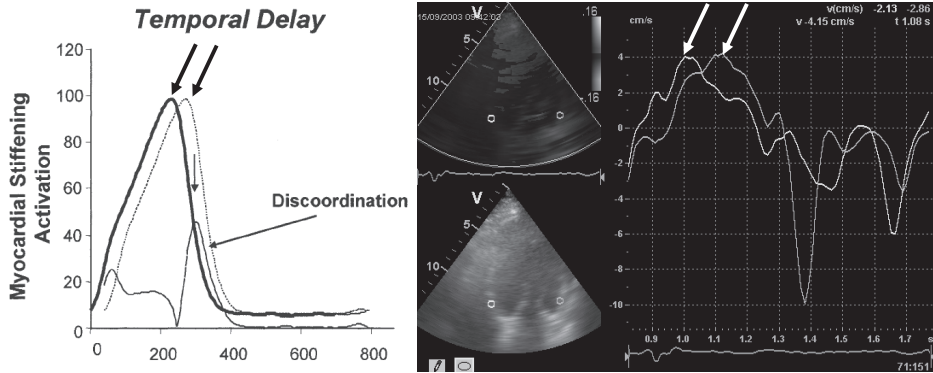


Figure 6. Mechanical dyssynchrony. The left panel is a schematic representation of mechanical dyssynchrony. Two different regions of the heart contract with similar force (myocardial stiffening), but one region has a delay in contraction relative to the other. The net difference between the two regions determines the extent of discoordination in contraction, or mechanical dyssynchrony. The right panel shows echocardiographic dyssynchrony assessment with tissue Doppler imaging. Sample areas are placed at the basal parts of the septum and lateral wall of the LV. The difference in time-to-peak systolic velocity of the two regions (indicated with white arrows) represents mechanical dyssynchrony. Left panel adapted with permission from Kass DA. An epidemic of dyssynchrony: But what does it mean? *J Am Coll Cardiol* 2008;51:12–7.

between active contraction and passive motion of the myocardium. Again, by calculating differences in time-to-peak systolic strain of various segments, ventricular dyssynchrony can be assessed (29).

Importantly, it has been demonstrated that the presence of mechanical dyssynchrony has prognostic value in heart failure patients (30). However, the association between mechanical dyssynchrony and the deterioration of cardiac function and functional class in pacemaker patients has not been fully elucidated yet. Furthermore, in the past decade cardiac resynchronization therapy has become a well-established therapeutic option for patients with severe drug-refractory heart failure and signs of electrical or mechanical dyssynchrony (31,32). In cardiac resynchronization therapy, an LV pacing lead is added to a conventional pacing system, allowing simultaneously pacing of the RV and LV to re-synchronize the cardiac chambers. It may well be that cardiac resynchronization therapy is able to (partly) reverse the detrimental effects of conventional RV apical pacing.

New imaging techniques may be valuable tools for the detection of mechanical dyssynchrony, and may help in monitoring patients with conventional pacemakers and selecting potential candidates for upgrade of RV pacing to biventricular pacing. Accordingly, the current studies explore the possible association between deterioration of cardiac function and ventricular mechanical dyssynchrony after onset of RV pacing, and reversal of the detrimental effects and LV dyssynchrony with cardiac resynchronization therapy.

PERCUTANEOUS VALVE PROCEDURES

Valvular heart disease is an important entity in clinical cardiology. Aortic stenosis (AS) and mitral regurgitation (MR) are the most common native single-valve disease. In the general population, the prevalence of AS is estimated between 2 and 7% (33). Various pathophysiologic processes can attribute to the development of AS or MR, but most frequently the etiology is degenerative (Table 2). Importantly, the presence of severe AS (34) or MR (35) is associated with a substantially increased risk of cardiac morbidity and mortality. The poor natural history of untreated AS and MR emphasizes the importance of treatment of patients with these conditions (36,37).

Surgical aortic valve replacement is the treatment of choice in severe, symptomatic AS. Operative mortality is about 3-5%, and good long-term survival has been reported (Figure 7) (38). Importantly, the severity of symptoms, LV ejection fraction and age are important predictors of good outcome after surgical aortic valve replacement (39). For MR, surgical treatment

Table 2. Results from the Euro Heart Survey on Valvular Heart Disease on the etiology and surgical treatment of aortic stenosis and mitral regurgitation.

	Aortic stenosis	Mitral regurgitation
Etiology *		
Degenerative, %	82	61
Rheumatic, %	11	14
Endocarditis, %	1	4
Inflammatory, %	0	1
Congenital, %	5	5
Ischaemic, %	0	7
Other, %	1	8
Surgical intervention †		
Mechanical prosthesis, %	49	43
Bioprosthesis, %	50	10
Valve repair, %	0	47
Other, %	1	0

* Data on etiology from 1197 patients with aortic stenosis and 877 patients with mitral regurgitation. † Data on surgical intervention from 512 patients with aortic stenosis and 155 patients with mitral regurgitation. Adapted from Lung et al., reference (42).

is more complex, due to its variety in etiologies. Mitral valve repair using undersized mitral annuloplasty is most frequently used for degenerative and ischemic MR (40). The outcome of surgical mitral valve repair depends largely on the etiology of MR, but also severity of symptoms, LV ejection fraction and age are important predictors of outcome (33). In particular for organic MR (e.g. mitral valve prolapse), good long-term results have been reported (41).

Despite the good outcome after surgical treatment of AS and MR, a large proportion of patients does not undergo surgery. The Euro Heart Survey on Valvular Heart Disease explored the characteristics, treatment and outcome of 5001 patients with valvular heart disease from 25 countries in Europe (42). From this Euro Heart Survey, it has become apparent that up to 30%

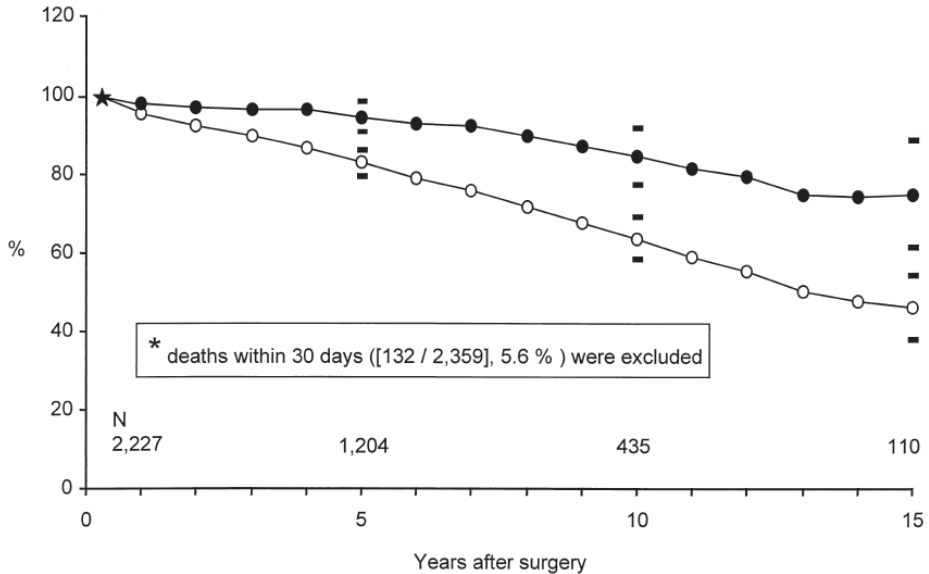


Figure 7. Long-term outcome after primary surgical aortic valve replacement in 2227 patients with severe aortic stenosis. The observed (open circles) and relative (solid circles) survival is shown in patients who survived the first postoperative month. Reprinted with permission from Kvidal P et al., reference (38).

of patients with severe symptomatic valvular disease do not undergo surgical intervention, while a clear indication exists. Most frequently, this is because of co-morbidity and age (42). Obviously, there is a need for a less invasive approach, in particular in elderly patients with co-morbidity and severe valvular heart disease.

In recent years, various new percutaneous procedures for the treatment of AS and MR have been introduced. The implantation of an aortic valve prosthesis through the femoral artery or the LV apex has become feasible (Figure 8). The feasibility of a balloon-expandable (43) and a self-expanding valve (44) for the percutaneous treatment of severe AS have been demonstrated. Importantly, large multi-center studies (45) and mid-term follow-up studies (46) have demonstrated the safety and efficacy of these procedures.

Furthermore, new percutaneous devices have been introduced for the percutaneous treatment of MR (Figure 8). The feasibility of a mitral valve clip mimicking edge-to-edge repair has been demonstrated (47), and different prostheses that target mitral annulus remodeling through the coronary sinus have been introduced (48,49). The safety and mid-term efficacy of these procedures have also been demonstrated (50,51).

However, percutaneous valve procedures still have limitations and severe complications can occur. An important issue is failure of the procedure as a result of unfavorable cardiac anatomy. For example, the close relation between the native valve leaflets, valve annulus and the coronary arteries may preclude safe percutaneous implantation of a device. In the Mitral Annuloplasty Device European Union Study (AMADEUS), the coronary sinus device was

recaptured because of potential coronary compromise in up to 30% of the non-implanted patients (51). Furthermore, acute coronary occlusion during percutaneous aortic valve implantation has been reported (43).

Imaging may be of great value in the percutaneous treatment of valvular heart disease. It may improve the selection of patients and may enhance real-time guidance of the procedures. In the studies described in the present thesis, the potential role of multi-slice computed tomography in the selection for candidates for new percutaneous valve procedures for AS and MR is explored.

OUTLINE OF THE PRESENT THESIS

The aim of this thesis is to evaluate the role of multimodality imaging to guide cardiac interventional procedures. In particular, catheter ablation procedures for AF, conventional pacing and cardiac resynchronization therapy, and percutaneous valve procedures are studied. Therefore, the present thesis consists of three distinct parts.

PART I: Catheter ablation for atrial fibrillation

In the first part, catheter ablation procedures for AF are studied. These procedures are considered a good treatment option in patients with drug-refractory AF, after at least one anti-arrhythmic drug has failed. Visualization of the PVs with different imaging modalities, the integration of various imaging techniques, and the effect of catheter ablation on LA and LV function are important issues in AF ablation. **Chapter 2** and **Chapter 3** provide two extensive reviews on the role of multimodality imaging in the assessment of PV and LA anatomy, and in catheter ablation procedures for AF. In **Chapter 4**, the first clinical experience with a new image integration system that allows integration of MSCT images and electroanatomic mapping is described. Subsequently, the integration of intracardiac echocardiography with electroanatomic mapping and multi-slice computed tomography is studied in **Chapter 5**. The assessment of PV anatomy with multi-slice computed tomography, and its impact on the outcome of catheter ablation procedures is explored in **Chapter 6**.

In the next chapters, the effect of catheter ablation for AF on LA and LV function is studied. In **Chapter 7**, conventional transthoracic two-dimensional echocardiography is used to assess the effect of catheter ablation on LA size. The findings of this study are further extended in the following chapters. In **Chapter 8**, real-time three-dimensional echocardiography is used to assess LA function after catheter ablation. Subsequently, the effect of catheter ablation on LA systolic and diastolic strain is investigated in **Chapter 9**. Furthermore, the predictive value of LA strain for LA reverse remodeling is studied. Finally, the effect of sinus rhythm maintenance after catheter ablation on LV function is studied in **Chapter 10**.

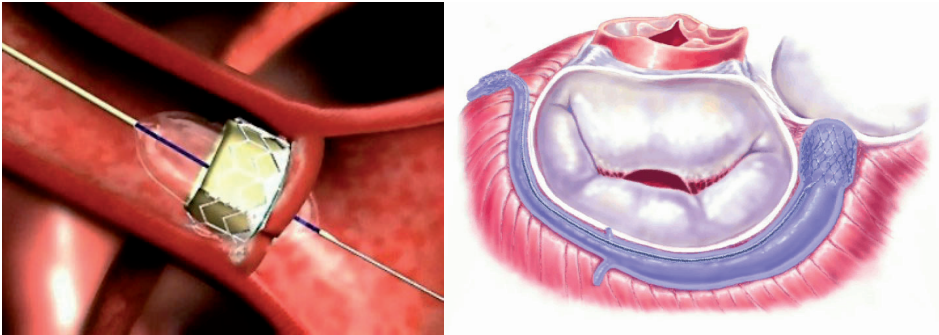


Figure 8. Percutaneous valve procedures for aortic stenosis (AS) and mitral regurgitation (MR). The left panel shows the percutaneous implantation of a balloon expandable aortic valve prosthesis. The catheter with the balloon and prosthesis is inserted retrograde through the femoral artery and aorta. The right panel shows a coronary sinus device that attempts to remodel the mitral valve annulus in severe MR. The device is inserted antegrade through the right atrium.

PART II: Ventricular pacing and dyssynchrony

In the second part, conventional RV apical pacing, cardiac resynchronization therapy and ventricular mechanical dyssynchrony are studied. In particular, the association between dyssynchrony and the deterioration of LV function after long-term RV apical pacing, and the reversal of the negative effects with cardiac resynchronization therapy are investigated. In **Chapter 11**, an extensive review of the available evidence on the effects of RV apical pacing on LV function is provided. **Chapter 12** describes the initial observation that long-term RV apical pacing can induce LV mechanical dyssynchrony assessed with conventional echocardiography and tissue Doppler imaging. Subsequently, the acute effects of RV apical pacing on ventricular dyssynchrony are studied with speckle-tracking echocardiography in **Chapter 13**. Furthermore, the effects of RV apical pacing on LV strain and LV twist are investigated in this study. Subsequently, speckle-tracking echocardiography is used to assess ventricular dyssynchrony, and in particular the site of latest activation in a cohort of patients with long-term RV apical pacing in **Chapter 14**. Importantly, the effect of upgrade to biventricular pacing is investigated in this study. In **Chapter 15**, the effect of RV apical pacing and ventricular dyssynchrony on myocardial oxidative metabolism and efficiency is studied with the use of positron emission tomography scanning. Finally, the prevalence of ventricular dyssynchrony in patients with arrhythmogenic right ventricular dysplasia/cardiomyopathy is studied in **Chapter 16**.

PART III: Percutaneous valve procedures

In the third part, the role of cardiac imaging in percutaneous valve procedures is explored. Recently, various percutaneous procedures for aortic valve and mitral valve disease have been introduced. The background of these procedures and the different prostheses are reviewed in **Chapter 17**. The relation between the mitral annulus, the LA posterior wall and the coronary arteries determines the feasibility of percutaneous mitral annuloplasty. The assessment of this critical relation with the use of multi-slice computed tomography is described in **Chapter 18**.

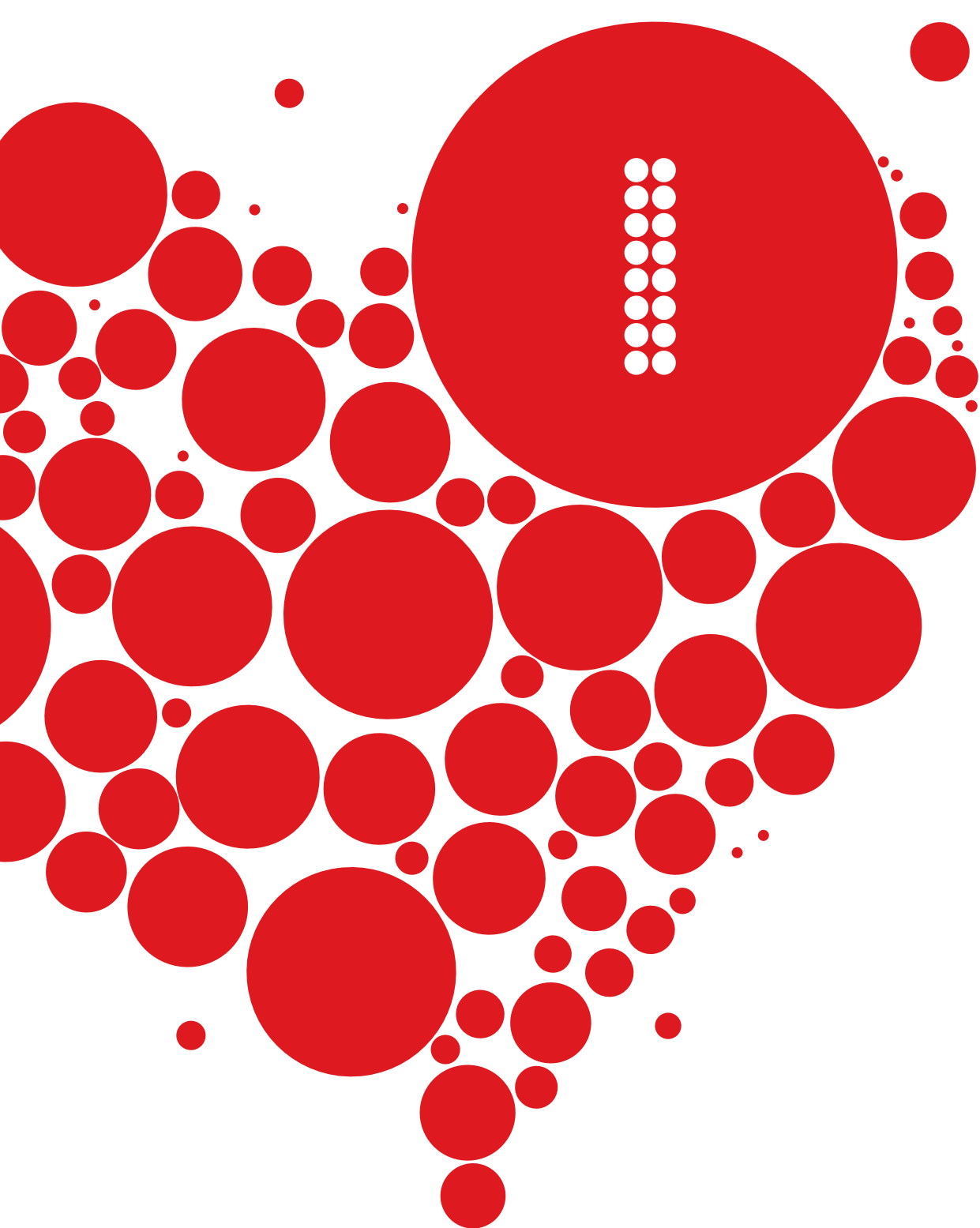
Subsequently, multi-slice computed tomography is used for the assessment of the mitral valve itself, and exploration of the anatomical mechanism underlying functional MR in **Chapter 19**. For percutaneous aortic valve procedures, other anatomical considerations are important. In particular, the extent and location of aortic valve calcifications, and the relation between the aortic valve annulus and the coronary arteries are important issues. The role of multimodality imaging in the selection of patients and performing percutaneous aortic valve procedures is discussed in **Chapter 20**. Furthermore, the clinical experience with percutaneous aortic valve procedures is extensively reviewed in this chapter. In **Chapter 21**, a systematic analysis with the use of multi-slice computed tomography of the aortic valve and the relation with the coronary arteries is performed in a large cohort of patients. Finally, this methodology is used in patients undergoing percutaneous aortic valve implantation in **Chapter 22**.

REFERENCES

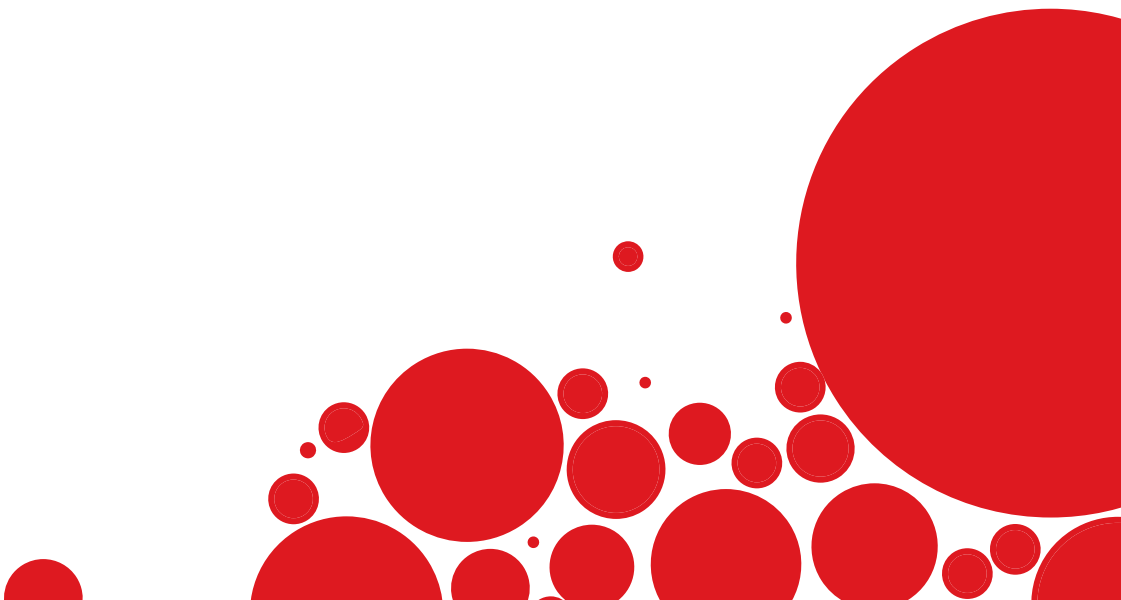
1. Go AS, Hylek EM, Phillips KA et al. Prevalence of diagnosed atrial fibrillation in adults: national implications for rhythm management and stroke prevention: the Anticoagulation and Risk Factors in Atrial Fibrillation (ATRIA) Study. *JAMA* 2001;285:2370-5.
2. Benjamin EJ, Wolf PA, D'Agostino RB, Silbershatz H, Kannel WB, Levy D. Impact of atrial fibrillation on the risk of death: the Framingham Heart Study. *Circulation* 1998;98:946-52.
3. Fuster V, Ryden LE, Cannom DS et al. ACC/AHA/ESC 2006 guidelines for the management of patients with atrial fibrillation—executive summary. *J Am Coll Cardiol* 2006;48:854-906.
4. Gage BF, Waterman AD, Shannon W, Boechler M, Rich MW, Radford MJ. Validation of clinical classification schemes for predicting stroke: results from the National Registry of Atrial Fibrillation. *JAMA* 2001;285:2864-70.
5. Wyse DG, Waldo AL, DiMarco JP et al. A comparison of rate control and rhythm control in patients with atrial fibrillation. *N Engl J Med* 2002;347:1825-33.
6. Van Gelder IC, Hagens VE, Bosker HA et al. A comparison of rate control and rhythm control in patients with recurrent persistent atrial fibrillation. *N Engl J Med* 2002;347:1834-40.
7. Haissaguerre M, Jais P, Shah DC et al. Spontaneous initiation of atrial fibrillation by ectopic beats originating in the pulmonary veins. *N Engl J Med* 1998;339:659-66.
8. Jais P, Cauchemez B, Macle L et al. Catheter ablation versus antiarrhythmic drugs for atrial fibrillation: the A4 study. *Circulation* 2008;118:2498-505.
9. Oral H, Pappone C, Chugh A et al. Circumferential pulmonary-vein ablation for chronic atrial fibrillation. *N Engl J Med* 2006;354:934-41.
10. Pappone C, Augello G, Sala S et al. A randomized trial of circumferential pulmonary vein ablation versus antiarrhythmic drug therapy in paroxysmal atrial fibrillation: the APAF Study. *J Am Coll Cardiol* 2006;48:2340-7.
11. Stabile G, Bertaglia E, Senatore G et al. Catheter ablation treatment in patients with drug-refractory atrial fibrillation: a prospective, multi-centre, randomized, controlled study (Catheter Ablation For The Cure Of Atrial Fibrillation Study). *Eur Heart J* 2006;27:216-21.
12. Cappato R, Calkins H, Chen SA et al. Up-dated Worldwide Survey on the Methods, Efficacy and Safety of Catheter Ablation for Human Atrial Fibrillation. *Circ Arrhythm Electrophysiol* 2010, in press.
13. Ho SY, Cabrera JA, Tran VH, Farre J, Anderson RH, Sanchez-Quintana D. Architecture of the pulmonary veins: relevance to radiofrequency ablation. *Heart* 2001;86:265-70.
14. Casacang-Verzosa G, Gersh BJ, Tsang TS. Structural and functional remodeling of the left atrium: clinical and therapeutic implications for atrial fibrillation. *J Am Coll Cardiol* 2008;51:1-11.
15. Chen MC, Chang JP, Guo GB, Chang HW. Atrial size reduction as a predictor of the success of radiofrequency maze procedure for chronic atrial fibrillation in patients undergoing concomitant valvular surgery. *J Cardiovasc Electrophysiol* 2001;12:867-74.
16. Hsu LF, Jais P, Sanders P et al. Catheter ablation for atrial fibrillation in congestive heart failure. *N Engl J Med* 2004;351:2373-83.
17. Mond HG, Irwin M, Morillo C, Ector H. The world survey of cardiac pacing and cardioverter defibrillators: calendar year 2001. *Pacing Clin Electrophysiol* 2004;27:955-64.
18. Sweeney MO, Hellkamp AS, Ellenbogen KA et al. Adverse effect of ventricular pacing on heart failure and atrial fibrillation among patients with normal baseline QRS duration in a clinical trial of pacemaker therapy for sinus node dysfunction. *Circulation* 2003;107:2932-7.
19. Wilkoff BL, Cook JR, Epstein AE et al. Dual-chamber pacing or ventricular backup pacing in patients with an implantable defibrillator: the Dual Chamber and VVI Implantable Defibrillator (DAVID) Trial. *JAMA* 2002;288:3115-23.
20. Tse HF, Lau CP. Long-term effect of right ventricular pacing on myocardial perfusion and function. *J Am Coll Cardiol* 1997;29:744-9.

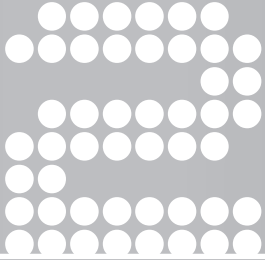
21. van Oosterhout MF, Prinzen FW, Arts T et al. Asynchronous electrical activation induces asymmetrical hypertrophy of the left ventricular wall. *Circulation* 1998;98:588-95.
22. Sweeney MO, Bank AJ, Nsah E et al. Minimizing ventricular pacing to reduce atrial fibrillation in sinus-node disease. *N Engl J Med* 2007;357:1000-8.
23. Vassallo JA, Cassidy DM, Miller JM, Buxton AE, Marchlinski FE, Josephson ME. Left ventricular endocardial activation during right ventricular pacing: effect of underlying heart disease. *J Am Coll Cardiol* 1986;7:1228-33.
24. Prinzen FW, Hunter WC, Wyman BT, McVeigh ER. Mapping of regional myocardial strain and work during ventricular pacing: experimental study using magnetic resonance imaging tagging. *J Am Coll Cardiol* 1999;33:1735-42.
25. Gomes JA, Damato AN, Akhtar M et al. Ventricular septal motion and left ventricular dimensions during abnormal ventricular activation. *Am J Cardiol* 1977;39:641-50.
26. Marsan NA, Breithardt OA, Delgado V, Bertini M, Tops LF. Predicting response to CRT. The value of two- and three-dimensional echocardiography. *Europace* 2008;10 Suppl 3:iii73-iii79.
27. Bax JJ, Bleeker GB, Marwick TH et al. Left ventricular dyssynchrony predicts response and prognosis after cardiac resynchronization therapy. *J Am Coll Cardiol* 2004;44:1834-40.
28. Leitman M, Lysyansky P, Sidenko S et al. Two-dimensional strain—a novel software for real-time quantitative echocardiographic assessment of myocardial function. *J Am Soc Echocardiogr* 2004;17:1021-9.
29. Suffoletto MS, Dohi K, Cannesson M, Saba S, Gorcsan J, III. Novel speckle-tracking radial strain from routine black-and-white echocardiographic images to quantify dyssynchrony and predict response to cardiac resynchronization therapy. *Circulation* 2006;113:960-8.
30. Bader H, Garrigue S, Lafitte S et al. Intra-left ventricular electromechanical asynchrony. A new independent predictor of severe cardiac events in heart failure patients. *J Am Coll Cardiol* 2004;43:248-56.
31. Bristow MR, Saxon LA, Boehmer J et al. Cardiac-resynchronization therapy with or without an implantable defibrillator in advanced chronic heart failure. *N Engl J Med* 2004;350:2140-50.
32. Cleland JG, Daubert JC, Erdmann E et al. The effect of cardiac resynchronization on morbidity and mortality in heart failure. *N Engl J Med* 2005;352:1539-49.
33. Vahanian A, Baumgartner H, Bax J et al. Guidelines on the management of valvular heart disease: The Task Force on the Management of Valvular Heart Disease of the European Society of Cardiology. *Eur Heart J* 2007;28:230-68.
34. Otto CM, Lind BK, Kitman DW, Gersh BJ, Siscovick DS. Association of aortic-valve sclerosis with cardiovascular mortality and morbidity in the elderly. *N Engl J Med* 1999;341:142-7.
35. Ling LH, Enriquez-Sarano M, Seward JB et al. Clinical outcome of mitral regurgitation due to flail leaflet. *N Engl J Med* 1996;335:1417-23.
36. Rosenhek R, Binder T, Porenta G et al. Predictors of outcome in severe, asymptomatic aortic stenosis. *N Engl J Med* 2000;343:611-7.
37. Grigioni F, Avierinos JF, Ling LH et al. Atrial fibrillation complicating the course of degenerative mitral regurgitation: determinants and long-term outcome. *J Am Coll Cardiol* 2002;40:84-92.
38. Kvidal P, Bergstrom R, Horte LG, Stahle E. Observed and relative survival after aortic valve replacement. *J Am Coll Cardiol* 2000;35:747-56.
39. Mihaljevic T, Nowicki ER, Rajeswaran J et al. Survival after valve replacement for aortic stenosis: implications for decision making. *J Thorac Cardiovasc Surg* 2008;135:1270-8.
40. Borger MA, Alam A, Murphy PM, Doenst T, David TE. Chronic ischemic mitral regurgitation: repair, replace or rethink? *Ann Thorac Surg* 2006;81:1153-61.
41. Mohty D, Orszulak TA, Schaff HV, Avierinos JF, Tajik JA, Enriquez-Sarano M. Very long-term survival and durability of mitral valve repair for mitral valve prolapse. *Circulation* 2001;104:11-17.
42. Iung B, Baron G, Butchart EG et al. A prospective survey of patients with valvular heart disease in Europe: The Euro Heart Survey on Valvular Heart Disease. *Eur Heart J* 2003;24:1231-43.
43. Webb JG, Chandavimol M, Thompson CR et al. Percutaneous aortic valve implantation retrograde from the femoral artery. *Circulation* 2006;113:842-50.

44. Grube E, Laborde JC, Gerckens U et al. Percutaneous implantation of the CoreValve self-expanding valve prosthesis in high-risk patients with aortic valve disease: the Siegburg first-in-man study. *Circulation* 2006;114:1616-24.
45. Piazza N, Grube E, Gerckens U et al. Procedural and 30-day outcomes following transcatheter aortic valve implantation using the third generation (18 Fr) corevalve revalving system: results from the multicentre, expanded evaluation registry 1-year following CE mark approval. *EuroIntervention* 2008;4:242-9.
46. Grube E, Buellesfeld L, Mueller R et al. Progress and Current Status of Percutaneous Aortic Valve Replacement: Results of Three Device Generations of the CoreValve Revalving System. *Circ Cardiovasc Intervent* 2008;1:167-75.
47. Feldman T, Wasserman HS, Herrmann HC et al. Percutaneous mitral valve repair using the edge-to-edge technique: six-month results of the EVEREST Phase I Clinical Trial. *J Am Coll Cardiol* 2005;46:2134-40.
48. Webb JG, Harenek J, Munt BI et al. Percutaneous transvenous mitral annuloplasty: initial human experience with device implantation in the coronary sinus. *Circulation* 2006;113:851-5.
49. Maniu CV, Patel JB, Reuter DG et al. Acute and chronic reduction of functional mitral regurgitation in experimental heart failure by percutaneous mitral annuloplasty. *J Am Coll Cardiol* 2004;44:1652-61.
50. Herrmann HC, Kar S, Siegel R et al. Effect of percutaneous mitral repair with the MitraClip device on mitral valve area and gradient. *EuroIntervention* 2009;4:437-42.
51. Schofer J, Siminiak T, Haude M et al. Percutaneous mitral annuloplasty for functional mitral regurgitation: results of the CARILLON Mitral Annuloplasty Device European Union Study. *Circulation* 2009;120:326-33.



Catheter ablation for atrial fibrillation





Multi-modality imaging to assess left atrial size, anatomy and function

Laurens F. Tops
Ernst E. van der Wall
Martin J. Schalij
Jeroen J. Bax

Department of Cardiology, Leiden University Medical Center, Leiden, the Netherlands

Heart 2007;93:1461-70

INTRODUCTION

The left atrium (LA) anterior-posterior diameter was one of the first standardized echocardiographic parameters. However, the clinical importance of LA size assessment has been neglected for a long time. Recent population-based studies have demonstrated the prognostic value of LA size for long-term outcome. Furthermore, with new dedicated techniques such as tissue Doppler imaging, it has become feasible to assess (regional) LA function. In addition, the introduction of catheter ablation procedures has changed the treatment of patients with drug-refractory atrial fibrillation (AF) dramatically. New image integration systems have become available for these catheter ablation procedures. With the use of image integration systems, a real anatomical 'roadmap' of the LA is provided for catheter ablation procedures. All these factors may explain the renewed interest in LA anatomy.

In the present manuscript, the importance of assessment of LA size and LA anatomy is discussed. Furthermore, the various imaging modalities that are available for the non-invasive visualization of the LA will be reviewed. In addition, the role of these imaging techniques in catheter ablation procedures for AF will be discussed.

CAUSES AND MECHANISMS OF LA DILATATION

In large population-based studies, it has been demonstrated that LA size is an important predictor of cardiovascular outcome (1-3). Tsang et al (3) recently demonstrated that a larger indexed LA volume predicted a higher risk of cardiovascular events after adjustment for age, gender and other covariates. Patients with a severely increased left atrium (≥ 40 ml/m²) had the highest risk for the development of cardiovascular events (hazard ratio 6.6) (3).

Left atrium dilatation can occur in a broad spectrum of cardiovascular diseases including hypertension, left ventricular dysfunction, mitral valve disease and AF. In general, two major conditions are associated with LA dilatation: pressure overload and volume overload (4). LA volume overload frequently occurs in the setting of mitral regurgitation. Pressure overload is most frequently caused by an increased LA afterload, secondary to mitral valve disease or LV dysfunction (4). Pritchett et al (5) demonstrated a close correlation between LA volume and the severity of diastolic dysfunction after adjusting for the presence of covariates including age, gender, cardiovascular disease, ejection fraction and left ventricular mass. Accordingly, it has been suggested that whereas LA volumes represent long-term exposure to elevated pressures, Doppler measures of filling pressures rather represent the actual LV filling pressures at one point in time (6).

Atrial fibrillation is another important factor associated with LA dilatation. Atrial fibrillation is the most commonly encountered cardiac arrhythmia, and the association of LA enlargement and AF has been well recognized (1,7-10). However, whether AF causes LA dilatation or vice

versa still remains controversial. Several studies suggest that LA enlargement may cause AF (1,7,8). In the Framingham Heart Study (7), M-mode derived LA size was an independent risk factor for development of AF. More recently, Tsang et al (1) demonstrated that LA volume (assessed with a modified biplane method) was a strong predictor of AF, incremental to clinical risk factors (1). However, other studies have revealed that LA enlargement may be the consequence of AF (9,10). Dittrich et al (10) demonstrated that AF was an independent predictor of LA size in a large cohort study with 3465 patients with AF.

32 THE IMPORTANCE OF LA SIZE AND ANATOMY ASSESSMENT

Assessment of LA size is important since it has been shown to provide strong prognostic information. The incremental value of LA size over conventional risk factors has been demonstrated in several studies (3,11-13). In the Framingham Heart study (13) it was demonstrated that LA enlargement was a significant predictor of death in both men and women. The relative risk of death per 10 mm increment in LA size was 1.3 for men (95% CI 1.0-1.5) and 1.4 for women (95% CI 1.1-1.7).

In particular, assessment of LA size is important in patients with AF. The guidelines on management of patients with AF recommend a standard 2-dimensional and Doppler echocardiogram, with assessment of LA size and function, in the clinical evaluation of all patients with AF (14). Osranek et al (12) demonstrated the predictive value of LA dilatation in patients with lone AF. In this population-based study with a median follow-up of 27 years, it was noted that in patients with lone AF, LA volume was a strong predictor of adverse events (cerebrovascular event/ acute myocardial infarction/ heart failure hospitalization/ death), independent of age and clinical risk factors (12).

The assessment of LA anatomy is important in the setting of catheter ablation procedures for AF. Although there is still debate concerning the best ablation strategy and the exact lesion set, knowledge on LA and pulmonary vein anatomy is mandatory, both before and during the ablation procedure. Both anatomical (15) and in vivo studies with different imaging modalities (16-18) have shown that LA and pulmonary vein anatomy is highly variable. Different non-invasive imaging modalities are available for assessment of LA size and anatomy. The various techniques and their clinical relevance/ applications will be discussed in the following paragraphs.

MULTI-MODALITY IMAGING OF THE LEFT ATRIUM

Echocardiography

For assessment of LA size various echocardiographic techniques are available, including transthoracic, transesophageal and intracardiac echocardiography. Transthoracic echocardiography is most commonly used in daily clinical practice to assess LA size. Both transesophageal and intracardiac echocardiography are mainly used during interventions for AF, such as cardioversion (transesophageal echocardiography) and catheter ablation procedures (intracardiac echocardiography).

Transthoracic echocardiography Feigenbaum was the first to demonstrate the correlation between LA dimension assessed with one-dimensional M-mode echocardiography and angiographic LA size (19). Afterwards, the development of two-dimensional echocardiography has expanded the insight in LA size and morphology. Nowadays, various established parameters for assessment of LA size are available (20). The LA anteroposterior diameter of the left atrium as assessed with M-mode is most commonly used in daily clinical practice and in large studies. However, it is not sufficient to determine true LA size, since M-mode represents only one dimension of the LA (21). In particular in LA enlargement, which may result in an asymmetrical geometry of the LA, M-mode echocardiography may underestimate LA size. Therefore, optimal assessment of LA size should include LA volume measurements (20,21). Various methods for the assessment of LA volume with two-dimensional echocardiography are available, including the cubical method, area-length method, ellipsoid method, and Modified Simpson's rule (Table 1 and Figure 1). In a prospective study including 631 patients (22), it was demonstrated that the biplane area-length method and the biplane Simpson's method compared closely (mean LA volume 39 ± 14 ml/m² and 38 ± 13 ml/m², correlation coefficient 0.98), whereas the ellipsoid method systematically underestimated LA volume (mean LA volume 32 ± 14 ml/m²). Recently,

Table 1. Methods for left atrial volume quantification with two-dimensional echocardiography

Method	Parameter	View	Equation	Assumption
Cube	Anterior-Posterior diameter (APD)	PSLAX	$4/3 \pi (APD/2)^3$	LA has a spherical shape
Ellipsoid	Anterior-Posterior diameter (APD)	PSLAX	$4/3 \pi (APD/2)(D1/2)$	LA has an ellipsoid geometry
	LA transversal diameter (D1)	4CH	(L/2)	
	LA length (L)	4CH		
Area-length	LA area planimetry (A2C)	2CH	$8/3 \pi [(A4C)(A2C)/L]$	LA has an ellipsoid geometry
	LA area planimetry (A4C)	4CH		
	LA length (L)	2CH or 4CH		
Modified Simpson's rule	LA planimetry	2CH	Summation of discs	Total volume can be calculated from sum of smaller volumes
		4CH		

LA = left atrium; PSLAX = parasternal long-axis; 2CH = 2-chamber view; 4CH = 4-chamber view

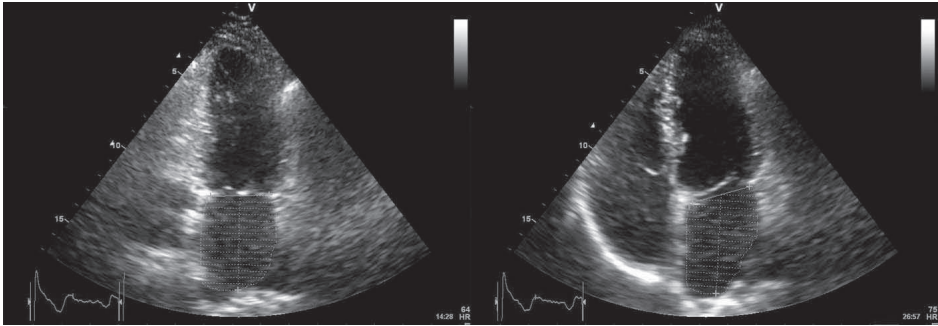


Figure 1. Measurement of LA volumes with transthoracic echocardiography using the modified biplane Simpson's rule. The maximum LA volume is assessed during ventricular systole in the apical 2-chamber (left panel) and apical 4-chamber (right panel) views. Maximal LA volume was 46 ml, minimal LA volume was 22 ml, resulting in an LA ejection fraction of 53%.

three-dimensional echocardiography has been introduced (Figure 2). A number of studies have demonstrated the feasibility of three-dimensional echocardiography for the assessment of LA volumes (23,24), and it has been validated against magnetic resonance imaging (25). Jenkins et al (23) have demonstrated that three-dimensional echocardiography allows accurate LA volume assessment, with a low test-retest variation, and a lower intra- and inter-observer variability as compared to two-dimensional echocardiography. However, there still remain some technical limitations such as the spatial and temporal resolution. In addition, since a relatively constant RR interval is needed, three-dimensional echocardiography may not be feasible in patients with AF and a high ventricular response rate.

Transesophageal echocardiography Transesophageal echocardiography (TEE) provides good views on the LA and the left atrial appendage (LAA). However, visualizing the complete left atrium to determine LA size with TEE may be hampered by the close proximity of the probe to the LA and the variable position of the esophagus to the posterior LA. As a result, measurements of LA size with TEE have not been standardized. Only few studies have compared the assessment of LA size with TEE and TTE. Block et al (26) assessed different LA dimensions with TEE and TTE in 109 patients. The authors noted that the 30- to 60-degree short-axis equivalent at the level of the aortic valve was the only view in which the entire LA dimension could be reliably obtained. Although TEE slightly underestimated LA size, it provided good correlation with TTE (26).

TEE is considered the procedure of choice for assessment of thrombi in the LA cavity or LAA. It can detect thrombi with a high degree of sensitivity and specificity varying from 93 - 100% (27). In addition, TEE is helpful in assessment of LAA emptying velocities, which are correlated with thrombus formation (velocities <20 cm/s) and with maintenance of sinus rhythm after cardioversion (velocities >40 cm/s) (28). Furthermore, TEE may be of great value in performing transseptal punctures in AF ablation procedures.

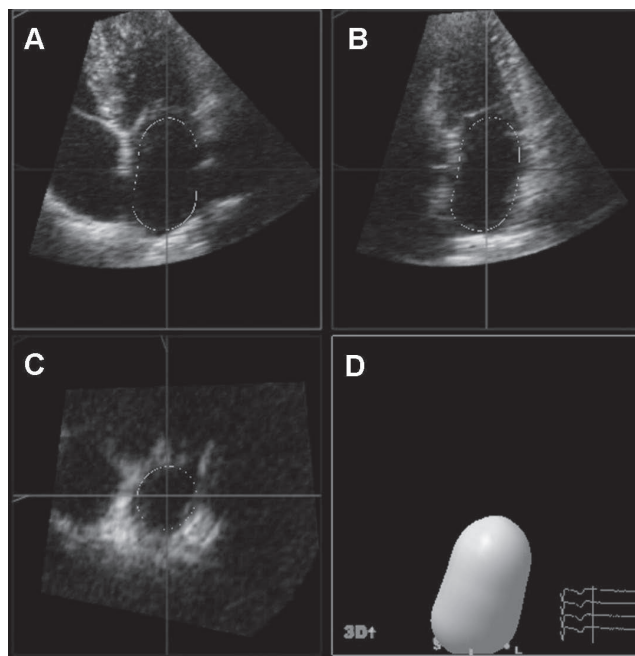


Figure 2. Real-time three-dimensional echocardiogram for the assessment of LA volumes. Panels A to C represent the coronal, sagittal and transverse planes, respectively. With the use of a 5-point tracing algorithm, LA volumes can be obtained throughout the cardiac cycle, represented by the 'shell' in panel D. In this example, LA maximum volume was 53 ml.

Intracardiac echocardiography Intracardiac echocardiography (ICE) is only used during interventional procedures, such as percutaneous closure of atrial septal defects and catheter ablation procedures. Therefore, no standardized measurements of LA size or volume are available. During these interventional procedures, ICE can accurately visualize LA anatomy and related structures (29). Furthermore, it allows visualization of intracardiac devices and catheters, and it is helpful in monitoring potential complications during catheter ablation procedures (30). Examples of intracardiac echocardiograms are shown in Figure 3.

In addition, the Doppler capacities of ICE allow for monitoring of pulmonary vein narrowing and may predict the recurrence of AF after ablation (31). Furthermore, LA function can be assessed with ICE. Rotter et al (32) demonstrated a good correlation between ICE and TEE for measurement of mitral E wave velocity (correlation coefficient 0.759, mean difference 6.9 cm/s) and LAA emptying velocity (correlation coefficient 0.991, mean difference 0.7 cm/s). Although ICE is limited by the monoplane character and the lack of standardized measurements of LA size, it is a valuable tool for interventional procedures.

Multi-slice computed tomography

The application of multi-slice computed tomography (MSCT) in cardiac imaging has rapidly expanded in the past few years. Since MSCT has an excellent spatial and temporal resolution,

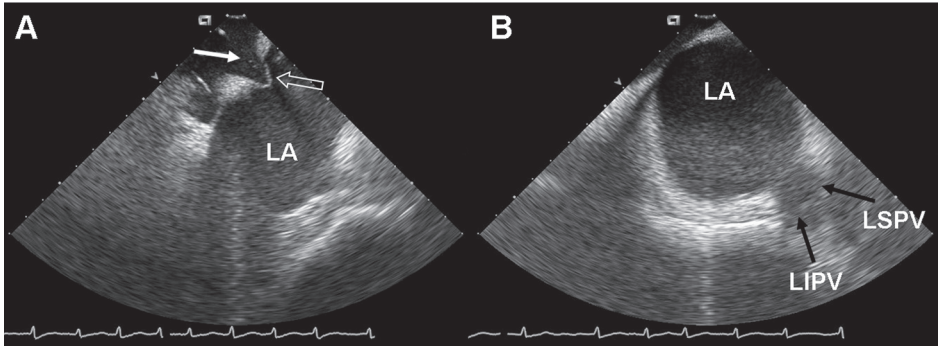


Figure 3. Intracardiac echocardiography during a catheter ablation procedure for AF. Panel A: The transseptal puncture is guided by ICE to gain access to the LA. The white arrow indicates the transseptal sheath aimed at the fossa ovalis, which is the preferred site for the transseptal puncture. The 'tenting' of the septum (open arrow) indicates stable contact of the sheath with the fossa ovalis. Panel B: The anatomy of the pulmonary veins can be assessed with ICE during the ablation procedure. In this patient, the left inferior pulmonary vein (LIPV) and the left superior pulmonary vein (LSPV) have a single insertion in the LA, a so-called 'common ostium' of the left-sided pulmonary veins.

it can accurately quantify LA volumes, by using the modified Simpson's method (33). However, because of the radiation exposure and the use of contrast agents, MSCT is not routinely used for the assessment of LA size.

For AF ablation procedures, MSCT is a valuable tool to depict LA anatomy (34). With the use of volume-rendered reconstructions, MSCT can provide detailed information on LA and pulmonary vein anatomy (Figure 4). Since LA and pulmonary vein anatomy is highly variable, MSCT may offer a 'road-map' for ablation. The exact role of MSCT in ablation procedures is discussed in one of the following paragraphs.

Magnetic resonance imaging

Magnetic resonance imaging (MRI) is considered the most accurate technique for the non-invasive assessment of atrial volumes, because of the high spatial resolution and the excellent myocardial border detection. Detailed information of LA size and volumes throughout the cardiac cycle can be acquired with MRI (Figure 5). Anderson et al (35) recently reported findings on LA dimensions and LA area assessed with MRI in 20 healthy controls and in 20 patients with cardiomyopathy. It was noted that a LA systolic area $<24 \text{ cm}^2$ was the upper 95th percentile of the normal range, and best discriminated normal from abnormal hearts (35). Similar to MSCT, a modified Simpson's method can be used to determine LA volumes. However, due to its relatively long acquisition times and the cumbersome data analysis, LA volume assessment with MRI is not performed in daily clinical practice. MRI can provide detailed information on LA and pulmonary vein anatomy before catheter ablation procedures, and is a useful tool in the follow-up of patients after the ablation procedure. This will be discussed in more depth in one of the following paragraphs.

Several studies have compared the value of the different imaging modalities for the assessment of LA size and volumes (23-26,36). Two-dimensional transthoracic echocardiography

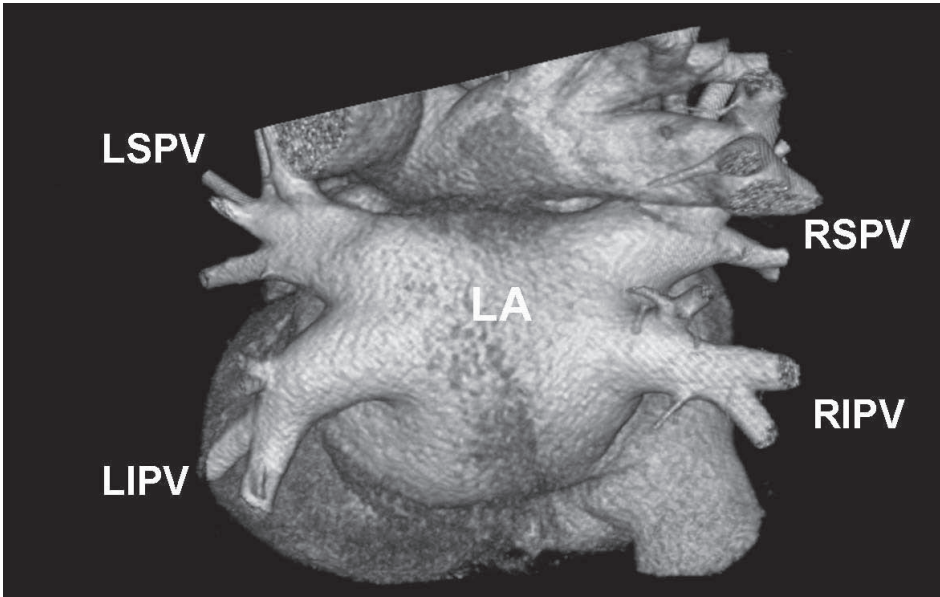


Figure 4. Volume-rendered three-dimensional reconstruction of a 64-slice MSCT scan. The dorsal view clearly demonstrates the anatomy of the LA and pulmonary veins. In this patient, normal pulmonary vein anatomy is present including four pulmonary veins, all with their own insertion into the LA. LIPV = left inferior pulmonary vein; LSPV = left superior pulmonary vein; RIPV = right inferior pulmonary vein; RSPV = right superior pulmonary vein.

(using the biplane methods) may underestimate true LA size, as compared with computed tomography (36) or magnetic resonance (25). However, these three-dimensional techniques are not preferred for LA size assessment in daily clinical practice. In this respect, new three-dimensional echocardiography is a promising technique that is widely available and provides accurate information on LA size (24).

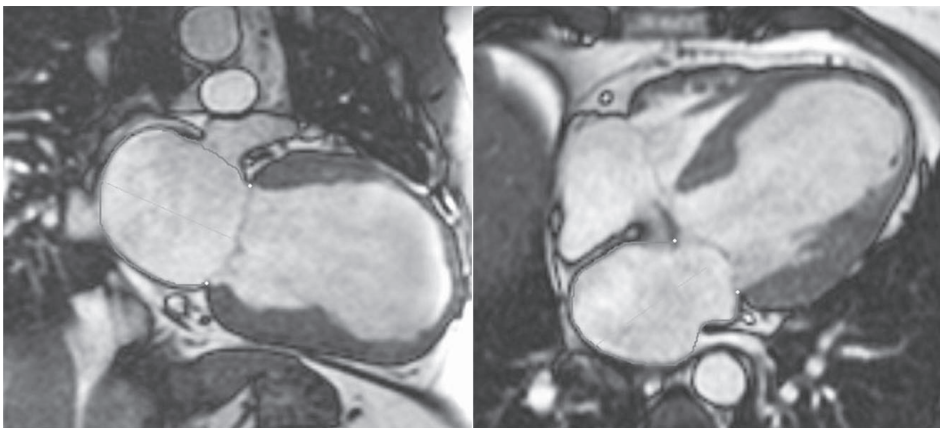


Figure 5. Assessment of LA volumes with MRI. The 2-chamber (left panel) and the 4-chamber (right panel) views are used to delineate the endocardial border of the LA, as well as the maximal diameter.

ASSESSMENT OF REGIONAL LA FUNCTION

38

Regional LA function is not routinely assessed, and therefore no standardized parameters for regional LA function are available. This can be partly explained by the fact that non-invasive evaluation of regional LA function may be hampered by the relative thin LA walls. However, assessment of regional LA function may provide more insight in atrial electromechanical remodeling and may be helpful in the management of AF with surgical or catheter ablation. New echocardiographic techniques, such as tissue Doppler imaging and strain (rate) imaging, allow non-invasive measurement of regional function of the myocardium. Tissue Doppler imaging quantifies regional tissue velocities of the myocardium. Strain and strain rate represent local tissue deformation and the rate (speed) of local deformation, respectively (37). Both techniques have been well validated for the assessment of regional left ventricular function. Recently, several studies (38-42) have applied these new techniques to the left atrium.

Tissue Doppler imaging allows quantification of regional myocardial velocities, and assessment of the timing of peak systolic and diastolic velocities of the myocardium (Figure 6, panel A). Thomas et al (38) used tissue Doppler imaging in 92 healthy volunteers to evaluate regional LA function. The authors noted that atrial contraction velocities were significantly increased in the annular segments, compared with the more superior segments.

Tissue Doppler imaging also provides information on the timing of regional velocities of the myocardium. Therefore, it may quantify regional electromechanical LA function, such as the total electromechanical activity of the atria (represented by the interval between the onset of the P-wave on the ECG to the end of the A' wave on the tissue Doppler images) (39). However, the clinical relevance and the exact correlation of these new tissue Doppler derived parameters of regional LA function with conventional parameters, such as mitral inflow A wave velocity and LA volumes, needs further investigation. Furthermore, a limitation of tissue Doppler imaging for evaluation of regional LA function is the angle dependency of the technique. Therefore, careful adjustment of the beam and gain settings should be made to avoid aliasing and to allow reliable measurement of tissue velocities of the LA.

Strain imaging and strain rate imaging are new tools for the assessment of regional myocardial deformation of the LA (40). An example of strain rate imaging of the LA is shown in Figure 6, panel B. In contrast to tissue Doppler imaging, strain imaging is not hampered by myocardial tethering. Furthermore, strain imaging allows for differentiation between active contraction and passive motion (37). However, the thin atrial walls may not generate clear strain curves and therefore require careful interpretation. Several studies have demonstrated the value of regional atrial strain in the analysis of patients with AF undergoing cardioversion (41,42). Di Salvo et al (41) studied 65 patients with AF and performed tissue Doppler imaging of standard apical images of the LA. It was noted that all tissue Doppler imaging derived parameters of the LA, including tissue velocities, strain and strain rate, were significantly reduced in patients with AF, compared with healthy controls. Of interest, multivariable analysis demonstrated that atrial

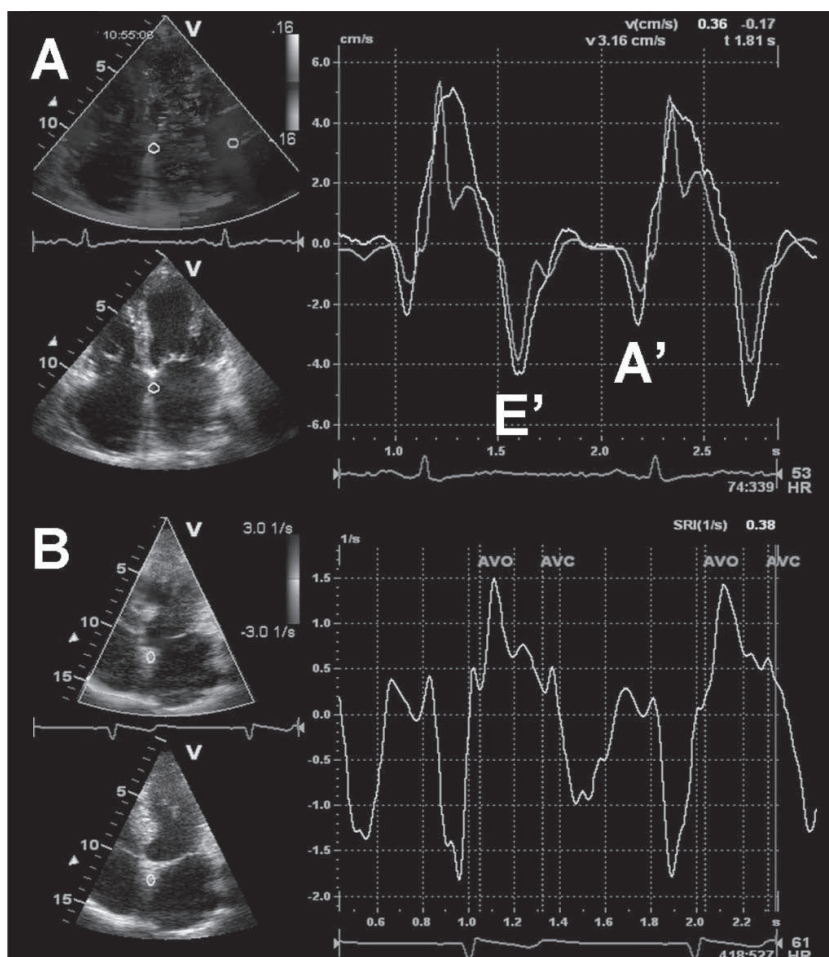


Figure 6. Panel A: Color-coded tissue Doppler imaging in the apical 4-chamber view for the assessment of regional LA function. The samples are placed in the basal atrial septum and the basal atrial lateral wall. From the myocardial velocity curves, peak systolic and diastolic velocities can be assessed. Early diastolic filling is indicated by E' and late diastolic filling is indicated by A'. Panel B: Strain rate imaging in the apical 4-chamber view in a patient with a history of paroxysmal atrial fibrillation. A sample is placed in the basal atrial septum. From the time-strain curves segmental atrial contraction and time-to-peak strain can be derived. The vertical green lines indicate aortic valve opening (AVO) and aortic valve closure (AVC).

inferior wall peak systolic strain rate and atrial septal peak systolic strain were the best predictors of maintenance of sinus rhythm after cardioversion (41). The assessment of regional LA function by tissue Doppler imaging or strain imaging may be of value in the clinical follow-up of patients with AF undergoing catheter ablation or cardioversion. It has been suggested that diminished regional atrial strain values may warrant prolonged use of anti-arrhythmic drugs and anti-coagulation (41,42). However, more studies are needed to appreciate the value of regional left atrial strain and its role to guide use of medication in patients with AF.

IMAGING OF LA FUNCTION IN THERAPY FOR AF

As previously discussed, the association between LA remodeling and AF has been well recognized. Restoration of normal sinus rhythm by catheter ablation or cardioversion may result in reverse remodeling of the LA, with subsequent improvement of LA function. However, electrical or pharmacological cardioversion may cause transient atrial mechanical dysfunction or 'stunning' (28,43). It has been demonstrated that conventional parameters of LA function, such as A wave velocity or A wave velocity time integral, are decreased immediately after cardioversion (43). The subsequent depressed LA appendage flow velocities increase the risk of thromboembolic events after cardioversion.

With the use of new techniques such as strain imaging, LA dysfunction following cardioversion can also be assessed (42). In 37 patients with chronic AF, it was noted that immediately after cardioversion regional LA function was depressed compared with healthy controls. However, 6 months after successful cardioversion a significant increase in LA strain was observed. The maximal increase in regional LA strain occurred within 1 month after cardioversion (42). This observation is in concordance with previous studies (43,44) and suggests that 'atrial stunning' following cardioversion is a function of the preceding AF, rather than the cardioversion itself.

Catheter ablation has been demonstrated to be successful in the restoration of sinus rhythm, and is performed in an increasing number of patients with symptomatic drug-refractory AF. It has been demonstrated that maintenance of sinus rhythm after catheter ablation is associated with a decrease in LA volumes (Figure 7) (45). Reant et al studied 48 patients with lone AF treated with catheter ablation (46). Serial echocardiograms up to 12 months after the procedure revealed a progressive decrease in LA dimensions. Interestingly, with the use of new tissue Doppler derived parameters it was noted that in parallel to the improvement in LA function, both LV systolic and diastolic function improved in the patients who maintained sinus rhythm (46). Furthermore, with the use of MRI it has been demonstrated that in addition to LA reverse remodeling, the area of the pulmonary venous ostia may decrease after successful catheter ablation procedures (47).

IMAGING IN CATHETER ABLATION PROCEDURES FOR AF

Multimodality imaging

Catheter ablation procedures are being performed in an increasing number of patients worldwide. The recent guidelines on management of patients with AF propose catheter ablation as a reasonable option when first-line anti-arrhythmic drugs have failed (14). Various ablation strategies have been proposed, including segmental ostial ablation and anatomically based circumferential ablation, and there is still debate concerning the exact lesion set. Regardless of the ablation strategy applied, knowledge on the complex LA and pulmonary vein anatomy is

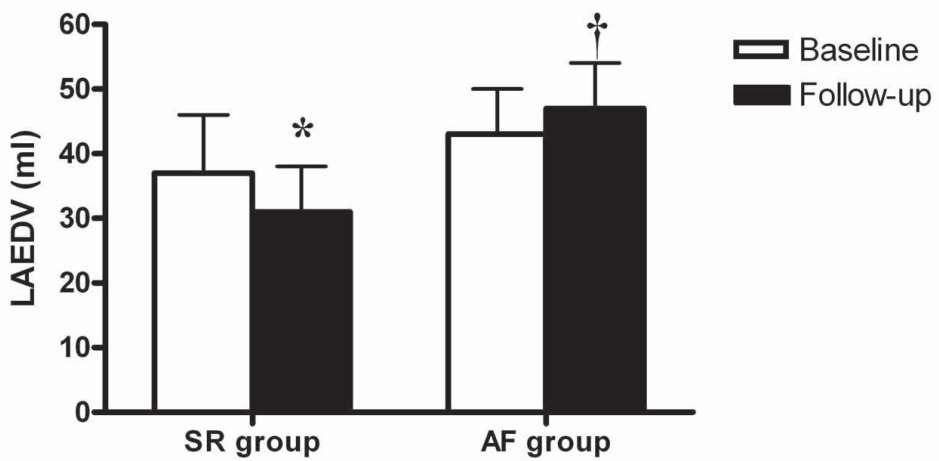


Figure 7. Reverse remodeling of the LA may occur after successful catheter ablation. A significant reduction in LA end-diastolic volume (LAEDV) was observed in the patients who maintained sinus rhythm after the catheter ablation procedure (SR group). In contrast, an increase in LA volumes was observed in the patients who had recurrence of atrial fibrillation (AF group). * = $p < 0.01$ baseline vs. 3 months of follow-up; † = $p < 0.05$ SR group vs. AF group.

essential during the ablation procedure. The veno-atrial junctions and anatomical landmarks in the LA, such as the ridge between the left superior pulmonary vein and the LAA, are critical structures to identify during catheter ablation procedures.

Anatomical studies have demonstrated that LA and pulmonary vein anatomy is highly variable (15). Most frequently, two left-sided pulmonary veins and two right-sided pulmonary veins drain separately into the LA (Figure 4). Anatomical variations include a single insertion or 'common ostium' of the pulmonary veins, and an additional pulmonary vein (Figure 8). A 'common ostium' is most frequently found on the left-sided pulmonary veins, whereas an additional pulmonary vein is most frequently noted on the right side. In 201 patients undergoing MSCT scanning, Marom et al (48) noted a left-sided 'common ostium' in 14% of the patients, and an additional right-sided pulmonary vein in 28% of the patients. In addition, variations in LAA morphology and LA roof anatomy may be present in patients with AF (49). Because of the complex anatomy of the LA and the variability in pulmonary vein anatomy, a detailed 'roadmap' for the ablation procedure is mandatory. The various imaging modalities that are available for assessment of LA and pulmonary vein anatomy in catheter ablation procedures include MSCT, MRI, ICE and electroanatomical mapping systems.

MSCT and MRI (Figures 8 and 9) provide detailed information on the anatomy of the LA and pulmonary veins. With the use of volume-rendered three-dimensional reconstructions and cross-sectional images, the number of pulmonary veins and their branching pattern can be accurately assessed (Figure 10). Furthermore, the diameters of the pulmonary vein ostia can be measured on the different orthogonal planes. In addition, MSCT may identify the presence of thrombi in the LAA and provide detailed information on surrounding structures, such as the

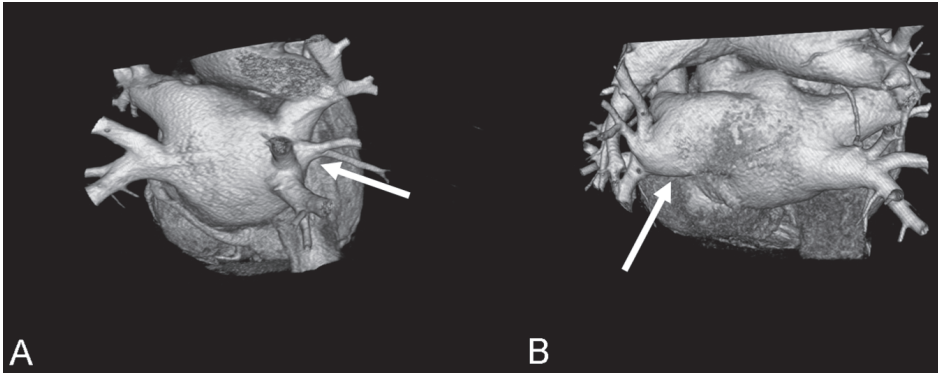


Figure 8. Variations in pulmonary vein (PV) anatomy shown on volume-rendered three-dimensional reconstructions of MSCT scans. Panel A demonstrates an additional PV on the right side. Panel B shows a 'common' ostium of the left-sided PVs.

esophagus and coronary arteries. However, the pre-procedural acquired MSCT and MRI images only provide off-line information.

In contrast to MSCT and MRI, ICE allows real-time assessment of the pulmonary veins and the veno-atrial junction during the ablation procedure. The Doppler capacities and the ability to monitor the catheter position in relation to the pulmonary veins are great advantages of this technique (29). In addition, ICE is helpful in assessment of the transmural extent of the ablation lesions (50) and ICE has been used to titrate ablation energy, thereby increasing the safety of the ablation procedure (30). Still, the major limitation of ICE is the mono-dimensional character of the technique. It has been demonstrated that three-dimensional imaging modalities

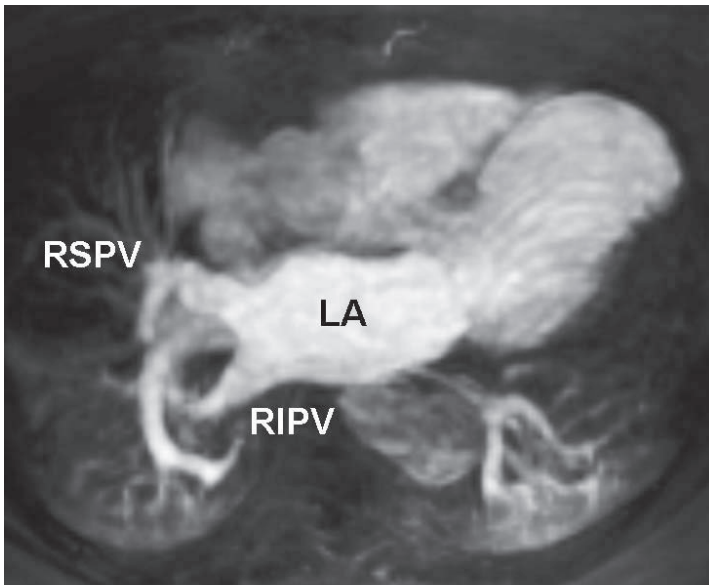


Figure 9. Maximum intensity projection of a gadolinium enhanced MRI angiogram of the pulmonary veins. LA = left atrium; RIPV = right inferior pulmonary vein; RSPV = right superior pulmonary vein

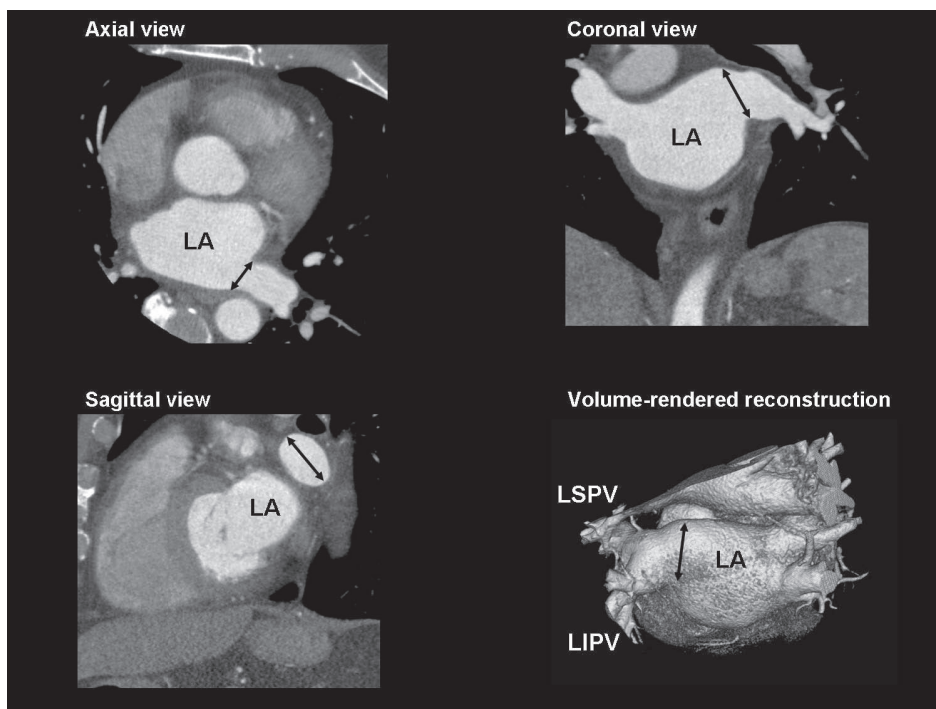


Figure 10. The different orthogonal planes (axial, coronal and sagittal) and three-dimensional volume rendered reconstructions of the MSCT scan can be used to assess LA and pulmonary vein anatomy. The black arrows indicate the large 'common ostium' of the left-sided pulmonary veins. LIPV = left inferior pulmonary vein; LSPV = left superior pulmonary vein

provide the most accurate information on LA and pulmonary vein anatomy (16,17). In a direct comparison between MSCT and ICE (Figure 11), it was noted that MSCT has a higher sensitivity for the detection of additional pulmonary veins and that ICE underestimated the size of the pulmonary venous ostia (16).

During the ablation procedure, electroanatomical mapping systems such as Carto™ (Biosense-Webster, Diamond Bar, California, USA) are available to assess LA and pulmonary vein anatomy. These systems combine on-line electrophysiological data with anatomical information, acquired with mapping catheters positioned in the LA (51). When performing the actual ablation, the ablation points can be marked on the acquired electroanatomical map. The major limitation of these systems is the use of reconstructed anatomy. Ideally, the detailed anatomical information acquired with three-dimensional imaging techniques (such as MSCT and MRI) could be combined with the on-line electrophysiological information. Recently, image integration systems have been introduced that allow the on-line use of MSCT or MRI images during the actual ablation procedures.

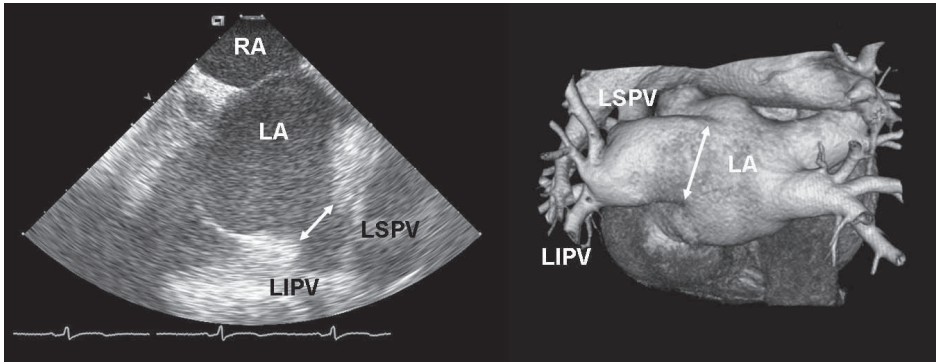


Figure 11. Comparison of MSCT and ICE to evaluate LA and pulmonary vein anatomy. In this patient, both techniques clearly visualize the 'common ostium' of the left-sided pulmonary veins (indicated with the white arrow). Whereas MSCT may provide more detailed three-dimensional information, ICE also provides on-line information on the relation between the ablation catheter and the pulmonary veins during the actual ablation. LIPV = left inferior pulmonary vein; LSPV = left superior pulmonary vein; RA = right atrium

Image integration

With the use of new image integration systems such as CartoMerge™ (Biosense-Webster, Diamond Bar, California, USA), it has become feasible to merge pre-procedural acquired three-dimensional MSCT or MRI images with on-line acquired electroanatomical maps. Before the ablation procedure, the MSCT or MRI images are segmented into different structures (Figure 12). During the ablation procedure, the MSCT or MRI images are 'registered' with the use of dedicated software algorithms that minimize the distance between the electroanatomical mapping points and the three-dimensional MSCT or MRI images (Figure 13). Both pre-clinical (52) and clinical studies (53-55) have demonstrated the accuracy of image integration systems. Advantages of the image integration systems include the possibility to monitor the exact catheter position in relation to the endocardial border, the pulmonary veins and the surrounding structures (Figure 14). Hereby, potential complications such as pulmonary vein stenosis and atrio-oesophageal fistula may be avoided.

Recently, Kistler et al (54) compared 47 patients treated using conventional mapping alone with 47 patients treated using MSCT image integration. In the image integration group, fluoroscopy times were significantly shorter (49 ± 27 minutes vs. 62 ± 26 minutes, $p < 0.05$) and the number of patients with maintenance of sinus rhythm without anti-arrhythmic medication was significantly higher in the image integration group (83% vs. 60%, $p < 0.05$) (54). However, these data have to be confirmed in larger, randomized trials.

One of the limitations of the new image integration technique is the time interval between the MSCT / MRI scan and the actual ablation procedure. Obviously, differences in fluid status, heart rate or rhythm are present between the two procedures, and may result in errors in the image fusion process. Furthermore, the accuracy of the image integration process may be affected by breathing during data acquisition and during the ablation procedure. In addition, variation of pulmonary vein location throughout the cardiac cycle may decrease the accuracy (56). Nonetheless, the various studies (52-55) have demonstrated the accuracy and the value

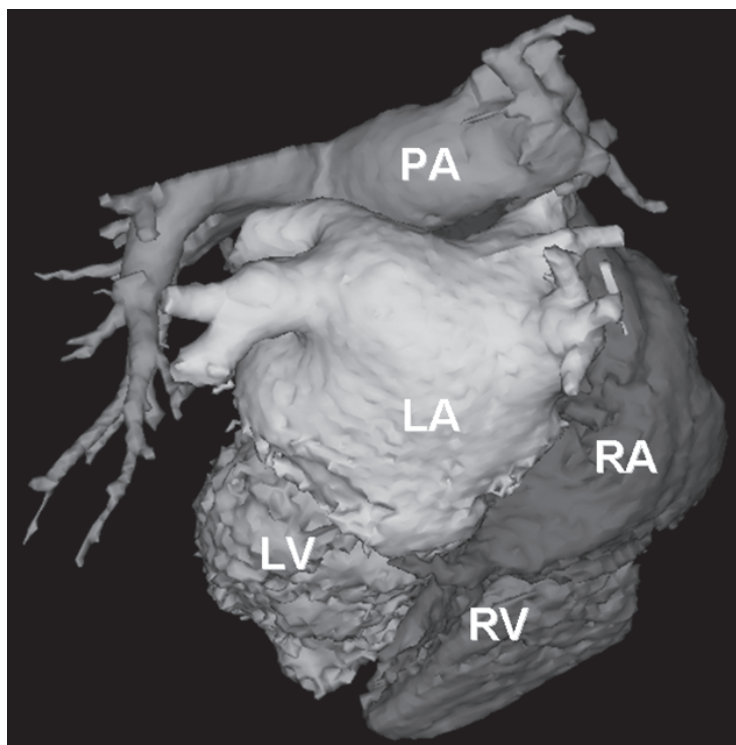


Figure 12. Segmentation of the MSCT scan into the different structures using the CartoMerge™ Image Integration Module. From the raw MSCT data, a three-dimensional volume is created. This volume is divided in the different chambers by placing anatomical landmarks and applying a dedicated software algorithm. The chamber of interest (LA in case of atrial fibrillation ablation) can then be used during the actual ablation procedure. LA = left atrium; LV = left ventricle; PA = pulmonary artery; RA = right atrium; RV = right ventricle

of image integration systems in guiding AF ablation procedures. By merging on-line acquired electrophysiological data with detailed anatomical information, these image integration systems are valuable tools in the invasive treatment of patients with AF.

SUMMARY

Assessment of LA size, anatomy and function is important in various clinical settings and can be performed with different imaging techniques. The assessment of LA size provides important prognostic information and is routinely performed with transthoracic echocardiography. Information on regional LA function can also be provided by transthoracic echocardiography and is important in the setting of treatment of atrial fibrillation. Catheter ablation procedures for AF require accurate imaging of LA and surrounding structures. Intracardiac echocardiography, MSCT and MRI provide detailed information on LA and pulmonary vein anatomy. New image integration systems allow the on-line use of pre-procedural acquired images and may facilitate the ablation procedures and potentially improve the outcome.

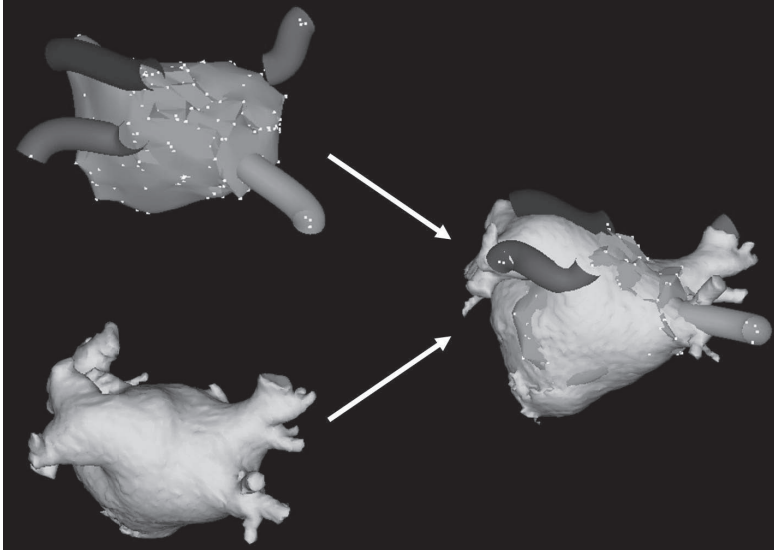


Figure 13. Image integration. The upper left panel demonstrates the conventional electroanatomical map with the reconstructed anatomy of the LA. The blue, purple, red and green 'tubes' represent the pulmonary veins. The lower left panel shows the segmented LA derived from MSCT (see also Figure 12). With the use of dedicated software, the CartoMerge™ Image Integration Module integrates the both modalities (right panel).

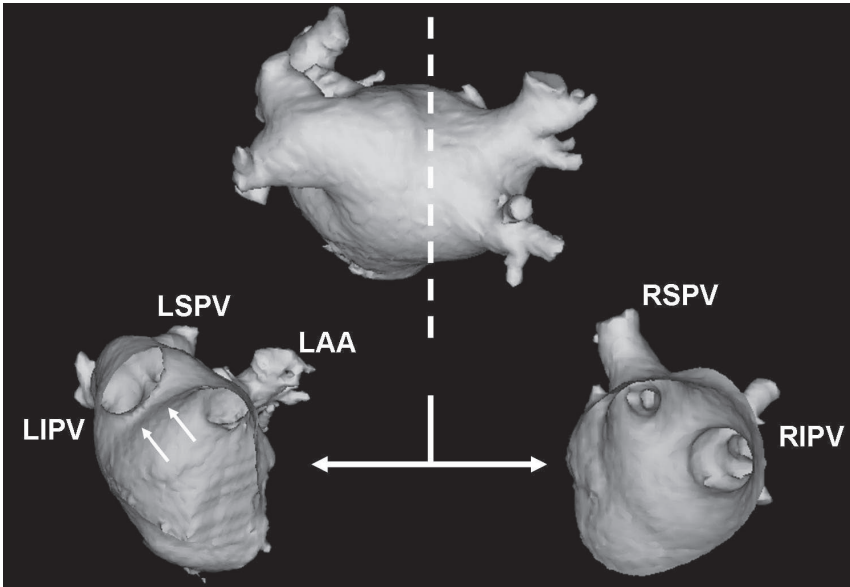


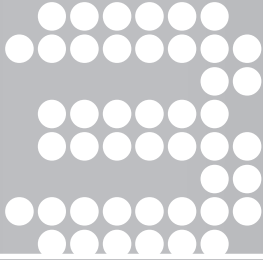
Figure 14. After the fusion process, the 'real' anatomy provided by the MSCT scan can be used to guide the actual catheter ablation. With the use of dedicated tools, such as a 'clipping plane' (represented by the dotted line), the ostium of the left-sided pulmonary veins (lower left panel) and the right-sided pulmonary veins (lower right panel) can be visualized. The relation between the ablation catheter and the ostium of the pulmonary veins can be monitored constantly. In this patient, a 'common ostium' of the left-sided pulmonary veins is present. The white arrows indicate the ridge between the left-sided pulmonary veins and the left atrial appendage (LAA). LIPV = left inferior pulmonary vein; LSPV = left superior pulmonary vein; RIPV = right inferior pulmonary vein; RSPV = right superior pulmonary vein.

REFERENCES

1. Tsang TS, Barnes ME, Bailey KR et al. Left atrial volume: important risk marker of incident atrial fibrillation in 1655 older men and women. *Mayo Clin Proc* 2001;76:467-75.
2. Pritchett AM, Jacobsen SJ, Mahoney DW, Rodeheffer RJ, Bailey KR, Redfield MM. Left atrial volume as an index of left atrial size: a population-based study. *J Am Coll Cardiol* 2003;41:1036-43.
3. Tsang TS, Abhayaratna WP, Barnes ME et al. Prediction of cardiovascular outcomes with left atrial size: is volume superior to area or diameter? *J Am Coll Cardiol* 2006;47:1018-23.
4. Abhayaratna WP, Seward JB, Appleton CP et al. Left atrial size: physiologic determinants and clinical applications. *J Am Coll Cardiol* 2006;47:2357-63.
5. Pritchett AM, Mahoney DW, Jacobsen SJ, Rodeheffer RJ, Karon BL, Redfield MM. Diastolic dysfunction and left atrial volume: a population-based study. *J Am Coll Cardiol* 2005;45:87-92.
6. Douglas PS. The left atrium: a biomarker of chronic diastolic dysfunction and cardiovascular disease risk. *J Am Coll Cardiol* 2003;42:1206-7.
7. Vaziri SM, Larson MG, Benjamin EJ, Levy D. Echocardiographic predictors of nonrheumatic atrial fibrillation. The Framingham Heart Study. *Circulation* 1994;89:724-30.
8. Psaty BM, Manolio TA, Kuller LH et al. Incidence of and risk factors for atrial fibrillation in older adults. *Circulation* 1997;96:2455-61.
9. Sanfilippo AJ, Abascal VM, Sheehan M et al. Atrial enlargement as a consequence of atrial fibrillation. A prospective echocardiographic study. *Circulation* 1990;82:792-7.
10. Dittrich HC, Pearce LA, Asinger RW et al. Left atrial diameter in nonvalvular atrial fibrillation: An echocardiographic study. Stroke Prevention in Atrial Fibrillation Investigators. *Am Heart J* 1999;137:494-9.
11. Tsang TS, Barnes ME, Gersh BJ et al. Prediction of risk for first age-related cardiovascular events in an elderly population: the incremental value of echocardiography. *J Am Coll Cardiol* 2003;42:1199-205.
12. Osranek M, Bursi F, Bailey KR et al. Left atrial volume predicts cardiovascular events in patients originally diagnosed with lone atrial fibrillation: three-decade follow-up. *Eur Heart J* 2005;26:2556-61.
13. Benjamin EJ, D'Agostino RB, Belanger AJ, Wolf PA, Levy D. Left Atrial Size and the Risk of Stroke and Death: The Framingham Heart Study. *Circulation* 1995;92:835-41.
14. Fuster V, Ryden LE, Cannom DS et al. ACC/AHA/ESC 2006 guidelines for the management of patients with atrial fibrillation—executive summary. *J Am Coll Cardiol* 2006;48:854-906.
15. Ho SY, Cabrera JA, Tran VH, Farre J, Anderson RH, Sanchez-Quintana D. Architecture of the pulmonary veins: relevance to radiofrequency ablation. *Heart* 2001;86:265-70.
16. Jongbloed MR, Bax JJ, Lamb HJ et al. Multislice computed tomography versus intracardiac echocardiography to evaluate the pulmonary veins before radiofrequency catheter ablation of atrial fibrillation: a head-to-head comparison. *J Am Coll Cardiol* 2005;45:343-50.
17. Wood MA, Wittkamp M, Henry D et al. A comparison of pulmonary vein ostial anatomy by computerized tomography, echocardiography, and venography in patients with atrial fibrillation having radiofrequency catheter ablation. *Am J Cardiol* 2004;93:49-53.
18. Mansour M, Holmvang G, Sosnovik D et al. Assessment of pulmonary vein anatomic variability by magnetic resonance imaging: implications for catheter ablation techniques for atrial fibrillation. *J Cardiovasc Electrophysiol* 2004;15:387-93.
19. Hirata T, Wolfe SB, Popp RL, Helmen CH, Feigenbaum H. Estimation of left atrial size using ultrasound. *Am Heart J* 1969;78:43-52.
20. Lang RM, Bierig M, Devereux RB et al. Recommendations for Chamber Quantification. *J Am Soc Echocardiogr* 2005;18:1440-63.
21. Lester SJ, Ryan EW, Schiller NB, Foster E. Best method in clinical practice and in research studies to determine left atrial size. *Am J Cardiol* 1999;84:829-32.
22. Ujino K, Barnes ME, Cha SS et al. Two-dimensional echocardiographic methods for assessment of left atrial volume. *Am J Cardiol* 2006;98:1185-8.

23. Jenkins C, Bricknell K, Marwick TH. Use of real-time three-dimensional echocardiography to measure left atrial volume: comparison with other echocardiographic techniques. *J Am Soc Echocardiogr* 2005;18:991-7.
24. Maddukuri PV, Vieira ML, DeCastro S et al. What is the best approach for the assessment of left atrial size? Comparison of various unidimensional and two-dimensional parameters with three-dimensional echocardiographically determined left atrial volume. *J Am Soc Echocardiogr* 2006;19:1026-32.
25. Rodevan O, Bjornerheim R, Ljosland M, Maehle J, Smith HJ, Ihlen H. Left atrial volumes assessed by three- and two-dimensional echocardiography compared to MRI estimates. *Int J Card Imaging* 1999;15:397-410.
26. Block M, Hourigan L, Bellows WH et al. Comparison of left atrial dimensions by transesophageal and transthoracic echocardiography. *J Am Soc Echocardiogr* 2002;15:143-9.
27. Klein AL, Murray RD, Grimm RA. Role of transesophageal echocardiography-guided cardioversion of patients with atrial fibrillation. *J Am Coll Cardiol* 2001;37:691-704.
28. Troughton RW, Asher CR, Klein AL. The role of echocardiography in atrial fibrillation and cardioversion. *Heart* 2003;89:1447-54.
29. Jongbloed MR, Schaliq MJ, Zeppenfeld K, Oemrawsingh PV, van der Wall EE, Bax JJ. Clinical applications of intracardiac echocardiography in interventional procedures. *Heart* 2005;91:981-90.
30. Marrouche NF, Martin DO, Wazni O et al. Phased-array intracardiac echocardiography monitoring during pulmonary vein isolation in patients with atrial fibrillation: impact on outcome and complications. *Circulation* 2003;107:2710-6.
31. Verma A, Marrouche NF, Yamada H et al. Usefulness of intracardiac Doppler assessment of left atrial function immediately post-pulmonary vein antrum isolation to predict short-term recurrence of atrial fibrillation. *Am J Cardiol* 2004;94:951-4.
32. Rotter M, Sanders P, Jais P et al. Prospective validation of phased array intracardiac echocardiography for the assessment of atrial mechanical function during catheter ablation of atrial fibrillation. *Heart* 2006;92:407-9.
33. Yamanaka K, Fujita M, Doi K et al. Multislice computed tomography accurately quantifies left atrial size and function after the MAZE procedure. *Circulation* 2006;114:15-19.
34. Jongbloed MR, Dirksen MS, Bax JJ et al. Atrial fibrillation: multi-detector row CT of pulmonary vein anatomy prior to radiofrequency catheter ablation--initial experience. *Radiology* 2005;234:702-9.
35. Anderson JL, Horne BD, Pennell DJ. Atrial dimensions in health and left ventricular disease using cardiovascular magnetic resonance. *J Cardiovasc Magn Reson* 2005;7:671-5.
36. Kircher B, Abbott JA, Pau S et al. Left atrial volume determination by biplane two-dimensional echocardiography: validation by cine computed tomography. *Am Heart J* 1991;121:864-71.
37. Marwick TH. Measurement of strain and strain rate by echocardiography: ready for prime time? *J Am Coll Cardiol* 2006;47:1313-27.
38. Thomas L, Levett K, Boyd A, Leung DY, Schiller NB, Ross DL. Changes in regional left atrial function with aging: evaluation by Doppler tissue imaging. *Eur J Echocardiogr* 2003;4:92-100.
39. Quintana M, Lindell P, Saha SK et al. Assessment of atrial regional and global electromechanical function by tissue velocity echocardiography: a feasibility study on healthy individuals. *Cardiovasc Ultrasound* 2005;3:4.
40. Sirbu C, Herbots L, D'hooge J et al. Feasibility of strain and strain rate imaging for the assessment of regional left atrial deformation: a study in normal subjects. *Eur J Echocardiogr* 2006;7:199-208.
41. Di Salvo G, Caso P, Lo PR et al. Atrial myocardial deformation properties predict maintenance of sinus rhythm after external cardioversion of recent-onset lone atrial fibrillation: a color Doppler myocardial imaging and transthoracic and transesophageal echocardiographic study. *Circulation* 2005;112:387-95.
42. Thomas L, McKay T, Byth K, Marwick TH. Abnormalities of left atrial function after cardioversion: an atrial strain rate study. *Heart* 2007;93:89-95.
43. Khan IA. Atrial stunning: basics and clinical considerations. *Int J Cardiol* 2003;92:113-28.
44. Stefanadis C, Dernelis J, Toutouzas P. A clinical appraisal of left atrial function. *Eur Heart J* 2001;22:22-36.

45. Tops LF, Bax JJ, Zeppenfeld K, Jongbloed MR, van der Wall EE, Schalij MJ. Effect of radiofrequency catheter ablation for atrial fibrillation on left atrial cavity size. *Am J Cardiol* 2006;97:1220-2.
46. Reant P, Lafitte S, Jais P et al. Reverse remodeling of the left cardiac chambers after catheter ablation after 1 year in a series of patients with isolated atrial fibrillation. *Circulation* 2005;112:2896-903.
47. Tsao HM, Wu MH, Huang BH et al. Morphologic remodeling of pulmonary veins and left atrium after catheter ablation of atrial fibrillation: insight from long-term follow-up of three-dimensional magnetic resonance imaging. *J Cardiovasc Electrophysiol* 2005;16:7-12.
48. Marom EM, Herndon JE, Kim YH, McAdams HP. Variations in pulmonary venous drainage to the left atrium: implications for radiofrequency ablation. *Radiology* 2004;230:824-9.
49. Wongcharoen W, Tsao HM, Wu MH et al. Morphologic characteristics of the left atrial appendage, roof, and septum: implications for the ablation of atrial fibrillation. *J Cardiovasc Electrophysiol* 2006;17:951-6.
50. Ren JF, Callans DJ, Schwartzman D, Michele JJ, Marchlinski FE. Changes in local wall thickness correlate with pathologic lesion size following radiofrequency catheter ablation: an intracardiac echocardiographic imaging study. *Echocardiography* 2001;18:503-7.
51. Gepstein L, Hayam G, Ben Haim SA. A novel method for nonfluoroscopic catheter-based electroanatomical mapping of the heart. In vitro and in vivo accuracy results. *Circulation* 1997;95:1611-22.
52. Dong J, Calkins H, Solomon SB et al. Integrated electroanatomic mapping with three-dimensional computed tomographic images for real-time guided ablations. *Circulation* 2006;113:186-94.
53. Tops LF, Bax JJ, Zeppenfeld K et al. Fusion of multislice computed tomography imaging with three-dimensional electroanatomic mapping to guide radiofrequency catheter ablation procedures. *Heart Rhythm* 2005;2:1076-81.
54. Kistler PM, Rajappan K, Jahngir M et al. The impact of CT image integration into an electroanatomic mapping system on clinical outcomes of catheter ablation of atrial fibrillation. *J Cardiovasc Electrophysiol* 2006;17:1093-101.
55. Heist EK, Chevalier J, Holmvang G et al. Factors affecting error in integration of electroanatomic mapping with CT and MR imaging during catheter ablation of atrial fibrillation. *J Interv Card Electrophysiol* 2006;17:21-7.
56. Noseworthy PA, Malchano ZJ, Ahmed J, Holmvang G, Ruskin JN, Reddy VY. The impact of respiration on left atrial and pulmonary venous anatomy: implications for image-guided intervention. *Heart Rhythm* 2005;2:1173-8.



Imaging and atrial fibrillation: the role of multimodality imaging in patient evaluation and management of atrial fibrillation

Laurens F. Tops
Martin J. Schalij
Jeroen J. Bax

Department of Cardiology, Leiden University Medical Center, Leiden, the Netherlands

Eur Heart J 2010, in press

ABSTRACT

Atrial fibrillation (AF) is the most common cardiac arrhythmia, and is associated with an increased risk of cardiac morbidity and mortality. In this review, the role of multimodality imaging in the evaluation and treatment of AF is discussed in two main parts. First, an overview of the initial assessment of an AF patient is provided, including the role of different imaging techniques. Conditions that are associated with AF (coronary artery disease, heart failure, valvular heart disease and left ventricular hypertrophy), and the assessment with various imaging modalities will be reviewed. Furthermore, left atrial size assessment and the screening for thrombus formation are addressed. Second, the role of imaging in the invasive treatment of AF with catheter ablation is reviewed. Issues that should be considered before the procedure including contra-indications and pulmonary vein and left atrial anatomy will be discussed. Furthermore, the integration of different imaging modalities during catheter ablation is explored. Finally, an overview of the role of imaging in the follow-up of patients treated with catheter ablation will be provided.

INTRODUCTION

Atrial fibrillation (AF) is the most commonly encountered arrhythmia, and its prevalence increases with advancing age. The prevalence of AF in the general population is estimated to be 0.4 to 1% (1). Importantly, AF is associated with an increased risk of cardiac morbidity and mortality (2). The 'Euro Heart Survey on Atrial Fibrillation' that included 5333 AF patients from 35 European countries, demonstrated that the evaluation and treatment of AF is associated with considerable costs (3). Therefore, continuous efforts are made to optimize the evaluation and treatment of AF patients (4).

The treatment of AF patients depends on various factors including but not limited to the type of AF, age and co-morbidity. These issues should therefore be evaluated in the initial assessment of a patient presenting with AF. In daily clinical practice, a 'rhythm control' strategy using anti-arrhythmic drugs is chosen in the majority of the patients (5). However in a large proportion of patients, anti-arrhythmic drugs fail to control AF. In these patients, the invasive treatment of AF with catheter ablation is a good option (6). The cornerstone of catheter ablation procedures is the electrical isolation of the pulmonary veins (PVs), since these are the main source of triggers initiating AF (7). In this review, we will explore the role of various imaging techniques in the evaluation and treatment of patients with AF. The manuscript will focus on relevant questions for daily clinical practice. The role of imaging in both the initial assessment of AF patients, and the invasive treatment of AF patients with catheter ablation will be reviewed.

CLINICAL EVALUATION OF PATIENTS WITH AF

Since the prevalence of AF is steadily increasing, an ever-growing number of patients in the outpatient clinic will present with AF. In the following paragraphs, we will focus on the role of imaging while answering the question *'What should be evaluated in patients presenting in the outpatient clinic with AF?'*

First, important factors associated with AF should be evaluated. A large number of (clinical) conditions, including structural heart disease, hypertension, surgery, hyperthyroidism and drugs are associated with AF. In order to diagnose these clinical conditions, medical history, physical examination and blood tests are often sufficient. However, other conditions associated with AF require (non-invasive) imaging for appropriate assessment. One of these conditions is underlying structural heart disease. Hence, an important question in the initial clinical evaluation of an AF patient is: *'Is there any underlying heart disease present?'* Subsequently, the question arises: *'Which imaging techniques can be used to detect the underlying heart disease?'*

Underlying heart disease

In the clinical evaluation of patients with AF, it is essential to evaluate underlying structural heart disease that may cause, or is associated with AF. Since the presence of 'true' lone AF is controversial, a potential reversible cause of AF (such as myocardial ischemia) should be excluded in the first assessment of a patient presenting with AF. In the Euro Heart Survey on Atrial Fibrillation, 90% of the AF patients had at least one associated medical condition (5). Most frequently, hypertension (up to 66%), coronary artery disease (up to 36%), heart failure (up to 49%), and valvular heart disease (up to 40%) was present. The prevalence of structural heart disease was highest in patients with persistent or permanent AF.

In daily clinical practice, conventional transthoracic echocardiography is most often used to detect underlying heart disease (5). However, other imaging modalities may provide important information that cannot be obtained with echocardiography. In the following paragraphs, the various cardiac conditions associated with AF, and the different imaging modalities to assess these conditions will be discussed.

Coronary artery disease The presence of coronary artery disease should be assessed in patients presenting with AF. Large cohort studies have reported a high prevalence of coronary artery disease among patients with AF (8). In 2768 patients with first detected AF, the incidence of coronary ischemic events was 31 per 1000 person-years (9). Furthermore, it has also been suggested that AF may be the first manifestation of cardiac ischemia (10). Typically, a stepwise approach starting with the evaluation of individual risk factors and exercise stress tests is applied when screening for coronary artery disease. However, non-invasive imaging modalities may have incremental value over traditional risk factors (11).

Various imaging modalities are available for the assessment of coronary artery disease in patients with AF. Conventional angiography remains the gold standard for detection of significant coronary artery stenosis. In recent years, non-invasive assessment of coronary artery disease with multi-slice computed tomography (MSCT) has become available. This technique enables non-invasive detection of significant coronary artery stenosis with a high sensitivity and specificity (12). It should be noted however that the diagnostic accuracy of MSCT may be limited in patients with AF during data acquisition (13). In addition, MSCT still is limited by higher radiation exposure as compared with conventional angiography. New techniques, such as the use of dose modulation during scanning may reduce radiation exposure. In a recent study, the presence of coronary artery disease was evaluated with MSCT in 150 patients with AF and 148 patients with similar age, gender, symptomatic status and pretest likelihood, but without a history of AF (14). Interestingly, a higher prevalence of obstructive coronary artery disease was noted in the AF patients, compared with the non-AF patients (41% in AF patients vs. 27% in non-AF patients, $p=0.01$). However, more studies are needed to fully appreciate the role of MSCT in the screening for coronary artery disease in AF patients.

Nuclear myocardial perfusion imaging provides information on the presence of ischemia, a surrogate marker for coronary artery disease; the diagnostic accuracy of nuclear perfusion imaging to detect significant coronary artery stenoses is high (15). It has been shown that nuclear imaging has similar diagnostic accuracy for detection of coronary artery disease in asymptomatic patients with AF as compared with patients without AF (16). Abidov et al. have demonstrated the prognostic value of ischemia detection with single-photon emission computed tomography in 384 AF patients and 15,664 patients without AF (17). The cardiac death rate was 6.3% per year in the AF patients with mildly abnormal myocardial perfusion scan, compared with 1.2% per year in the non-AF group with similar perfusion findings. This finding further underlines the importance of screening for coronary artery disease in AF patients.

Heart failure The presence of left ventricular (LV) systolic dysfunction or heart failure should be assessed in AF patients. The close relation between AF and heart failure has been well appreciated (18). In the Euro Heart Survey on Atrial Fibrillation 135 patients (5%) developed new onset heart failure during 1-year follow-up, while 314 patients (24.7%) experienced worsening of existing heart failure (5). Conversely, the Framingham Heart study demonstrated a 4.5-fold to 5.9-fold increased risk for the development of AF in men and women with LV systolic dysfunction (19). The exact pathophysiologic mechanism underlying the association between AF and LV dysfunction is only partially understood, but includes electromechanical factors, cellular and extra-cellular changes, and neurohumoral modulation (20).

For the assessment of LV systolic function, conventional two-dimensional transthoracic echocardiography is typically used. Using standard apical images, LV volumes can be assessed and subsequently LV ejection fraction can be calculated (21). Although conventional echocardiography is most frequently used in daily clinical practice, the accuracy of this technique largely depends on the operator and LV morphology. Therefore, in general magnetic resonance imaging (MRI) is considered the gold standard for assessment of LV volumes. However, it should be noted that pacemakers still are a contra-indication for cardiac MRI. In addition, gadolinium for delayed-enhancement MRI should not be used in patients with severely impaired renal function, due to the risk of nephrogenic systemic fibrosis. Nuclear imaging and MSCT can also be used for the assessment of LV function (12), but these techniques are associated with radiation. Novel real-time three-dimensional echocardiography allows accurate assessment of LV volumes and systolic function (22), and good agreement between this technique and MRI has been reported (23). However, more studies on the accuracy of this technique in patients with AF are needed.

Valvular heart disease Another condition that is associated with AF is valvular heart disease. In the Euro Heart Survey, about 20% of AF patients had valvular heart disease, with the highest prevalence among patients with persistent or permanent AF (5). Most often, mitral valve disease is present, resulting in elevated left atrial (LA) pressures and subsequently in a higher susceptibility to AF.

Transthoracic echocardiography is typically used for the assessment of valvular disease in patients with AF. It allows a comprehensive anatomical and functional evaluation of the different valves. Recently, the feasibility of both MRI (24) and MSCT (25) to assess valvular heart disease have been demonstrated. However, in daily clinical practice conventional echocardiography remains the technique of choice to assess valvular heart disease in AF patients.

LV hypertrophy The presence of LV hypertrophy should be evaluated in the initial assessment of AF patients. Long-lasting hypertension may result in LV hypertrophy and may expose the LA to elevated pressures. Since hypertension may be present in up to 66% of patients presenting with AF (5), screening for LV hypertrophy is essential. In 1924 patients of the Framingham Heart Study, increased LV wall thickness was one of the predictors for the development of AF over a 7.2-year period (HR 1.28 per 4-mm increment, 95% CI, 1.03 to 1.60) (26). Importantly, it has been suggested that antihypertensive therapy targeted at regression or prevention of LV hypertrophy may reduce the incidence of new-onset AF (27).

In addition to conventional criteria using electrocardiography, various imaging modalities can be used for the screening for LV hypertrophy in AF patients. In daily clinical practice, transthoracic echocardiography is most frequently used. Using standard echocardiographic images, LV wall thickness and LV mass can be assessed (21). However, three-dimensional imaging techniques such as MRI may provide a more accurate quantification of LV hypertrophy (28). Real-time three-dimensional echocardiography may overcome the limitations of conventional echocardiography and may be comparable with MSCT and MRI for assessment of LV hypertrophy (22).

Left atrial size

In addition to underlying structural heart disease, LA size should be assessed in the initial evaluation of patients with AF (1). In particular LA dilatation, as a marker of LA remodeling, should be identified. The association between AF and LA remodeling is well appreciated (29), but it remains controversial whether AF causes LA dilatation, or rather is its consequence. It has been demonstrated that LA size is a strong predictor of cardiovascular events in patients with lone AF, independent of age and clinical risk factors (30). Therefore, LA size should be assessed in the initial evaluation of AF patients, but the question is: *'How should LA size be assessed?'*

Magnetic resonance imaging still is considered the gold standard for quantification of LA size. Its three-dimensional character and high spatial resolution allow accurate assessment of the LA. Typically, the modified Simpson's rule is applied, using LA areas from subsequent cross-sectional images (31). However, MRI is limited by the relatively time-consuming data acquisition and cumbersome data analysis. Therefore, in daily clinical practice, MRI is not often used for the assessment of LA size. Similarly, MSCT allows three-dimensional assessment of LA size, with high spatial and temporal resolution (32). The modified Simpson's rule and simplified linear methods can be used to quantify LA size (33). MSCT however, is not routinely used for assessment of LA size, because of radiation exposure and the need for contrast agents.

Transthoracic echocardiography is widely used for assessment of LA size in daily clinical practice. In randomized clinical trials and large cohort studies, linear methods such as the M-mode derived LA diameter are typically used for LA size assessment because of the good reproducibility. However, it has been well recognized that the M-mode derived LA diameter may underestimate true LA size (34). In particular when LA dilatation is present, resulting in an asymmetric shape of the LA, linear methods are not the preferred method. Instead, LA volumes should be assessed for quantification of LA size (21).

Various methods are available for quantification of LA volumes using transthoracic echocardiography (Figure 1). The ellipsoid method and biplane area-length method use various LA diameters and/or areas to calculate LA volumes, assuming that the LA has an ellipsoid shape (35). The modified biplane Simpson's rule using planimetry is considered the most accurate method and is most frequently used. Good agreement between the biplane area-length method and the biplane Simpson's rule has been demonstrated (36). However, all these methods still use geometric assumptions and are operator dependent. Real-time three-dimensional echocardiography allows more accurate assessment of LA volumes (Figure 2) (22). In addition, because

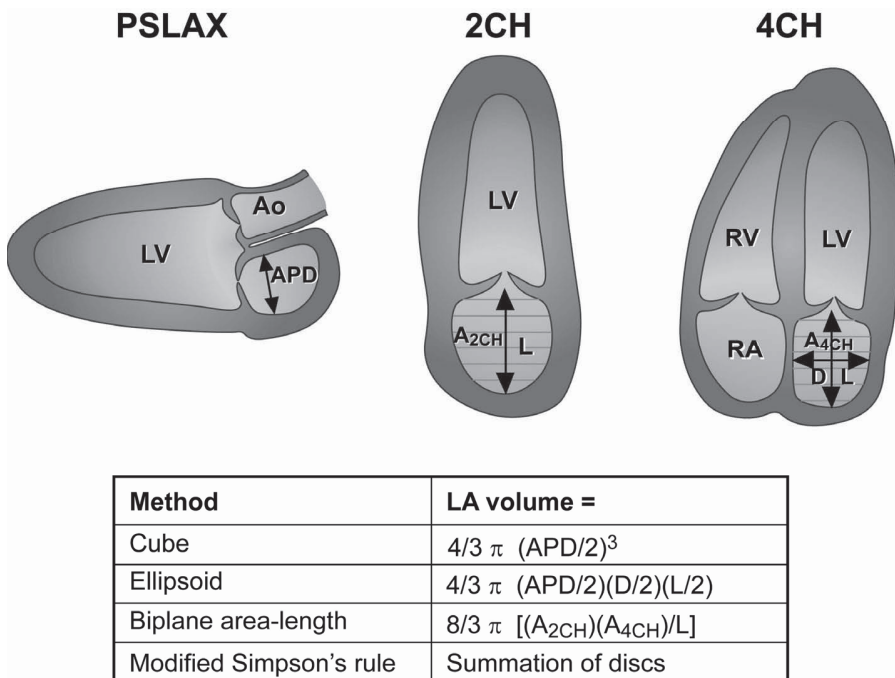


Figure 1. Using transthoracic echocardiography, various methods are available to assess LA size. The standard parasternal long-axis view (PSLAX) and the apical 2-chamber (2CH) and 4-chamber (4CH) views are used to assess LA diameters and LA area (using planimetry). Subsequently, LA volume can be calculated with the different equations. APD, D, L = LA diameter; A_{2CH} = LA area on 2-chamber view; A_{4CH} = LA area on 4-chamber view.

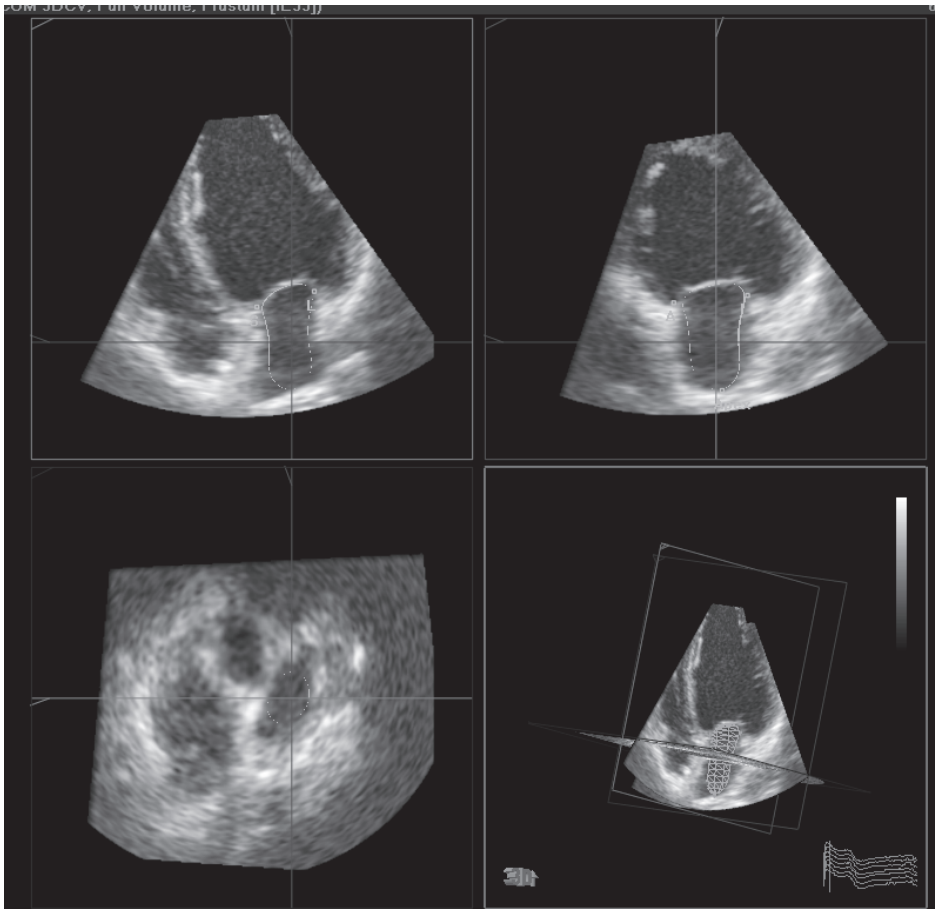


Figure 2. Real-time three-dimensional echocardiography for the assessment of LA volumes. Automatic border detection can be applied to the apical 4-chamber and 2-chamber view (upper panels) for quantification of LA volumes.

of its semi-automatic character, resulting in high reproducibility, real-time three-dimensional echocardiography is of great value in the follow-up of AF patients (37).

Left atrial thrombus

In addition to underlying structural heart disease and LA size, the presence of thrombus should be assessed in selected patients presenting with AF. Although there are various sources of embolism in patients with ischemic stroke, the majority of strokes occurring in patients with AF can be attributed to the presence of thromboembolism in the LA (1). Therefore, screening for thrombus formation is of critical importance, in particular in patients undergoing cardioversion or catheter ablation for AF. The question arises: *'Which imaging technique should be used for the screening for LA thrombi?'*

Conventional transthoracic echocardiography can be used to assess LA dilatation and severe LV dysfunction, both associated with the presence of LA thrombi and stroke (38,39). However, this technique has only moderate sensitivity and specificity for the detection of LA thrombi (40). In contrast, transesophageal echocardiography has a very high sensitivity and specificity for detection of cardiogenic sources of thromboembolism (41). In addition, spontaneous echo contrast and reduced LA appendage flow velocity, associated with LA thrombus formation, can be assessed with transesophageal echocardiography. Importantly, it has been demonstrated that the use of transesophageal echocardiography may result in less hemorrhagic complications after cardioversion, compared with a conventional strategy using anticoagulation prior to cardioversion (42).

Non-invasive three-dimensional imaging techniques such as MRI and MSCT have also been used for the detection of thrombi in the LA and LA appendage. However, both techniques have low inter-observer agreement, and moderate sensitivity and specificity compared with transesophageal echocardiography (43,44). Therefore, at present transesophageal echocardiography is still considered the gold standard for the detection of thrombi in the LA and LA appendage in patients with AF (1).

PATIENTS WITH AF UNDERGOING CATHETER ABLATION

After the initial assessment as described before, a tailored treatment strategy should be planned for each AF patient. Radiofrequency catheter ablation is a good therapeutic option when at least one anti-arrhythmic drug has failed (1). A recent study including 1404 AF patients undergoing PV isolation demonstrated that 78% of patients with paroxysmal AF and 67% of patients with non-paroxysmal AF ($p < 0.001$) maintain sinus rhythm after a single catheter ablation procedure (45). Although various ablation strategies exist, the majority of approaches target electrical isolation of the PVs (6). In the following paragraphs, the question *'What is the role of imaging in catheter ablation for AF?'* will be answered. Before the procedure, during the actual ablation and during follow-up various imaging modalities play a different role (Table 1). The different processes and the preferred imaging modalities will be reviewed in the following paragraphs.

Pre-procedural issues: Contra-indications and assessment of anatomy

The first step in the work-up of a patient referred for AF ablation is to exclude any contra-indication. The most important is to rule out the presence of LA thrombi. In particular in patients with persistent AF, or patients who are in AF at the time of the procedure, this is of critical importance (6). As discussed previously, transesophageal echocardiography is considered the gold standard for detection of LA thrombi. In addition, extreme LA dilatation and long-lasting permanent AF are relative contra-indications for AF ablation, since these conditions are associated with a low

Table 1. The role of imaging in AF ablation

Process	Imaging modality	Comment
Before catheter ablation		
Assessment of LA / LAA thrombus	TEE	Considered gold standard for detection of thrombi
Assessment of LA size and anatomy	TTE	Most often used in daily clinical practice
	RT3DE	New technique allowing accurate assessment of LA volumes
	MSCT or MRI	Allow three-dimensional assessment of LA volumes and specific anatomic features. Considered gold standard for assessment of LA volumes
Assessment of PV anatomy	MSCT or MRI	Provide detailed three-dimensional information on PV anatomy as a 'road-map to ablation'
During catheter ablation		
Positioning catheters	Fluoroscopy	Standard imaging modality in the electrophysiology laboratory. Enables visualization of catheters and devices.
Transseptal puncture	ICE	May enhance safety of transseptal puncture by direct visualization of inter-atrial septum and puncture needle
Visualization of LA and PVs	Fluoroscopy	New rotational angiography technique accurately identifies PV anatomy and PV diameters
	ICE	Allows real-time assessment of PV ostium, but underestimates PV diameter
	Mapping system	Provides real-time electroanatomic information, and guides ablation. Limited by the use of reconstructed anatomy
Image integration	Fluoroscopy & MSCT / MRI	Combines real-time fluoroscopy with detailed LA and PV anatomy from MSCT or MRI
	Mapping system & MSCT / MRI	Combines electroanatomic map with detailed LA and PV anatomy from MSCT or MRI
	Mapping system & ICE	Combines electroanatomic map with real-time anatomic information from ICE
Follow-up after catheter ablation		
Assessment of PV stenosis	MSCT or MRI	Preferably, these three-dimensional techniques are correlated with pre-procedural images for detection of PV stenosis
Detection of pericardial effusion	TTE	Routine echocardiography should be performed before discharge and during follow-up
Esophageal injury	MSCT or MRI	Should be performed when atrio-esophageal fistula is suspected
Assessment of LA size and function	TTE	Conventional method for detection of LA volumes and function
	RT3DE	Three-dimensional assessment of LA volumes allows detection of LA reverse remodeling
	MSCT	Three-dimensional assessment of LA volumes allows detection of LA reverse remodeling
	MRI	Preliminary studies demonstrate feasibility of LA scar detection with gadolinium enhanced MRI

ICE = intracardiac echocardiography; LA = left atrium/atrial; LAA = left atrial appendage; MRI = magnetic resonance imaging; MSCT = multi-slice computed tomography; PV = pulmonary vein; RT3DE = real-time 3-dimensional echocardiography; TEE = transesophageal echocardiography; TTE = transthoracic echocardiography.

probability of successful outcome (46). Therefore, LA size assessment should be performed routinely, as described in the previous section. After exclusion of any contra-indication, LA and PV anatomy should be assessed, since the PVs are the main target during the ablation procedure. Therefore, an important question is: 'How can LA and PV anatomy best be assessed?'

From anatomical studies it has become apparent that LA and PV anatomy is highly variable (47). Typically, four separate PVs are present: two right-sided and two left-sided PVs. Large *in vivo* studies using MSCT and MRI scanning have demonstrated that a single PV ostium on the left side or an additional right-sided PV are the most common variations (Figure 3) (48,49). These anatomical variants may be present in up to 30% of patients, and may affect the planned ablation strategy. In general, three-dimensional imaging techniques such as MSCT and MRI are used for assessment of PV anatomy. Using three-dimensional reconstructions and cross-sectional images, these techniques provide the most detailed information on PV anatomy.

In addition to the number of PVs, the exact diameter and shape of the PVs should be assessed. Knowledge on PV diameter may be very helpful, especially for new ablation strategies

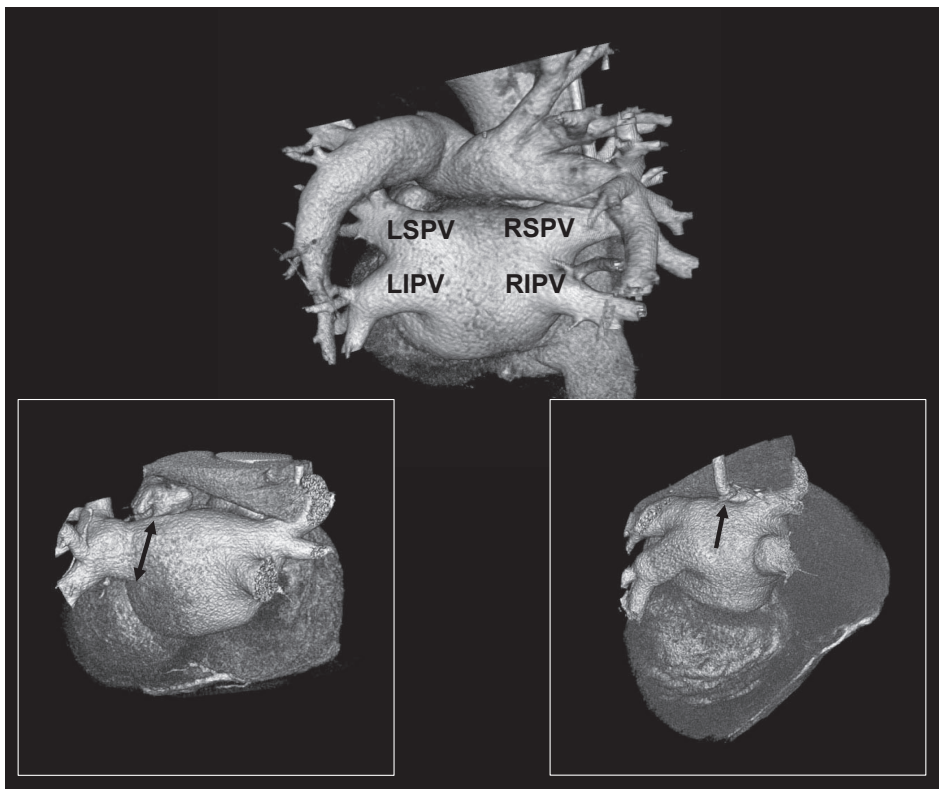


Figure 3. Three-dimensional volume-rendered reconstructions of MSCT images are created to assess LA and PV anatomy. Normal PV anatomy includes four PVs draining separately into the LA (upper panel). Variations of PV anatomy include a single (or 'common') ostium of the left-sided PVs (lower left panel, black double-headed arrow), and an additional right-sided PV (lower right panel, black arrow). LIPV = left inferior pulmonary vein; LSPV = left superior pulmonary vein; RIPV = right inferior pulmonary vein; RSPV = right superior pulmonary vein.

using balloon-catheters (50). In addition, comparison of PV diameters at baseline and during follow-up allows detection of PV stenosis after catheter ablation (51).

Finally, specific anatomical features of the LA, such as the LA appendage, variations in LA roof anatomy and the 'Coumadin ridge' between the left-sided PVs and the LA appendage, can be assessed prior to the ablation procedure (52). Surrounding structures that may be important during catheter ablation can be identified including coronary veins, coronary arteries and the course of the esophagus (25,53). For these issues, MSCT and MRI are the preferred imaging modalities (6).

62 **During catheter ablation: visualization of structures and image integration**

During the actual catheter ablation procedure, mapping and ablation catheters are introduced into the LA after a transseptal puncture. This is typically performed under fluoroscopy guidance, but intracardiac echocardiography can be used to better visualize the inter-atrial septum and puncture needle (54). After gaining access to the LA, the exact location and anatomy of the PV ostia is determined, and the position of the mapping/ablation catheters in relation to them. For this purpose, various imaging modalities are available.

Fluoroscopy is the most widely used imaging technique in the electrophysiology laboratory. However, correct visualization of cardiac structures may be limited with fluoroscopy alone. In recent years, a new application of conventional fluoroscopy has been introduced: rotational angiography uses a C-arm flat-panel fluoroscopy system and contrast medium to create three-dimensional images of the LA and PVs (55). It has been demonstrated that this technique correctly identifies PVs and provides PV diameters that correlate well with those derived from pre-procedural acquired MSCT images (56).

Intracardiac echocardiography can be used in addition to fluoroscopy to visualize the PVs. This technique provides real-time images of the PVs and neighboring structures. In addition, it may be very helpful in avoiding complications during the ablation (57). A limitation of intracardiac echocardiography is its two-dimensional character. As a result, PV diameters may be underestimated as compared with three-dimensional imaging techniques (58,59).

Electroanatomic mapping systems may also be used in addition to fluoroscopy. These systems provide on-line electrophysiologic data, and allow tracking of mapping/ablation catheters and annotation of ablation points (60). A limitation of electroanatomic mapping systems however is the use of reconstructed anatomy. Finally, three-dimensional imaging techniques such as MSCT and MRI can provide very detailed information on LA and PV anatomy. However, scanning is performed before the ablation procedure, and therefore these techniques cannot provide real-time images.

Although the various imaging modalities all provide important information during the catheter ablation procedure, each technique has its own limitations. Integration of the different modalities may overcome the limitations of each separate modality. Hence, the question is: *'Is it possible to integrate different imaging modalities during AF ablation?'*

In recent years, various image integration systems have been introduced, allowing integration of different imaging modalities. Dedicated software has been developed to integrate biplane fluoroscopy and MSCT or MRI images (61). Angiographic reconstructions of the LA and PVs from fluoroscopy and three-dimensional volume rendered reconstructions from pre-procedural acquired MSCT or MRI images are merged with the use of calibration, translation and rotation processes. Several studies have demonstrated the feasibility of this new technique and its value during AF ablation (62,63).

In the past years, large clinical experience has been obtained with the integration of electroanatomic maps and three-dimensional techniques such as MSCT and MRI (64). This image integration strategy uses algorithms that minimize the distance between the reconstructed anatomy from the electroanatomic map and the MSCT or MRI image (65,66). Importantly, it has been demonstrated that the use of image integration may improve the outcome of the ablation procedure (67). In a cohort of 290 patients (145 patients with image integration, 145 patients with conventional mapping and ablation approach), the AF-free survival rate was significantly higher in patients with image integration (Figure 4) (68). However, this finding was not confirmed in a smaller, randomized study: single procedure success after 6 months follow-up was similar in patients with image integration and conventional mapping approach (50% vs. 56%, $p=0.65$) (69). More randomized controlled trials are needed to fully appreciate the role of integration of electroanatomic maps and MSCT or MRI images in catheter ablation procedures, and the impact on procedure/ fluoroscopy times and outcome. Nonetheless, image integration facilitates AF ablation by combining on-line electrophysiologic and detailed anatomic information.

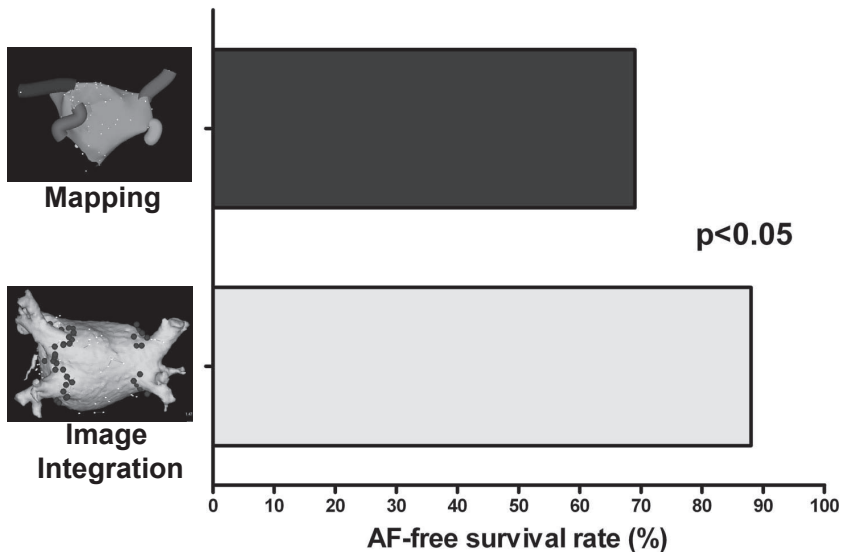


Figure 4. The use of image integration during catheter ablation may significantly improve the outcome of the procedure. In patients treated with catheter ablation using image integration, the AF-free survival rate was significantly higher compared with patients who were treated with conventional electroanatomic mapping alone (AF-free survival rate 88% vs. 69%, $p < 0.05$). Adapted from Della Bella et al., reference 68.

More recently, integration of intracardiac echocardiography, electroanatomic mapping and MSCT has become available (70) (Figure 5). With the use of an intracardiac echocardiography probe that is tracked by the electroanatomic mapping system, a real-time electrophysiologic and anatomic reconstruction of the LA and PVs is created. Subsequently, it is integrated with MSCT images, adding detailed anatomic information. Although it is a promising strategy, more studies are needed to appreciate the role of this new technique and its effect on the outcome of catheter ablation for AF.

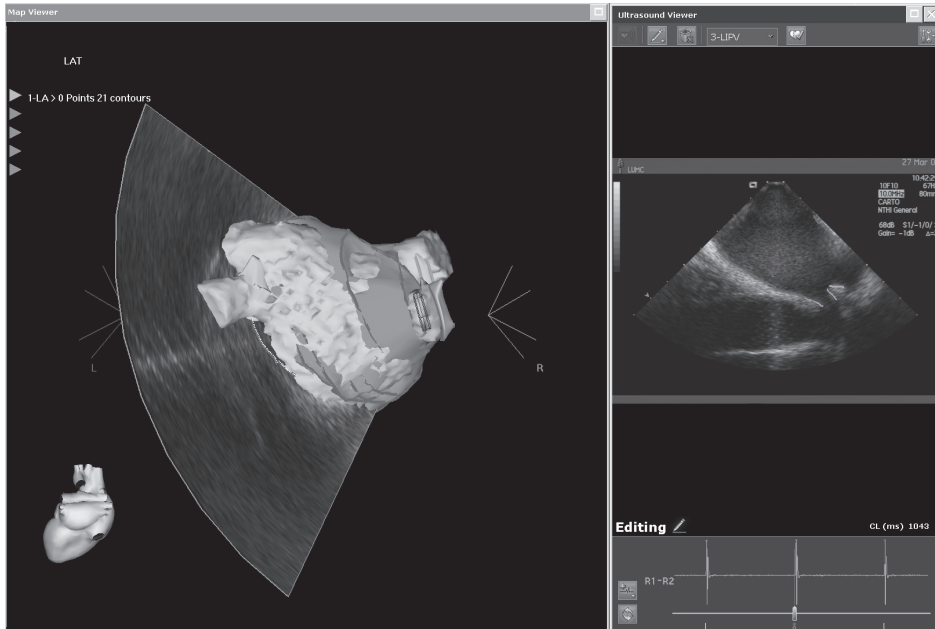


Figure 5. The feasibility of the integration of electroanatomic mapping, intracardiac echocardiography and MSCT has recently been demonstrated. A dedicated intracardiac echocardiography probe provides real-time anatomic images that are integrated with pre-procedural acquired MSCT images. On the ECG-gated intracardiac echocardiography images, the anatomy of the LA and PVs can be annotated, creating a three-dimensional shell (right panel). Subsequently, the three imaging modalities are integrated with dedicated algorithms (left panel).

Follow-up issues: assessment of complications and evaluation of LA function

Immediately after the procedure and during follow-up, patients should be screened for complications. A large survey revealed that serious complications occur in up to 6% of patients (71). Therefore, it is important to know: *'Which complications can be expected and how can they be assessed?'*

Pulmonary vein stenosis is one of the most frequently occurring complications of AF ablation (6). Fortunately, the prevalence is decreasing due to more proximal ablation strategies. Asymptomatic PV stenosis may occur in up to 19% of patients, whereas symptomatic PV stenosis requiring intervention occurs in less than 1% of patients (72). Conventional invasive angiography assessing PV diameters may be used for the detection of PV stenosis. However,

three-dimensional imaging techniques such as MSCT or MRI are recommended for accurate assessment of PV stenosis (73).

Severe pericardial effusion or cardiac tamponade is another serious complication after AF ablation. In a recent meta-analysis with 70 studies including approximately 15,500 AF patients, cardiac tamponade was reported in up to 5% of the patients (median from all studies 1%) (72). During the procedure, invasive blood pressure measurement, fluoroscopy, and transthoracic echocardiography are helpful tools to detect pericardial effusion. In addition, intracardiac echocardiography can be used during the procedure (74). Conventional transthoracic echocardiography is the preferred imaging modality for screening during follow-up (6).

Finally, injury to the esophagus may occur after ablation, since the esophagus has a close relation with the posterior LA wall and PVs. A rare but severe complication is an atrio-esophageal fistula (75). MSCT or MRI should be performed when this complication is suspected (6).

In addition to the detection of complications, the effects of catheter ablation on cardiac function may be assessed during follow-up. It has been demonstrated that AF ablation has favorable effects on LV systolic function in patients with heart failure (76). In contrast, in patients with preserved LV systolic function, LV ejection fraction does not change after successful catheter ablation (77). However, it may be that LV ejection fraction is not a sensitive marker to detect subtle changes in LV systolic function. Recently, it has been demonstrated that global LV systolic strain does improve in patients with preserved LV systolic function who maintain sinus rhythm after catheter ablation (78). In contrast, patients who had recurrence of AF did not show a significant improvement in LV systolic strain.

Furthermore, since extensive ablation in the LA may result in scar formation and subsequently in changes in LA anatomy, one could wonder: *'What is the effect of catheter ablation on LA size and function?'* As previously described, there is a strong association between AF and LA enlargement. Interestingly, it has been demonstrated that restoration of sinus rhythm may result in reversal of LA enlargement (29). Several studies have demonstrated a decrease in LA volumes after successful catheter ablation (79-81). Typically, transthoracic echocardiography is used for the follow-up of LA volumes. However, three-dimensional techniques may provide more accurate information, as previously described. With the use of real-time three-dimensional echocardiography, it has been shown that LA maximum volume decreases in patients who maintain in sinus rhythm during follow-up (82). Similarly, LA reverse remodeling has also been demonstrated with MSCT (32) and MRI (83).

Furthermore, AF ablation may affect LA function. Three distinct phases can be distinguished in LA function: LA reservoir function (during ventricular systole), LA conduit function (during early ventricular diastole) and LA booster pump function (during late ventricular diastole). In general, LA function parameters are derived from trans-mitral flow patterns using Doppler echocardiography. However, using real-time three-dimensional echocardiography the different phases in LA function can be derived from LA volumes throughout the cardiac cycle. Marsan et

al. demonstrated that LA booster pump function significantly improves in AF ablation patients who maintain sinus rhythm during follow-up (Figure 6) (37).

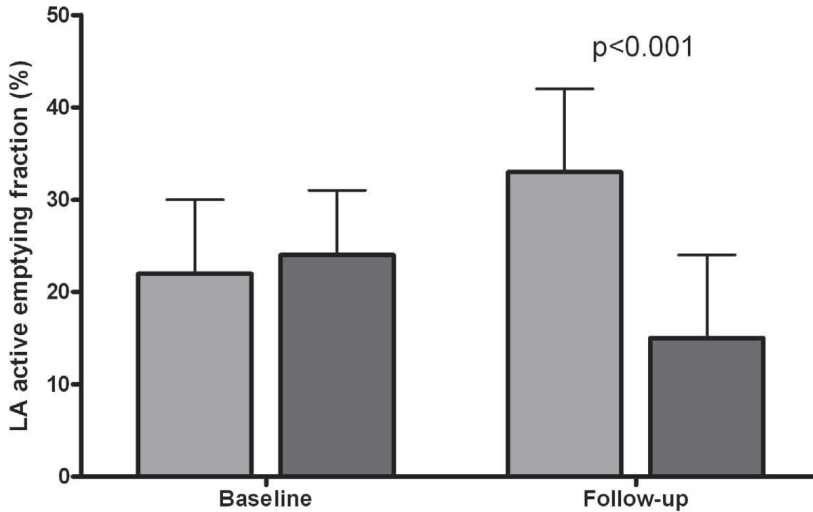


Figure 6. Left atrial active emptying fraction (representing LA active function) improves in patients who maintain sinus rhythm during follow-up (green bars). In contrast, a deterioration of LA active emptying fraction is noted in patients who have recurrence of AF during follow-up (red bars). Adapted from Marsan et al., reference 37.

With the use of tissue Doppler echocardiography, LA strain and strain rate can be assessed. These parameters represent myocardial mechanical function, allowing quantification of LA segmental function (84). Schneider et al. used this technique to assess LA function in 118 patients undergoing AF ablation (85). After 3 months follow-up, an improvement in the different LA functions was noted, but only in patients who maintained sinus rhythm during follow-up.

Finally, the feasibility of LA scar assessment with gadolinium enhanced MRI has recently been demonstrated. In 53 patients undergoing AF ablation, MRI images were acquired before the procedure and after 3 months follow-up. Interestingly, the extent of LA scar as assessed with MRI was a strong predictor of freedom from AF during follow-up (OR 18.5, 95% CI 1.27 to 268, $p=0.032$) (86). However, more studies are needed to appreciate the role of LA scar assessment with MRI in the follow-up of AF ablation patients.

CONCLUSIONS

Multimodality imaging plays an important role in the initial assessment of AF patients, and during subsequent invasive treatment with catheter ablation (Figure 7). An important issue to consider in the first evaluation of AF patients is the presence of any underlying heart disease that is associated with AF: coronary artery disease, heart failure, valvular heart disease and LV

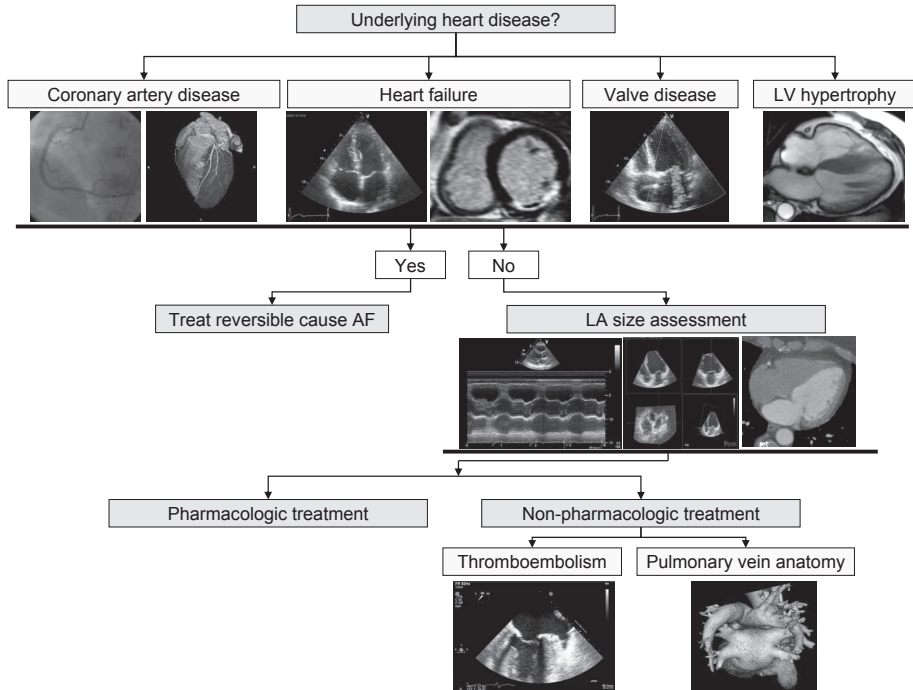


Figure 7. Multimodality imaging plays an important role in the evaluation of AF patients, and in the management of AF. Various modalities are available for screening for underlying heart disease causing AF. For LA size assessment, various methods are available; three-dimensional imaging techniques provide the most accurate estimation. In particular in the non-pharmacologic treatment of AF, imaging plays an important role in patient selection and guidance of the procedure. See also text for explanation.

hypertrophy. Any (reversible) underlying disease that causes AF should be treated first. Furthermore, LA size should be assessed in the initial evaluation of AF patients. For the routine assessment of LA size transthoracic echocardiography is the technique of choice. Preferably, LA volumes are assessed for estimation of LA size.

After the initial assessment of the AF patient, a treatment strategy is chosen (pharmacologic vs. non-pharmacologic). Multimodality imaging is of particular value in the non-pharmacologic treatment of AF. In patients undergoing electrocardioversion or catheter ablation, LA thrombi should be excluded with transesophageal echocardiography. Before catheter ablation, PV anatomy should be evaluated, preferably with three-dimensional imaging techniques such as MSCT or MRI. During the actual ablation procedure, different imaging modalities are available for visualization of cardiac anatomy. New dedicated systems allow integration of the various modalities, further facilitating catheter ablation procedures. After the ablation procedure, imaging plays an important role in the detection of complications. Finally, the effects of the catheter ablation procedure on LA size and function can be assessed with various imaging modalities.

REFERENCES

1. Fuster V, Ryden LE, Cannom DS et al. ACC/AHA/ESC 2006 guidelines for the management of patients with atrial fibrillation: full text. *Europace* 2006;8:651-745.
2. Benjamin EJ, Wolf PA, D'Agostino RB, Silbershatz H, Kannel WB, Levy D. Impact of atrial fibrillation on the risk of death: the Framingham Heart Study. *Circulation* 1998;98:946-52.
3. Ringborg A, Nieuwlaar R, Lindgren P et al. Costs of atrial fibrillation in five European countries: results from the Euro Heart Survey on atrial fibrillation. *Europace* 2008;10:403-11.
4. Kirchhof P, Bax J, Blomstrom-Lundquist C et al. Early and comprehensive management of atrial fibrillation: proceedings from the 2nd AFNET/EHRA consensus conference on atrial fibrillation entitled 'research perspectives in atrial fibrillation'. *Europace* 2009;11:860-85.
5. Nieuwlaar R, Capucci A, Camm AJ et al. Atrial fibrillation management: a prospective survey in ESC member countries: the Euro Heart Survey on Atrial Fibrillation. *Eur Heart J* 2005;26:2422-34.
6. Calkins H, Brugada J, Packer DL et al. HRS/EHRA/ECAS expert consensus statement on catheter and surgical ablation of atrial fibrillation: recommendations for personnel, policy, procedures and follow-up. *Europace* 2007;9:335-79.
7. Haissaguerre M, Jais P, Shah DC et al. Spontaneous initiation of atrial fibrillation by ectopic beats originating in the pulmonary veins. *N Engl J Med* 1998;339:659-66.
8. Lip GY, Beevers DG. ABC of atrial fibrillation. History, epidemiology, and importance of atrial fibrillation. *BMJ* 1995;311:1361-3.
9. Miyasaka Y, Barnes ME, Gersh BJ et al. Coronary ischemic events after first atrial fibrillation: risk and survival. *Am J Med* 2007;120:357-63.
10. Schoonderwoerd BA, Van Gelder IC, Crijns HJ. Left ventricular ischemia due to coronary stenosis as an unexpected treatable cause of paroxysmal atrial fibrillation. *J Cardiovasc Electrophysiol* 1999;10:224-8.
11. van Werkhoven JM, Schuijff JD, Gaemperli O et al. Prognostic value of multislice computed tomography and gated single-photon emission computed tomography in patients with suspected coronary artery disease. *J Am Coll Cardiol* 2009;53:623-32.
12. Schroeder S, Achenbach S, Bengel F et al. Cardiac computed tomography: indications, applications, limitations, and training requirements: report of a Writing Group deployed by the Working Group Nuclear Cardiology and Cardiac CT of the European Society of Cardiology and the European Council of Nuclear Cardiology. *Eur Heart J* 2008;29:531-56.
13. Tsimikas I, Drosch T, Brodoefel H et al. Diagnostic accuracy and image quality of cardiac dual-source computed tomography in patients with arrhythmia. *Int J Cardiol* 2009.
14. Nucifora G, Schuijff JD, Tops LF et al. Prevalence of coronary artery disease assessed by multislice computed tomography coronary angiography in patients with paroxysmal or persistent atrial fibrillation. *Circ Cardiovasc Imaging* 2009;2:100-6.
15. Marcassa C, Bax JJ, Bengel F et al. Clinical value, cost-effectiveness, and safety of myocardial perfusion scintigraphy: a position statement. *Eur Heart J* 2008;29:557-63.
16. Askew JW, Miller TD, Hodge DO, Gibbons RJ. The value of myocardial perfusion single-photon emission computed tomography in screening asymptomatic patients with atrial fibrillation for coronary artery disease. *J Am Coll Cardiol* 2007;50:1080-5.
17. Abidov A, Hachamovitch R, Rozanski A et al. Prognostic implications of atrial fibrillation in patients undergoing myocardial perfusion single-photon emission computed tomography. *J Am Coll Cardiol* 2004;44:1062-70.
18. Anter E, Jessup M, Callans DJ. Atrial fibrillation and heart failure: treatment considerations for a dual epidemic. *Circulation* 2009;119:2516-25.
19. Benjamin EJ, Levy D, Vaziri SM, D'Agostino RB, Belanger AJ, Wolf PA. Independent risk factors for atrial fibrillation in a population-based cohort. The Framingham Heart Study. *JAMA* 1994;271:840-4.
20. Cha YM, Redfield MM, Shen WK, Gersh BJ. Atrial fibrillation and ventricular dysfunction: a vicious electromechanical cycle. *Circulation* 2004;109:2839-43.

21. Lang RM, Bierig M, Devereux RB et al. Recommendations for Chamber Quantification. *J Am Soc Echocardiogr* 2005;18:1440-63.
22. Mor-Avi V, Sugeng L, Lang RM. Real-time 3-dimensional echocardiography: an integral component of the routine echocardiographic examination in adult patients? *Circulation* 2009;119:314-29.
23. Jenkins C, Bricknell K, Hanekom L, Marwick TH. Reproducibility and accuracy of echocardiographic measurements of left ventricular parameters using real-time three-dimensional echocardiography. *J Am Coll Cardiol* 2004;44:878-86.
24. Cawley PJ, Maki JH, Otto CM. Cardiovascular magnetic resonance imaging for valvular heart disease: technique and validation. *Circulation* 2009;119:468-78.
25. Tops LF, Krishnan SC, Schuijff JD, Schalij MJ, Bax JJ. Noncoronary Applications of Cardiac Multidetector Row Computed Tomography. *J Am Coll Cardiol* 2008;1:94-106.
26. Vaziri SM, Larson MG, Benjamin EJ, Levy D. Echocardiographic predictors of nonrheumatic atrial fibrillation. The Framingham Heart Study. *Circulation* 1994;89:724-30.
27. Okin PM, Wachtell K, Devereux RB et al. Regression of electrocardiographic left ventricular hypertrophy and decreased incidence of new-onset atrial fibrillation in patients with hypertension. *JAMA* 2006;296:1242-8.
28. Lyne JC, Pennell DJ. Cardiovascular magnetic resonance in the quantitative assessment of left ventricular mass, volumes and contractile function. *Coron Artery Dis* 2005;16:337-43.
29. Casacalang-Verzosa G, Gersh BJ, Tsang TS. Structural and functional remodeling of the left atrium: clinical and therapeutic implications for atrial fibrillation. *J Am Coll Cardiol* 2008;51:1-11.
30. Osranek M, Bursi F, Bailey KR et al. Left atrial volume predicts cardiovascular events in patients originally diagnosed with lone atrial fibrillation: three-decade follow-up. *Eur Heart J* 2005;26:2556-61.
31. Jarvinen V, Kupari M, Hekali P, Poutanen VP. Assessment of left atrial volumes and phasic function using cine magnetic resonance imaging in normal subjects. *Am J Cardiol* 1994;73:1135-8.
32. Lemola K, Sneider M, Desjardins B et al. Effects of left atrial ablation of atrial fibrillation on size of the left atrium and pulmonary veins. *Heart Rhythm* 2004;1:576-81.
33. Hof I, Arbab-Zadeh A, Dong J, Scherr D, Chilukuri K, Calkins H. Validation of a simplified method to determine left atrial volume by computed tomography in patients with atrial fibrillation. *Am J Cardiol* 2008;102:1567-70.
34. Lester SJ, Ryan EW, Schiller NB, Foster E. Best method in clinical practice and in research studies to determine left atrial size. *Am J Cardiol* 1999;84:829-32.
35. Abhayaratna WP, Seward JB, Appleton CP et al. Left atrial size: physiologic determinants and clinical applications. *J Am Coll Cardiol* 2006;47:2357-63.
36. Ujino K, Barnes ME, Cha SS et al. Two-dimensional echocardiographic methods for assessment of left atrial volume. *Am J Cardiol* 2006;98:1185-8.
37. Marsan NA, Tops LF, Holman ER et al. Comparison of left atrial volumes and function by real-time three-dimensional echocardiography in patients having catheter ablation for atrial fibrillation with persistence of sinus rhythm versus recurrent atrial fibrillation three months later. *Am J Cardiol* 2008;102:847-53.
38. Tsang TS, Abhayaratna WP, Barnes ME et al. Prediction of cardiovascular outcomes with left atrial size: is volume superior to area or diameter? *J Am Coll Cardiol* 2006;47:1018-23.
39. Echocardiographic predictors of stroke in patients with atrial fibrillation: a prospective study of 1066 patients from 3 clinical trials. *Arch Intern Med* 1998;158:1316-20.
40. Omran H, Jung W, Rabahieh R et al. Imaging of thrombi and assessment of left atrial appendage function: a prospective study comparing transthoracic and transoesophageal echocardiography. *Heart* 1999;81:192-8.
41. Pearson AC, Labovitz AJ, Tatineni S, Gomez CR. Superiority of transesophageal echocardiography in detecting cardiac source of embolism in patients with cerebral ischemia of uncertain etiology. *J Am Coll Cardiol* 1991;17:66-72.

42. Klein AL, Grimm RA, Murray RD et al. Use of transesophageal echocardiography to guide cardioversion in patients with atrial fibrillation. *N Engl J Med* 2001;344:1411-20.
43. Mohrs OK, Nowak B, Petersen SE et al. Thrombus detection in the left atrial appendage using contrast-enhanced MRI: a pilot study. *AJR Am J Roentgenol* 2006;186:198-205.
44. Gottlieb I, Pinheiro A, Brinker JA et al. Diagnostic accuracy of arterial phase 64-slice multidetector CT angiography for left atrial appendage thrombus in patients undergoing atrial fibrillation ablation. *J Cardiovasc Electrophysiol* 2008;19:247-51.
45. Bhargava M, Di Biase L, Mohanty P et al. Impact of type of atrial fibrillation and repeat catheter ablation on long-term freedom from atrial fibrillation: Results from a multicenter study. *Heart Rhythm* 2009;6:1403-12.
46. Berrueto A, Tamborero D, Mont L et al. Pre-procedural predictors of atrial fibrillation recurrence after circumferential pulmonary vein ablation. *Eur Heart J* 2007;28:836-41.
47. Ho SY, Cabrera JA, Tran VH, Farre J, Anderson RH, Sanchez-Quintana D. Architecture of the pulmonary veins: relevance to radiofrequency ablation. *Heart* 2001;86:265-70.
48. Marom EM, Herndon JE, Kim YH, McAdams HP. Variations in pulmonary venous drainage to the left atrium: implications for radiofrequency ablation. *Radiology* 2004;230:824-9.
49. Mansour M, Holmvang G, Sosnovik D et al. Assessment of pulmonary vein anatomic variability by magnetic resonance imaging: implications for catheter ablation techniques for atrial fibrillation. *J Cardiovasc Electrophysiol* 2004;15:387-93.
50. Reddy VY, Neuzil P, Themistoclakis S et al. Visually-guided balloon catheter ablation of atrial fibrillation: experimental feasibility and first-in-human multicenter clinical outcome. *Circulation* 2009;120:12-20.
51. Packer DL, Keelan P, Munger TM et al. Clinical presentation, investigation, and management of pulmonary vein stenosis complicating ablation for atrial fibrillation. *Circulation* 2005;111:546-54.
52. Wongcharoen W, Tsao HM, Wu MH et al. Morphologic characteristics of the left atrial appendage, roof, and septum: implications for the ablation of atrial fibrillation. *J Cardiovasc Electrophysiol* 2006;17:951-6.
53. Lemola K, Sneider M, Desjardins B et al. Computed tomographic analysis of the anatomy of the left atrium and the esophagus: implications for left atrial catheter ablation. *Circulation* 2004;110:3655-60.
54. Jongbloed MR, Schalij MJ, Zeppenfeld K, Oemrawsingh PV, van der Wall EE, Bax JJ. Clinical applications of intracardiac echocardiography in interventional procedures. *Heart* 2005;91:981-90.
55. Thiagalingam A, Manzke R, d'Avila A et al. Intraprocedural volume imaging of the left atrium and pulmonary veins with rotational X-ray angiography: implications for catheter ablation of atrial fibrillation. *J Cardiovasc Electrophysiol* 2008;19:293-300.
56. Kriatselis C, Tang M, Roser M, Fleck E, Gerds-Li H. A new approach for contrast-enhanced X-ray imaging of the left atrium and pulmonary veins for atrial fibrillation ablation: rotational angiography during adenosine-induced asystole. *Europace* 2009;11:35-41.
57. Saad EB, Cole CR, Marrouche NF et al. Use of intracardiac echocardiography for prediction of chronic pulmonary vein stenosis after ablation of atrial fibrillation. *J Cardiovasc Electrophysiol* 2002;13:986-9.
58. Jongbloed MR, Bax JJ, Lamb HJ et al. Multislice computed tomography versus intracardiac echocardiography to evaluate the pulmonary veins before radiofrequency catheter ablation of atrial fibrillation: a head-to-head comparison. *J Am Coll Cardiol* 2005;45:343-50.
59. Wood MA, Wittkamp M, Henry D et al. A comparison of pulmonary vein ostial anatomy by computerized tomography, echocardiography, and venography in patients with atrial fibrillation having radiofrequency catheter ablation. *Am J Cardiol* 2004;93:49-53.
60. Gepstein L, Hayam G, Ben Haim SA. A novel method for nonfluoroscopic catheter-based electroanatomical mapping of the heart. In vitro and in vivo accuracy results. *Circulation* 1997;95:1611-22.
61. Ector J, De Buck S, Huybrechts W et al. Biplane three-dimensional augmented fluoroscopy as single navigation tool for ablation of atrial fibrillation: accuracy and clinical value. *Heart Rhythm* 2008;5:957-64.

62. Ector J, De Buck S, Adams J et al. Cardiac three-dimensional magnetic resonance imaging and fluoroscopy merging: a new approach for electroanatomic mapping to assist catheter ablation. *Circulation* 2005;112:3769-76.
63. Sra J, Krum D, Malloy A et al. Registration of three-dimensional left atrial computed tomographic images with projection images obtained using fluoroscopy. *Circulation* 2005;112:3763-8.
64. Tops LF, Schalij MJ, den Uijl DW, Abraham TP, Calkins H, Bax JJ. Image integration in catheter ablation of atrial fibrillation. *Europace* 2008;10 Suppl 3:iii48-iii56.
65. Dong J, Calkins H, Solomon SB et al. Integrated electroanatomic mapping with three-dimensional computed tomographic images for real-time guided ablations. *Circulation* 2006;113:186-94.
66. Tops LF, Bax JJ, Zeppenfeld K et al. Fusion of multislice computed tomography imaging with three-dimensional electroanatomic mapping to guide radiofrequency catheter ablation procedures. *Heart Rhythm* 2005;2:1076-81.
67. Kistler PM, Rajappan K, Jahngir M et al. The impact of CT image integration into an electroanatomic mapping system on clinical outcomes of catheter ablation of atrial fibrillation. *J Cardiovasc Electro-physiol* 2006;17:1093-101.
68. Della Bella P, Fassini G, Cireddu M et al. Image integration-guided catheter ablation of atrial fibrillation: a prospective randomized study. *J Cardiovasc Electrophysiol* 2009;20:258-65.
69. Kistler PM, Rajappan K, Harris S et al. The impact of image integration on catheter ablation of atrial fibrillation using electroanatomic mapping: a prospective randomized study. *Eur Heart J* 2008;29:3029-36.
70. den Uijl DW, Tops LF, Tolosana JM et al. Real-time integration of intracardiac echocardiography and multislice computed tomography to guide radiofrequency catheter ablation for atrial fibrillation. *Heart Rhythm* 2008;5:1403-10.
71. Cappato R, Calkins H, Chen SA et al. Worldwide survey on the methods, efficacy, and safety of catheter ablation for human atrial fibrillation. *Circulation* 2005;111:1100-5.
72. Terasawa T, Balk EM, Chung M et al. Systematic Review: Comparative Effectiveness of Radiofrequency Catheter Ablation for Atrial Fibrillation. *Ann Intern Med* 2009;151:191-202.
73. Holmes DR, Jr., Monahan KH, Packer D. Pulmonary vein stenosis complicating ablation for atrial fibrillation: clinical spectrum and interventional considerations. *JACC Cardiovasc Interv* 2009;2:267-76.
74. Hijazi ZM, Shivkumar K, Sahn DJ. Intracardiac echocardiography during interventional and electrophysiological cardiac catheterization. *Circulation* 2009;119:587-96.
75. Pappone C, Oral H, Santinelli V et al. Atrio-esophageal fistula as a complication of percutaneous transcatheter ablation of atrial fibrillation. *Circulation* 2004;109:2724-6.
76. Khan MN, Jais P, Cummings J et al. Pulmonary-vein isolation for atrial fibrillation in patients with heart failure. *N Engl J Med* 2008;359:1778-85.
77. Lutomsy BA, Rostock T, Koops A et al. Catheter ablation of paroxysmal atrial fibrillation improves cardiac function: a prospective study on the impact of atrial fibrillation ablation on left ventricular function assessed by magnetic resonance imaging. *Europace* 2008;10:593-9.
78. Tops LF, den Uijl DW, Delgado V et al. Long-term improvement in left ventricular strain after successful catheter ablation for atrial fibrillation in patients with preserved left ventricular systolic function. *Circ Arrhythmia Electrophysiol* 2009;2:249-57.
79. Beukema WP, Elvan A, Sie HT, Misier AR, Wellens HJ. Successful radiofrequency ablation in patients with previous atrial fibrillation results in a significant decrease in left atrial size. *Circulation* 2005;112:2089-95.
80. Reant P, Lafitte S, Jais P et al. Reverse remodeling of the left cardiac chambers after catheter ablation after 1 year in a series of patients with isolated atrial fibrillation. *Circulation* 2005;112:2896-903.
81. Tops LF, Bax JJ, Zeppenfeld K, Jongbloed MR, van der Wall EE, Schalij MJ. Effect of radiofrequency catheter ablation for atrial fibrillation on left atrial cavity size. *Am J Cardiol* 2006;97:1220-2.
82. Delgado V, Vidal B, Sitges M et al. Fate of left atrial function as determined by real-time three-dimensional echocardiography study after radiofrequency catheter ablation for the treatment of atrial fibrillation. *Am J Cardiol* 2008;101:1285-90.

83. Tsao HM, Wu MH, Huang BH et al. Morphologic remodeling of pulmonary veins and left atrium after catheter ablation of atrial fibrillation: insight from long-term follow-up of three-dimensional magnetic resonance imaging. *J Cardiovasc Electrophysiol* 2005;16:7-12.
84. Leung DY, Boyd A, Ng AA, Chi C, Thomas L. Echocardiographic evaluation of left atrial size and function: current understanding, pathophysiologic correlates, and prognostic implications. *Am Heart J* 2008;156:1056-64.
85. Schneider C, Malisius R, Krause K et al. Strain rate imaging for functional quantification of the left atrium: atrial deformation predicts the maintenance of sinus rhythm after catheter ablation of atrial fibrillation. *Eur Heart J* 2008;29:1397-409.
86. McGann CJ, Kholmovski EG, Oakes RS et al. New magnetic resonance imaging-based method for defining the extent of left atrial wall injury after the ablation of atrial fibrillation. *J Am Coll Cardiol* 2008;52:1263-71.



Fusion of multi-slice computed tomography imaging with three-dimensional electroanatomical mapping to guide radiofrequency catheter ablation procedures

Laurens F. Tops¹

Jeroen J. Bax¹

Katja Zeppenfeld¹

Monique R.M. Jongbloed¹

Hildo J. Lamb²

Ernst E. van der Wall¹

Martin J. Schalij¹

¹*Department of Cardiology, Leiden University Medical Center, Leiden, the Netherlands*

²*Department of Radiology, Leiden University Medical Center, Leiden, the Netherlands*

Heart Rhythm 2005;2:1076-81

ABSTRACT

Background: The outcome of catheter ablation procedures of cardiac arrhythmias depends on the ability to evaluate the underlying mechanism and to depict target sites for ablation. Fusion of different imaging modalities within one system may improve electroanatomic modeling and facilitate ablation procedures.

Objectives: To study the feasibility of fusion of multi-slice computed tomography (MSCT) with electroanatomic mapping to guide radiofrequency catheter ablation of atrial arrhythmias.

Methods: Sixteen patients (15 men, age 54 ± 7 years) with drug-refractory atrial fibrillation (AF) underwent 64-slice MSCT within 2 days before radiofrequency catheter ablation. MSCT data were imported in the Carto™ electroanatomic mapping system. Using the new CartoMerge™ Image Integration Module, the MSCT images and the electroanatomical map were aligned. A statistical algorithm provided information about the accuracy of the fusion process.

Results: In all patients MSCT images could be fused with the electroanatomic map. Mean distance between the mapping points and the MSCT surface ranged from 1.7 ± 1.2 mm to 2.8 ± 1.8 mm. This resulted in an average of 2.1 ± 0.2 mm for the patient group as a whole.

Conclusion: MSCT images can be fused with the 3D electroanatomic mapping system in an accurate manner. Anatomy-based catheter ablation procedures for atrial arrhythmias may be facilitated by integration of different imaging modalities.

INTRODUCTION

Ectopic beats originating from the pulmonary veins have been identified as a potential cause of atrial fibrillation (AF) (1). Catheter ablation focused on isolation of the pulmonary veins is a curative treatment modality of AF. Different strategies for pulmonary vein isolation have been proposed, including segmental (2) and circumferential (3) ablation. Electrical isolation of the pulmonary veins has proved to be a safe technique with a reasonable long-term success rate (4,5). To plan and guide these ablation procedures, detailed anatomic information is needed. Several imaging modalities are available to visualize the anatomy of the left atrium and the pulmonary veins.

Both magnetic resonance imaging and multi-slice computed tomography (MSCT) are non-invasive imaging modalities that can provide the requested information and both imaging modalities have been used to provide road maps prior to ablation (6,7). These techniques provide detailed information on the precise number, location and anatomy of the pulmonary veins and have been demonstrated useful in the planning of ablation procedures (8,9). In addition, detailed information is also needed during the ablation procedure; fluoroscopy alone is not accurate enough and may result in a prolonged radiation exposure. For this purpose, 3D electroanatomic mapping systems that facilitate ablation procedures have been introduced (10). However, a realistic anatomical representation of the left atrium and pulmonary veins is still difficult to obtain. Therefore, fusion of an anatomical imaging technique (e.g. MSCT) with 3D electroanatomic mapping may further facilitate ablation procedures. In the current study, the feasibility of fusion of MSCT with electroanatomic mapping is demonstrated in patients undergoing radiofrequency ablation for AF.

METHODS

Study population

The study population consisted of 16 consecutive patients (15 men, mean age 54 ± 7 years) with symptomatic drug-refractory AF who were admitted for radiofrequency catheter ablation. AF was present for 54 ± 12 months, and was paroxysmal in 5 patients, persistent in 9 and permanent in 2 patients. Mean number of anti-arrhythmic drugs used was 3.7 ± 1.6 per patient. Mean left atrial size was 4.4 ± 0.3 cm; mean left ventricular ejection fraction was $57 \pm 10\%$. Seven patients were treated for hypertension; none of the patients had clinically relevant valvular disease. Six patients underwent coronary angiography for suspected coronary artery disease; in none of the patients significant coronary artery stenoses were detected. One patient had a pacemaker. In two patients a catheter ablation procedure for atrial flutter was performed previously.

Multi-slice computed tomography

All patients underwent MSCT using a 64-detector row system (Toshiba Medical Systems, Otawara, Japan) 2 days prior to the ablation procedure, as previously reported (8). Collimation was 64 x 0.5 mm, rotation time 400 ms, and tube voltage 100 kV at 250 mA. Cranio-caudal scanning was performed during an inspiratory breathhold, without electrocardiographic gating. Non-ionic contrast material (Iomeron 400, Bracco Altana Pharma, Konstanz, Germany) was infused through the antecubital vein with an infusion rate of 5 ml/s. A total amount of 70 ml contrast was given. Automatic detection of the contrast bolus in the ascending aorta was used to time the scan. All MSCT images were evaluated by two experienced observers in consensus. To assess the number of pulmonary veins, the number of ostia (common or separate ostia), and the branching pattern of the pulmonary veins, 2D viewing modes and 3D reconstructions were used. Diameters of the pulmonary vein ostia were measured in the anterior-posterior and superior-inferior direction, as previously described (8). Furthermore, thrombi in the left atrial appendage and extra-cardiac anomalies were excluded.

Image processing

Before the ablation procedure, raw MSCT data were loaded into the 3D electroanatomic mapping system (Carto XP™, Biosense Webster, California, USA) equipped with the newly developed CartoMerge™ Image Integration Module. The accuracy of this new technique has been validated in animal studies previously (11). To depict the structures of interest (left atrium and pulmonary veins) out of the raw data set, a segmentation process was performed manually.

This process consisted of several phases. First, the borders of the structures of interest were delineated by setting the threshold intensity range. The presence of contrast in the left atrium allowed differentiation between endocardium (low intensity level) and blood pool (high intensity level). Subsequently, a 3D volume was created by labeling all volume units of the raw MSCT data within the set threshold intensity range. To segment this volume into different structures, anatomical markers were placed in the middle of the different areas of the volume. An algorithm was then implemented to automatically depict the different structures of interest based on the placement of the anatomical markers and the borders (Figure 1). Finally, the result of the segmentation process was verified on axial slices. When an adequate segmentation of the MSCT images was achieved, the surface images were stored in the Carto™ system.

Mapping and radiofrequency ablation

The aim of the radiofrequency catheter ablation procedure for AF was to obtain an electrical disconnection of all pulmonary veins. With the use of intracardiac echocardiography an intracardiac thrombus was excluded and a transseptal puncture was guided (12). Mapping and ablation was performed with a 4 mm quadripolar mapping/ablation catheter (7F Thermocool, Biosense Webster, California, USA). A 6F reference catheter was placed in the right atrium.

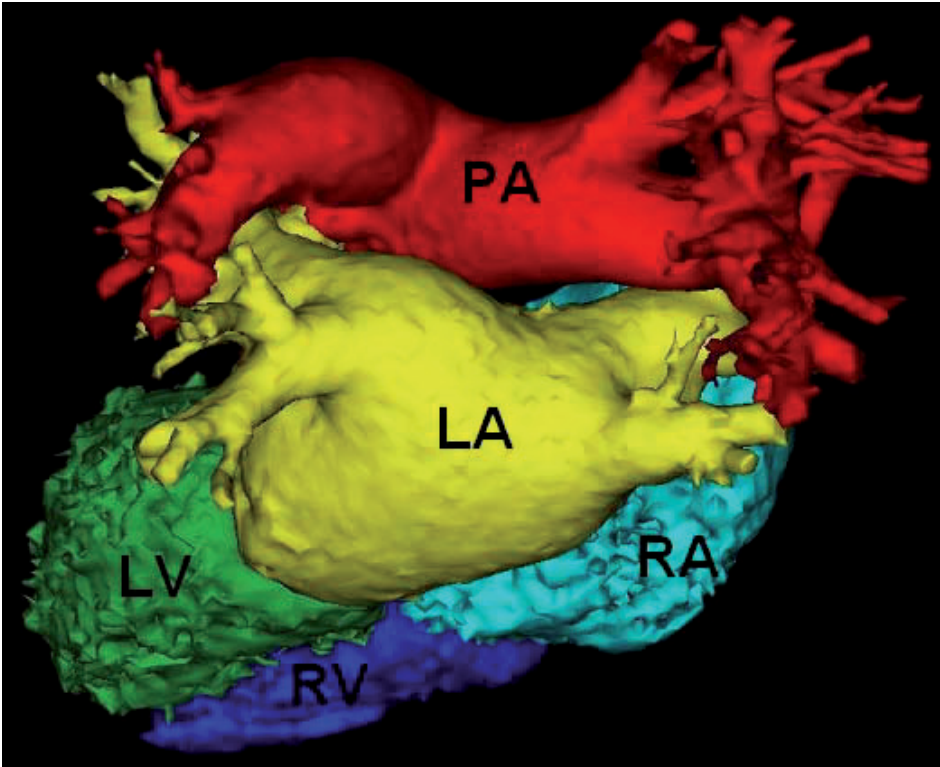


Figure 1. Multislice computed tomography image after segmentation using the CartoMerge™ Image Integration Module. Segmentation included: creation of a 3D volume, placement of anatomical markers on different structures and implementation of an algorithm that creates the different structures of interest (see text). LA = left atrium; LV = left ventricle; PA = pulmonary arteries; RA = right atrium; RV = right ventricle.

After completion of the electroanatomic map, a registration process was performed manually to fuse the MSCT images and the electroanatomic map. First, the 3D surface image of the MSCT was displayed on the Carto™ system next to the electroanatomic map. A landmark was then placed on the electroanatomic map on a certain point (e.g. left atrial appendage), confirmed with intracardiac echocardiography and fluoroscopy. A second landmark was placed on the MSCT image at the same location (Figure 2). Next, the surface registration algorithm was performed to align the MSCT surface image and the electroanatomic map. This algorithm composed the best fit of the two structures based on minimizing distance between the two landmarks and the distance between all mapping points and the MSCT surface image.

The accuracy of the registration process was then reviewed. The algorithm used for fusion provided information about the accuracy of the registration: mean distance, standard deviation and range between all mapping points and the MSCT surface image were reviewed. Furthermore, the catheter position in the fused electroanatomic map and MSCT was reviewed using intracardiac echocardiography and fluoroscopy.

After registration of the MSCT surface image radiofrequency current was applied outside the ostia of the pulmonary veins, using the ablation catheter with a 4 mm open loop irrigated

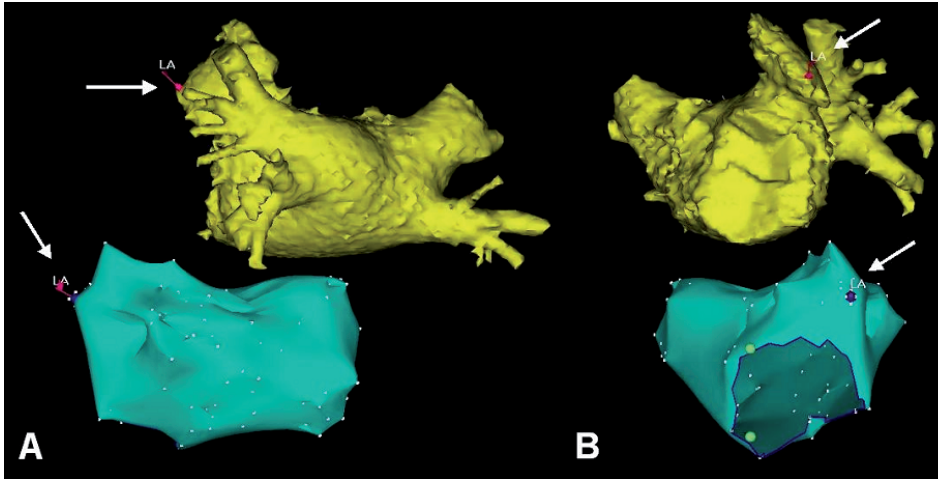


Figure 2. During the ablation procedure, a registration process was performed to fuse the electroanatomic map and the MSCT image. After completion of the electroanatomic map of the left atrium, landmarks were placed on the electroanatomic map and the MSCT surface image. In this case, a landmark (LA) was placed on the left atrial appendage, based on fluoroscopy and intracardiac echocardiography. Panel A: posterior view, Panel B: lateral view.

tip. The following power and temperature settings were used: irrigation rate 20 mL/min, maximum temperature 50°C, maximum radiofrequency energy 30 W. At each point, radiofrequency current was applied until a voltage <0.1 mV was achieved, with a maximum of 60 seconds per point. If a separate pulmonary venous insertion was noted on the MSCT image, radiofrequency current was targeted to form separate circles surrounding the pulmonary venous ostia. If a common ostium was observed, ablation points were targeted in a large circle surrounding the common ostium. The procedure was considered successful when pulmonary vein isolation was confirmed by recording entrance block during sinus rhythm or pacing in the coronary sinus. All patients received heparin intravenously (activated clotting time > 300 sec) to avoid thromboembolic complications.

After the ablation procedure, patients received heparin intravenously until INR was adequate with oral anticoagulants. Transthoracic 2D echocardiography was performed within 24 hours to detect pericardial effusion. Electrocardiographic monitoring (including 12-lead surface and 24-hour Holter monitoring) was obtained to assess the maintenance of sinus rhythm after the ablation procedure.

Statistical analysis

The statistical algorithm of the new CartoMerge™ Image Integration Module provides statistical information (mean, standard deviation and range) about the distances between all mapping points and the MSCT surface image. All data are presented as mean ± standard deviation or number (%).

RESULTS

MSCT and image processing

In the 16 patients, a total number of 67 pulmonary veins were identified by MSCT (4.2 ± 0.4 per patient). In 3 patients (19%), an additional pulmonary vein on the right side was observed. A common ostium of the left-sided pulmonary veins was noted in 6 patients (38%), and a common ostium of the right-sided pulmonary veins in 1 patient (6%). In 9 patients (63%), early branching pattern of a pulmonary vein was observed, all in the right inferior pulmonary vein.

The anterior-posterior and superior-inferior diameters were as follows: left superior pulmonary vein 15.8 ± 2.3 mm and 19.0 ± 2.1 mm respectively, left inferior pulmonary vein 13.2 ± 2.0 mm and 18.4 ± 1.9 mm, right superior pulmonary vein 17.7 ± 2.7 mm and 20.1 ± 3.3 mm, right inferior pulmonary vein 17.3 ± 2.7 mm and 17.6 ± 2.4 mm, respectively.

Image processing of the raw MSCT data could be performed within 10 minutes in all patients. Good contrast timing during the CT scan favored the segmentation process: the presence of contrast allowed excellent differentiation between the endocardium (low intensity level) and the blood pool (high intensity level). In all patients, an adequate segmentation of the MSCT was achieved.

Mapping and radiofrequency ablation

Eventually, all patients were treated with radiofrequency catheter ablation for AF. In all patients a transseptal puncture could be performed guided by intracardiac echocardiography. Mean mapping time was 43 ± 15 minutes, and a mean of 224 ± 59 mapping points was used to create an electroanatomic map of the left atrium and pulmonary veins. There was no difference in heart rhythm during MSCT scanning and the mapping / ablation procedure.

After placement of the landmarks, the MSCT image and the electroanatomic map were fused. This registration process could be performed within 5 - 7 minutes in all patients. After the registration, the distances between all mapping points and the MSCT surface image were reviewed. Results of the registration processes are listed in Table 1. Mean distance between the mapping points and the MSCT surface ranged from 1.7 ± 1.2 mm to 2.8 ± 1.8 mm. This resulted in an average of 2.1 ± 0.2 mm for the patient group as a whole.

The fused electroanatomic map and MSCT surface image were used to guide the catheter during the actual ablation. Exact catheter position and relation to the pulmonary veins and the endocardium could be adequately visualized (Figure 3). Radiofrequency current was applied outside the ostia of all the pulmonary veins. Mean ablation time was 89 ± 20 minutes, and mean fluoroscopy time was 48 ± 7 minutes. Procedural success was achieved in all patients. No complications occurred during the ablation procedures, in 2 patients mild pericardial effusion was observed after the procedure, without hemodynamic consequences. After the ablation procedure all patients were in sinus rhythm.

Table 1. Results of the registration process per patient

Patient	Age	Gender	No. of Mapping points	Distance between mapping points and MSCT (mm)		
				Mean	SD	Range
1	64	M	217	2.2	1.8	0.0 - 9.1
2	56	M	204	2.2	1.7	0.0 - 9.3
3	58	M	185	1.9	1.4	0.0 - 6.7
4	54	M	220	2.8	1.8	0.0 - 8.3
5	43	M	248	2.1	1.5	0.1 - 7.4
6	56	M	328	2.0	1.6	0.0 - 7.1
7	51	M	117	1.7	1.2	0.0 - 4.9
8	58	F	151	1.9	1.3	0.0 - 6.5
9	55	M	165	1.9	1.5	0.0 - 7.1
10	58	M	316	2.2	1.6	0.0 - 9.9
11	35	M	294	2.3	1.7	0.0 - 7.9
12	65	M	219	2.4	1.5	0.0 - 5.6
13	56	M	282	2.1	1.4	0.0 - 6.3
14	56	M	245	1.9	1.2	0.0 - 5.1
15	56	M	205	2.1	1.7	0.0 - 8.9
16	50	M	191	2.0	1.4	0.0 - 6.8
Mean	53.7		224.2	2.1		
SD	7.2		59.0	0.2		

DISCUSSION

The results of this study illustrate the feasibility of fusion of MSCT images with 3D electroanatomic mapping in patients undergoing catheter ablation for AF. The mean distance between the MSCT image and the electroanatomic map was only 2 mm, allowing accurate visualization of the catheter position on real surface anatomy during the ablation procedure. The integration of MSCT images and 3D electroanatomic mapping is a promising technique which may facilitate ablation procedures.

Image processing and registration

The introduction of 3D electroanatomic mapping systems has facilitated the anatomical based ablation procedures for AF (10). However, the surrogate anatomy is reconstructed from multiple catheter recordings along the endocardium (13). Therefore, the use of reconstructed maps may be limited by the complex anatomy of the left atrium and pulmonary veins.

Registration of previously acquired 3D images is a new technique, which offers the ability of using real surface anatomy to guide anatomical based catheter ablation procedures (14,15). Reddy et al (15) demonstrated the feasibility of fusion of magnetic resonance images and 3D electroanatomic mapping in an animal study. After manual segmentation of the magnetic resonance image of the left ventricle, the authors performed a similar registration process. Mean distance between the electroanatomic map and the surface image of the left ventricle was 4.9 ± 1.8 mm. The registration process was limited by the rotation of the left ventricle around its

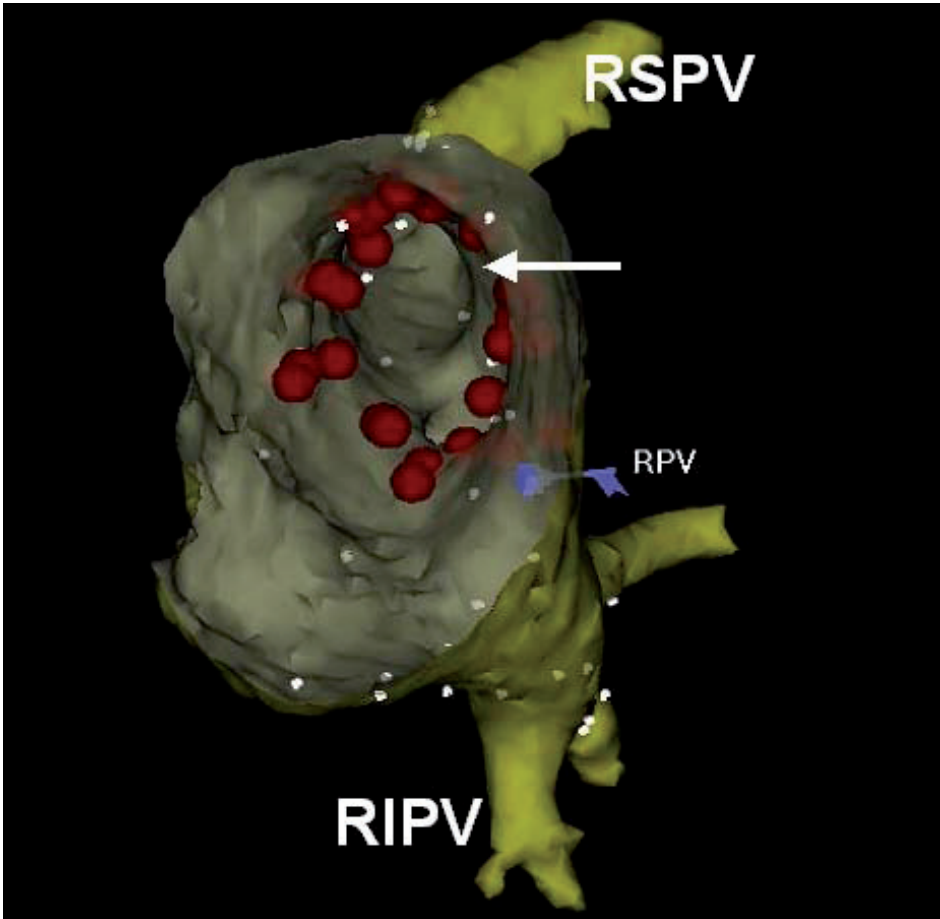


Figure 3. After registration, the fused electroanatomic map and MSCT surface image are used to guide catheter ablation. In this view from inside the left atrium, the ostium (arrow) of the right superior pulmonary vein (RSPV) is visualized. Radiofrequency current was applied outside the ostia of the pulmonary veins. Red tags indicate sites of radiofrequency current delivery. RPV = landmark used for registration; RSPV = right superior pulmonary vein; RIPV = right inferior pulmonary vein.

symmetric long axis. To assess an accurate registration, part of the ascending aorta had to be included in the electroanatomic map (15). In the current study, the mean distance between the MSCT image and the electroanatomic map was only 2.1 ± 0.2 mm for the patient group as a whole. Furthermore, the specific anatomy of the left atrium and the pulmonary veins made improper registration due to rotation impossible. The current *in vivo* study demonstrates that fusion of previously acquired MSCT images of the left atrium and 3D electroanatomic mapping can be performed accurately.

Clinical implications

Anatomy-based catheter ablation for AF is nowadays a safe procedure, and is performed in a large number of centers worldwide (5). Infrequent serious complications, such as pulmonary

vein stenosis, have been reported (16). MSCT can accurately depict the anatomy of the left atrium and the pulmonary veins (8,17), and complications can be avoided to some extent by integration of pre-procedural acquired MSCT images and the 3D mapping images. Furthermore, isolation of all pulmonary veins is necessary to achieve good long-term results. The number and anatomy of the pulmonary veins can be highly variable (18), and the small right middle pulmonary vein has been associated with the initiation of AF (19). Using the electroanatomic mapping system alone, additional or small pulmonary veins are difficult to identify. Detailed information on number, location and branching pattern of all pulmonary veins (as provided by MSCT) during the ablation procedure may improve outcome.

Furthermore, the use of integration of different imaging modalities may reduce procedure time and fluoroscopy time. The introduction of non-fluoroscopic systems reduced fluoroscopy time during AF ablation procedures. However, incorrect geometry of the reconstructed anatomy may limit the use of non-fluoroscopy systems (20). Recently, stereotactic systems have become available to guide ablation procedures (21,22). Although initial results are promising, the high costs of stereotactic systems limit their use in clinical practice. Alternatively, fusion of MSCT images and 3D electroanatomic mapping is easy to perform as demonstrated in the current study and allows visualization of real surface anatomy during the ablation procedure.

Limitations

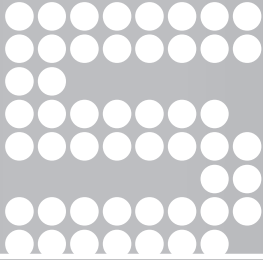
The present study has some limitations. Scanning was performed during breath-hold, whereas patients were breathing normally during the ablation procedure. Furthermore, heart rate is variable during the ablation procedure. As a consequence, different volumes of the left atrium during the MSCT scan and the ablation procedure may limit the fusion process. However, using a 64-slice MSCT scanner, data acquisition was completed in only 4 seconds. This short breath-hold may minimize the possible difference in left atrial volumes. Reddy et al (15) also observed differences in volume between the surface image and the electroanatomic map of the left ventricle. This resulted in a mean distance of approximately 5 mm between the magnetic resonance surface image and the electroanatomic map. However, ablation based on the magnetic resonance surface image alone resulted in exact ablation lesions in their porcine model (15). We speculate that volume differences in the left atrium and pulmonary veins may be smaller than in the left ventricle, limiting the possible error and allowing precise ablation. Furthermore, the mean distance between the MSCT surface image and the electroanatomic map was only 2.1 ± 0.2 mm for the patient group as a whole. More validation studies in well-controlled animal models are needed to fully appreciate the strengths and limitations of this new fusion approach.

CONCLUSION

The current study demonstrates that integration of pre-procedural acquired MSCT images and the 3D electroanatomic mapping system can be performed accurately. This new technique allows the use of real surface anatomy to guide anatomy-based catheter ablation procedures. The fusion of different imaging modalities may facilitate catheter ablation for AF.

REFERENCES

1. Haissaguerre M, Jais P, Shah DC et al. Spontaneous initiation of atrial fibrillation by ectopic beats originating in the pulmonary veins. *N Engl J Med* 1998;339:659-66.
2. Oral H, Scharf C, Chugh A et al. Catheter ablation for paroxysmal atrial fibrillation: segmental pulmonary vein ostial ablation versus left atrial ablation. *Circulation* 2003;108:2355-60.
3. Pappone C, Rosanio S, Oreto G et al. Circumferential radiofrequency ablation of pulmonary vein ostia: A new anatomic approach for curing atrial fibrillation. *Circulation* 2000;102:2619-28.
4. Pappone C, Rosanio S, Augello G et al. Mortality, morbidity, and quality of life after circumferential pulmonary vein ablation for atrial fibrillation: outcomes from a controlled nonrandomized long-term study. *J Am Coll Cardiol* 2003;42:185-97.
5. Cappato R, Calkins H, Chen SA et al. Worldwide survey on the methods, efficacy, and safety of catheter ablation for human atrial fibrillation. *Circulation* 2005;111:1100-5.
6. Ghaye B, Szapiro D, Dacher JN et al. Percutaneous ablation for atrial fibrillation: the role of cross-sectional imaging. *Radiographics* 2003;23:S19-S33.
7. Mansour M, Holmvang G, Sosnovik D et al. Assessment of pulmonary vein anatomic variability by magnetic resonance imaging: implications for catheter ablation techniques for atrial fibrillation. *J Cardiovasc Electrophysiol* 2004;15:387-93.
8. Jongbloed MR, Dirksen MS, Bax JJ et al. Atrial fibrillation: multi-detector row CT of pulmonary vein anatomy prior to radiofrequency catheter ablation--initial experience. *Radiology* 2005;234:702-9.
9. Schwartzman D, Lacomis J, Wigginton WG. Characterization of left atrium and distal pulmonary vein morphology using multidimensional computed tomography. *J Am Coll Cardiol* 2003;41:1349-57.
10. Packer DL. Evolution of mapping and anatomic imaging of cardiac arrhythmias. *Pacing Clin Electrophysiol* 2004;27:1026-49.
11. Dickfeld T, Dong J, Solomon SB et al. Assessment of position error of catheter mapping system (Bio-sense Carto® V8) with CT/MR image integration capabilities. *Heart Rhythm* 2005;2:S278.
12. Jongbloed MR, Schalijs MJ, Zeppenfeld K, Oemrawsingh PV, van der Wall EE, Bax JJ. Clinical applications of intracardiac echocardiography in interventional procedures. *Heart* 2005;91:981-90.
13. Gepstein L, Hayam G, Ben Haim SA. A novel method for nonfluoroscopic catheter-based electroanatomical mapping of the heart. In vitro and in vivo accuracy results. *Circulation* 1997;95:1611-22.
14. Sra J, Krum D, Hare J et al. Feasibility and validation of registration of three-dimensional left atrial models derived from computed tomography with a noncontact cardiac mapping system. *Heart Rhythm* 2005;2:55-63.
15. Reddy VY, Malchano ZJ, Holmvang G et al. Integration of cardiac magnetic resonance imaging with three-dimensional electroanatomic mapping to guide left ventricular catheter manipulation: feasibility in a porcine model of healed myocardial infarction. *J Am Coll Cardiol* 2004;44:2202-13.
16. Packer DL, Keelan P, Munger TM et al. Clinical presentation, investigation, and management of pulmonary vein stenosis complicating ablation for atrial fibrillation. *Circulation* 2005;111:546-54.
17. Cronin P, Sneider MB, Kazerooni EA et al. MDCT of the left atrium and pulmonary veins in planning radiofrequency ablation for atrial fibrillation: a how-to guide. *AJR Am J Roentgenol* 2004;183:767-78.
18. Marom EM, Herndon JE, Kim YH, McAdams HP. Variations in pulmonary venous drainage to the left atrium: implications for radiofrequency ablation. *Radiology* 2004;230:824-9.
19. Tsao HM, Wu MH, Yu WC et al. Role of right middle pulmonary vein in patients with paroxysmal atrial fibrillation. *J Cardiovasc Electrophysiol* 2001;12:1353-7.
20. Rotter M, Takahashi Y, Sanders P et al. Reduction of fluoroscopy exposure and procedure duration during ablation of atrial fibrillation using a novel anatomical navigation system. *Eur Heart J* 2005.
21. Dickfeld T, Calkins H, Zviman M et al. Anatomic stereotactic catheter ablation on three-dimensional magnetic resonance images in real time. *Circulation* 2003;108:2407-13.
22. Solomon SB, Dickfeld T, Calkins H. Real-time cardiac catheter navigation on three-dimensional CT images. *J Interv Card Electrophysiol* 2003;8:27-36.



Real-time integration of intracardiac echocardiography and multi-slice computed tomography to guide radiofrequency catheter ablation for atrial fibrillation

Dennis W. den Uijl¹
Laurens F. Tops¹
José M. Tolosana^{1,2}
Joanne D. Schuijf¹
Serge A.I.P. Trines¹
Katja Zeppenfeld¹
Jeroen J. Bax¹
Martin J. Schalij¹

¹*Department of Cardiology, Leiden University Medical Center, Leiden, the Netherlands*

²*Thorax institute, Hospital Clinic, University of Barcelona, Barcelona, Spain*

Heart Rhythm 2008;5:1403-10

ABSTRACT

Background: Multi-slice computed tomography (MSCT) integration is commonly used to guide radiofrequency catheter ablation (RFCA) for atrial fibrillation (AF). MSCT provides detailed anatomical information but lacks the ability to provide real-time anatomy during RFCA. Intra-cardiac echocardiography (ICE) allows real-time visualization of cardiac structures.

Objective: The purpose of this study was to investigate the feasibility of three-dimensional (3D) anatomical mapping of the left atrium (LA) with ICE and integrating the 3D map with MSCT to facilitate RFCA for AF.

86

Methods: In 17 patients undergoing RFCA for AF, 3D mapping of the LA was performed with ICE using a new mapping system (CARTOSOUND™, Biosense Webster) which allows tracking of a new ICE probe. On each ICE image endocardial contours were traced and used to generate a 3D map of the LA and pulmonary veins (PVs). A preprocedural acquired MSCT image of the LA was then integrated with the 3D map. Additionally, PV assessment with ICE was compared with MSCT.

Results: Accurate 3D mapping could be performed in all patients with a mean number of 31.1 ± 8.5 contours. Integration with MSCT resulted in a mean distance between MSCT and ICE contours of 2.2 ± 0.3 mm for the LA and PVs together and of 1.7 ± 0.2 mm around the PV ostia specifically. Agreement in assessment of PV anatomy and diameters between ICE and MSCT was excellent.

Conclusion: Three-dimensional ICE mapping of the LA is feasible. The 3D map created with ICE can be merged with MSCT to facilitate RFCA for AF.

INTRODUCTION

Ectopic beats originating from the pulmonary veins (PVs) can initiate atrial fibrillation (AF) (1). Radiofrequency catheter ablation (RFCA) is considered a reasonable option in the treatment of patients with AF, when at least one anti-arrhythmic drug has failed (2). Ablation strategies targeting the PVs are the cornerstone of these RFCA procedures. To plan and guide these ablation procedures, non-invasive three-dimensional (3D) imaging modalities like magnetic resonance imaging and multi-slice computed tomography (MSCT) are available to visualize the left atrium (LA) and PVs (3,4). Electrophysiological navigation systems allowing the integration of MSCT with electroanatomical maps combine accurate real-time navigation with detailed anatomical information thereby facilitating the ablation procedure (5) and reducing fluoroscopy time and procedural duration (6).

However, a limiting factor of using MSCT to guide the ablation procedure is the time interval between image acquisition and the ablation procedure which may result in differences in heart rhythm, heart rate and fluid status potentially causing an inaccurate registration process. Because the quality of the registration process determines the accuracy of navigating (7), this could result in less accurate lesion placement during RFCA. Recently, a new electroanatomical mapping system has been released that allows integration of 3D mapping and real-time intracardiac echocardiography (ICE). Using this system, a registered 3D shell of the LA and PV anatomy can be generated from two-dimensional (2D) ICE images.

The aim of this study was to investigate the feasibility of creating a 3D map of the LA and PVs with ICE and integrating this map with a MSCT surface image in order to facilitate RFCA for AF. In addition, a direct comparison between this new ICE technique and MSCT for the assessment of PV anatomy was performed.

METHODS

Study population and protocol

The study population comprised 17 consecutive patients with symptomatic drug refractory AF, who underwent RFCA in our institution. In all patients a MSCT was acquired two days before the ablation. Prior to the procedure, the raw MSCT data was loaded into an electroanatomical mapping system (CARTO XP™, Biosense Webster, Diamond Bar, California) equipped with a newly developed image integration module (CARTOSOUND™, Biosense Webster). During the ablation procedure 3D maps of the LA and PVs were created using an ICE catheter with an imbedded CARTO navigation sensor (10Fr Soundstar™, Biosense Webster) allowing the mapping system to detect its position and generate a registered 3D shell from the recorded two-dimensional (2D) images. After completion of the mapping procedure a registration process was performed

to integrate the MSCT image with the 3D map made with ICE. Thereafter the merged MSCT image and 3D maps were used to guide the RFCA procedure.

Multi-Slice Computed Tomography

The MSCT examination was performed with a 64-slice Toshiba Aquilion 64 system (Toshiba Medical Systems, Otawara, Japan) (7 patients) or a 320-slice Toshiba Aquilion One system (Toshiba Medical Systems) (10 patients). Craniocaudal scanning was performed during breath holding. For the Aquilion 64 system collimation was 64 x 0.5 mm, rotation time 400 ms and tube voltage between 100 and 135 kV at 250 to 400 mA. For the Aquilion One system collimation was 320 x 0.5 mm, rotation time 350 ms and tube voltage 120 kV at 400 to 500 mA. In all patients nonionic contrast material (Iomeron 400, Bracco, Milan, Italy; 105 ml for Aquilion 64 and 50 ml for Aquilion One scanning) was infused through the antecubital vein at a rate of 5 ml/s followed by 50 ml saline solution flush. Automatic detection of the contrast bolus was used to time the start of the scan. Before the ablation procedure, all MSCT data were analyzed on a dedicated workstation (Vitrea 2; Vital Images, Minnetonka, Minnesota).

Image processing and segmentation

Prior to the ablation procedure, the raw MSCT data were loaded into the image integration module of the mapping system (CartoMerge™, Biosense Webster) and a segmentation process was performed. The segmentation process consisted of three phases as described previously (5). The first step was to delineate the borders of interest on the MSCT (LA and PVs) by manually setting the threshold intensity range. A 3D volume was subsequently created of all structures within the set threshold range. The second step was to segment this 3D volume into different structures by placing markers in the middle of the different areas. An algorithm was used to automatically depict the different structures based on the placement of the markers and the border of the 3D volume. Finally, the segmented surface images were exported to the mapping system.

Anatomical mapping with ICE

During the catheter ablation procedure, a 3D anatomical map was created with ICE images. A new mapping system was used, equipped with a new image integration module that allows the integration of ICE and 3D mapping (CARTOSOUND™). This system is able to detect the position and direction of a specifically designed ICE catheter with an imbedded CARTO navigation sensor located at its tip (Soundstar™). By positioning the ICE catheter inside the right atrium, ECG gated images of the LA and PVs were acquired. To provide ECG gating, either a quadripolar electrophysiological catheter placed inside the right atrium or the body surface ECG was used as a reference signal in patients with sinus rhythm or AF, respectively. In order to correct for respiratory phase, all ICE images were acquired during expiratory breath hold. Intra-cardiac echocardiography was performed using a Sequoia ultrasound system (Siemens Medical

Solutions USA, Mountain View, California) which transferred real-time ICE data to the mapping system. On the mapping system, the endocardial contours were traced manually after which they were assigned to a map (Figure 1A). All contours within a map were used to generate a registered 3D shell (Figure 1B and 1C). For each map a separate shell was generated. Different maps were created for the LA and for each of the PVs (Figure 1D).

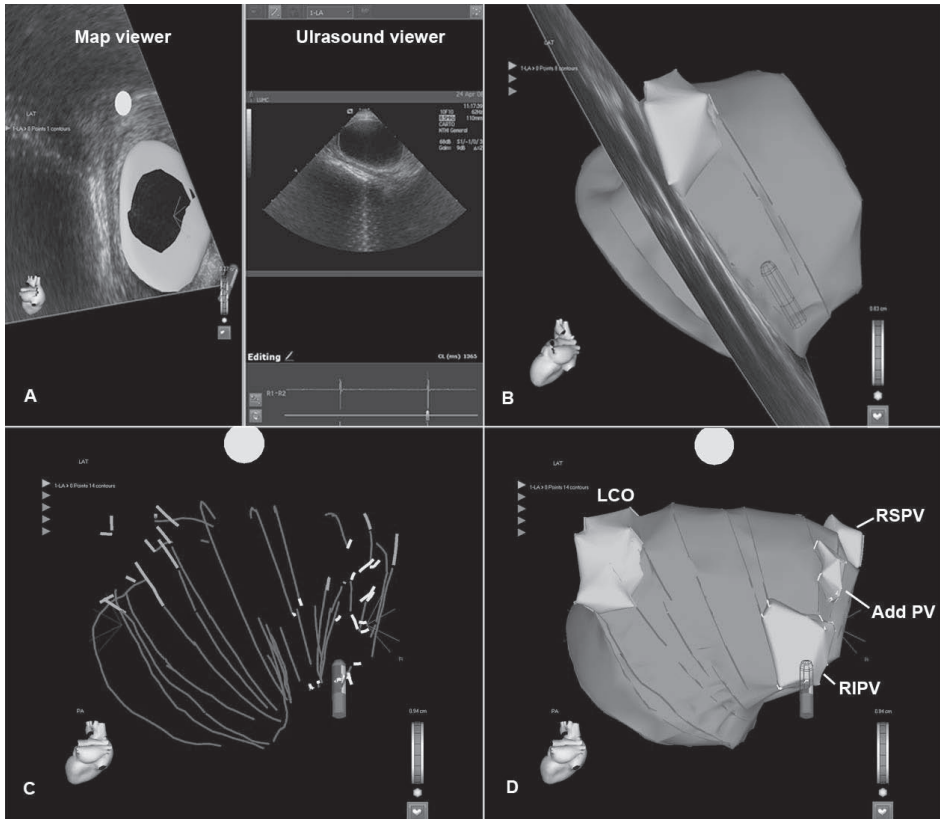


Figure 1. Three-dimensional (3D) mapping with intracardiac echocardiographic (ICE). Ultrasound images of the left atrium (LA) are acquired. The endocardial contour of the LA is traced on the ultrasound viewer of the mapping system. After assigning the contour to a map, it appears on the map viewer (A). By acquiring more contours and reconstructing them into a registered 3D shell (B), the shape of the LA and pulmonary veins (PVs) is depicted. Systematically, the LA and PVs are visualized (C) until a complete 3D map of the LA and PVs is acquired (D). Add PV = additional pulmonary vein, LCO = left common ostium, RIPV = right inferior pulmonary vein, RSPV = right superior pulmonary vein.

Registration

After creating a map with ICE, a registration process was performed to integrate the MSCT surface image and the 3D map. First, the MSCT surface image was displayed next to the anatomical map (Figure 2A). A landmark was placed at a distinct anatomical structure on the anatomical map and at a corresponding point on the MSCT model. Then 'visual alignment' was performed by minimizing the distance between both landmarks. Next, the maps created during the

mapping procedure were each assigned to the corresponding MSCT surface image and a 'surface registration' was performed. During this process the ICE contours were represented as a line of adjacent mapping points. An internal algorithm was used to minimize the distance between these points and the MSCT surface image (Figure 2B).

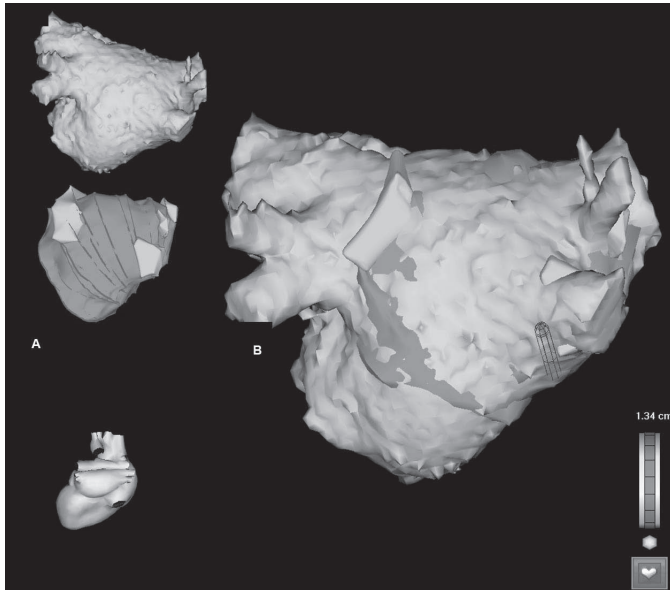


Figure 2. After 3D mapping with ICE, the 3D map and multi-slice computed tomography (MSCT) image are displayed next to each other (A). Then a manual registration process is performed. This results in the integration of the 3D map and the MSCT image in order to anatomically guide the ablation procedure (B).

The accuracy of the registration process was then reviewed. The mean value, standard deviation and range of the distance between the points along the ICE contours and the MSCT surface were provided by the algorithm. The accuracy of the registration process at the level of the PVs was evaluated by measuring the distance between the contours and MSCT surface at 5 representative points around each PV ostium (Figure 3).

PV anatomy and quantitative measurements

After an accurate registration had been acquired the PVs and their atrial insertion were evaluated on both MSCT and ICE. Pulmonary vein anatomy was classified according to the presence or absence of a common ostium/trunk and/or additional veins. As described previously, a common ostium was defined as a PV carina located outside the extrapolated endocardial border of the LA (4). A common trunk was defined as a clearly recognizable common part in which both superior and inferior PV drain before emptying into the LA (8). An additional vein was defined as a supranumerical vein entering the LA with a separate ostium. The same criteria for PV classification were used for MSCT and ICE evaluation.

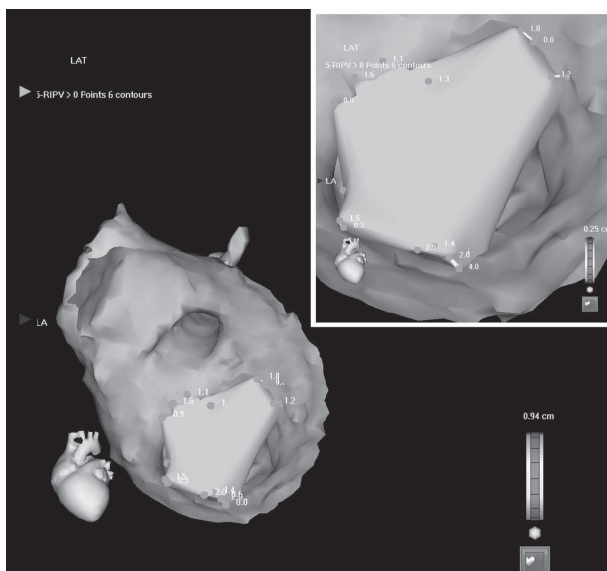


Figure 3. The quality of the registration process was reviewed at the level of the PV ostium by measuring the distance between the MSCT and the 3D map at 5 representative points.

Pulmonary vein diameters on MSCT were measured in anterior-posterior (AP) and superior-inferior (SI) direction inside the PV ostium, as previously described (4). Pulmonary vein diameters on ICE were measured at the widest point. Left atrial diameter was measured in AP direction on both MSCT and the 3D map created with ICE.

Radiofrequency catheter ablation

Radiofrequency catheter ablation was performed by creating two circumferential lesions around the left and right PV antrum (Figure 4). Additional lesions consisting of a roofline, a mitral valve isthmus line or sites exhibiting fractionated activity were created if deemed necessary. After excluding an intracardiac thrombus, and in the absence of a patent foramen ovale, a transseptal puncture was performed under ICE guidance. All patients received a bolus of intravenous heparin (5000 IU) with an additional bolus to maintain an activated clotting time between 300-400 s. The ablation procedure was guided by the 3D map created with ICE and integrated with the MSCT image. An open loop irrigated 4-mm tip quadripolar mapping/ablation catheter (7Fr Navistar™, Biosense Webster) was introduced in the LA and used to apply radiofrequency current outside the ostia of all PVs. At each point, radiofrequency current was applied at 30-35 W (maximum tip temperature 45 °C) until a voltage of <0.1 mV was achieved, with a maximum of 60 seconds per point.

Statistical analysis

Data are presented as mean \pm SD or as number (percentage). Statistical analysis was performed using SPSS 14.0 software (SPSS Inc., Chicago, Illinois). Statistical comparisons were performed

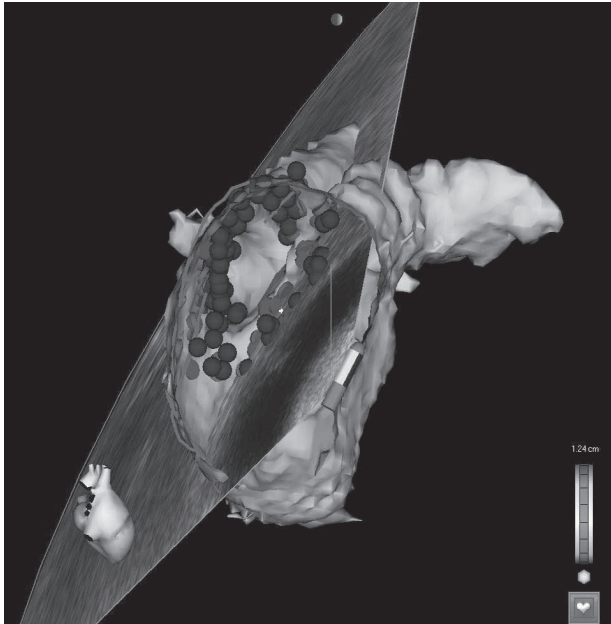


Figure 4. After registration, the 3D map created with ICE and integrated MSCT image were used to facilitate the ablation procedure. Circumferential lesions were created outside the PV ostia. Red tags represent the sites of radiofrequency current application.

with two tailed Student's T-test, paired or unpaired as appropriate. Kappa analysis was used to quantify the level of agreement in PV anatomy classification with MSCT and ICE. Bland-Altman analysis was used to quantify the level of agreement between measurements of PV diameter with ICE and MSCT. A P value <0.05 was considered statistically significant.

RESULTS

Study population

Seventeen patients were studied (13 men, mean age 56 ± 8 years). Atrial fibrillation was paroxysmal in 11 patients and persistent in 6 according to the ACC/AHA/ESC Guidelines definition (9). Mean duration of AF was 72 ± 58 months and the mean number of anti-arrhythmic drugs used was 3.7 ± 1.3 per patient. Mean LA size measured by transthoracic echocardiography was 41.8 ± 5.3 mm; mean left ventricular ejection fraction was 58 ± 7 %. Four patients had undergone another radiofrequency catheter ablation procedure for AF previously.

Mapping and registration accuracy

In order to acquire a good geometry of LA and PVs a mean of 31.1 ± 8.5 ICE contours were drawn per patient (range 18-43 contours). The mean time needed to make a 3D map with ICE was 76 ± 27 minutes (range 25-126 minutes). It was noted that the time needed to make a

map significantly decreased from 97 ± 20 minutes during the first 4 procedures to 39 ± 10 minutes during the last 13 procedures ($p < 0.001$). After the registration process the mean distance between the drawn ICE contours and the MSCT surface image ranged from 1.7 to 2.8 mm (mean 2.2 ± 0.3 mm). The standard deviation of the ICE-MSCT difference ranged from 1.4 mm to 1.9 mm (mean 1.7 ± 0.2 mm). Individual results of the registration process are given in Table 1.

The accuracy of the registration process at the level of the PVs was evaluated by calculating the mean value of the distance between the contours and MSCT surface at 5 representative points around each PV ostium. The mean distance between the drawn contours and the MSCT surface image at the level of the PV ostia ranged from 0.7 to 4.4 mm (mean 1.7 ± 1.1 mm) and was smallest around the left inferior PV (mean 1.5 ± 1.1 mm) and largest around the left superior PV (mean 2.1 ± 1.3 mm) (Table 2).

Table 1. Result of the registration process per patient

Patient	Age (years)	Gender	No. of contours	Distance between contours and MSCT surface image (mm)		
				Mean	SD	Range
1	46	F	20	2.1	1.6	0.00-8.45
2	55	M	19	1.9	1.4	0.00-8.91
3	61	M	27	2.3	1.6	0.00-8.82
4	72	M	23	2.5	1.9	0.01-10.27
5	57	M	18	2.1	1.7	0.01-10.17
6	40	F	36	1.8	1.4	0.01-7.19
7	58	M	39	2.6	1.9	0.00-9.99
8	48	M	38	2.0	1.5	0.00-7.68
9	61	F	29	1.9	1.4	0.15-6.45
10	47	M	42	1.7	1.4	0.00-7.44
11	68	M	22	2.3	1.5	0.01-7.03
12	50	M	40	2.1	1.6	0.01-9.15
13	53	F	38	1.9	1.7	0.00-12.50
14	58	M	31	2.8	1.9	0.02-11.56
15	60	M	43	2.5	1.8	0.00-8.57
16	54	M	30	2.5	1.7	0.01-8.36
17	58	M	34	2.3	1.6	0.01-8.38
Mean	55.6		31.1	2.2	1.7	
SD	8.0		8.5	0.3	0.2	

MSCT = multi-slice computed tomography; No. = number; SD = standard deviation.

Table 2. Result of the registration process at pulmonary vein ostia

Pulmonary vein (PV)	Distance between contours and MSCT surface image (mm)		
	Mean	SD	Range
Right superior PV	1.7	1.0	0.8-3.2
Right inferior PV	1.6	1.0	0.7-3.2
Left superior PV	2.1	1.3	0.8-4.4
Left inferior PV	1.5	1.1	1.0-2.4
Left common trunk	1.7	1.2	1.3-1.9
Both right PVs	1.7	1.0	0.7-3.2
Both Left PVs	1.8	1.2	0.8-4.4
All PVs	1.7	1.1	0.7-4.4

Classification of PV anatomy

An equal number of 70 PVs were visualized with MSCT and ICE (4.12 ± 0.49 per patient). The most common PV variant consisted of 2 left sided PVs with separate ostia and 2 right sided PVs with separate ostia (7 patients, 41%). A common ostium of the left PVs was noted in 8 patients (47%) with MSCT and in 10 patients (59%) with ICE. A common trunk of the left superior and left inferior PV was recognized in 3 patients (18%) with both MSCT and ICE. An additional PV was identified in 5 patients (29%). All additional PVs were located at the right side of the LA. Using kappa analysis, an excellent agreement between MSCT and ICE for the classification of the left-sided PVs ($\text{kappa} = 0.77$) and the right-sided PVs ($\text{kappa} = 1.00$) was observed.

Quantitative measurements

Pulmonary vein diameters were measured in two directions on MSCT (AP and SI) and in the direction of the largest diameter possible on ICE, as previously described (4). Superior-inferior diameters measured on MSCT were significantly larger for all PVs compared to the diameters measured on ICE (Table 3). The AP diameters of the right superior PV, left superior PV and additional veins measured on MSCT were not significantly different from the diameters measured on ICE. In contrast, the AP diameters of the right inferior PV on MSCT were significantly larger than the PV diameters on ICE (Table 3). Bland-Altman analysis demonstrated that there was a good overall agreement between ICE and MSCT for the assessment of the PV ostium diameter (Figure 5).

Table 3. Measurements of pulmonary vein ostium diameter: MSCT vs. ICE

	MSCT SI (mm)	MSCT AP (mm)	ICE (mm)	SI diameter MSCT vs. ICE (p-value)	AP diameter MSCT vs. ICE (p-value)
Right superior PV	24.0 ± 3.5	19.2 ± 3.3	18.3 ± 3.3	<0.01	NS
Right inferior PV	20.8 ± 3.0	17.9 ± 3.3	15.3 ± 2.4	<0.01	<0.05
Left superior PV	21.6 ± 3.9	15.4 ± 3.0	15.2 ± 2.2	<0.01	NS
Left inferior PV	19.0 ± 2.1	11.9 ± 2.3	14.6 ± 2.4	<0.01	<0.05
Left common trunk	38.2 ± 3.8	22.4 ± 1.0	28.2 ± 0.4	<0.05	<0.05
Additional PV	9.6 ± 1.9	8.5 ± 2.4	8.5 ± 0.9	<0.05	NS
All PVs	21.5 ± 5.7	16.2 ± 4.5	16.0 ± 4.3	<0.01	NS

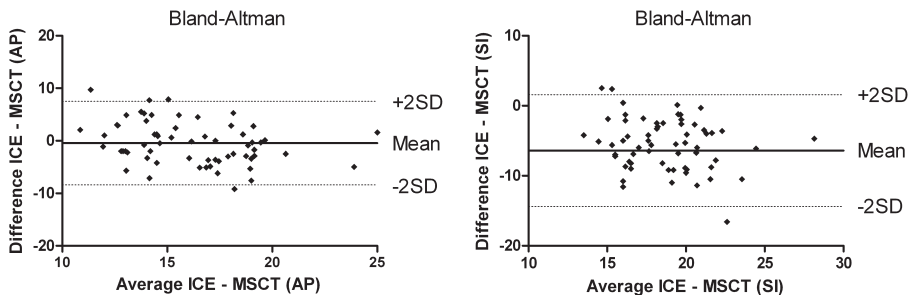


Figure 5. Bland-Altman analysis of measurements performed with MSCT and ICE in AP (left panel) and SI (right panel) directions.

Left atrial diameter was measured in AP direction on both MSCT and ICE. Mean AP diameter of the LA on MSCT was 39.6 ± 7.2 mm compared to 35.9 ± 7.2 mm on ICE. The mean difference between AP diameter on MSCT and ICE was 3.7 ± 5.0 mm ($p < 0.01$) and ranged from 0.3 to 15.6 mm.

Radiofrequency catheter ablation

Transseptal puncture was performed under ICE guidance in 13 patients. A patent foramen ovale existed in 4 patients. The mean ablation time was 80 ± 34 minutes and mean fluoroscopy time was 35 ± 6 minutes. Radiofrequency catheter ablation was targeted at the PVs in all patients. No differences between heart rhythm during MSCT acquisition and ablation procedure were observed. No complications occurred during and after the ablation procedure.

DISCUSSION

The present study is the first to report on the feasibility of creating a 3D map of the LA and PVs with ICE and integrating this map with MSCT in order to facilitate RFCA for AF. This study has three main findings: 1) It is feasible to create an anatomical map of the LA and PVs using ICE contours; 2) The anatomical map created by ICE can accurately be merged with a MSCT surface image and 3) Anatomical ICE mapping is a sensitive imaging modality to visualize PVs and classify LA and PV anatomy.

Three-dimensional mapping with ICE and MSCT integration

In the present study, a novel mapping system was used that enables detection of a specifically designed ICE catheter with an imbedded CARTO navigation sensor. This mapping system allows acquisition of ECG gated ICE images and reconstructs them into a registered 3D shell. With this new technology, it has become possible to acquire accurate real-time anatomical information of the LA and PVs without entering the left side of the heart. Khaykin et al first reported on the use of 3D mapping with ICE during the ablation of a right free wall accessory pathway (10). Okumura et al demonstrated the accuracy of navigation based on 3D mapping with ICE in animal experiments (11). Both groups subsequently demonstrated the feasibility of creating a 3D map with ICE to guide RFCA for AF (11-13). The present study supports these findings and additionally demonstrates the accuracy of creating a 3D map of the LA and PVs with ICE by comparing LA and PV geometry on the 3D ICE map with MSCT.

In addition, the current study is the first to demonstrate the feasibility of integrating a 3D map created with ICE and a MSCT image. Integration of MSCT images with conventional electroanatomical mapping is commonly used to guide RFCA for AF (14). In an animal study, Dong et al (15) demonstrated that the integration of MSCT and electroanatomical mapping allows accurate placement of anatomically guided ablation lesions in all cardiac chambers. Furthermore, several studies demonstrated the feasibility of the integration of MSCT and

electroanatomical mapping to guide RFCA for AF (5,16-18). Importantly, Kistler et al (6) showed that the integration of a MSCT image to guide RFCA for AF is associated with reduced fluoroscopy time and an improved outcome of the procedure.

However, the time interval between the MSCT data acquisition and the ablation procedure is a limitation of MSCT image integration. This delay may result in differences in heart rhythm, heart rate and fluid status which may cause errors in the image integration process, thereby compromising the accuracy of lesion placement. By integrating real-time ICE, MSCT and electroanatomical mapping, it has become possible to combine real-time anatomical and electrophysiological information with highly detailed anatomical information, thereby potentially increasing the accuracy of the placement of ablation lesions. The present study demonstrates the accuracy of integrating a MSCT image with a 3D map created with ICE. This was illustrated by a mean distance of only 2.2 mm between the MSCT image and the ICE contours, which is comparable with the integration results between an electroanatomical map and MSCT (5,16-18).

However, despite acquiring a good overall match between ICE and MSCT, the distance between the represented points along the ICE contours and MSCT ranged from 0.00 to 12.50 mm (Table 1). Similar ranges have been reported for the integration of electroanatomical maps and MSCT (5,16). This wide range may be related to differences in reconstructed LA and PV anatomy between MSCT and ICE in areas that are strongly influenced by cardiac and respiratory movement.

Pulmonary vein visualization

Left atrial and PV anatomy are highly variable (3,4,19). Importantly, accurate visualization of the PV ostia during RFCA for AF is required to avoid ablation within the PVs (2). In the present study, the PV ostia were visualized with ICE and MSCT. Both imaging modalities recorded an equal number of PVs, which suggests that 3D mapping with ICE has a high sensitivity for detecting PVs. Furthermore, there was good agreement between ICE and MSCT for classification of the PV anatomy.

In the present study, ICE slightly underestimated PV diameter, as compared with MSCT. This observation is in agreement with a study by Jongbloed et al (4) who found that ICE underestimated PV diameter for all PVs by 3.5 mm in SI direction and 0.2 mm in AP direction. An explanation for the underestimation of left sided PV diameters on ICE may be the fact that these PVs are visualized in longitudinal cross-sections thereby potentially missing the middle and widest part of the PVs. In contrast, the underestimation of the right sided PV diameters may be due to the fact that the exact PV-LA junction can be challenging to visualize in transversal cross-sections. However, since radiofrequency current is typically applied outside the PVs, this should have little implications for the safety of the ablation procedure.

The present study shows that 3D mapping with ICE provides an accurate visualization of PV ostia and PV anatomy with a high sensitivity for detecting additional PVs and gives a good estimation of PV dimensions, as compared with MSCT.

Clinical implications

The integration of MSCT with electroanatomical mapping allows accurate placement of ablation lesions (15) and has improved the outcome of anatomically guided RFCA targeting the PVs (6). However, it is reported that the accuracy of navigating with MSCT integration depends on the quality of the registration process (7). With the release of a new electroanatomical mapping system that allows integration of ICE it has become possible to acquire calibrated real-time 3D anatomical information without performing a manual registration process.

The ablation procedures in this study were guided by a 3D map made with ICE, integrated with a MSCT surface image. Importantly, this study demonstrates that 3D mapping with ICE alone provides accurate visualization of the LA geometry and PV ostia which is required to safely perform RFCA for AF targeting the PVs. Therefore it should be possible to perform an anatomically guided ablation procedure targeting the PVs on 3D mapping with ICE alone. This may result in a considerable reduction in radiation exposure for the patient. Further studies are therefore needed to fully explore the value of this promising new technique.

Limitations

This study represents an initial experience with 3D mapping using ICE to guide RFCA for AF. The time necessary to make a map with ICE was therefore relatively long. However, due to a clear learning curve, this time decreased in the later procedures. Therefore, it can be expected that the time needed to make a 3D ICE map can be shortened significantly. In this study RFCA was guided by the 3D map made with ICE and integrated with the MSCT image. As a consequence no data has been acquired on guidance by 3D ICE mapping alone. Furthermore, at present no data is available on the outcome of the ablation procedures.

Intracardiac echocardiography allows real-time visualization of important cardiac structures. However, some areas of the LA may be challenging to visualize with ICE due to their parallel orientation to the ultrasound beam. Examples of these areas are the right sided PV-LA junction and the left side of the anterior wall. By positioning the ICE catheter inside the right ventricle these structures can be visualized from another angle thereby providing more insight in LA and PV anatomy. Additionally, conventional electroanatomical mapping can also be used to acquire anatomical information in these and other areas.

Three-dimensional mapping with ICE is very sensitive to respiratory phase. Small differences in respiratory phase during image acquisition may result in contours situated outside the interpolated continuity of the other contours of the 3D map. However, by acquiring all ICE images during expiratory breath hold, consistent sets of contours could be acquired in all patients.

Three-dimensional mapping with ICE is a very promising but expensive technique. The ICE catheters used in this study are single-use only and a dedicated mapping system with image integration modules is needed to integrate ICE with the electroanatomical mapping and MSCT images. Furthermore this technology is only available on one electroanatomical mapping system (CARTO XP) and on limited echocardiographic machines (Sequoia ultrasound system and

Cypress ultrasound system, Siemens Medical Solutions). Nonetheless, integration of ICE provides accurate anatomical information that could potentially replace MSCT integration in RFCA for AF. Replacing MSCT would render the use of ICE cost-efficient and would reduce radiation exposure to the patient. Furthermore, the ability to acquire registered real-time anatomical information of important structures with ICE has a significant additional value compared to MSCT integration.

CONCLUSIONS

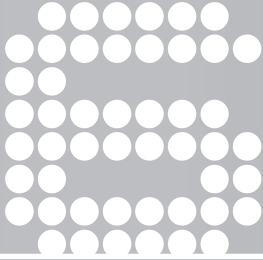
98

Using a novel mapping system that allows integration of ICE and electroanatomical mapping it is feasible to create a real-time registered 3D shell of LA and PV anatomy. Furthermore, the 3D map created with ICE can accurately be integrated with a MSCT surface image. This approach combines real-time anatomy with high detailed anatomy potentially providing highly accurate lesion placement during anatomical ablation procedures.

REFERENCES

1. Haissaguerre M, Jais P, Shah DC et al. Spontaneous initiation of atrial fibrillation by ectopic beats originating in the pulmonary veins. *N Engl J Med* 1998;339:659-66.
2. Calkins H, Brugada J, Packer DL et al. HRS/EHRA/ECAS expert Consensus Statement on catheter and surgical ablation of atrial fibrillation: recommendations for personnel, policy, procedures and follow-up. *Heart Rhythm* 2007;4:816-61.
3. Mansour M, Holmvang G, Sosnovik D et al. Assessment of pulmonary vein anatomic variability by magnetic resonance imaging: implications for catheter ablation techniques for atrial fibrillation. *J Cardiovasc Electrophysiol* 2004;15:387-93.
4. Jongbloed MR, Bax JJ, Lamb HJ et al. Multislice computed tomography versus intracardiac echocardiography to evaluate the pulmonary veins before radiofrequency catheter ablation of atrial fibrillation: a head-to-head comparison. *J Am Coll Cardiol* 2005;45:343-50.
5. Tops LF, Bax JJ, Zeppenfeld K et al. Fusion of multislice computed tomography imaging with three-dimensional electroanatomic mapping to guide radiofrequency catheter ablation procedures. *Heart Rhythm* 2005;2:1076-81.
6. Kistler PM, Rajappan K, Jahngir M et al. The impact of CT image integration into an electroanatomic mapping system on clinical outcomes of catheter ablation of atrial fibrillation. *J Cardiovasc Electrophysiol* 2006;17:1093-101.
7. Fahmy TS, Mlcochova H, Wazni OM et al. Intracardiac echo-guided image integration: optimizing strategies for registration. *J Cardiovasc Electrophysiol* 2007;18:276-82.
8. Marom EM, Herndon JE, Kim YH, McAdams HP. Variations in pulmonary venous drainage to the left atrium: implications for radiofrequency ablation. *Radiology* 2004;230:824-9.
9. Fuster V, Ryden LE, Cannom DS et al. ACC/AHA/ESC 2006 guidelines for the management of patients with atrial fibrillation—executive summary. *J Am Coll Cardiol* 2006;48:854-906.
10. Khaykin Y, Klemm O, Verma A. First human experience with real-time integration of intracardiac echocardiography and 3D electroanatomical imaging to guide right free wall accessory pathway ablation. *Europace* 2008;10:116-7.
11. Okumura Y, Henz BD, Johnson SB et al. Three-Dimensional ultrasound for image-guided mapping and intervention: methods, quantitative validation, and clinical feasibility of a novel multimodality image mapping system. *Circ Arrhythmia Electrophysiol* 2008;1:110-9.
12. Khaykin Y, Klemm O, Whaley B, Seabrook C, Beardsall M, Wulffhart ZA et al. First human experience with real time integration of intracardiac echocardiography and 3D electroanatomical imaging to guide pulmonary vein antrum isolation. *J Am Coll Cardiol* 2008;51:A15
13. Khaykin Y, Skanes A, Wulffhart ZA et al. Intracardiac echo integration with three-dimensional mapping: role in AF ablation. *JAFIB* 2008;1:74-9.
14. Tops LF, van der Wall EE, Schalij MJ, Bax JJ. Multi-modality imaging to assess left atrial size, anatomy and function. *Heart* 2007;93:1461-70.
15. Dong J, Calkins H, Solomon SB et al. Integrated electroanatomic mapping with three-dimensional computed tomographic images for real-time guided ablations. *Circulation* 2006;113:186-94.
16. Kistler PM, Earley MJ, Harris S et al. Validation of three-dimensional cardiac image integration: use of integrated CT image into electroanatomic mapping system to perform catheter ablation of atrial fibrillation. *J Cardiovasc Electrophysiol* 2006;17:341-8.
17. Martinek M, Nesser HJ, Aichinger J, Boehm G, Purerfellner H. Accuracy of integration of multislice computed tomography imaging into three-dimensional electroanatomic mapping for real-time guided radiofrequency ablation of left atrial fibrillation-influence of heart rhythm and radiofrequency lesions. *J Interv Card Electrophysiol* 2006;17:85-92.
18. Dong J, Dalal D, Scherr D et al. Impact of heart rhythm status on registration accuracy of the left atrium for catheter ablation of atrial fibrillation. *J Cardiovasc Electrophysiol* 2007;18:1269-76.

19. Wood MA, Wittkamp M, Henry D et al. A comparison of pulmonary vein ostial anatomy by computerized tomography, echocardiography, and venography in patients with atrial fibrillation having radiofrequency catheter ablation. *Am J Cardiol* 2004;93:49-53.



Impact of pulmonary vein anatomy and left atrial dimensions on the outcome of circumferential radiofrequency catheter ablation for atrial fibrillation

Dennis W. den Uijl¹
Laurens F. Tops¹
Victoria Delgado¹
Joanne D. Schuijf¹
Lucia J.M. Kroft²
Albert de Roos²
Eric Boersma³
Serge A.I.P. Trines¹
Katja Zeppenfeld¹
Martin J. Schalij¹
Jeroen J. Bax¹

¹Department of Cardiology, Leiden University Medical Center, Leiden, the Netherlands

²Department of Radiology, Leiden University Medical Center, Leiden, the Netherlands

³Department of Epidemiology and Statistics, Erasmus University, Rotterdam, the Netherlands

Submitted

ABSTRACT

Background: Multi-slice computed tomography (MSCT) is commonly acquired prior to radio-frequency catheter ablation (RFCA) for atrial fibrillation (AF) in order to plan and guide the procedure. Importantly, MSCT allows accurate measurement of left atrial (LA) and pulmonary vein (PV) dimensions and classification of PV anatomy.

Objective: The aim of this study was to investigate the impact of LA dimensions, PV dimensions and PV anatomy on the outcome of circumferential RFCA for AF.

Methods: One hundred consecutive patients undergoing RFCA for AF (paroxysmal 72%, persistent 28%) were studied. Left atrial dimensions, PV dimensions and PV anatomy were assessed in multiple directions on MSCT. Pulmonary vein anatomy was classified as normal or atypical based on the absence/presence of a common trunk or additional vein(s).

Results: After a mean follow up of 11.6 ± 2.8 months, 65 patients (65%) maintained sinus rhythm. Enlargement of the LA in anterior-posterior direction on MSCT was related to a higher risk for AF recurrence. No relation was found between PV dimensions and outcome of RFCA. In contrast, the presence of atypical right-sided PV anatomy was related to a reduced risk for AF recurrence. Multivariate analysis showed that anterior-posterior LA diameter on MSCT (OR=1.083, $p=0.027$), atypical right-sided PV anatomy (OR=0.149, $p=0.006$), and persistent AF (OR=3.004, $p=0.035$) were independent predictors of AF recurrence after RFCA.

Conclusions: Enlargement of anterior-posterior LA diameter and presence of atypical anatomy of the right PVs are independent risk factor for AF recurrence.

INTRODUCTION

Radiofrequency catheter ablation (RFCA) is considered a reasonable treatment option for patients with symptomatic drug-refractory atrial fibrillation (AF) (1). However, this treatment modality is associated with a considerable recurrence rate and a small risk for serious complications (2). Identification of pre-procedural risk factors for AF recurrence is mandatory to improve the outcome of RFCA.

Multi-slice computed tomography (MSCT) is nowadays commonly acquired prior to RFCA for AF. It provides important information about left atrial (LA) and pulmonary vein (PV) anatomy which can be used to plan and guide the RFCA procedure (3). Moreover, MSCT allows accurate multidirectional assessment of LA and PV dimensions (4,5). It has been demonstrated that LA and PV dimensions are enlarged in patients with AF (6,7). However, whereas LA size is a well-known risk factor for AF recurrence after RFCA (8-11), little is known about the prognostic importance of PV dilatation. Similarly, the impact of PV anatomy on the outcome of RFCA has not been studied extensively. Potentially, different anatomical drainage patterns could be accompanied by different tissue characteristics of the surrounding myocardium rendering the PV area more or less resistant to electrical isolation. Moreover, certain anatomical variants could pose a technical difficulty to achieve stable catheter position during ablation thereby compromising effective lesion formation. The aim of this study was to investigate the impact of multidirectional LA dimensions, PV dimensions and PV anatomy assessed by MSCT on the outcome of circumferential RFCA for AF.

METHODS

Study population

The study population comprised 100 consecutive patients with symptomatic drug-refractory AF, undergoing circumferential RFCA. After RFCA, all patients were evaluated on a regular basis at the outpatient clinic during a 12-month follow-up period. Routine electrocardiograms (ECG) were recorded each visit and 24-hour Holter registrations were scheduled at 3, 6 and 12 months after the ablation. All medications were continued for at least 3 months. Afterwards, anti-arrhythmic drugs were discontinued at the discretion of the physician. After a post-ablation blanking period of 3 months, recurrence of AF was defined as any recording of AF on ECG or an episode longer than 30 seconds on 24-hour Holter monitoring (1). After 12-month follow-up, the study population was divided into two groups: patients with maintenance of sinus rhythm (SR) (non-recurrence group) and patients who had recurrence of AF (recurrence group).

Multi-Slice Computed Tomography

Multi-slice computed tomography data were acquired prior to the ablation in order to guide the procedure (3). The MSCT scan was performed with a 64-slice Toshiba Aquilion 64 system (Toshiba Medical Systems, Otawara, Japan). A bolus of 70 ml nonionic contrast material (Iomeron 400, Bracco, Milan, Italy) was infused through the antecubital vein at a rate of 5 ml/s followed by 50 ml saline solution flush. Automatic detection of the contrast bolus in the descending aorta was used to time the start of the scan. Craniocaudal scanning was performed during breath-hold, without ECG-gating. Collimation was 64 x 0.5 mm, rotation time 400 ms and the tube voltage 100 kV at 250 mA. After acquisition, the raw MSCT data were exported, post-processed and analyzed on a dedicated workstation (Vitrea 2, Vital Images, Minnetonka, Minnesota, USA).

Pulmonary vein ostium dimensions were evaluated using a two-dimensional viewing mode. To allow accurate assessment, multiplanar reformatting was used by placing two orthogonal planes parallel to the course of the vein (Figure 1, panel A and B). The third orthogonal plane, orientated perpendicular to the course of the vein, was then used to measure the diameter of the PV ostium in anterior-posterior (AP) and superior-inferior (SI) direction (Figure 1, panel C). The ratio between the largest and smallest diameter was calculated in order to obtain information on the oval shape of the ostium. Similarly, multiplanar reformatting was used to assess LA dimensions in 3 orthogonal directions: AP, longitudinal and transversal direction (Figure 2).

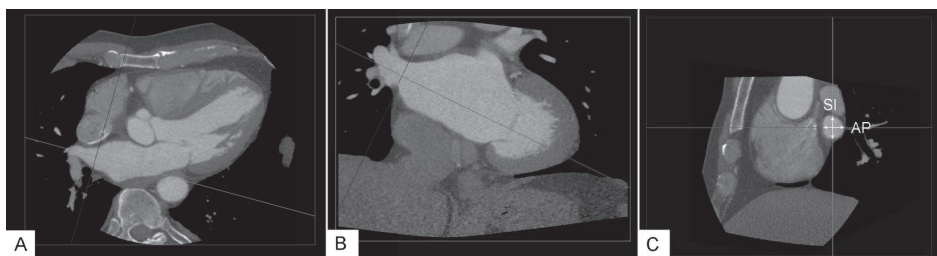


Figure 1. To assess pulmonary vein diameters, two orthogonal planes were placed parallel to the course of the vein (panel A and B). A third orthogonal plane (panel C), oriented perpendicular to the course of the vein, was then used to measure the anterior-posterior (AP) and superior-inferior (SI) pulmonary vein diameter (white arrows).

Pulmonary vein anatomy was analyzed from an external view using a 3D volume-rendered reconstruction. Pulmonary vein classification was based on the presence or absence of a common trunk and/or additional vein(s) (Figure 3). A common trunk was defined as a conjoined part of more than 5 mm in which both superior and inferior PV drain before entering the LA. An additional vein was defined as a supernumerary vein directly entering the LA.

To evaluate the impact of PV anatomy on the outcome of RFCA for AF, left- and right-sided anatomy was additionally classified as normal or atypical. Atypical anatomy was defined as the presence of a common trunk or an additional PV.

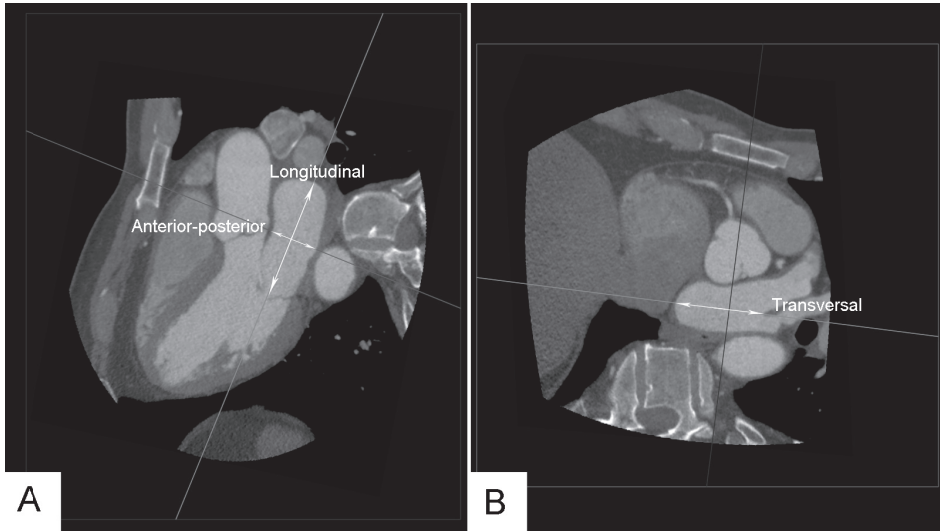


Figure 2. The left atrial (LA) dimensions (white arrows) were assessed in three orthogonal directions by using multiplanar reformatting. Panel A: LA dimensions in anterior-posterior (AP) (red line) and longitudinal direction (green line). Panel B: LA dimension in transversal direction (green line). Panel B is a cross-section of panel A at the level of the crosshair and parallel to the red line.

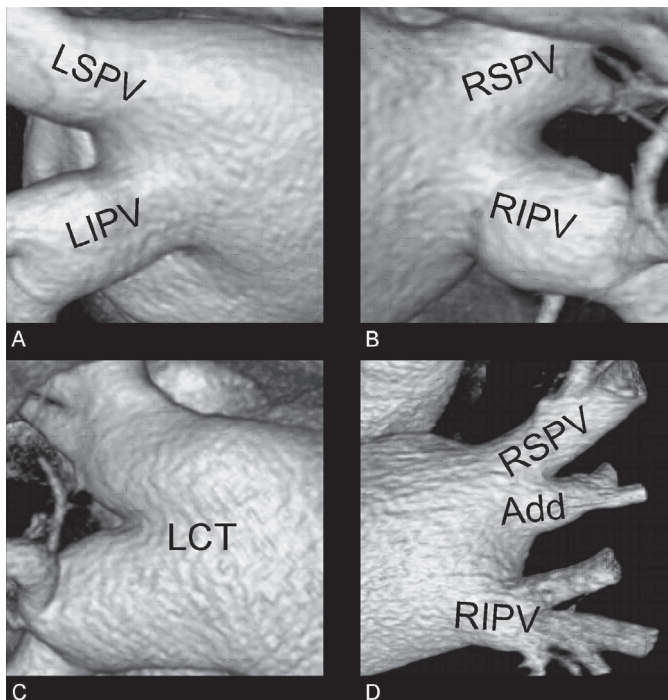


Figure 3. Panel A: Separate ostia of the left-sided pulmonary veins; Panel B: Separate ostia of the right-sided pulmonary veins; Panel C: Common trunk of the left-sided pulmonary veins (defined as a conjoined part of more than 5 mm); Panel D: Additional right-sided pulmonary vein (defined as a supernumerary vein directly entering the left atrium). Add = additional pulmonary vein, LIPV = left inferior pulmonary vein, LSPV = left superior pulmonary vein, RIPV = right inferior pulmonary vein, RSPV = right superior pulmonary vein.

Radiofrequency catheter ablation

The RFCA procedure was aimed at creating two circumferential lesions around the left- and right-sided ipsilateral PVs approximately 1 cm outside the ostia. All patients received intravenous heparin to maintain an activated clotting time of 300–400 s. Intracardiac echocardiography was used to guide the transseptal puncture. To guide the ablation, a non-fluoroscopic electroanatomical mapping system with MSCT integration was used (CARTO XP™ with Cartomerge™, Biosense Webster, Diamond Bar, California, USA). Contact mapping and ablation was performed using a 4-mm quadripolar open-loop irrigated mapping/ablation catheter (7Fr Navistar™, Biosense Webster). A 6Fr quadripolar diagnostic catheter placed inside the right atrium served as a temporal reference. Radiofrequency current was applied at 30–35 W with a maximum temperature of 45°C and an irrigation flow of 20 ml/min until a bipolar voltage of <0.1 mV was achieved, with a maximum of 60 s per point. The end-point of the procedure was PV isolation as confirmed by recording entrance block during SR or pacing from inside the coronary sinus (1).

Statistical analysis

Data are presented as mean \pm SD or as number (percentage). Statistical comparisons for continuous variables were performed with the two tailed Student's t-test, paired or unpaired as appropriate. Statistical comparisons for categorical variables were performed with the Chi-square test. Univariate and multivariate logistic regression analyses were performed to study the impact of PV anatomy, PV dimensions, LA dimensions and clinical characteristics on the incidence of AF recurrence after RFCA. Variables with a p-value <0.05 in the univariate analyses were included into the multivariate analysis. Multivariate analysis was performed using an 'enter' method. All statistical analyses were performed with SPSS software (version 16.0, SPSS Inc., Chicago, Illinois, USA). A p-value of <0.05 was considered statistically significant.

RESULTS

One hundred consecutive patients were included (77 men, mean age 56 ± 9 years), from an ongoing clinical registry (12). Atrial fibrillation was paroxysmal in 72 patients and persistent in 28 patients according to American College of Cardiology/American Heart Association/European Society of Cardiology guidelines definitions (13). None of the patients had previously undergone RFCA for AF. Median duration of AF was 48 months (interquartile range: 24–84) and the mean number of anti-arrhythmic drugs used was 3.1 ± 1.3 per patient. The mean AP diameter of the LA was 43 ± 6 mm and the mean left ventricular ejection fraction was $58 \pm 8\%$ on transthoracic echocardiography (Table 1). The procedural end-point of PV isolation was achieved in all patients.

After a mean follow-up of 11.6 ± 2.8 months, 65 patients (65%) had maintained SR (non-recurrence group), whereas 35 patients (35%) had recurrence of AF (recurrence group). In

Table 1. Baseline characteristics

	Total study population (n = 100)
Age (years)	56.4 ± 8.6
Gender (male/female)	77/23
Body Surface Area (m ²)	2.1 ± 0.2
Type of AF (paroxysmal/persistent)	72/28
Duration of AF (months)	64 ± 60
Anti-arrhythmic drugs used per patient	3.1 ± 1.3
Hypertension, n (%)	53 (53)
Coronary artery disease, n (%)	8 (8)
Diabetes, n (%)	8 (8)
Echocardiography	
Anterior-posterior LA diameter (mm)	43 ± 6
Left ventricular ejection fraction (%)	58 ± 8

AF = atrial fibrillation; LA = left atrium.

the recurrence group a higher prevalence of persistent AF was found compared to the non-recurrence group (14 [22%] vs 14 [40%], $p=0.049$).

Left atrial dimensions

Left atrial dimensions were measured in three orthogonal directions on MSCT: AP, longitudinal and transversal (Figure 2). Mean AP diameter was 41 ± 7 mm, mean longitudinal diameter was 65 ± 8 mm and mean transversal diameter was 59 ± 7 mm. Anterior-posterior LA diameter was significantly larger in the recurrence group than in the non-recurrence group (43 ± 6 mm vs. 39 ± 7 mm, $p=0.02$). Interestingly, no differences were found between the recurrence group and non-recurrence group in longitudinal (64 ± 7 mm vs. 65 ± 9 mm, $p=0.45$) and transversal (59 ± 7 mm vs. 60 ± 7 mm, $p=0.57$) LA diameter.

Pulmonary vein dimensions

Pulmonary vein ostial dimensions were assessed in AP and SI direction on MSCT (Table 2). Pulmonary vein dimensions were larger in SI direction than in AP direction (21.1 ± 2.3 mm vs. 16.3 ± 2.5 mm, $p<0.001$). Overall, right-sided PVs had a larger diameter than left-sided PVs (20.0

Table 2. Pulmonary vein measurements on MSCT

	AP diameter (mm)	SI diameter (mm)	Mean diameter (mm)	Ratio
RSPV	18.8 ± 4.2	23.3 ± 4.5	21.0 ± 4.0	0.80 ± 0.11
RIPV	17.7 ± 2.9	20.3 ± 3.2	19.0 ± 2.8	0.87 ± 0.10
LSPV	14.3 ± 2.6	21.1 ± 3.6	17.7 ± 2.4	0.67 ± 0.13
LIPV	12.1 ± 2.7	18.8 ± 2.5	15.4 ± 2.0	0.65 ± 0.15
ADD	8.9 ± 3.1	10.1 ± 2.4	9.5 ± 2.5	0.82 ± 0.11
LCT	19.5 ± 4.5	33.5 ± 4.7	26.5 ± 3.4	0.59 ± 0.15
All RPV	18.2 ± 2.5	21.8 ± 2.8	20.0 ± 2.4	0.83 ± 0.08
All LPV	13.2 ± 2.5	19.9 ± 2.0	16.6 ± 1.6	0.66 ± 0.11
All PV	16.3 ± 2.5	21.1 ± 2.3	18.7 ± 2.2	0.77 ± 0.09

ADD = additional pulmonary vein; AP = anterior-posterior; LCT = left common trunk; LIPV = left inferior pulmonary vein; LPV = left pulmonary veins; LSPV = left superior pulmonary vein; RIPV = right inferior pulmonary vein; RPV = right pulmonary veins; RSPV = right superior pulmonary vein; SI = superior-inferior

± 2.4 mm vs. 16.6 ± 1.6 mm, $p < 0.001$). Similarly, superior PVs had a larger diameter than inferior PVs (19.6 ± 3.8 mm vs. 17.5 ± 3.1 mm, $p < 0.001$). With regard to the shape of the PV ostium, left-sided PVs had a more pronounced oval shape than right-sided PV ostia indicated by a lower ratio between the largest and smallest PV diameter (ratio 0.65 ± 0.09 vs. 0.84 ± 0.09 , $p < 0.001$).

In contrast to AP LA dimension, PV dimensions were not related to the recurrence of AF during follow-up: no differences were found in mean PV diameter between the recurrence and non-recurrence group (18.8 ± 2.2 mm vs. 18.6 ± 2.2 mm, $p = 0.74$). In addition, a similar oval shape of the PV ostia was found in the both groups (non-recurrence group vs. recurrence group: 0.77 ± 0.09 vs. 0.77 ± 0.09 , $p = 0.73$).

Pulmonary vein anatomy

Pulmonary vein anatomy was classified based on the presence or absence of a common trunk and/or additional PV. A total of 174 left-sided PVs and 226 right-sided PVs were identified on MSCT. Separate ostia of the left superior PV and left inferior PV were present in 74 patients (74%) and a common trunk of the left PVs was present in the remaining 26 patients (26%). Separate ostia of the right superior PV and right inferior PV were observed in 78 patients (78%), an additional right-sided PV in 18 patients (18%) and 2 additional right-sided veins in 4 patients (4%). Accordingly, atypical anatomy of the left-sided PVs was present in 26 patients (26%) and atypical anatomy of the right-sided PVs was observed in 22 patients (22%).

Atypical anatomy of the right-sided PVs was associated with a significantly lower risk for AF recurrence than normal anatomy of the right-sided PVs (unadjusted OR: 0.136, $p = 0.010$). In contrast, the presence of atypical anatomy of the left-sided PVs had no significant impact on the outcome of RFCA (unadjusted OR: 0.466, $p = 0.14$).

Predictors of AF recurrence

Univariate logistic regression analyses were performed to study the impact of LA dimensions, PV dimensions and PV anatomy, as well as clinical risk factors (e.g. type of AF, hypertension) on the outcome of RFCA for AF (Table 3). A large AP LA diameter was related to a higher risk for recurrent AF after RFCA (unadjusted OR: 1.082, $p = 0.021$). Similarly, patients with persistent AF had a higher risk for AF recurrence (unadjusted OR: 2.429, $p = 0.049$). In contrast, the presence of atypical right-sided PV anatomy was related to a lower risk for AF recurrence (unadjusted OR: 0.136, $p = 0.010$). Subsequent multivariate analyses demonstrated that AP LA diameter, type of AF and right-sided PV anatomy were independent predictors of AF recurrence (OR: 1.083, $p = 0.027$, OR: 3.004, $p = 0.035$ and OR: 0.149, $p = 0.006$, respectively) (Table 4).

Table 3. Univariate logistic regression analysis of clinical and anatomical characteristics on MSCT as risk factors for recurrence of AF after RFCA

	OR	95% CI	P-value
Clinical characteristics			
Age (years)	1.027	0.978-1.079	0.28
Male gender	1.012	0.381-2.691	0.98
AF duration (months)	1.032	0.952-1.118	0.45
Failed anti-arrhythmic drugs (n)	1.109	0.802-1.532	0.53
Persistent AF	2.429	0.989-5.963	0.05*
Hypertension	0.908	0.399-2.067	0.82
Left atrial AP diameter (TTE)	1.042	0.966-1.125	0.29
Left ventricular ejection fraction (%)	0.971	0.920-1.026	0.30
MSCT characteristics			
Right atypical anatomy	0.136	0.030-0.624	0.010*
Left atypical anatomy	0.466	0.167-1.297	0.14*
Mean PV diameter	1.033	0.856-1.247	0.73
Left atrial diameter			
AP (mm)	1.082	1.012-1.156	0.021*
Longitudinal (mm)	1.021	0.967-1.078	0.45
Transversal (mm)	1.018	0.958-1.082	0.57

* included in multivariate logistic regression analysis; ECV = electrocardioversion; TTE = transthoracic echocardiography; other abbreviations as in Table 2.

Table 4. Multivariate logistic regression analysis of clinical and anatomical characteristics on MSCT as risk factors for recurrence of AF after RFCA

	OR	95% CI	P-value
Clinical characteristics			
Persistent AF	3.004	1.082-8.345	0.035
MSCT characteristics			
Right complex anatomy	0.149	0.038-0.576	0.006
Left atrial AP diameter (mm)	1.083	1.009-1.162	0.027

DISCUSSION

The present study investigated the impact of LA dimensions, PV dimensions and PV anatomy on the outcome of circumferential RFCA for AF. The main findings can be summarized as follows: enlargement of the LA in AP direction on MSCT is an independent predictor of AF recurrence after RFCA. In contrast, PV dimensions are not related to the outcome of RFCA. Finally, atypical anatomy of the right-sided PVs is independently associated with less recurrences of AF after RFCA.

Left atrial dimensions

Left atrial enlargement is an important risk factor for the development of AF in the general population (14) and has been identified as an independent predictor of AF recurrence after RFCA (8-11). Heavily dilated atria are thought to contain a large extent of atrial remodeling thereby limiting the efficacy of RFCA. Multislice CT allows accurate measurement of LA dimensions and is commonly acquired prior to RFCA in order to plan and guide the procedure (3). The present

study evaluated LA dimensions in three orthogonal directions on MSCT: AP, longitudinal and transversal. Anterior-posterior LA diameter on MSCT was identified as an independent predictor of AF recurrence, whereas longitudinal and transversal LA diameters were not. Interestingly, atrial dilatation is thought to be predominantly oriented in longitudinal and transversal direction and not in AP direction (15). A potential explanation for our finding is that dilatation of the LA in AP direction occurs at a more advanced stage of atrial enlargement and reflects a higher extent of atrial remodeling, thereby explaining its prognostic value. Importantly, AP LA diameter was a strong predictor of AF recurrence even after correction for type of AF.

110

Pulmonary vein dimensions

Similar to LA dimensions, PV dimensions are enlarged in patients with AF (6,7). However, little is known about the prognostic importance of PV dilatation in patients undergoing RFCA for AF. The present study evaluated the impact of PV ostial dimensions assessed by MSCT on the outcome of RFCA for AF. No differences were found in PV dimensions or shape between patients with AF recurrence and patients without AF recurrence during follow-up. These results suggest that PV dilatation has no prognostic importance for the outcome of circumferential RFCA. Most likely, PV dilatation is caused by the presence of AF and can be best considered an epiphenomenon.

Pulmonary vein anatomy

The observations by Haïssaguerre et al. that ectopic beats originating from the PVs can initiate AF, have led to an increasing interest in the PVs as target for RFCA (16). Nowadays, isolation of the PV region is the cornerstone for most ablation strategies (1). However, the relation between the anatomy of the PV region and the efficacy RFCA for AF has not been studied extensively. Several studies have shown that large variations in pulmonary venous drainage pattern into the LA exist (5,17-20). Potentially, certain anatomical variants could pose a technical challenge to achieve stable catheter position thereby influencing the outcome of RFCA. Moreover, different venous drainage patterns could be accompanied by different tissue characteristics of the surrounding myocardium rendering the PV area more or less resistant to electrical isolation.

In the present study, the relation between PV anatomy and outcome of AF ablation was studied in 100 consecutive patients undergoing circumferential RFCA. Pulmonary vein anatomy was analyzed on MSCT and classified according to the presence or absence of a common trunk and/or additional PV as either normal or atypical. Atypical anatomy of the right-sided PVs was associated with a decreased risk for AF recurrence after RFCA. After correction for AP LA diameter and type of AF, right-sided PV anatomy remained an independent predictor of AF recurrence after RFCA. Potential explanations for these results include that an atypical PV drainage pattern may be accompanied by an increased susceptibility of the surrounding myocardial tissue for electrical isolation or a lower likelihood for PV ectopy originating from the right-sided PVs. Furthermore an atypical PV drainage pattern may pose less technical difficulty

to achieve stable catheter position, resulting in a more effective lesion formation and a lower risk for electrical reconnection.

Recently, Hof et al reported on the impact of PV anatomy on the efficacy of RFCA in 146 patients (9). Interestingly, no relation was found between PV anatomy and outcome of RFCA. However, several differences can be identified between their work and the present study that could have caused this discrepancy. Most importantly, the definition of outcome used by Hof et al included three categories (failure, improvement of AF burden and complete success) (9), whereas the present study only considered two (AF recurrence and non-recurrence). The use of this definition of outcome may also explain why type of AF, which is a commonly accepted risk factor for AF recurrence (1) was not related to outcome in their study (9).

Clinical implications

Despite the introduction of new devices to perform PV isolation, circumferential RFCA remains a widely used ablation strategy. Multi-slice computed tomography is commonly performed prior to these procedures. The present study demonstrates that AP LA dimension and PV anatomy on MSCT have an important impact on the likelihood to maintain SR after RFCA. In patients undergoing RFCA for AF, information about LA size and PV anatomy on MSCT can be used to decide whether circumferential RFCA alone is sufficient or additional ablation lesions (e.g. PV carina ablation) may be needed to improve outcome.

Limitations

The present study represents a single center experience. In addition, the number of evaluated patients is relatively small; nonetheless, statistical significance was reached. The applicability of MSCT as a pre-procedural patient selection tool is limited by the radiation exposure of this technique. However, since MSCT is commonly acquired prior to RFCA to plan and guide the procedure, the present results may help determine whether additional ablation is needed in patients who are undergoing circumferential ablation.

CONCLUSIONS

Right-sided PV anatomy is an independent predictor of AF recurrence after circumferential RFCA for AF. In addition, enlargement of the LA in AP direction and type of AF are independent pre-procedural risk factors for recurrence of AF after circumferential RFCA.

REFERENCES

1. Calkins H, Brugada J, Packer DL et al. HRS/EHRA/ECAS expert Consensus Statement on catheter and surgical ablation of atrial fibrillation: recommendations for personnel, policy, procedures and follow-up. *Heart Rhythm* 2007;4:816-61.
2. Cappato R, Calkins H, Chen SA et al. Worldwide survey on the methods, efficacy, and safety of catheter ablation for human atrial fibrillation. *Circulation* 2005;111:1100-5.
3. Tops LF, Bax JJ, Zeppenfeld K et al. Fusion of multislice computed tomography imaging with three-dimensional electroanatomic mapping to guide radiofrequency catheter ablation procedures. *Heart Rhythm* 2005;2:1076-81.
4. Hof I, Arbab-Zadeh A, Scherr D et al. Correlation of left atrial diameter by echocardiography and left atrial volume by computed tomography. *J Cardiovasc Electrophysiol* 2009;20:159-63.
5. Jongbloed MR, Bax JJ, Lamb HJ et al. Multislice computed tomography versus intracardiac echocardiography to evaluate the pulmonary veins before radiofrequency catheter ablation of atrial fibrillation: a head-to-head comparison. *J Am Coll Cardiol* 2005;45:343-50.
6. Tsao HM, Yu WC, Cheng HC et al. Pulmonary vein dilation in patients with atrial fibrillation: detection by magnetic resonance imaging. *J Cardiovasc Electrophysiol* 2001;12:809-13.
7. Kato R, Lickfett L, Meiningner G et al. Pulmonary vein anatomy in patients undergoing catheter ablation of atrial fibrillation: lessons learned by use of magnetic resonance imaging. *Circulation* 2003;107:2004-10.
8. Berrueto A, Tamborero D, Mont L et al. Pre-procedural predictors of atrial fibrillation recurrence after circumferential pulmonary vein ablation. *Eur Heart J* 2007;28:836-41.
9. Hof I, Chilukuri K, Arbab-Zadeh A et al. Does left atrial volume and pulmonary venous anatomy predict the outcome of catheter ablation of atrial fibrillation? *J Cardiovasc Electrophysiol* 2009;20:1005-10.
10. Shin SH, Park MY, Oh WJ et al. Left atrial volume is a predictor of atrial fibrillation recurrence after catheter ablation. *J Am Soc Echocardiogr* 2008;21:697-702.
11. Abecasis J, Dourado R, Ferreira A et al. Left atrial volume calculated by multi-detector computed tomography may predict successful pulmonary vein isolation in catheter ablation of atrial fibrillation. *Europace* 2009;11:1289-94.
12. Tops LF, Bax JJ, Zeppenfeld K, Jongbloed MR, van der Wall EE, Schalij MJ. Effect of radiofrequency catheter ablation for atrial fibrillation on left atrial cavity size. *Am J Cardiol* 2006;97:1220-2.
13. Fuster V, Ryden LE, Cannom DS et al. ACC/AHA/ESC 2006 guidelines for the management of patients with atrial fibrillation--executive summary. *J Am Coll Cardiol* 2006;48:854-906.
14. Vaziri SM, Larson MG, Benjamin EJ, Levy D. Echocardiographic predictors of nonrheumatic atrial fibrillation. The Framingham Heart Study. *Circulation* 1994;89:724-30.
15. Lang RM, Bierig M, Devereux RB et al. Recommendations for Chamber Quantification. *J Am Soc Echocardiogr* 2005;18:1440-63.
16. Haissaguerre M, Jais P, Shah DC et al. Spontaneous initiation of atrial fibrillation by ectopic beats originating in the pulmonary veins. *N Engl J Med* 1998;339:659-66.
17. Mansour M, Holmvang G, Sosnovik D et al. Assessment of pulmonary vein anatomic variability by magnetic resonance imaging: implications for catheter ablation techniques for atrial fibrillation. *J Cardiovasc Electrophysiol* 2004;15:387-93.
18. Schwartzman D, Lacomis J, Wigginton WG. Characterization of left atrium and distal pulmonary vein morphology using multidimensional computed tomography. *J Am Coll Cardiol* 2003;41:1349-57.
19. Marom EM, Herndon JE, Kim YH, McAdams HP. Variations in pulmonary venous drainage to the left atrium: implications for radiofrequency ablation. *Radiology* 2004;230:824-9.
20. Cronin P, Kelly AM, Desjardins B et al. Normative analysis of pulmonary vein drainage patterns on multidetector CT with measurements of pulmonary vein ostial diameter and distance to first bifurcation. *Acad Radiol* 2007;14:178-88.



Effect of radiofrequency catheter ablation for atrial fibrillation on left atrial cavity size

Laurens F. Tops

Jeroen J. Bax

Katja Zeppenfeld

Monique R.M. Jongbloed

Ernst E. van der Wall

Martin J. Schalij

Department of Cardiology, Leiden University Medical Center, Leiden, the Netherlands

Am J Cardiol 2006;97:1220-2

ABSTRACT

Left atrial (LA) remodeling is associated with atrial fibrillation (AF). Radiofrequency catheter ablation offers a good treatment option for AF, with reasonable long-term results. The purpose of the current study was to assess whether LA reverse remodeling occurs after successful catheter ablation. Fifty-seven consecutive patients (45 men, age 53 ± 8 years) with symptomatic drug-refractory AF were treated with radiofrequency catheter ablation. Patients were divided in 2 groups based on recurrence of AF on Holter monitoring and 12-lead ECG at 6 weeks and 3 months follow-up (SR-group: no recurrence; AF-group: recurrence of AF). At baseline and 3 months follow-up, 2-dimensional echocardiography was performed to assess LA size and dimensions. Furthermore, LA volumes were measured at end-systole (LAESV) and end-diastole (LAEDV). After 3 months 39 of 57 patients (68%) maintained sinus rhythm. At 3 months follow-up, LA anteroposterior diameter showed a significant reduction in the SR-group (4.5 ± 0.3 cm vs. 4.2 ± 0.2 cm, $p < 0.01$), whereas a further increase was observed in the AF-group (4.5 ± 0.3 cm vs. 4.8 ± 0.3 cm, $p < 0.05$). Furthermore, LAESV and LAEDV decreased significantly in the SR-group from baseline to follow-up (LAESV 59 ± 12 ml vs. 50 ± 11 ml, $p < 0.01$; LAEDV 37 ± 9 ml vs. 31 ± 7 ml, $p < 0.01$), whereas a tendency towards an increase in LA volumes was observed in the AF-group. In conclusion, this study demonstrates that LA reverse remodeling occurs after successful radiofrequency catheter ablation for AF.

INTRODUCTION

Radiofrequency catheter ablation offers a curative treatment modality for patients with drug-refractory atrial fibrillation (AF) (1). Anatomical based electrical isolation of pulmonary veins has proven to be a safe method with reasonable long-term results (2). However, the effect of radiofrequency catheter ablation on left atrial (LA) size has not been evaluated extensively. Accordingly, the purpose of the current study was to assess whether LA reverse remodeling occurs after successful radiofrequency catheter ablation for AF.

METHODS

The study population consisted of 57 consecutive patients (45 men, age 53 ± 8 years) with symptomatic drug-refractory AF, who were referred for radiofrequency catheter ablation. AF was present for 6 ± 5 years and was paroxysmal in 35 (61%), persistent in 18 (32%) and permanent in 4 (7%). In 17 patients ablation of atrial flutter was performed previously.

Radiofrequency ablation

The ablation procedure was aimed at electrical isolation of all pulmonary veins from the LA. With the use of phased-array intracardiac echocardiography an intracardiac thrombus was excluded and a transseptal puncture was guided. Endocardial mapping was performed with a 4 mm quadripolar mapping/ablation catheter (7F Thermocool, Biosense Webster, California, USA), using a 3-dimensional electroanatomical mapping system (CARTO™, Biosense Webster). A 6F diagnostic catheter placed in the right atrium served as a temporal reference.

Radiofrequency current was applied outside the ostia of all pulmonary veins, using the ablation catheter with a 4 mm open loop irrigated tip. Additional lines were targeted between the mitral annulus and the left inferior pulmonary vein (mitral isthmus line) and between the ostia of the left and right superior pulmonary veins (roof line). The following power and temperature settings were used: irrigation rate 20 mL/min, maximum temperature 50°C, maximum radiofrequency energy 30 W. At each point, radiofrequency current was applied until a voltage <0.1 mV was achieved, with a maximum of 60 seconds per point. The procedure was considered successful when pulmonary vein isolation was confirmed by recording entrance block during sinus rhythm or pacing in the coronary sinus. All patients received heparin intravenously (activated clotting time > 300 sec) to avoid thrombo-embolic complications.

Follow-up

After the ablation procedure rhythm was continuously monitored until discharge. Patients received heparin intravenously until INR was adequate with oral anticoagulants. Transthoracic

2-dimensional echocardiography was performed within 24 hours after the ablation procedure to detect pericardial effusion.

Follow-up was scheduled at 6 weeks and 3 months after the ablation procedure. Follow-up at 6 weeks consisted of an outpatient clinic visit with a 12-lead surface ECG. At 3 months follow-up, 24-hour Holter monitoring, a 12-lead surface ECG, and a standard 2-dimensional echocardiogram were performed. During the 3 months follow-up all medication, including anti-arrhythmic drugs, was continued in all patients. Patients were divided into 2 groups based on their rhythm during follow-up. Group 1 maintained sinus rhythm during the 3 months follow-up (SR-group) whereas group 2 had recurrence of AF during follow-up (AF-group).

Echocardiography

Two-dimensional echocardiography was performed 2 days before the ablation procedure, and at 3 months follow-up. Two-dimensional images were recorded with patients in the left lateral decubitus position using a commercially available system (Vingmed system Seven, General Electric-Vingmed, Milwaukee, Wisconsin, USA). Images were obtained using a 3.5-MHz transducer at a depth of 16 cm in the parasternal and apical views (standard long-axis and 2- and 4-chamber images). Standard 2-dimensional images and color Doppler data triggered to the QRS complex were saved in cine loop format.

LA measurements were performed off-line using commercial software (Echopac 6.1, General Electric-Vingmed). LA anteroposterior diameter was measured at end-systole on the M-mode image obtained from the parasternal long-axis view (3). Short- and long-axis of the LA were measured on apical 4-chamber views at end-systole. Furthermore, LA volumes were measured on apical 2- and 4-chamber views using the biplane Simpson's rule (4,5). Measurements on LA volumes were acquired from 3 consecutive beats, and subsequently averaged. Left atrial end-systolic volume (LAESV) was defined as the largest LA volume in ventricular systole; left atrial end-diastolic volume (LAEDV) was defined as the smallest possible LA volume in ventricular diastole (5). Inter- and intraobserver agreement for the assessment of LA volumes were 92% and 95%, respectively.

Statistical analysis

Data are expressed as mean \pm SD or number (%), as appropriate. Continuous variables were compared using the nonparametric Mann-Whitney U test for unpaired variables or the nonparametric Wilcoxon signed-ranks test for paired variables. The chi-square test was used to test categorical variables. All statistical tests were performed using SPSS 12.0 software for Windows. A p-value <0.05 was considered significant.

RESULTS

A total number of 57 patients were treated with radiofrequency catheter ablation for AF. Immediate success of the procedure was achieved in all patients. In 3 patients (5%) mild pericardial effusion (<1.0 cm) was observed within 24 hours after the ablation procedure, without hemodynamic consequences. No acute complications were observed. Complete rhythm and echocardiography follow-up data was available in all patients.

After 3 months follow-up, 39 of 57 patients (68%) maintained sinus rhythm. The study population was divided in 2 groups (with maintained sinus rhythm or relapsed AF). Baseline characteristics of the 2 groups are listed in Table 1. There were no significant differences in baseline characteristics between the AF-group and the SR-group. Only the proportion of patients with non-paroxysmal AF at baseline was higher in the AF-group as compared to the SR-group (72% versus 23%, $p < 0.05$).

Table 1. Clinical characteristics of patients with maintenance of sinus rhythm (SR-group) and recurrence of atrial fibrillation (AF-group)

Variable	SR-group (n=39)	AF-group (n=18)
Age (years)	53 ± 9	54 ± 8
Men/Women	32/7	13/5
Body surface area (m ²)	2.07 ± 0.16	2.07 ± 0.17
Non-paroxysmal AF	9 (23%)	13 (72%)*
Duration AF (years)	7 ± 5	5 ± 4
Number of anti-arrhythmic drugs per patient	3.5 ± 1.8	4.0 ± 1.5
Left ventricular ejection fraction (%)	55 ± 9	54 ± 6
Valvular disease	4 (10%)	2 (11%)
Hypertension	13 (33%)	4 (22%)
Coronary artery disease	2 (5%)	2 (11%)

* $p < 0.05$ SR-group vs AF-group.

Left atrial dimensions and volumes

The LA dimensions (anteroposterior diameter, short- and long-axis) and volumes at baseline and 3 months follow-up are listed in Table 2. Baseline echocardiographic parameters were

Table 2. Left atrial dimensions and volumes at baseline and 3 months follow-up

Variable	SR-group (n=39)	AF-group (n=18)
Baseline		
LA anteroposterior diameter (cm)	4.5 ± 0.3	4.5 ± 0.3
LA short axis (cm)	4.5 ± 0.3	4.6 ± 0.2
LA long axis (cm)	5.1 ± 0.3	5.2 ± 0.4
LAEDV (ml)	59 ± 12	63 ± 7
LAESV (ml)	37 ± 9	43 ± 7*
3 months follow-up		
LA anteroposterior diameter (cm)	4.2 ± 0.2 [†]	4.8 ± 0.3**
LA short axis (cm)	4.2 ± 0.3 [†]	4.8 ± 0.3**
LA long axis (cm)	4.6 ± 0.4 [†]	5.3 ± 0.3*
LAEDV (ml)	50 ± 11 [†]	68 ± 8*
LAESV (ml)	31 ± 7 [†]	47 ± 7*

* $p < 0.05$ SR-group vs AF-group; [†] $p < 0.01$ baseline vs 3 months follow-up; [‡] $p < 0.05$ baseline vs 3 months follow-up.

similar in both groups, except that the LAEDV was significantly smaller in the SR-group as compared to the AF-group (37 ± 9 ml vs. 43 ± 7 ml, $p < 0.05$).

At 3 months follow-up, the LA anteroposterior diameter had decreased significantly in the SR-group (baseline 4.5 ± 0.3 cm vs. follow-up 4.2 ± 0.2 cm, $p < 0.01$). In contrast, in the AF-group, the LA anteroposterior diameter increased significantly from 4.5 ± 0.3 cm to 4.8 ± 0.3 cm ($p < 0.05$) (Figure 1). In addition, at 3 months follow-up LAESV and LAEDV had decreased

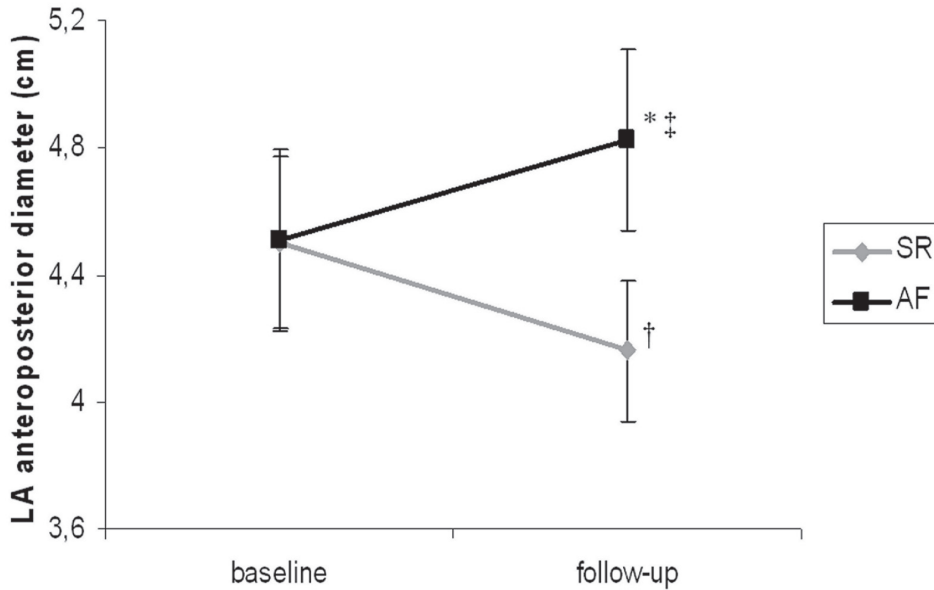


Figure 1. Left atrial anteroposterior diameter at baseline and 3 months follow-up in the SR-group and the AF-group. * $p < 0.05$ SR-group vs. AF-group; † $p < 0.01$ baseline vs. 3 months follow-up; ‡ $p < 0.05$ baseline vs. 3 months follow-up.

significantly in the SR-group in comparison to baseline measurements (Table 2). In contrast, in the AF-group, LAESV and LAEDV showed a tendency to increase, although the differences were not significantly different (Table 2). As a consequence, at 3 months follow-up all LA dimensions and volumes were significantly larger in the AF-group as compared to the SR-group (Table 2).

DISCUSSION

The findings in current study demonstrate that reverse remodeling of the LA occurs after successful radiofrequency catheter ablation for AF. In patients who maintained sinus rhythm, LA dimensions showed a significant decrease at 3 months follow-up. In contrast, in patients with recurrence of AF during follow-up, an increase in LA dimensions was observed. Furthermore, LA volumes decreased significantly in the SR-group, whereas a tendency towards a further increase in LA volumes was observed in the AF-group.

In the current study, LA dimensions and volumes were measured using standard 2-dimensional echocardiography to determine LA size at baseline and 3 months follow-up. A significant decrease in LA anteroposterior diameter was observed in the SR-group. Although M-mode is used commonly in clinical practice to measure LA dimension, it may not be sufficient to determine true LA size (6). Since M-mode represents only 1 dimension of the LA, it may underestimate LA size. Therefore, short- and long-axis of the LA were also evaluated on the apical 4- and 2-chamber images. The short- and long-axis measurements confirmed the findings observed on M-mode echocardiography (LA anteroposterior diameter). A significant decrease was observed in patients who maintained sinus rhythm, and an increase in LA dimensions was observed in patients with recurrence of AF.

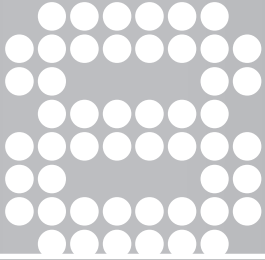
LA enlargement may result in an asymmetrical geometry of the LA. Therefore, optimal assessment of LA size should include LA volume measurements (6). In the current study the biplane Simpson's rule (4,5) was used to assess LAEDV and LAESV. Several reports have demonstrated that this method is an accurate technique for assessment of LA volumes using echocardiography (6,7). Furthermore, this method has been validated against CT (4) and MRI techniques (8) in previous studies. Using the biplane Simpson's rule, a significant decrease in LA volumes was demonstrated in the SR-group at 3 months follow-up, whereas a tendency towards an increase in LA volumes was noted in the AF-group.

CONCLUSIONS

In conclusion, LA cavity size decreases in patients who maintain sinus rhythm after radiofrequency catheter ablation, whereas LA size increases in patients with recurrence of AF.

REFERENCES

1. Haissaguerre M, Jais P, Shah DC et al. Spontaneous initiation of atrial fibrillation by ectopic beats originating in the pulmonary veins. *N Engl J Med* 1998;339:659-66.
2. Pappone C, Rosanio S, Augello G et al. Mortality, morbidity, and quality of life after circumferential pulmonary vein ablation for atrial fibrillation: outcomes from a controlled nonrandomized long-term study. *J Am Coll Cardiol* 2003;42:185-97.
3. Sahn DJ, DeMaria A, Kisslo J, Weyman A. Recommendations regarding quantitation in M-mode echocardiography: results of a survey of echocardiographic measurements. *Circulation* 1978;58:1072-83.
4. Kircher B, Abbott JA, Pau S et al. Left atrial volume determination by biplane two-dimensional echocardiography: validation by cine computed tomography. *Am Heart J* 1991;121:864-71.
5. Gutman J, Wang YS, Wahr D, Schiller NB. Normal left atrial function determined by 2-dimensional echocardiography. *Am J Cardiol* 1983;51:336-40.
6. Lester SJ, Ryan EW, Schiller NB, Foster E. Best method in clinical practice and in research studies to determine left atrial size. *Am J Cardiol* 1999;84:829-32.
7. Khankirawatana B, Khankirawatana S, Porter T. How should left atrial size be reported? Comparative assessment with use of multiple echocardiographic methods. *Am Heart J* 2004;147:369-74.
8. Sievers B, Kirchberg S, Addo M, Bakan A, Brandts B, Trappe HJ. Assessment of left atrial volumes in sinus rhythm and atrial fibrillation using the biplane area-length method and cardiovascular magnetic resonance imaging with TrueFISP. *J Cardiovasc Magn Reson* 2004;6:855-63.



Comparison of left atrial volumes and function by real-time three-dimensional echocardiography in patients having catheter ablation for atrial fibrillation with persistence of sinus rhythm versus recurrent atrial fibrillation three months later

Nina Ajmone Marsan^{1,2}

Laurens F. Tops¹

Eduard R. Holman¹

Nico R. Van de Veire¹

Katja Zeppenfeld¹

Eric Boersma³

Ernst E. van der Wall¹

Martin J. Schalij¹

Jeroen J. Bax¹

¹Department of Cardiology, Leiden University Medical Center, Leiden, the Netherlands

²Department of Cardiology, IRCCS Policlinico S. Matteo, Pavia, Italy

³Department of Epidemiology and Statistics, Erasmus University, Rotterdam, the Netherlands

Am J Cardiol 2008;102:847-53

ABSTRACT

Real-time 3-dimensional echocardiography (RT3DE) can provide a unique combination of accurate left atrium (LA) volume quantification and rapid, automatic assessment of LA function. The aim of the study was to evaluate the changes in LA volumes and function in patients with atrial fibrillation (AF) undergoing radiofrequency catheter ablation (RFCA), using RT3DE.

Fifty-seven consecutive patients referred for RFCA were studied. Paroxysmal AF was present in 43 patients (75%), and persistent AF in 14 (25%). After a mean follow-up of 7.9 ± 2.7 months, patients were divided into 2 groups: successful RFCA (SR group) and recurrence of AF (AF group). RT3DE was performed before, within 3 days and 3 months after RFCA to assess LA volumes (maximum, minimum and preA) and LA functions (passive, active and reservoir). A total of 38 patients (67%) had successful RFCA (SR group). Immediately after RFCA, no significant changes in LA volumes and function were observed. After 3 months, a significant reduction in LA volumes (maximum: from 26 ± 8 to 23 ± 7 mL/m², $p < 0.01$) was noted only in the SR group, together with a significant improvement in LA active (from 22 ± 8 to $33 \pm 9\%$, $p < 0.01$) and reservoir functions (from 116 ± 45 to $152 \pm 54\%$, $p < 0.01$). Conversely, the AF group showed a trend towards a deterioration of LA volumes and function. In conclusion, in patients who maintain sinus rhythm after RFCA, a significant reverse remodeling and functional improvement of the LA is observed using RT3DE.

INTRODUCTION

Recently, real-time 3-dimensional echocardiography (RT3DE) has been validated against magnetic resonance imaging and has been shown to be more accurate and reproducible than 2-dimensional (2D) echocardiography for the quantification of left atrial (LA) volumes (1,2). Furthermore, RT3DE may be a novel, reliable technique for the assessment of LA function, providing unique information about phasic changes of LA volumes during the cardiac cycle (3,4). In the present study, RT3DE was used to evaluate the changes in LA volumes and function in atrial fibrillation (AF) patients treated with radiofrequency catheter ablation (RFCA).

METHODS

In a 10 months period, 57 consecutive patients (44 men; age 56 ± 9 years) with symptomatic drug-refractory AF, referred to our institution for RFCA in accordance to the current guidelines criteria, were included in this study. According to the ACC/AHA/ESC Guidelines definition (5), paroxysmal AF was present in 43 patients (75%), while persistent AF was present in the remaining 14 patients (25%); none of the patients had permanent AF. Mean AF duration (calculated from the time of the first episode) was 4.6 ± 4.1 years and the patients had an unsuccessful treatment with 3 ± 1 anti-arrhythmic drugs (mainly flecainide, propafenone, sotalol and amiodarone).

After RFCA, the patients were evaluated at the out-patient clinic on a regular basis. During follow-up, all medication, including anti-arrhythmic drugs, were continued in all patients for 3 months after the RFCA procedure. Afterwards, anti-arrhythmic drugs were discontinued at discretion of the physician. At the latest follow-up, successful RFCA was defined as the absence of symptomatic recurrences lasting more than 3 minutes (6) and/or the absence of AF episodes lasting more than 30 seconds (detected with 24-hours Holter ECG recording and surface ECG) during follow-up, after a blanking period of 1 month (5,7). Accordingly, the study population was divided into 2 groups: patients with successful RFCA (SR group) and patients who had recurrence of AF (AF group). Before and within 3 days after the ablation procedure, RT3DE was performed to assess LA and left ventricular (LV) size and function. In addition, conventional 2D color-Doppler echocardiography was performed to assess mitral regurgitation (MR) and LV filling pattern. After 3 months follow-up, the echocardiograms were repeated to assess the effect of the RFCA on LA volumes and function.

Real-time 3-dimensional echocardiography

Patients were imaged with a commercially available system (iE33, Philips Medical Systems, Bothell, Washington) equipped with X3, fully sampled matrix transducer. Apical full-volume data sets were obtained in all patients, combining 7 small real-time sub-volumes to provide a

larger pyramidal volume. The acquisition was performed during end-expiratory apnea within 1 breath hold. Frame rate ranged from 20 to 35 frames/sec. The RT3DE data sets were stored digitally and quantitative analyses were performed off-line using a semi-automated contour tracing algorithm (Q-Lab, version 5.0, Philips Medical Systems) based on 5 reference points. In all patients the image quality was sufficient for quantitative analysis and the post-processing of the images was performed within 10 minutes. Left ventricular volumes and function were assessed as previously described in detail (8).

Quantification of LA volumes was performed using the semi-automated contour tracing algorithm developed for the LV, but marking 5 atrial reference points: 4 at the anterior, inferior, lateral and septal part of atrial dome and 1 at the level of the mitral annulus (Figure 1). The position of the reference points was chosen to avoid changes in the view orientation that the software automatically generates, since the position of the dome of the LA is opposite of the apex of the LV. Manual corrections of the automatic trace were made to exclude the LA appendage and the pulmonary vein ostia. Left atrial volumes were measured at 3 time points during the cardiac cycle: 1) maximum volume (LA_{max}) at end-systole, just before mitral valve opening; 2) minimum volume (LA_{min}) at end-diastole, just before mitral valve closure; 3) volume before atrial active contraction (LA_{preA}) obtained from the last frame before mitral valve reopening or

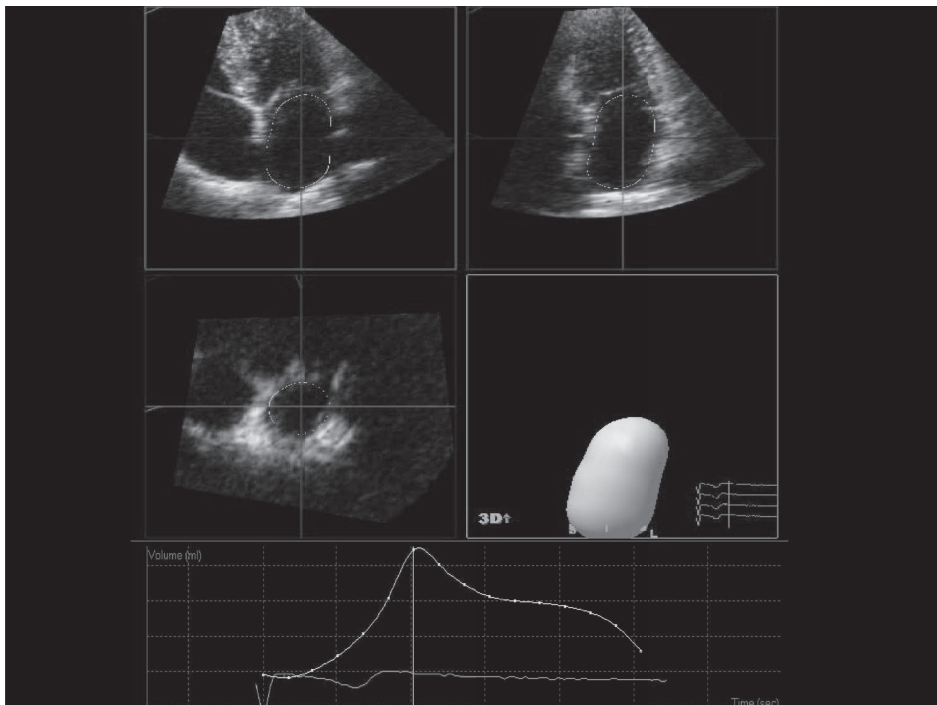


Figure 1. Assessment of LA volumes using RT3DE. An automatic border detection is obtained marking 5 reference points in the apical 2- and 4-chamber views (upper panel) and the LA 3D model is provided by the software. The changes of LA volumes during the heart cycle are plotted as a curve (lower panel).

at time of the P wave on the surface ECG. All LA volumes were indexed to the body surface area, as recommended (9).

Twenty patients were randomly identified for inter- and intra-observer agreement. According to the Bland-Altman analysis, intra-observer variability was excellent with a mean differences of 1.2 ± 2.9 mL for LA_{max} , 0.1 ± 1.1 mL for LA_{min} and 0.8 ± 2.3 mL for LA_{preA} ($p = NS$). Inter-observer variability was also good with a mean difference for LA_{max} , LA_{min} and LA_{preA} of 3.6 ± 5.6 mL, 0.7 ± 5.4 mL and 1.9 ± 3.4 mL, respectively ($p = NS$).

The LA function was derived from the LA volumes and expressed with the following parameters (10,11): 1) Total atrial emptying fraction: $LA_{EF} = ([LA_{max} - LA_{min}]/LA_{max}) \times 100$; 2) Active atrial emptying fraction: $LA_{active} = ([LA_{preA} - LA_{min}]/LA_{preA}) \times 100$, which is considered an index of LA active contraction; 3) Passive atrial emptying fraction: $LA_{passive} = ([LA_{max} - LA_{preA}]/LA_{max}) \times 100$, which is considered an index of LA conduit function; 4) Atrial expansion index: $LA_{reservoir} = ([LA_{max} - LA_{min}]/LA_{min}) \times 100$, which is considered an index of LA reservoir function.

The severity of MR was graded semi-quantitatively from color-Doppler images in the conventional parasternal long-axis and apical 4-chamber view and characterized as follows: absent, mild (ratio jet area/LA area $<20\%$), moderate (jet area/LA area 20% to 40%) and severe (jet area/LA area $>40\%$) (12). Left ventricular diastolic function was evaluated according to the Canadian Consensus recommendations (13) through the following Doppler measurements: ratio of early (E) to late (A) diastolic filling velocities (E/A) and deceleration time (DT) of the E wave.

Radiofrequency catheter ablation procedure

The RFCA procedure was aimed at electrical isolation of all pulmonary veins from the LA. Endocardial mapping was performed with a 4-mm quadripolar mapping/ablation catheter (7Fr Thermocool, Biosense Webster, Diamond Bar, California, USA), using a 3D electroanatomic mapping system (CARTO, Biosense Webster). A 6Fr diagnostic catheter placed in the right atrium served as a temporal reference. Radiofrequency current was applied outside the ostia of all pulmonary veins, using the ablation catheter with a 4-mm open loop irrigated tip. The following power and temperature settings were used: irrigation rate 20 ml/min, maximum temperature $50^\circ C$, and maximum radiofrequency energy 30W. At each point, the radiofrequency current was applied until a voltage of <0.1 mV was achieved, with a maximum of 60 s/point. The procedure was considered successful when pulmonary vein isolation was confirmed by the recording of entrance block during SR or pacing in the coronary sinus. All patients received heparin intravenously (activated clotting time >300 sec) to avoid thrombo-embolic complications during the catheter ablation procedure. After RFCA, the rhythm was continuously monitored until discharge.

Statistical analysis

Continuous data are presented as mean \pm standard deviation. Categorical data are presented as absolute numbers or percentages. Independent-samples T test and Wilcoxon rank-test were used to compare continuous variables, as appropriate, and χ^2 test was used to compare

categorical variables. Sequential data measurements were analyzed by the general linear model (GLM) procedure for repeated measures. For all tests, a p value <0.05 was considered significant. A statistical software program SPSS 15.0 (SPSS Inc, Chicago, IL, USA) was used for statistical analysis.

RESULTS

Baseline clinical characteristics of the study population are summarized in Table 1. At baseline, RT3DE revealed a mild enlargement of LA volume and a moderate reduction in LA_{EF}, LA_{active} and LA_{reservoir} (Table 2), as compared to the reference values for a normal LA (9,14). Left ventricular systolic and diastolic functions were normal and in 27 patients MR was present (mild n = 24; moderate n = 3) (Table 3). Six patients were in AF at the baseline evaluation and all had a recurrence of AF during follow-up. In these patients, LA_{preAF}, LA_{active}, LA_{passive} and LV diastolic function could therefore not be assessed.

Table 1. Baseline clinical characteristics of the total study population and of patients with and without recurrence of AF after radiofrequency catheter ablation

Variable	Total study population n = 57	Sinus rhythm group n = 38	Atrial fibrillation group n = 19
Age (years)	56 ± 9	57 ± 9	53 ± 9
Male/Female	44/13	28/10	16/3
Body surface area (m ²)	2.1 ± 0.2	2.1 ± 0.3	2.1 ± 0.1
Atrial fibrillation: Paroxysmal/Persistent	45 (79%) / 12 (21%)	34 (89%) / 4 (11%)	11 (58%) / 8 (42%)*
Duration atrial fibrillation (years)	4.6 ± 4.1	4.5 ± 4.1	4.6 ± 4.1
Number of anti-arrhythmic drugs per patient	3 ± 1	3 ± 1	3 ± 1
ACE-inhibitor and/or Angiotensin receptor blocker	26 (46%)	17 (45%)	9 (47%)
Heart rate (beats/minute)	62 ± 20	60 ± 13	66 ± 36
Hypertension	25 (44%)	13 (34%)	11 (58%)
Diabetes mellitus	6 (11%)	6 (15%)	0 (0%)
Coronary artery disease	3 (5%)	2 (5%)	1 (5%)

*p <0.05 SR group versus AF group.

After a mean follow-up of 7.9 ± 2.7 months, 38 patients (67%) had successful RFCA (SR group), whereas 19 patients (33%) had recurrence of AF (AF group). Of note, these patients were classified in the same group also at 3 months follow-up evaluation. No significant differences were found in the baseline clinical characteristics between the AF and SR groups, except for the percentage of patients with persistent AF (Table 1). At baseline, RT3DE showed larger LA_{max} in the AF group than in the SR group (31 ± 8 vs. 26 ± 8 mL/m², p <0.05), but no significant differences in LA and LV function (Table 2 and 3). Conventional 2D color-Doppler echocardiography revealed a comparable LV diastolic function and prevalence of MR (mild/ moderate) between

Table 2. Left atrium (LA) volumes and function at baseline, immediately after and 3 months after the ablation procedure in the total study population and in patients with or without recurrence of AF

Variable	Total study population n = 57	Sinus rhythm group n = 38	Atrial fibrillation group n = 19	p value
LA volumes				
LA maximum volume (mL/m²)				
Baseline	28 ± 9	26 ± 8	31 ± 8	<0.01 [§]
After ablation		26 ± 8	31 ± 8	<0.05
3 months follow-up		23 ± 7*	32 ± 8	<0.001
LA minimum volume (mL/m²)				
Baseline	14 ± 6	13 ± 5	16 ± 7	NS
After ablation		12 ± 5	17 ± 6	<0.01
3 months follow-up		10 ± 4*	18 ± 6	<0.001
LA volume preA (mL/m²)				
Baseline	16 ± 5	16 ± 5	18 ± 6	NS
After ablation		16 ± 5	18 ± 4	NS
3 months follow-up		14 ± 5*	20 ± 6*	<0.01
LA function				
LA total emptying fraction (%)				
Baseline	50 ± 11	52 ± 10	47 ± 13	NS
After ablation		52 ± 10	44 ± 12	<0.05
3 months follow-up		58 ± 10*	42 ± 11*	<0.001
LA passive emptying fraction (%)				
Baseline	39 ± 9	39 ± 9	38 ± 10	NS [§]
After ablation		39 ± 9	35 ± 10	NS
3 months follow-up		38 ± 9	35 ± 9	NS
LA active emptying fraction (%)				
Baseline	22 ± 8	22 ± 8	24 ± 7	NS
After ablation		21 ± 6	17 ± 7	NS
3 months follow-up		33 ± 9*	15 ± 9*	<0.001
LA expansion index (%)				
Baseline	110 ± 48	116 ± 45	101 ± 55	NS
After ablation		117 ± 43	92 ± 49	NS
3 months follow-up		152 ± 54*	78 ± 35*	<0.001

*p < 0.01 (GLM for repeated measures within subjects); § p value derived from GLM for repeated measures between subjects (sinus rhythm vs. atrial fibrillation).

the 2 groups (Table 3). Immediately after the RFCA procedure, no significant changes in LA volumes were observed (Table 2). However, after 3 months of follow-up, a significant decrease in LA volumes was noted in the SR group, involving LA_{max}, LA_{min} and LA_{preA} volumes. Conversely, the AF group showed a trend towards an increase in LA volumes during follow-up (Table 2). An example of a patient in the SR group with a significant reduction of LA_{max} and LA_{min} is shown in Figure 2. In both groups, no significant changes in LA function were noted immediately after the RFCA procedure. However, after 3 months of follow-up, a significant improvement of LA_{active} and LA_{reservoir} was noted in the SR group, whereas in the AF group these parameters showed a significant deterioration (Figure 3). In contrast, LA_{passive} function did not change significantly in both groups. In concordance with the changes in LA_{active}, a significant improvement in LA_{EF} was observed in the SR group, while a significant deterioration in LA_{EF} was observed in the AF group (Table 2).

Table 3. Left ventricular function at baseline and 3 months after the ablation procedure in the total study population and in patients with or without recurrence of atrial fibrillation

Variable	Total study population n = 57	Sinus rhythm group n = 38	Atrial fibrillation group n = 19
Left ventricular ejection fraction (%)			
Baseline	57 ± 9	58 ± 9	57 ± 11
3 months follow-up		59 ± 10	57 ± 8
E/A			
Baseline	1.2 ± 0.6	1.1 ± 0.4	1.4 ± 0.6
3 months follow-up		1.2 ± 0.2	1.3 ± 0.7
Deceleration time (ms)			
Baseline	194 ± 53	196 ± 51	192 ± 48
3 months follow-up		199 ± 40	195 ± 42
Mitral regurgitation, n (absent/mild/moderate/severe)			
Baseline	30/24/3/0	21/16/1/0	9/8/2/0
3 months follow-up		25/13/0/0*	9/8/2/0

* p < 0.01 baseline vs. follow-up.

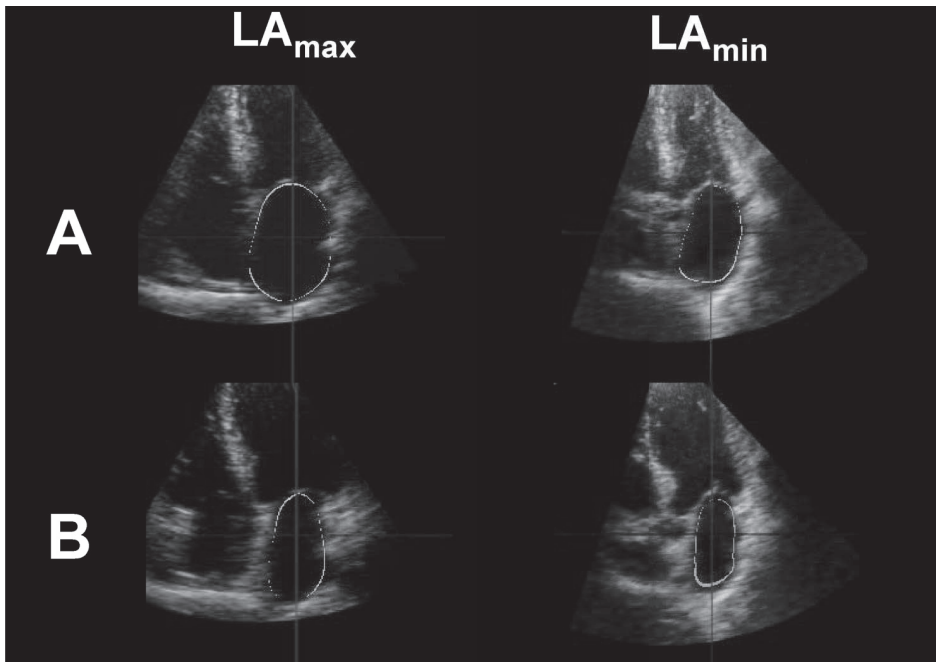


Figure 2. Example of a patient with significant reduction of LA_{max} and LA_{min} 3 months after the RFCA (panel B vs. panel A). LA_{max} decreased from 83 to 66 mL/m² and LA_{min} decreased from 44 to 33 mL/m².

Mean LV ejection fraction was 58 ± 9% in the SR group and 57 ± 11% in the AF group (p = NS) and no significant changes were observed during follow-up. Similarly, LV diastolic function was normal in both groups before the RFCA procedure and did not change during follow-up (Table 3). However, 12 patients in the SR group and 3 patients in the AF group had an abnormal

LV relaxation based on $E/A < 1$. For these patients an improvement in LV filling pattern was noted in the SR group only (E/A ratio from 0.7 ± 0.2 to 1.6 ± 0.5 , $p < 0.01$). Only 3 patients had clinically relevant MR (moderate or severe) and a significant improvement in the degree of MR after RFCA was only observed in the SR group (Table 3).

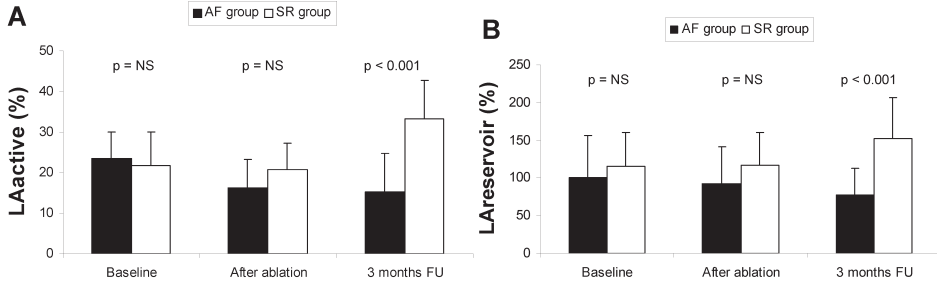


Figure 3. Left atrium active emptying fraction (LA_{active} ; panel A) and expansion index ($LA_{reservoir}$; panel B) at baseline, immediately after catheter ablation and at 3 months follow-up (FU) in SR and AF groups.

DISCUSSION

The main findings of the current study can be summarized as follows: 1) three months after RFCA, a significant reduction in LA volumes and a clear improvement of LA active contraction and LA reservoir function was observed in patients with a successful RFCA procedure; 2) patients with recurrence of AF after RFCA showed a trend towards a worsening of LA volumes and function

Real-time 3-dimensional echocardiography

In the present study, RT3DE was used to assess LA volumes and function in patients treated with RFCA for AF. The assessment of LA size is fundamental in the management of patients with AF, since it has important prognostic value and is used as a surrogate marker of therapy success (15-18). The most recent recommendations for cardiac chamber quantification indicate LA volume as the preferred measurement of LA size (9). However, the majority of the previous studies only evaluated LA diameter and LA area, using conventional 2D echocardiography (16,18,19). Although most frequently used, 2D echocardiography is limited for the assessment of LA volume by significant geometric assumptions and low reproducibility due to diverging position and orientation of imaging planes. RT3DE has been demonstrated to be more accurate for LA volumes quantification, with the most favorable test-retest variation (1,2,4). In addition to LA volumes, assessment of LA function is of particular significance in patients treated with RFCA for AF. However, accurate non-invasive measurements for LA function are still lacking. Recently, initial studies have proposed tissue Doppler imaging (TDI) and 2D strain as new modalities to assess LA myocardial function (20,21). However, these techniques need to be further validated for this purpose and have some limitations related to the angle dependency of TDI (21) and the

difficult analysis of LA systole with 2D strain (20). In contrast, RT3DE is well validated (3,4,22) and provides a unique combination of an accurate measurement of LA volumes together with a rapid and automatic detection of phasic changes of LA volumes that provides detailed information of the different LA functions.

Effect of RFCA on LA volumes and function

The relationship between LA enlargement and AF is complex: structural changes of the LA may be related several factors including 1) pressure or volume overload due to underlying structural heart disease; 2) the increased LV filling pressure induced by the tachyarrhythmia; 3) AF itself (23,24). Supporting the latter hypothesis, abnormal atrial histology (fibrosis, necrosis and inflammation) has been found uniformly in patients with lone AF (25). Furthermore, LA dilatation has been directly correlated with the duration of AF, as a result of LA electrical and structural remodeling (18). In the present study, mild dilatation of the LA was noted at baseline using RT3DE. This may be explained by the relatively low prevalence of patients with persistent AF and with structural heart disease (Table 1). Of note, the AF group, compared to the SR group, demonstrated larger baseline LA volumes, probably related to the higher percentage of persistent AF. Furthermore, after 3 months a significant decrease in LA volumes was noted in patients with successful RFCA. These results are in agreement with previous studies that showed a significant reduction in LA volumes after conversion of AF to SR, either by electrical cardioversion or RFCA (6,14,26). The reduction in LA_{min} as observed in the present study is most probably the direct result of the improvement of LA active contraction; whereas the reduction in LA_{max} is reflecting a true reverse remodeling that is related with the long-lasting restoration of SR. Although LA reverse remodeling may also be ascribed to atrial scarring caused by RFCA, this is very unlikely since LA volumes tended to worsen in patients with recurrence of AF during follow-up.

In addition, an improvement in LA function was observed in patients who maintained SR after RFCA. The LA serves multiple functions. During LV systole and isovolumic relaxation, it operates as a “reservoir” that receives blood from pulmonary veins and stores energy in the form of pressure; during the early diastole, it operates as a “conduit” for transfer blood into the LV after mitral valve opening; during the late diastole the “active” contraction of LA contributes to LV stroke volume by 20-30% (22,23). To interpret the baseline and follow-up findings of the present study, it is important to consider that the major determinants of LA_{active} are the heart rhythm, the atrial contractility and the LA_{preA} (Frank-Starling effect) (3,11). The $LA_{reservoir}$ is rather influenced by LV systolic function (mitral annulus displacement) and by LA wall stiffness (11,27). On the contrary, $LA_{passive}$ is mainly related to LV diastolic function (11,28).

In the present study, a moderate reduction of LA_{active} and $LA_{reservoir}$ was noted at baseline evaluation. Conversely, no significant impairment of $LA_{passive}$ was observed. Since LV systolic and diastolic functions were normal on average and LA_{preA} was even decreased compared to

the normal values, the reduction in LA_{active} and $LA_{reservoir}$ is most probably related to the effect of AF itself on the contractility and the stiffness of atrial walls.

Immediately after RFCA, no significant changes in LA functions were found, but LA_{active} tended to worsen. This finding occurred in both the SR and AF groups and can be related to the phenomenon of atrial “stunning” (29). After 3 months of follow-up, a significant improvement in LA_{active} and $LA_{reservoir}$ was noted in the SR group, whereas in the AF group these parameters showed a significant deterioration. Since LV systolic and diastolic functions did not change after RFCA and LA_{preA} was even decreased, the functional improvement in the SR group is most probably related to a favorable effect of the long-lasting restoration of SR on the intrinsic characteristics of the atrial myocardium (24). These findings are in line with previous studies (6,14) and carry important clinical implications, since they may translate into a reduced risk of AF recurrences and thrombo-embolic complications at long-term follow-up (24). However, the exact impact of LA reverse remodeling and improvement of LA function on cardiovascular outcomes remains to be determined.

The results of the present study need to be confirmed in a larger population with longer clinical and echocardiographic follow-up. In addition, in patients with paroxysmal AF, asymptomatic recurrences cannot be excluded and may have influenced the success rate in the present study.

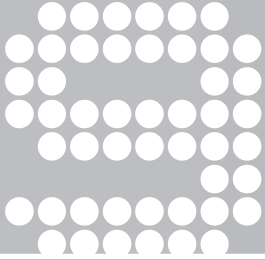
CONCLUSIONS

In conclusion, the effect of RFCA on LA size and function can be accurately evaluated with RT3DE. In the present study, a significant reverse remodeling and functional improvement of the LA was noted in patients who maintain sinus rhythm after RFCA. In contrast, a deterioration of LA volumes and function was observed in patients with recurrence of AF.

REFERENCES

1. Khankirawatana B, Khankirawatana S, Lof J, Porter TR. Left atrial volume determination by three-dimensional echocardiography reconstruction: validation and application of a simplified technique. *J Am Soc Echocardiogr* 2002;15:1051-6.
2. Poutanen T, Ikonen A, Vainio P, Jokinen E, Tikanoja T. Left atrial volume assessed by transthoracic three dimensional echocardiography and magnetic resonance imaging: dynamic changes during the heart cycle in children. *Heart* 2000;83:537-42.
3. Anwar AM, Geleijnse ML, Soliman OI, Nemes A, ten Cate FJ. Left atrial Frank-Starling law assessed by real-time, three-dimensional echocardiographic left atrial volume changes. *Heart* 2007;93:1393-7.
4. Anwar AM, Soliman OI, Geleijnse ML, Nemes A, Vletter WB, ten Cate FJ. Assessment of left atrial volume and function by real-time three-dimensional echocardiography. *Int J Cardiol* 2008;123:155-61.
5. Fuster V, Ryden LE, Cannom DS et al. ACC/AHA/ESC 2006 guidelines for the management of patients with atrial fibrillation--executive summary. *J Am Coll Cardiol* 2006;48:854-906.
6. Reant P, Lafitte S, Jais P et al. Reverse remodeling of the left cardiac chambers after catheter ablation after 1 year in a series of patients with isolated atrial fibrillation. *Circulation* 2005;112:2896-903.
7. Calkins H, Brugada J, Packer DL et al. HRS/EHRA/ECAS expert Consensus Statement on catheter and surgical ablation of atrial fibrillation: recommendations for personnel, policy, procedures and follow-up. *Heart Rhythm* 2007;4:816-61.
8. Soliman OI, Krenning BJ, Geleijnse ML et al. A comparison between QLAB and TomTec full volume reconstruction for real time three-dimensional echocardiographic quantification of left ventricular volumes. *Echocardiography* 2007;24:967-74.
9. Lang RM, Bierig M, Devereux RB et al. Recommendations for chamber quantification. *Eur J Echocardiogr* 2006;7:79-108.
10. Poutanen T, Jokinen E, Sairanen H, Tikanoja T. Left atrial and left ventricular function in healthy children and young adults assessed by three dimensional echocardiography. *Heart* 2003;89:544-9.
11. Spencer KT, Mor-Avi V, Gorcsan J, III et al. Effects of aging on left atrial reservoir, conduit, and booster pump function: a multi-institution acoustic quantification study. *Heart* 2001;85:272-7.
12. Bonow RO, Carabello BA, Kanu C et al. ACC/AHA 2006 guidelines for the management of patients with valvular heart disease. *Circulation* 2006;114:e84-231.
13. Rakowski H, Appleton C, Chan KL et al. Canadian consensus recommendations for the measurement and reporting of diastolic dysfunction by echocardiography: from the Investigators of Consensus on Diastolic Dysfunction by Echocardiography. *J Am Soc Echocardiogr* 1996;9:736-60.
14. Thomas L, Thomas SP, Hoy M, Boyd A, Schiller NB, Ross DL. Comparison of left atrial volume and function after linear ablation and after cardioversion for chronic atrial fibrillation. *Am J Cardiol* 2004;93:165-70.
15. Benjamin EJ, D'Agostino RB, Belanger AJ, Wolf PA, Levy D. Left atrial size and the risk of stroke and death: The Framingham Heart Study. *Circulation* 1995;92:835-41.
16. Berrueto A, Tamborero D, Mont L et al. Pre-procedural predictors of atrial fibrillation recurrence after circumferential pulmonary vein ablation. *Eur Heart J* 2007;28:836-41.
17. Kirchhof P, Auricchio A, Bax J et al. Outcome parameters for trials in atrial fibrillation: executive summary: Recommendations from a consensus conference organized by the German Atrial Fibrillation Competence Network (AFNET) and the European Heart Rhythm Association (EHRA). *Eur Heart J* 2007;28:2803-17.
18. Petersen P, Kastrup J, Brinch K, Godtfredsen J, Boysen G. Relation between left atrial dimension and duration of atrial fibrillation. *Am J Cardiol* 1987;60:382-4.
19. Beukema WP, Elvan A, Sie HT, Misier AR, Wellens HJ. Successful radiofrequency ablation in patients with previous atrial fibrillation results in a significant decrease in left atrial size. *Circulation* 2005;112:2089-95.

20. D'Andrea A, Caso P, Romano S et al. Different effects of cardiac resynchronization therapy on left atrial function in patients with either idiopathic or ischaemic dilated cardiomyopathy: a two-dimensional speckle strain study. *Eur Heart J* 2007;28:2738-48.
21. Yu CM, Fang F, Zhang Q et al. Improvement of atrial function and atrial reverse remodeling after cardiac resynchronization therapy for heart failure. *J Am Coll Cardiol* 2007;50:778-85.
22. Thomas L. Assessment of atrial function. *Heart Lung Circ* 2007;16:234-42.
23. Abhayaratna WP, Seward JB, Appleton CP et al. Left atrial size: physiologic determinants and clinical applications. *J Am Coll Cardiol* 2006;47:2357-63.
24. Casaciang-Verzosa G, Gersh BJ, Tsang TS. Structural and functional remodeling of the left atrium: clinical and therapeutic implications for atrial fibrillation. *J Am Coll Cardiol* 2008;51:1-11.
25. Frustaci A, Chimenti C, Bellocci F, Morgante E, Russo MA, Maseri A. Histological substrate of atrial biopsies in patients with lone atrial fibrillation. *Circulation* 1997;96:1180-4.
26. Tops LF, Bax JJ, Zeppenfeld K, Jongbloed MR, van der Wall EE, Schalij MJ. Effect of radiofrequency catheter ablation for atrial fibrillation on left atrial cavity size. *Am J Cardiol* 2006;97:1220-2.
27. Barbier P, Solomon SB, Schiller NB, Glantz SA. Left atrial relaxation and left ventricular systolic function determine left atrial reservoir function. *Circulation* 1999;100:427-36.
28. Nikitin NP, Witte KK, Thackray SD, Goodge LJ, Clark AL, Cleland JG. Effect of age and sex on left atrial morphology and function. *Eur J Echocardiogr* 2003;4:36-42.
29. Khan IA. Atrial stunning: basics and clinical considerations. *Int J Cardiol* 2003;92:113-28.



Left atrial strain predicts reverse remodeling after catheter ablation for atrial fibrillation

Laurens F. Tops
Victoria Delgado
Matteo Bertini
Nina Ajmone Marsan
Dennis W. den Uijl
Serge A.I.P. Trines
Katja Zeppenfeld
Eduard R. Holman
Martin J. Schalij
Jeroen J. Bax

Department of Cardiology, Leiden University Medical Center, Leiden, the Netherlands

Submitted

ABSTRACT

Background: The association between LA reverse remodeling and improvement in LA strain after catheter ablation has not been investigated thus far.

Objectives: The purpose of this study was to assess left atrial (LA) strain during long-term follow-up after catheter ablation for atrial fibrillation (AF), and find predictors for LA reverse remodeling.

Methods: In 148 patients undergoing catheter ablation for AF, LA volumes and LA strain were assessed with echocardiography at baseline and after a mean of 13.2 ± 6.7 months follow-up. The study population was divided according to LA reverse remodeling at follow-up: 'Responders' were defined as patients who exhibited $\geq 15\%$ reduction in maximum LA volume at long-term follow-up. LA systolic (LAs) strain was assessed with tissue Doppler imaging.

Results: At follow-up, 93 patients (63%) were classified as a responder, whereas 55 patients (37%) were non-responders. At baseline, LAs strain was significantly higher in the responders as compared with the non-responders ($19 \pm 8\%$ vs. $14 \pm 6\%$, $p=0.001$). In the responders, a significant increase in LAs strain was noted from baseline to follow-up (from $19 \pm 8\%$ to $22 \pm 9\%$, $p<0.05$), whereas no change was noted in the non-responders. LAs strain at baseline was the strongest predictor of LA reverse remodeling (Odds ratio 1.089; 95% CI 1.014-1.169, $p=0.019$).

Conclusions: In the present study, 63% of the patients exhibited LA reverse remodeling after catheter ablation for AF, with a concomitant improvement in LA strain. Left atrial strain at baseline was the strongest predictor of LA reverse remodeling.

INTRODUCTION

Left atrial (LA) enlargement is associated with cardiac morbidity and is a robust predictor of cardiovascular outcome (1,2). The relation between LA enlargement and atrial fibrillation (AF) has been well recognized. However, it still remains controversial whether LA enlargement causes AF (3), or vice versa (4).

Reversal of LA enlargement, or 'reverse remodeling', has been demonstrated with drug therapy and after restoration of sinus rhythm with cardioversion (5). In addition, it has been shown that LA reverse remodeling may occur after successful catheter ablation for AF (6).

At the same time, LA function may improve after restoration of sinus rhythm with catheter ablation (7). Using tissue Doppler imaging, it has been demonstrated that LA strain may improve at three months after successful catheter ablation for AF (8). However, it is unclear whether these changes in LA strain remain during long-term follow-up. More importantly, the association between LA reverse remodeling and the improvement in LA strain has not been investigated thus far. Accordingly, the purpose of the present study was to evaluate reverse remodeling and LA strain during long-term follow-up after catheter ablation for AF. In addition, predictors for LA reverse remodeling were studied.

METHODS

Study population and study protocol

The study population comprised 148 patients from an ongoing clinical registry (6) with symptomatic drug-refractory AF, who were referred for radiofrequency catheter ablation. Before the ablation procedure and after 12 months follow-up, an extensive echocardiographic evaluation was performed to assess LA strain. In a subgroup of patients with an available echocardiogram during sinus rhythm both at baseline and at follow-up (n=122), LA late diastolic strain (representing LA active contraction) and LV systolic strain was assessed. At long-term follow-up, the study population was divided according to reverse remodeling of the LA after the catheter ablation procedure.

Catheter ablation procedure

The protocol of the catheter ablation procedure has been described in more detail elsewhere (9). In brief, electrical isolation of all pulmonary veins from the LA was attempted using an electroanatomic mapping system with an image integration module (CARTO™ and CartoMerge™, Biosense Webster, Diamond Bar, California). Endocardial mapping and ablation was performed with a 4 mm quadripolar mapping/ablation catheter, with an open loop irrigated tip (7F Thermocool, Biosense Webster). A 6F diagnostic catheter placed in the right atrium served as a temporal reference. Radiofrequency current was applied outside the ostia of all pulmonary

veins using the following settings: irrigation rate 20 mL/min, maximum temperature 50°C, maximum radiofrequency energy 30 W. At each point, radiofrequency current was applied until a voltage <0.1 mV was achieved, with a maximum of 60 seconds per point. The procedure was considered successful when pulmonary vein isolation was confirmed by recording entrance block during sinus rhythm or pacing in the coronary sinus. All patients received heparin intravenously (activated clotting time > 300 sec) to avoid thrombo-embolic complications.

After the catheter ablation procedure, all patients were evaluated at the out-patient clinic on a regular basis. All medication, including anti-arrhythmic drugs, was continued in all patients during the first 3 months of follow-up. Afterwards, anti-arrhythmic drugs were discontinued at the discretion of the physician. A surface ECG was acquired at every follow-up visit, and 24-hours Holter monitoring was performed at 3 to 6 months intervals. Maintenance of sinus rhythm during follow-up was defined as the absence of symptomatic recurrences lasting more than 3 minutes and/or the absence of AF episodes lasting more than 30 seconds detected with 24-hour Holter monitoring or surface ECG, after a blanking period of 1 month (10).

Echocardiography

Two-dimensional echocardiography was performed within 2 days before the ablation procedure, and at 12 months follow-up. Two-dimensional images were recorded with the patient in the left lateral decubitus position using a commercially available system (Vivid 7, General Electric-Vingmed, Milwaukee, Wisconsin, USA). Images were acquired using a 3.5-MHz transducer at a depth of 16 cm in the parasternal and apical views (standard long-axis and 2- and 4-chamber images). Standard 2-dimensional images and color Doppler data were saved in cine loop format. All analyses were performed off-line using commercial software (Echopac 7.0.0, General Electric-Vingmed).

Left ventricular end-diastolic and end-systolic volumes were assessed from the apical 2- and 4-chamber images, and indexed to body surface area; LV ejection fraction (LVEF) was calculated using the biplane Simpson's rule (11). Left ventricular diastolic function was evaluated using the following Doppler measurements: ratio of early (E) to late (A) diastolic filling velocities (E/A) and deceleration time of the E wave (12). In addition, LV systolic strain and strain rate was assessed using color-coded tissue Doppler imaging in a subgroup of patients, as previously described (13).

Left atrial volumes and ejection fraction The LA anteroposterior diameter was measured at end-systole on the M-mode image obtained from the parasternal long-axis view. Furthermore, LA volumes were measured on apical 2- and 4-chamber views. Maximum LA volume (LA_{max}) was defined as the largest LA volume just prior to mitral valve opening; minimum LA volume (LA_{min}) was defined as the smallest possible LA volume in ventricular diastole. All LA volumes were indexed to body surface area, as recommended (14). Left atrial total emptying (LA_{EF}) was calculated using the biplane Simpson's rule (14).

Definition of LA reverse remodeling To study the determinants of reverse remodeling of the LA after catheter ablation, the study population was divided into 2 groups according to the extent of decrease in LA_{max} during follow-up (15). ‘Responders’ were defined as patients who exhibited $\geq 15\%$ reduction in LA_{max} at long-term follow-up. The ‘non-responders’ were patients who demonstrated a decrease in $LA_{max} < 15\%$, or an increase in LA_{max} during follow-up.

Left atrial strain analysis Left atrial deformation properties were studied using color-coded tissue Doppler imaging, by offline analysis of standard apical 2- and 4-chamber images of 3 consecutive heart beats. Frame rates were at least 115 frames/s, and the sector width was adjusted to allow the highest possible frame rate.

A sample volume (6 x 4 mm) was placed at the basal to mid parts of the LA septum and lateral wall (4-chamber view), and the LA anterior and inferior wall (2-chamber view). If necessary, Gaussian smoothing was applied to create clear strain curves. From the reconstructed strain curves, myocardial LA longitudinal lengthening or LAs strain (representing LA expansion function) was identified as the peak positive strain value during LV systole. In a subgroup of patients with an available echocardiogram during sinus rhythm both at baseline and at follow-up (n=122), myocardial LA shortening, or LAa strain (representing LA active contraction) was identified as the peak negative strain value during LV diastole occurring after the P-wave on the ECG.

Peak LAs strain and LAa strain was assessed for the 4 regions (septal, lateral, anterior, inferior), and averaged to acquire global LAs strain and LAa strain values. Similar, LAs strain rate and LAa strain rate, representing the speed at which LA deformation occurs, was assessed in the 4 regions and averaged (Figure 1).

Statistical analysis

All continuous variables had normal distribution (as evaluated by Kolmogorov-Smirnov tests). Summary statistics for these variables are therefore presented as mean \pm standard deviation (SD). Categorical data are summarized as frequencies and percentages.

Differences in clinical and echocardiographic variables between the responders and the non-responders were evaluated using unpaired Student t-tests (continuous variables), Chi-square tests or Fisher’s exact tests (dichotomous variables), as appropriate. Differences in continuous variables between baseline and follow-up were evaluated using paired Student t-test.

Intra- and inter-observer reproducibility for the assessment of LA strain and LA strain rate was determined by intraclass correlation coefficient and Bland-Altman analysis. Intra-observer reproducibility was determined by repeating the strain and strain rate measurements at 2 different time points by one experienced reader in 15 randomly selected patients. A second experienced reader performed the strain analysis in the same 15 patients, providing the inter-observer reproducibility data. Intra-class correlation coefficient and the mean bias with limits of agreement (2 SD) from Bland-Altman analysis are reported.

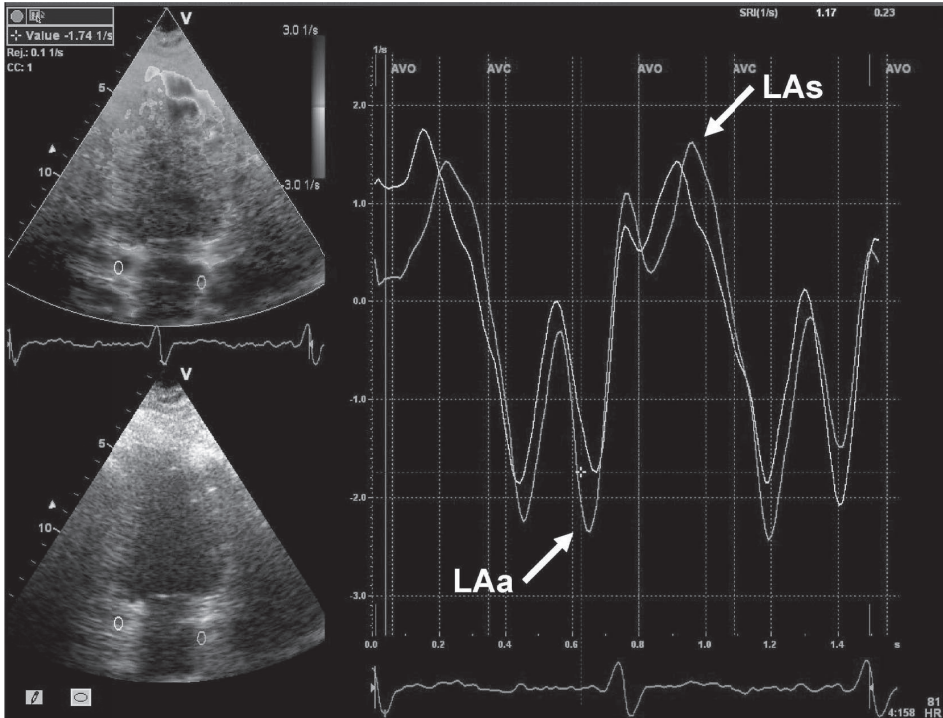


Figure 1. Strain rate imaging in the apical 2-chamber view in a patient at baseline. Samples are placed in the basal-mid atrial inferior (yellow) and anterior (green) atrial walls. With the use of the vertical green lines indicating aortic valve opening (AVO) and aortic valve closure (AVC), peak strain rate values of the different segments can be obtained (white arrows). LAa indicates peak LA strain rate during late ventricular diastole, representing the speed at which LA deformation during active contraction occurs. LAs indicates peak LA strain rate during ventricular systole, representing the speed at which LA deformation during LA expansion occurs.

To explore potential predictors of response, univariate analysis of baseline clinical and echocardiographic characteristics was performed first. Odds ratios were calculated with 95% confidence intervals as an estimate of the risk associated with each variable. Independent predictors of LA reverse remodeling were obtained by performing a multivariate logistic regression analysis based on enter model. Those variables with $p < 0.1$ at the univariate analysis were included. Statistical analyses were performed using SPSS software (version 15.0, SPSS Inc. Chicago, Illinois). All statistical tests were two-sided, and a p -value < 0.05 was considered significant.

RESULTS

Study population

A total of 148 patients were treated with radiofrequency catheter ablation. Baseline characteristics of the total study population are summarized in Table 1. Atrial fibrillation was paroxysmal in 112 patients (76%) and persistent in 36 patients (24%). Mean duration of follow-up was $13.2 \pm$

Table 1. Baseline characteristics of the study population

	All patients (n=148)	Responders (n=93)	Non-responders (n=55)	P-value *
Clinical characteristics				
Age, years	54 ± 9	55 ± 8	54 ± 10	0.5
Gender, M / F	117 / 31	75 / 18	42 / 13	0.5
Body surface area, m ²	2.1 ± 0.2	2.1 ± 0.2	2.1 ± 0.2	0.4
Type of AF				
Paroxysmal, n (%)	112 (76)	76 (82)	36 (65)	0.03
Persistent, n (%)	36 (24)	17 (18)	19 (35)	0.03
Duration of AF, years	5.3 ± 4.5	5.4 ± 4.2	5.2 ± 4.9	0.9
Previous anti-arrhythmic drugs, n	3.2 ± 1.5	3.3 ± 1.6	3.1 ± 1.3	0.4
ACE inhibitor / ATII, n (%)	72 (49)	46 (49)	26 (47)	0.9
Hypertension, n (%)	62 (42)	42 (30)	20 (36)	0.3
Coronary artery disease, n (%)	9 (6)	6 (6)	3 (5)	1.0
Echocardiographic characteristics				
LVEDV, ml/m ²	54 ± 12	54 ± 12	53 ± 12	0.4
LVESV, ml/m ²	23 ± 7	23 ± 7	23 ± 6	0.9
LVEF, %	57 ± 7	57 ± 8	56 ± 7	0.4
E/A	1.3 ± 0.4	1.3 ± 0.4	1.3 ± 0.4	0.8
Deceleration time (ms)	243 ± 70	247 ± 67	237 ± 77	0.5

* Responders vs. non-responders. ACE = angiotensin converting enzyme; AF = atrial fibrillation; ATII = angiotensin II receptor blocker; LVEDV = left ventricular end-diastolic volume; LVEF = left ventricular ejection fraction; LVESV = left ventricular end-systolic volume.

6.7 months. During follow-up, 99 patients (67%) remained in sinus rhythm, whereas 49 patients (33%) had recurrence of AF. None of the patients underwent a repeat procedure during follow-up.

Left atrial volumes and strain analysis

In the overall study population, LA diameter decreased from 43 ± 5 mm to 42 ± 5 mm ($p=0.003$) during follow-up. In addition, LA_{max} decreased significantly from baseline to follow-up (from 30 ± 7 ml/m² to 25 ± 7 ml/m², $p<0.001$). In parallel, LA_{min} decreased from 18 ± 6 ml/m² to 15 ± 7 ml/m² ($p<0.001$). Finally, there was a modest but statistically significant improvement in LA_{Ef} from baseline to follow-up in the overall study population (from $41 \pm 13\%$ to $45 \pm 14\%$, $p=0.002$).

Left atrial strain and strain rate measurements were feasible in 2078 of 2160 attempted segments (96%). In 15 randomly selected patients, reproducibility data for LA strain and LA strain rate measurements was assessed. Intra-observer agreement for the assessment of LA strain and LA strain rate was good. Intra-class correlation coefficients were: 0.8 for LA strain and 0.6 for LA strain rate. For LA strain, mean bias was 0.98 (limits of agreement: -4.39 – 6.34) without significant trend. For LA strain rate, mean bias was -0.02 (limits of agreement: -0.34 – 0.31) without significant trend. Similar, inter-observer agreement for LA strain and LA strain rate was good. Intra-class correlation coefficients were: 0.7 for LA strain and 0.8 for LA strain rate. For LA strain, mean bias was -0.14 (limits of agreement: -5.91 – 5.64). For LA strain rate, mean bias was -0.10 (limits of agreement: -0.21 – 0.42).

In the overall study population, LA deformation properties showed a significant improvement during follow-up. LAs strain increased from $17 \pm 7\%$ to $19 \pm 9\%$ ($p=0.001$), and LAs strain rate increased from 1.1 ± 0.4 1/s to 1.2 ± 0.5 1/s ($p=0.001$). Similar, LAa strain improved from

$-4 \pm 3\%$ to $-6 \pm 6\%$ ($p=0.03$), and LAa strain rate improved from -1.4 ± 0.7 1/s to -1.6 ± 0.7 1/s ($p=0.03$).

Left atrial reverse remodeling

Based on the cut-off value ($\geq 15\%$ decrease in LA_{max}), 93 patients (63%) were classified as a responder, whereas 55 patients (37%) were non-responders. Baseline characteristics of the two groups are listed in Table 1. The proportion of patients with paroxysmal AF was significantly higher among the responders compared with the non-responders (82% vs. 65%, $p=0.03$).

142

Responders vs. non-responders Mean follow-up duration was comparable in the 2 groups (responders 12.7 ± 5.2 months vs. non-responders 13.8 ± 8.6 months, $p=0.3$). Importantly, 69% ($n=38$) of the non-responders experienced recurrence of AF, as compared to 12% ($n=11$) of the responders ($p<0.001$). At follow-up, 34 responders (37%) and 17 non-responders (31%) were off anti-arrhythmic drugs ($p=0.6$). The majority of the patients were on either beta-blockers or class IC anti-arrhythmic drugs. There were no differences between the 2 groups regarding the use of beta-blockers (27% vs. 22%, respectively, $p=0.6$) and class IC anti-arrhythmic drugs (32% vs. 31%, $p=1.0$) at follow-up.

Left ventricular systolic strain significantly improved in the responders during follow-up (from $-20 \pm 5\%$ to $-22 \pm 4\%$, $p<0.05$), whereas it decreased in the non-responders (from $-20 \pm 5\%$ to $-18 \pm 5\%$, $p<0.05$). Similar, an improvement in LV systolic strain rate was noted in the responders, and an impairment was noted in the non-responders (Table 2).

Left atrial volume and strain analysis By definition, LA_{max} decreased significantly in the responders (from 31 ± 7 ml/m² to 22 ± 6 ml/m², $p<0.001$), whereas a small increase was observed in the non-responders (from 29 ± 5 ml/m² to 31 ± 6 ml/m², $p=0.002$). Left atrial diameter and LA_{min} were comparable in the 2 groups at baseline. However, a significant decrease was observed in the responders during follow-up, resulting in significant differences between the two groups at follow-up (Table 2). Finally, LA_{EF} increased significantly in the responders, whereas no change was noted in the non-responders (Table 2).

Left atrial deformation properties demonstrated different trends during follow-up according to the presence of LA reverse remodeling. LAs strain was significantly higher at baseline in the responders, as compared to the non-responders (Table 2). In addition, a significant increase in LAs strain was noted in the responders, whereas no change was observed in the non-responders (Figure 2). Similarly, LAs strain rate at baseline was significantly higher in the responders, as compared with the non-responders (Table 2). During follow-up, LAs strain rate increased significantly in the responders, whereas no change was observed in the non-responders (Table 2). Similar trends were noted for LAa strain and LAa strain rate. Whereas LAa strain and strain rate improved significantly in the responders, LAa strain remained similar and LAa strain rate decreased in the non-responders (Table 2 and Figure 2).

Table 2. Echocardiographic results of the study population at baseline and follow-up

	Responders	Non-responders	P-value *
LA diameter, mm			
Baseline	43 ± 4	43 ± 5	0.6
Follow-up	40 ± 4 †	45 ± 6 †	<0.001
LA _{max} , ml/m ²			
Baseline	31 ± 7	29 ± 5	0.04
Follow-up	22 ± 6 †‡	31 ± 6 †	<0.001
LA _{min} , ml/m ²			
Baseline	19 ± 6	17 ± 5	0.2
Follow-up	12 ± 5 †	19 ± 8	<0.001
LA _{EP} , %			
Baseline	41 ± 14	41 ± 12	0.9
Follow-up	46 ± 11 †	42 ± 18	0.1
LA _s strain, %			
Baseline	19 ± 8	14 ± 6	0.001
Follow-up	22 ± 9 †	15 ± 8	<0.001
LA _s strain rate, 1/s			
Baseline	1.2 ± 0.4	1.0 ± 0.4	0.02
Follow-up	1.4 ± 0.4 †	1.0 ± 0.4	<0.001
LA _a strain, % §			
Baseline	-4 ± 3	-4 ± 3	0.4
Follow-up	-6 ± 6 †	-4 ± 3	0.03
LA _a strain rate, 1/s §			
Baseline	-1.4 ± 0.7	-1.3 ± 0.9	0.3
Follow-up	-1.7 ± 0.7 †	-1.1 ± 0.7	<0.001
LV strain, % §			
Baseline	-20 ± 5	-20 ± 5	0.6
Follow-up	-22 ± 4 †	-18 ± 5 †	<0.001
LV strain rate, 1/s §			
Baseline	-1.2 ± 0.4	-1.1 ± 0.3	0.1
Follow-up	-1.4 ± 0.5 †	-1.0 ± 0.3	<0.001

* Responders vs. non-responders; † p<0.05 baseline vs. follow-up; ‡ by definition; § data available in 76 responders and 46 non-responders.

LA = left atrial; LA_{EP} = left atrial total emptying fraction; LA_{max} = maximum left atrial volume; LA_{min} = minimum left atrial volume; LV = left ventricular.

Prediction of LA reverse remodeling

Univariate and multivariate logistic regression analysis was performed to determine the predictors of LA reverse remodeling. The results of the logistic regression analysis are shown in Table 3. At multivariate analysis, the strongest predictors of LA reverse remodeling after catheter ablation were LA_s strain at baseline (Odds ratio 1.089; 95% CI 1.014-1.169, p=0.019) and LA_{max} (Odds ratio 1.086; 95% CI 1.018-1.159, p=0.012).

DISCUSSION

In the present study, LA reverse remodeling and LA strain were studied in 148 patients undergoing catheter ablation for AF. In 93 patients (63%), LA reverse remodeling was noted at long-term follow-up. In these patients, LA systolic and late diastolic strain and strain rate increased significantly from baseline to follow-up. In patients without LA reverse remodeling, no significant

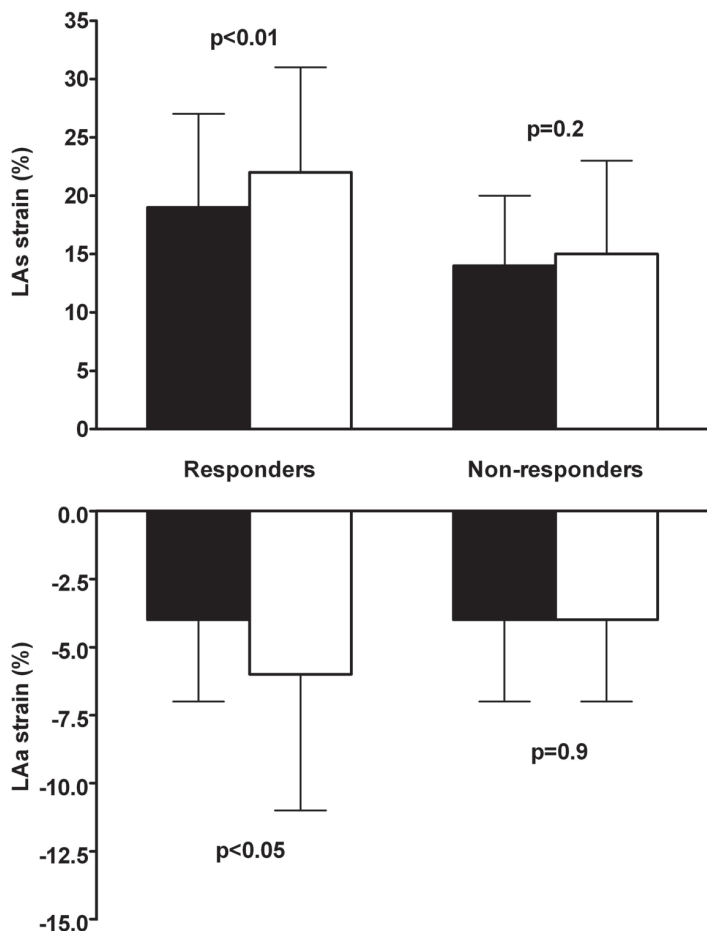


Figure 2. Changes in LAs strain and LAa strain according to LA reverse remodeling. From baseline (black bars) to follow-up (white bars), different changes in LAs strain (upper panel) and LAa strain (lower panel) were observed in the 2 groups. In the responders, a significant improvement in LAs strain and LAa strain was observed. In contrast, the non-responders did not show an improvement in LAs strain or LAa strain from baseline to follow-up.

changes in LA strain and strain rate were noted. Importantly, LAs strain at baseline was the strongest predictor of LA reverse remodeling.

Left atrial reverse remodeling

Left atrial remodeling includes structural, electrical, metabolic and neurohumoral changes, and may occur in response to several pathologic processes. Atrial dilatation is an important aspect of LA structural remodeling (1). Recently, it has been suggested that the extent of LA structural remodeling may play an important role in the success of AF ablation (16). Interestingly, several studies have demonstrated that this atrial enlargement is, at least partially, reversible. Reverse LA remodeling has been demonstrated with drug therapy (17), after mitral valve surgery (15),

Table 3. Univariate and multivariate logistic regression analysis for prediction of reverse remodeling after catheter ablation

	Univariate analysis		Multivariate analysis	
	OR (95% CI)	P-value	OR (95% CI)	P-value
Age	1.015 (0.977-1.054)	0.457
Hypertension	1.441 (0.727-2.858)	0.295
Type of AF	2.359 (1.098-5.071)	0.028	1.937 (0.846-4.438)	0.118
LVEF	1.022 (0.976-1.071)	0.349
LA _{max}	1.058 (1.003-1.117)	0.040	1.086 (1.018-1.159)	0.012
LAs strain	1.102 (1.039-1.168)	0.001	1.089 (1.014-1.169)	0.019
LAs strain rate	2.996 (1.163-7.716)	0.023	1.422 (0.502-4.027)	0.508

C-statistic: 0.712; OR = Odds ratio, other abbreviations as in Tables 1 and 2.

and with cardiac resynchronization therapy (18). In addition, successful catheter ablation for AF may result in reversal of LA dilatation (6).

Although the exact underlying pathophysiology of LA reverse remodeling remains unclear, it has been suggested that reversal of LA dilatation may have prognostic implications and may reduce the risk of AF (5). Therefore, LA reverse remodeling may become a surrogate marker of success after AF ablation. Typically, maintenance of sinus rhythm during follow-up is used to define successful catheter ablation (10). However, asymptomatic AF recurrence may result in overestimation of success. Importantly, in the present study, there is an overlap between responders and patients who maintained sinus rhythm (82 out of 93 responders), and non-responders and patients with recurrence of AF (38 out of 55 non-responders). Therefore, LA reverse remodeling may be a more robust marker for successful AF ablation that can easily be quantified.

Interestingly, in the patients that exhibited LA reverse remodeling, an improvement in LA function was observed in the present study. The concordance of LA reverse remodeling and improvement in LA function has previously been demonstrated (7). In addition, predictors for LA reverse remodeling were studied in the present study. Although the proportion of patients with paroxysmal and persistent AF was different among the responders and the non-responders, the type of AF was not predictive for LA reverse remodeling at multivariate analysis. This indicates that the type of AF is not an independent determinant of LA structural changes that deteriorate LA myocardial deformation and reduce the ability of the LA to reverse remodel. Interestingly, at multivariate analysis, LA systolic strain (as a novel marker of LA reservoir function) was the strongest predictor of LA reverse remodeling during follow-up.

Left atrial strain analysis

Recent studies have demonstrated the feasibility of strain analysis to assess segmental LA function (19). In LA function, three different phases can be distinguished: 1) LA reservoir function, during ventricular systole; 2) LA conduit function, during early ventricular diastole; 3) LA booster pump function, during late ventricular diastole. In the present study, tissue Doppler imaging was used to assess LA peak systolic and late diastolic strain, which represent LA reservoir function and LA booster pump function, respectively (20). At baseline, LA strain was impaired

as compared with previously reported values for healthy controls (21,22). Left atrial reservoir function is mainly determined by LV systolic function and LA wall stiffness (23). In patients with AF and preserved LVEF, subtle changes in LV and LA myocardium may already be present (24,25). Indeed, myocardial deformation imaging techniques may reveal these subtle changes. Impaired LAs strain and strain rate indicate reduced compliance of the LA, and may indirectly reflect high fibrosis content. These functional changes may therefore reflect structural changes that may determine the ability of the LA to reverse remodel after catheter ablation for AF.

Interestingly, an improvement in LA strain was observed in patients with LA reverse remodeling during follow-up. Several other studies have demonstrated improvements in LA strain in response to therapy. In a cohort of 107 heart failure patients undergoing cardiac resynchronization therapy, LA strain was assessed at baseline and after 3 months follow-up. In patients who exhibited LV reverse remodeling after cardiac resynchronization therapy, LA systolic strain improved from $16.8 \pm 9.8\%$ to $21.8 \pm 9.4\%$ ($p=0.002$), in parallel with LA reverse remodeling (26). Thomas et al. (27) noted improvements in LA strain and strain rate in 37 patients with AF who maintained sinus rhythm during 6 months after cardioversion. Similarly, it has been demonstrated that LA strain and strain rate may improve after catheter ablation for AF (8). Schneider et al. demonstrated a significant increase in LA systolic strain in patients who maintained sinus rhythm after catheter ablation, whereas it remained unchanged in patients with recurrence of AF. In addition, it was demonstrated that LA systolic strain and strain rate may predict the maintenance of sinus rhythm during 3 months follow-up (8).

In the present study, similar improvements in LA strain and strain rate were observed in 148 patients after long-term follow-up. In addition, it was demonstrated that LA strain at baseline was the strongest predictor for LA reverse remodeling during follow-up. Previously, it has been demonstrated that LA systolic strain may predict the maintenance of sinus rhythm after cardioversion (24). Although the exact mechanism remains to be elucidated, it may well be that the degree of impairment in atrial compliance (represented by LA systolic strain) plays an important role in the ability to reverse LA enlargement and maintain sinus rhythm during follow-up.

Interestingly, the improvements in LA strain and strain rate in the responders were accompanied by improvements in LV systolic strain. These findings suggest that LA and LV myocardial deformations are closely related. Restoration of sinus rhythm with catheter ablation results in an improved LA function and subsequent more efficient LV filling pattern and LV mechanics (7,28). At the same time, the improvement in LV systolic function and diastolic filling pattern due to heart rhythm normalization may result in an improved LA function, and may therefore be a determinant of LA reverse remodeling. Additional studies are warranted to elucidate whether the improvement in LV mechanics precedes the improvement in LA function or vice versa.

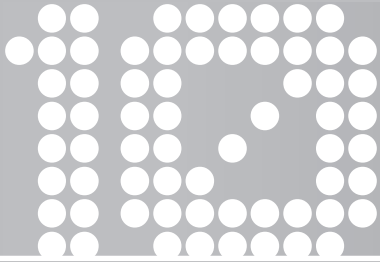
CONCLUSIONS

In the present study, 63% of the patients exhibited LA reverse remodeling after catheter ablation for AF. In these responders, LA strain and strain rate increased significantly from baseline to follow-up. In contrast, no changes in LA strain and strain rate were noted in the non-responders. Left atrial systolic strain at baseline was the strongest predictor of LA reverse remodeling.

REFERENCES

1. Abhayaratna WP, Seward JB, Appleton CP et al. Left atrial size: physiologic determinants and clinical applications. *J Am Coll Cardiol* 2006;47:2357-63.
2. Rossi A, Cicoira M, Zanolla L et al. Determinants and prognostic value of left atrial volume in patients with dilated cardiomyopathy. *J Am Coll Cardiol* 2002;40:1425.
3. Vaziri SM, Larson MG, Benjamin EJ, Levy D. Echocardiographic predictors of nonrheumatic atrial fibrillation. The Framingham Heart Study. *Circulation* 1994;89:724-30.
4. Sanfilippo AJ, Abascal VM, Sheehan M et al. Atrial enlargement as a consequence of atrial fibrillation. A prospective echocardiographic study. *Circulation* 1990;82:792-7.
5. Casaciang-Verzosa G, Gersh BJ, Tsang TS. Structural and functional remodeling of the left atrium: clinical and therapeutic implications for atrial fibrillation. *J Am Coll Cardiol* 2008;51:1-11.
6. Tops LF, Bax JJ, Zeppenfeld K, Jongbloed MR, van der Wall EE, Schalij MJ. Effect of radiofrequency catheter ablation for atrial fibrillation on left atrial cavity size. *Am J Cardiol* 2006;97:1220-2.
7. Marsan NA, Tops LF, Holman ER et al. Comparison of left atrial volumes and function by real-time three-dimensional echocardiography in patients having catheter ablation for atrial fibrillation with persistence of sinus rhythm versus recurrent atrial fibrillation three months later. *Am J Cardiol* 2008;102:847-53.
8. Schneider C, Malisius R, Krause K et al. Strain rate imaging for functional quantification of the left atrium: atrial deformation predicts the maintenance of sinus rhythm after catheter ablation of atrial fibrillation. *Eur Heart J* 2008;29:1397-409.
9. Tops LF, Bax JJ, Zeppenfeld K et al. Fusion of multislice computed tomography imaging with three-dimensional electroanatomic mapping to guide radiofrequency catheter ablation procedures. *Heart Rhythm* 2005;2:1076-81.
10. Calkins H, Brugada J, Packer DL et al. HRS/EHRA/ECAS expert Consensus Statement on catheter and surgical ablation of atrial fibrillation: recommendations for personnel, policy, procedures and follow-up. *Heart Rhythm* 2007;4:816-61.
11. Schiller NB, Shah PM, Crawford M et al. Recommendations for quantitation of the left ventricle by two-dimensional echocardiography. *J Am Soc Echocardiogr* 1989;2:358-67.
12. Rakowski H, Appleton C, Chan KL et al. Canadian consensus recommendations for the measurement and reporting of diastolic dysfunction by echocardiography: from the Investigators of Consensus on Diastolic Dysfunction by Echocardiography. *J Am Soc Echocardiogr* 1996;9:736-60.
13. Abraham TP, Dimaano VL, Liang HY. Role of tissue Doppler and strain echocardiography in current clinical practice. *Circulation* 2007;116:2597-609.
14. Lang RM, Bierig M, Devereux RB et al. Recommendations for Chamber Quantification. *J Am Soc Echocardiogr* 2005;18:1440-63.
15. Westenberg JJ, van der Geest RJ, Lamb HJ et al. MRI to evaluate left atrial and ventricular reverse remodeling after restrictive mitral annuloplasty in dilated cardiomyopathy. *Circulation* 2005;112:1437-1442.
16. Oakes RS, Badger TJ, Kholmovski EG et al. Detection and quantification of left atrial structural remodeling with delayed-enhancement magnetic resonance imaging in patients with atrial fibrillation. *Circulation* 2009;119:1758-67.
17. Tsang TS, Barnes ME, Abhayaratna WP et al. Effects of quinapril on left atrial structural remodeling and arterial stiffness. *Am J Cardiol* 2006;97:916-20.
18. Marsan NA, Bleeker GB, Ypenburg C et al. Real-time three-dimensional echocardiography as a novel approach to assess left ventricular and left atrium reverse remodeling and to predict response to cardiac resynchronization therapy. *Heart Rhythm* 2008;5:1257-64.
19. Leung DY, Boyd A, Ng AA, Chi C, Thomas L. Echocardiographic evaluation of left atrial size and function: current understanding, pathophysiologic correlates, and prognostic implications. *Am Heart J* 2008;156:1056-64.

20. Zhang Q, Yip GW, Yu CM. Approaching regional left atrial function by tissue Doppler velocity and strain imaging. *Eurpace* 2008;10 Suppl 3:iii62-iii69.
21. Gulel O, Yuksel S, Soylu K et al. Evaluation of left atrial functions by color tissue Doppler imaging in adults with body mass indexes ≥ 30 kg/m² versus those < 30 kg/m². *Int J Cardiovasc Imaging* 2009;25:371-7.
22. Wang Z, Tan H, Zhong M, Jiang G, Zhang Y, Zhang W. Strain rate imaging for noninvasive functional quantification of the left atrium in hypertensive patients with paroxysmal atrial fibrillation. *Cardiology* 2008;109:15-24.
23. Barbier P, Solomon SB, Schiller NB, Glantz SA. Left atrial relaxation and left ventricular systolic function determine left atrial reservoir function. *Circulation* 1999;100:427-36.
24. Di Salvo G, Caso P, Lo PR et al. Atrial myocardial deformation properties predict maintenance of sinus rhythm after external cardioversion of recent-onset lone atrial fibrillation: a color Doppler myocardial imaging and transthoracic and transesophageal echocardiographic study. *Circulation* 2005;112:387-95.
25. Boyd AC, Schiller NB, Ross DL, Thomas L. Differential recovery of regional atrial contraction after restoration of sinus rhythm after intraoperative linear radiofrequency ablation for atrial fibrillation. *Am J Cardiol* 2009;103:528-34.
26. Yu CM, Fang F, Zhang Q et al. Improvement of atrial function and atrial reverse remodeling after cardiac resynchronization therapy for heart failure. *J Am Coll Cardiol* 2007;50:778-85.
27. Thomas L, McKay T, Byth K, Marwick TH. Abnormalities of left atrial function after cardioversion: an atrial strain rate study. *Heart* 2007;93:89-95.
28. Tops LF, den Uijl DW, Delgado V et al. Long-term improvement in left ventricular strain after successful catheter ablation for atrial fibrillation in patients with preserved left ventricular systolic function. *Circ Arrhythmia Electrophysiol* 2009;2:249-57.



Long-term improvement in left ventricular strain after successful catheter ablation for atrial fibrillation in patients with preserved left ventricular systolic function

Laurens F. Tops
Dennis W. Den Uijl
Victoria Delgado
Nina Ajmone Marsan
Katja Zeppenfeld
Eduard R. Holman
Ernst E. van der Wall
Martin J. Schalij
Jeroen J. Bax

Department of Cardiology, Leiden University Medical Center, Leiden, the Netherlands

Circ Arrhythmia Electrophysiol 2009;2:249-57

ABSTRACT

Background: The effect of successful catheter ablation on left ventricular (LV) strain in patients with preserved LV systolic function is unknown. The aim of the present study was to assess the long-term effects of catheter ablation for atrial fibrillation (AF) on LV strain and strain rate in patients with preserved LV ejection fraction.

Methods and Results: In 78 patients undergoing catheter ablation for AF, speckle tracking strain imaging was performed to assess LV strain in 3 directions (radial, circumferential and longitudinal) at baseline and after 12 months follow-up. The study population was divided into 2 groups, according to the maintenance of sinus rhythm during follow-up. After 13.8 ± 4.7 months follow-up, 54 patients (69%) were in sinus rhythm (SR-group), whereas 24 patients (31%) had recurrence of AF (AF-group). No significant changes in LV ejection fraction from baseline to follow-up were noted ($60 \pm 7\%$ vs. $59 \pm 7\%$, $p=NS$). Circumferential strain improved significantly in the SR-group ($-18.3 \pm 3.2\%$ vs. $-20.4 \pm 3.8\%$, $p<0.001$), whereas it remained unchanged in the AF-group ($-18.9 \pm 3.5\%$ vs. $-17.9 \pm 3.1\%$, $p=NS$). In the SR-group, significant improvements in LV longitudinal strain and strain rate were noted, whereas in the AF-group, LV longitudinal strain and strain rate deteriorated significantly at long-term follow-up.

Conclusion: After successful catheter ablation, LV circumferential and longitudinal strain and strain rate improve significantly in patients who maintain sinus rhythm. In contrast, a decrease in LV longitudinal strain and strain rate is observed in patients with recurrence of AF.

INTRODUCTION

Radiofrequency catheter ablation procedures are considered a reasonable option in the treatment of patients with highly symptomatic, drug-refractory atrial fibrillation (AF). It has been demonstrated that these procedures can effectively restore sinus rhythm and provide long-term relief of symptoms (1). Furthermore, reverse remodeling and functional improvement of the left atrium (LA) has been reported after successful catheter ablation for AF (2,3).

In addition, the restoration of sinus rhythm may result in an improvement in left ventricular (LV) systolic function. It has been demonstrated that LV ejection fraction improves following successful catheter ablation in patients with systolic heart failure (4-6). In patients with preserved systolic function however, studies have failed to demonstrate a change in LV ejection fraction after catheter ablation (7). It is likely however, that LV ejection fraction does not reflect subtle changes in systolic LV function, and therefore the effect of catheter ablation on LV systolic function cannot be detected by measuring LV ejection fraction. Recently, two-dimensional (2D) speckle tracking strain imaging has been introduced (8,9). This novel technique may detect more subtle abnormalities in LV systolic function, as compared with conventional parameters such as LV ejection fraction (10). In addition, it allows angle-independent evaluation of LV systolic strain in 3 directions: radial, circumferential, and longitudinal (11).

Accordingly, the purpose of the present study was to assess the long-term effects of catheter ablation for AF on LV function and deformation properties. Two-dimensional speckle tracking strain imaging was used to study LV strain and strain rate in patients with maintenance of sinus rhythm and patients with recurrence of AF after radiofrequency catheter ablation.

METHODS

Study population and study protocol

The study population comprised selected patients with symptomatic drug-refractory AF, who were referred for radiofrequency catheter ablation. Before the ablation procedure and after 12 months follow-up, an extensive echocardiographic evaluation was performed. To minimize the confounding effect of variations in heart rhythm on LV deformation properties, only patients with an available echocardiogram during sinus rhythm at baseline and at follow-up were studied. In addition, patients with moderate or severe valvular disease, or patients with a history of heart failure or coronary artery bypass graft were excluded from the study. Out of 98 patients who underwent radiofrequency catheter ablation, 20 patients were excluded because of the presence of AF during the baseline or follow-up echocardiogram. The remaining 78 patients formed the study population of the present study.

To study the effect of successful catheter ablation on LV function and deformation properties, the study population was divided into 2 groups, according to the maintenance of sinus

rhythm during the 12 months follow-up. In addition, LV function and deformation properties were assessed in a group of 20 healthy controls matched for age, gender, body surface area who were selected from an echocardiographic database.

Radiofrequency catheter ablation

The catheter ablation procedure was aimed at electrical isolation of all pulmonary veins from the LA, and has been described in more detail elsewhere (12). In brief, endocardial mapping and ablation was performed with a 4 mm quadripolar mapping/ablation catheter (7F Thermo-cool, Biosense Webster, Diamond Bar, California), using an electroanatomical mapping system (CARTO™, Biosense Webster). A 6F diagnostic catheter placed in the right atrium served as a temporal reference. Radiofrequency current was applied outside the ostia of all pulmonary veins, using the ablation catheter with a 4 mm open loop irrigated tip (maximum flow 20 mL/min, maximum temperature 50°C, maximum radiofrequency energy 30 W). At each ablation point, radiofrequency current was applied until a voltage <0.1 mV was achieved, with a maximum of 60 seconds per point. Pulmonary vein isolation was confirmed by recording entrance block during sinus rhythm or pacing in the coronary sinus (1). All patients received heparin intravenously (activated clotting time 300-400 sec) to avoid thrombo-embolic complications.

Follow-up

After the catheter ablation procedure, patients were evaluated at the out-patient clinic on a regular basis. All medication, including anti-arrhythmic drugs, was continued in all patients during the first 3 months after the ablation procedure. Thereafter, anti-arrhythmic drugs were discontinued at the discretion of the physician. A surface ECG was acquired at every follow-up visit, and 24-hours Holter monitoring was performed at 3 to 6 months intervals. A successful catheter ablation was defined as the absence of symptomatic recurrences lasting more than 3 minutes and/or the absence of AF episodes lasting more than 30 seconds detected with 24-hours Holter monitoring or surface ECG, after a blanking period of 1 month (1).

Subsequently, the study population was divided into 2 groups according to the absence or presence of AF during follow-up. The 'SR-group' comprised patients with maintenance of sinus rhythm during follow-up, whereas patients in the 'AF-group' had recurrence of AF during follow-up. Clinical and echocardiographic variables at baseline and at 12 months follow-up were compared between the 2 groups.

Echocardiography

Two-dimensional echocardiography was performed within 2 days before the ablation procedure, and after 12 months follow-up. Images were recorded with patients in the left lateral decubitus position using a commercially available system (Vivid 7, General Electric Vingmed, Milwaukee, Wisconsin).

Images acquisition was performed using a 3.5-MHz transducer at a depth of 16 cm in the standard parasternal and apical views (standard long-axis and 2- and 4-chamber images). Standard M-mode and 2D images including color Doppler data from 3 consecutive heart beats were saved in cine loop format. All analyses were performed off-line using commercial software (Echopac 6.1, General Electric Vingmed).

The anteroposterior diameter of the LA was measured at end-systole on the M-mode image obtained from the parasternal long-axis view (13). Left atrial volume was calculated using the biplane area-length method (13). In addition, LV end-diastolic and end-systolic diameters were acquired from the parasternal long-axis view (13). Left ventricular end-diastolic and end-systolic volumes were assessed from the apical 2- and 4-chamber images, and LV ejection fraction was calculated using the biplane Simpson's rule (14). Finally, LV diastolic function was assessed using the mitral inflow pattern from the pulsed-wave Doppler images (15), and tissue Doppler imaging. The ratio of early (E) to late (A) diastolic filling velocities (E/A), deceleration time of the E wave, the septal early diastolic mitral annular motion velocity (E'), and the E/E' ratio were assessed. Subsequently, LV diastolic function was classified as being normal, abnormal relaxation (mild diastolic dysfunction, grade 1), pseudonormal filling (moderate diastolic dysfunction, grade 2) or restrictive filling pattern (severe diastolic dysfunction, grade 3) (16,17).

Left ventricular strain analysis

On standard gray-scale images (frame rate 75 ± 11 frames/s), 2D speckle tracking strain imaging was used to study LV deformation. Novel speckle-tracking software was used, as previously described (8,9,18). Briefly, this technique permits angle-independent measurement of myocardial strain in 3 different directions (radial, circumferential, and longitudinal). It tracks the characteristic pattern of natural acoustic markers present in the myocardial wall ('speckles') from frame-to-frame throughout the cardiac cycle. Myocardial strain is then calculated by the change in position of the speckle pattern with respect to the initial position (8,9).

Three distinct patterns of LV deformation were assessed: 1) radial strain; representing myocardial thickening/thinning in the short-axis plane; 2) circumferential strain; representing myocardial shortening/lengthening in the short-axis plane; and 3) longitudinal strain; representing myocardial shortening/lengthening in the long-axis plane. Peak systolic radial and circumferential strain/strain rate were calculated by averaging the peak systolic values of the 6 segments from the LV mid ventricular short-axis view. Peak systolic longitudinal strain/strain rate was calculated by averaging the peak systolic values of the 18 segments, derived from the 6 segments of the 3 apical views (2-, 4-chamber and apical long axis views) (Figure 1). For myocardial strain, regional thickening or lengthening is expressed as a positive value, and thinning or shortening as a negative value (19). Finally, strain rate (expressed in 1/s) was calculated in all 3 directions, representing the speed at which myocardial deformation occurs (19).

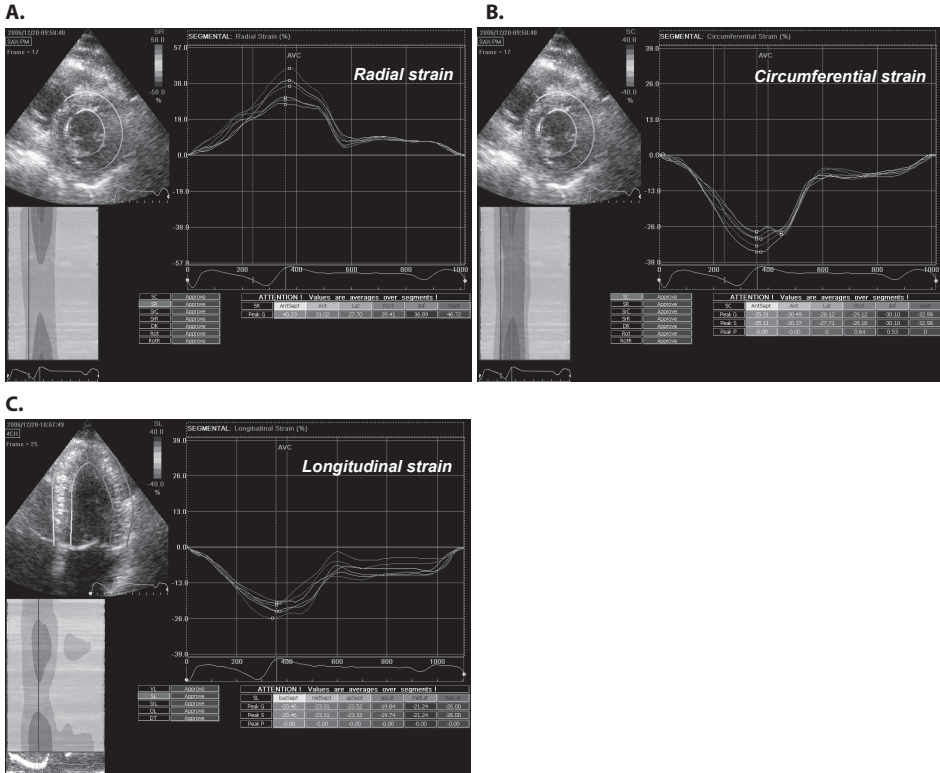


Figure 1. Assessment of left ventricular strain. Left ventricular strain was assessed in 3 directions: radial strain (upper panel) and circumferential strain (middle panel) were assessed on short-axis images. Longitudinal strain (lower panel) was assessed on standard apical images.

Statistical analysis

All continuous variables had normal distribution (as evaluated by Kolmogorov-Smirnov tests). Summary statistics for these variables are therefore presented as mean values ± one standard deviation (SD). Categorical data are summarized as frequencies and percentages. Differences in clinical and echocardiographic variables between the SR-group and the AF-group were evaluated using unpaired Student t-tests (continuous variables), Chi-square tests or Fisher’s exact tests (dichotomous variables), as appropriate. Changes in echocardiographic variables from baseline to follow-up were evaluated using paired Student t-tests.

Intra- and inter-observer reproducibility of strain and strain rate measurements by 2-dimensional speckle tracking strain analysis was determined by linear regression (Pearson’s correlation coefficient) and Bland-Altman analysis. Intra-observer reproducibility was determined by repeating the strain and strain rate measurements at two different time points by one experienced reader in 20 randomly selected patients. A second experienced reader performed the strain analysis in the same 20 patients, providing the inter-observer reproducibility data.

Multivariate logistic regression analysis based on enter model was performed for the prediction of the maintenance of sinus rhythm at follow-up. The dependent variable was the

maintenance of sinus rhythm. As independent variables, the number of antiarrhythmic drugs, LA remodeling (represented by the change in LA volume), change in mean arterial pressure and LV mass index, change in longitudinal strain and change in circumferential strain after catheter ablation were entered in the model. Model discrimination was assessed using c-statistic. All analyses were performed using SPSS software (version 12.0, SPSS Inc. Chicago, Illinois, USA). All statistical tests were two-sided, and a p-value <0.05 was considered significant.

RESULTS

Study population

The baseline characteristics of the study population are summarized in Table 1. The majority of the patients had paroxysmal AF (67 patients, 86%), in 11 patients (14%) persistent AF was present. Mean time from the first documented AF episode to the radiofrequency catheter ablation procedure was 5.9 ± 3.9 years. A mean of 3.4 ± 1.4 different anti-arrhythmic drugs per patient had been used previously.

Table 1. Baseline characteristics of the study population

	All patients (n=78)	SR-group (n=54)	AF-group (n=24)	P value *
Age, yrs	54 ± 9	54 ± 9	54 ± 8	NS
Gender, M/F	63 / 15	43 / 11	20 / 4	NS
Body surface area, m ²	2.1 ± 0.2	2.1 ± 0.2	2.1 ± 0.1	NS
Heart rate, bpm	62 ± 11	61 ± 9	63 ± 15	NS
Blood pressure				
Systolic, mmHg	133 ± 16	133 ± 16	135 ± 16	NS
Diastolic, mmHg	81 ± 12	81 ± 12	82 ± 11	NS
LV mass index, g/m ²	111 ± 24	109 ± 26	117 ± 20	NS
Type of AF				
Paroxysmal, n (%)	67 (86)	49 (91)	18 (75)	NS
Persistent, n (%)	11 (14)	5 (9)	6 (25)	NS
Duration of AF, yrs	5.9 ± 3.9	6.0 ± 4.2	4.2 ± 3.0	NS
Anti-arrhythmic drugs used per patient	3.4 ± 1.4	3.6 ± 1.4	3.1 ± 1.3	NS
Beta-blocker, n (%)	36 (46)	23 (43)	13 (54)	NS
Calcium channel blocker, n (%)	7 (9)	4 (7)	3 (13)	NS
Class IC anti-arrhythmic drug, n (%)	27 (35)	19 (35)	8 (33)	NS
Amiodarone, n (%)	25 (32)	19 (35)	6 (25)	NS
ACE inhibitor / ATII, n (%)	40 (51)	27 (50)	13 (54)	NS
Statin, n (%)	20 (26)	14 (26)	6 (25)	NS
Hypertension, n (%)	36 (46)	22 (41)	14 (58)	NS
Diabetes Mellitus, n (%)	4 (5)	3 (6)	1 (4)	NS
Coronary artery disease, n (%)	5 (6)	4 (7)	1 (4)	NS

* SR-group vs. AF-group; ACE = Angiotensin converting enzyme; AF = atrial fibrillation; ATII = Angiotensin II receptor blocker.

After a mean of 13.8 ± 4.7 months follow-up, 54 patients (69%) were in sinus rhythm (SR-group), whereas 24 patients (31%) had recurrence of AF (AF-group). The study population was subsequently divided into 2 groups, according to the success of the catheter ablation procedure. No significant differences in baseline characteristics were noted between the 2 groups (Table 1).

In the total study population, no significant differences in heart rate between the baseline and follow-up echocardiogram were noted (baseline 62 ± 11 bpm vs. follow-up 63 ± 20 bpm, $p=NS$). In addition, no differences between the 2 groups at the follow-up echocardiogram were noted (SR-group 64 ± 9 bpm vs. AF-group 62 ± 10 bpm, $p=NS$). In the overall study population, no differences in mean systolic (from 133 ± 16 mmHg to 131 ± 16 mmHg, $p=NS$) or diastolic (from 81 ± 12 mmHg to 80 ± 9 mmHg, $p=NS$) blood pressure was noted during follow-up.

In addition, there were no differences between the SR-group and the AF-group with regard to the use of anti-arrhythmic drugs at baseline (Table 1). At follow-up, 27 patients (35%) used beta-blockers (including Sotalol), 1 patient (1%) used a calcium channel blocker, 17 patients (22%) used a class IC anti-arrhythmic drug, and 6 patients (8%) used Amiodarone. At follow-up, there were no significant differences in the use of anti-arrhythmic drugs between the SR-group and the AF-group, except for the use of beta-blockers (SR-group $n=12$ [35%] vs. AF-group $n=15$ [63%], $p<0.01$). By definition of the study protocol, all patients were in sinus rhythm during both echocardiographic evaluations.

Echocardiographic changes during follow-up

In the overall study population, a decrease in LA diameter and LA volume was noted from baseline to follow-up (Table 2). Interestingly, this decrease in LA diameter was more pronounced in the SR-group (baseline 43 ± 5 mm vs. follow-up 40 ± 5 mm, $p<0.01$), as compared with the AF-group (baseline 45 ± 5 mm vs. follow-up 45 ± 5 mm, $p=NS$). Similar, LA volumes decreased significantly in the SR-group from baseline to follow-up (from 58 ± 18 ml to 51 ± 14 ml, $p<0.01$), whereas no changes in LA volumes were noted in the AF-group (from 65 ± 17 ml to 64 ± 21 ml, $p=NS$).

Table 2. Echocardiographic parameters at baseline and at long-term follow-up in the total study population

	Baseline (n=78)	Follow-up (n=78)	P value
LA diameter, mm	44 ± 5	42 ± 5	<0.05
LA volume, ml	60 ± 18	55 ± 17	<0.01
E/A ratio	1.3 ± 0.5	1.4 ± 0.5	<0.05
Deceleration time, ms	236 ± 48	234 ± 56	NS
E/E' ratio	8.8 ± 3.4	8.8 ± 4.2	NS
LV end-diastolic diameter, mm	54 ± 5	54 ± 5	NS
LV end-systolic diameter, mm	32 ± 6	32 ± 6	NS
LV end-diastolic volume, ml	124 ± 29	124 ± 28	NS
LV end-systolic volume, ml	49 ± 17	50 ± 15	NS
LV ejection fraction, %	60 ± 7	59 ± 7	NS

LA = left atrial; LV = left ventricular.

In addition, an improvement in diastolic function was observed in the overall study population (Table 2). Mean E/A ratio increased from 1.3 ± 0.5 to 1.4 ± 0.5 ($p < 0.05$). At baseline, 48 patients (62%) had normal diastolic function, whereas 21 patients (27%) had mild diastolic dysfunction and 9 patients (11%) had moderate diastolic dysfunction. At long-term follow-up, 16 patients improved in diastolic function: 59 patients (76%) had normal diastolic function, and 12 patients (15%) had mild, and 7 patients (9%) had moderate diastolic dysfunction.

Finally, LV dimensions and volumes were similar at baseline and at follow-up in the overall study population (Table 2). In addition, there was no significant change in LV ejection fraction (from $60 \pm 7\%$ to $59 \pm 7\%$, $p = \text{NS}$). Both in the SR-group and in the AF-group, no significant changes were noted in LV volumes and LV ejection fraction from baseline to follow-up (Table 3).

Table 3. Left ventricular systolic function and strain/ strain rate at baseline and follow-up in the SR-group and the AF-group

	SR-group (n=54)	AF-group (n=24)	P value
LV end-diastolic diameter, mm			
Baseline	53 ± 6	55 ± 4	NS
Follow-up	53 ± 6	55 ± 5	NS
LV end-systolic diameter, mm			
Baseline	32 ± 6	33 ± 5	NS
Follow-up	32 ± 5	34 ± 7	NS
LV end-diastolic volume, ml			
Baseline	123 ± 30	127 ± 26	NS
Follow-up	124 ± 30	123 ± 23	NS
LV end-systolic volume, ml			
Baseline	49 ± 17	49 ± 17	NS
Follow-up	51 ± 15	49 ± 13	NS
LV ejection fraction, %			
Baseline	60 ± 7	62 ± 7	NS
Follow-up	59 ± 7	61 ± 6	NS
GRS, %			
Baseline	40.1 ± 17.0	39.1 ± 13.1	NS
Follow-up	37.2 ± 15.2	38.3 ± 15.3	NS
GRSr, 1/s			
Baseline	1.9 ± 0.6	1.7 ± 0.5	NS
Follow-up	1.9 ± 0.6	1.7 ± 0.4	NS
GCS, %			
Baseline	-18.3 ± 3.2	-18.9 ± 3.5	NS
Follow-up	$-20.4 \pm 3.8 \ddagger$	-17.9 ± 3.1	<0.05
GCSr, 1/s			
Baseline	-1.1 ± 0.3	-1.1 ± 0.2	NS
Follow-up	$-1.2 \pm 0.3 \dagger$	-1.1 ± 0.2	<0.05
GLS, %			
Baseline	-18.8 ± 2.7	-19.1 ± 1.5	NS
Follow-up	$-19.6 \pm 2.6 \ddagger$	$-17.9 \pm 1.8 \dagger$	<0.05
GLSr, 1/s			
Baseline	-0.9 ± 0.1	-1.0 ± 0.1	NS
Follow-up	$-1.0 \pm 0.1 \dagger$	$-0.9 \pm 0.1 *$	<0.001

* $p < 0.05$ vs. baseline; † $p < 0.01$ vs. baseline; ‡ $p < 0.001$ vs. baseline; GCS = Global circumferential strain; GCSr = Global circumferential strain rate; GLS = Global longitudinal strain; GLSr = Global longitudinal strain rate; GRS = Global radial strain; GRSr = Global radial strain rate; LV = left ventricular.

Left ventricular strain and strain rate

Linear regression analysis demonstrated good intra- and inter-observer agreement for the radial, circumferential and longitudinal strain and strain rate measurements (Table 4). In addition, Bland-Altman analysis showed a small bias for all strain and strain rate measurements performed by the same observer (intra-observer variability) and the two different observers (inter-observer variability) (Table 4).

Table 4. Intra- and inter-observer reproducibility of myocardial strain and strain rate

	Intra-observer		Inter-observer	
	Mean difference \pm 2SD *	r^\dagger	Mean difference \pm 2SD *	r^\dagger
Radial strain (%)	1.40 \pm 11.52	0.94	-4.83 \pm 12.80	0.89
Radial strain rate (1/s)	0.14 \pm 0.36	0.94	-0.14 \pm 0.64	0.88
Circumferential strain (%)	-0.35 \pm 3.96	0.85	-1.21 \pm 4.51	0.88
Circumferential strain rate (1/s)	-0.02 \pm 0.26	0.87	-0.01 \pm 0.30	0.86
Longitudinal strain (%)	-0.51 \pm 2.66	0.91	0.57 \pm 3.40	0.87
Longitudinal strain rate (1/s)	-0.06 \pm 0.12	0.91	0.01 \pm 0.24	0.86

* As assessed with Bland-Altman analysis; † as assessed with linear regression analysis.

Strain and strain rate values for the overall study population at baseline were compared with a group of 20 healthy controls (mean LV ejection fraction $60 \pm 7\%$). Radial strain and radial strain rate were not significantly different between the overall study population and the healthy controls ($40.1 \pm 15.6\%$ vs. $40.8 \pm 11.7\%$, $p=NS$; and 1.8 ± 0.6 1/s vs. 1.9 ± 0.6 1/s, $p=NS$, respectively). In contrast, both circumferential strain and circumferential strain rate were significantly reduced in the study population, as compared to the controls ($-18.4 \pm 3.1\%$ vs. $-20.1 \pm 3.3\%$, $p<0.05$; and -1.1 ± 0.2 1/s vs. -1.3 ± 0.3 1/s, $p<0.05$). Similar, both longitudinal strain and longitudinal strain rate were significantly lower in the overall study population, as compared to the healthy controls ($-18.9 \pm 2.4\%$ vs. $-20.4 \pm 2.1\%$, $p<0.05$; and -0.9 ± 0.1 1/s vs. -1.1 ± 0.2 1/s, $p<0.01$).

In the overall study population, radial strain did not change significantly from baseline to follow-up (from $40.6 \pm 15.1\%$ to $37.5 \pm 15.1\%$, $p=NS$). In addition, radial strain rate was similar at baseline and follow-up (1.8 ± 0.6 1/s and 1.8 ± 0.6 1/s, respectively; $p=NS$). Within the 2 groups, no differences were noted for radial strain and radial strain rate at baseline and at long-term follow-up (Table 3). Radial strain at long-term follow-up was comparable in the SR-group and the AF-group (Figure 2).

In contrast, circumferential strain improved significantly from baseline to follow-up in the total study population (from $-18.6 \pm 3.2\%$ to $-19.7 \pm 3.6\%$, $p<0.01$). Similar, circumferential strain rate improved significantly from baseline to follow-up (from -1.1 ± 0.2 1/s to -1.2 ± 0.3 1/s, $p<0.05$). Baseline values for circumferential strain and strain rate were comparable for the SR-group and the AF-group (Table 3). Importantly, circumferential strain and strain rate improved only in the SR-group from baseline to follow-up (from $-18.3 \pm 3.2\%$ to $-20.4 \pm 3.8\%$, $p<0.001$; and from -1.1 ± 0.3 1/s to -1.2 ± 0.3 1/s, $p<0.01$, respectively), whereas no significant changes

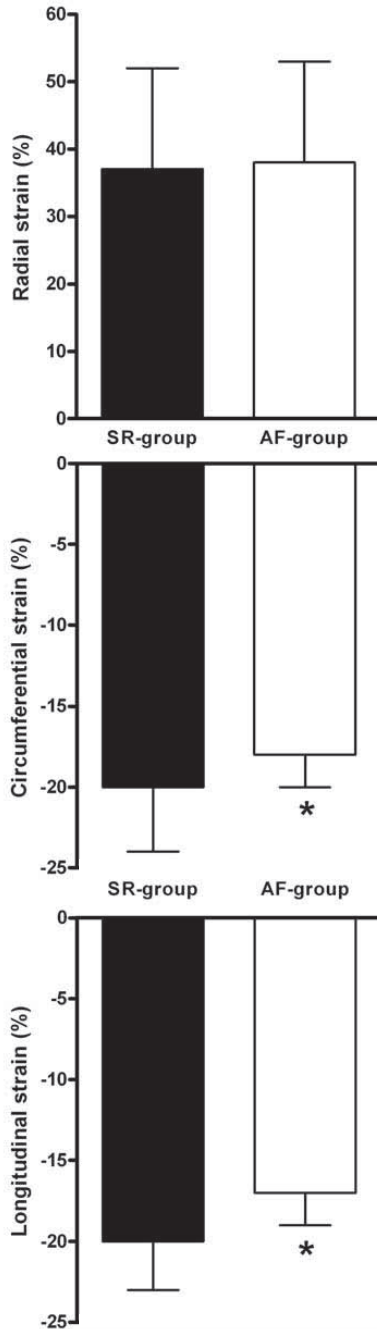


Figure 2. The strain values at follow-up are demonstrated for both the SR-group (black bars) and the AF-group (white bars). After long-term follow-up, radial strain (upper panel) was comparable in the SR-group ($37.2 \pm 15.2\%$) and the AF-group ($38.3 \pm 15.3\%$). However, circumferential strain (middle panel) and longitudinal strain (lower panel) were significantly lower in the AF-group ($-17.9 \pm 3.1\%$ and $-17.9 \pm 1.8\%$, respectively), as compared with the SR-group ($-20.4 \pm 3.8\%$ and $-19.6 \pm 2.6\%$, respectively). * $p < 0.05$

were noted in the AF-group (Table 3). As a result, circumferential strain at long-term follow-up was significantly higher in the SR-group, as compared with the AF-group (Figure 2).

Longitudinal strain was not significantly different at baseline and follow-up in the total study population ($-18.9 \pm 2.4\%$ and $-19.1 \pm 2.5\%$ respectively, $p=NS$). In addition, longitudinal strain rate was similar at baseline -1.0 ± 0.1 1/s and follow-up -1.0 ± 0.1 1/s, $p=NS$). However, the changes in longitudinal strain and strain rate from baseline to follow-up were different in the 2 groups: Whereas longitudinal strain improved significantly in the SR-group (from $-18.8 \pm 2.7\%$ to $-19.6 \pm 2.6\%$, $p<0.001$), it deteriorated significantly in the AF-group (from $-19.1 \pm 1.5\%$ to $-17.9 \pm 1.8\%$, $p<0.01$). At long-term follow-up longitudinal strain was significantly different between the 2 groups (Figure 2). In the SR-group, 37 of the 54 patients (69%) demonstrated an improvement in longitudinal strain (from $-18.5 \pm 2.8\%$ to $-20.0 \pm 2.6\%$, $p<0.001$), whereas 17 of the 37 patients (31%) in the SR-group showed no improvement (from $-19.6 \pm 2.4\%$ to $-18.9 \pm 2.4\%$, $p<0.01$). In the AF-group, 18 of the 24 patients (75%) exhibited deterioration in longitudinal strain (from $-19.7 \pm 1.6\%$ to $-17.6 \pm 1.7\%$, $p<0.001$), whereas 6 of the 24 patients (25%) did not exhibit deterioration in longitudinal strain (from $-18.3 \pm 1.7\%$ to $-18.8 \pm 1.8\%$, $p=NS$). Similarly, longitudinal strain rate improved significantly in the SR-group, whereas it deteriorated in the AF-group (Table 3). An example of a patient from the SR-group demonstrating improvements in LV circumferential and longitudinal strain is shown in Figure 3.

A multivariate logistic regression analysis was performed to study the predictors of the maintenance of sinus rhythm after catheter ablation. The results of the multivariate logistic regression analysis are shown in Table 5. Interestingly, the change in longitudinal strain and circumferential strain at follow-up were the only independent predictors for maintenance of

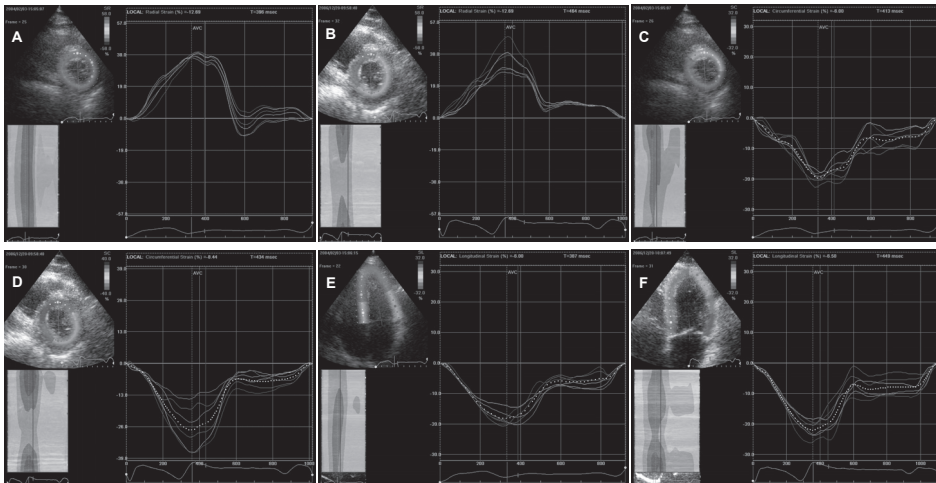


Figure 3. In this patient, global radial strain did not improve from baseline (38.1%, panel A) to 12 months follow-up (37.3%, panel B). In contrast, a significant improvement in global circumferential strain (baseline -19.4%, panel C; follow-up -26.5%, panel D) and global longitudinal strain (baseline -17.3%, panel E; follow-up -22.5%, panel F) was observed.

Table 5. Logistic regression analysis for predictors of maintenance of sinus rhythm after catheter ablation

	Odds ratio	95% confidence interval	p-value
Number of anti-arrhythmic drugs	2.267	0.508 – 10.121	0.284
Change in LV mass index	0.996	0.952 – 1.043	0.878
Change in mean arterial pressure	1.011	0.926 – 1.104	0.808
Change in maximum LA volume	1.015	0.965 – 1.067	0.566
Change in circumferential strain	0.537	0.339 – 0.849	0.008
Change in longitudinal strain	0.338	0.155 – 0.737	0.006

C-statistic: 0.934.

sinus rhythm: Change in circumferential strain: Odds ratio 0.537, 95% confidence interval 0.339 to 0.849, $p = 0.008$; change in longitudinal strain: Odds ratio 0.338, 95% confidence interval 0.155 to 0.737, $p = 0.006$.

DISCUSSION

In the present study, 78 patients with preserved LV systolic function, undergoing radiofrequency catheter ablation for AF, were studied. At long-term follow-up, a significant improvement in circumferential and longitudinal strain and strain rate was observed. Importantly, these improvements were only present in patients who maintained sinus rhythm during follow-up, whereas patients who had recurrence of AF did not exhibit improvements in circumferential and longitudinal strain.

Left ventricular function after catheter ablation

Significant improvements in LV strain were observed after successful catheter ablation in the current study in patients with preserved LV systolic function. The beneficial effect of catheter ablation on LV function has been demonstrated previously in patients with impaired LV systolic function (4-6). Interestingly, in patients with preserved LV systolic function, the favorable effects of catheter ablation on LV function are less clear. In 52 patients with an LV ejection fraction >50% undergoing catheter ablation, Lutomsky et al. noted that LV ejection fraction remained unchanged after 6 months follow-up (from $60 \pm 6\%$ to $59 \pm 9\%$, $p=0.22$) (7). It was concluded that successful catheter ablation may be less beneficial in patients with normal LV ejection fraction (7).

However, it may well be that the positive effects of the restoration of sinus rhythm on LV systolic function are present, but cannot be detected by conventional parameters such as LV ejection fraction. The evaluation of LV strain may detect more subtle abnormalities in LV systolic function (20), which can improve after AF ablation. Indeed, preliminary data in 25 patients with normal LV ejection fraction suggest that LV deformation may improve after catheter ablation for AF (21). In the present study, 2D speckle tracking strain imaging was used to assess LV function after catheter ablation for AF in 78 patients. Similar to previous data (7), mean LV

ejection fraction did not improve after long-term follow-up. However, significant changes in LV circumferential and longitudinal strain and strain rate were noted, in particular in the patients who maintained sinus rhythm during follow-up.

The improvement in LV function (according to strain and strain rate) after successful catheter ablation can be attributed to the normalization of the heart rate, or to the restoration of sinus rhythm and subsequent more efficient LV filling. However, at present it remains unclear what mechanism contributes most (1,22). In the current study, the mean heart rate did not change significantly from baseline to follow-up. Per study protocol, both echocardiograms were acquired during sinus rhythm, and therefore the differences in LV strain cannot be attributed to changes in heart rhythm during image acquisition. Furthermore, significant changes in circumferential and longitudinal strain and strain rate were only noted in the patients who maintained sinus rhythm during follow-up. Therefore, the current results suggest that the improvement in LV function after catheter ablation may be more related to restoration and long-term maintenance of sinus rhythm than to normalization of heart rate.

At the same time, it may also be that an improvement in LV function ultimately results in favorable reverse remodeling of the left atrium and subsequently in a reduced risk of recurrent AF (23). Interestingly, in the present study, improvements in circumferential and longitudinal strain were the only predictors for maintenance of sinus rhythm during follow-up (Table 5). Although the restoration of sinus rhythm and the improvement in LV function after catheter ablation are clearly related, it remains unclear which factor is the exact cause and which is the consequence.

Left ventricular strain

In the present study, 3 distinct patterns of LV deformation were studied: radial, circumferential and longitudinal strain. Interestingly, different responses during long-term follow-up were noted among the various strain patterns. Previously, several studies have demonstrated the effects of different clinical settings on these strain patterns (24-27). In an animal model of myocardial ischemia, it was noted that circumferential and longitudinal strain, as assessed with speckle tracking echocardiography, were most sensitive to reduced coronary flow (24). In addition, in 53 patients with diabetes, Fang et al. demonstrated a significant impairment of longitudinal strain as compared with controls, while radial strain was compensatory increased (25). Finally, in patients with hypertrophic cardiomyopathy but normal LV systolic function, marked reductions in longitudinal strain have been demonstrated (26,27). From anatomical studies, it is known that there is a difference in orientation of the endocardial and epicardial myocardial fibers. It has been suggested that the LV myocardial architecture is a transmural continuum of two helical fiber geometries, with a right-handed helical geometry in the subendocardial region gradually changing into a left-handed geometry in the subepicardial region (28). The discrepancy among the various strain patterns as found in the abovementioned studies may be explained by the fact that the longitudinal fibers located in the subendocardium, mediating the long axis deformation, may be more susceptible to pathologic changes (29).

In the present study, baseline values for LV strain were comparable in the SR-group and the AF-group, and modestly reduced as compared with previously reported values for healthy controls (25,26). Interestingly, circumferential and longitudinal strain improved significantly in patients who maintained sinus rhythm after catheter ablation. In contrast, in patients with recurrence of AF, circumferential strain remained unchanged and longitudinal strain even deteriorated. No significant changes in radial strain were noted in both groups. It may be that, similar to detrimental effects of various pathologic changes, the longitudinal fibers may be more prone to the beneficial effect of restoration of normal sinus rhythm and subsequent more efficient LV filling and contraction.

Limitations

Some limitations of the present study need to be addressed. First, the study population was divided into two groups, based on recurrence of symptomatic AF episodes and/or detection of AF with surface ECG and 24-hours Holter monitoring on a regular basis. Asymptomatic AF recurrence during follow-up may therefore have been missed. Second, no data on the exact AF burden before the ablation procedure and during follow-up are available in the present study. Although potential asymptomatic AF recurrences may affect the results, and exact AF burden assessment may provide more information on the relation between improvement in LV function and AF recurrence, the definition of AF recurrence in the present study is according to the recommendations from the Heart Rhythm Society Expert Consensus Statement (1).

In addition, only a small number of patients with persistent AF was included in the study. Therefore, no comparisons between patients with paroxysmal and persistent AF could be performed. However, to minimize the confounding effect of variations in heart rhythm on LV deformation properties, only patients with an available echocardiogram during sinus rhythm at baseline and at follow-up were included in the present study. A larger population in future studies may allow comparison between paroxysmal and persistent AF patients.

Finally, in the present study, LV dyssynchrony was not routinely assessed. Future studies may investigate if LV dyssynchrony is present in patients undergoing catheter ablation, and if the improvement in LV function as demonstrated in the present study is associated with an improvement in LV dyssynchrony.

CONCLUSIONS

In patients with preserved LV systolic function undergoing catheter ablation for AF, improvements in LV strain were noted, without significant changes in LV ejection fraction. Longitudinal and circumferential strain and strain rate improved in patients who maintained sinus rhythm during follow-up. In contrast, patients who had recurrence of AF exhibited no improvements in circumferential or longitudinal strain.

REFERENCES

1. Calkins H, Brugada J, Packer DL et al. HRS/EHRA/ECAS expert Consensus Statement on catheter and surgical ablation of atrial fibrillation: recommendations for personnel, policy, procedures and follow-up. *Heart Rhythm* 2007;4:816-61.
2. Tops LF, Bax JJ, Zeppenfeld K, Jongbloed MR, van der Wall EE, Schalij MJ. Effect of radiofrequency catheter ablation for atrial fibrillation on left atrial cavity size. *Am J Cardiol* 2006;97:1220-2.
3. Reant P, Lafitte S, Jais P et al. Reverse remodeling of the left cardiac chambers after catheter ablation after 1 year in a series of patients with isolated atrial fibrillation. *Circulation* 2005;112:2896-903.
4. Hsu LF, Jais P, Sanders P et al. Catheter ablation for atrial fibrillation in congestive heart failure. *N Engl J Med* 2004;351:2373-83.
5. Gentlesk PJ, Sauer WH, Gerstenfeld EP et al. Reversal of left ventricular dysfunction following ablation of atrial fibrillation. *J Cardiovasc Electrophysiol* 2007;18:9-14.
6. Chen MS, Marrouche NF, Khaykin Y et al. Pulmonary vein isolation for the treatment of atrial fibrillation in patients with impaired systolic function. *J Am Coll Cardiol* 2004;43:1004-9.
7. Lutomsky BA, Rostock T, Koops A et al. Catheter ablation of paroxysmal atrial fibrillation improves cardiac function: a prospective study on the impact of atrial fibrillation ablation on left ventricular function assessed by magnetic resonance imaging. *Europace* 2008;10:593-9.
8. Leitman M, Lysyansky P, Sidenko S et al. Two-dimensional strain—a novel software for real-time quantitative echocardiographic assessment of myocardial function. *J Am Soc Echocardiogr* 2004;17:1021-9.
9. Reisner SA, Lysyansky P, Agmon Y, Mutlak D, Lessick J, Friedman Z. Global longitudinal strain: a novel index of left ventricular systolic function. *J Am Soc Echocardiogr* 2004;17:630-3.
10. Edvardsen T, Helle-Valle T, Smiseth OA. Systolic dysfunction in heart failure with normal ejection fraction: speckle-tracking echocardiography. *Prog Cardiovasc Dis* 2006;49:207-14.
11. Delgado V, Ypenburg C, van Bommel RJ et al. Assessment of left ventricular dyssynchrony by speckle tracking strain imaging comparison between longitudinal, circumferential, and radial strain in cardiac resynchronization therapy. *J Am Coll Cardiol* 2008;51:1944-52.
12. Tops LF, Bax JJ, Zeppenfeld K et al. Fusion of multislice computed tomography imaging with three-dimensional electroanatomic mapping to guide radiofrequency catheter ablation procedures. *Heart Rhythm* 2005;2:1076-81.
13. Lang RM, Bierig M, Devereux RB et al. Recommendations for Chamber Quantification: *J Am Soc Echocardiogr* 2005;18:1440-63.
14. Schiller NB, Shah PM, Crawford M et al. Recommendations for quantitation of the left ventricle by two-dimensional echocardiography. *J Am Soc Echocardiogr* 1989;2:358-67.
15. Quinones MA, Otto CM, Stoddard M, Waggoner A, Zoghbi WA. Recommendations for quantification of Doppler echocardiography. *J Am Soc Echocardiogr* 2002;15:167-84.
16. Ommen SR, Nishimura RA, Appleton CP et al. Clinical utility of Doppler echocardiography and tissue Doppler imaging in the estimation of left ventricular filling pressures: A comparative simultaneous Doppler-catheterization study. *Circulation* 2000;102:1788-94.
17. Lester SJ, Tajik AJ, Nishimura RA, Oh JK, Khandheria BK, Seward JB. Unlocking the mysteries of diastolic function: deciphering the Rosetta Stone 10 years later. *J Am Coll Cardiol* 2008;51:679-89.
18. Tops LF, Suffoletto MS, Bleeker GB et al. Speckle-tracking radial strain reveals left ventricular dyssynchrony in patients with permanent right ventricular pacing. *J Am Coll Cardiol* 2007;50:1180-8.
19. Kowalski M, Kukulski T, Jamal F et al. Can natural strain and strain rate quantify regional myocardial deformation? A study in healthy subjects. *Ultrasound Med Biol* 2001;27:1087-97.
20. Abraham TP, Dimaano VL, Liang HY. Role of tissue Doppler and strain echocardiography in current clinical practice. *Circulation* 2007;116:2597-609.
21. Reant P, Lafitte S, Jais P, Sacher F, Derval N, Deplagne A et al. Improvement of left ventricular deformation after catheter ablation for isolated paroxysmal atrial fibrillation in patients with normal ejection fraction: a 2-dimensional strain study. *Eur Heart J* 2007;28(Suppl):1-250.

22. Cha YM, Redfield MM, Shen WK, Gersh BJ. Atrial fibrillation and ventricular dysfunction: a vicious electromechanical cycle. *Circulation* 2004;109:2839-43.
23. Casaclang-Verzosa G, Gersh BJ, Tsang TS. Structural and functional remodeling of the left atrium: clinical and therapeutic implications for atrial fibrillation. *J Am Coll Cardiol* 2008;51:1-11.
24. Reant P, Labrousse L, Lafitte S et al. Experimental validation of circumferential, longitudinal, and radial 2-dimensional strain during dobutamine stress echocardiography in ischemic conditions. *J Am Coll Cardiol* 2008;51:149-57.
25. Fang ZY, Leano R, Marwick TH. Relationship between longitudinal and radial contractility in subclinical diabetic heart disease. *Clin Sci (Lond)* 2004;106:53-60.
26. Serri K, Reant P, Lafitte M et al. Global and regional myocardial function quantification by two-dimensional strain: application in hypertrophic cardiomyopathy. *J Am Coll Cardiol* 2006;47:1175-81.
27. Kato TS, Noda A, Izawa H et al. Discrimination of nonobstructive hypertrophic cardiomyopathy from hypertensive left ventricular hypertrophy on the basis of strain rate imaging by tissue Doppler ultrasonography. *Circulation* 2004;110:3808-14.
28. Sengupta PP, Korinek J, Belohlavek M et al. Left ventricular structure and function: basic science for cardiac imaging. *J Am Coll Cardiol* 2006;48:1988-2001.
29. Jones CJ, Raposo L, Gibson DG. Functional importance of the long axis dynamics of the human left ventricle. *Br Heart J* 1990;63:215-20.



Ventricular pacing and dyssynchrony





The effects of right ventricular apical pacing on ventricular function and dyssynchrony: implications for therapy

Laurens F. Tops
Martin J. Schalij
Jeroen J. Bax

Department of Cardiology, Leiden University Medical Center, Leiden, the Netherlands

J Am Coll Cardiol 2009;54:764-76

ABSTRACT

Cardiac pacing is the only effective treatment for patients with sick sinus syndrome and atrioventricular conduction disorders. In cardiac pacing, the endocardial pacing lead is typically positioned at the right ventricular (RV) apex. At the same time, there is increasing indirect evidence, derived from large pacing mode selection trials and observational studies, that conventional RV apical pacing may have detrimental effects on cardiac structure and left ventricular (LV) function, which is associated with development of heart failure. These detrimental effects may be related to the abnormal electrical and mechanical activation pattern of the ventricles (or ventricular dyssynchrony) caused by RV apical pacing. Still, it remains uncertain if the deterioration of LV function as noted in a proportion of patients receiving RV apical pacing is directly related to acutely induced LV dyssynchrony. The upgrade from RV pacing to cardiac resynchronization therapy (CRT) may partially reverse the deleterious effects of RV pacing. It has even been suggested that selected patients with a conventional pacemaker indication should receive CRT to avoid the deleterious effects. This review will provide a contemporary overview of the available evidence on the detrimental effects of RV apical pacing. Furthermore, the available alternatives for patients with a standard pacemaker indication will be discussed. In particular, the role of CRT and alternative RV pacing sites in these patients will be reviewed.

INTRODUCTION

For decades, cardiac pacing has been an effective treatment in the management of patients with brady- and tachy-arrhythmias (1). New indications for pacing such as drug-refractory heart failure have been introduced (2). However, sick sinus syndrome and atrioventricular (AV) conduction disorders still remain the most important indications for cardiac pacing (3). The endocardial pacing lead is typically positioned at the right ventricular (RV) apex. In general RV apical pacing is very well tolerated and effective. However, it has been suggested that RV apical pacing may have detrimental effects on cardiac structure and left ventricular (LV) function (4). This may be related to the abnormal electrical and mechanical activation pattern of the ventricles (or ventricular dyssynchrony) caused by RV apical pacing. In recent years, the association between RV apical pacing and mechanical dyssynchrony, and their effects on cardiac function have been studied by electrophysiologists, cardiac imaging experts and physiologists. Although the approach to this complex problem may differ among them, the overlapping perspectives have provided important pathophysiologic information.

In this manuscript, the potential detrimental effects of RV apical pacing, and the underlying pathophysiology will be reviewed. In particular, the role of ventricular dyssynchrony will be discussed. Furthermore, the therapeutic options in patients with a pacemaker indication will be reviewed; including the role of CRT and alternative RV pacing sites.

THE EFFECTS OF RV APICAL PACING

Cardiac pacing is the only effective treatment for symptomatic sinus node disease, and can improve symptomatic chronotropic incompetence (1). In addition, numerous studies have demonstrated symptomatic and functional improvement by cardiac pacing in patients with AV block (5). Furthermore, conventional dual-chamber pacing can improve cardiac function in selected patients with LV dysfunction (6). Finally, cardiac pacing is an effective treatment in controlling symptoms of chronic, drug-refractory atrial fibrillation (7). In the last decades, there have been significant increases in the incidence of pacemaker implantations (8).

A number of large randomized clinical trials have provided important information for selection of the optimal pacing mode (9-11). But more importantly, these trials have suggested an association between RV apical pacing and cardiac morbidity and mortality. In addition, a number of clinical (12,13) and pre-clinical (14,15) studies have investigated the exact effects of RV apical pacing on cardiac function. Furthermore, it has been suggested that pacing-induced mechanical dyssynchrony is associated with a deterioration of LV function and clinical status in patients with permanent RV apical pacing (16).

Evidence from pacing mode trials

Several large, randomized clinical trials on pacing mode selection have suggested an association between a high percentage of RV apical pacing and a worse clinical outcome (17). A substudy of the MDe Selection Trial (MOST) demonstrated a strong association between RV pacing and the risk of heart failure hospitalization and atrial fibrillation in both 'physiologic pacing' (DDDR: n=707) and ventricular pacing (VVIR: n=632) (10). It was noted that >40% of ventricular pacing in the DDDR group was associated with an increased risk of heart failure hospitalization (hazard ratio 2.60; 95% CI 1.05 - 6.47; p<0.05) and that >80% of ventricular pacing in the VVIR group was associated with an increased risk of heart failure hospitalization (hazard ratio 2.50; 95% CI 1.44 - 4.36; p<0.05). In the Dual Chamber and VVI Implantable Defibrillator (DAVID) trial patients with a standard indication for a defibrillator implantation, but without an indication for anti-bradycardia pacing, were randomized between 'physiologic pacing' (DDDR mode, lower rate of 70 bpm) or ventricular back-up pacing (VVIR mode, lower rate of 40 bpm) (11). After a median follow-up of 8.4 months, the primary outcome measure (freedom from death and absence of hospitalization for new or worsened heart failure) was lower in the VVIR-40 group than in the DDDR-70 group (relative hazard 1.61; 95% CI 1.06 - 2.44; p=0.03). Interrogation of the defibrillator device revealed a significantly higher percentage of ventricular paced beats in the DDDR-70 group at 3 months follow-up. Importantly, a trend towards a worse survival at 12 months was noted in patients with a high percentage of pacing at 3 months follow-up (11). It should be noted however that not only RV apical pacing itself may have resulted in this worse outcome, but also the higher mean heart rate, and the changes in AV coupling in the DDDR group may have detrimental effects.

These trials suggest that there is no clinical benefit of 'physiologic' DDDR pacing over VVIR. This may be explained by the higher percentage of ventricular pacing in the DDDR groups, as a result of the short programmed AV interval. Thus, the beneficial effect of maintaining AV synchrony by 'physiologic' DDDR pacing may be reduced by the deleterious effects of RV apical pacing itself.

Unfortunately, the exact amount of RV apical pacing that negatively affects cardiac function remains unclear from these trials. A certain amount of ventricular pacing may actually be beneficial since it maintains physiologic AV conduction (6). At the same time, the negative effects of RV apical pacing may be more pronounced in certain patient populations. In particular, patients with underlying conduction disease (18) and patients with ischemic heart disease (19) may be at risk. Furthermore, it has been suggested that in patients who require pacing for a longer period of time, and patients with depressed LV function at baseline are more susceptible for the deleterious effects of RV apical pacing (4). More studies are therefore needed to fully understand the beneficial and deleterious effects of RV apical pacing, and to better identify the patients who are at risk for the detrimental effects of RV pacing. The available studies in which the underlying pathophysiology is studied will be reviewed in the following paragraphs.

Pathophysiology of detrimental effects

In general, the negative effects of RV apical pacing have been attributed to the abnormal electrical and mechanical activation pattern of the ventricles (14). During RV apical pacing, the conduction of the electrical wave front propagates through the myocardium, rather than through the His-Purkinje conduction system. As a result, the electrical wave front propagates more slowly and induces heterogeneity in electrical activation of the myocardium, comparable to left bundle branch block. This is characterized by a single breakthrough at the interventricular septum, and the latest activation at the inferoposterior base of the LV (20-22).

Similar to the changes in electrical activation of the ventricles, the mechanical activation pattern of the LV is changed during RV apical pacing. Importantly, not only the onset of mechanical contraction is changed, but also the pattern of mechanical contraction (14). In several animal studies, it has been demonstrated that the early-activated regions near the pacing site exhibit rapid early systolic shortening, resulting in pre-stretch of the late activated regions (15,23). As a result, these regions exhibit an increase in (delayed) systolic shortening, imposing systolic stretch to the early activated regions exhibiting pre-mature relaxation. This abnormal contraction pattern of the various regions of the LV may result in a redistribution of myocardial strain and work and subsequent less effective contraction (15).

Both the abnormal electrical and mechanical activation pattern of the ventricles can result in changes in cardiac metabolism and perfusion, remodeling, hemodynamics and mechanical function. An overview of the potential harmful effects of RV apical pacing on cardiac function is provided in Table 1. The effects on cardiac metabolism and perfusion have been demonstrated in both clinical and pre-clinical studies (24). Even in the absence of coronary artery disease, myocardial perfusion defects may be present in up to 65% of the patients after long-term RV apical pacing, and are mainly located near the pacing site (12,25).

Table 1. Acute and long-term effects of RV apical pacing

Changes in electrical activation and mechanical activation
Metabolism / perfusion
Changes in regional perfusion
Changes in oxygen demand
Remodeling
Asymmetric hypertrophy
Histopathological changes
Ventricular dilation
Functional mitral regurgitation
Hemodynamics
Decreased cardiac output
Increased LV filling pressures
Mechanical function
Changes in myocardial strain
Interventricular mechanical dyssynchrony
Intraventricular mechanical dyssynchrony

Long-term RV pacing may also result in structural changes, and LV remodeling. Endomyocardial biopsies in 14 patients with congenital complete AV block revealed cellular and intracellular alterations, including mitochondrial variations and degenerative fibrosis, after long-term permanent RV pacing (26). In addition, changes in LV wall thickness (27), and LV remodeling (28) may occur after long-term RV pacing. In addition, functional mitral regurgitation and left atrial remodeling may occur during RV apical pacing (29,30).

Moreover, hemodynamic properties and global mechanical function may be affected by the abnormal electrical and mechanical activation of the LV. Pacing at the RV apex may result in a decrease in cardiac output and may alter LV filling properties (13). Changes in myocardial strain and timing of regional strain may occur during RV apical pacing. Using magnetic resonance imaging in an animal model of cardiac pacing, Prinzen et al. noted a significant decrease in strain in the regions close to the pacing site, whereas an increase in myocardial strain was noted in remote regions (15). Importantly, timing of peak regional strain is also changed during pacing. This is often referred to as 'mechanical dyssynchrony' (31).

Mechanical dyssynchrony during RV apical pacing

Right ventricular apical pacing can induce both interventricular dyssynchrony (between the RV and the LV), as well as intraventricular dyssynchrony (within the LV) (16). It has been demonstrated that the presence of ventricular dyssynchrony is associated with an increased risk of cardiac morbidity (32) and mortality (33) in heart failure patients. In addition, it has been suggested that the presence of mechanical dyssynchrony after long-term RV apical pacing is associated with reduced LV systolic function and deterioration in functional capacity (16). However, there are only a few studies that have demonstrated a direct relation between (pacing-induced) ventricular dyssynchrony and clinical heart failure. At the same time, it has been shown that restoration of normal conduction and 'cardiac synchrony' by cardiac resynchronization therapy (CRT) results in normalization of LV systolic function (34,35). This suggests that an abnormal activation pattern (left bundle branch block during RV apical pacing) or ventricular dyssynchrony may be directly related to a deterioration of LV function. Therefore, the assessment of ventricular dyssynchrony may provide important information in patients with permanent RV apical pacing.

Several echocardiographic techniques are available for the assessment of cardiac mechanical dyssynchrony. These include conventional Doppler techniques, tissue Doppler imaging, strain analysis and novel three-dimensional echocardiography. The majority of the techniques have been used to quantify inter- and intraventricular dyssynchrony in heart failure patients referred for CRT (36). Likewise, these techniques can be used to detect the presence of ventricular mechanical dyssynchrony during acute and long-term RV apical pacing.

For the quantification of interventricular dyssynchrony, conventional Doppler techniques are typically used (Figure 1). For both ventricles, the electromechanical delay is calculated as the time from onset of the QRS complex to the onset of pulmonary systolic flow (RV electromechanical delay) or aortic systolic flow (LV electromechanical delay). The time difference

between the RV and LV electromechanical delay represents interventricular dyssynchrony (37). From previous studies, it has become clear that RV apical pacing can induce significant interventricular dyssynchrony (16,38).

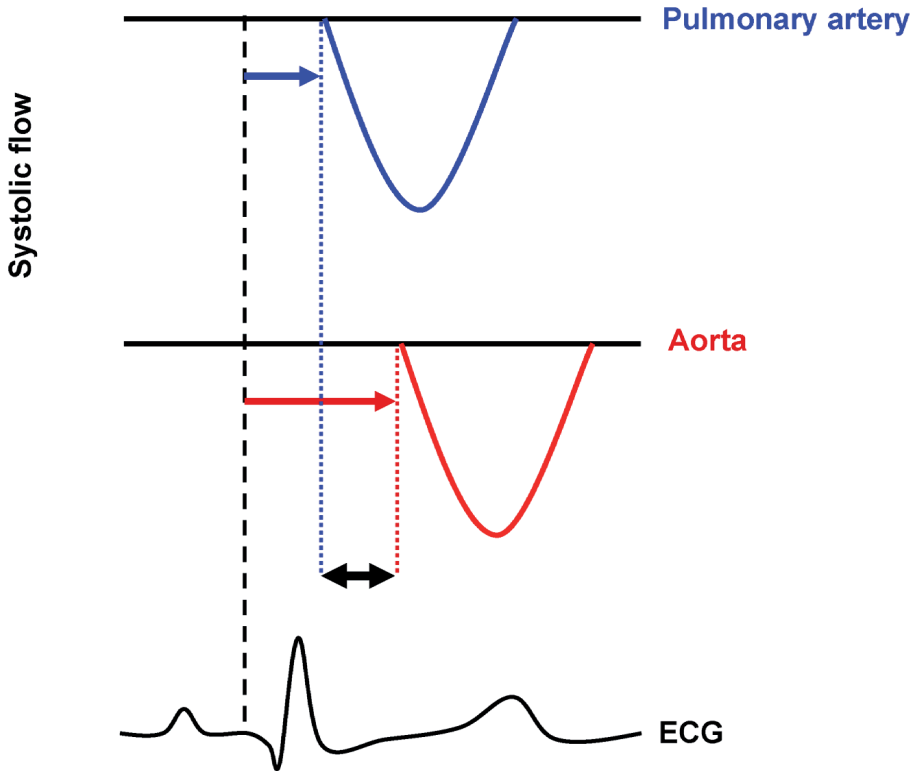


Figure 1. Schematic representation of interventricular dyssynchrony during RV apical pacing. For assessment of interventricular dyssynchrony, the ECG and systolic flow through the pulmonary artery and aorta (assessed with Doppler echocardiography) are typically used. Both the RV and LV electromechanical delay are measured from the onset of QRS (dashed black line). The RV electromechanical delay is the time from the onset of QRS to the onset of pulmonary systolic flow (blue arrow). The LV electromechanical delay is the time from the onset of QRS to the onset of aortic systolic flow (red arrow). Subsequently, the interventricular dyssynchrony can be calculated as the difference between the RV and the LV electromechanical delays (black arrow).

For the assessment of intraventricular (or LV) dyssynchrony, several echocardiographic techniques are available, including tissue Doppler imaging, two-dimensional speckle-tracking strain analysis, and real-time three-dimensional echocardiography (39). In general, LV dyssynchrony is represented by the delay in mechanical activation between the interventricular septum and the posterior or lateral wall (Figure 2). Already in 1977, Gomes et al. demonstrated the effect of RV apical pacing on the mechanical delay between the septum and the posterior wall (40). During the acute onset of cardiac pacing in 12 patients, it was noted that there was an early rapid pre-ejection posterior motion of the interventricular septum. In addition, the posterior wall of the LV exhibited a delayed contraction, resulting in a significant delay between

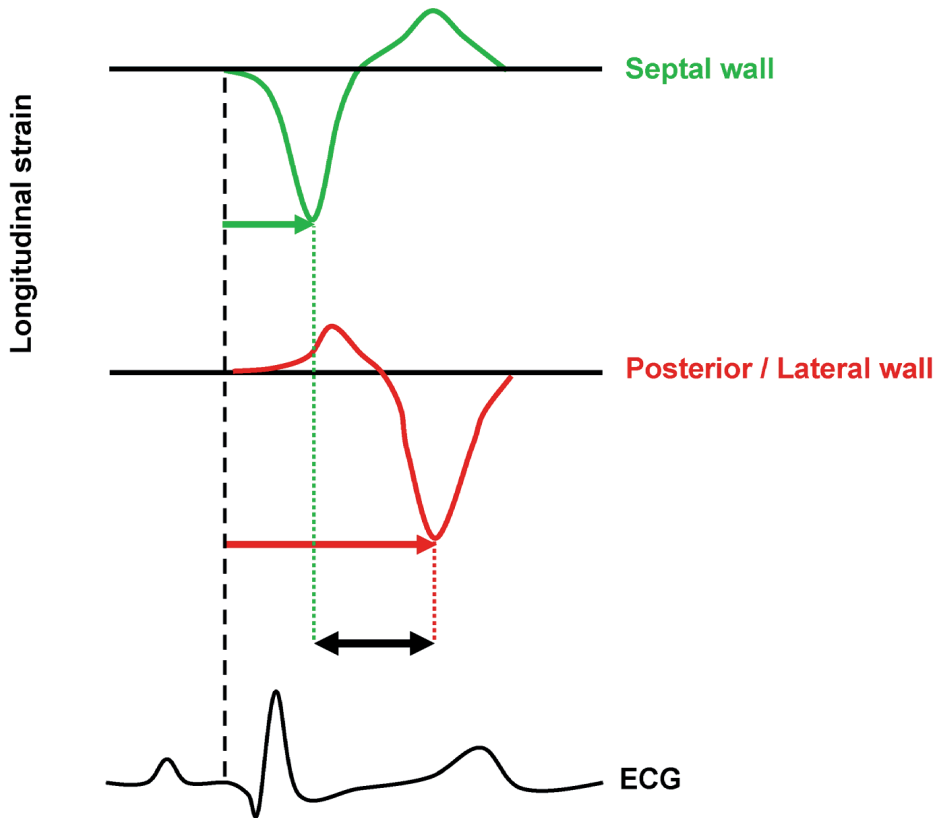


Figure 2. Schematic representation of intraventricular dyssynchrony during RV apical pacing. Intraventricular dyssynchrony is represented by the delay in mechanical activation between different segments within the LV. In this example, longitudinal strain curves of the septum and the posterior or lateral wall are demonstrated. The time from onset of QRS to peak systolic strain for the septum (green arrow) and the posterior or lateral wall (red arrow) is indicated. The difference in time-to-peak strain for the various segments is the delay in mechanical activation, or LV intraventricular dyssynchrony (indicated by the black arrow).

the activation of the septum (61 ± 5 ms) and the posterior wall (116 ± 18 ms) (40). More recently, these findings have been confirmed with dedicated echocardiographic techniques (41–44). From these studies, it has become apparent that RV apical pacing can induce significant intraventricular mechanical dyssynchrony, which has been related to reduced LV function.

CLINICAL IMPLICATIONS

From the large pacing-mode selection trials and observational studies, it has become apparent that conventional RV apical pacing is associated with an increased risk of adverse events (e.g. development of LV dilatation and heart failure). However, in daily clinical practice not all patients who receive RV apical pacing will experience these adverse events (19). In a retrospective study including 286 patients with permanent pacing after AV junction ablation, it was noted that LV

ejection fraction (LVEF) decreased significantly in only 9% of the patients during follow-up (45). In another retrospective study of 304 patients with pacemaker implantation for high degree AV block, the clinical outcome after at least one year of RV apical pacing was studied (46). A total of 79 patients (26%) developed new-onset heart failure after a mean of 6.5 ± 5.7 years of pacing. It appears that some patients are more susceptible to the detrimental effects of RV apical pacing than others, possibly related to mechanical ventricular dyssynchrony.

Ventricular dyssynchrony may be present in up to 50% of the patients after long-term RV apical pacing (38,41,47). Importantly, it has been demonstrated that the presence of mechanical dyssynchrony after long-term RV apical pacing is associated with LV dilatation, and a deterioration of LV systolic function and functional capacity (16). However, it remains unclear if LV dyssynchrony is an acute phenomenon, which may then induce deterioration of LV function at longer follow-up and subsequent development of heart failure.

A recent study in patients with structurally normal hearts, undergoing electrophysiologic testing revealed that significant LV dyssynchrony may be induced acutely in up to 36% of individuals (Figure 3) (48). A concomitant impairment in LV systolic function was observed, reflected by a reduction in LVEF (from $56 \pm 8\%$ to $48 \pm 9\%$, $p=0.001$) and LV longitudinal strain (from -18.3



Figure 3. Right ventricular apical pacing acutely induces LV dyssynchrony. Echocardiographic analysis of LV dyssynchrony during intrinsic rhythm (panel A) and immediately after onset of RV apical pacing (panel B). Speckle-tracking strain analysis enables the evaluation of the timing of systolic strain. The color-coded curves represent the time-strain curves of 6 mid-ventricular segments of the LV. During intrinsic rhythm (panel A), a synchronous contraction of all LV segments is present. In contrast, during RV apical pacing, significant LV dyssynchrony is present: there is a significant delay (130 ms) between the time-to-peak strain of the antero-septum (yellow arrow) and the posterolateral segment (purple arrow).

$\pm 3.5\%$ to $-11.8 \pm 3.6\%$, $p<0.001$) (48). In 153 patients undergoing pacemaker implantation for standard indications, Pastore et al. assessed LV dyssynchrony using tissue Doppler echocardiography at baseline and after at least 24 hours (mean 1.7 ± 0.3 days) of continuous RV apical pacing (49). A total of 101 patients (66%) exhibited significant LV dyssynchrony. Interestingly, the amount of pacing-induced LV dyssynchrony was related to the presence of LV dysfunction at baseline (Figure 4). It has been demonstrated previously that the conduction abnormalities induced by RV apical pacing may be enhanced by accompanying conduction disease at

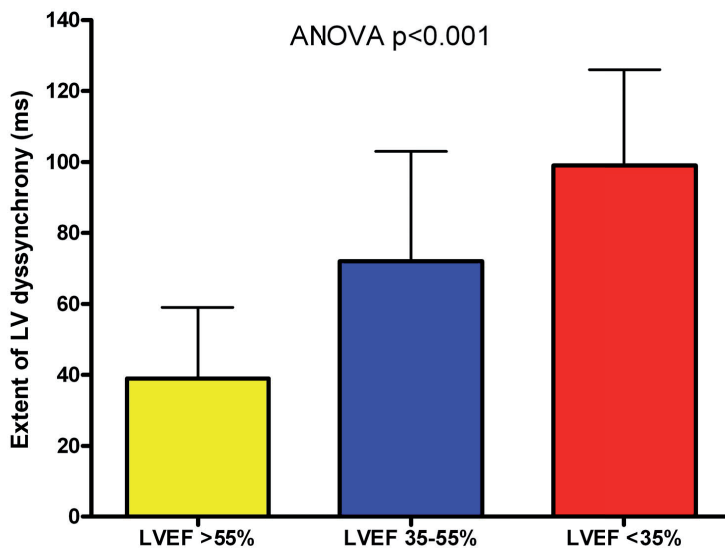


Figure 4. Left ventricular dyssynchrony during RV pacing according to baseline LVEF. In 153 patients undergoing pacemaker implantation, LV dyssynchrony was assessed during RV apical pacing. Patients were classified according to baseline LVEF: normal (LVEF >55%), moderately depressed (LVEF 35-55%), or severely depressed (LVEF <35%). The extent of LV dyssynchrony was strongly related with baseline LVEF. In patients with normal LVEF, 45% of the patients developed LV dyssynchrony (40 out of 89), whereas 39 of the 42 patients (93%) with moderately depressed LVEF developed LV dyssynchrony. In patients with severely depressed LVEF (n=22), all patients exhibited LV dyssynchrony during RV apical pacing (49). LV = left ventricular; LVEF = left ventricular ejection fraction; RV = right ventricular

baseline (18). Unfortunately, the abovementioned studies only assessed LV dyssynchrony and LV function in the acute phase. Although it has been demonstrated that the negative effects of the abnormal LV activation sequence may sustain even after termination of RV apical pacing (50), it still remains unclear whether the acutely induced LV dyssynchrony is the basis for the development of LV dysfunction and heart failure after long-term RV apical pacing. In addition, it is still unclear why some patients acutely develop ventricular dyssynchrony, and others do not. This may be due to subtle differences in the location of the pacing lead within the RV apex, and thus the proximity of the Purkinje system. At the same time, some echocardiographic techniques used to assess ventricular dyssynchrony may not be sensitive enough to detect small changes in electromechanical activation (51). Therefore, more studies are needed on acutely induced ventricular dyssynchrony, and its long-term effects.

When future studies show that the acutely induced LV dyssynchrony is associated with deterioration of LV function during follow-up, ventricular dyssynchrony assessment during pacemaker implantation may have important clinical implications. If LV dyssynchrony is present immediately after onset of RV apical pacing, a CRT device may be preferred over conventional RV apical pacing. In contrast, if no LV dyssynchrony is present, conventional RV apical pacing alone may be accepted. Monitoring of LV dyssynchrony and LV function is then warranted.

At the same time, with the increasing evidence of the detrimental effects of RV apical pacing, it has been suggested that the percentage of ventricular pacing should be kept to a

minimum (4). However, in a large proportion of patients, RV pacing is inevitable (1). For these patients, a number of alternative strategies to minimize the induction of mechanical dyssynchrony and other deleterious effects have been proposed. These therapeutic options, including the upgrade from RV pacing to CRT, 'de novo' CRT, and alternative pacing sites, will be discussed in the following paragraphs.

THERAPEUTIC OPTIONS IN PATIENTS WITH RV APICAL PACING

The detrimental effects of RV apical pacing related to cardiac metabolism, remodeling, hemodynamics and mechanical function may be prevented or partially reversed by CRT or alternative RV pacing sites. In the subset of patients who experience detrimental effects of RV apical pacing, CRT may restore the synchronous contraction of the LV and subsequently improve LV function. Alternatively, a number of strategies, including alternative RV pacing sites, have been suggested to avoid the deleterious effects of RV apical pacing. All these therapeutic options will be discussed in the following paragraphs.

Upgrade of RV apical pacing to CRT

Several studies have demonstrated beneficial effects of the upgrade from RV apical pacing to CRT (Table 2). Reverse remodeling of the LV (defined as a reduction in LV end-diastolic or end-systolic volume) after upgrade from RV apical to CRT has been demonstrated in several studies (47,52,53). In addition, the severity of mitral regurgitation may improve after upgrade to CRT (54-57).

Furthermore, LV hemodynamics and mechanical function may improve after upgrade to CRT. In an invasive hemodynamic study in 18 patients with congenital complete AV block who had received RV apical pacing for a mean of 81 ± 10 months, CRT resulted in a significant increase in LV dP/dt_{max} (58). In parallel, a significant decrease in LV end-diastolic pressure and isovolumic pressure half-time was observed (58). Improvements in global LVEF have been demonstrated in various studies, including four prospective studies with more than 110 patients with previous AV junction ablation and pacemaker implantation (52,54,59,60) (Table 2).

Finally, it has been demonstrated that the upgrade from RV apical pacing to CRT may result in a significant improvement in exercise capacity and NYHA functional class (57) (Figure 5). Unfortunately, at present it remains uncertain if the upgrade to CRT in previously paced patients results in an improved prognosis.

Effect on ventricular dyssynchrony In parallel with the improvements in LV function, LV dyssynchrony may improve after upgrade from RV apical to CRT. An acute reduction in the LV pre-ejection interval after onset of CRT in previously paced patients has been demonstrated in several studies (61,62). Importantly, this effect is maintained during mid- and long-term follow-up (47,53,55). In 32 patients receiving upgrade to CRT after a minimum of one year RV apical

Table 2. Studies on mid- and long-term effects of upgrade from RV apical pacing to CRT

Study (reference)	Number of patients	Inclusion criteria	RV pacing		CRT		Outcome after upgrade: RV pacing vs. CRT		
			Indication	Duration	Follow-up duration	QRS duration (ms)	LVEF (%)	NYHA class	Other outcome parameters
Randomized, cross over studies									
Leclercq et al. (57)	44	NYHA III/IV LVEF <35% Ventricular dyssynchrony	Conventional indications	49 ± 34 mo	6 mo	200 ± 20 vs. 154 ± 26 *	30 ± 11 vs. 29 ± 11	2.5 ± 0.7 vs. 2.1 ± 0.4 *	Improvement in 6MWT, QOL Reduction of LV dyssynchrony
Höjjer et al. (90)	10	NYHA III/IV No LBBB in pre-pacing ECG	AVB SND Bradycardia	Median 68 mo	6 mo	N/A	N/A	N/A	Improvement in 6MWT, pro-BNP, QOL No changes in echocardiographic parameters
Observational studies									
Leclercq et al. (59)	20	NYHA III/IV LVEF ≤35% Paced QRS ≥200 ms	Conventional indications	N/A	15 ± 10 mo	222 ± 18 vs. 163 ± 30 *	20 ± 6 vs. 24 ± 13 *	3.8 ± 0.4 vs. 2.6 ± 0.5 *	N/A
Baker et al. (60)	60	NYHA III/IV	SND AVB AVJ ablation	N/A	7.7 mo	206 ± 36 vs. 170 ± 34 *	23 ± 8 vs. 29 ± 11 *	3.4 ± 0.5 vs. 2.4 ± 0.7 *	Improvement in QOL
Leon et al. (52)	20	NYHA III/IV LVEF ≤35%	AVJ ablation	26 ± 12 mo	17 ± 5 mo	213 ± 40 vs. 172 ± 31 *	22 ± 7 vs. 31 ± 12 *	3.4 ± 0.5 vs. 2.4 ± 0.6 *	Improvement in QOL
Valls-Bertault et al. (54)	16	NYHA III/IV LVEF ≤35%	AVJ ablation	20 ± 19 mo	6 mo	192 ± 28 vs. 177 ± 23	24 ± 9 vs. 28 ± 12	3.4 ± 0.5 vs. 2.6 ± 1.1 *	No changes in 6MWT and peak VO2
Eldadah et al. (55)	12	NYHA III	AVB Bradycardia	> 1 yr	4 – 6 wks	N/A	31 ± 5 vs. 36 ± 5 *	3.0 ± 0.0 vs. 2.0 ± 0.7 *	Reduction of LV dyssynchrony Improvement in LV systolic strain
Laurenzi et al. (91)	38	NYHA III/IV LVEF <35% QRS >150 ms	N/A	4.7 ± 2.0 yrs	6 mo	179 ± 19 vs. 124 ± 20 *	27 ± 6 vs. 38 ± 10 *	3.1 ± 0.4 vs. 2.0 ± 0.6 *	Reduction of LV dyssynchrony

* Indicates a significant difference after upgrade ($p < 0.05$ RV pacing vs. CRT). AVB = atrioventricular block; AVJ ablation = atrioventricular junction ablation; CRT = cardiac resynchronization therapy; LBBB = left bundle branch block; LV = left ventricular; LVEF = left ventricular ejection fraction; NYHA = New York Heart Association; mo = months; QOL = quality of life; RV = right ventricular; SND = sinus node dysfunction; wk = week; yr = year; 6MWT = 6 minute walking-test.

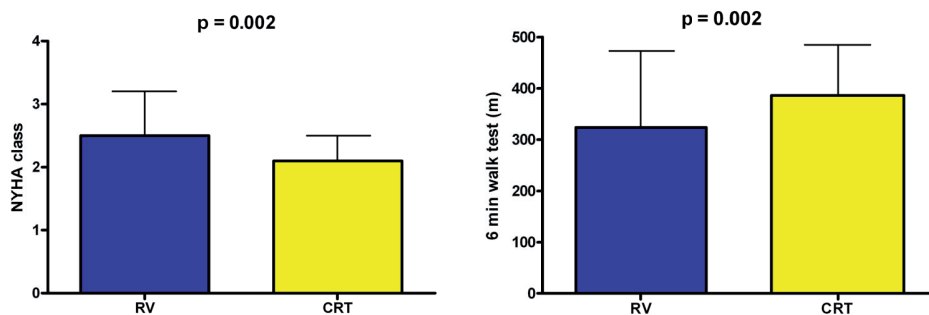


Figure 5. Changes in NYHA functional class and 6 minute walking-test after upgrade from RV pacing to CRT. In 44 patients with conventional pacemaker indications, an upgrade to CRT was performed after a mean of 49 ± 34 months of RV apical pacing. After 6 months of CRT, NYHA class improved from 2.5 ± 0.7 to 2.1 ± 0.4 (left panel), and the distance walked during the 6 minute walking-test increased from 324 ± 20 m to 386 ± 99 m (right panel) (57). CRT = cardiac resynchronization therapy; NYHA = New York Heart Association; RV = right ventricular pacing.

pacing, tissue Doppler imaging was used to assess LV dyssynchrony. After a mean of 144 ± 17 days, a significant decrease in the mean septal-to-lateral delay was noted from 101 ± 12 ms to 10 ± 9 ms ($p < 0.001$) (53). Likewise, with the use of novel speckle-tracking echocardiography it has been demonstrated that the difference in time-to-peak strain of various LV segments (as a measure of LV dyssynchrony) decreases significantly after upgrade to CRT (47).

RV apical pacing versus CRT

With the promising results of upgrading patients from RV apical pacing to CRT, it has been suggested that patients with moderate to severe LV dysfunction and a standard pacemaker indication may actually benefit from CRT instead of RV apical pacing alone. A number of observational studies and randomized trials have performed a head-to-head comparison between the two pacing modes.

The effects of the two pacing modes on LV remodeling have been studied in the Homburg Biventricular Pacing Evaluation (HOBIPACE) trial (63). In this trial, 30 patients with standard indications for permanent pacing and a LVEF $\leq 40\%$, were randomized between RV pacing and CRT. After 3 months of pacing, cross-over to the other pacing modality was performed. The LV end-systolic volume was 177.3 ± 68.7 ml at baseline, and decreased modestly with RV pacing (160.2 ± 73.4 ml, $p < 0.05$). When compared with RV pacing, CRT significantly reduced LV end-systolic volume by 17% (133.1 ± 66.5 ml, $p < 0.001$) (63).

In addition to LV remodeling, improvements in LV hemodynamics (64,65) and LV mechanical function (66) during CRT have been demonstrated. In the Post AV Nodal Ablation Evaluation (PAVE) trial, 184 patients were randomized after AV junction ablation in two parallel arms (conventional RV pacing or CRT) (66). Mean LVEF at follow-up was significantly lower in the 81 patients who underwent RV pacing as compared with the 103 patients with CRT ($41 \pm 13\%$ vs. $46 \pm 13\%$, $p < 0.05$) (66). However, it should be noted that other trials, including the Optimal Pacing SITE (OPSITE) trial (67), demonstrated only modest improvement in LVEF during CRT compared to RV pacing.

A number of randomized trials have compared conventional RV apical pacing and CRT (Table 3). Although some trials have demonstrated clear long-term benefit of CRT over RV pacing with regard to peak VO₂ or the distance walked during the 6 minute walking-test (63,66), others have demonstrated only modest (67,68) or no benefit at all (69). The ongoing Biventricular Pacing for Atrioventricular Block to Prevent Cardiac Desynchronization (BioPace) trial will demonstrate if CRT actually provides benefit in morbidity and mortality over conventional RV apical pacing (70).

Table 3. Randomized clinical trials comparing RV apical pacing versus CRT

Trial (reference)	Number of patients	Design	Inclusion criteria	Primary end-point	Secondary end-point	Comment
MUSTIC (68)	43	Cross-over	Chronic heart failure LV systolic dysfunction Persistent AF Ventricular pacing QRS >200 ms 6MWT <450 m	6MWT	Peak VO ₂ QOL Heart failure hospitalization Mortality Patient pacing preference	CRT modestly superior over RV pacing for 6MWT and peak VO ₂ No difference in QOL
OPSITE (67)	56	Cross-over	AVN ablation and PM implantation CRT	QOL 6MWT	Subgroup analysis of: QOL 6MWT	CRT modestly superior over RV pacing for QOL and 6MWT
PAVE (66)	184	Parallel arms	AVN ablation and PM implantation	6MWT	QOL LVEF	CRT superior over RV pacing for 6MWT and LVEF No differences in QOL
HOBIPACE (63)	30	Cross-over	LV systolic dysfunction Permanent ventricular pacing	LVESV LVEF peak VO ₂	NYHA class QOL NT-proBNP Exercise capacity LV dyssynchrony	CRT superior over RV pacing for LVESV, LVEF, peak VO ₂ CRT superior over RV pacing for secondary end-points
Albertsen et al. (69)	50	Parallel arms	High-grade AV block	LVEF	LV dyssynchrony LV diastolic function LA volumes LV dimensions NT-proBNP 6MWT	No difference in LVEF No differences in secondary end-points

AF = atrial fibrillation; AV = atrioventricular; AVN = atrioventricular node; CRT = cardiac resynchronization therapy; LA = left atrial; LV = left ventricular; LVEF = left ventricular ejection fraction; LVESV = left ventricular end-systolic volume; NYHA = New York Heart Association; PM = pacemaker; QOL = quality of life; RV = right ventricular; 6MWT = 6 minute walking-test.

Effect on ventricular dyssynchrony For mechanical dyssynchrony, only a few studies have systematically compared RV apical pacing and CRT. In 6 heart failure patients referred for CRT, Matsushita et al. assessed dyssynchrony during RV apical pacing and during CRT (71). During CRT, a decrease in both LV intraventricular dyssynchrony (RV pacing 322 ± 101 ms vs. CRT 209 ± 88 ms, $p < 0.05$) and interventricular dyssynchrony (RV pacing 37.2 ± 44.7 ms vs. CRT 16.2 ± 47.4 ms, $p < 0.05$) was noted (71). In a randomized study comparing DDDR pacing and CRT in 50 patients with high degree AV block, Albertsen et al. assessed ventricular dyssynchrony using tissue Doppler imaging (69). After 12 months follow-up, the number of LV segments displaying delayed longitudinal contraction (representing LV dyssynchrony) was significantly lower in the patients with CRT, as compared with the patients with DDDR pacing (69). These studies suggest that CRT may be superior over RV apical pacing with regard to the induction of LV dyssynchrony. Together with the promising results on LV remodeling and LV function, it may well be that CRT is a good therapeutic option in patients with moderate to severe LV dysfunction and a conventional indication for cardiac pacing. However, it should be noted that although CRT reduces the amount of ventricular dyssynchrony, normal electromechanical activation is not completely restored (72,73). In addition, it remains uncertain if there is a significant improvement in long-term outcome with CRT, as compared with conventional RV apical pacing. Therefore, more studies are needed to fully appreciate the role of CRT in these patients (1).

Pacing strategies and alternative pacing sites

Alternatives for RV apical pacing may be important in patients who have a depressed LV function at baseline or patients who are expected to be paced frequently (complete AV block) or for a longer period of time (young patients, congenital AV block). Various pacing strategies have been suggested to minimize the amount of RV apical pacing. In addition, strategies to minimize de-synchronization of ventricular contraction using alternative pacing sites have been proposed.

Atrial-based pacing Atrial-based pacing may be preferred over RV apical pacing in selected patient groups, since it prevents cardiac de-synchronization by maintaining normal ventricular electrical activation. Nielsen et al. randomized 177 patients with sinus node disease between AAIR pacing or DDDR pacing with a short AV delay or DDDR pacing with a fixed long AV delay (74). During a mean follow-up of 2.9 ± 1.1 years, left atrial and LV diameters increased and LV fractional shortening decreased in the DDDR groups, whereas no changes occurred in the AAIR group. In addition, atrial fibrillation was less common in the AAIR group as compared to the two DDDR groups (7.4% vs. 23.3% and 17.5%, respectively; $p = 0.03$) (74). However, other large randomized trials have not been able to consistently demonstrate an improved outcome of atrial-based pacing. In a recent meta-analysis from 5 randomized clinical trials comparing atrial-based and ventricular pacing, no significant reduction in mortality with atrial-based pacing could be demonstrated (hazard ratio 0.95; 95% CI 0.87 – 1.03; $p = 0.19$). In addition, no

differences were found in the composite end-point of stroke, cardiovascular death, and heart failure hospitalization between the different pacing modes (Figure 6). However, a significant reduction in atrial fibrillation was noted with atrial-based pacing (hazard ratio 0.80; 95% CI 0.72 – 0.89; $p < 0.001$) (75).

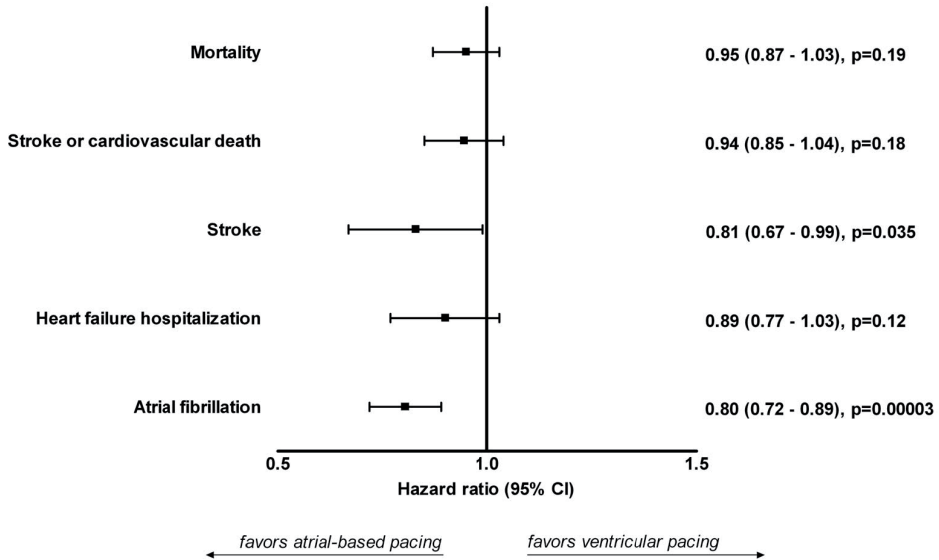


Figure 6. Meta-analysis on atrial-based pacing versus ventricular pacing. A meta-analysis of 5 randomized clinical trials including more than 7000 patients compared atrial-based pacing with ventricular based pacing. This figure demonstrates the effect of the pacing modes on the different outcome parameters (mortality, stroke or cardiovascular death, stroke, heart failure hospitalization, atrial fibrillation), expressed as the hazard ratio and 95% confidence interval (CI). A significant reduction in the incidence of stroke and atrial fibrillation was observed, in favor of atrial-based pacing. The remaining outcome parameters did not show a significant difference between the two pacing modes (75).

Atrial-based pacing to prevent cardiac de-synchronization may only be feasible in selected patients. There is still concern about atrial-based pacing in patients with sinus node disease, because of the development of AV block in these patients (76). In the abovementioned trial, the incidence of progression to symptomatic AV block was 1.9% per year (74). Therefore, atrial-based pacing for the maintenance of ventricular synchrony is only recommended in patients with sinus node disease without AV conduction abnormalities (1).

Minimal ventricular pacing algorithms In addition, specific pacing algorithms have been introduced to minimize unnecessary RV pacing. These algorithms promote normal AV conduction and target maintenance of intrinsic ventricular conduction (77,78). Thereby, the algorithms avoid the induction of LV dyssynchrony. In the Inhibition of unnecessary RV pacing with AVSH in ICDs Study (INTRINSIC RV), the effects of the use of an AV search hysteresis algorithm was studied (77). A total of 988 patients with an indication for an Implantable Cardioverter Defibrillator were randomized between VVI-40 back-up pacing or DDDR pacing with the AV search hysteresis

algorithm. In the DDDR group, 32 patients (6.4%) met the composite primary end-point of all-cause mortality and heart failure hospitalization, as compared with 46 patients (9.5%) in the VVI group ($p < 0.001$). It was concluded that the use of the AV search hysteresis algorithm was associated with similar clinical outcomes compared with VVIR backup pacing (77).

Similar, in the Search AV Extension and Managed Ventricular Pacing for Promoting Atrio-ventricular Conduction (SAVE PACE) trial, 1065 patients with sinus node disease and intact AV conduction were randomized between conventional dual-chamber pacing and dual-chamber minimal ventricular pacing (78). With the use of the minimal RV pacing algorithm, the percentage of paced ventricular beats was significantly reduced, as compared with conventional dual-chamber ventricular pacing (9.1 vs. 99.0%, $p < 0.001$). After a mean of 1.7 ± 1.0 years, the development of persistent atrial fibrillation was significantly reduced with minimal ventricular pacing (7.9% in minimal RV pacing vs. 12.7% in conventional dual-chamber pacing, $p = 0.004$). Although these results suggest that this reduction is directly related to the decrease in RV apical pacing, a better AV coupling may have contributed as well. Unfortunately, no significant difference in mortality or heart failure hospitalizations between the two groups was observed (78). These studies suggest a favorable effect of minimizing ventricular pacing algorithms. However, more studies are needed to fully appreciate the exact clinical benefits in daily practice (1).

Alternative RV pacing sites Pacing at the RV outflow tract, septal pacing and direct His bundle pacing have been suggested as alternatives to the RV apex when pacing is inevitable (79). Because of the closer proximity to the normal conduction system, these sites may result in less electrical activation delay (represented by a shorter QRS duration) and less mechanical dyssynchrony.

From all alternative RV pacing sites, the RV outflow tract has been studied the most extensively. A meta-analysis of 9 studies with 217 patients comparing RV outflow tract and RV apical pacing demonstrated a favorable effect of RV outflow tract pacing on hemodynamics (80). Unfortunately, the majority of the studies involved short-term follow-up studies. A recent retrospective study demonstrated a better survival in patients with RV outflow tract pacing as compared with RV apical pacing (81). The favorable effect of RV outflow tract pacing may be related to the more physiologic activation pattern, resulting in less LV dyssynchrony. However, a small study with 14 patients could not demonstrate a benefit of RV outflow tract pacing over RV apical pacing with regard to LV dyssynchrony (82). More studies with dyssynchrony analysis and long-term follow-up comparing RV outflow pacing and RV apical pacing are therefore needed.

Septal pacing may be another good alternative for RV apical pacing. Short-term studies have suggested good results compared with RV apical pacing (83), with good pacing thresholds and lead stability (84). In addition, less ventricular dyssynchrony may be present during septal pacing as compared with RV apical pacing (85). However, at long-term follow-up, septal pacing may not be superior over RV apical pacing. In a randomized study including 98 patients with AV

block (53 septal pacing vs. 45 apical pacing), no differences in LVEF and exercise capacity were found after 18 months follow-up (86).

Direct His bundle pacing or para-Hisian pacing has also been suggested as an alternative for RV apical pacing. In one of the first clinical studies with permanent direct His bundle pacing, Deshmukh et al. demonstrated the feasibility of this strategy (87). Implantation was successful in 12 of 14 patients (86%), with maintenance of His bundle capture at long-term follow-up in 11 patients (92%). After a mean of 23.4 ± 8.3 months, LV end-diastolic diameter had decreased from 51 ± 10 mm to 43 ± 8 mm ($p < 0.01$) and LVEF had increased from $18.2 \pm 9.8\%$ to $28.6 \pm 11.2\%$ ($p < 0.05$) (87). Importantly, it has been demonstrated that His bundle pacing may result in less inter- and intraventricular dyssynchrony (88,89). In a randomized study comparing RV apical pacing and para-Hisian pacing in 16 patients, Occhetta et al. noted a significant reduction in interventricular dyssynchrony during para-Hisian pacing as compared with RV apical pacing (34 ± 18 ms vs. 47 ± 19 ms, $p < 0.05$) (89).

Although the various studies have demonstrated beneficial effects of the alternative pacing sites, at present septal and direct His bundle pacing are still not recommended in patients requiring permanent cardiac pacing because of difficulties with lead positioning, and concerns about lead stability and threshold (1). In addition, it should be remembered that any electrical stimulation outside the normal conduction system may ultimately result in electromechanical changes with deleterious effects on LV function. Furthermore, the majority of the studies on alternative pacing sites were non-randomized studies with small study populations and short-term follow-up. Nonetheless, there is increasing evidence that these alternative sites may provide benefit over conventional RV apical pacing.

CONCLUSIONS

From large pacing mode selection trials and observational studies, it has become apparent that a high amount of RV apical pacing may be associated with a worse clinical outcome (deterioration of LV systolic function, development of heart failure and atrial fibrillation). Unfortunately, it remains unclear if there is an 'optimal amount' of RV pacing, and which patients at most susceptible for the deleterious effects of RV pacing. The negative effects may be related to the induction of ventricular dyssynchrony by RV apical pacing. Future studies are needed to address these remaining questions.

Various therapeutic options have been suggested in patients with a conventional pacemaker indication. The upgrade to CRT may partially reverse the deleterious effects of RV apical pacing. New pacing strategies and alternative RV pacing sites may prevent the induction of ventricular dyssynchrony and the deterioration of LV function.

REFERENCES

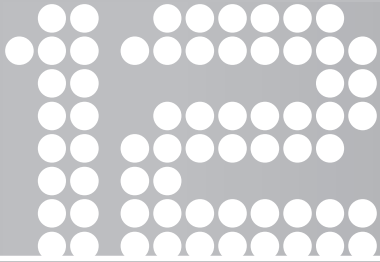
1. Epstein AE, DiMarco JP, Ellenbogen KA et al. ACC/AHA/HRS 2008 Guidelines for Device-Based Therapy of Cardiac Rhythm Abnormalities. *J Am Coll Cardiol* 2008;51:e1-62.
2. Vardas PE, Auricchio A, Blanc JJ et al. Guidelines for cardiac pacing and cardiac resynchronization therapy. *Eur Heart J* 2007;28:2256-95.
3. Mond HG, Irwin M, Morillo C, Ector H. The world survey of cardiac pacing and cardioverter defibrillators: calendar year 2001. *Pacing Clin Electrophysiol* 2004;27:955-64.
4. Sweeney MO, Prinzen FW. A new paradigm for physiologic ventricular pacing. *J Am Coll Cardiol* 2006;47:282-8.
5. Barold SS. Indications for permanent cardiac pacing in first-degree AV block: class I, II, or III? *Pacing Clin Electrophysiol* 1996;19:747-51.
6. Brecker SJ, Xiao HB, Sparrow J, Gibson DG. Effects of dual-chamber pacing with short atrioventricular delay in dilated cardiomyopathy. *Lancet* 1992;340:1308-12.
7. Brignole M, Gianfranchi L, Menozzi C et al. Assessment of atrioventricular junction ablation and DDDR mode-switching pacemaker versus pharmacological treatment in patients with severely symptomatic paroxysmal atrial fibrillation: a randomized controlled study. *Circulation* 1997;96:2617-24.
8. Uslan DZ, Tleyjeh IM, Baddour LM et al. Temporal trends in permanent pacemaker implantation: a population-based study. *Am Heart J* 2008;155:896-903.
9. Hayes DL, Furman S. Cardiac pacing: how it started, where we are, where we are going. *J Cardiovasc Electrophysiol* 2004;15:619-27.
10. Sweeney MO, Hellkamp AS, Ellenbogen KA et al. Adverse effect of ventricular pacing on heart failure and atrial fibrillation among patients with normal baseline QRS duration in a clinical trial of pacemaker therapy for sinus node dysfunction. *Circulation* 2003;107:2932-7.
11. Wilkoff BL, Cook JR, Epstein AE et al. Dual-chamber pacing or ventricular backup pacing in patients with an implantable defibrillator: the Dual Chamber and VVI Implantable Defibrillator (DAVID) Trial. *JAMA* 2002;288:3115-23.
12. Tse HF, Lau CP. Long-term effect of right ventricular pacing on myocardial perfusion and function. *J Am Coll Cardiol* 1997;29:744-9.
13. Lieberman R, Padeletti L, Schreuder J et al. Ventricular pacing lead location alters systemic hemodynamics and left ventricular function in patients with and without reduced ejection fraction. *J Am Coll Cardiol* 2006;48:1634-41.
14. Prinzen FW, Peschar M. Relation between the pacing induced sequence of activation and left ventricular pump function in animals. *Pacing Clin Electrophysiol* 2002;25:484-98.
15. Prinzen FW, Hunter WC, Wyman BT, McVeigh ER. Mapping of regional myocardial strain and work during ventricular pacing: experimental study using magnetic resonance imaging tagging. *J Am Coll Cardiol* 1999;33:1735-42.
16. Tops LF, Schalij MJ, Holman ER, van Erven L, van der Wall EE, Bax JJ. Right ventricular pacing can induce ventricular dyssynchrony in patients with atrial fibrillation after atrioventricular node ablation. *J Am Coll Cardiol* 2006;48:1642-8.
17. Gillis AM. Redefining physiologic pacing: lessons learned from recent clinical trials. *Heart Rhythm* 2006;3:1367-72.
18. Varma N. Left ventricular conduction delays induced by right ventricular apical pacing: effect of left ventricular dysfunction and bundle branch block. *J Cardiovasc Electrophysiol* 2008;19:114-22.
19. Sweeney MO, Hellkamp AS. Heart failure during cardiac pacing. *Circulation* 2006;113:2082-8.
20. Vassallo JA, Cassidy DM, Miller JM, Buxton AE, Marchlinski FE, Josephson ME. Left ventricular endocardial activation during right ventricular pacing: effect of underlying heart disease. *J Am Coll Cardiol* 1986;7:1228-33.
21. Rodriguez LM, Timmermans C, Nabar A, Beatty G, Wellens HJ. Variable patterns of septal activation in patients with left bundle branch block and heart failure. *J Cardiovasc Electrophysiol* 2003;14:135-41.

22. Auricchio A, Fantoni C, Regoli F et al. Characterization of left ventricular activation in patients with heart failure and left bundle-branch block. *Circulation* 2004;109:1133-9.
23. Badke FR, Boinay P, Covell JW. Effects of ventricular pacing on regional left ventricular performance in the dog. *Am J Physiol* 1980;238:H858-H867.
24. Prinzen FW, Augustijn CH, Arts T, Allesie MA, Reneman RS. Redistribution of myocardial fiber strain and blood flow by asynchronous activation. *Am J Physiol* 1990;259:H300-H308.
25. Skolidis EI, Kochiadakis GE, Koukouraki SI et al. Myocardial perfusion in patients with permanent ventricular pacing and normal coronary arteries. *J Am Coll Cardiol* 2001;37:124-9.
26. Karpawich PP, Rabah R, Haas JE. Altered cardiac histology following apical right ventricular pacing in patients with congenital atrioventricular block. *Pacing Clin Electrophysiol* 1999;22:1372-7.
27. van Oosterhout MF, Prinzen FW, Arts T et al. Asynchronous electrical activation induces asymmetrical hypertrophy of the left ventricular wall. *Circulation* 1998;98:588-95.
28. Vernooy K, Dijkman B, Cheriex EC, Prinzen FW, Crijns HJ. Ventricular remodeling during long-term right ventricular pacing following His bundle ablation. *Am J Cardiol* 2006;97:1223-7.
29. Barold SS, Ovsyshcher IE. Pacemaker-induced mitral regurgitation. *Pacing Clin Electrophysiol* 2005;28:357-60.
30. Maurer G, Torres MA, Corday E, Haendchen RV, Meerbaum S. Two-dimensional echocardiographic contrast assessment of pacing-induced mitral regurgitation: relation to altered regional left ventricular function. *J Am Coll Cardiol* 1984;3:986-91.
31. Kass DA. An epidemic of dyssynchrony: but what does it mean? *J Am Coll Cardiol* 2008;51:12-7.
32. Bader H, Garrigue S, Lafitte S et al. Intra-left ventricular electromechanical asynchrony. A new independent predictor of severe cardiac events in heart failure patients. *J Am Coll Cardiol* 2004;43:248-56.
33. Cho GY, Song JK, Park WJ et al. Mechanical dyssynchrony assessed by tissue Doppler imaging is a powerful predictor of mortality in congestive heart failure with normal QRS duration. *J Am Coll Cardiol* 2005;46:2237-43.
34. Castellant P, Fatemi M, Bertault-Valls V, Etienne Y, Blanc JJ. Cardiac resynchronization therapy: "nonresponders" and "hyperresponders". *Heart Rhythm* 2008;5:193-7.
35. Ypenburg C, van Bommel RJ, Borleffs CJ et al. Long-term prognosis after cardiac resynchronization therapy is related to the extent of left ventricular reverse remodeling at midterm follow-up. *J Am Coll Cardiol* 2009;53:483-90.
36. Bax JJ, Abraham T, Barold SS et al. Cardiac resynchronization therapy: Part 1—issues before device implantation. *J Am Coll Cardiol* 2005;46:2153-67.
37. Rouleau F, Merheb M, Geffroy S et al. Echocardiographic assessment of the interventricular delay of activation and correlation to the QRS width in dilated cardiomyopathy. *Pacing Clin Electrophysiol* 2001;24:1500-6.
38. Schmidt M, Bromsen J, Herholz C et al. Evidence of left ventricular dyssynchrony resulting from right ventricular pacing in patients with severely depressed left ventricular ejection fraction. *Europace* 2007;9:34-40.
39. Marsan NA, Breithardt OA, Delgado V, Bertini M, Tops LF. Predicting response to CRT. The value of two- and three-dimensional echocardiography. *Europace* 2008;10 Suppl 3:iii73-iii79.
40. Gomes JA, Damato AN, Akhtar M et al. Ventricular septal motion and left ventricular dimensions during abnormal ventricular activation. *Am J Cardiol* 1977;39:641-50.
41. Thambo JB, Bordachar P, Garrigue S et al. Detrimental ventricular remodeling in patients with congenital complete heart block and chronic right ventricular apical pacing. *Circulation* 2004;110:3766-72.
42. Lupi G, Sassone B, Badano L et al. Effects of right ventricular pacing on intra-left ventricular electromechanical activation in patients with native narrow QRS. *Am J Cardiol* 2006;98:219-22.
43. Liu WH, Chen MC, Chen YL et al. Right ventricular apical pacing acutely impairs left ventricular function and induces mechanical dyssynchrony in patients with sick sinus syndrome: a real-time three-dimensional echocardiographic study. *J Am Soc Echocardiogr* 2008;21:224-9.

44. Albertsen AE, Nielsen JC, Poulsen SH et al. DDD(R)-pacing, but not AAI(R)-pacing induces left ventricular desynchronization in patients with sick sinus syndrome: tissue-Doppler and 3D echocardiographic evaluation in a randomized controlled comparison. *Europace* 2008;10:127-33.
45. Chen L, Hodge D, Jahangir A et al. Preserved left ventricular ejection fraction following atrioventricular junction ablation and pacing for atrial fibrillation. *J Cardiovasc Electrophysiol* 2008;19:19-27.
46. Zhang XH, Chen H, Siu CW et al. New-onset heart failure after permanent right ventricular apical pacing in patients with acquired high-grade atrioventricular block and normal left ventricular function. *J Cardiovasc Electrophysiol* 2008;19:136-41.
47. Tops LF, Suffoletto MS, Bleeker GB et al. Speckle-tracking radial strain reveals left ventricular dyssynchrony in patients with permanent right ventricular pacing. *J Am Coll Cardiol* 2007;50:1180-8.
48. Delgado V, Tops LF, Trines SA et al. Acute effects of right ventricular apical pacing on left ventricular synchrony and mechanics. *Circ Arrhythmia Electrophysiol* 2009;2:135-45.
49. Pastore G, Noventa F, Piovesana P et al. Left ventricular dyssynchrony resulting from right ventricular apical pacing: relevance of baseline assessment. *Pacing Clin Electrophysiol* 2008;31:1456-62.
50. Nahlawi M, Waligora M, Spies SM, Bonow RO, Kadish AH, Goldberger JJ. Left ventricular function during and after right ventricular pacing. *J Am Coll Cardiol* 2004;44:1883-8.
51. Chung ES, Leon AR, Tavazzi L et al. Results of the Predictors of Response to CRT (PROSPECT) trial. *Circulation* 2008;117:2608-16.
52. Leon AR, Greenberg JM, Kanuru N et al. Cardiac resynchronization in patients with congestive heart failure and chronic atrial fibrillation: effect of upgrading to biventricular pacing after chronic right ventricular pacing. *J Am Coll Cardiol* 2002;39:1258-63.
53. Witte KK, Pipes RR, Nanthakumar K, Parker JD. Biventricular pacemaker upgrade in previously paced heart failure patients--improvements in ventricular dyssynchrony. *J Card Fail* 2006;12:199-204.
54. Valls-Bertault V, Fatemi M, Gilard M, Pennec PY, Etienne Y, Blanc JJ. Assessment of upgrading to biventricular pacing in patients with right ventricular pacing and congestive heart failure after atrioventricular junctional ablation for chronic atrial fibrillation. *Europace* 2004;6:438-43.
55. Eldadah ZA, Rosen B, Hay I et al. The benefit of upgrading chronically right ventricle-paced heart failure patients to resynchronization therapy demonstrated by strain rate imaging. *Heart Rhythm* 2006;3:435-42.
56. Marai I, Gurevitz O, Carasso S et al. Improvement of congestive heart failure by upgrading of conventional to resynchronization pacemakers. *Pacing Clin Electrophysiol* 2006;29:880-4.
57. Leclercq C, Cazeau S, Lellouche D et al. Upgrading from single chamber right ventricular to biventricular pacing in permanently paced patients with worsening heart failure: The RD-CHF Study. *Pacing Clin Electrophysiol* 2007;30 Suppl 1:S23-S30.
58. Shimano M, Tsuji Y, Yoshida Y et al. Acute and chronic effects of cardiac resynchronization in patients developing heart failure with long-term pacemaker therapy for acquired complete atrioventricular block. *Europace* 2007;9:869-74.
59. Leclercq C, Cazeau S, Ritter P et al. A pilot experience with permanent biventricular pacing to treat advanced heart failure. *Am Heart J* 2000;140:862-70.
60. Baker CM, Christopher TJ, Smith PF, Langberg JJ, DeLurgio DB, Leon AR. Addition of a left ventricular lead to conventional pacing systems in patients with congestive heart failure: feasibility, safety, and early results in 60 consecutive patients. *Pacing Clin Electrophysiol* 2002;25:1166-71.
61. Horwich T, Foster E, De Marco T, Tseng Z, Saxon L. Effects of resynchronization therapy on cardiac function in pacemaker patients "upgraded" to biventricular devices. *J Cardiovasc Electrophysiol* 2004;15:1284-9.
62. Cazeau S, Bordachar P, Jauvert G et al. Echocardiographic modeling of cardiac dyssynchrony before and during multisite stimulation: a prospective study. *Pacing Clin Electrophysiol* 2003;26:137-43.
63. Kindermann M, Hennen B, Jung J, Geisel J, Bohm M, Frohlig G. Biventricular versus conventional right ventricular stimulation for patients with standard pacing indication and left ventricular dysfunction: the Homburg Biventricular Pacing Evaluation (HOBIPACE). *J Am Coll Cardiol* 2006;47:1927-37.

64. Kass DA, Chen CH, Curry C et al. Improved left ventricular mechanics from acute VDD pacing in patients with dilated cardiomyopathy and ventricular conduction delay. *Circulation* 1999;99:1567-73.
65. Simantirakis EN, Vardakis KE, Kochiadakis GE et al. Left ventricular mechanics during right ventricular apical or left ventricular-based pacing in patients with chronic atrial fibrillation after atrioventricular junction ablation. *J Am Coll Cardiol* 2004;43:1013-8.
66. Doshi RN, Daoud EG, Fellows C et al. Left ventricular-based cardiac stimulation post AV nodal ablation evaluation (the PAVE study). *J Cardiovasc Electrophysiol* 2005;16:1160-5.
67. Brignole M, Gammage M, Puggioni E et al. Comparative assessment of right, left, and biventricular pacing in patients with permanent atrial fibrillation. *Eur Heart J* 2005;26:712-22.
68. Leclercq C, Walker S, Linde C et al. Comparative effects of permanent biventricular and right-univentricular pacing in heart failure patients with chronic atrial fibrillation. *Eur Heart J* 2002;23:1780-7.
69. Albertsen AE, Nielsen JC, Poulsen SH et al. Biventricular pacing preserves left ventricular performance in patients with high-grade atrio-ventricular block: a randomized comparison with DDD(R) pacing in 50 consecutive patients. *Europace* 2008;10:314-20.
70. Funck RC, Blanc JJ, Mueller HH, Schade-Brittinger C, Bailleul C, Maisch B. Biventricular stimulation to prevent cardiac desynchronization: rationale, design, and endpoints of the 'Biventricular Pacing for Atrioventricular Block to Prevent Cardiac Desynchronization (BioPace)' study. *Europace* 2006;8:629-35.
71. Matsushita K, Ishikawa T, Sumita S et al. Assessment of regional wall motion by strain Doppler during biventricular pacing in patients with conventional indications for a pacemaker. *Pacing Clin Electrophysiol* 2004;27:1284-91.
72. Wyman BT, Hunter WC, Prinzen FW, McVeigh ER. Mapping propagation of mechanical activation in the paced heart with MRI tagging. *Am J Physiol* 1999;276:H881-H891.
73. Wyman BT, Hunter WC, Prinzen FW, Faris OP, McVeigh ER. Effects of single- and biventricular pacing on temporal and spatial dynamics of ventricular contraction. *Am J Physiol Heart Circ Physiol* 2002;282:H372-H379.
74. Nielsen JC, Kristensen L, Andersen HR, Mortensen PT, Pedersen OL, Pedersen AK. A randomized comparison of atrial and dual-chamber pacing in 177 consecutive patients with sick sinus syndrome: echocardiographic and clinical outcome. *J Am Coll Cardiol* 2003;42:614-23.
75. Healey JS, Toff WD, Lamas GA et al. Cardiovascular outcomes with atrial-based pacing compared with ventricular pacing: meta-analysis of randomized trials, using individual patient data. *Circulation* 2006;114:11-7.
76. Rosenqvist M, Obel IW. Atrial pacing and the risk for AV block: is there a time for change in attitude? *Pacing Clin Electrophysiol* 1989;12:97-101.
77. Olshansky B, Day JD, Moore S et al. Is dual-chamber programming inferior to single-chamber programming in an implantable cardioverter-defibrillator? Results of the INTRINSIC RV (Inhibition of Unnecessary RV Pacing With AVSH in ICDs) study. *Circulation* 2007;115:9-16.
78. Sweeney MO, Bank AJ, Nsah E et al. Minimizing ventricular pacing to reduce atrial fibrillation in sinus-node disease. *N Engl J Med* 2007;357:1000-8.
79. Manolis AS. The deleterious consequences of right ventricular apical pacing: time to seek alternate site pacing. *Pacing Clin Electrophysiol* 2006;29:298-315.
80. de Cock CC, Giudici MC, Twisk JW. Comparison of the haemodynamic effects of right ventricular outflow-tract pacing with right ventricular apex pacing: a quantitative review. *Europace* 2003;5:275-8.
81. Vanerio G, Vidal JL, Fernandez BP, Banina AD, Viana P, Tejada J. Medium- and long-term survival after pacemaker implant: Improved survival with right ventricular outflow tract pacing. *J Interv Card Electrophysiol* 2008;21:195-201.
82. Ten Cate TJ, Scheffer MG, Sutherland GR, Fred VJ, van Hemel NM. Right ventricular outflow and apical pacing comparably worsen the echocardiographic normal left ventricle. *Eur J Echocardiogr* 2008;9:672-7.
83. Victor F, Mabo P, Mansour H et al. A randomized comparison of permanent septal versus apical right ventricular pacing: short-term results. *J Cardiovasc Electrophysiol* 2006;17:238-42.

84. Burri H, Sunthorn H, Dorsaz PA, Viera I, Shah D. Thresholds and complications with right ventricular septal pacing compared to apical pacing. *Pacing Clin Electrophysiol* 2007;30 Suppl 1:S75-S78.
85. Yu CC, Liu YB, Lin MS, Wang JY, Lin JL, Lin LC. Septal pacing preserving better left ventricular mechanical performance and contractile synchronism than apical pacing in patients implanted with an atrioventricular sequential dual chamber pacemaker. *Int J Cardiol* 2007;118:97-106.
86. Kypta A, Steinwender C, Kammler J, Leisch F, Hofmann R. Long-term outcomes in patients with atrioventricular block undergoing septal ventricular lead implantation compared with standard apical pacing. *Europace* 2008;10:574-9.
87. Deshmukh P, Casavant DA, Romanyshyn M, Anderson K. Permanent, direct His-bundle pacing: a novel approach to cardiac pacing in patients with normal His-Purkinje activation. *Circulation* 2000;101:869-77.
88. Zanon F, Bacchiega E, Rampin L et al. Direct His bundle pacing preserves coronary perfusion compared with right ventricular apical pacing: a prospective, cross-over mid-term study. *Europace* 2008;10:580-7.
89. Occhetta E, Bortnik M, Magnani A et al. Prevention of ventricular desynchronization by permanent para-Hisian pacing after atrioventricular node ablation in chronic atrial fibrillation: a crossover, blinded, randomized study versus apical right ventricular pacing. *J Am Coll Cardiol* 2006;47:1938-45.
90. Hoijer CJ, Meurling C, Brandt J. Upgrade to biventricular pacing in patients with conventional pacemakers and heart failure: a double-blind, randomized crossover study. *Europace* 2006;8:51-5.
91. Laurenzi F, Achilli A, Avella A et al. Biventricular upgrading in patients with conventional pacing system and congestive heart failure: results and response predictors. *Pacing Clin Electrophysiol* 2007;30:1096-104.



Right ventricular pacing can induce ventricular dyssynchrony in patients with atrial fibrillation after atrioventricular node ablation

Laurens F. Tops
Martin J. Schalij
Eduard R. Holman
Lieselot van Erven
Ernst E. van der Wall
Jeroen J. Bax

Department of Cardiology, Leiden University Medical Center, Leiden, the Netherlands

J Am Coll Cardiol 2006;48:1642-8

ABSTRACT

Background: Atrioventricular (AV) node ablation and subsequent long-term RV pacing is a well-established treatment option in patients with atrial fibrillation (AF).

Objectives: To assess the effects of long-term right ventricular (RV) pacing on left ventricular (LV) dyssynchrony, LV function and heart failure symptoms.

Methods: In 55 patients with drug-refractory AF, AV node ablation and implantation of a pacemaker was performed. At baseline and after a mean of 3.8 ± 1.7 years, LV dyssynchrony (by M-mode echocardiography and tissue Doppler imaging), LV function and volumes and functional status were assessed.

Results: After long-term RV pacing, 27 patients (49%) had developed LV dyssynchrony. Concomitantly, these patients worsened in heart failure symptoms (NYHA class increased from 1.8 ± 0.6 to 2.2 ± 0.7 , $p < 0.05$), with a decrease in LV ejection fraction (from $48 \pm 7\%$ to $43 \pm 7\%$, $p < 0.05$) and an increase in LV end-diastolic volume (from 116 ± 39 ml to 130 ± 52 ml, $p < 0.05$). Conversely, patients without LV dyssynchrony did not deteriorate in heart failure symptoms, LV function or LV volumes.

Conclusions: Long-term RV pacing can induce LV dyssynchrony in almost 50% of patients treated with AV node ablation for chronic AF. The development of LV dyssynchrony was associated with deterioration in heart failure symptoms, systolic LV function and LV dilatation.

INTRODUCTION

Chronic atrial fibrillation (AF) represents the most commonly encountered cardiac arrhythmia, and contributes substantially to cardiac morbidity and mortality (1). Although pharmacological therapy still is considered first-line therapy (2), anti-arrhythmic drugs are frequently ineffective and may have serious side-effects. Therefore, several non-pharmacological therapies have been introduced (3).

Atrioventricular (AV) node ablation and subsequent permanent pacing is a well-established treatment option in patients with chronic, drug-refractory AF (4). AV node ablation and permanent pacing may improve quality of life and exercise capacity (5), and may be superior to pharmacological therapy in controlling symptoms of AF (4,6).

However, recent studies have shown detrimental effects of long-term right ventricular (RV) pacing (7,8). Left ventricular (LV) dilatation (remodeling) (7) with a decrease in LV ejection fraction (8) after long-term RV pacing have been reported.

The underlying cause of these adverse effects is unknown but may be related to induction of LV dyssynchrony after long-term RV pacing, with subsequent deterioration of LV function. To evaluate this hypothesis, the effects of long-term RV pacing on LV function and dyssynchrony were evaluated in patients with chronic AF with normal LV function and without valvular disease undergoing AV node ablation and RV pacing.

METHODS

Study population

We retrospectively studied 55 patients who suffered from permanent AF, despite optimal pharmacological therapy. Accordingly, all patients were scheduled for AV node ablation and pacemaker implantation. All patients had preserved LV systolic function without significant valvular disease. At baseline and after a minimum period of one year RV pacing, New York Heart Association (NYHA) functional class was assessed and echocardiography was performed.

Ablation and pacemaker implantation

Atrioventricular node ablation was performed with a 4 mm quadripolar mapping / ablation catheter (EPT, Boston Scientific, Natick, Massachusetts, USA), accessed through the femoral vein. A temporary pacing electrode was placed in the RV apex for back-up pacing. Radiofrequency energy was applied at the AV node until complete AV-block was achieved. Thereafter the pacemaker was implanted. Pacemaker leads were inserted through the subclavian vein using standard implantation techniques. The RV leads were positioned in the RV apex in all patients. After implantation, pacemakers were routinely programmed to VVIR mode.

Echocardiography

All patients underwent echocardiography before the ablation procedure and after long-term RV pacing. Images were recorded with patients in the left lateral decubitus position using a commercially available system (Vingmed Vivid Seven, General Electric-Vingmed, Milwaukee, Wisconsin, USA). Images were obtained using a 3.5-MHz transducer at a depth of 16 cm in the parasternal (long- and short-axis) and apical (two-chamber and four-chamber) views. Standard two-dimensional images and color Doppler data triggered to the QRS complex were saved in cine-loop format.

LV end-diastolic and end-systolic volumes and LV ejection fraction were calculated from apical two- and four-chamber images using the biplane Simpson's rule (9). Furthermore, LV end-diastolic diameter was measured from the parasternal long-axis images.

The severity of mitral regurgitation was graded semi-quantitatively using color-flow Doppler in the conventional parasternal long-axis and apical four-chamber images (10). Mitral regurgitation was characterized as: minimal = 1+ (jet area/left atrial area <10%), moderate = 2+ (jet area/left atrial area 10-20%), moderate-severe = 3+ (jet area/left atrial area 20-45%), or severe = 4+ (jet area/left atrial area >45%) (10).

Ventricular dyssynchrony

At baseline and after long-term RV pacing, LV dyssynchrony was assessed. Septal-to-posterior wall motion delay (SPWMD) was assessed using an M-mode recording from the parasternal short-axis view at the papillary muscle level. The interval between the maximal posterior displacement of the septum and the maximal displacement of the LV posterior wall was calculated (11). As reported by Pitzalis et al, SPWMD ≥ 130 ms was used as the cut-off value for LV dyssynchrony (11,12).

Furthermore, interventricular dyssynchrony was calculated as the difference between LV electromechanical delay (time from QRS onset to aortic systolic flow onset) and RV electromechanical delay (time from QRS onset to pulmonary systolic flow onset) (13). An interventricular delay ≥ 40 ms was used as a cut-off value for interventricular dyssynchrony, as previously described (13,14).

In addition, LV dyssynchrony was assessed using color-coded tissue Doppler imaging (TDI) after long-term RV pacing in 52 patients. The frame rates ranged from 80 to 115 frames/s, depending on the sector width of the range of interest; pulse repetition frequencies ranged from 0.5 to 1 kHz, resulting in aliasing velocities ranging from 16 to 32 cm/s. TDI parameters were measured from color-coded images of three consecutive heart beats by off-line analysis. Data were analyzed using commercially available software (Echopac 6.1, General Electric-Vingmed). To assess LV dyssynchrony, the sample volume was placed in the basal portions of the septum and lateral wall; the time to peak systolic velocity was obtained in the septum and lateral wall, and the septal-to-lateral delay in peak velocity was calculated as an indicator of LV dyssynchrony. A septal-to-lateral delay ≥ 65 ms was used as a cut-off value for LV dyssynchrony

assessed with TDI, as previously reported (15). The interventricular dyssynchrony and TDI images were evaluated by two independent observers, blinded to the results of the SPWMD.

Statistical analysis

Results are presented as mean values \pm SD, or number (%). Continuous data were compared using paired or unpaired Student *t* test when appropriate. Correlation between SPWMD and TDI was assessed using Pearson's linear correlation. Agreement between SPWMD and TDI was expressed in a 2X2 table using κ statistics. A κ value of <0.4 represents poor agreement, a κ between 0.4 and 0.75 represents fair to good agreement, and a κ value of >0.75 is considered an excellent agreement based on the Fleiss classification (16). A *p* value <0.05 was considered statistically significant.

RESULTS

Study population

Fifty-five patients were studied. Baseline characteristics of the patients are listed in Table 1. All patients had preserved LV systolic function at baseline. None of the patients had significant mitral regurgitation or LV dysfunction. In all patients AV node ablation with subsequent pacemaker implantation was performed successfully. No complications related to the ablation procedure or pacemaker implantation were observed. Mean follow-up was 3.8 ± 1.7 years (range 1.2 to 8.7 years).

Table 1. Baseline characteristics of the study population

	All patients (n= 55)	Dyssynchrony absent (n = 28)	Dyssynchrony present (n = 27)
Age (yrs)	61 \pm 11	60 \pm 11	62 \pm 12
Gender (M/F)	27/28	15/13	12/15
Duration AF (yrs)	7 \pm 5	8 \pm 5	7 \pm 5
Anti-arrhythmic drugs used per patient	3.3 \pm 1.3	3.4 \pm 1.5	3.2 \pm 1.2
Hypertension	27 (49%)	14 (50%)	13 (48%)
Coronary artery disease	5 (9%)	2 (7%)	3 (11%)
Clinically relevant MR (grade \geq 2+)	0	0	0
Previous myocardial infarction	3 (6%)	1 (4%)	2 (7%)
NYHA functional class			
I	22 (40%)	13 (46%)	9 (33%)
II	26 (47%)	11 (39%)	15 (56%)
III	7 (13%)	4 (14%)	3 (11%)
IV	0	0	0
QRS duration (ms)	99 \pm 12	100 \pm 13	98 \pm 10
SPWMD (ms)	63 \pm 31	60 \pm 36	67 \pm 22
IVD (ms)	25 \pm 13	24 \pm 14	25 \pm 12

AF = atrial fibrillation; IVD = interventricular delay; MR = mitral regurgitation; NYHA = New York Heart Association; SPWMD = septal-to-posterior wall motion delay.

At baseline, mean interventricular delay was 25 ± 13 ms. None of the patients had an interventricular delay ≥ 40 ms, representing interventricular dyssynchrony. Mean SPWMD before AV node ablation and pacemaker implantation was 63 ± 31 ms (range 4 to 122 ms). In none of the patients, a SPWMD ≥ 130 ms was present at baseline, indicating absence of LV dyssynchrony in all patients.

After long-term RV pacing, mean SPWMD was 121 ± 64 ms (range 11 to 240 ms). In 27 patients (49%) a SPWMD ≥ 130 ms was present, indicating LV dyssynchrony. Accordingly, the study population was divided into two groups: with or without LV dyssynchrony at follow-up, based on a SPWMD delay ≥ 130 ms after long-term RV pacing. Baseline characteristics of the two groups are listed in Table 1. There were no differences in baseline characteristics between the two groups (Table 1).

Intraventricular dyssynchrony

Intraventricular dyssynchrony as assessed with TDI was available in 52 patients after long-term RV pacing. The patients who did not develop LV dyssynchrony on M-mode echocardiography after long-term RV pacing, did also not exhibit LV dyssynchrony on TDI (mean septal-to-lateral delay 37 ± 45 ms). In contrast, the patients who had developed LV dyssynchrony as assessed by M-mode echocardiography also displayed LV dyssynchrony on TDI (mean septal-to-lateral delay 109 ± 26 ms, $p < 0.05$ vs. patients without LV dyssynchrony). Of note, all patients with SPWMD ≥ 130 ms on M-mode had a septal-to-lateral delay ≥ 65 ms assessed with TDI (Table 2). In contrast, there were 4 patients without dyssynchrony on M-mode, that had a septal-to-lateral delay ≥ 65 ms assessed with TDI. A linear relation was found between SPWMD and septal-to-lateral delay ($R = 0.66$, $p < 0.01$) (Figure 1). When applying the cut-off values (SPWMD ≥ 130 ms, septal-to-lateral delay ≥ 65 ms) for LV dyssynchrony, an excellent agreement ($\kappa = 0.85$) between SPWMD and TDI to detect LV dyssynchrony was observed (Figure 2). Disagreement between SPWMD and TDI was based on 4 (8%) patients, in which LV dyssynchrony could only be detected with TDI (Table 2).

Table 2. Agreement between SPWMD and septal-to-lateral delay

		Septal-to-lateral delay ≥ 65 ms		Total
		present	absent	
SPWMD ≥ 130 ms	present	25	0	25
	absent	4	23	27
Total		29	23	52

There is an excellent agreement (92%) between the two methods to assess LV dyssynchrony ($\kappa = 0.85$, $p < 0.01$). The disagreement is related to 4 (8%) patients, in which LV dyssynchrony could only be detected with TDI. LV = left ventricle; TDI = tissue Doppler imaging; SPWMD = septal-to-posterior wall motion delay.

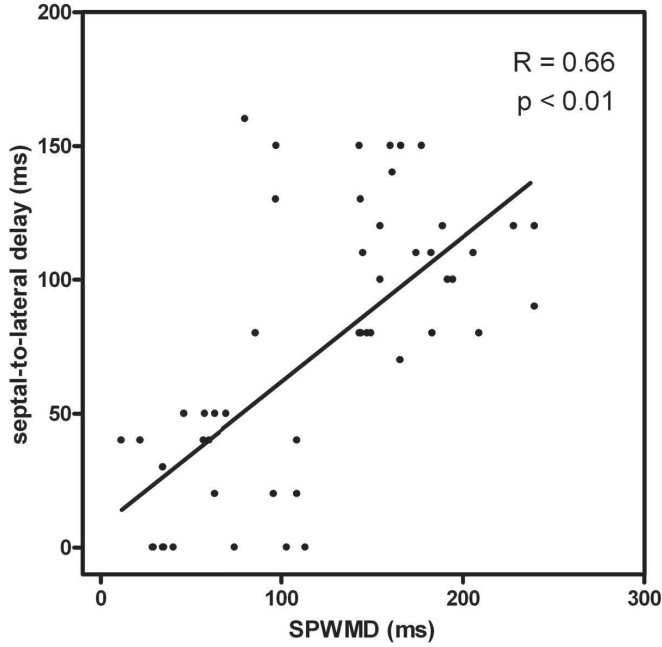


Figure 1. A linear relation was found between SPWMD and septal-to-lateral delay after chronic RV pacing. RV = right ventricle; SPWMD = septal-to-posterior wall motion delay.

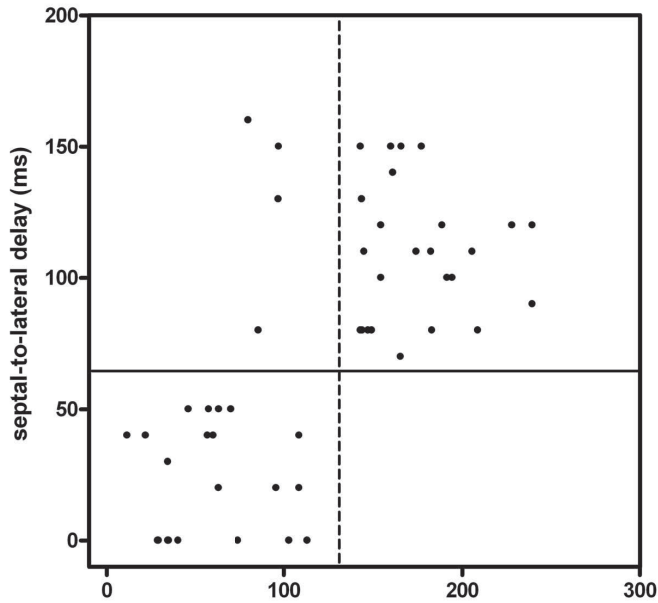


Figure 2. SPWMD and septal-to-lateral delay after chronic RV pacing. For LV dyssynchrony, a cut-off value of SPWMD >130 ms (dashed line), and septal-to-lateral delay >65 ms (solid line) was used. There is a good agreement between SPWMD and septal-to-lateral delay. In only 4 patients, there was a disagreement between SPWMD and septal-to-lateral delay. LV = left ventricle; RV = right ventricle; SPWMD = septal-to-posterior wall motion delay.

Interventricular dyssynchrony

At baseline, none of the patients exhibited interventricular dyssynchrony (mean interventricular delay 25 ± 13 ms). After long-term RV pacing, mean interventricular delay did not increase significantly in the patients without LV dyssynchrony (24 ± 14 ms vs. 35 ± 25 ms, $p=NS$). In contrast, interventricular delay revealed a significant increase in the patients with LV dyssynchrony after long-term RV pacing (25 ± 12 ms vs. 49 ± 19 ms, $p<0.05$). In 19 patients (70%) with LV dyssynchrony, an interventricular delay ≥ 40 ms was present after long-term RV pacing, indicating the presence of interventricular dyssynchrony. In contrast, in only 5 patients (17%) without LV dyssynchrony, an interventricular delay ≥ 40 ms was present ($p<0.01$ vs. patients with LV dyssynchrony).

Clinical and echocardiographic effects of long-term RV pacing

After long-term RV pacing, functional status and LV parameters were re-assessed in all patients. In patients without LV dyssynchrony, NYHA class improved from 1.7 ± 0.7 to 1.4 ± 0.5 ($p<0.01$), whereas NYHA class deteriorated in patients who had developed LV dyssynchrony (from 1.8 ± 0.6 to 2.2 ± 0.7 , $p<0.05$) (Figure 3). Furthermore, LV ejection fraction decreased significantly in patients with LV dyssynchrony ($48 \pm 7\%$ vs. $43 \pm 7\%$, $p<0.05$), whereas LV ejection fraction remained unchanged in patients without LV dyssynchrony (Figure 3).

Also, in patients with LV dyssynchrony, an increase in LV end-diastolic volume (116 ± 39 ml vs. 130 ± 52 ml, $p<0.05$) and LV end-systolic volume (62 ± 26 ml vs. 75 ± 35 ml, $p<0.05$) was observed after long-term RV pacing (Table 3). In addition, LV end-diastolic diameter increased significantly in patients with LV dyssynchrony (5.3 ± 0.8 cm vs. 5.6 ± 0.7 cm, $p<0.05$), whereas no difference in LV diameter was observed in patients without LV dyssynchrony after long-term RV pacing (Table 3).

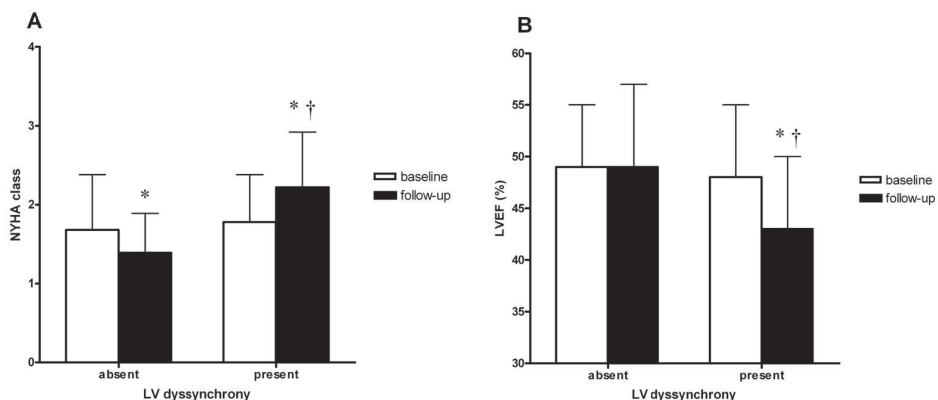


Figure 3. Effects of chronic RV pacing on clinical status and LV ejection fraction. Panel A: In patients with LV dyssynchrony, NYHA functional class deteriorated significantly, whereas NYHA functional class improved significantly in patients without LV dyssynchrony. Panel B: LV ejection fraction decreased significantly in patients with LV dyssynchrony after chronic RV pacing. * $p < 0.05$ baseline vs follow-up; † $p < 0.05$ with dyssynchrony vs without dyssynchrony. LV = left ventricle; LVEF = left ventricular ejection fraction; NYHA = New York Heart Association; RV = right ventricle.

Table 3. LV parameters at baseline and after chronic RV pacing

	Dyssynchrony absent (n = 28)	Dyssynchrony present (n = 27)
LVEF (%)		
Baseline	49 ± 6	48 ± 7
Follow-up	49 ± 8	43 ± 7* †
LVEDV (ml)		
Baseline	119 ± 46	116 ± 39
Follow-up	121 ± 31	130 ± 52*
LVESV (ml)		
Baseline	61 ± 25	62 ± 26
Follow-up	62 ± 19	75 ± 35*
LVEDD (cm)		
Baseline	5.2 ± 0.6	5.3 ± 0.8
Follow-up	5.3 ± 0.4	5.6 ± 0.7* †
Clinically relevant MR (grade ≥ 2+)		
Baseline	0	0
Follow-up	2 (7%)	5 (18%)

* $p < 0.05$ baseline vs. follow-up; † $p < 0.05$ with dyssynchrony vs. without dyssynchrony. LV = left ventricle; LVEDD = left ventricular end-diastolic diameter, LVEDV = left ventricular end-diastolic volume, LVEF = left ventricular ejection fraction, LVESV = left ventricular end-systolic volume, MR = mitral regurgitation, RV = right ventricle.

DISCUSSION

The current observations demonstrate the adverse effects of long-term RV pacing on LV synchrony and LV function. In 49% of the patients treated with AV node ablation and pacemaker implantation, LV dyssynchrony was induced after long-term RV pacing associated with an increase in heart failure symptoms, a decrease in global LV function and LV dilatation.

Effects of long-term RV pacing

In patients with drug-refractory AF, ablation of the AV node and permanent pacing has proven to be effective (4). However, the beneficial effect of the therapy may (partially) be reversed by the non-physiological activation pattern of the interventricular septum. Several studies (7,17-20) have reported negative effects of permanent RV pacing. Regional perfusion defects (17,18), asymmetrical hypertrophy of the ventricular wall (19) and an impairment of LV ejection fraction (20) have been reported after permanent RV pacing.

Furthermore, Thambo et al (7) recently demonstrated the induction of LV dyssynchrony after long-term RV pacing in 23 patients with congenital complete AV-block. Following long-term RV pacing, the mean SPWMD, as a measure of LV dyssynchrony, had significantly increased as compared to baseline (41 ± 16 ms vs. 84 ± 26 ms, $p < 0.05$). In addition, the septal-to-lateral delay as measured by TDI was significantly larger in patients with permanent pacing as compared to controls (59 ± 18 ms vs. 19 ± 9 ms, $p < 0.01$). Similar results were demonstrated in the current study, showing an increase in SPWMD from 63 ± 31 ms to 121 ± 64 ms ($p < 0.05$) after long-term RV pacing, and in 27 (49%) patients the SPWMD exceeded 130 ms, indicating substantial LV dyssynchrony.

The presence of LV dyssynchrony may result in systolic LV dysfunction (21,22). Tambo et al (7) reported a significantly lower cardiac output in patients with LV dyssynchrony after long-term RV pacing, as compared to healthy controls. In addition, LV end-diastolic diameter had significantly increased in these patients as compared to controls (5.5 ± 0.7 cm vs. 4.6 ± 0.6 cm, $p < 0.05$). The observations in the present study are in line with these previous results: patients with LV dyssynchrony after long-term RV pacing showed a decrease in LV ejection fraction, with an increase in LV volumes and LV end-diastolic diameter (Table 3) indicating LV dilatation.

Assessment of LV dyssynchrony

In the current study, LV dyssynchrony was measured by M-mode echocardiography. With M-mode echocardiography the SPWMD can be measured as recently introduced by Pitzalis et al (11). The SPWMD indicates the delay between the maximal systolic motion of the septum and the LV free wall, reflecting intraventricular dyssynchrony (11). At baseline, none of the patients in the current study had SPWMD exceeding 130 ms, which is used as the upper limit of normal LV synchrony. After long-term RV pacing however, 27 (49%) patients had developed LV dyssynchrony, as illustrated by a SPWMD ≥ 130 ms.

In addition to SPWMD, TDI was used to assess the septal-to-lateral delay. TDI is a sophisticated echocardiographic technique that permits measurement and timing of myocardial systolic (and diastolic) velocities. By comparing the differences in time to peak systolic velocities of different LV regions, TDI can identify LV dyssynchrony (23).

Both M-mode using SPWMD and TDI using the septal-to-lateral delay have proven to be effective in the detection of LV dyssynchrony (11,15). In the current study, a good agreement was detected between the SPWMD and septal-to-lateral delay (Figure 2). In particular, all patients with LV dyssynchrony on M-mode also exhibited LV dyssynchrony on TDI, and only 4 patients (8%) without LV dyssynchrony on M-mode had LV dyssynchrony on TDI, indicating minimal underestimation of LV dyssynchrony by SPWMD. Marcus et al (24) have recently demonstrated substantial underestimation of LV dyssynchrony by M-mode echocardiography as compared to TDI in patients with severe LV dysfunction. In particular, in patients with ischemic LV dysfunction and akinesia of the (antero-)septum, assessment of SPWMD may not be feasible and TDI may be preferred for accurate detection of LV dyssynchrony (25). In the current study however, all patients had preserved LV function without significant valvular disease, explaining the better agreement between the two techniques.

Clinical implications

The observations in the current study demonstrate that RV pacing may induce LV dyssynchrony in a substantial percentage of patients with preserved LV function who undergo AV node ablation. In addition, the induction of LV dyssynchrony was associated with a deterioration of LV function and clinical status. Therefore, it needs to be considered whether these patients should have undergone biventricular pacing rather than RV pacing. Recently, several studies

have compared different pacing strategies for patients with AF treated with AV node ablation and permanent pacing. In the PAVE trial (8), 184 patients treated with AV node ablation and pacemaker implantation were randomly assigned to RV pacing or biventricular pacing. After 6 months follow-up, the LV ejection fraction was significantly lower in 81 patients who underwent RV pacing as compared to 103 patients with biventricular pacing ($41 \pm 13\%$ vs. $46 \pm 13\%$, $p < 0.05$). Unfortunately, LV dyssynchrony was not assessed in the PAVE study.

The OPSITE-study (26) compared RV pacing and biventricular pacing in patients with permanent AF undergoing AV node ablation. After 6 months, patients with RV pacing had a significant lower LV ejection fraction as compared to biventricular pacing ($43 \pm 11\%$ vs. $45 \pm 13\%$, $p < 0.05$). In addition, NYHA functional class was significantly lower with RV pacing as compared to biventricular pacing (1.6 ± 0.7 vs. 1.8 ± 0.7 , $p < 0.05$).

In addition, a positive effect of upgrading long-term RV pacing to biventricular pacing has recently been demonstrated. Leon et al (27) reported an improvement in NYHA functional class and LV function after upgrading to biventricular pacing in 20 heart failure patients with chronic AF, previous AV node ablation and RV pacing.

The aforementioned studies provide evidence for the benefit of biventricular pacing, as compared to RV pacing in patients with chronic AF and AV node ablation (8,26,27). The observations in the present study illustrate that in a substantial part of the patients with preserved LV function who undergo AV node ablation, long-term RV pacing can induce LV dyssynchrony, which appears associated with adverse effects, including an increase in heart failure symptoms, and a decrease in LV function with LV dilatation. Whether LV dyssynchrony results in LV dilatation or vice versa, remains unclear. The abnormal electrical activation pattern induced by RV pacing may result in LV dyssynchrony, with subsequent LV dilatation and regional contraction abnormalities (20,22). Conversely, Yu et al demonstrated that a large LV end-systolic diameter predicted the severity of LV dyssynchrony in patients with heart failure (28). However, in the present study, no differences in baseline LV dimensions or volumes were found between the patients with and without LV dyssynchrony after long-term RV pacing. Therefore, no predictors for the induction of LV dyssynchrony could be identified. It may well be that the patients who develop LV dyssynchrony may benefit from biventricular pacing, whereas the patients who do not develop LV dyssynchrony may not need biventricular pacing. Accordingly, patients should be evaluated after RV pacing for development of LV dyssynchrony, and if LV dyssynchrony is induced, biventricular pacing should be considered. Ideally, patients who are at risk for development of LV dyssynchrony should be identified at baseline (before AV node ablation and pacemaker implantation), but the results of the current study could not demonstrate any difference in baseline variables (Table 1). Clearly, additional studies in large populations are needed to confirm the current findings, and to develop selection criteria for patients with normal LV function who may require biventricular pacing rather than RV pacing after AV node ablation for chronic, drug-refractory AF.

Study limitations

Some limitations of the present study need to be addressed. First, it is a retrospective study, and it has a relatively small study population. Larger, prospective studies on the development (and prediction) of LV dyssynchrony after AV node ablation are needed. Furthermore, relatively soft end-points (NYHA functional class and ventricular remodeling) were used to assess clinical efficacy. However, these parameters are often used as markers for clinical efficacy (8,26,27). Finally, the changes in LV ejection fraction and LV end-diastolic volume in the patients with LV dyssynchrony in the present study are relatively small, but statistically significant.

206

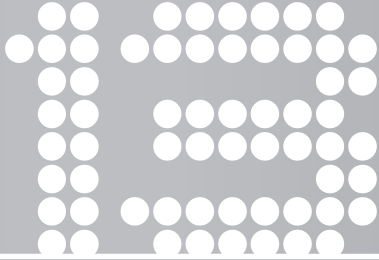
CONCLUSIONS

In patients treated with AV node ablation, long-term RV pacing induced LV dyssynchrony in 49% of patients. These patients appear to develop heart failure symptoms with a reduction in LV systolic function and LV dilatation. These patients may benefit from biventricular pacing rather than RV pacing.

REFERENCES

1. Benjamin EJ, Wolf PA, D'Agostino RB, Silbershatz H, Kannel WB, Levy D. Impact of atrial fibrillation on the risk of death: the Framingham Heart Study. *Circulation* 1998;98:946-52.
2. Fuster V, Ryden LE, Asinger RW et al. ACC/AHA/ESC guidelines for the management of patients with atrial fibrillation: executive summary. *J Am Coll Cardiol* 2001;38:1231-66.
3. Scheinman MM, Morady F. Nonpharmacological approaches to atrial fibrillation. *Circulation* 2001;103:2120-5.
4. Brignole M, Gianfranchi L, Menozzi C et al. Assessment of atrioventricular junction ablation and DDDR mode-switching pacemaker versus pharmacological treatment in patients with severely symptomatic paroxysmal atrial fibrillation: a randomized controlled study. *Circulation* 1997;96:2617-24.
5. Wood MA, Brown-Mahoney C, Kay GN, Ellenbogen KA. Clinical outcomes after ablation and pacing therapy for atrial fibrillation : a meta-analysis. *Circulation* 2000;101:1138-44.
6. Marshall HJ, Harris ZI, Griffith MJ, Holder RL, Gammage MD. Prospective randomized study of ablation and pacing versus medical therapy for paroxysmal atrial fibrillation: effects of pacing mode and mode-switch algorithm. *Circulation* 1999;99:1587-92.
7. Thambo JB, Bordachar P, Garrigue S et al. Detrimental ventricular remodeling in patients with congenital complete heart block and chronic right ventricular apical pacing. *Circulation* 2004;110:3766-72.
8. Doshi RN, Daoud EG, Fellows C et al. Left ventricular-based cardiac stimulation post AV nodal ablation evaluation (the PAVE study). *J Cardiovasc Electrophysiol* 2005;16:1160-5.
9. Schiller NB, Shah PM, Crawford M et al. Recommendations for quantitation of the left ventricle by two-dimensional echocardiography. *J Am Soc Echocardiogr* 1989;2:358-67.
10. Thomas JD. How leaky is that mitral valve? Simplified Doppler methods to measure regurgitant orifice area. *Circulation* 1997;95:548-50.
11. Pitzalis MV, Iacoviello M, Romito R et al. Cardiac resynchronization therapy tailored by echocardiographic evaluation of ventricular asynchrony. *J Am Coll Cardiol* 2002;40:1615-22.
12. Pitzalis MV, Iacoviello M, Romito R et al. Ventricular asynchrony predicts a better outcome in patients with chronic heart failure receiving cardiac resynchronization therapy. *J Am Coll Cardiol* 2005;45:65-9.
13. Porciani MC, Puglisi A, Colella A et al. Echocardiographic evaluation of the effect of biventricular pacing: The InSync Italian Registry. *European Heart Journal, Supplement* 2000;2:J23-J30.
14. Rouleau F, Merheb M, Geffroy S et al. Echocardiographic assessment of the interventricular delay of activation and correlation to the QRS width in dilated cardiomyopathy. *Pacing Clin Electrophysiol* 2001;24:1500-6.
15. Bax JJ, Bleeker GB, Marwick TH et al. Left ventricular dyssynchrony predicts response and prognosis after cardiac resynchronization therapy. *J Am Coll Cardiol* 2004;44:1834-40.
16. Fleiss JL, Levin B, Paik MC. *Statistical methods for rates and proportions*. 3rd ed. New York: Wiley, 2003.
17. Tse HF, Lau CP. Long-term effect of right ventricular pacing on myocardial perfusion and function. *J Am Coll Cardiol* 1997;29:744-9.
18. Skalidis EI, Kochiadakis GE, Koukouraki SI et al. Myocardial perfusion in patients with permanent ventricular pacing and normal coronary arteries. *J Am Coll Cardiol* 2001;37:124-9.
19. van Oosterhout MF, Prinzen FW, Arts T et al. Asynchronous electrical activation induces asymmetrical hypertrophy of the left ventricular wall. *Circulation* 1998;98:588-95.
20. Tse HF, Yu C, Wong KK et al. Functional abnormalities in patients with permanent right ventricular pacing: the effect of sites of electrical stimulation. *J Am Coll Cardiol* 2002;40:1451-8.
21. Burkhoff D, Oikawa RY, Sagawa K. Influence of pacing site on canine left ventricular contraction. *Am J Physiol* 1986;251:H428-H435.
22. Prinzen FW, Hunter WC, Wyman BT, McVeigh ER. Mapping of regional myocardial strain and work during ventricular pacing: experimental study using magnetic resonance imaging tagging. *J Am Coll Cardiol* 1999;33:1735-42.

23. Yu CM, Bax JJ, Monaghan M, Nihoyannopoulos P. Echocardiographic evaluation of cardiac dyssynchrony for predicting a favourable response to cardiac resynchronisation therapy. *Heart* 2004;90 Suppl 6:vi17-vi22.
24. Marcus GM, Rose E, Vioria EM et al. Septal to Posterior Wall Motion Delay Fails to Predict Reverse Remodeling or Clinical Improvement in Patients Undergoing Cardiac Resynchronization Therapy. *J Am Coll Cardiol* 2005;46:2208-14.
25. Bax JJ, Ansalone G, Breithardt OA et al. Echocardiographic evaluation of cardiac resynchronization therapy: ready for routine clinical use? A critical appraisal. *J Am Coll Cardiol* 2004;44:1-9.
26. Brignole M, Gammage M, Puggioni E et al. Comparative assessment of right, left, and biventricular pacing in patients with permanent atrial fibrillation. *Eur Heart J* 2005;26:712-22.
27. Leon AR, Greenberg JM, Kanuru N et al. Cardiac resynchronization in patients with congestive heart failure and chronic atrial fibrillation: effect of upgrading to biventricular pacing after chronic right ventricular pacing. *J Am Coll Cardiol* 2002;39:1258-63.
28. Yu CM, Lin H, Zhang Q, Sanderson JE. High prevalence of left ventricular systolic and diastolic asynchrony in patients with congestive heart failure and normal QRS duration. *Heart* 2003;89:54-60.



Acute effects of right ventricular apical pacing on left ventricular synchrony and mechanics

Victoria Delgado*
Laurens F. Tops*
Serge A.I.P. Trines
Katja Zeppenfeld
Nina Ajmone Marsan
Matteo Bertini
Eduard R. Holman
Martin J. Schalij
Jeroen J. Bax

Department of Cardiology, Leiden University Medical Center, Leiden, the Netherlands

Circ Arrhythmia Electrophysiol 2009;2:135-45

** Victoria Delgado and Laurens F. Tops contributed equally to this article and are shared first author.*

ABSTRACT

Background: Long-term right ventricular (RV) apical pacing has a detrimental effect on left ventricular (LV) function. However, the acute effects of RV apical pacing on LV mechanics remain unclear. The purpose of this study was to assess the acute impact of RV apical pacing on global LV function, evaluating LV contraction synchrony and LV shortening and twist, using 2-dimensional (2D) speckle-tracking strain imaging.

Methods and Results: A group of 25 patients with structural normal hearts referred for electrophysiological (EP) study were studied. Two-dimensional echocardiography was performed at baseline and during RV apical pacing at the time of the EP study. Changes in LV synchrony and mechanics (longitudinal shortening and twist) were assessed using speckle-tracking strain imaging. In addition, 25 controls matched by age, gender and LV function were studied during sinus rhythm. The group of patients (44 ± 12 years, 10 men) and the group of controls (48 ± 3 years, 8 men) showed comparable LV synchrony, LV longitudinal shortening and LV twist at baseline. However, during RV apical pacing, a more dyssynchronous LV contraction was observed in the patients (from 21 ms [$Q_1:10, Q_3:53$] to 91 ms [$Q_1:40, Q_3:204$], $p < 0.001$) together with an impairment in LV longitudinal shortening (from $-18.3 \pm 3.5\%$ to $-11.8 \pm 3.6\%$, $p < 0.001$) and in LV twist (from $12.4 \pm 3.7^\circ$ to $9.7 \pm 2.6^\circ$, $p = 0.001$).

Conclusions: During RV apical pacing, an acute induction of LV dyssynchrony is observed. In addition, LV longitudinal shortening and LV twist are acutely impaired.

INTRODUCTION

Several animal and human studies have demonstrated detrimental effects of right ventricular (RV) apical pacing on cardiac function (1-4). The direct electrical stimulation of the RV apex induces an abnormal activation sequence and asynchronous ventricular contraction (3-5). Subsequently, left ventricular (LV) performance is impaired with a decrease in stroke volume and an abnormal LV relaxation (2). In patients with severe LV dysfunction, these effects are more pronounced and permanent RV apical pacing may result in a higher risk of morbidity and mortality at long-term follow-up (6,7). Recently, it has been shown that patients with long-term RV pacing and LV dysfunction also had LV dyssynchrony (8,9). The question that arises from this observation is whether RV pacing induced LV dyssynchrony resulted in LV dysfunction with heart failure, or whether RV pacing resulted in LV dysfunction and heart failure with subsequent development of LV dyssynchrony.

Importantly, in the majority of the studies that thus far have evaluated the long-term effects of RV apical pacing, the study population comprised patients with structural heart disease, which is a confounding factor that may amplify the detrimental effects of RV pacing on LV function (6,10,11). The exact effects of RV apical pacing on LV function in patients without structural heart disease have not been studied extensively (12). In addition, primarily the long-term effects of RV apical pacing have been studied, and not much information is available on the acute effects of RV pacing on LV function and LV dyssynchrony.

The recently introduced echocardiographic speckle-tracking analysis enables comprehensive evaluation of LV mechanics (LV synchrony, LV systolic function and LV twist) by studying LV deformation in 3 directions (radial, longitudinal and circumferential) (13-16). Importantly, this technique may reveal more subtle changes in LV systolic function, as compared to conventional measures such as LV ejection fraction.

Accordingly, the purpose of the present study was to assess the acute impact of RV apical pacing on global LV function in a group of patients without structural heart disease, evaluating LV contraction synchrony and LV global longitudinal shortening and twist, using 2-dimensional (2D) speckle-tracking strain imaging.

METHODS

Study population

Twenty-five patients, who were referred for an electrophysiological (EP) study for evaluation of supraventricular arrhythmias, were included in the present study. Inclusion criteria were: age > 18 years old, no evidence of structural heart disease by 2D echocardiography, QRS duration on surface electrocardiogram < 120 ms and New York Heart Association functional class I.

Study protocol

In the patient group, echocardiography was performed during sinus rhythm before the EP study, and during RV apical pacing at the end of the EP study. During the EP study, a standard diagnostic catheter (6F, Quadripolar catheter, Biosense-Webster, Diamond Bar, CA, USA) allowing temporary pacing was positioned in the RV apex. Constant RV apical overdrive pacing was performed for 5 minutes. To ensure continuous capture, RV apical pacing was performed with a cycle length of at least 100 ms shorter than the baseline cycle length. After 5 minutes, the echocardiogram was acquired during RV apical pacing. Surface electrocardiograms were recorded during sinus rhythm and RV pacing.

In addition, 25 controls frequency-matched for age, gender, body surface area and LV systolic function were selected from an echocardiographic database. The control group comprised patients referred for echocardiography with atypical chest pain, palpitations or syncope without murmur. In particular, only patients with normal LV systolic function without LV dilatation were selected. Furthermore, subjects who were referred for echocardiographic evaluation of known valvular disease, murmur, or heart failure were excluded.

Therefore, all subjects (both patients and controls), had normal echocardiograms, without structural heart disease. Patients underwent 2D echocardiography during sinus rhythm and during RV apical pacing (at the EP laboratory) whereas controls were imaged at the echocardiography laboratory during sinus rhythm only. Informed consent to participate was obtained from all subjects.

Echocardiography

A commercially available system was used (Vingmed Vivid 7 or Vivid-I, General Electric-Vingmed, Milwaukee, Wisconsin) and data were obtained using a 3.5-MHz transducer at a depth of 16 cm in the parasternal (long- and short-axis) and apical (2-, 3- and 4-chamber) views. Data acquisition was performed by an experienced sonographer during sinus rhythm and RV apical pacing with the patients in the supine position. Special care was taken to avoid either oblique parasternal short-axis views of the LV or foreshortened LV apical views.

Acquired data were transferred to an off-line workstation for further analysis (EchoPac version 6.0.1, General Electric-Vingmed). Left ventricular dimensions (end-diastolic and end-systolic diameter, septum and posterior wall thickness) were measured from the M-mode recordings derived from parasternal long-axis views. Furthermore, LV volumes and LV ejection fraction were measured from the 2- and 4-chamber apical views using the biplane Simpson's rule (17).

Speckle-tracking strain analysis

From standard gray-scale images, 2D speckle-tracking strain analysis was performed to study several aspects of LV mechanics: LV synchrony, global longitudinal shortening and LV twist. For this purpose, novel speckle-tracking software was used, as previously described (16). In

brief, this technique allows angle-independent measurement of myocardial strain in 3 different directions: circumferential shortening and radial thickening in the short-axis views and longitudinal shortening in the apical views. Natural acoustic markers (or speckles), equally distributed in the myocardial wall, form a characteristic pattern that is tracked from frame-to-frame along the cardiac cycle. The change in the position of the speckle pattern with respect to the initial position is used to calculate myocardial strain (16). In the selected views, the endocardial border is traced manually at an end-systolic frame. Next, a region of interest, that includes the myocardial wall, is displayed automatically. The software allows for further adjustment of the region of interest in order to fit the entire myocardial wall within the boundaries. Then, the tracking quality can be evaluated and validated. Finally, the region of interest is divided in 6 segments and the time-strain curves along the cardiac cycle for each segment are displayed.

LV synchrony To evaluate LV synchrony, mid ventricular short-axis images at the level of the papillary muscles were selected and 2D speckle-tracking radial strain analysis was performed, as previously described (15). The time from the onset of QRS to the peak strain value was measured for each segment (anteroseptal, anterior, lateral, posterior, inferior and septal). Subsequently, the difference between the earliest and the latest segments was calculated. LV dyssynchrony was defined as a time difference ≥ 130 ms between the earliest and the latest segments, as previously described (5,15). To compare differences between sinus rhythm and RV apical pacing, LV dyssynchrony was normalized to RR interval, as previously described (18).

LV longitudinal shortening In addition to conventional measurements of LV systolic function based on 2D echocardiography, LV longitudinal shortening was evaluated. For this purpose, automated function imaging, a method based on 2D speckle-tracking strain imaging, was used (16). The selected views were the apical 2-, 3- and 4-chamber views. In brief, from an end-systolic frame of each view, 2 basal points at the mitral annulus, and 1 point at the apex, were used as reference points to trace the region of interest spanning the entire myocardial wall. Using a 17-segment model, the peak systolic longitudinal strain for each LV segment was calculated and presented as a “polar map”, with the average value of peak systolic longitudinal strain for each view and the averaged global longitudinal peak systolic strain for the complete LV (Figure 1). Conventionally, longitudinal shortening is presented in negative values.

LV twist The helical disposition of the myocardial fibers determines the characteristic wringing motion of the LV. As previously described, viewed from the LV apex, the apical segments of the LV show a systolic counter-clockwise rotation whereas the basal segments of the LV show a clockwise rotation (19). The assessment of LV rotation by 2D speckle-tracking strain imaging requires the acquisition of the LV short-axis at the apical level (the most distal level from the papillary muscles) and at the basal level (the level where the leaflets of the mitral valve are visualized) (14). In each short-axis image, the region of interest including the entire myocardial wall

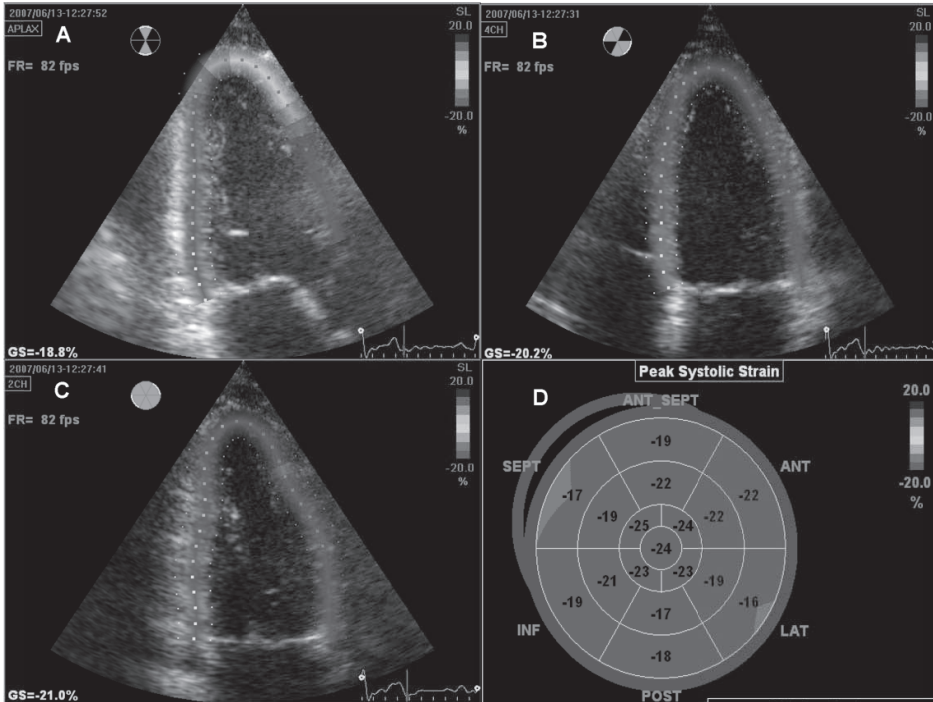


Figure 1. The automated function imaging algorithm enables the measurement of global LV longitudinal strain from 3 standard apical views of the LV. The apical long-axis view of the LV (panel A) should be measured first, defining the aortic valve closure. The time interval between the R wave and the aortic valve closure is used as a reference for the measurement of LV shortening at 4- and 2-chamber view loops (panels B and C respectively). Finally, the algorithm provides the peak systolic longitudinal strain for each LV segment in a “bull’s eye” plot, with the average value of peak systolic longitudinal strain for each view and the averaged global longitudinal peak systolic strain for the complete LV (panel D).

is traced at an end-systolic frame and divided into 6 segments. Subsequently, the time-rotation curves are displayed along the cardiac cycle. The counter-clockwise rotation is conventionally presented as positive values and the clockwise rotation as negative values. The difference between the systolic apical and basal rotation results in LV twist (Figure 2)(14).

Reproducibility of the assessment of LV rotation was analyzed with repeated measurements by an experienced observer at two different time points and by a second experienced observer. Intra- and inter-observer agreements for these measurements were evaluated by Bland-Altman analysis. Intra-observer variability was good, with an excellent agreement (mean \pm 2SD was $-0.1 \pm 2.2^\circ$) between two repeated measurements. Similarly, inter-observer variability showed an excellent agreement (mean \pm 2SD was $0.14 \pm 3.4^\circ$).

Statistical analysis

All variables were normally distributed (as assessed by Kolmogorov-Smirnov test), except LV dyssynchrony indexed to RR interval. Continuous variables are presented as mean \pm SD, when normally distributed, and as median (25th and 75th percentiles: Q_1 , Q_3) when non-normally distributed. Comparisons between the patients and the matched controls were performed

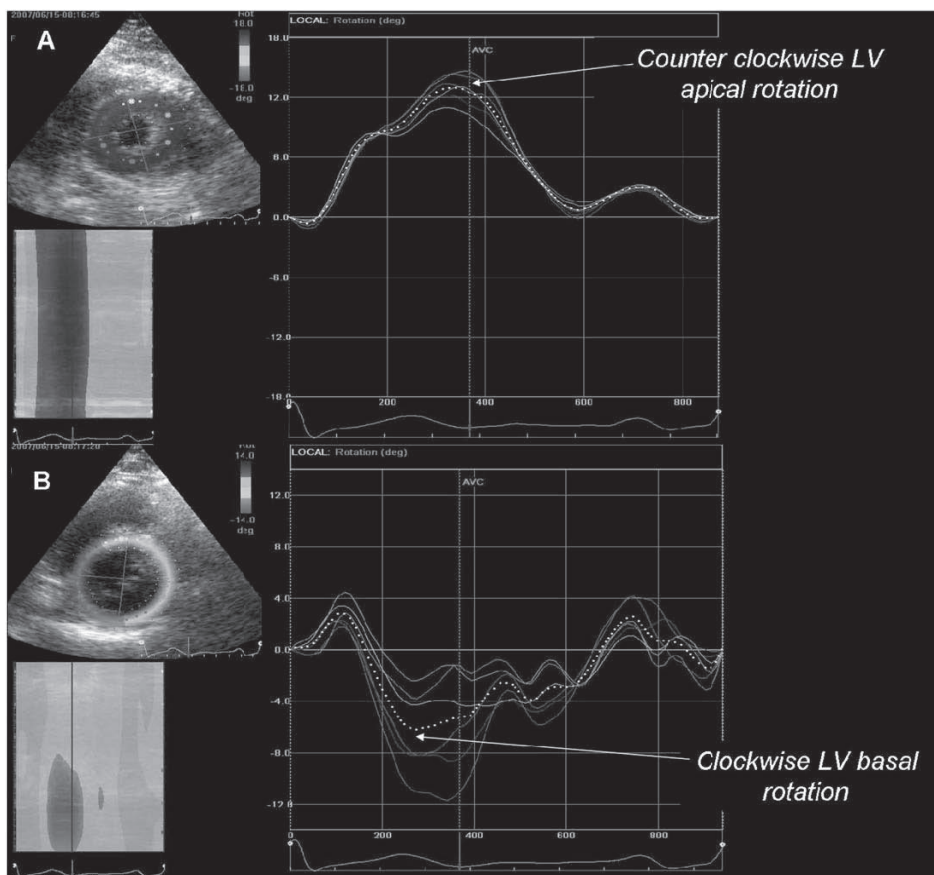


Figure 2. Assessment of LV twist by 2D speckle-tracking strain imaging. LV twist was calculated using 2D speckle-tracking strain imaging applied to LV apical (panel A) and basal (panel B) short-axis view. The LV apex demonstrates a counter clockwise systolic peak rotation, whereas the LV base shows a clockwise systolic peak rotation. The difference between the apical and the basal systolic peak rotation results in LV twist.

using the unpaired Student t-test (for normally distributed variables) and Mann-Whitney U-test (for non-normally distributed variables). Comparisons within the group of patients during sinus rhythm and RV apical pacing were performed using the paired Student t-test (for normally distributed variables) and Wilcoxon Signed Ranks test (for non-normally distributed variables). All statistical analyses were performed with SPSS software (version 16.0, SPSS Inc., Chicago, Illinois). All statistical tests were two-sided, and a p-value <0.05 was considered statistically significant.

RESULTS

The study protocol could be completed in all 25 patients (mean age 44 ± 12 years, 10 men/15 women). In 15 (60%) patients, atrioventricular nodal reentry tachycardia was demonstrated

during the EP study, whereas in the remaining 10 patients, no tachyarrhythmia was documented. In all individuals, echocardiographic image quality was sufficient for quantitative analysis. Echocardiographic data acquisition was performed at a mean frame rate of 84 ± 13 frames/sec. By definition, at baseline all the patients and matched controls showed structural normal hearts with synchronous LV systolic contraction as evaluated by 2D speckle-tracking radial strain imaging.

To acquire the echocardiographic data during RV apical pacing, continuous capture was ensured by pacing with a cycle length of at least 100 ms shorter than the baseline cycle length. Mean heart rate was 69 ± 14 bpm at baseline and 106 ± 11 bpm during RV apical pacing ($p < 0.001$). During RV apical pacing, the QRS duration on the surface electrocardiogram was significantly longer as compared to baseline (131 ± 18 ms vs. 92 ± 7 ms; $p = 0.001$).

Effects of RV apical pacing on LV dimensions and volumes

Baseline LV dimensions and volumes were comparable between the patients and the matched controls (Table 1). During RV apical pacing, a significant decrease in LV end-diastolic diameter and volume were observed in the patients, whereas LV end-systolic diameter and volume did not change (Table 2). Consequently, LV ejection fraction decreased significantly from $56 \pm 8\%$ to $48 \pm 9\%$ ($p = 0.001$).

Effect of RV apical pacing on LV mechanics

LV synchrony With the use of 2D speckle-tracking radial strain, LV synchrony was assessed in the study population. Median time difference between the earliest and latest segments (corrected by RR interval) was similar in the patient group and the matched controls at baseline (Table

Table 1. Echocardiographic characteristics of the study population

	Patients (n=25)	Controls (n=25)	p-value
Age, yrs	44 ± 12	48 ± 3	0.100
Gender, M/F	10/15	8/17	0.556
Heart rate, bpm	69 ± 14	72 ± 12	0.469
LV dimensions and volumes			
LV end-diastolic diameter (mm)	49 ± 5	49 ± 4	0.567
LV end-systolic diameter (mm)	30 ± 5	27 ± 4	0.126
Interventricular septum thickness (mm)	10 ± 2	10 ± 2	0.816
Posterior wall thickness (mm)	10 ± 2	10 ± 2	0.787
LV end-diastolic volume (ml)	99 ± 26	95 ± 22	0.538
LV end-systolic volume (ml)	44 ± 16	38 ± 11	0.183
LV ejection fraction (%)	56 ± 8	60 ± 6	0.069
LV mechanics			
LV synchrony (RR-indexed) (ms) *	21 (10, 53)	20 (0, 68)	0.953
LV longitudinal shortening (%)	-18.3 ± 3.5	-18.5 ± 4.1	0.947
LV apical rotation (°)	7.1 ± 3.5	6.4 ± 3.5	0.507
LV basal rotation (°)	-5.4 ± 2.7	-6.6 ± 2.4	0.084
LV twist (°)	12.4 ± 3.7	13.0 ± 3.2	0.538

*expressed as median (25th, 75th percentiles); LV = left ventricular.

Table 2. Changes in LV dimensions, volumes and mechanics during RV apical pacing in the 25 patients undergoing electrophysiological testing

	Sinus Rhythm	RV apical pacing	Difference (RV-SR)	p-value (RV vs. SR)
LV dimensions and function				
LV end-diastolic diameter (mm)	49 ± 5	45 ± 6	-4.0 ± 5.2	<0.001
LV end-systolic diameter (mm)	30 ± 5	29 ± 6	-0.2 ± 4.5	0.827
LV end-diastolic volume (ml)	99 ± 26	88 ± 25	-11.0 ± 12.2	<0.001
LV end-systolic volume (ml)	44 ± 16	45 ± 16	1.0 ± 11.4	0.615
LV ejection fraction (%)	56 ± 8	48 ± 9	-8.0 ± 10.2	0.001
LV mechanics				
LV synchrony (RR-indexed) (ms)*	21 (10, 53)	91 (40, 204)	50 (12,174)	<0.001
LV longitudinal shortening (%)	-18.3 ± 3.5	-11.8 ± 3.6	7.0 ± 4.0	<0.001
LV apical rotation (°)	7.1 ± 3.5	6.7 ± 2.6	-0.4 ± 3.2	0.573
LV basal rotation (°)	-5.4 ± 2.7	-3.0 ± 2.1	2.4 ± 2.8	<0.001
LV twist (°)	12.4 ± 3.7	9.7 ± 2.6	-2.7 ± 3.6	0.001

*expressed as median (25th, 75th percentiles); LV= left ventricular; RV= right ventricular; SR= sinus rhythm.

1). In contrast, during RV apical pacing, the time difference between the earliest and the latest segments increased significantly from 21 ms (Q₁: 10, Q₃: 53) to 91 ms (Q₁: 40, Q₃: 204) (p<0.001). In 9 (36%) patients, a time difference >130 ms between the earliest and the latest activated segments was present during RV apical pacing, indicating the presence of LV dyssynchrony. An example of a patient with LV dyssynchrony during RV pacing is shown in Figure 3.

LV longitudinal shortening At baseline, the LV longitudinal shortening assessed by automated function imaging was comparable between patients and matched controls. Mean peak systolic global longitudinal strain was -18.3 ± 3.5% in the patients and -18.5 ± 4.1% in the matched controls (p=0.9). However, the LV global longitudinal strain value decreased significantly during RV apical pacing from -18.3 ± 3.5% to -11.8 ± 3.6% (p<0.001). Representative examples of LV longitudinal shortening during sinus rhythm and RV pacing are shown in Figure 4.

LV twist At baseline, no significant differences in LV rotation and twist between the patients and matched controls were observed (Table 1). However, during RV apical pacing, LV rotation showed significant changes. While the LV apex showed a slight decrease in rotation (from 7.1 ± 3.5° to 6.7 ± 2.6°, p=0.6), the base of the LV showed a significant decrease in rotation (from -5.4 ± 2.7° to -3.0 ± 2.1°, p<0.001). Consequently, LV twist was significantly impaired during RV apical pacing (from 12.4 ± 3.7° to 9.7 ± 2.6°, p=0.001). An example of a patient with a significant decrease in LV twist during RV pacing is shown in Figure 5.

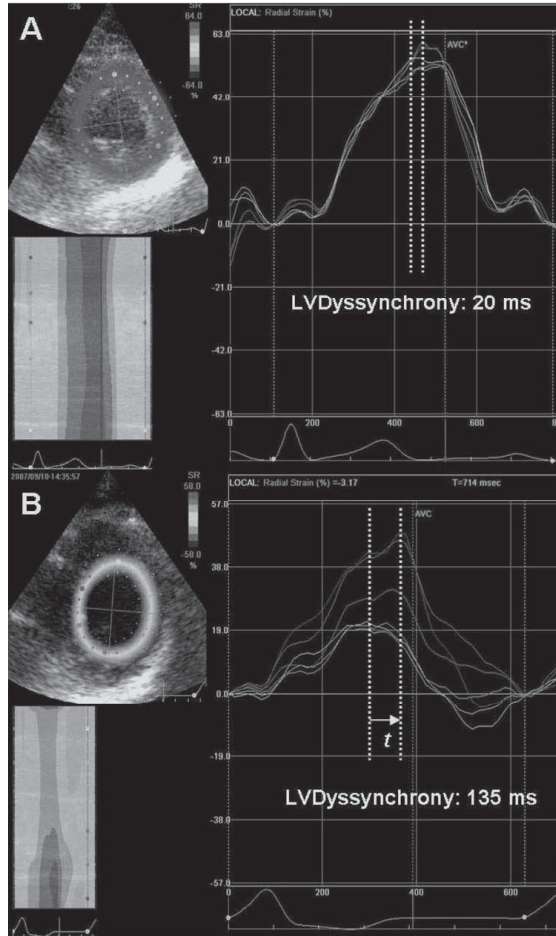


Figure 3. Changes in LV synchrony during RV apical pacing. LV dyssynchrony was measured using 2D speckle-tracking radial strain applied to midventricular short-axis images. A synchronous contraction was observed in sinus rhythm (panel A). During RV apical pacing, the time delay between the earliest and latest segments increased significantly, showing a more dyssynchronous LV contraction (panel B).

DISCUSSION

The present study provides more insight into the acute effects of RV apical pacing on cardiac mechanics in patients with structural normal hearts. Right ventricular apical pacing acutely induced dyssynchronous LV contraction associated with impairment in LV longitudinal systolic function. Furthermore, a deleterious effect on the characteristic torsional deformation of the LV during systole was noted.

Changes in LV dimensions induced by RV apical pacing

The baseline LV dimensions observed in the present study were comparable in patients and controls. However, during RV apical pacing a decrease in LV end-diastolic diameter and volume

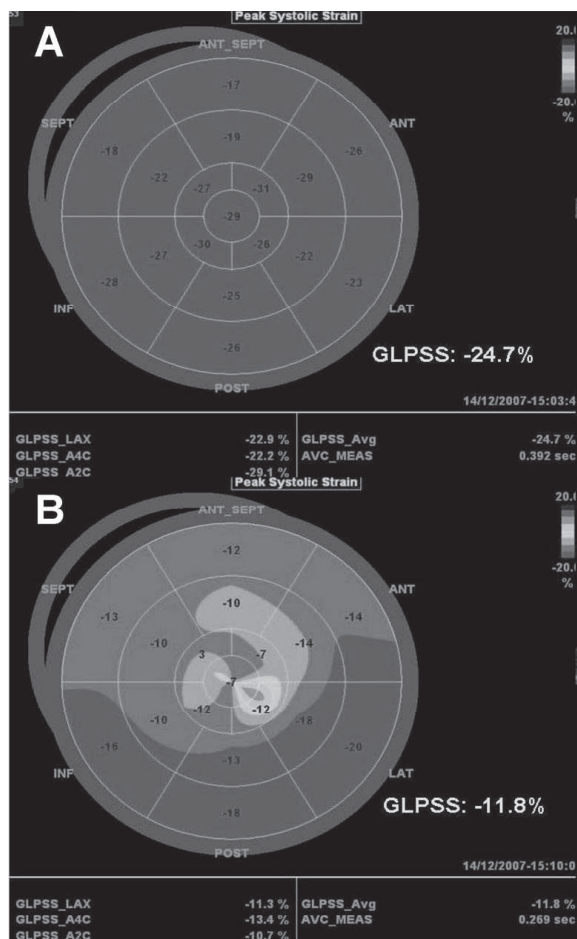


Figure 4. This figure shows the changes in global longitudinal peak systolic strain (GLPSS) in the same patient as in Figure 2. The LV longitudinal shortening was assessed on standard apical views using automated function imaging. Panel A shows the polar map with a normal and homogeneous GLPSS during sinus rhythm. However, during RV apical pacing, a significant decrease in GLPSS was observed (panel B).

was observed, whereas the LV end-systolic dimensions remained unchanged. Consequently, LV ejection fraction showed a significant impairment during RV pacing.

In general, information on the acute effects of RV apical pacing on LV dimensions and volumes in patients with preserved LV function is scarce (2,10). Recently, Liu et al. studied the acute effects of RV apical pacing on LV function in a group of 35 patients with sick sinus syndrome using real-time 3-dimensional echocardiography (10). During RV apical pacing, patients showed a decrease in LV end-diastolic volume (from 79 ± 22 ml to 76 ± 20 ml, $p=0.07$) and in LV ejection fraction (from $57 \pm 8\%$ to $54 \pm 8\%$, $p=0.01$) (10). In addition, in a group of patients with preserved LV ejection fraction studied by Lieberman et al. RV apical pacing induced a moderate decrease in LV ejection fraction (from $51 \pm 12\%$ to $48 \pm 14\%$, $p=NS$) whereas the LV dimensions remained unchanged (2).

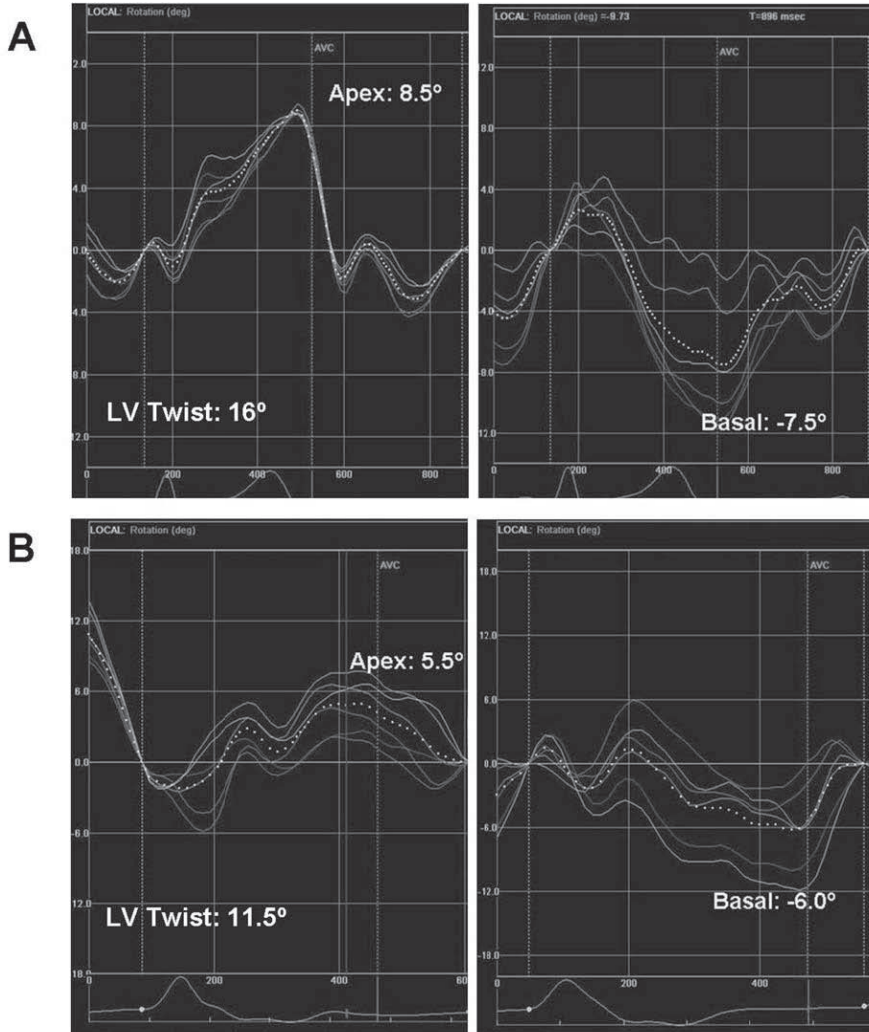


Figure 5. Changes in left ventricular (LV) rotation during RV apical pacing. LV rotation was assessed by applying 2D speckle-tracking strain imaging at the LV apex and base. Subsequently, LV twist is derived from the difference between the apical and basal rotations. This figure demonstrates LV rotation and twist in the same patient as in Figure 3 and 4. Panel A shows both apical and basal LV rotations during sinus rhythm. During RV apical pacing (panel B), a decrease in both apical and basal LV rotations was observed, with a subsequent significant decrease in LV twist.

Several factors may contribute to the decrease in LV end-diastolic dimension and volume and LV ejection fraction during RV apical pacing. Normal LV diastolic filling may be impaired by the loss of normal atrioventricular conduction and subsequent decrease in left atrial contribution to diastolic filling (20,21). In addition, the earlier activation of the RV may hamper LV filling that is accomplished by the shared interventricular septum (20-22). Both mechanisms may result in a decrease in LV pre-load during RV apical pacing and, according to the Frank-Starling law, result in a lower LV stroke volume.

Changes in LV synchrony during RV apical pacing

In the present study, the synchronicity of the LV was evaluated by 2D speckle-tracking radial strain imaging, measuring the time difference between the earliest and the latest activated segments. Using this technique, synchronous contraction of the LV was observed in both the controls and the patients at baseline. During RV apical pacing, the time difference between the earliest and the latest activated segments increased significantly, reflecting a more dyssynchronous contraction pattern of the LV. In particular, 9 (36%) patients exhibited significant LV dyssynchrony (>130 ms between the earliest and the latest activated segments) during RV pacing.

Several animal and human studies have reported the acute effects of RV apical pacing on LV synchrony (10,12,23). Wymann et al. demonstrated the changes in LV mechanical activation synchrony during RV apical pacing using tagged-magnetic resonance imaging in an experimental study (23). During RV apical pacing, the breakthrough of the mechanical activation was located at the interventricular septum and spread along the LV walls ending at the lateral wall (23). As a result, the mechanical activation delay was significantly higher during RV apical pacing (77.6 ± 16.4 ms) as compared to right atrial pacing (43.6 ± 17.1 ms).

Similarly, clinical studies have observed an acute induction of LV systolic dyssynchrony by RV apical pacing (10,12). Fornwalt et al. assessed the effects of RV apical pacing on systolic dyssynchrony using tissue Doppler imaging in 14 pediatric patients with normal cardiac structure and function (12). After 1 minute of RV apical pacing significant LV systolic dyssynchrony was noted, compared with sinus rhythm (from 49 ± 28 ms to 94 ± 47 ms, $p < 0.05$). In addition, Liu et al. demonstrated an acute increase of LV systolic dyssynchrony index assessed with real-time 3-dimensional echocardiography during RV apical pacing in a group of patients with sick sinus syndrome (from $5.3 \pm 2.1\%$ to $7.0 \pm 2.5\%$) (10).

The induction of LV dyssynchrony by RV apical pacing, as observed in the present and previous studies may be explained by changes in the electro-mechanical activation pattern during pacing. During ectopic activation of the LV by RV apical pacing, the depolarization impulse spreads through the slower-conducting myocardium rather than through the His-Purkinje system, resulting in a heterogeneous electrical and mechanical activation of the LV (24). However, it remains undetermined why some patients develop LV dyssynchrony during RV pacing while other patients do not.

Changes in LV shortening and twist induced by RV apical pacing

In the present study, changes in LV systolic mechanics were evaluated, focusing on LV longitudinal shortening and LV twist. In sinus rhythm, patients and controls showed comparable values of LV shortening and LV twist. However, during RV apical pacing, a significant decrease in both parameters was observed. The complex architecture of the LV determines a characteristic deformation pattern consisting of systolic shortening in the longitudinal and circumferential directions together with thickening in the radial direction (25). When viewed from the LV apex, this deformation pattern results in a typical wringing movement with a net counter-clockwise

rotation of the apex relative to the base of the heart (14). Any abnormality in this complex pattern of deformation and twist could significantly affect cardiac performance.

Several experimental studies have demonstrated changes in LV strain during RV pacing (3,23,25,26). Prinzen et al. described the non-uniformity of myocardial fiber strain during RV pacing as compared to the uniformity observed during right atrial pacing using sonomicrometry technique in a dog-model (3). Interestingly, in the early-activated LV areas the amount of shortening was lower than in the remote areas, resulting in a decrease in the net LV strain pattern during RV pacing (3). In addition, Liakopoulos et al. evaluated the effects of RV apical pacing on LV segmental shortening in a swine-model with sonomicrometry technique as well (25). The authors observed a pronounced decrease in LV segmental shortening during RV apical pacing at the posterior wall (from $18.8 \pm 6.1\%$ in sinus rhythm to $13.6 \pm 9.6\%$ during RV apical pacing, $p < 0.05$) (25).

In the present study, the novel automated function imaging algorithm was used to assess global LV systolic shortening. Similar to the aforementioned studies, a significant decrease in LV longitudinal shortening was observed acutely during RV apical pacing. In addition, the resultant torsional movement of the LV showed a significant decrease during RV apical pacing. A decrease in both apical and basal rotation was observed during RV pacing in the present study. However, this decrease was more pronounced in the LV basal level.

A reduction in LV strain and LV twist has been previously reported in several clinical situations (hypertrophic cardiomyopathy, aortic stenosis and myocardial infarction) (27-29). However, the effect of RV apical pacing on LV twist has only been studied in animal experiments (30,31). Buchalter et al. demonstrated that the LV torsional movement depends on the sequence of LV depolarization, showing significant reduction in the LV twist during RV apical pacing (30). Furthermore, Sorger et al., in a tagged magnetic resonance study, observed a dramatic decrease in LV twist during RV apical pacing as compared to atrial pacing ($6.1 \pm 1.7^\circ$ vs. $11.1 \pm 3.5^\circ$, $p < 0.001$) (31). The results of the current study are in agreement with these previous studies. Moreover, the present findings illustrate that the decrease in LV twist is simultaneous to the impairment in LV longitudinal shortening. The long-term effects of RV apical pacing on LV strain and twist however are still unclear and need further study.

Clinical implications

Previous studies demonstrated that long-term RV apical pacing may increase the risk of LV dysfunction and heart failure associated with the presence of LV dyssynchrony by 25-30% (9,32). The precise time course of development of these phenomena (LV dysfunction, heart failure and LV dyssynchrony) after RV pacing is currently unclear. In the present study, 36% of the patients developed significant LV dyssynchrony acutely during RV apical pacing, as assessed by 2-dimensional speckle-tracking strain imaging. In addition, significant impairment in LV systolic function was observed reflected by reduced LV ejection fraction, but also an impaired LV

longitudinal shortening and reduced LV twist. Whether this acutely induced LV dyssynchrony is the basis for the development of heart failure after long-term RV pacing needs further study.

Study Limitations

Some limitations need to be addressed. First, short-term effects of RV apical pacing on LV mechanics were assessed in the present study and, to avoid intrinsic ventricular conduction, pacing rate was set to 25% over the normal sinus rhythm, resulting in a high heart rate. These non-physiological conditions may preclude us to draw conclusions about the long-term effects of chronic RV pacing on LV performance. Second, all patients were considered to have structural normal hearts according to the clinical history, physical examination and the results of the complementary diagnostic exams performed. Unfortunately, endomyocardial biopsies were not available to confirm the absence of structural heart disease. Finally, additional studies evaluating different pacing sites and longer follow-up are needed to better understand the long-term effects of the acutely induced changes in LV mechanics by RV pacing.

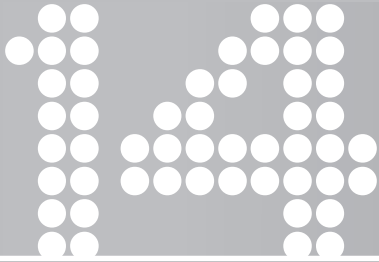
CONCLUSIONS

In the present study, speckle-tracking analysis applied to conventional 2D echocardiography was used to study the acute effects of RV apical pacing on LV mechanics. Right ventricular apical pacing acutely induced a dyssynchronous LV contraction together with a decrease LV longitudinal function. In addition, the characteristic torsional deformation of the LV during systole was impaired acutely by RV apical pacing.

REFERENCES

1. Boerth RC, Covell JW. Mechanical performance and efficiency of the left ventricle during ventricular stimulation. *Am J Physiol* 1971;221:1686-91.
2. Lieberman R, Padeletti L, Schreuder J et al. Ventricular pacing lead location alters systemic hemodynamics and left ventricular function in patients with and without reduced ejection fraction. *J Am Coll Cardiol* 2006;48:1634-41.
3. Prinzen FW, Augustijn CH, Arts T, Allesie MA, Reneman RS. Redistribution of myocardial fiber strain and blood flow by asynchronous activation. *Am J Physiol* 1990;259:H300-H308.
4. Victor F, Mabo P, Mansour H et al. A randomized comparison of permanent septal versus apical right ventricular pacing: short-term results. *J Cardiovasc Electrophysiol* 2006;17:238-42.
5. Tops LF, Suffoletto MS, Bleeker GB et al. Speckle-tracking radial strain reveals left ventricular dyssynchrony in patients with permanent right ventricular pacing. *J Am Coll Cardiol* 2007;50:1180-8.
6. Lamas GA, Lee KL, Sweeney MO et al. Ventricular pacing or dual-chamber pacing for sinus-node dysfunction. *N Engl J Med* 2002;346:1854-62.
7. Wilkoff BL, Cook JR, Epstein AE et al. Dual-chamber pacing or ventricular backup pacing in patients with an implantable defibrillator: the Dual Chamber and VVI Implantable Defibrillator (DAVID) Trial. *JAMA* 2002;288:3115-23.
8. Schmidt M, Bromsen J, Herholz C et al. Evidence of left ventricular dyssynchrony resulting from right ventricular pacing in patients with severely depressed left ventricular ejection fraction. *Europace* 2007;9:34-40.
9. Sweeney MO, Hellkamp AS, Ellenbogen KA et al. Adverse effect of ventricular pacing on heart failure and atrial fibrillation among patients with normal baseline QRS duration in a clinical trial of pacemaker therapy for sinus node dysfunction. *Circulation* 2003;107:2932-7.
10. Liu WH, Chen MC, Chen YL et al. Right ventricular apical pacing acutely impairs left ventricular function and induces mechanical dyssynchrony in patients with sick sinus syndrome: a real-time three-dimensional echocardiographic study. *J Am Soc Echocardiogr* 2008;21:224-9.
11. Tantengco MV, Thomas RL, Karpawich PP. Left ventricular dysfunction after long-term right ventricular apical pacing in the young. *J Am Coll Cardiol* 2001;37:2093-100.
12. Fornwalt BK, Cummings RM, Arita T et al. Acute pacing-induced dyssynchronous activation of the left ventricle creates systolic dyssynchrony with preserved diastolic synchrony. *J Cardiovasc Electrophysiol* 2008;19:483-8.
13. Korinek J, Wang J, Sengupta PP et al. Two-dimensional strain—a Doppler-independent ultrasound method for quantitation of regional deformation: validation in vitro and in vivo. *J Am Soc Echocardiogr* 2005;18:1247-53.
14. Kim HK, Sohn DW, Lee SE et al. Assessment of left ventricular rotation and torsion with two-dimensional speckle tracking echocardiography. *J Am Soc Echocardiogr* 2007;20:45-53.
15. Suffoletto MS, Dohi K, Cannesson M, Saba S, Gorcsan J, III. Novel speckle-tracking radial strain from routine black-and-white echocardiographic images to quantify dyssynchrony and predict response to cardiac resynchronization therapy. *Circulation* 2006;113:960-8.
16. Delgado V, Mollema SA, Ypenburg C et al. Relation between global left ventricular longitudinal strain assessed with novel automated function imaging and biplane left ventricular ejection fraction in patients with coronary artery disease. *J Am Soc Echocardiogr* 2008;21:1244-50.
17. Schiller NB, Shah PM, Crawford M et al. Recommendations for quantitation of the left ventricle by two-dimensional echocardiography. *J Am Soc Echocardiogr* 1989;2:358-67.
18. Lafitte S, Bordachar P, Lafitte M et al. Dynamic ventricular dyssynchrony: an exercise-echocardiography study. *J Am Coll Cardiol* 2006;47:2253-9.
19. Helle-Valle T, Crosby J, Edvardsen T et al. New noninvasive method for assessment of left ventricular rotation: speckle tracking echocardiography. *Circulation* 2005;112:3149-56.

20. Leclercq C, Gras D, Le HA, Nicol L, Mabo P, Daubert C. Hemodynamic importance of preserving the normal sequence of ventricular activation in permanent cardiac pacing. *Am Heart J* 1995;129:1133-41.
21. Rosenqvist M, Isaaz K, Botvinick EH et al. Relative importance of activation sequence compared to atrioventricular synchrony in left ventricular function. *Am J Cardiol* 1991;67:148-56.
22. Bleasdale RA, Turner MS, Mumford CE et al. Left ventricular pacing minimizes diastolic ventricular interaction, allowing improved preload-dependent systolic performance. *Circulation* 2004;110:2395-400.
23. Wyman BT, Hunter WC, Prinzen FW, Faris OP, McVeigh ER. Effects of single- and biventricular pacing on temporal and spatial dynamics of ventricular contraction. *Am J Physiol Heart Circ Physiol* 2002;282:H372-H379.
24. Vassallo JA, Cassidy DM, Marchlinski FE et al. Endocardial activation of left bundle branch block. *Circulation* 1984;69:914-23.
25. Liakopoulos OJ, Tomioka H, Buckberg GD, Tan Z, Hristov N, Trummer G. Sequential deformation and physiological considerations in unipolar right or left ventricular pacing. *Eur J Cardiothorac Surg* 2006;29 Suppl 1:S188-S197.
26. Waldman LK, Covell JW. Effects of ventricular pacing on finite deformation in canine left ventricles. *Am J Physiol* 1987;252:H1023-H1030.
27. Fuchs E, Muller MF, Oswald H, Thony H, Mohacsi P, Hess OM. Cardiac rotation and relaxation in patients with chronic heart failure. *Eur J Heart Fail* 2004;6:715-22.
28. Nagel E, Stuber M, Burkhard B et al. Cardiac rotation and relaxation in patients with aortic valve stenosis. *Eur Heart J* 2000;21:582-9.
29. Takeuchi M, Borden WB, Nakai H et al. Reduced and delayed untwisting of the left ventricle in patients with hypertension and left ventricular hypertrophy: a study using two-dimensional speckle tracking imaging. *Eur Heart J* 2007;28:2756-62.
30. Buchalter MB, Rademakers FE, Weiss JL, Rogers WJ, Weisfeldt ML, Shapiro EP. Rotational deformation of the canine left ventricle measured by magnetic resonance tagging: effects of catecholamines, ischaemia, and pacing. *Cardiovasc Res* 1994;28:629-35.
31. Sorger JM, Wyman BT, Faris OP, Hunter WC, McVeigh ER. Torsion of the left ventricle during pacing with MRI tagging. *J Cardiovasc Magn Reson* 2003;5:521-30.
32. Zhang XH, Chen H, Siu CW et al. New-onset heart failure after permanent right ventricular apical pacing in patients with acquired high-grade atrioventricular block and normal left ventricular function. *J Cardiovasc Electrophysiol* 2008;19:136-41.



Speckle-tracking radial strain reveals left ventricular dyssynchrony in patients with permanent right ventricular pacing

Laurens F. Tops¹
Matthew S. Suffoletto²
Gabe B. Bleeker¹
Eric Boersma³
Ernst E. van der Wall¹
John Gorcsan III²
Martin J. Schalij¹
Jeroen J. Bax¹

¹Department of Cardiology, Leiden University Medical Center, Leiden, the Netherlands

²Cardiovascular Institute, University of Pittsburgh, Pittsburgh, USA

³Department of Epidemiology and Statistics, Erasmus University, Rotterdam, the Netherlands

J Am Coll Cardiol 2007;50:1180-8

ABSTRACT

Background: Recent studies have shown detrimental effects of RV pacing, possibly related to the induction of LV dyssynchrony.

Objectives: Speckle-tracking strain analysis was used to assess the effects of permanent right ventricular (RV) pacing on the heterogeneity in timing of regional wall strain and left ventricular (LV) dyssynchrony.

Methods: Fifty-eight patients treated with His bundle ablation and pacemaker implantation were studied. To assess the effect of RV pacing on time-to-peak radial strain of different LV segments, speckle-tracking analysis was applied to standard LV short-axis images. In addition, NYHA functional class, LV volumes and systolic function were assessed at baseline and after long-term RV pacing.

Results: At baseline, similar time-to-peak strain for the 6 segments was observed (mean 371 ± 114 ms). In contrast, after a mean of 3.8 ± 2.0 years of RV pacing, there was a marked heterogeneity in time-to-peak strain of the 6 segments. In 33 patients (57%) LV dyssynchrony, represented by a time difference ≥ 130 ms between the time-to-peak strain of the (antero)septal and the posterolateral segments, was present. In these patients, a deterioration of LV systolic function and NYHA class was observed. In 11 patients 'upgrade' of the conventional pacemaker to a biventricular pacemaker resulted in partial reversal of the detrimental effects of RV pacing.

Conclusions: Speckle-tracking analysis revealed that permanent RV pacing induced heterogeneity in time-to-peak strain, resulting in LV dyssynchrony in 57% of patients, associated with deterioration of LV systolic function and NYHA class. Biventricular pacing may reverse these adverse effects of RV pacing.

INTRODUCTION

Cardiac pacing is the only effective treatment in patients with symptomatic sinus node dysfunction or atrioventricular block. In order to maintain atrioventricular synchrony, dual-chamber pacing has been introduced. Surprisingly, large randomized trials have not been able to prove substantial benefit of DDDR pacing over conventional VVIR pacing (1). More importantly, evidence emerges that ventricular pacing should be kept to a minimum (2). Recently, several trials (3-5) have shown that conventional right ventricular (RV) pacing is associated with an increased risk for development of heart failure and death. Furthermore, left ventricular (LV) dilatation (6) and LV dysfunction (7) following RV apical pacing have been demonstrated.

Currently, little data on the exact cause of the deleterious effects of RV pacing exist. Few animal studies have been performed on the effect of the abnormal ventricular activation pattern on regional wall strain (8-10). In a recent study, tissue Doppler imaging was used to demonstrate the possible relation between LV dyssynchrony and the detrimental effects of RV apical pacing (11). Tissue Doppler imaging however is not an ideal method, because with this technique myocardial velocities are assessed, but no information on myocardial strain and active deformation is obtained. We hypothesized that the detrimental effects of RV pacing may be related to the induction of heterogeneity in time-to-peak radial strain of the LV walls, ultimately resulting in LV dyssynchrony. Strain imaging with MRI tagging may be the most accurate technique to assess radial strain and LV dyssynchrony (9); this technique however is technically demanding and is not feasible for patients with pacemakers. However, with the recently introduced speckle tracking analysis applied to standard echocardiograms (12,13), accurate strain imaging using echocardiography has become available.

Therefore, in the current study speckle tracking radial strain was used to evaluate the effect of permanent RV pacing on the heterogeneity in timing of regional strain and LV dyssynchrony. For this purpose, we studied patients with permanent RV apical pacing after His bundle ablation for drug-refractory atrial fibrillation. In addition, the effect of long-term RV pacing on LV systolic function, LV dilatation and functional class was evaluated. Finally, we evaluated whether upgrading RV pacing to biventricular reversed LV dyssynchrony, with an improvement in LV systolic function and functional class.

METHODS

Study sample and study design

Sixty-three patients treated with His bundle ablation and pacemaker implantation were initially screened for the study. All patients had preserved LV systolic function and had no significant valvular disease. Of the 63 patients, 5 patients (8%) were excluded because the echocardiogram image quality was unsuitable for quantitative speckle tracking strain analysis. Eventually, the

study sample comprised 58 patients with drug-refractory, permanent atrial fibrillation. Ten patients were included in a previous study on the effects of permanent RV pacing (11). In all patients a clinical decision to perform a His bundle ablation had been made. Before the His bundle ablation and pacemaker implantation procedure, and after a minimum of 1 year RV pacing, New York Heart Association (NYHA) functional class was assessed and an extensive echocardiographic evaluation was performed. Novel speckle tracking radial strain was used to evaluate the presence of LV dyssynchrony at baseline and after long-term RV pacing. LV systolic function, LV volumes and LV dimensions were assessed at baseline and after long-term RV apical pacing to determine the effect of pacing on global LV function and LV size. Furthermore, the effect of biventricular pacing on LV dyssynchrony and LV function in previously RV paced patients was assessed in 11 patients who received an 'upgrade' of the conventional pacemaker to biventricular pacing because of the presence of LV dyssynchrony and heart failure symptoms.

Ablation and pacemaker implantation

His bundle ablation was performed with a 4 mm quadripolar mapping / ablation catheter (EPT, Boston Scientific, Natick, Massachusetts, USA), accessed through the femoral vein. A temporary pacing electrode was placed in the RV apex for back-up pacing. After the detection of a clear His bundle signal, radiofrequency energy was applied until complete AV-block was achieved. Thereafter the permanent pacemaker was implanted. Pacemaker leads were inserted through the subclavian vein using standard implantation techniques. The RV leads were positioned in the RV apex in all patients. After implantation, pacemakers were routinely programmed to VVIR mode. The day after the procedure an echocardiogram and a standard X-ray was performed to exclude pericardial effusion and lead dislocation.

Echocardiography

All patients underwent echocardiography before the ablation procedure and after long-term permanent RV pacing. Images were recorded with patients in the left lateral decubitus position using a commercially available system (Vingmed Vivid 5 or 7, General Electric-Vingmed, Milwaukee, Wisconsin, USA). Images were obtained using a 3.5-MHz transducer at a depth of 16 cm in the parasternal (long- and short-axis) and apical (2- and 4-chamber) views. Standard two-dimensional images and color Doppler data were digitally stored in cine-loop format.

LV end-diastolic and end-systolic volumes were assessed from the apical 2- and 4-chamber images, and LV ejection fraction was calculated using the biplane Simpson's rule (14). Furthermore, LV end-diastolic and end-systolic diameters were measured from the M-mode recordings derived from the parasternal long-axis images. The severity of mitral regurgitation was graded semi-quantitatively using color-flow Doppler in the conventional parasternal long-axis and apical 4-chamber images (15). Mitral regurgitation was characterized as: minimal = grade 1 (jet area/left atrial area < 10%), moderate = grade 2 (jet area/left atrial area 10-20%), moderate-

severe = grade 3 (jet area/left atrial area 20-45%), or severe = grade 4 (jet area/left atrial area >45%) (15).

Strain analysis

Radial strain was assessed on LV short-axis images at the papillary muscle level, using speckle tracking analysis (12,13). Off-line analysis of radial strain was performed on digitally stored images (EchoPac version 6.0.1, General Electric-Vingmed) by 2 independent observers blinded to the clinical and other echocardiographic information. The novel speckle tracking software tracks frame-to-frame movement of natural acoustic markers, or speckles, on standard gray scale images of the myocardium (frame rate varied from 40 to 80 frames/s), as previously described (12,13). In brief, myocardial strain is assessed from temporal differences in the mutual distance of neighboring speckles. The change in length / initial length of the speckle pattern over the cardiac cycle can be used to calculate radial strain, with myocardial thickening represented as positive strain, and myocardial thinning as negative strain. Regional LV strain is assessed using a region of interest that spans the entire LV myocardium throughout the cardiac cycle. The traced endocardium is automatically divided into 6 standard segments: septal, anteroseptal, anterior, lateral, posterior, and inferior, respectively (16).

Time-strain curves for all the 6 segments were constructed. Both peak radial strain values and time from QRS onset to peak radial strain were obtained. Consequently, the location of the earliest and latest activated segments and the heterogeneity in time-to-peak radial strain for the 6 segments were determined. LV dyssynchrony was defined as an interval ≥ 130 ms for the absolute difference in time-to-peak radial strain for the septal or anteroseptal wall versus the posterior or lateral wall (16). In addition, the time difference between the earliest and latest activated segments was calculated. Furthermore, intra- and interobserver variability for determining the time-to-peak radial strain were evaluated on short-axis images of 15 randomly selected patients. Intraobserver variability for determining the time-to-peak radial strain of all 6 segments was $10 \pm 11\%$, and interobserver variability was $8 \pm 7\%$. The presence or absence of LV dyssynchrony after long-term RV apical pacing was confirmed by tissue Doppler imaging (17).

Upgrading permanent RV pacing to biventricular pacing

Biventricular pacing is able to resynchronize the asynchronous contracting heart. To test the hypothesis that LV dyssynchrony induced by RV apical pacing can be reversed by biventricular pacing, we studied 11 RV paced patients of the study sample who were 'upgraded' to biventricular pacing. In these patients, an upgrade of the conventional pacemaker to a biventricular pacing device (Contak Renewal, Guidant Corporation, St. Paul, Minnesota, USA; or Insync Centry, Medtronic Inc., Minneapolis, Minnesota, USA) was performed because of development of heart failure (NYHA class III or IV) and the presence of LV dyssynchrony. The LV pacing lead was inserted transvenously via the subclavian route. First, a coronary sinus venogram was obtained during occlusion of the coronary sinus using a balloon catheter. Next, the LV pacing lead was

inserted in the coronary sinus with the help of an 8Fr-guiding catheter, and positioned as far as possible in the venous system, preferably in the (postero)lateral vein. After a minimum of 6 months of biventricular pacing, functional class of the patients was re-evaluated, and an extensive echocardiographic study was performed.

Statistical analysis

All continuous variables had normal distribution (as evaluated by Kolmogorov-Smirnov tests). Summary statistics for these variables are therefore presented as mean values \pm one standard deviation (SD). Categorical data are summarized as frequencies and percentages. Differences in baseline characteristics between patients with and without LV dyssynchrony are evaluated using unpaired Student t-tests (continuous variables), Chi-square tests or Fisher's exact tests (dichotomous variables), as appropriate.

One-way Analysis of variance (ANOVA) with repeated measures was applied to evaluate differences in time-to-peak radial strain between the 6 segments at baseline and at follow-up within the separate cohorts of patients with and without LV dyssynchrony. Changes that occurred in the time-to-peak value between the baseline and follow-up visit were quantified, and differences in changes according to the presence or absence of LV dyssynchrony were then analyzed by one-way ANOVA as well. Subsequently, two-way ANOVA (with repeated measures for segments) was applied to study differences in time-to-peak radial strain patterns between patients with and without LV dyssynchrony. Univariable and multivariable logistic regression analyses were performed to identify possible predictors of LV dyssynchrony. The following variables were investigated: age, duration of atrial fibrillation, coronary artery disease, QRS duration at baseline, LV ejection fraction and follow-up duration. All variables entered the multivariable stage, irrespective of the results of the univariable analyses. Subsequently, the backward deletion method was applied to build the final regression model, and we intended to keep all variables with a p-value <0.15 in the model. We intended to report adjusted Odds Ratios (OR), however since no variable reached the pre-specified p <0.15 we report only the crude unadjusted OR with their corresponding 95% confidence intervals (CI).

Changes in LV function and LV size between the baseline and follow-up visit were quantified, and differences in these changes between patients with and without LV dyssynchrony were studied by unpaired Student t-tests. Changes in LV ejection fraction over the 3 different time points (baseline, RV pacing, biventricular pacing) for 11 patients who were upgraded to biventricular pacing, were analyzed with one-way ANOVA with Bonferroni post-hoc testing (3 repeated tests; p <0.0167 was considered significant for each test).

Analyses were performed using SPSS software (version 12.0, SPSS Inc. Chicago, Illinois, USA). All statistical tests were two-sided, and a p-value <0.05 was considered significant.

RESULTS

Study sample

Fifty-eight patients treated with His bundle ablation and pacemaker implantation were studied. The baseline characteristics of the study sample are listed in Table 1. In all patients the ablation and pacemaker implantation procedures were performed successfully. No complications related to the procedures were observed. Mean follow-up was 3.8 ± 2.0 years (range 1.2 to 8.7 years).

Table 1. Baseline characteristics of the study sample

	All patients (n=58)	LV dyssynchrony absent (n=25)	LV dyssynchrony present (n=33)	P value *
Age, years	61 ± 11	59 ± 11	63 ± 12	0.1
Gender, M/F	33 / 25	15 / 10	18 / 15	0.8
Duration of AF, years	7 ± 5	7 ± 5	6 ± 5	0.3
Previous used anti-arrhythmic drugs, n	3.2 ± 1.3	3.2 ± 1.5	3.2 ± 1.1	0.9
Hypertension, n (%)	26 (45%)	12 (48%)	14 (42%)	0.8
Severe MR (grade 3-4), n (%)	0 (0%)	0 (0%)	0 (0%)	1.0
Coronary artery disease, n (%)	8 (14%)	3 (12%)	5 (15%)	1.0
Previous myocardial infarction, n (%)	4 (7%)	1 (4%)	3 (9%)	0.6
NYHA functional class	1.7 ± 0.6	1.7 ± 0.6	1.8 ± 0.7	0.5
QRS duration, ms	99 ± 10	100 ± 11	99 ± 11	0.8

* As assessed with unpaired Student t-tests (continuous variables), Chi-square or Fisher's Exact tests (dichotomous variables), as appropriate. AF = atrial fibrillation; MR = mitral regurgitation; NYHA = New York Heart Association.

Strain analysis: Heterogeneity in time-to-peak radial strain

Time-to-peak radial strain was assessed for the 6 standard segments: septal, anteroseptal, anterior, lateral, posterior and inferior. A total of 762 segments were analyzed on the LV short-axis images. Of the 762 segments, 35 segments (5%) were excluded because of poor tracking scores. Subsequently, the site of earliest and latest mechanical activation throughout the cardiac cycle was determined. At baseline, there was a homogeneous distribution of the earliest and latest mechanical activated sites among the 6 segments (Figure 1, panel A). In contrast, after long-term permanent RV pacing, a marked heterogeneity in time-to-peak radial strain of the 6 segments was observed (Figure 1, panel B). The septal and the anteroseptal segments were most frequently the earliest activated segments (34% and 30% of the total earliest activated segments, respectively); whereas the lateral and posterior segments were only seldom the earliest activated sites (7% and 6%, respectively). In contrast, the lateral and posterior segments were most frequently the latest activated segments (31% and 25%, respectively); whereas the septal (5%) and the anteroseptal (6%) were rarely the latest activated segments (Figure 1).

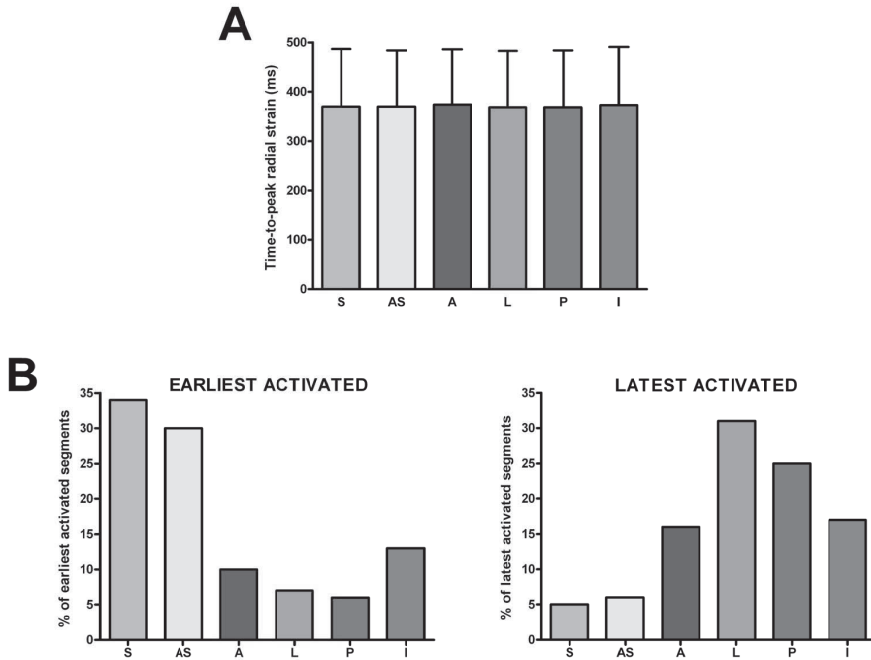


Figure 1. Distribution of time-to-peak radial strain among the 6 segments. Panel A: Time-to-peak radial strain was similar among the 6 standard segments at baseline. Panel B: Distribution of the sites of earliest and latest mechanical activation after permanent right ventricular pacing. The septal and antero-septal segments were most frequently the sites of earliest mechanical activation, whereas the lateral and posterior segments were most frequently the sites of latest mechanical activation. A= anterior; AS = antero-septal; I = inferior; L= lateral; P = posterior; S = septal.

LV dyssynchrony assessment with speckle tracking radial strain

The difference in time-to-peak radial strain between the 6 segments can be used to assess LV dyssynchrony. A time difference ≥ 130 ms between the time-to-peak radial strain of the (antero) septal and the posterolateral segments has been found to predict the response to cardiac resynchronization therapy (16). Therefore, we used this cut-off value to determine the presence of LV dyssynchrony. In Table 2, the time-to-peak radial strain values at baseline and at follow-up are shown with the study sample divided according to the presence or absence of LV dyssynchrony.

At baseline, strain curves revealed similar time-to-peak radial strain among the 6 segments (Table 2). Mean time-to-peak radial strain was 371 ± 114 ms for the 6 segments in all patients. There were no significant differences in time-to-peak radial strain among the 6 segments at baseline (Table 2). Accordingly, there was no significant delay between the (antero)septal and posterolateral segments (mean difference 26 ± 25 ms). Furthermore, the time difference between the earliest and the latest activated segments was 37 ± 31 ms. In none of the patients LV dyssynchrony, as represented by a time difference ≥ 130 ms between the (antero)septal and posterolateral segments, was present at baseline.

Table 2. Time-to-peak radial strain for the 6 segments at baseline and after permanent RV pacing

	Septal	Anteroseptal	Anterior	Lateral	Posterior	Inferior	P value among 6 segments *	P value between 2 groups †
Baseline								
LV dyssynchrony absent (n=25), ms	375 ± 100	371 ± 101	373 ± 96	365 ± 98	365 ± 103	373 ± 104	0.06	0.5
LV dyssynchrony present (n=33), ms	366 ± 131	369 ± 125	375 ± 125	370 ± 129	371 ± 126	373 ± 130	0.8	
Follow-up								
LV dyssynchrony absent, ms	375 ± 72	389 ± 63	395 ± 64	389 ± 54	394 ± 57	379 ± 77	0.2	<0.001
LV dyssynchrony present, ms	280 ± 120	287 ± 100	407 ± 76	453 ± 77	445 ± 93	374 ± 124	<0.001	
Δ								
LV dyssynchrony absent, ms	+ 7 ± 126	+ 26 ± 128	+ 31 ± 119	+ 30 ± 113	+ 37 ± 116	+ 12 ± 145	0.09	<0.001
LV dyssynchrony present, ms	- 80 ± 159	- 79 ± 164	+ 38 ± 154	+ 87 ± 157	+ 81 ± 144	+ 9 ± 148	<0.001	

* As assessed with one-way ANOVA. † As assessed with two-way ANOVA.

In contrast, after a mean of 3.8 ± 2.0 years of permanent RV pacing, radial strain curves revealed significant differences in time-to-peak radial strain among the 6 segments. In 33 (57%) patients there was a difference of ≥ 130 ms between the (antero)septal and posterolateral segments, indicating the presence of LV dyssynchrony. The study sample was subsequently divided in 2 groups: patients without LV dyssynchrony ($n=25$) and patients with LV dyssynchrony ($n=33$) after permanent RV pacing. There were no significant differences in baseline characteristics between the 2 groups (Table 1), and none of the variables that we considered were significantly associated with the development of LV dyssynchrony (Table 3). Duration of follow-up was similar between the patients with and without LV dyssynchrony (4.0 ± 2.0 years and 3.8 ± 2.0 years, respectively) and paced QRS duration at follow-up was not different between the patients with and without LV dyssynchrony (169 ± 20 ms vs. 167 ± 21 ms, $p=0.8$).

Table 3. Multivariable regression analysis for prediction of LV dyssynchrony

	OR (95% CI)	P value
Age *	0.97 (0.92 – 1.01)	0.1
Duration of AF *	1.06 (0.94 – 1.19)	0.3
Coronary artery disease	0.61 (0.14 – 2.74)	0.5
QRS duration	1.01 (0.96 – 1.06)	0.8
LV ejection fraction	0.98 (0.88 – 1.09)	0.7
Follow-up duration *	0.92 (0.71 – 1.20)	0.5

* ratio per year.

Radial strain after long-term permanent RV pacing

In the patients with LV dyssynchrony, time-to-peak radial strain was significantly shorter in the septal and anteroseptal segments, as compared to baseline values (septal 280 ± 120 ms vs. 366 ± 131 ms, $p=0.014$; anteroseptal 287 ± 100 ms vs. 369 ± 125 ms, $p=0.019$). In contrast, time-to-peak radial strain in the lateral and posterior segments was significantly longer, as compared to baseline values (lateral 453 ± 77 ms vs. 370 ± 129 ms, $p=0.008$; posterior 445 ± 93 ms vs. 371 ± 126 ms, $p=0.007$).

Conversely, in the patients without LV dyssynchrony, no significant differences in time-to-peak radial strain among the 6 segments were observed. Time-to-peak radial strain was longer for all 6 segments as compared to baseline, but no significant differences were detected (Table 2).

In addition to time-to-peak strain, peak radial strain was assessed for the 6 standard segments. At baseline, no differences were noted in peak radial strain among the 6 segments (septal $31 \pm 14\%$, anteroseptal $32 \pm 13\%$, anterior $32 \pm 15\%$, lateral $33 \pm 16\%$, posterior $33 \pm 17\%$ and inferior $33 \pm 14\%$). In contrast, after long-term RV pacing, peak radial strain was significantly lower in the septal and the anteroseptal segments ($21 \pm 13\%$, $p=0.007$, and $24 \pm 16\%$, $p=0.039$ respectively) and significantly higher in the lateral and posterior segments ($43 \pm 20\%$, $p=0.030$, and $42 \pm 20\%$, $p=0.040$ respectively), whereas peak radial strain remained similar in the anterior ($32 \pm 20\%$) and inferior ($32 \pm 18\%$) segments, as compared to baseline. Interest-

ingly, no significant differences were noted between the patients with LV dyssynchrony and the patients without LV dyssynchrony.

Thirty-eight patients underwent echocardiography within 1 day after the pacemaker implantation as part of the clinical evaluation. Of these patients, 14 (37%) showed LV dyssynchrony immediately after pacemaker implantation. In addition, at follow-up tissue Doppler imaging was performed to confirm the presence or absence of LV dyssynchrony. All patients with LV dyssynchrony on speckle tracking analysis also had LV dyssynchrony on tissue Doppler imaging (mean 103 ± 21 ms). All patients without LV dyssynchrony on speckle tracking analysis also had no LV dyssynchrony on tissue Doppler imaging (mean 29 ± 22 ms).

At baseline and follow-up, NYHA functional class was assessed and echocardiographic evaluation was performed to assess LV volumes, diameters and LV systolic function. In the patients with LV dyssynchrony, NYHA functional class deteriorated from 1.8 ± 0.7 to 2.4 ± 0.7 ($p < 0.001$), whereas NYHA class improved in the patients without LV dyssynchrony (from 1.7 ± 0.6 to 1.4 ± 0.6 , $p = 0.008$). The LV parameters as assessed with standard echocardiograms are listed in Table 4.

Table 4. Echocardiographic parameters of LV function and LV size at baseline and after RV pacing

	LV dyssynchrony absent (n=25)			LV dyssynchrony present (n=33)			P value *
	Baseline	Follow-up	Δ	Baseline	Follow-up	Δ	
LV ejection fraction, %	48 ± 5	51 ± 7	$+4 \pm 8$	48 ± 5	39 ± 10	-10 ± 11	<0.001
LV end-diastolic volume, ml	115 ± 27	119 ± 29	$+3 \pm 18$	124 ± 38	158 ± 70	$+34 \pm 50$	0.004
LV end-systolic volume, ml	60 ± 17	58 ± 18	-3 ± 14	65 ± 24	99 ± 59	$+37 \pm 50$	<0.001
LV end-diastolic diameter, cm	5.2 ± 0.7	5.4 ± 0.4	$+0.1 \pm 0.7$	5.5 ± 0.9	6.0 ± 1.0	$+0.4 \pm 0.7$	0.5
LV end-systolic diameter, cm	3.4 ± 0.6	3.5 ± 0.5	$+0.1 \pm 0.7$	3.8 ± 0.9	4.4 ± 1.3	$+0.5 \pm 1.0$	0.2
Fractional shortening, %	35 ± 9	35 ± 7	$+1 \pm 9$	32 ± 11	27 ± 12	-4 ± 13	0.8
Clinically relevant mitral regurgitation (grade 3-4), n (%)	0	2 (8%)	+2	0	5 (15%)	+5	0.7

* Difference between Δ values of patients with LV dyssynchrony vs. patients without LV dyssynchrony, as assessed with unpaired t tests for continuous variables and Fisher's Exact test for dichotomous variable.

Upgrading permanent RV pacing to biventricular pacing

In 11 patients, an upgrade of the conventional pacemaker to a biventricular pacing device was performed 4.1 ± 2.0 years after the His bundle ablation and pacemaker implantation procedure because of heart failure symptoms and the presence of LV dyssynchrony. The LV pacing lead was positioned in the mid lateral region in 3 patients (27%), and in the postero-lateral region in 8 patients (73%). After a mean of 11 ± 8 months, an extensive echocardiogram was performed to assess LV function and LV dyssynchrony.

In all patients, radial strain curves revealed disappearance of the LV dyssynchrony after upgrade to biventricular pacing. Time-to-peak radial strain for the different segments were: septal 373 ± 56 ms, anteroseptal 362 ± 53 ms, anterior 369 ± 53 ms, lateral 367 ± 54 ms, posterior 386 ± 43 ms, inferior 374 ± 48 ms. In none of the patients, a difference in time-to-peak radial strain ≥ 130 ms between the (antero)septal and posterolateral segments was present. A

representative example of the speckle tracking strain curves of a patient at the different time points is shown in Figure 2.

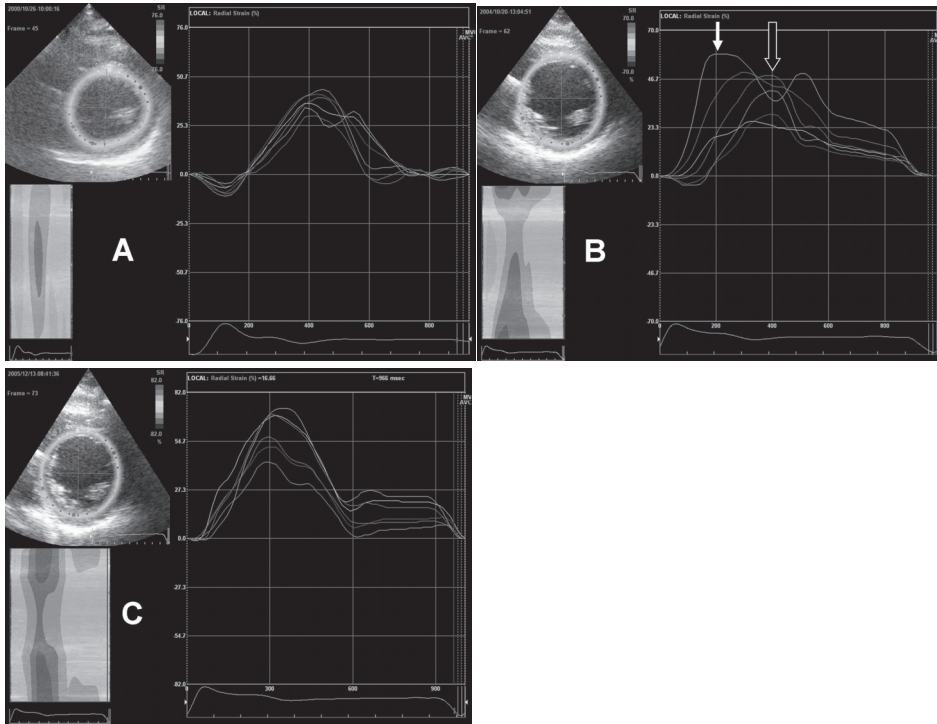


Figure 2. Radial strain curves assessed with speckle tracking analysis of a representative patient. The color-coded curves represent the 6 segments (light blue = septal; yellow = anteroseptal; red = anterior; green = lateral; purple = posterior; dark blue = inferior). Panel A: Before His bundle ablation and pacemaker implantation, there was no significant delay in time-to-peak radial strain among the 6 segments. Panel B: After 4 years of permanent RV pacing, a marked heterogeneity in time-to-peak strain for the 6 segments was observed. A time difference >130 ms was present between the time-to-peak radial strain of the septal (arrow) and posterolateral (open arrow) segments. Panel C: In this patient, upgrade of the conventional pacemaker to a biventricular pacemaker was performed. More than 1 year after 'upgrade', the radial strain curves revealed restoration of synchronous LV activation, with no significant delay between the time-to-peak radial strain of the different segments.

Of interest, mean LV ejection fraction improved from $30 \pm 8\%$ to $39 \pm 7\%$ ($p < 0.001$) after upgrade to biventricular pacing. In all patients, an increase in LV ejection fraction $\geq 5\%$ was observed. LV ejection fractions for the different time points in the 11 patients are demonstrated in Figure 3. In addition, the deleterious effects of RV apical pacing on LV volumes were partially reversed after upgrade to biventricular pacing. LV end-diastolic volume had decreased from 224 ± 66 ml to 167 ± 47 ml ($p = 0.001$), and LV end-systolic volume had decreased from 160 ± 58 ml to 103 ± 34 ml ($p < 0.001$) after upgrade to biventricular pacing. In all patients, a decrease in end-systolic volume $\geq 15\%$ was observed. In addition, NYHA functional class improved after upgrade to biventricular pacing from 3.1 ± 0.3 to 2.1 ± 0.5 ($p < 0.001$).

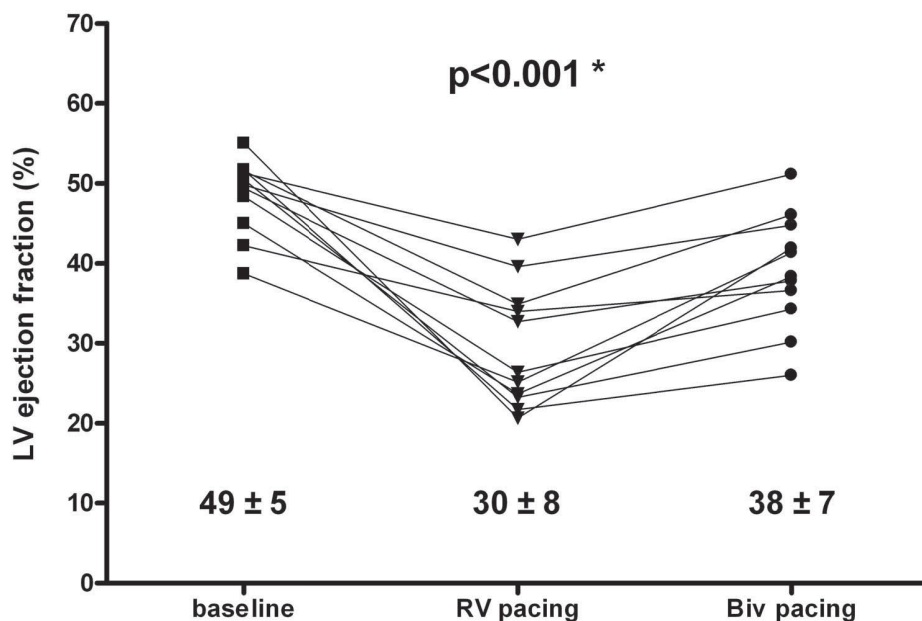


Figure 3. Effect of upgrading to biventricular pacing on left ventricular ejection fraction. LV ejection fraction at different time points for 11 patients who were upgraded to biventricular (BiV) pacing after a mean of 4.1 ± 2.0 years of permanent RV pacing. After permanent RV pacing, LV ejection fraction had significantly decreased. This was partly reversed after upgrade to biventricular pacing. * As assessed with repeated measures analysis of variance. Bonferroni post-hoc testing revealed significant differences between baseline and RV pacing ($p < 0.001$) and between RV pacing and BiV pacing ($p < 0.01$).

DISCUSSION

In the present study, speckle tracking revealed heterogeneity in time-to-peak radial strain and LV dyssynchrony in 57% of the patients with permanent RV pacing after His bundle ablation. The present study further extends our previous findings (11). Whereas previously myocardial velocities were assessed with tissue Doppler imaging (11), in the present study timing of regional LV strain was assessed with the use of speckle tracking. Frequently, strain analysis allows for more accurate analysis of LV function/dyssynchrony since it may permit differentiation between active contraction and passive motion. In addition, using this novel technique, accurate evaluation of LV dyssynchrony at baseline was possible, whereas in the previous study the M-mode derived septal-to-posterior wall motion delay was used (11). Most importantly, in the present study it was demonstrated that LV dyssynchrony induced by RV apical pacing could be reversed in patients receiving an 'upgrade' to biventricular pacing, with a concomitant improvement in LV function and functional class.

Strain analysis

In the present study, novel speckle tracking software applied to standard short-axis images was used to assess timing of regional wall strain, and identify regions of early and late activation in permanent RV paced patients. Speckle tracking radial strain is a novel technique that allows angle-independent measurement of regional strain and time-to-peak radial strain of different segments among the LV wall (12,13). This new technique has recently been validated using sonomicrometry and magnetic resonance imaging (18,19). Furthermore, it has been demonstrated that speckle tracking can quantify LV dyssynchrony, and accurately predict responders to cardiac resynchronization therapy (16). In addition, speckle tracking analysis allows for an accurate quantification of regional wall strain and time-to-peak wall strain, with a high reproducibility (20,21). In the current study, a good inter- and intra-observer agreement for this novel technique was noted.

Using speckle tracking radial strain, induction of heterogeneity in strain after RV pacing was demonstrated, with a short time-to-peak radial strain of the anteroseptal segments and a long time-to-peak radial strain of the posterolateral segments. At present, no studies have been reported concerning the effects of permanent RV apical pacing on timing of regional wall strain in patients. In contrast, several animal studies have reported wall strain analysis during RV pacing (8-10). Wyman et al (8) used magnetic resonance imaging tagging to evaluate regional wall strain in 7 dogs during RV apical pacing. Similar to the present findings, the authors demonstrated an early activation of the septum with late activation of the lateral wall during RV apical pacing. Dohi et al (10) studied the effect of RV and biventricular pacing in 8 dogs using angle-corrected tissue Doppler strain imaging. The authors reported similar heterogeneity in activation with short time-to-peak strain in the septal segments (189 ± 55 ms) and long time-to-peak strain in the free wall (487 ± 37 ms) during RV pacing.

Furthermore, in the present study regional wall strain analysis revealed that the site of earliest mechanical activation was mainly located at the (antero)septum, whereas the site of latest activation was mainly located at the posterolateral wall. In a mapping study in 40 patients, Vassallo et al (22) demonstrated that the site of earliest activation in the left ventricle during RV pacing was consistently located in the septum. In addition, the authors demonstrated that the site of latest activation during RV apical pacing varied (22), but was predominantly located in the posterior wall. The current observations are in line with this study: 64% of the earliest activated segments were located in the (antero)septum, and 56% of the latest activated segments were located in the posterolateral wall (Figure 1).

A significant time difference between the earliest and latest time-to-peak radial strain represents intraventricular conduction delay or LV dyssynchrony. Previously, a time difference ≥ 130 ms between the (early) septal and the (late) posterior wall, as assessed with speckle tracking radial strain, has been demonstrated to be a good predictor for response to cardiac resynchronization therapy (16). Interestingly, in the present study not all patients exhibited a significant delay between the earliest activated (antero)septum and the latest activated posterolateral

wall. In 53% of the patients, significant LV dyssynchrony was present after long-term RV pacing. Furthermore, time-to-peak radial strain in the patients without LV dyssynchrony was later in all segments as compared to the non-paced baseline value. Thus, the exact effect of RV apical pacing may differ per patient. This may be related to the fact that the electrical impulses propagate more slowly through the myocardium during RV pacing than through the Purkinje system during normal sinus rhythm. However, it remains unclear why some patients develop significant LV dyssynchrony, and others do not. There were no differences in baseline characteristics between the two groups, and mean follow-up duration was similar in the two groups. Importantly, a multivariable logistic regression analysis including age, duration of atrial fibrillation, coronary artery disease, QRS duration at baseline, LV ejection fraction and follow-up duration was not able to identify any predictor for the development of LV dyssynchrony in the present study. Future studies are needed to identify the patients who are more vulnerable for the detrimental effects of permanent RV apical pacing. Furthermore, more studies are needed to determine whether LV dyssynchrony is induced acutely with RV apical pacing or develops over time.

Impact of RV pacing on LV function and heart failure symptoms

Recently, several trials have stressed the deleterious effects of RV apical pacing. In the DAVID trial (3), DDDR pacing increased the risk of death or heart failure hospitalization, as compared to VVIR back-up pacing in 506 patients with an indication for implantable cardioverter defibrillator therapy. Similarly, the MOST trial (4) demonstrated that the cumulative percent ventricular pacing was a strong predictor of heart failure hospitalization in patients with DDDR and VVIR pacing. The aforementioned studies suggest that RV apical pacing should be avoided. However, the exact mechanism of the detrimental effect of RV apical pacing remains unclear in these studies. The present study shows that the decrease in LV systolic function and NYHA functional class is directly related to the presence of LV dyssynchrony. Previously, it has been suggested that the detrimental effects of RV apical pacing may be more pronounced in patients with LV dysfunction before pacemaker implantation (4). However, in the present study no differences in baseline characteristics between the patients with and the patients without LV dyssynchrony were found.

Effects of upgrade to biventricular pacing

To reverse the abnormal activation pattern (i.e. LV dyssynchrony) induced by RV pacing, biventricular pacing could be considered. In the present study, 11 patients received 'upgrade' of the conventional pacemaker to biventricular pacing. LV dyssynchrony, induced by RV apical pacing, largely resolved with a concomitant improvement in LV function and NYHA functional class. Leon et al (23) reported similar results in 20 patients with severe heart failure and prior atrioventricular node ablation and permanent RV pacing. Following upgrade to biventricular pacing, LV ejection fraction improved from $22 \pm 7\%$ to $31 \pm 12\%$, and NYHA class improved from 3.4 ± 0.5 to 2.4 ± 0.6 . The HOBIPACE trial (24) recently demonstrated that in 30 patients

with standard pacemaker indication and LV dysfunction, biventricular pacing was superior to conventional RV pacing regarding LV systolic function (ejection fraction biventricular $34.8 \pm 8.9\%$ vs. RV pacing $28.5 \pm 11.2\%$, $p < 0.001$), NYHA functional class (biventricular 1.9 ± 0.6 vs. RV pacing 2.5 ± 0.7 , $p < 0.05$) and exercise capacity (peak oxygen consumption biventricular 14.0 ± 3.0 ml/min/kg vs. RV pacing 12.5 ± 2.9 ml/min/kg, $p < 0.001$).

In addition, alternate pacing sites (such as RV outflow tract, paraHisian or direct His bundle pacing) have been proposed to replace RV apical pacing (2). Several short-term studies have reported a modest benefit of RV outflow tract, as compared to RV apical pacing (25). Furthermore, paraHisian (26) and direct His bundle pacing (27) have been proven to be feasible. However, concerns about long-term lead stability at the various sites exist, and no large randomized trials on long-term benefit over RV apical pacing have been reported. Still, alternate pacing sites may prevent the occurrence of LV dyssynchrony as induced by RV apical pacing, and therefore could be considered in patients who need permanent pacing.

Limitations

In the present study only 6 segments at the mid-ventricular level were analyzed using radial strain analysis. Analysis at more basal and apical levels and analysis of circumferential or longitudinal strain may provide additional information on the effects of RV apical pacing on LV function. Nonetheless, it has been demonstrated that radial strain analysis at the mid-ventricular level is of great value for the detection of LV dyssynchrony and the prediction of response to cardiac resynchronization therapy (16). Additional head-to-head comparisons are needed to determine which type of strain analysis (radial, longitudinal or circumferential) provides optimal information.

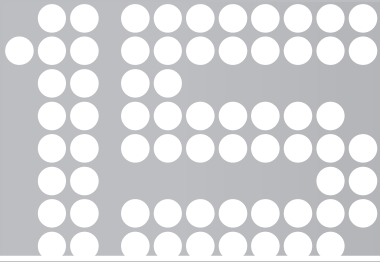
CONCLUSIONS

Speckle tracking radial strain revealed that permanent RV pacing induced heterogeneity in time-to-peak strain among the LV walls (with early activation in the (antero)septal and late activation in the posterolateral segments). In 57% of patients, this resulted in the presence of LV dyssynchrony. In these patients a deterioration of LV systolic function and NYHA functional class was observed. Upgrade to biventricular pacing resulted in (partial) reversal of these detrimental effects of RV pacing.

REFERENCES

1. Healey JS, Toff WD, Lamas GA et al. Cardiovascular outcomes with atrial-based pacing compared with ventricular pacing: meta-analysis of randomized trials, using individual patient data. *Circulation* 2006;114:11-7.
2. Manolis AS. The deleterious consequences of right ventricular apical pacing: time to seek alternate site pacing. *Pacing Clin Electrophysiol* 2006;29:298-315.
3. Wilkoff BL, Cook JR, Epstein AE et al. Dual-chamber pacing or ventricular backup pacing in patients with an implantable defibrillator: the Dual Chamber and VVI Implantable Defibrillator (DAVID) Trial. *JAMA* 2002;288:3115-23.
4. Sweeney MO, Hellkamp AS, Ellenbogen KA et al. Adverse effect of ventricular pacing on heart failure and atrial fibrillation among patients with normal baseline QRS duration in a clinical trial of pace-maker therapy for sinus node dysfunction. *Circulation* 2003;107:2932-7.
5. Steinberg JS, Fischer A, Wang P et al. The clinical implications of cumulative right ventricular pacing in the multicenter automatic defibrillator trial II. *J Cardiovasc Electrophysiol* 2005;16:359-65.
6. Vernoooy K, Dijkman B, Cheriex EC, Prinzen FW, Crijns HJ. Ventricular remodeling during long-term right ventricular pacing following His bundle ablation. *Am J Cardiol* 2006;97:1223-7.
7. Tse HF, Yu C, Wong KK et al. Functional abnormalities in patients with permanent right ventricular pacing: the effect of sites of electrical stimulation. *J Am Coll Cardiol* 2002;40:1451-8.
8. Wyman BT, Hunter WC, Prinzen FW, McVeigh ER. Mapping propagation of mechanical activation in the paced heart with MRI tagging. *Am J Physiol* 1999;276:H881-H891.
9. Prinzen FW, Hunter WC, Wyman BT, McVeigh ER. Mapping of regional myocardial strain and work during ventricular pacing: experimental study using magnetic resonance imaging tagging. *J Am Coll Cardiol* 1999;33:1735-42.
10. Dohi K, Pinsky MR, Kanzaki H, Severyn D, Gorcsan J, III. Effects of radial left ventricular dyssynchrony on cardiac performance using quantitative tissue Doppler radial strain imaging. *J Am Soc Echocardiogr* 2006;19:475-82.
11. Tops LF, Schalij MJ, Holman ER, van Erven L, van der Wall EE, Bax JJ. Right ventricular pacing can induce ventricular dyssynchrony in patients with atrial fibrillation after atrioventricular node ablation. *J Am Coll Cardiol* 2006;48:1642-8.
12. Reisner SA, Lysyansky P, Agmon Y, Mutlak D, Lessick J, Friedman Z. Global longitudinal strain: a novel index of left ventricular systolic function. *J Am Soc Echocardiogr* 2004;17:630-3.
13. Leitman M, Lysyansky P, Sidenko S et al. Two-dimensional strain—a novel software for real-time quantitative echocardiographic assessment of myocardial function. *J Am Soc Echocardiogr* 2004;17:1021-9.
14. Schiller NB, Shah PM, Crawford M et al. Recommendations for quantitation of the left ventricle by two-dimensional echocardiography. *J Am Soc Echocardiogr* 1989;2:358-67.
15. Thomas JD. How leaky is that mitral valve? Simplified Doppler methods to measure regurgitant orifice area. *Circulation* 1997;95:548-50.
16. Suffoletto MS, Dohi K, Cannesson M, Saba S, Gorcsan J, III. Novel speckle-tracking radial strain from routine black-and-white echocardiographic images to quantify dyssynchrony and predict response to cardiac resynchronization therapy. *Circulation* 2006;113:960-8.
17. Bax JJ, Bleeker GB, Marwick TH et al. Left ventricular dyssynchrony predicts response and prognosis after cardiac resynchronization therapy. *J Am Coll Cardiol* 2004;44:1834-40.
18. Langeland S, Wouters PF, Claus P et al. Experimental assessment of a new research tool for the estimation of two-dimensional myocardial strain. *Ultrasound Med Biol* 2006;32:1509-13.
19. Notomi Y, Lysyansky P, Setser RM et al. Measurement of ventricular torsion by two-dimensional ultrasound speckle tracking imaging. *J Am Coll Cardiol* 2005;45:2034-41.
20. Amundsen BH, Helle-Valle T, Edvardsen T et al. Noninvasive myocardial strain measurement by speckle tracking echocardiography: validation against sonomicrometry and tagged magnetic resonance imaging. *J Am Coll Cardiol* 2006;47:789-93.

21. Cho GY, Chan J, Leano R, Strudwick M, Marwick TH. Comparison of two-dimensional speckle and tissue velocity based strain and validation with harmonic phase magnetic resonance imaging. *Am J Cardiol* 2006;97:1661-6.
22. Vassallo JA, Cassidy DM, Miller JM, Buxton AE, Marchlinski FE, Josephson ME. Left ventricular endocardial activation during right ventricular pacing: effect of underlying heart disease. *J Am Coll Cardiol* 1986;7:1228-33.
23. Leon AR, Greenberg JM, Kanuru N et al. Cardiac resynchronization in patients with congestive heart failure and chronic atrial fibrillation: effect of upgrading to biventricular pacing after chronic right ventricular pacing. *J Am Coll Cardiol* 2002;39:1258-63.
24. Kindermann M, Hennen B, Jung J, Geisel J, Bohm M, Frohlig G. Biventricular versus conventional right ventricular stimulation for patients with standard pacing indication and left ventricular dysfunction: the Homburg Biventricular Pacing Evaluation (HOBIPACE). *J Am Coll Cardiol* 2006;47:1927-37.
25. de Cock CC, Giudici MC, Twisk JW. Comparison of the haemodynamic effects of right ventricular outflow-tract pacing with right ventricular apex pacing: a quantitative review. *Europace* 2003;5:275-8.
26. Occhetta E, Bortnik M, Magnani A et al. Prevention of ventricular desynchronization by permanent para-Hisian pacing after atrioventricular node ablation in chronic atrial fibrillation: a crossover, blinded, randomized study versus apical right ventricular pacing. *J Am Coll Cardiol* 2006;47:1938-45.
27. Deshmukh P, Casavant DA, Romanyshyn M, Anderson K. Permanent, direct His-bundle pacing: a novel approach to cardiac pacing in patients with normal His-Purkinje activation. *Circulation* 2000;101:869-77.



The effect of right ventricular pacing on myocardial oxidative metabolism and efficiency: relation with left ventricular dyssynchrony

Heikki Ukkonen¹

Laurens F. Tops²

Antti Saraste¹

Alexander Naum³

Juhani Koistinen¹

Jeroen J. Bax²

Juhani Knuuti³

¹Department of Medicine, Turku University Hospital, Turku, Finland

²Department of Cardiology, Leiden University Medical Center, Leiden, the Netherlands

³Turku PET Center, University of Turku, Turku, Finland

ABSTRACT

Purpose: Right ventricular (RV) apical pacing induces dyssynchrony by left bundle branch block type electrical activation sequence in the heart, and may impair left ventricular (LV) function. Whether these functional changes are accompanied with changes in myocardial perfusion, oxidative metabolism and efficiency, and the relation with the induction of LV dyssynchrony are unknown. Our study was designed to study the acute effects of RV pacing on these parameters.

Methods: Ten patients with normal LV ejection fraction and VVI/DDD pacemaker were studied during AAI-pacing/sinus rhythm without RV pacing (pacing-OFF) and with RV pacing (pacing-ON) at the same heart rate. Dynamic [^{15}O]water and [^{11}C]acetate positron emission tomography was used to measure perfusion and oxidative metabolism (k_{mono}) of the LV. An echocardiographic examination was used to assess LV stroke volume (SV) and LV dyssynchrony. Myocardial efficiency of forward work was calculated as systolic blood pressure \times cardiac output/LV mass/ k_{mono} .

Results: RV pacing decreased SV in all subjects (mean decrease 13%, from 76 ± 7 to 66 ± 7 ml, $p=0.004$) but global perfusion and k_{mono} were unchanged. The efficiency tended to be lower with pacing-ON (70 ± 20 vs. 81 ± 21 mmHg-L/g, $p=0.066$). In patients with dyssynchrony during pacing ($n=6$) efficiency decreased by 23% (from 78 ± 25 to 60 ± 14 mmHg-L/g, $p=0.02$) but in patients without dyssynchrony no change in efficiency was detected. Accordingly, heterogeneity in myocardial perfusion and oxidative metabolism was detected during pacing in patients with dyssynchrony but not in those without dyssynchrony.

Conclusions: RV pacing resulted in a significant decrease in SV. However, deleterious effects on LV oxidative metabolism and efficiency were observed only in patients with dyssynchrony during RV pacing.

INTRODUCTION

Right ventricular (RV) apical pacing induces a left bundle branch block (LBBB) type electrical activation sequence in the heart (1). This abnormal activation pattern of the ventricles may have detrimental effects on cardiac structure and function. Several clinical trials have demonstrated an association between RV pacing and an increased risk of heart failure and death (2,3). In addition, RV pacing has been shown to impair left ventricular (LV) function both in normal and failing hearts (4-6). Importantly, it has been demonstrated that this deterioration in LV function is related to the presence of LV dyssynchrony during RV pacing (7).

The exact effects of RV pacing on myocardial perfusion, oxidative metabolism and cardiac efficiency have not been fully elucidated. In experimental LBBB, significant changes in regional myocardial perfusion and glucose metabolism have been observed (8). Similarly, RV pacing may result in regional alterations in glucose metabolism (9). Importantly, the relation between the presence of LV dyssynchrony during RV pacing and changes in myocardial perfusion, oxidative metabolism and cardiac efficiency has not been studied.

Therefore, the objective of the present study was to evaluate the effect of RV pacing on both global and regional oxidative metabolism and perfusion, and myocardial efficiency. In addition, the effect of RV pacing-induced LV dyssynchrony on myocardial oxidative metabolism and efficiency was studied.

METHODS

Study population and study protocol

Ten patients (5 men, mean age 62 ± 17 years) with previously implanted RV or dual-chamber pacemaker and normal LV function were included in the study. None of the patients had ventricular conduction abnormality during atrial rhythm. All the vasoactive medications were withheld 24 hours prior the study. Patient characteristics are summarized in Table 1. [^{11}C]acetate PET imaging was used to measure oxidative metabolism, [^{15}O]H₂O to measure myocardial perfusion and an echocardiographic examination to measure LV volumes, stroke work and dyssynchrony. Patients were studied both during AAI pacing or sinus rhythm without RV pacing (pacing-OFF) and during RV pacing (pacing-ON) at the same heart rate. During pacing-ON, AV delay was kept shorter (mean 129 ± 30 ms) than natural AV delay (mean 262 ± 79 ms) to ensure successful RV pacing (Table 1).

The sequence was pacing-OFF – pacing-ON in seven patients and pacing-ON – pacing-OFF in three patients. The device was programmed to the desired setting at least 1 hour prior to the PET and echocardiographic studies. The PET and echocardiographic examinations were performed during the same day approximately 2 hours apart (Figure 1). A standard 12-lead ECG was recorded every 10 minutes during PET imaging to ensure the appropriate pacing

Table 1. Patient characteristics

Patient	Gender	Age (years)	RV lead location	Dyssynchrony with RV pacing	AV delay pacing-OFF (ms)	AV delay pacing-ON (ms)	QRS duration pacing-OFF (ms)	QRS duration pacing-ON (ms)
1	F	87	septal	yes	170	90	100	140
2	F	47	inferobasal	no	350	120	100	170
3	M	54	septal	no	190	160	110	100
4	M	66	basal	no	270	150	100	160
5	F	62	septum	yes	240	100	100	170
6	M	77	apical	yes	380	180	90	170
7	M	62	septal	no	270	140	110	180
8	M	68	basal	yes	350	120	110	180
9	F	28	apical	yes	250	140	80	180
10	F	73	apical	yes	150	90	80	150
Mean ± SD		62 ± 17			262 ± 79	129 ± 30*	98 ± 11	160 ± 25*

* $p < 0.001$ vs. pacing-OFF; AV = atrioventricular; RV = right ventricular.

mode during the study. Maximal time interval between the initiation of atrial and ventricular activations (AV delay) and maximal QRS duration were measured both during pacing-ON and pacing-OFF. The protocol was approved by the institutional ethic review board of Turku University Hospital and was carried out in accordance with institutional guidelines.

Echocardiography

Images were recorded with patients in the left lateral decubitus position using a commercially available system (Vingmed Vivid 7, General Electric-Vingmed, Milwaukee, Wisconsin, USA). Images were obtained using a 3.5-MHz transducer at a depth of 16 cm in the parasternal

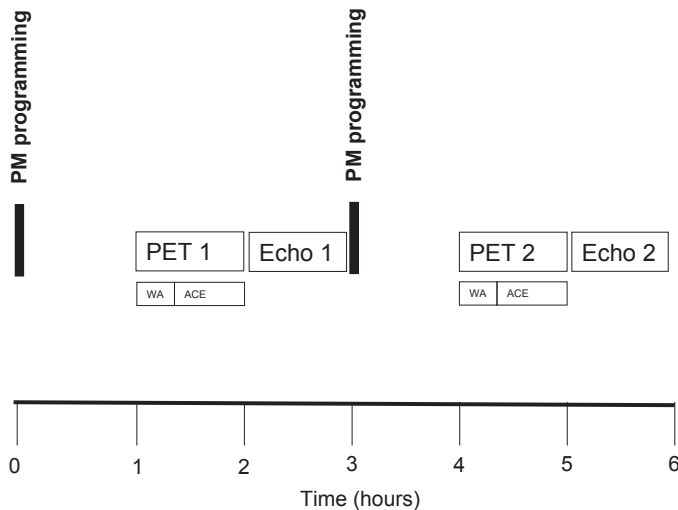


Figure 1. Study flow chart. The sequence was pacing-OFF – pacing-ON in 7 patients and pacing-ON – pacing-OFF in 3 patients. PM = pacemaker; WA = [^{15}O]H $_2$ O PET; ACE = [^{11}C] acetate; PET 1 = first PET study; PET 2 = second PET study; Echo 1 = first echocardiography study; Echo 2 = second echocardiography study.

(long- and short-axis) and apical (2- and 4-chamber) views. Standard two-dimensional images and color Doppler data triggered to the QRS complex were digitally stored in cine-loop format.

Cardiac output and LV work power Cardiac output (CO) was derived from pulsed-wave Doppler analysis. The LV outflow tract velocity-time integral was obtained from the LV long-axis apical view with the sample volume positioned approximately 5 mm proximal to the aortic valve. By measuring the diameter of the LV outflow tract and the heart rate, CO was derived (10). External, or forward, LV work power was calculated (LV work power = systolic blood pressure (SBP) \times CO); and subsequently forward LV work power per gram of tissue was calculated as: forward LV work power / LV mass (11).

Left ventricular dyssynchrony Left ventricular dyssynchrony was assessed with the use of speckle-tracking analysis and color-coded tissue Doppler imaging (TDI). Off-line analysis of LV dyssynchrony was performed on digitally stored images (EchoPac version 6.1, General Electric-Vingmed) by an independent observer blinded to all other results; the echocardiographic studies during pacing-OFF and pacing-ON were evaluated in random order.

The assessment of LV dyssynchrony with speckle-tracking analysis has been described in more detail previously (12,13). In brief, speckle-tracking analysis is a technique that tracks frame-to-frame movement of natural acoustic markers on standard gray scale images of the myocardium. With the use of dedicated algorithms, time-strain curves are constructed to assess myocardial strain throughout the cardiac cycle (14,15). Short-axis images of the LV at the level of the papillary muscles were used and automatically divided into 6 standard segments: septal, anteroseptal, anterior, lateral, posterior, and inferior, respectively. Time-strain curves for all the 6 segments were then constructed. Subsequently, the time from QRS onset to peak radial strain of each segment was obtained. Left ventricular dyssynchrony was defined as an interval ≥ 130 ms for the absolute difference in time-to-peak radial strain for the septal or anteroseptal wall versus the posterior or lateral wall (12,13).

In addition, LV dyssynchrony was assessed using color-coded TDI by placing sample volumes in the basal portions of the septum, lateral, anterior and inferior wall (16). The time-to-peak systolic velocity was obtained in these 4 regions and the maximum difference among the 4 regions was used as an indicator of LV dyssynchrony. A delay >65 ms was used as a cut-off value for LV dyssynchrony assessed with TDI, as previously reported (16).

To study the effects of RV pacing and LV dyssynchrony on myocardial oxidative metabolism and efficiency, the PET data were first analyzed based on RV pacing mode only, comparing the two pacing conditions (pacing-ON vs. pacing-OFF). Thereafter, the study population was divided into two groups, according to the presence of LV dyssynchrony during RV pacing.

Positron Emission Tomography

Patients were positioned in a whole body PET scanner (GE Advance Milwaukee, WI, USA) and [^{11}C]acetate and [^{15}O]H $_2$ O PET imaging was performed as previously described (11). The Carimas software package (17) for cardiac image analysis (Carimas, Turku PET Center, Turku, Finland) was used to sample the LV myocardium into polar maps. The resulting polar map represents the tracer uptake in the LV myocardium. Values of regional myocardial blood flow (MBF) expressed in millilitres per gram of tissue per minute and oxidative metabolism (clearance rate constant, k_{mono} , 1/min) were automatically generated on a pixel-by-pixel basis, based on the previously published tracer kinetic models (18-22). Regional values of MBF and oxidative metabolism were then obtained using the conventional 17 segment model. The average values of the septal [2, 3, 8, 9, 14] and the lateral [5, 6, 11, 12 and 16] myocardial segments were used to calculate the septal-to-lateral wall ratios. In addition, myocardial efficiency (the relation between the forward work and oxygen consumption) was estimated as: forward LV work power per gram / LV k_{mono} (SBP x CO/LV mass/LV k_{mono}).

Statistical Analysis

All continuous data are expressed as mean \pm SD. Comparisons between pacing-OFF and pacing-ON were performed using a two-sided paired t-test; comparisons between dyssynchrony vs. no dyssynchrony were performed using unpaired univariate repeated measurements ANOVA. A p -value < 0.05 was considered statistically significant.

RESULTS

Effects of RV pacing

The patient characteristics, pacing lead positions and the presence of LV dyssynchrony as well as the ECG parameters during pacing-OFF and pacing-ON are presented in Table 1. By definition, AV delay was significantly shorter during pacing-ON than pacing-OFF (129 ± 30 vs. 262 ± 79 ms, $p < 0.001$). RV pacing induced clear widening of QRS complex in all except one patient and QRS duration was significantly longer during pacing-ON than pacing-OFF (160 ± 25 vs. 98 ± 11 ms, $p < 0.001$).

The hemodynamic, echocardiographic and PET results during pacing-OFF and pacing-ON are summarized in Table 2. There was no significant difference in heart rate and blood pressures during pacing-OFF and pacing-ON (Table 2). In contrast, CO was 13% lower during pacing-ON as compared to pacing-OFF, and LV work power was 13% lower during pacing-ON (Table 2).

For the total study population, the absolute global MBF was comparable during pacing-ON and pacing-OFF, but septal-to-lateral wall MBF ratio was 19% lower during pacing-ON than during pacing-OFF ($p = 0.017$) (Table 2). Global myocardial oxidative metabolism (k_{mono}) was comparable during pacing-ON and pacing-OFF. However, the septal-to-lateral wall k_{mono} ratio

Table 2. The effects of RV pacing on hemodynamics, LV function and PET-derived parameters

Measure	Pacing-OFF	Pacing-ON	p-value
Heart rate, bpm	63 ± 8	67 ± 10	0.053
Systolic BP, mmHg	129 ± 25	130 ± 24	0.42
Diastolic BP, mmHg	69 ± 11	72 ± 9	0.27
CO, l/min	4.87 ± 0.69	4.24 ± 0.80	0.0003
LV work power, mmHg-l/min/g	5.17 ± 1.80	4.56 ± 1.78	0.013
MBF, ml/min/g	1.04 ± 0.21	1.05 ± 0.15	0.52
MBF septal/lateral ratio	0.81 ± 0.13	0.66 ± 0.07	0.017
k_{mono} , min ⁻¹	0.069 ± 0.016	0.069 ± 0.016	0.94
k_{mono} septal/lateral ratio	1.10 ± 0.19	0.90 ± 0.13	0.009
Efficiency, mmHg-l/g	80.67 ± 20.54	69.93 ± 20.34	0.066

CO = cardiac output; LV = left ventricular; MBF = myocardial blood flow.

was 18% lower during pacing-ON than during pacing-OFF ($p=0.009$) (Table 2). These changes in LV function and oxidative metabolism resulted in a tendency for lower myocardial efficiency during pacing-ON than during pacing-OFF ($p=0.066$) (Table 2).

Effects of RV pacing-induced LV dyssynchrony

For the total study population, mean LV dyssynchrony significantly increased during pacing-ON, both assessed with speckle-tracking imaging (pacing-OFF 18 ± 18 ms vs. pacing-ON 121 ± 83 ms, $p=0.003$) and with TDI (pacing-OFF 12 ± 11 ms vs. pacing-ON 76 ± 39 ms, $p=0.001$). Using the previously reported cut-off values (12,16), 6 of the 10 patients (60%) developed significant LV dyssynchrony during RV pacing as assessed by echocardiography. The results in patients with dyssynchrony and without dyssynchrony are summarized in Table 3. The blood pressures and heart rates were comparable during pacing-ON and pacing-OFF. In patients with dyssynchrony, CO decreased significantly during pacing-ON as compared with pacing-OFF (from 4.91 ± 0.55 to 4.20 ± 0.69 l/min, $p=0.006$). In contrast, in the patients without dyssynchrony a moderate decrease in CO was observed during pacing-ON (Table 3). A significant decrease in LV work power was noted only in the patients with LV dyssynchrony during RV pacing (Table 3).

In patients with dyssynchrony, global MBF was not different between the pacing conditions but septal-to-lateral wall MBF ratio was 24% lower during pacing-ON ($p=0.016$). In patients without dyssynchrony, no difference in global MBF as well as in septal-to-lateral wall MBF ratio was detected between pacing-OFF and pacing-ON (Table 3). Similar to the changes in MBF, in patients with dyssynchrony global k_{mono} was comparable during pacing-ON and pacing-OFF, but the septal-to-lateral wall k_{mono} ratio was 22% lower during pacing-ON than during pacing-OFF ($p=0.038$). In patients without dyssynchrony, both global k_{mono} as well as the septal-to-lateral wall k_{mono} ratio were not different between pacing-OFF and pacing-ON (Table 3).

Finally, in patients with dyssynchrony myocardial efficiency was 23% lower during pacing-ON than during pacing-OFF ($p=0.023$). In contrast, in patients without dyssynchrony myocardial efficiency was comparable during pacing-ON and pacing-OFF ($p=0.70$) (Figure 2).

Table 3. The effects of RV pacing on hemodynamic, LV function and PET-derived parameters according to the development of dyssynchrony during pacing

	All patients (n=10)	With dyssynchrony (n=6)	Without dyssynchrony (n=4)
MBF, ml/g/min			
Pacing-OFF	1.04 ± 0.21	1.03 ± 0.16	1.07 ± 0.31
Pacing-ON	1.05 ± 0.15	1.03 ± 0.16	1.07 ± 0.15
p-value*	0.5	0.9	0.5
MBF septal-to-lateral ratio			
Pacing-OFF	0.81 ± 0.13	0.85 ± 0.15	0.75 ± 0.08
Pacing-ON	0.66 ± 0.07	0.65 ± 0.07	0.71 ± 0.04 †
p-value*	0.02	0.02	0.8
k_{mono} , min ⁻¹			
Pacing-OFF	0.069 ± 0.017	0.071 ± 0.022	0.068 ± 0.003
Pacing-ON	0.069 ± 0.016	0.074 ± 0.029	0.061 ± 0.006
p-value*	0.9	0.7	0.2
k_{mono} septal-to-lateral ratio			
Pacing-OFF	1.10 ± 0.19	1.11 ± 0.22	1.09 ± 0.17
Pacing-ON	0.90 ± 0.13	0.87 ± 0.05	0.95 ± 0.20
p-value*	0.009	0.04	0.19
CO, l/min			
Pacing-OFF	4.87 ± 0.69	4.91 ± 0.55	4.82 ± 0.95
Pacing-ON	4.24 ± 0.80	4.20 ± 0.68	4.30 ± 1.06
p-value*	<0.001	0.006	0.05
LV work power, mmHg-l/min/g			
Pacing-OFF	5.17 ± 1.80	5.32 ± 2.06	4.95 ± 1.61
Pacing-ON	4.56 ± 1.78	4.52 ± 1.83	4.61 ± 1.97
p-value*	0.013	0.04	0.2
Efficiency, mmHg-l/g			
Pacing-OFF	76.29 ± 23.82	78.11 ± 25.35	73.55 ± 24.78
Pacing-ON	66.37 ± 22.24	60.40 ± 13.93	75.32 ± 31.33 †
p-value*	0.07	0.02	0.7

* Pacing-OFF vs. Pacing-ON; † p < 0.05 with dyssynchrony vs. without dyssynchrony; CO = cardiac output; MBF = myocardial blood flow; LV = left ventricular

DISCUSSION

RV pacing, myocardial oxidative metabolism and efficiency

To our knowledge, this is the first study to investigate the effect of RV pacing on myocardial oxidative metabolism and efficiency of work. We found that the global LV perfusion and oxidative metabolism remained unchanged despite reduction in LV function during RV pacing. This tended to impair efficiency of cardiac work. Concordantly with the previous study on glucose metabolism, we found an altered distribution of perfusion and oxidative metabolism as septal-to-lateral wall ratios were reduced during RV pacing (9).

In agreement with earlier findings, RV pacing in the present study resulted in a reduction in cardiac output and LV work power and this occurred without changes in hemodynamics and heart rate. Right ventricular pacing causes an activation pattern similar to LBBB, and it reduces the septal-to-lateral wall ratio of mechanical work in the healthy canine heart (23). In a study by Preumont et al. with eight candidates for permanent pacemaker implantation, RV pacing

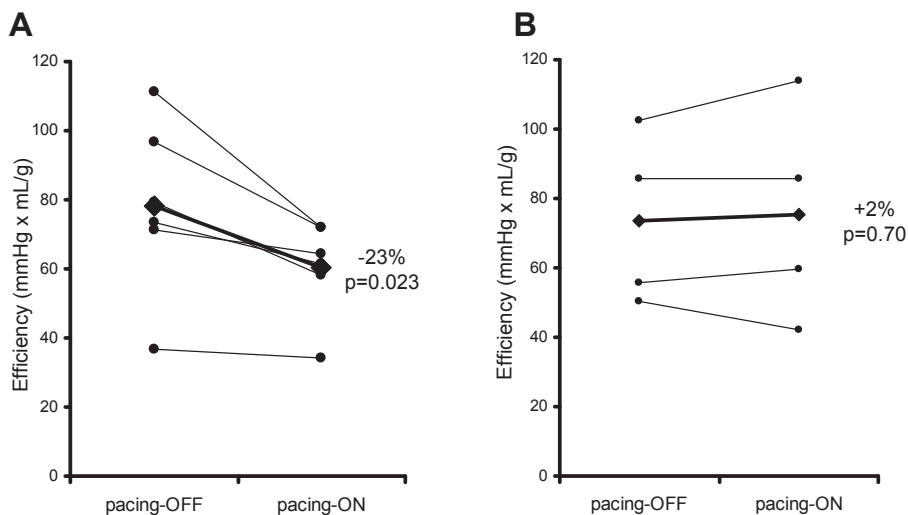


Figure 2. Myocardial efficiency with pacing-OFF and pacing-ON in patients developing dysynchrony with RV pacing (panel A) and in patients not developing dysynchrony with RV pacing (panel B). ● = individual values, ◆ = group mean

induced heterogeneity in regional glucose metabolism (9). The defects in glucose uptake were found in the left ventricle near the stimulation site, primarily in the inferior, apical and septal wall. However, the results in the distribution of myocardial perfusion have been more variable either showing no abnormalities (9) or corresponding decrease in septal-to-lateral perfusion (24,25). On the other hand, it was found that regional myocardial perfusion defects may be present in up to 65% of the patients after long-term RV pacing (24,25).

LV dyssynchrony, myocardial oxidative metabolism and efficiency

In the present study, 60% of the patients exhibited significant LV dyssynchrony during RV pacing. Previously, it has been demonstrated that RV pacing may result in significant LV dyssynchrony in a substantial proportion of patients (13). In the present study, speckle-tracking strain analysis was used to assess if patients developed LV dyssynchrony during RV pacing, and cardiac metabolism and efficiency data were analyzed accordingly. Interestingly, during RV pacing QRS duration increased significantly in nine out of ten patients, but significant LV dyssynchrony was noted only in 60% of the patients. This is in agreement with earlier notion that approximately one third of the heart failure patients with prolonged QRS do not demonstrate ventricular dyssynchrony (26).

Importantly, in the patients with LV dyssynchrony during RV pacing, significant changes in septal-to-lateral ratio of MBF and k_{mono} were observed. In contrast, in patients without LV dyssynchrony during RV pacing, no significant changes were noted. These findings emphasize that the perfusion, metabolic and work efficiency abnormalities are paralleling with induced mechanical changes (or LV dyssynchrony). The magnitude of the deterioration of myocardial efficiency in patients who developed dyssynchrony during RV pacing was 23%. Of note, this

large effect was detected in patients with preserved systolic function. In patients with a failing heart, similar degree of effect would likely be clinically significant.

Previous studies in patients with LBBB have demonstrated that LV dyssynchrony is linked with adverse effects on MBF, metabolism and efficiency (27-29). Significant heterogeneity (decreased septal-to-lateral wall ratio) was reported for both MBF (28,29) and oxidative metabolism (11,27,29). Restoration of the normal contraction sequence of the LV by cardiac resynchronization therapy abolishes the heterogeneity and improves myocardial efficiency (11,27). The present study suggests that altered myocardial metabolism and cardiac efficiency may be the underlying mechanism for the deterioration in LV function in patients with LV dyssynchrony during RV pacing.

Study limitations

In the present study a shortened AV delay was used during pacing-ON. This was necessary to enable successful pacing without increasing heart rate. Liebold and coworkers (30) investigated the effect of PR interval during pacing on cardiac function and found that when this interval is shorter LV performance was deteriorated. However, this happened only with very short PR intervals (40 ms) and the optimal interval was 80 ms or higher. In the present study, all PR intervals were 90 ms or higher and, therefore, it is unlikely that a slightly shorter PR interval during RV pacing would contribute to the reduced LV function. In the present study quite a small number of patients was studied. This is especially true for prespecified subgroup analysis. However, each patient was studied twice to allow direct measurement of the effects of RV pacing. Relatively many measurements were performed in a relatively small number of patients. Advanced and very accurate but laborious techniques were applied and we believe that this patients group was large enough to obtain reliable findings.

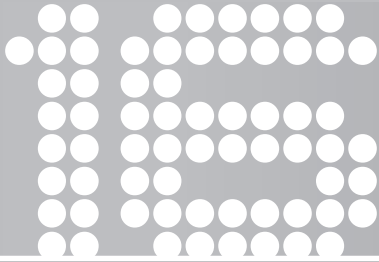
CONCLUSIONS

RV pacing may result in a significant decrease in LV performance. However, LV oxidative metabolism and efficiency become abnormal only in patients who exhibit LV dyssynchrony during RV pacing. This study emphasizes the importance of synchronous LV contraction also in the non-failing heart. Further studies are needed to assess whether altered myocardial efficiency contributes to the previously suggested unfavorable effects of RV pacing in patients with a failing heart.

REFERENCES

1. Vassallo JA, Cassidy DM, Miller JM, Buxton AE, Marchlinski FE, Josephson ME. Left ventricular endocardial activation during right ventricular pacing: effect of underlying heart disease. *J Am Coll Cardiol* 1986;7:1228-33.
2. Wilkoff BL, Cook JR, Epstein AE et al. Dual-chamber pacing or ventricular backup pacing in patients with an implantable defibrillator: the Dual Chamber and VVI Implantable Defibrillator (DAVID) Trial. *JAMA* 2002;288:3115-23.
3. Sweeney MO, Hellkamp AS, Ellenbogen KA et al. Adverse effect of ventricular pacing on heart failure and atrial fibrillation among patients with normal baseline QRS duration in a clinical trial of pacemaker therapy for sinus node dysfunction. *Circulation* 2003;107:2932-7.
4. Kass DA, Chen CH, Curry C et al. Improved left ventricular mechanics from acute VDD pacing in patients with dilated cardiomyopathy and ventricular conduction delay. *Circulation* 1999;99:1567-73.
5. Auricchio A, Stellbrink C, Block M et al. Effect of pacing chamber and atrioventricular delay on acute systolic function of paced patients with congestive heart failure. The Pacing Therapies for Congestive Heart Failure Study Group. The Guidant Congestive Heart Failure Research Group. *Circulation* 1999;99:2993-3001.
6. Lieberman R, Padeletti L, Schreuder J et al. Ventricular pacing lead location alters systemic hemodynamics and left ventricular function in patients with and without reduced ejection fraction. *J Am Coll Cardiol* 2006;48:1634-41.
7. Tops LF, Schalij MJ, Holman ER, van Erven L, van der Wall EE, Bax JJ. Right ventricular pacing can induce ventricular dyssynchrony in patients with atrial fibrillation after atrioventricular node ablation. *J Am Coll Cardiol* 2006;48:1642-8.
8. Ono S, Nohara R, Kambara H, Okuda K, Kawai C. Regional myocardial perfusion and glucose metabolism in experimental left bundle branch block. *Circulation* 1992;85:1125-31.
9. Preumont N, Jansens JL, Berkenboom G, van de BP, Stoupel E, Goldman S. Effects of right ventricular pacing on regional myocardial glucose metabolism. *Europace* 2005;7:584-91.
10. Quinones MA, Otto CM, Stoddard M, Waggoner A, Zoghbi WA. Recommendations for quantification of Doppler echocardiography. *J Am Soc Echocardiogr* 2002;15:167-84.
11. Sundell J, Engblom E, Koistinen J et al. The effects of cardiac resynchronization therapy on left ventricular function, myocardial energetics, and metabolic reserve in patients with dilated cardiomyopathy and heart failure. *J Am Coll Cardiol* 2004;43:1027-33.
12. Suffoletto MS, Dohi K, Cannesson M, Saba S, Gorcsan J, III. Novel speckle-tracking radial strain from routine black-and-white echocardiographic images to quantify dyssynchrony and predict response to cardiac resynchronization therapy. *Circulation* 2006;113:960-8.
13. Tops LF, Suffoletto MS, Bleeker GB et al. Speckle-tracking radial strain reveals left ventricular dyssynchrony in patients with permanent right ventricular pacing. *J Am Coll Cardiol* 2007;50:1180-8.
14. Reisner SA, Lysyansky P, Agmon Y, Mutlak D, Lessick J, Friedman Z. Global longitudinal strain: a novel index of left ventricular systolic function. *J Am Soc Echocardiogr* 2004;17:630-3.
15. Leitman M, Lysyansky P, Sidenko S et al. Two-dimensional strain—a novel software for real-time quantitative echocardiographic assessment of myocardial function. *J Am Soc Echocardiogr* 2004;17:1021-9.
16. Bax JJ, Bleeker GB, Marwick TH et al. Left ventricular dyssynchrony predicts response and prognosis after cardiac resynchronization therapy. *J Am Coll Cardiol* 2004;44:1834-40.
17. <http://www.turkupetcentre.net/carimasturku>
18. Iida H, Kanno I, Takahashi A et al. Measurement of absolute myocardial blood flow with H215O and dynamic positron-emission tomography. Strategy for quantification in relation to the partial-volume effect. *Circulation* 1988;78:104-15.
19. Iida H, Rhodes CG, de Silva R et al. Use of the left ventricular time-activity curve as a noninvasive input function in dynamic oxygen-15-water positron emission tomography. *J Nucl Med* 1992;33:1669-77.

20. Armbrecht JJ, Buxton DB, Schelbert HR. Validation of [1-11C]acetate as a tracer for noninvasive assessment of oxidative metabolism with positron emission tomography in normal, ischemic, postischemic, and hyperemic canine myocardium. *Circulation* 1990;81:1594-605.
21. Brown M, Marshall DR, Sobel BE, Bergmann SR. Delineation of myocardial oxygen utilization with carbon-11-labeled acetate. *Circulation* 1987;76:687-96.
22. Buxton DB, Schwaiger M, Nguyen A, Phelps ME, Schelbert HR. Radiolabeled acetate as a tracer of myocardial tricarboxylic acid cycle flux. *Circ Res* 1988;63:628-34.
23. Prinzen FW, Hunter WC, Wyman BT, McVeigh ER. Mapping of regional myocardial strain and work during ventricular pacing: experimental study using magnetic resonance imaging tagging. *J Am Coll Cardiol* 1999;33:1735-42.
24. Tse HF, Lau CP. Long-term effect of right ventricular pacing on myocardial perfusion and function. *J Am Coll Cardiol* 1997;29:744-9.
25. Skolidis EI, Kochiadakis GE, Koukouraki SI et al. Myocardial perfusion in patients with permanent ventricular pacing and normal coronary arteries. *J Am Coll Cardiol* 2001;37:124-9.
26. Emkanjoo Z, Esmaeilzadeh M, Mohammad HN, Alizadeh A, Tayyebi M, Sadr-Ameli MA. Frequency of inter- and intraventricular dyssynchrony in patients with heart failure according to QRS width. *Europace* 2007;9:1171-6.
27. Ukkonen H, Beanlands RS, Burwash IG et al. Effect of cardiac resynchronization on myocardial efficiency and regional oxidative metabolism. *Circulation* 2003;107:28-31.
28. Knaapen P, van Campen LM, de Cock CC et al. Effects of cardiac resynchronization therapy on myocardial perfusion reserve. *Circulation* 2004;110:646-51.
29. Lindner O, Vogt J, Kammeier A et al. Effect of cardiac resynchronization therapy on global and regional oxygen consumption and myocardial blood flow in patients with non-ischaemic and ischaemic cardiomyopathy. *Eur Heart J* 2005;26:70-6.
30. Liebold A, Rodig G, Merk J, Birnbaum DE. Short atrioventricular delay dual-chamber pacing early after coronary artery bypass grafting in patients with poor left ventricular function. *J Cardiothorac Vasc Anesth* 1998;12:284-7.



Prevalence and pathophysiologic attributes of ventricular dyssynchrony in arrhythmogenic right ventricular dysplasia/ cardiomyopathy

Laurens F. Tops^{1,2}, Kalpana Prakasa¹, Harikrishna Tandri¹, Darshan Dalal¹
Rahul Jain¹, Veronica L. Dimaano¹, David Dombroski³, Cynthia James¹
Crystal Tichnell¹, Amy Daly¹, Frank Marcus⁴, Martin J. Schalij², Jeroen J. Bax²
David Bluemke³, Hugh Calkins¹, Theodore P. Abraham¹

¹*Division of Cardiology, Department of Medicine, Johns Hopkins University, Baltimore, USA*

²*Department of Cardiology, Leiden University Medical Center, Leiden, the Netherlands*

³*Department of Radiology, Johns Hopkins University, Baltimore, USA*

⁴*Sarver Heart Center, University of Arizona College of Medicine, Tucson, USA*

J Am Coll Cardiol 2009;54:445-51

ABSTRACT

Background: ARVD/C is characterized by fibrofatty replacement of RV myocardium and RV dilatation. These pathologic changes may result in electromechanical dyssynchrony.

Objectives: To study the prevalence and mechanisms underlying right ventricular (RV) dyssynchrony in Arrhythmogenic Right Ventricular Dysplasia/Cardiomyopathy (ARVD/C) using tissue Doppler echocardiography (TDE).

Methods: Electrocardiography, conventional and TDE was performed in 52 ARVD/C patients fulfilling Task Force criteria and 25 controls. RV end-diastolic and end-systolic areas, RV fractional area change (RVFAC), and left ventricular (LV) volumes and function were assessed. Mechanical synchrony was assessed by measuring differences in time-to-peak systolic velocity (T_{SV}) between the RV free wall, ventricular septum and LV lateral wall. RV dyssynchrony was defined as the difference in T_{SV} between the RV free wall and the ventricular septum, >2 SD above the mean value for controls.

Results: Mean difference in RV T_{SV} was higher in ARVD/C compared to controls (55 ± 34 ms vs. 26 ± 15 ms, $p < 0.001$). Significant RV dyssynchrony was not noted in any of the controls. Based on a cut-off value of 56 ms, significant RV dyssynchrony was present in 26 ARVD/C patients (50%). Patients with RV dyssynchrony had larger RV end-diastolic area (22 ± 5 vs. 19 ± 4 cm², $p = 0.02$), and lower RVFAC (29 ± 8 vs. $34 \pm 8\%$, $p = 0.03$) compared to ARVD/C patients without RV dyssynchrony. No differences in QRS duration, LV volumes and function were present between the two groups.

Conclusions: RV dyssynchrony may occur in up to 50% of ARVD/C patients, and is associated with RV remodeling. This finding may have therapeutic and prognostic implications in ARVD/C.

INTRODUCTION

Arrhythmogenic right ventricular dysplasia cardiomyopathy (ARVD/C) is an inherited disease characterized by fibrofatty replacement of right ventricular (RV) myocardium (1). The diagnosis is established based on the presence of a conglomeration of factors (2,3). Other than ventricular arrhythmias, ARVD/C results in progressive RV dilatation and systolic dysfunction leading to heart failure (4,5).

Ventricular electro-mechanical delay (or mechanical dyssynchrony) has been well described in left ventricular (LV) failure and has formed the basis of cardiac resynchronization therapy leading to significant improvements in symptoms, functional capacity and survival in heart failure patients (6). Although RV mechanical dyssynchrony has been described in pulmonary hypertension (7), there are no data on whether a primary RV cardiomyopathy such as ARVD/C is associated with mechanical dyssynchrony. Tissue Doppler (TDE) and strain (SE) echocardiography have emerged as the predominant means of evaluating ventricular mechanics (8,9).

Several components of the ARVD/C disease process could potentially lead to the development of RV mechanical dyssynchrony. Fibrofatty infiltration could involve the RV conduction system resulting in electrical and electro-mechanical delays. Similar to LV failure, RV dilatation and dysfunction may cause dyssynchrony. Lastly, other factors such as pulmonary pressures and LV involvement may influence RV mechanical properties. Importantly, ventricular electro-mechanical dyssynchrony has prognostic and therapeutic implications (10,11).

Accordingly, the aims of this study were to determine the prevalence of mechanical dyssynchrony in a large cohort of ARVD/C patients and to better elucidate the factors influencing RV mechanics in ARVD/C.

METHODS

Study population and protocol

This study was approved by the institutional review board with written informed consent obtained in all subjects. The study population comprised 52 ARVD/C patients with diagnosis confirmed by Task Force criteria (2) and 25 control subjects. All control subjects were healthy volunteers, recruited on campus, with no history of medical illness, not on any cardioactive medications, who had a normal echo Doppler examination (18 men, 7 women; mean age 32 ± 6 years). All patients underwent a detailed history and physical examination, 12 lead electrocardiogram (ECG), signal averaged ECG, conventional echocardiography and TDE/SE.

Echocardiography

Conventional and TDE/SE images were acquired from at least 3 consecutive heart beats and digitally stored for off-line analysis using a Vivid 7 ultrasound machine (GE Healthcare,

Waukesha, WI). Offline analysis was performed using EchoPAC PC version 6.1 (GE Healthcare). During image acquisition, special care was taken to acquire accurate images of the RV free wall. Off-plane images of the RV were acquired to maximize visualization of RV morphology.

The RV outflow tract dimension was measured in the parasternal short-axis view at the level of the aortic valve plane (12). In addition, RV end-diastolic area (RVEDA) and RV end-systolic area (RVESA) were measured by tracing the RV endocardial border on the apical 4-chamber view and RV fractional area change (RVFAC) was calculated as a measure of RV systolic function using the following equation: $RVFAC = (RVEDA - RVESA) / RVEDA \times 100\%$ (12). Biplane LV end-diastolic and -systolic volumes were assessed from the apical 2- and 4-chamber images, and LV ejection fraction was calculated using the biplane Simpson's formula (13).

Tissue Doppler/strain echocardiography

Standard apical 4-chamber images and narrow-angle-sector images were acquired for tissue Doppler and strain analysis. Adjustments to the sector width were made to visualize one myocardial wall at a time (RV free wall, interventricular septum, LV lateral wall), in order to obtain an optimal alignment between the wall and the ultrasound beam, and to maximize frame rates (mean frame rate 253 ± 46 frames/s). The gain settings, filters and pulse repetition frequency were adjusted to optimize color saturation and to avoid aliasing.

Off-line analysis was performed by placing the Doppler sample at the basal segment of the RV free wall, interventricular septum and LV lateral wall, as previously described (14). Semi-automated tissue tracking was used to maintain the sample area within the region of interest throughout the cardiac cycle. Peak systolic tissue velocity of each segment was obtained and averaged from 3 cardiac cycles. For peak systolic strain analysis, an offset (strain) distance of 12 mm was used; for all segments the time-to-peak systolic strain was similarly assessed. Off-line analyses were performed by two observers, blinded to the results of the echocardiographic RV function analysis.

Ventricular dyssynchrony

For the assessment of ventricular dyssynchrony, the time from the onset of the QRS complex to the peak systolic tissue velocity of different segments was measured (T_{SV}). The difference between the T_{SV} of the septum and the T_{SV} of the RV free wall was calculated as an indicator of RV dyssynchrony. Significant RV dyssynchrony was defined as a septal to RV free wall T_{SV} delay exceeding 2 standard deviation (SD) above the mean value for the control group.

Similarly, for LV dyssynchrony the difference in T_{SV} between the septum and the LV lateral wall was calculated. A value > 2 SD above the mean value derived from the control group, was used as a cut-off value for the presence of significant LV dyssynchrony. Finally, interventricular dyssynchrony was calculated as the difference in T_{SV} between the RV free wall and the LV lateral wall. The cut-off value for significant interventricular dyssynchrony was defined similar to RV and LV dyssynchrony.

Statistical analysis

Continuous data are presented as mean \pm SD; categorical data are presented as frequencies and percentages. Differences between the ARVD/C patients and the controls, and between the ARVD/C patients with and without ventricular dyssynchrony, were evaluated using unpaired student t test (continuous variables), or Chi-square tests (dichotomous variables). Differences in continuous variables between controls and ARVD/C patients with and without ventricular dyssynchrony were evaluated with one-way ANOVA. Correlations between echocardiographic variables and the extent of RV dyssynchrony were assessed with Pearson's correlation test.

Inter- and intra-observer variability for the assessment of T_{SV} of the RV free wall and the interventricular septum and RV dyssynchrony were assessed using Bland-Altman analysis, in 10 random ARVD/C patients that were analyzed by two independent observers (inter-observer variability) and by a single observer at two different time points (intra-observer variability); mean differences \pm SD and 95% confidence intervals are reported. In addition, kappa statistic was used to assess the inter- and intra-observer variability for the classification of the presence or absence of RV dyssynchrony.

All statistical analyses were performed using SPSS software (version 12.0, SPSS Inc. Chicago, Illinois). All statistical tests were two-sided, and a p-value <0.05 was considered statistically significant.

RESULTS

Baseline characteristics of the 52 ARVD/C patients are summarized in Table 1. In none of the patients, symptoms of right-sided heart failure were present. Right ventricular areas (RVEDA and RVESA) were higher and RVFAC significantly lower in ARVD/C compared to the controls (Table 2). There were no significant inter-group differences in LV volumes and function. Peak systolic velocities and strain values in the interventricular septum and the LV lateral wall were comparable between the ARVD/C patients and controls (Table 2). In contrast, RV free wall peak systolic velocity (7.4 ± 2.1 cm/s vs. 9.9 ± 1.2 cm/s, $p < 0.001$) and RV free wall peak systolic strain ($-19 \pm 7\%$ vs. $-25 \pm 9\%$, $p = 0.002$) were significantly lower in ARVD/C patients compared to controls, respectively.

Ventricular dyssynchrony

In all subjects, echocardiographic images were of sufficient quality to assess time-to-peak systolic velocity. Mean T_{SV} of the septum and the RV free wall in the ARVD/C patients was 159 ± 40 ms and 210 ± 42 ms, respectively. In the controls, mean T_{SV} of the septum and the RV free wall was 135 ± 39 ms and 160 ± 33 ms, respectively. Mean time-to-peak strain of the septum and RV free wall was 387 ± 67 ms and 434 ± 73 ms in the ARVD/C patients and 345 ± 88 ms and 368 ± 75 ms in the controls.

Table 1. Baseline characteristics

	ARVD/C patients (n=52)
Age, yrs	41 ± 12
Gender, M/F	22 / 30
Symptomatic, n (%)	45 (87)
Syncope, n (%)	13 (25)
Palpitations, n (%)	18 (35)
Ventricular tachycardia, n (%)	14 (27)
Other symptoms, n (%)	9 (17)
Implantable cardioverter-defibrillator, n (%)	45 (87)
Filtered QRS duration, ms	131 ± 36
Right bundle branch block, n (%)	10 (19)
Epsilon waves, n (%)	0 (0)
T wave inversion in right precordial leads, n (%)	39 (75)
RV systolic pressure, mmHg	29 ± 6

RV = right ventricular.

The mean difference in T_{sv} between the septum and the RV free wall, representing RV dyssynchrony, was 55 ± 34 ms in the ARVD/C patients, and 26 ± 15 ms in the controls ($p < 0.001$). Based on a cut-off value of ≥ 56 ms, significant RV dyssynchrony was present in 26 ARVD/C patients (50%). In these patients, mean RV dyssynchrony was 84 ± 20 ms, whereas it was 26 ± 16 ms in the remaining patients ($p < 0.001$). An example of a patient with significant RV dyssynchrony is shown in Figure 1.

Table 2. Echocardiographic data

Variable	Controls (n=25)	ARVD/C patients (n=52)	P value
RVOT diameter (cm)	2.6 ± 0.2	2.9 ± 0.4	0.001
RVEDA (cm ²)	17 ± 3	20 ± 5	<0.001
RVESA (cm ²)	9 ± 2	14 ± 4	<0.001
RVFAC (%)	44 ± 7	32 ± 8	<0.001
LVEDV (ml)	108 ± 31	104 ± 27	0.5
LVESV (ml)	45 ± 14	45 ± 14	0.9
LVEF (%)	59 ± 5	57 ± 5	0.1
Septum			
Peak systolic velocity (cm/s)	5.9 ± 1.1	5.4 ± 1.1	0.1
Peak systolic strain (%)	-24 ± 6	-21 ± 7	0.1
RV free wall			
Peak systolic velocity (cm/s)	9.9 ± 1.2	7.4 ± 2.1	<0.001
Peak systolic strain (%)	-25 ± 9	-19 ± 7	0.002
LV lateral wall			
Peak systolic velocity (cm/s)	7.0 ± 2.1	6.5 ± 1.4	0.2
Peak systolic strain (%)	-18 ± 8	-18 ± 6	0.2

LV = left ventricular; LVEDV = left ventricular end-diastolic volume; LVEF = left ventricular ejection fraction; LVESV = left ventricular end-systolic volume; RV = right ventricular; RVEDA = right ventricular end-diastolic area; RVESA = right ventricular end-systolic area; RVFAC = right ventricular fractional area change; RVOT = right ventricular outflow tract.

Mean T_{SV} for the LV lateral wall in the ARVD/C patients and the controls was 171 ± 47 ms and 155 ± 47 ms, respectively. Mean time-to-peak strain of the LV lateral wall was 398 ± 70 ms in the ARVD/C patients and 370 ± 86 ms in the controls. There was no significant difference in LV dyssynchrony between the ARVD/C patients and the controls (21 ± 18 ms vs. 22 ± 19 ms, $p=0.7$). Using a cut-off value of ≥ 60 ms (>2 SD of the controls), 2 ARVD/C patients (4%) demonstrated significant LV dyssynchrony.

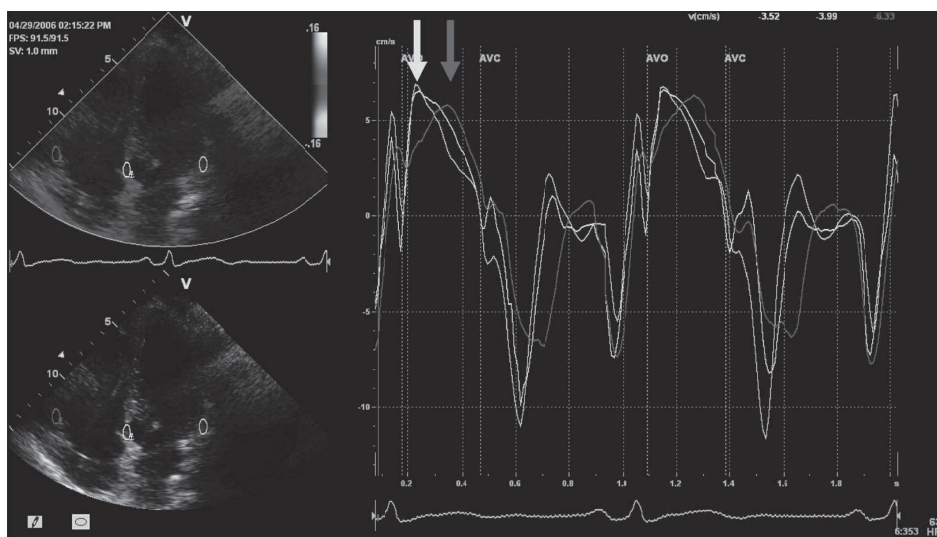


Figure 1. Example of an ARVD/C patient with significant RV dyssynchrony. Samples are placed at the basal parts of the septum (yellow curve), RV free wall (red curve) and LV lateral wall (green curve). In this patient, a significant delay between the septum and the RV free wall was present (110 ms), indicated by the yellow and red arrows.

Interventricular dyssynchrony, calculated as the difference in T_{SV} between the RV free wall and the LV lateral wall, was 53 ± 36 ms in the ARVD/C patients and 21 ± 15 ms in the controls ($p<0.001$). Based on a cut-off value of ≥ 51 ms (>2 SD of the controls), significant interventricular dyssynchrony was present in 22 patients (42%) with ARVD/C. In these patients, mean interventricular dyssynchrony was 88 ± 17 ms, whereas it was 27 ± 21 ms in the remaining patients ($p<0.001$). In 19 of the 26 patients with RV dyssynchrony (73%), significant interventricular dyssynchrony was present. Conversely, in 23 of the 26 patients without RV dyssynchrony (88%), no significant interventricular dyssynchrony was present.

Factors influencing RV dyssynchrony

We examined several morphologic and functional factors that could potentially impact RV mechanical synchrony. These included 1) Electrocardiographic: presence of RV conduction abnormalities as typified by QRS duration and presence of right bundle branch block; 2) Morphologic: RV volumes and LV volumes; 3) Functional: RV function and LV function. To study

these factors, ARVD/C patients were divided into those with RV dyssynchrony (n=26) and those without RV dyssynchrony (n= 26).

No differences in RV conduction abnormalities, evaluated by signal averaged and surface ECG, were noted between the two groups: filtered QRS duration on signal averaged ECG was similar in ARVD/C patients with versus those without RV dyssynchrony (134 ± 41 ms vs. 128 ± 32 ms, respectively; $p=0.6$). No difference in the prevalence of T wave inversion in right precordial leads was noted between the two groups (with RV dyssynchrony n=18; without RV dyssynchrony n=21, $p=0.5$). Similarly, there were no differences in the prevalence of right bundle branch block noted in 5 patients (19%) with RV dyssynchrony and in 5 patients (19%) without RV dyssynchrony ($p=1.0$). In addition, there was no difference in the number of patients with documented ventricular tachycardia at baseline between the group with and the group without RV dyssynchrony (10 patients vs. 4 patients, $p=0.1$).

Compared to patients without RV dyssynchrony, the patients with RV dyssynchrony had larger RVEDA (Table 3), and a lower RVFAC (Figure 2). No significant differences in LV volumes, function, and peak systolic velocities and peak systolic strain were noted between patients with and without RV dyssynchrony. In contrast, peak systolic strain of the RV free wall was significantly decreased in patients with RV dyssynchrony, compared with patients without RV dyssynchrony (Figure 2).

A modest, but significant correlation was found between FAC and RV dyssynchrony ($r=-0.38$, $p=0.001$), and between RVEDA and RV dyssynchrony ($r=0.38$, $p=0.001$). In addition, a modest, but significant correlation was found between peak systolic strain of the RV free wall and RV dyssynchrony ($r=0.40$, $p<0.001$).

Table 3. Echocardiographic data in ARVD/C patients with and without right ventricular dyssynchrony

Variable	Without RV dyssynchrony (n=26)	With RV dyssynchrony (n=26)	P value
RVOT diameter (cm)	2.9 ± 0.4	2.9 ± 0.4	0.9
RVEDA (cm ²)	19 ± 4	22 ± 5	0.02
RVESA (cm ²)	12 ± 3	16 ± 5	0.005
RVFAC (%)	34 ± 8	29 ± 8	0.03
LVEDV (ml)	104 ± 28	103 ± 26	1.0
LVESV (ml)	45 ± 13	45 ± 15	1.0
LVEF (%)	57 ± 4	57 ± 6	0.8
Septum			
Peak systolic velocity (cm/s)	5.4 ± 1.3	5.4 ± 1.0	1.0
Peak systolic strain (%)	-21 ± 7	-22 ± 7	0.8
RV free wall			
Peak systolic velocity (cm/s)	7.4 ± 2.5	7.3 ± 1.7	0.9
Peak systolic strain (%)	-22 ± 7	-16 ± 6	0.001
LV lateral wall			
Peak systolic velocity (cm/s)	6.4 ± 1.5	6.6 ± 1.4	0.5
Peak systolic strain (%)	-19 ± 7	-16 ± 5	0.1

Abbreviations as in Table 2.

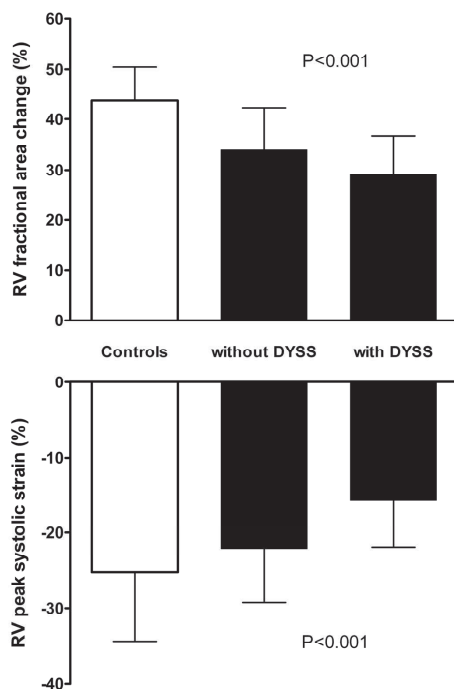


Figure 2. Right ventricular fractional area change (upper panel) and RV peak systolic strain (lower panel) in the 25 controls, 26 ARVD/C patients without RV dyssynchrony and 26 ARVD/C patients with RV dyssynchrony. Both RV fractional area change and RV peak systolic strain were significantly decreased in the ARVD/C patients with RV dyssynchrony.

Reproducibility of RV dyssynchrony

The intra-observer and inter-observer variability for time-to-peak systolic velocity for the RV free wall were 1.0 ± 16.6 ms (95% CI -31.6 to 33.6), and 0 ± 26.7 ms (95% CI -52.3 to 52.3), respectively. The intra-observer and inter-observer variability for RV dyssynchrony were 0 ± 18.9 ms (95% CI -36.9 to 36.9) and -5.0 ± 29.5 ms (95% CI -62.9 to 52.9), respectively. For the classification of the presence or absence of RV dyssynchrony, an excellent agreement was noted between the two observers ($\kappa=0.80$) and within the same observer ($\kappa=1.0$).

DISCUSSION

We present a previously unreported finding of significant ventricular mechanical dyssynchrony in patients with a primary RV cardiomyopathy, ARVD/C. In a relatively large cohort of ARVD/C patients we demonstrate RV dyssynchrony in 50% and interventricular dyssynchrony in 42% of the patients. Patients with RV dyssynchrony had larger RV volumes and lower RV function compared to controls.

Right ventricular dyssynchrony

The presence of LV and interventricular dyssynchrony has been studied in a broad spectrum of clinical settings (9). In contrast, RV dyssynchrony has not been studied extensively. The presence of RV dyssynchrony was first reported by Lopez-Candales et al. in 20 patients with pulmonary hypertension (7). Using time-to-peak strain between the septum and RV free wall, RV dyssynchrony was found to be more pronounced in patients with pulmonary hypertension as compared to controls (92 ± 78 ms vs. 11 ± 23 ms, $p < 0.001$). In contrast, there were no differences in LV dyssynchrony between the two groups (7). Similarly, intra- and inter-ventricular dyssynchrony was examined in 34 patients with LV systolic heart failure, mean LV ejection fraction $22 \pm 7\%$ (56% with non-ischemic cardiomyopathy) (15). Mean RV dyssynchrony was 59 ± 45 ms and mean LV dyssynchrony was 80 ± 62 ms.

In a larger unselected cohort of patients with a primary RV cardiomyopathy (ARVD/C), we report for the first time the occurrence of significant RV and interventricular mechanical dyssynchrony. As opposed to previous studies, dyssynchrony in this population occurred in the absence of confounding factors such as pulmonary hypertension and LV failure. Our data also established a cutoff value for mechanical dyssynchrony in the RV using 25 healthy controls. Interestingly, our cutoff value of 56 ms is close to the previously reported cut-off values for LV dyssynchrony (16).

Factors influencing RV dyssynchrony in ARVD/C

The presence of RV dyssynchrony is not surprising given previous and recent knowledge about the pathophysiology of ARVD/C. Recent data on potential causal genes suggest that most mutations involve genes that encode desmosomal proteins and include but are not limited to desmoplakin, plakophilin 2 and desmoglein (17-19). Thus ARVD/C is considered a desmopathy that is likely associated with abnormal cell to cell coupling, both electrically and mechanically, providing the substrate for the RV dyssynchrony.

Akin to LV dysfunction, electrical conduction abnormalities in the RV could be associated with mechanical delays. However, in our cohort we found no differences in QRS duration and/or the presence of right bundle branch block between patients with and without RV dyssynchrony. Although in general the presence of mechanical dyssynchrony is related to intra-ventricular conduction abnormalities, substantial LV ventricular dyssynchrony has been previously demonstrated in the absence of QRS prolongation (20,21). Thus ARVD/C may be another example of dyssynchrony with a narrow QRS. Another potential explanation may be that in ARVD/C, ventricular dyssynchrony is more related to regional and heterogeneous abnormalities in conduction and contractility, not evident on a surface ECG (22).

In contrast to the lack of association between electrocardiographic abnormalities and dyssynchrony, RV morphology and function appeared to be related to RV dyssynchrony. Larger RVEDA and RVESA were noted in the patients with RV dyssynchrony. However, this relationship was not as strong as previously reported in patients with pulmonary hypertension ($r=0.70$,

$p < 0.001$ between RVEDA and RV dyssynchrony) (23). One potential reason for a weaker relationship could be the difference in pathology. ARVD/C is a patchy infiltrative process with regional dilatation while pulmonary hypertension (pressure overload) affects the RV globally and is more likely to cause uniform chamber dilatation in the load-sensitive RV (24).

Similar to dyssynchrony associated with LV failure (20,25), our data indicate a relationship between RV function, as determined by RVFAC and RV peak systolic strain, and RV dyssynchrony in ARVD/C. These findings are also in line with previous studies in patients with pulmonary hypertension (7,23) and systolic heart failure (15). Finally, fibrofatty infiltration in ARVD/C could involve the conduction system and thereby introduce electro-mechanical delays resulting in dyssynchrony. Similar relationships have been examined in ischemic cardiomyopathy where significant amounts of fibrosis result in the presence of mechanical dyssynchrony (22).

Our findings present several incremental points of knowledge concerning ARVD/C that could be potentially used for prognostic and therapeutic purposes. In patients with LV failure, the presence of significant ventricular dyssynchrony is associated with a worse prognosis (10). Dyssynchrony in ARVD/C may similarly predict worse clinical outcomes. Serial monitoring of RV dyssynchrony may identify patients at higher risk and deserving of aggressive therapy. Cardiac resynchronization therapy has improved symptoms and survival in dyssynchronous left heart failure (8,26). The presence of significant RV or interventricular dyssynchrony may introduce the possibility of resynchronization therapy for right sided failure in patients with ARVD/C who would otherwise be transplant candidates. However, more prospective studies are needed to further elucidate the clinical implications of the presence of RV dyssynchrony in ARVD/C.

Limitations

The mean age of the control group was lower than the ARVD/C patients. This may affect the definition of RV dyssynchrony for the ARVD/C patients. However, it has been demonstrated that ventricular dyssynchrony does not depend on age (27). In addition, LV dyssynchrony was comparable between the controls and the ARVD/C patients in the present study. Lastly, we strictly selected healthy normal controls since a previous definition for RV dyssynchrony was not available. Older controls tended to have medical conditions such as hypertension and diabetes, whose effects on RV dyssynchrony are unclear and were therefore excluded from the normal group. Larger studies with the power to assess the influence of other co-morbidities should ideally include an age-matched control group.

Furthermore, in the present study only TDE was used to define interventricular dyssynchrony. Interventricular dyssynchrony, calculated as the time difference between RV and LV pre-ejection intervals may have also provided additional information. However, RV outflow Doppler was not consistently performed in a fair number of subjects and we are unable to assess this parameter in our population.

Duration of disease is likely an important factor in the development of RV dyssynchrony in ARVD/C. However, determining the onset and duration of disease in this relatively asymptomatic group is challenging. We are therefore unable to evaluate its influence on RV dyssynchrony.

Similarly, the extent of fibrofatty infiltration may be an important factor in the pathogenesis of RV dyssynchrony in ARVD/C patients. In a small subset of patients enrolled in the present study, who also had clinical magnetic resonance imaging, we found no correlation between the extent of fibrofatty infiltration (as assessed by gadolinium enhancement) and RV dyssynchrony. These data were not presented due to the small sample size and lack of statistical power to offer reliable conclusions.

Finally, although the present study is the first observational study that demonstrates the presence of RV dyssynchrony in ARVD/C patients, unfortunately, this cross-sectional analysis does not provide insights into the clinical significance of the presence of RV dyssynchrony, and its exact role in ARVD/C management remains unclear. However, our findings prompt larger longitudinal studies to evaluate the influence of dyssynchrony on diagnosis, treatment and prognostication of ARVD/C patients including prediction of clinical outcomes such as heart failure, potential for arrhythmias and response to treatment. In particular, future studies may allow a more systematic assessment of several important factors including but not limited to duration of disease and genotype.

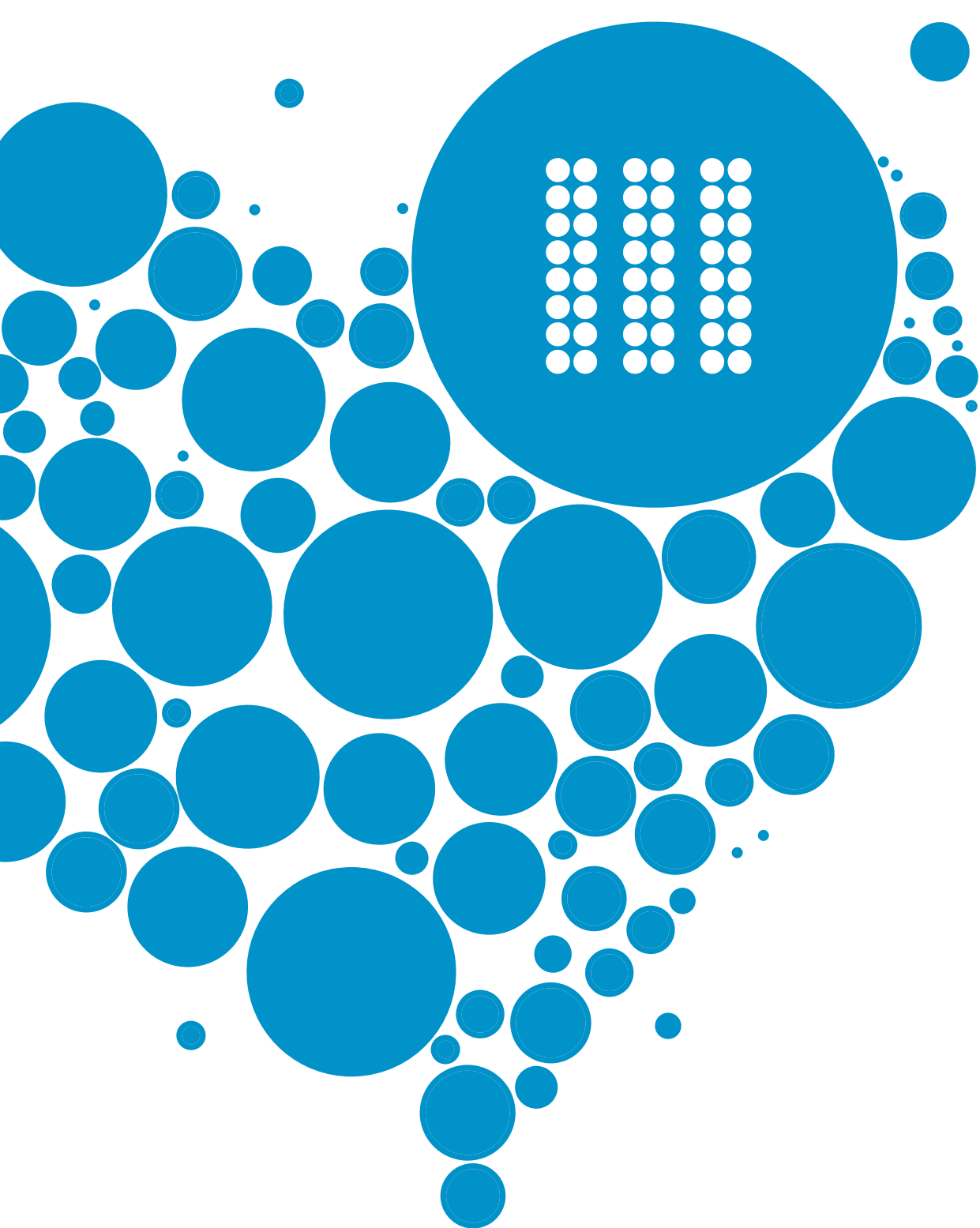
CONCLUSIONS

Significant RV dyssynchrony may occur in up to 50% of ARVD/C patients and is associated with RV remodeling and dysfunction rather than electrocardiographic abnormalities. This finding may have therapeutic and prognostic implications in ARVD/C.

REFERENCES

1. Corrado D, Basso C, Thiene G et al. Spectrum of clinicopathologic manifestations of arrhythmogenic right ventricular cardiomyopathy/dysplasia: a multicenter study. *J Am Coll Cardiol* 1997;30:1512-20.
2. McKenna WJ, Thiene G, Nava A et al. Diagnosis of arrhythmogenic right ventricular dysplasia/cardiomyopathy. *Br Heart J* 1994;71:215-8.
3. Kies P, Bootsma M, Bax J, Schalij MJ, van der Wall EE. Arrhythmogenic right ventricular dysplasia/cardiomyopathy: screening, diagnosis, and treatment. *Heart Rhythm* 2006;3:225-34.
4. Dalal D, Nasir K, Bomma C et al. Arrhythmogenic right ventricular dysplasia: a United States experience. *Circulation* 2005;112:3823-32.
5. Hulot JS, Jouven X, Empana JP, Frank R, Fontaine G. Natural history and risk stratification of arrhythmogenic right ventricular dysplasia/cardiomyopathy. *Circulation* 2004;110:1879-84.
6. Bax JJ, Ansalone G, Breithardt OA et al. Echocardiographic evaluation of cardiac resynchronization therapy: ready for routine clinical use? A critical appraisal. *J Am Coll Cardiol* 2004;44:1-9.
7. Lopez-Candales A, Dohi K, Bazaz R, Edelman K. Relation of right ventricular free wall mechanical delay to right ventricular dysfunction as determined by tissue Doppler imaging. *Am J Cardiol* 2005;96:602-6.
8. Bax JJ, Abraham T, Barold SS et al. Cardiac resynchronization therapy: Part 1--issues before device implantation. *J Am Coll Cardiol* 2005;46:2153-67.
9. Abraham TP, Dimaano VL, Liang HY. Role of tissue Doppler and strain echocardiography in current clinical practice. *Circulation* 2007;116:2597-609.
10. Bader H, Garrigue S, Lafitte S et al. Intra-left ventricular electromechanical asynchrony. A new independent predictor of severe cardiac events in heart failure patients. *J Am Coll Cardiol* 2004;43:248-56.
11. Gorcsan J, III, Abraham T, Agler DA et al. Echocardiography for cardiac resynchronization therapy: recommendations for performance and reporting--a report from the American Society of Echocardiography Dyssynchrony Writing Group endorsed by the Heart Rhythm Society. *J Am Soc Echocardiogr* 2008;21:191-213.
12. Lang RM, Bierig M, Devereux RB et al. Recommendations for Chamber Quantification. *J Am Soc Echocardiogr* 2005;18:1440-63.
13. Schiller NB, Shah PM, Crawford M et al. Recommendations for quantitation of the left ventricle by two-dimensional echocardiography. *J Am Soc Echocardiogr* 1989;2:358-67.
14. Prakasa KR, Wang J, Tandri H et al. Utility of tissue Doppler and strain echocardiography in arrhythmogenic right ventricular dysplasia/cardiomyopathy. *Am J Cardiol* 2007;100:507-12.
15. Rajagopalan N, Dohi K, Simon MA et al. Right ventricular dyssynchrony in heart failure: a tissue Doppler imaging study. *J Card Fail* 2006;12:263-7.
16. Bax JJ, Bleeker GB, Marwick TH et al. Left ventricular dyssynchrony predicts response and prognosis after cardiac resynchronization therapy. *J Am Coll Cardiol* 2004;44:1834-40.
17. Rampazzo A, Nava A, Malacrida S et al. Mutation in human desmoplakin domain binding to plakoglobin causes a dominant form of arrhythmogenic right ventricular cardiomyopathy. *Am J Hum Genet* 2002;71:1200-6.
18. Gerull B, Heuser A, Wichter T et al. Mutations in the desmosomal protein plakophilin-2 are common in arrhythmogenic right ventricular cardiomyopathy. *Nat Genet* 2004;36:1162-4.
19. Pillichou K, Nava A, Basso C et al. Mutations in desmoglein-2 gene are associated with arrhythmogenic right ventricular cardiomyopathy. *Circulation* 2006;113:1171-9.
20. Ghio S, Constantin C, Klersy C et al. Interventricular and intraventricular dyssynchrony are common in heart failure patients, regardless of QRS duration. *Eur Heart J* 2004;25:571-8.
21. Bleeker GB, Schalij MJ, Molhoek SG et al. Relationship between QRS duration and left ventricular dyssynchrony in patients with end-stage heart failure. *J Cardiovasc Electrophysiol* 2004;15:544-9.
22. Kass DA. An epidemic of dyssynchrony: but what does it mean? *J Am Coll Cardiol* 2008;51:12-7.

23. Lopez-Candales A, Dohi K, Rajagopalan N et al. Right ventricular dyssynchrony in patients with pulmonary hypertension is associated with disease severity and functional class. *Cardiovasc Ultrasound* 2005;3:23.
24. Haddad F, Doyle R, Murphy DJ, Hunt SA. Right ventricular function in cardiovascular disease, part II: pathophysiology, clinical importance, and management of right ventricular failure. *Circulation* 2008;117:1717-31.
25. Ghio S, Freemantle N, Serio A et al. Baseline echocardiographic characteristics of heart failure patients enrolled in a large European multicentre trial (CArdiac RESynchronisation Heart Failure study). *Eur J Echocardiogr* 2006;7:373-8.
26. Bradley DJ, Bradley EA, Baughman KL et al. Cardiac resynchronization and death from progressive heart failure: a meta-analysis of randomized controlled trials. *JAMA* 2003;289:730-40.
27. Ng AC, Tran dT, Newman M et al. Left ventricular longitudinal and radial synchrony and their determinants in healthy subjects. *J Am Soc Echocardiogr* 2008;21:1042-8.



Percutaneous valve procedures





Percutaneous valve procedures: an update

Laurens F. Tops¹
Samir R. Kapadia²
E. Murat Tuzcu²
Alec Vahanian³
Ottavio Alfieri⁴
John G. Webb⁵
Jeroen J. Bax¹

¹*Department of Cardiology, Leiden University Medical Center, the Netherlands*

²*Department of Cardiovascular Medicine, Cleveland Clinic, Cleveland, USA*

³*Department of Cardiology, Bichat Hospital, Paris, France*

⁴*Department of Cardiac Surgery, San Raffaele University Hospital, Milan, Italy*

⁵*Division of Cardiology, St Paul's Hospital, University of British Columbia, Vancouver, Canada*

ABSTRACT

Valvular heart disease is an important cause of morbidity and mortality. Aortic stenosis and mitral regurgitation account for the majority of patients with native valve disease. Although surgical treatment provides satisfactory outcome, a large proportion of patients do not undergo a surgical intervention, because of the high estimated operative risk and multiple co-morbidities.

Recently, new techniques that enable percutaneous treatment of valvular heart disease have been developed and their feasibility has been reported in several studies. All techniques target a minimal invasive procedure with a low risk of procedure related complications. In this manuscript, an overview of the various percutaneous procedures for mitral and aortic valve disease will be provided. In addition, an update on the ongoing trials in percutaneous valve procedures will be presented. Finally, the role of imaging in performing percutaneous valve procedures will be discussed.

INTRODUCTION

Valvular heart disease is an important cause of morbidity and mortality. Aortic stenosis (AS) and mitral regurgitation (MR) account for the majority of native valve disease (1,2). Although surgical treatment has good outcome in most patients, operative risk may be high due to age and co-morbidity. Importantly, a large proportion of patients (in particular with AS) are not referred for surgery. Data from the recent Euro Heart Survey on valvular heart disease, revealed that up to 30% of the patients with severe valvular disease did not undergo surgery, although an indication existed (3). The high estimated operative risk, multiple co-morbidities and patient's age are the main reasons for denial of surgery. Therefore, there is a need for alternative procedures, particularly in the elderly.

Over the past few years, techniques for percutaneous valve repair and replacement have been developed and feasibility has been reported in numerous studies, both in animal models and randomized trials in patients (4). All techniques target a minimal invasive procedure with a low risk of complications. This review provides an overview of the various percutaneous procedures for mitral and aortic valve disease and a summary of the ongoing trials. Moreover, the role of imaging in these percutaneous valve procedures is also discussed.

PERCUTANEOUS MITRAL PROCEDURES

Several percutaneous approaches for the treatment of mitral valve (MV) stenosis and MR are available. The field of percutaneous MV repair has many important differences compared to percutaneous aortic valve (AV) replacement. The anatomy or mechanism of MR may involve one or more elements of the MV apparatus. The patient population, depending on the mechanism of regurgitation, can vary in age, co-morbidities and symptomatology. The timing of intervention and the goals (or endpoints) of treatment are also less well defined. The surgical "gold standard" is not as readily identifiable when different mechanisms of MR are critically analyzed. Therefore, the development and evaluation of MV technologies pose unique challenges compared to the percutaneous AV replacement. The different percutaneous MV procedures are summarized in Table 1, and will be discussed in the following paragraphs.

Percutaneous mitral commissurotomy

Balloon commissurotomy is now an accepted therapy for selected patients with rheumatic mitral stenosis (1,2). It has been shown that percutaneous mitral commissurotomy provides excellent early hemodynamic effects, and a lower rate of residual stenosis and restenosis as compared with surgical mitral commissurotomy (5). Currently, percutaneous mitral commissurotomy is typically performed utilizing the Inoue technique with transseptal access to the left atrium and antegrade access to the MV and the use of a self-seating balloon (6). The goal

Table 1. Percutaneous mitral valve procedures reported to date

Approach	Device	Feature	Company	Status
Leaflet repair	MitraClip	Edge-to-edge clip	Evalve	Pivotal
	Mobius	Edge-to-edge suture	Edwards Lifesciences	On hold
Coronary sinus annuloplasty	MONARC	Delayed effect	Edwards Lifesciences	Clinical data
	PTMA	Late adjustment	Viacor	Clinical data
	Carillon	Adjustable	Cardiac Dimensions	Clinical data
Direct remodeling	Coapsys	Transmyocardial cord (minimal invasive)	Myocor	Clinical data
	iCoapsys	Transmyocardial cord	Myocor	Clinical data
	PS ³	Transatrial cord	Ample Medical	Clinical data
Annular plication	Mitralign	Left ventricular procedure	Mitralign	Preclinical
	Accucinch	Left ventricular procedure	Guided Delivery Systems	Preclinical
Annular shrinking	QuantumCor	Radiofrequency	QuantumCor	Preclinical
Valve replacement	Endovalve	Catheter delivered valve	Endovalve	Preclinical

is to produce a controlled tear of the fused MV commissures. Since this is a well-established procedure, and has been studied extensively, percutaneous balloon mitral commissurotomy will not be reviewed in detail here.

Paravalvular leak closure

Paravalvular leaks may occur following surgical valve replacement due to suture dehiscence, endocarditis or technical errors. When regurgitation is hemodynamically significant or results in clinically important hemolysis, percutaneous closure may offer an alternative to re-operation in high risk patients and patients with contraindications for surgery (7). Only selected defects are suitable for percutaneous closure. In general, multiple defects, defects that measure above 8 mm in diameter, or extend over a broad circumference of the valve, cannot be effectively dealt with. A variety of implantable devices have been utilized. At present, coils are favored for very small defects, patent ductus devices for medium defects and atrial septal occluders for larger defects. However, more experience is needed to fully understand the best strategy and optimal approach for patients with paravalvular leakage (7).

Leaflet repair (Edge-to-edge)

The most advanced percutaneous mitral repair procedure is the edge-to-edge repair procedure with the Evalve Percutaneous Mitral Repair System or MitraClip® device (Evalve Inc., Menlo

Park, CA) modeled after a surgical procedure which has been shown to be effective in selected patients (8). Alfieri surgical repair involves suturing a small segment of the anterior mitral leaflet to the posterior leaflet. The result is a double-orifice MV with improved leaflet coaptation. The percutaneous procedure using the MitraClip device (Figure 1) involves transeptal cannulation of the left atrium, and positioning of the delivery catheter perpendicular to the MV. During echocardiographic guidance, a clip is placed to appose the anterior and posterior MV leaflets, creating a double-orifice valve (9). An example of the percutaneous edge-to-edge repair with the use of the MitraClip is shown in Figure 2.

A similar procedure utilizing percutaneously placed sutures (Mobius™, Edwards Lifesciences Inc., Irvine, CA) has been reported (10). However clinical trials have been put on hold due to the technical difficulty of suture placement and poor durability.

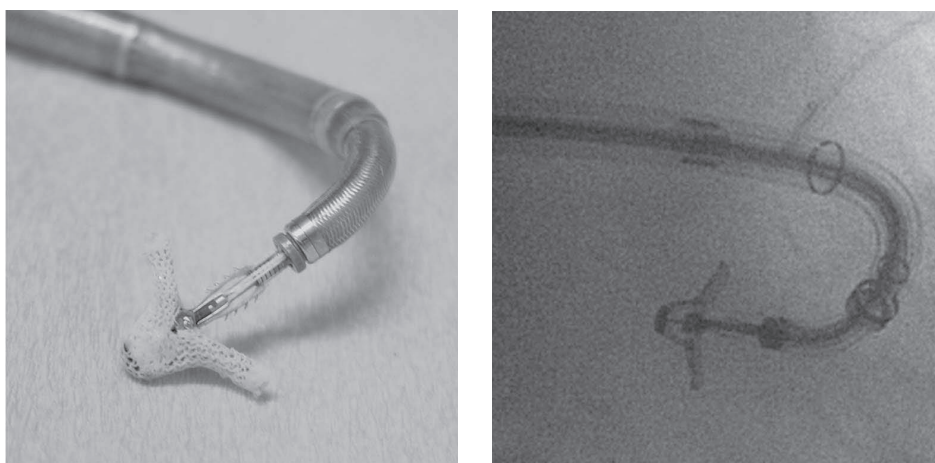


Figure 1. The MitraClip device is a 2-armed, polyester-covered, soft tissue-fixation device (left panel). The outside dimension when closed is 4 mm; in the grasping position, the 2 “arms” span about 20 mm. In the open position, it is used to grasp and immobilize the central mitral leaflet scallops by retraction of the delivery catheter. Each arm has an opposing “gripper” that aids in securing the leaflets in the clip by means of small, multipronged friction elements. All these elements are clearly visible on fluoroscopy (right panel).

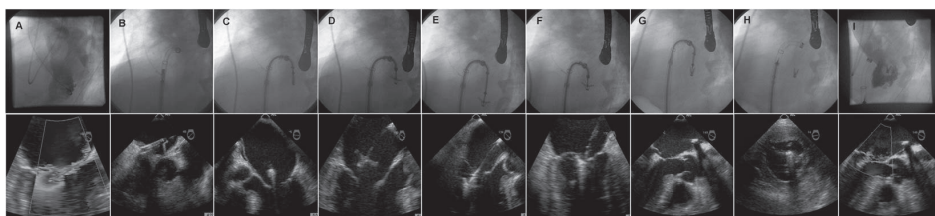


Figure 2. Outline of the percutaneous MV repair procedure (MitraClip) using fluoroscopic and echo guidance. Severe MR is seen by transthoracic and transesophageal echocardiography (panel A). The device sheath is placed in the left atrium after transeptal puncture (panel B). The clip is advanced just above the MV in the closed configuration (panel C). The MitraClip is then opened in the left atrium (panel D) and advanced into the left ventricle (panel E). Subsequently, the clip is pulled back in systole to stabilize the MV leaflets (panel F), the grippers are quickly lowered and the clip is closed (panel G). After confirming that the leaflets are adequately captured between an arm on the ventricular side and a gripper on the atrial side, the clip is closed in a locked position. Once a functioning double-orifice mitral valve is confirmed with echocardiography, the clip is detached (panel H). There is minimal MR after the procedure with excellent procedural outcome.

Coronary sinus annuloplasty

This approach is based on the close anatomical relation of the mitral annulus with the coronary sinus. Several devices for this approach exist. The MONARC™ device (Edwards Lifesciences Inc.) consists of a nickel titanium alloy (nitinol) implant (11). The implant itself is comprised of three sections; a distal self-expanding anchor, a spring-like 'bridge', and a proximal self-expanding anchor (Figure 3). The distal anchor is deployed in the great cardiac vein and the proximal anchor is deployed in the proximal coronary sinus. The bridge has shape memory properties that result in shortening forces at body temperature. Biodegradable suture is interwoven in the spring like bridge section, initially preventing shortening. Following implantation the suture degrades allowing the bridge section to shorten. The anchors draw the proximal coronary sinus and distal great cardiac vein together while the bridge section tenses and straightens indirectly displacing the posterior annulus anteriorly and reducing mitral annulus diameter and septal-lateral distance.

The Percutaneous Transvenous Mitral Annuloplasty system (PTMA™, Viacor Inc., Wilmington, MA) utilizes an indwelling catheter placed within the coronary sinus (12). Wire-like implants can be placed into the coronary sinus via the catheter system. A potential advantage of the system is the ability to add or remove rods to vary the effect of the device. Late adjustment is possible by surgically accessing the closed system from a subclavicular pocket.

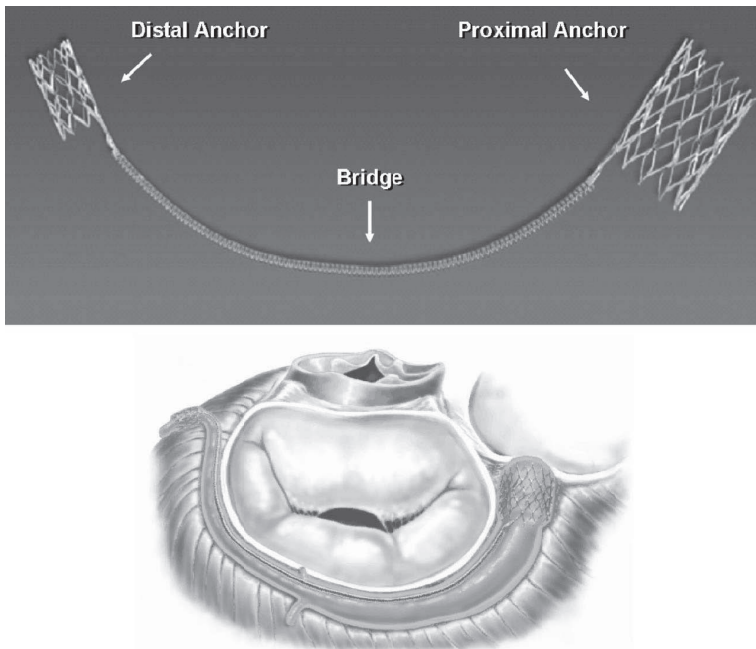


Figure 3. The MONARC device consists of two self-expanding stent-like anchors which are implanted in the coronary sinus (upper panel). The anchors are joined by a longer bridge segment which is designed to gradually shorten after implantation. As this occurs the anchors are drawn together shortening the coronary sinus and the adjacent posterior mitral annulus. The lower panel demonstrates the position of the MONARC device in the coronary sinus.

The CARILLON™ Mitral Contour System (Cardiac Dimensions Inc., Kirkland, WA) consists of a steel wire shaped with distal and proximal stent like anchors (13). The length of the central connector segment can be varied at the time of implantation to adapt the degree of shortening of the coronary sinus. Advantages of the device include the ability to adjust or remove the device at the time of implantation.

Direct remodeling

Several percutaneous techniques for direct remodeling of the left ventricle and the MV for the treatment of MR are in early testing stages. The Coapsys® and iCoapsys™ devices (Myocor® Inc., Maple Grove, MN) target remodeling of the left ventricle as well as the mitral annulus and subvalvular apparatus by implantation of a transventricular cord. The Coapsys device (Figure 4) consists of three epicardial pads implanted on the exterior surface of the heart at the level of the mitral annulus using a surgical approach (14,15). A tether connecting the three anchors can be

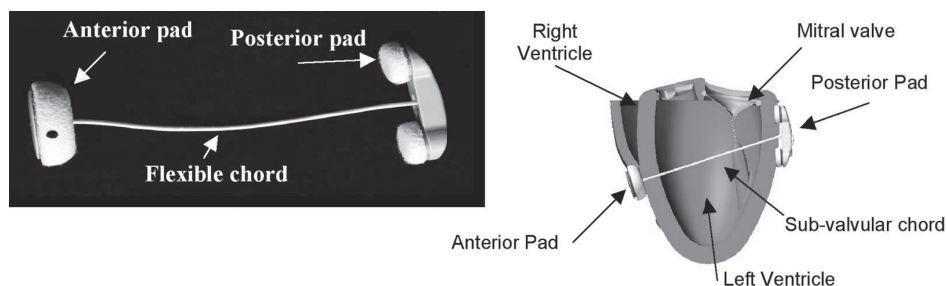


Figure 4. The Coapsys device consists of three epicardial pads and a flexible chord connecting them (left panel). The right panel schematically shows the implantation of the Coapsys device and the final position of the epicardial pads.

shortened to cause a conformational change in the left ventricle and mitral annulus. Recently, a truly percutaneous implanted version of the device entitled iCoapsys has been introduced (16). For implantation of the iCoapsys device, a specifically designed needle, guidewire and sheath are used to obtain controlled access in to the pericardial space. The posterior target zone is between the papillary muscle and the P2 segment of the mitral annulus, about two centimeters apical to the atrioventricular groove. Once proper alignment is achieved, a needle is passed from each catheter into the ventricle. A flexible wire introduced through the posterior catheter is captured by a snare from the anterior catheter. The flexible wire is used to place the transventricular cord, which is exteriorized through the delivery sheath. Then, the permanent implant device is placed over the cord, posterior pad first. Finally, the cord is tightened to achieve the desired effect, trimmed and the catheters are removed.

The Percutaneous Septal Shortening System PS³ (Ample Medical Inc., Foster City, CA) delivers an implant into the posterior annulus with a tether attached to an atrial septal closure device. Both produce anterior movement of the posterior annulus, thereby restoring the line of coaptation (17,18). The PS³ system differs from the Coapsys system in that it creates a transatrial

bridge as opposed to a transventricular bridge. The advantages of the PS³ system when compared to the transventricular cinching devices include the relative ease of placement and avoidance of left circumflex coronary artery impingement. However, this transatrial approach may not result in additional advantages, such as left ventricular remodeling, as compared with the transventricular devices.

Other percutaneous mitral procedures

Several other percutaneous procedures in the treatment of MR are being evaluated in pre-clinical studies (Table 1). Percutaneous procedures that replicate surgical suture plication of the posterior mitral annulus have been developed. The Mitralign Direct Annuloplasty SystemTM (Mitralign Inc., Salem, NH) and the Accucinch Annuloplasty SystemTM (Guided Delivery Systems Inc., Santa Clara, CA) involve catheter access through the AV in order to place various types of anchors into the left ventricular aspect of the posterior mitral annulus. These anchors are attached by sutures which can then be pulled tight drawing the anchors together and plicating the mitral annulus.

The QuantumCor catheter device (QuantumCor Inc., Lake Forest, CA) targets remodeling of the MV annulus by delivery of radiofrequency energy directly to the tissue.

The EndoValve Mitral Valve Replacement System (EndoValve Inc., Princeton, NJ) is a prosthetic valve folded in into a catheter and delivered antegrade through transseptal access. The first animal study has shown the feasibility of the device, and more results are eagerly awaited.

PERCUTANEOUS AORTIC PROCEDURES

The different percutaneous AV procedures will be discussed in the following paragraphs and are summarized in Table 2.

Aortic valvuloplasty

Current guidelines indicate that aortic valvuloplasty might be useful as a bridge to surgery or as palliation in non-surgical candidates (1,2). The procedure is generally performed utilizing retrograde access from the femoral artery, although some operators prefer an antegrade, transseptal approach. Since the first reports of this procedure more than 20 years ago (19), various procedural enhancements such as lower profile balloons and sheaths, more appropriate

Table 2. Percutaneous aortic valve procedures reported to date

Approach	Device	Feature	Company	Status
Valve implantation	Cribier-Edwards valve	Balloon expandable	Edwards Lifesciences	Clinical data
	SAPIEN valve	Balloon expandable	Edwards Lifesciences	Clinical data
	CoreValve	Self-expanding	CoreValve	Clinical data

balloon sizing in relation to annulus diameter, and burst pacing to reduce balloon and cardiac movement during balloon inflation, may have improved outcome beyond that encountered in the early reported experience (6). Nonetheless, no survival benefit after balloon valvuloplasty has been shown (20). Therefore, at present AV balloon valvuloplasty plays a limited role in the management of degenerative AS.

Aortic valve implantation

The balloon expandable percutaneous AV was first tested in 1992 by Andersen et al. in an animal model (21). The subsequent initial human implantation was performed by Cribier et al. in 2002, via an antegrade approach, in a 57-year old man with calcific AS and cardiogenic shock (22). Immediately after valve implantation, the patient's hemodynamic conditions improved markedly with good valve function. The valve performed well over the next four months, although the patient died from complications unrelated to the procedure or the prosthetic valve. At present, two types of catheter delivered aortic prosthetic valves are available and have seen extensive clinical use.

The first is the balloon-expandable Edwards SAPIEN valve (Edwards Lifesciences Inc.), successor of the initially used Cribier-Edwards valve (Figure 5). It incorporates a balloon-expandable stainless steel stent, fabric sealing cuff and bovine pericardial leaflets. Current prosthesis sizes include 23 and 26 mm expanded size for aortic annulus diameters between 18 to 22 mm and 21 to 25 mm, respectively. Typically, a balloon valvuloplasty is performed first, and subsequently the prosthesis is deployed; both processes are performed during rapid right ventricular pacing (23). Initial procedures were performed utilizing femoral venous puncture, transseptal access to the left atrium and passage through the MV to reach the AV (22,24). However, the antegrade delivery of the AV has a potential drawback of damaging the anterior mitral leaflet as the valve traverses through the left atrium to the aorta. Currently, a retrograde approach from the femoral artery is preferred (25,26). Recently an alternative, transapical approach has been proposed



Figure 5. The Edwards balloon expandable prosthetic valve is constructed of a stainless steel stent, bovine pericardial leaflets and a fabric sealing cuff.

in patients with extensive femoral artery disease. After an intercostal incision, direct puncture of the apical portion of the left ventricular free wall is performed to gain catheter access to the left ventricle and AV (27).

The other type of catheter delivered aortic prosthetic valve is the CoreValve ReValving system™ (CoreValve Inc, Irvine, CA), consisting of a self-expanding nitinol alloy stent with a pericardial sealing cuff and leaflets (Figure 6). The device is constrained within a delivery sheath, expanding to its predetermined shape when the sheath is withdrawn (28). The CoreValve total length is 50 mm, and it has a specific design features with a waist in the middle part. The lower part of the valve is designed to expand using high radial forces; the middle part includes the pericardial tissue valve and is constrained to avoid coronary occlusion. The

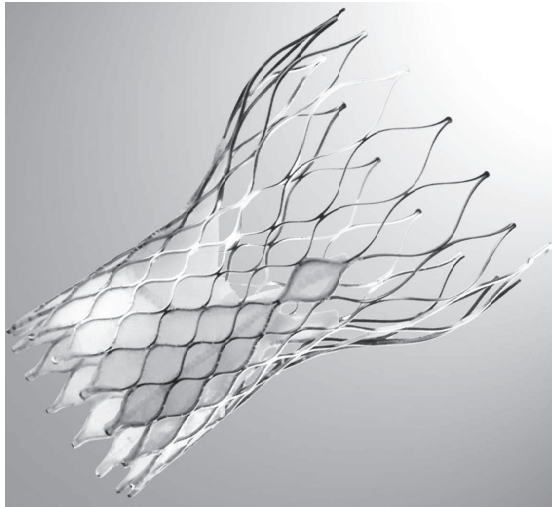


Figure 6. The CoreValve self-expanding prosthetic valve is constructed of a nitinol stent and pericardial leaflets and sealing cuff.

upper part of the prosthesis enables fixation in the ascending aorta. While the first-generation device used bovine pericardial tissue and was constrained within a 24F delivery sheath, the second-generation device incorporated a porcine pericardial tissue valve within a 21F sheath. The first generation CoreValve was limited to an ascending aorta diameter of 30 mm, whereas the broader upper section of the second-generation device allowed for its deployment in an ascending aorta up to 45 mm diameter. Currently, third-generation (18F) prostheses are available with an inner valve diameter of 21 mm. The CoreValve is typically implanted retrograde from the femoral artery under fluoroscopic guidance, and a cardiac assist device, extracorporeal membrane oxygenation or a full-bypass support was used in the first series (29). However, at present, the CoreValve is implanted without cardiac assist or full-bypass support. In May 2007, the CoreValve became the first percutaneous valve to receive CE mark approval in Europe.

Finally, many new percutaneous valves such as Lotus™ Valve System (Sadra Medical Inc., Campbell, CA), and the percutaneous AV from Direct Flow Inc. (Santa Rosa, CA), AorTx Inc. (Palo

Alto, CA) and Heart Leaflet Inc. (Maple Grove, MN) are also entering early human studies. The hope is that these newer valve technologies will improve on first-generation devices by using collapsible, inflatable valve frames for repositioning before final deployment and hopefully a smaller size for easy deliverability.

(PRE)CLINICAL STUDIES AND TRIALS ON PERCUTANEOUS VALVE PROCEDURES

The introduction of new technology typically involves preclinical developmental studies, phase I and phase II clinical trials. In general, it should be noted that only limited numbers of patients have been treated with percutaneous valve procedures, and that a clear learning curve for performing these procedures is present. In the following paragraphs, the reported studies and ongoing clinical trials for both percutaneous MV and AV procedures will be discussed.

Percutaneous mitral valve procedures

Leaflet repair (Edge-to-edge) For this percutaneous MV repair approach, the MitraClip is the most commonly used device. Preclinical data from a porcine model was first published in 2003 (9). Complete endothelialization and encapsulation of the clip was seen with no clip embolization or thromboembolism. The phase I prospective, multi-center safety and feasibility trial entitled EVEREST (Endovascular Valve Edge-to-Edge Repair Study) has been reported in 2005, with short-term and six-month results in the first 27 patients (30). All patients enrolled were candidates for MV surgery and had MR that was centered between A2 and P2, meeting prespecified parameters for flail dimensions or leaflet tethering to ensure device capture of the leaflets. Most patients had degenerative MV disease ($n = 25$, 93%). Successful deployment of the clips was achieved in 24 of the 27 patients (89%). Partial clip detachment ($n = 3$), severe residual MR ($n = 2$) and device malfunction ($n = 1$), required MV surgery after initial successful percutaneous clip implantation. Now that the capability to place two clips has been introduced, residual MR may become less common. Of the 27 initial patients in the EVEREST trial, 13 patients (48%) remained with MR grade 2+ or less at six months follow-up. One year follow-up on these patients shows a durable reduction in MR if initial procedural success is achieved (Figure 7) (31). The primary safety endpoint of EVEREST I was freedom from death, myocardial infarction, cardiac tamponade, cardiac surgery for failed clip, clip detachment, stroke or septicemia. A prespecified event rate of 34.4% was expected based on comparison to surgical event rates, however only 15% of patients had a major adverse event (clip detachment $n = 3$; stroke $n = 1$). The pivotal phase II trial has been initiated (EVEREST II) comparing percutaneous MV repair approach to standard cardiac surgery. The study design is a prospective, multicenter, randomized, controlled trial with a 2:1 randomization to study and control arms, respectively (Table 3).

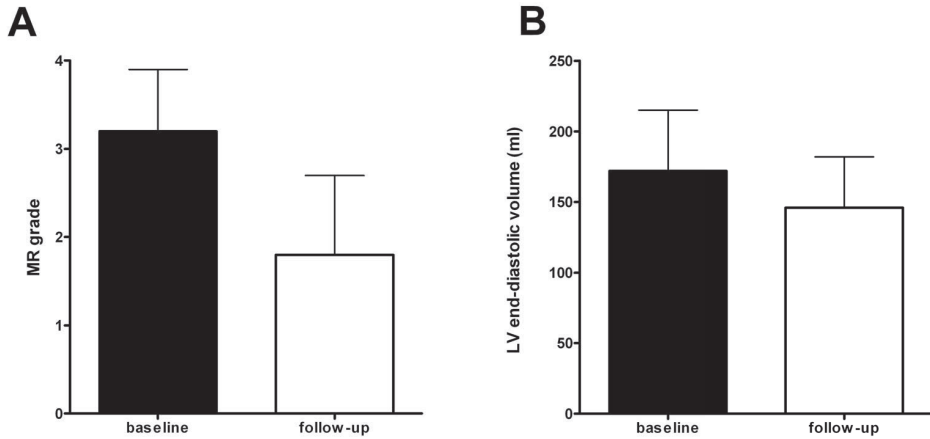


Figure 7. After 12 months follow-up, a significant improvement in MR grade (panel A) and left ventricular (LV) end-diastolic volume (panel B) was observed in 46 patients with severe MR treated with percutaneous edge-to-edge repair (MitraClip). Mitral regurgitation grade decreased from 3.2 ± 0.7 to 1.8 ± 0.9 ($p < 0.001$), and LV end-diastolic volume decreased from 172 ± 43 to 146 ± 36 ($p < 0.001$) indicating a sustained benefit of successful percutaneous MV repair at long-term follow-up.

Coronary sinus annuloplasty As discussed in previous paragraphs, several devices are available, each with specific features. The MONARC system has recently been implanted in patients with chronic ischemic MR. Initial results in humans showed successful implantation in four of five patients, with one failure leading to coronary sinus perforation. However, separation of the nitinol bridge segment was observed in three of four patients, and no significant changes in MR grade or mitral annulus diameter were found at follow-up (11). With additional animal experience showing improved results with the new device design, a trial using the MONARC device has started enrolling functional MR patients. The EVOLUTION trial, a multi-center feasibility and safety study in Europe and Canada, has begun with a primary safety objective of procedural success and 30-day safety, and a 90-day efficacy endpoint of reduction in MR by one grade (Table 3). Preliminary results were recently presented, showing successful implantation in 32 of 36 patients (89%). Preliminary efficacy data indicate the efficacy endpoint (MR reduction by 1 grade at 90 days) was met in 9 of 17 patients analyzed (53%) (32).

The PTMA system has also been reported to effectively reduce severe MR. In a sheep model of ischemic MR a single rod resulted in immediate reduction of MR from grade 3+ or 4+ to grade 0 or 1+ in all animals. A reduction of the mitral annulus diameter was observed (pre-insertion 30 ± 2 mm vs. post-insertion 24 ± 2 mm, $p < 0.03$), without any sign of mitral stenosis (12). Human implantation has been performed in patients undergoing open heart surgery for ischemic MR (33). In four patients who had attempted implantation of the multi-lumen device, there was successful delivery in only three patients. The mitral annulus anterior-posterior diameter decreased from 41 ± 4 mm to 35 ± 2 mm, resulting in a reduction in MR from grade 2 or 3+ to 1+. Unfortunately, the PTMA device could not be implanted permanently (33). Further short- and long-term human data, including the PTOLEMY trial (Table 3), are pending.

Table 3. Ongoing trials on percutaneous valve procedures

Name	Device	Type	Design	Sample Size	Primary Endpoint	Comment
Percutaneous mitral valve procedures						
EVEREST II	MitraClip device	Randomized	Percutaneous Edge-to-Edge repair vs. surgical MV repair / replacement	390	Safety: Freedom from MAE (30 days) Efficacy: Freedom from surgery for valve dysfunction, death, and 3+ or 4+ MR	Up to 42 US and Canadian sites
EVEREST – High Risk Registry	MitraClip device	Single arm Non-randomized	Percutaneous Edge-to-Edge repair	70	Safety: Freedom from MAE (30 days) Efficacy: Freedom from surgery for valve dysfunction, death, and 3+ or 4+ MR	May continue enrollment beyond initial allocation
EVOLUTION	MONARC system	Single arm Uncontrolled	Safety and feasibility	120	Clinical Endpoints and quality of life indicators	19 sites in Europe and Canada
PTOLEMY	PTMA system	Single arm Uncontrolled	Safety and feasibility	20	Device related MAE (30 days)	Feasibility study
AMADEUS	CARILLON system	Single arm Non-randomized	Safety and feasibility	n/a	n/a	European study
COMPETENT	CARILLON system	Single arm Non-randomized	Safety and feasibility	n/a	n/a	US study
RESTOR-MV	Coapsys device	Randomized	Coapsys device vs. surgical MV repair	250	Safety: Freedom from MAE (12 months) Efficacy: Mean change in MR grade	Concomitant coronary artery bypass graft surgery
VIVID	i-Coapsys device	Single arm Uncontrolled	Safety and feasibility	30	Intra- and peri-procedural safety Intra-procedural efficacy	Enrollment not yet started
Percutaneous aortic valve procedures						
PARTNER	Edwards SAPIEN Valve	Randomized	Percutaneous AVR vs. surgical AVR	350	1-year mortality	Group A: High risk surgical patients
	Edwards SAPIEN Valve	Randomized	Percutaneous AVR vs. no AVR	250	1-year mortality	Group B: Inoperable patients

AMADEUS = cArillon Mitral Annuloplasty Device European Union Study; AVR = aortic valve replacement; EVEREST = Endovascular Valve Edge-to-Edge REpair SStudy; MAE = major adverse events; MR = mitral regurgitation; PARTNER = Placement of AoRTic TraNscatheter Valve trial; RESTOR-MV = Randomized Evaluation of a Surgical Treatment for Off-pump Repair of the Mitral Valve; VIVID = Valvular and Ventricular Improvement Via iCoapsys Delivery.

The initial preclinical testing of the CARILLON system indicated that there were anatomical, design and safety issues with this coronary sinus device, as three of twelve dogs had left circumflex coronary artery ischemia, causing fatality in two dogs (13). Nonetheless, in the seven dogs with successful implantation, a reduction in mitral annular size at four weeks follow-up was observed compared to those with unsuccessful implantation (33.7 ± 2.3 mm vs. 37.3 ± 1.1 mm, $p < 0.05$) (13). Subsequent experiments were done in an ovine model, demonstrating favorable acute hemodynamic effects and no mortality (34). A multi-center human safety and feasibility study is currently underway in Europe entitled AMADEUS (cArillon Mitral Annuloplasty Device European Union Study), enrolling patients with grade 2+ to 4+ functional MR and NYHA class II to IV. A Phase I investigational device exemption study entitled COMPETENT targets a similar patient population in the United States and is designed to assess hemodynamics, quality of life, and exercise tolerance (Table 3).

Direct remodeling There are several other approaches to percutaneous treatment of MR that are being evaluated (Table 1). The Coapsys, iCoapsys and PS³ system have both proven feasible in animal and human studies and therefore are discussed at some length in the following paragraphs.

The Coapsys system involves surgical placement of pericardial implants off-pump. These implants are placed on each side of the heart, with a tethering subvalvular cord that crosses the ventricle directly. This cord is then cinched up to decrease the septal-to-lateral diameter and eliminate MR. In initial animal studies using a canine tachycardia-model of functional MR ($n = 10$), this device reduced the mean MR grade from 2.9 ± 0.7 to 0.6 ± 0.7 ($p < 0.001$), without adverse consequence on ventricular function (14). The safety and efficacy of the Coapsys device has also been demonstrated in humans. In 11 patients a sustained benefit after 12 months follow-up on the severity of MR (from grade 2.9 ± 0.5 to 1.1 ± 0.6 , $p < 0.05$) and NYHA functional class (from 2.5 ± 0.5 to 1.2 ± 0.4 , $p < 0.05$) has been shown (15). The Randomized Evaluation of a Surgical Treatment for Off-pump Repair of the Mitral Valve trial (RESTOR-MV) is enrolling patients with coronary artery disease and ischemic MR, who undergo coronary artery bypass grafting combined with either traditional MV repair or Coapsys device placement (Table 3). Intra-operative results from this trial have been reported in the first 19 patients receiving the implant, showing a reduction in MR after implantation from grade 2.7 ± 0.8 to 0.4 ± 0.7 ($p < 0.001$). All implants were performed successfully without cardiopulmonary bypass and no hemodynamic compromise or structural damage to the mitral apparatus was experienced (35). A similar system is currently under development for percutaneous use (iCoapsys). The device is implanted percutaneously through a pericardial access sheath, as previously described. The device was initially tested in a canine model ($n = 8$), achieving a reduction in MR grade from 3.2 to 0.7 (16). However, in the first animal studies, device placement was complicated and it has been redesigned to more closely mimic the surgically-placed device. The iCoapsys system allows for the ability to intervene in non-surgical candidates and those undergoing

percutaneous coronary intervention. This device theoretically provides a more comprehensive mechanism of action, preserving normal valve dynamics, and addressing the mitral annulus as well as the subvalvular space and abnormal left ventricular geometry. This geometric reshaping of the ventricle may be advantageous to ventricular function and remodeling and is unique to this device. The Valvular and Ventricular Improvement Via iCoapsys Delivery (VIVID) Feasibility Study will assess the safety and efficacy of the iCoapsys device in humans and is expected to be launched soon (Table 3).

The PS³ system utilizes the coronary sinus and a septal closure device to place a cord across the atrium, create tension on the annulus, and subsequently reduce the septal-to-lateral dimension. This device has been applied to an ovine model of tachycardia-induced cardiomyopathy created by rapid right ventricular pacing (17). The degree of reduction in functional MR, and in the septal-lateral systolic distance, was the primary efficacy measure of this study. Sheep underwent short-term (n = 19) and long-term (n = 4) evaluation after implantation. The PS³ system was successfully implanted in all animals with no evidence of left circumflex coronary artery impingement and maintenance of coronary sinus patency. The short-term results indicated a significant reduction in septal-lateral diameter from 32.5 ± 3.5 mm to 24.6 ± 2.4 mm post-procedure ($p < 0.001$). This was maintained at 30-days in the long-term animals (septal-lateral diameter 25.3 ± 0.8 mm after 30 days). The results for reduction in MR in the short-term animals were similar, with an MR grade of 2.1 ± 0.6 pre-procedure versus 0.4 ± 0.4 post-procedure ($p < 0.001$). This result was maintained at 30-days follow-up (mean MR grade 0.2 ± 0.1). Additional hemodynamic and laboratory data were consistent with improved cardiac function (17).

Recently, the results of the first-in-human feasibility study of the PS³ system have been reported. In two patients with MR referred for surgical MV repair, the percutaneous PS³ system was implanted successfully before the conventional surgical procedure. Both MR severity and septal-to-lateral diameter decreased after device implantation. No coronary impingement was noted and surgery confirmed good device position, without complications (18). Larger studies are needed to fully appreciate the strengths and limitations of the PS³ system.

Percutaneous aortic valve procedures

Balloon-expanding valve: Cribier-Edwards Valve After extensive testing in animal models (21) and a successful first-in-man experience (22), a single center Phase 1 project was started in 2003 for compassionate use of the Cribier-Edwards valve in patients with end-stage AS (24,36). These patients had been formally evaluated by two cardiothoracic surgeons and deemed to be unsuitable for surgical AV replacement. Thirty-six patients were enrolled in the Initial Registry of Endovascular Implantation of Valves in Europe (I-REVIVE) trial which was followed by the Registry of Endovascular Critical Aortic Stenosis Treatment (RECAST) trial (36). Twenty seven of these patients underwent successful percutaneous AV implantation without coronary

occlusion or disruption of MV architecture. Of these, antegrade approach was successful in 85% (23 of 26 patients) and retrograde approach in 57% (4 of 7 patients). The noteworthy procedural limitations were prosthesis migration/embolization, failure to cross the stenotic AV and para-valvular aortic regurgitation. Anatomic and functional success was obtained as evidenced by an improvement in aortic valve area (AVA) from $0.60 \pm 0.11 \text{ cm}^2$ to $1.70 \pm 0.10 \text{ cm}^2$ ($p < 0.001$), an increase in left ventricular ejection fraction (from $45 \pm 18\%$ to $53 \pm 14\%$, $p < 0.05$), and an improved NYHA functional class (from IV to I-II in over 90% of patients). Importantly, the improvement in AVA and mean aortic gradient was maintained at 24 months and the maximum improvement in left ventricular ejection fraction was observed in patients with depressed systolic function at baseline. The 30-day mortality was 22% (6 of 27 patients). Eleven patients were alive at nine months follow-up, and no device related deaths occurred up to 26 months after implantation (36).

In their first cohort, Webb et al. successfully implanted the Cribier-Edwards valve in 14 of 18 patients who had previously been deemed unsuitable for surgical valve replacement (25). The AVA increased from 0.6 ± 0.2 to $1.6 \pm 0.4 \text{ cm}^2$ ($p < 0.001$), and remained stable at one month follow-up. The early mortality was 11% (2 of 18) and short-term survival was 89% (16 of 18) at a mean of 75 days follow-up (25). The same group subsequently reported both short- and mid-term outcomes in an extended cohort of 50 patients who underwent percutaneous Cribier-Edwards valve implantation via a retrograde approach (26). Valve implantation was successful in 43 patients (86%) and the reasons for procedural failure were similar to those previously reported (36). The main difference was in the frequency of the vascular complications with the retrograde approach. In 43 patients who had successful implant, the 30-day mortality was 12% (5 of 43 patients) compared to expected mortality of 28% according to the logistic EuroScore. Of interest, there was a clear dichotomy in both procedural success and 30-day mortality, representing the learning curve. Procedural success increased from 76% in the first 25 patients to 96% in the second 25, and 30-day mortality fell from 16% to 8%. Importantly, no patients needed open heart surgery in the first 30 days. There were no subsequent deaths and at median follow-up of 359 days, 81% of the patients who underwent successful transcatheter AV replacement were alive. Additionally, there was a significant improvement in AVA and NYHA functional class (Figure 8) with durability of these parameters at one-year follow-up (26).

In addition, the feasibility of transapical implantation of the Cribier-Edwards valve has been shown. Lichtenstein et al. successfully implanted the valve in seven patients unsuitable for open heart surgery and for percutaneous transfemoral AV implantation, secondary to severe aorto-iliac disease (27). This was a very high-risk elderly population (mean age 77 ± 9 years) with poor functional class (mean NYHA III) and high logistic EuroScore (mean $35 \pm 26\%$). After implantation, the AVA increased from $0.7 \pm 0.1 \text{ cm}^2$ to $1.8 \pm 0.8 \text{ cm}^2$ and the mean AV gradient decreased from 31 ± 10 to $9 \pm 6 \text{ mmHg}$. These parameters remained stable up to six months after implantation and four of the seven patients were alive after six months (27).

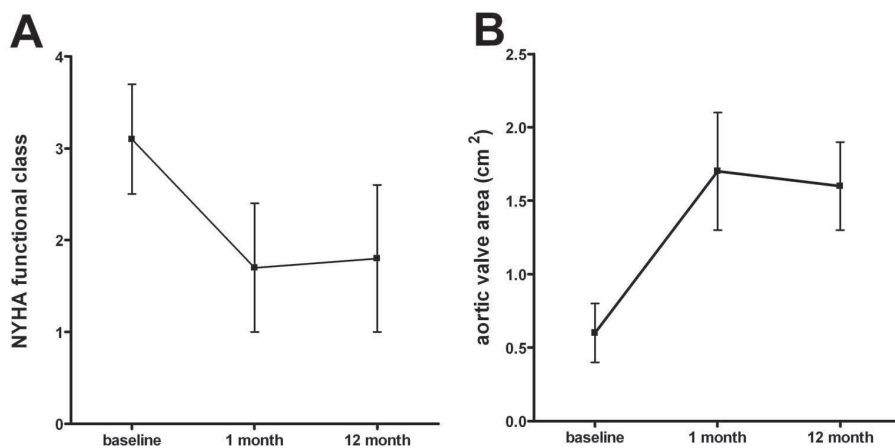


Figure 8. In 50 patients undergoing percutaneous AV replacement, a significant improvement in NYHA functional class was observed after 1 month (from 3.1 ± 0.6 to 1.7 ± 0.7 , $p < 0.001$). This improvement was maintained after 12 months follow-up (panel A). Similarly, aortic valve area significantly improved after 1 month (from 0.6 ± 0.2 to 1.7 ± 0.4 , $p < 0.001$) and 12 months follow-up (panel B).

In another recent study, Walther et al. successfully used the transapical approach for implantation of the prosthesis in 55 of 59 (93.2%) elderly patients (mean age 81 ± 6 years) with a poor functional class (NYHA III-IV), high mean logistic EuroScore ($27 \pm 14\%$), and severe calcified AS (mean AVA 0.5 ± 0.2 cm²) (37). After successful implantation, echocardiography revealed good valve function (mean AV gradient 9 ± 6 mmHg) with minor paravalvular leakage in 17 patients. At a mean follow-up of 110 ± 77 days (range 1 - 255 days) 78% of the patients were alive. It is evident from these series that device and technique related shortcomings can be readily addressed and to date over 500 Edwards percutaneous valves have been deployed worldwide, with high technical success. Importantly, use of the larger valve (26 mm) seems to be related to less para-valvular aortic regurgitation.

Balloon-expanding valve: Edwards SAPIEN valve Initial results of the feasibility trial in the United States were presented at the 2007 TCT meeting (38). In this series, retrograde delivery was successful in 47 of 54 patients (87%). The intent-to-treat analysis of all 54 patients showed a 30-day mortality of 7.4% with a 30-day major adverse cardiac events rate of 16.7%. After this initial feasibility trial, a pivotal randomized multi-center trial, entitled PARTNER (Placement of AoRTic tranScathetER valves) has been started in North America and Europe and is projected to complete enrollment by the end of 2008 (Table 3). This prospective randomized clinical trial will enroll 600 patients in 2 separate treatment arms. The surgical arm of the trial is comparing the SAPIEN valve to standard surgical AV replacement in 350 patients, with the objective of demonstrating non-inferiority. The medical management arm of the trial will compare the SAPIEN valve to appropriate medical therapy (including balloon valvuloplasty) in 250 patients who are considered too high risk for conventional open heart surgery, with the objective of demonstrating superiority of the SAPIEN valve. The primary endpoint in both arms of the trial is

mortality at one year with secondary endpoints that focus on long-term adverse cardiovascular events composite, valve performance and quality-of-life indicators.

Self-expanding valve: CoreValve In 2005, the CoreValve aortic prosthesis was first implanted in a patient. The subject was a 73-year old woman with severe calcified AS, NYHA class IV heart failure and reduced left ventricular systolic function who was declined surgical AV replacement because of extensive co-morbidity (39). At two weeks follow-up her initial hemodynamic improvement persisted and she improved to NYHA class II.

Subsequently, Grube et al. have reported significant advancement in the CoreValve ReValving system from first-generation to third-generation (28,29). In the pilot study, 25 patients underwent CoreValve implantation under general anesthesia with extracorporeal support (extracorporeal percutaneous femoro-femoral bypass) using the retrograde approach via a surgical arterial cut-down (28). These patients had been deemed unsuitable for open heart surgery by a cardiologist and cardiovascular surgeon. Only first- and second-generation devices were used in the pilot study. The patient cohort was elderly (mean age 80 ± 5 years) with NYHA class III-IV (96%), a mean AVA of 0.72 ± 0.13 cm², and a median logistic EuroScore of 11%. Acute procedural success was achieved in 21 of 25 patients (84%) with a reduction in mean AV gradient, and a functional improvement in NYHA class at 30-days follow-up (Figure 9). Interestingly at 30-days follow-up, 17 of 18 patients (94%) had none or only mild aortic regurgitation. Procedural limitations and complications were similar to the Cribier-Edwards valve. Major in-hospital cardiovascular and cerebral events occurred in 8 patients (32%) whereas major bleeding occurred in 5 of 10 patients (50%) treated with the first-generation device and in 1 of 15 patients (7%) treated with the second-generation prosthesis. Among 18 patients with device success (82%), no further adverse events occurred within 30 days after hospital discharge (28).

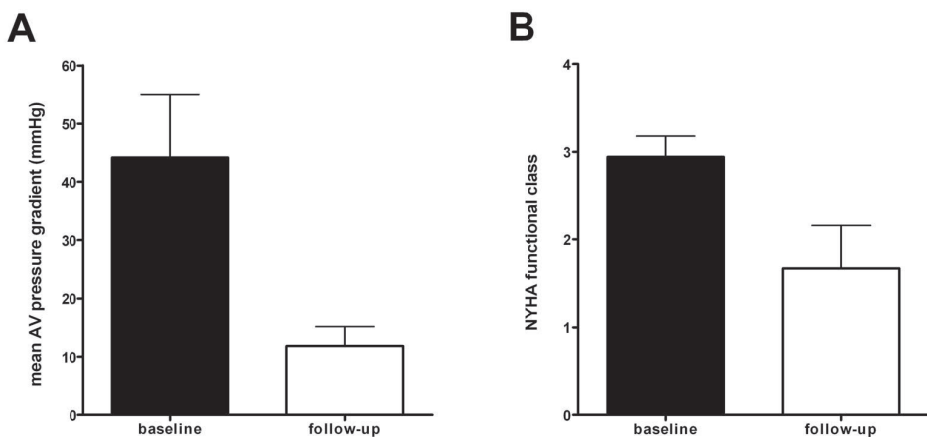


Figure 9. After percutaneous implantation of the CoreValve prosthesis, a significant improvement of mean AV pressure gradient (panel A) and NYHA class (panel B) was observed. Mean AV pressure gradient decreased from 44.2 ± 10.8 to 11.8 ± 3.4 mmHg ($p < 0.001$) and NYHA class decreased from 2.9 ± 0.2 to 1.7 ± 0.5 ($p < 0.001$) after 30 days of follow-up.

In the second series, the CoreValve was implanted in 50 and 36 patients using second- and third-generation devices, respectively (29). The study population included elderly patients (mean age 82 ± 6 years) with a poor functional class (83% NYHA class III-IV), high logistic EuroScore (22%), and severe calcified AS. Acute device success, which was similar in both groups, was achieved in 76 of 86 (88%) patients. After implantation the mean AVA increased significantly (from $0.60 \pm 0.16 \text{ cm}^2$ to $1.67 \pm 0.41 \text{ cm}^2$, $p < 0.05$) along with an improvement in NYHA functional class (from 2.85 ± 0.73 to 1.85 ± 0.60 , $p < 0.001$). Peri-procedural rate of death, stroke, and myocardial infarction was 14%. Overall 30-day mortality rate was 12%, while the combined rate of death, stroke, and myocardial infarction was 22%. Impressively, in patients with device and procedural success, the mortality was 9% and 5%, respectively.

Valve-in-valve concept While the experience with percutaneous AV procedures increases rapidly, a new concept has emerged also. Recently, the feasibility of a 'valve-in-valve' model has been reported for replacement of a aortic and mitral valve xenograft (40). Walther et al. implanted conventional aortic and mitral valve prostheses (23 or 25-mm Carpentier Edwards) in seven pigs. Subsequently, a transapical puncture was performed for positioning of the repeat 23 mm transcatheter valve (Edwards SAPIEN). All transcatheter 'valve-in-valve' implantations were performed successfully and good valve function was demonstrated after the procedure.

Recently, Grube and coworkers reported the first use of the CoreValve to treat severe aortic regurgitation of a degenerated aortic bioprosthesis in an 80-year old man with extensive comorbidity and a logistic EuroScore of 36% (41). The insertion of the percutaneous AV using the CoreValve resulted in a complete resolution of severe, symptomatic aortic regurgitation of the seven-year old aortic bio-prosthesis placed by open heart surgery for severe calcified AS. After one year follow-up, the patient is still free of symptoms with good 'valve-in-valve' prosthesis function (no aortic regurgitation, mean gradient 12 mmHg) (41).

The 'valve-in-valve' concept is of particular interest since re-operation for degenerated xenografts may be challenging. The mortality risk for re-operation is significantly higher than for first isolated aortic valve replacement (42). Performing a percutaneous procedure when the initial AV xenograft has failed does not require re-sternotomy, cardiopulmonary bypass or cardioplegic arrest and thus has the potential for a lower morbidity and mortality rate. The initial results of the 'valve-in-valve concept' in animal models and in humans are promising.

PERFORMING PERCUTANEOUS VALVE PROCEDURES

In percutaneous valve therapy, both careful selection of potential candidates and thorough follow-up after the procedure are of critical importance. In the following paragraphs, the selection of patients, procedural issues and strategies for follow-up are discussed.

Selection of patients

The success of percutaneous valve procedures depends heavily upon appropriate selection of patients for a particular device. Both for percutaneous MV and AV procedures, a comprehensive assessment of valve pathology, vascular access and co-morbidity are critical for patient selection.

Percutaneous mitral procedures Mitral regurgitation can result from many different anatomical and functional aberrations of the MV, mainly related to annulus dilatation, leaflet prolapse or restricted leaflet motion. While percutaneous leaflet edge-to-edge repair is appropriate for patients with MR related to leaflet prolapse, the percutaneous coronary sinus mitral annuloplasty is more suitable for patients with mitral annulus dilatation (43). Therefore, anatomical selection of patients for percutaneous MV procedures is directly dependent on the echocardiographic analysis including the mechanism of MR, leaflet size, coaptation height, annular dimension and severity of prolapse (44). In addition, for percutaneous coronary sinus annuloplasty, proper imaging to define the proximity of the coronary sinus to the mitral annulus and the left circumflex coronary artery is mandatory (13).

Percutaneous aortic valve procedures In general, the selection of patients for percutaneous aortic valve procedures includes several issues. The severity and prognosis of the AS should be assessed first. Afterwards, the presence of co-morbidity and surgical risk should be thoroughly investigated. If the patient is no surgical candidate, the feasibility of a percutaneous AV procedure should be evaluated, including assessment of vascular access.

A comprehensive assessment of the patient's surgical risk with input from cardiologists, cardiac surgeons and cardiac anesthesiologists is crucial in the selection of potential candidates. The initial feasibility experience of percutaneous AV replacement was appropriately restricted to patients that were deemed not to be candidates for surgical AV replacement (22,25). However, in the ongoing PARTNER trial (Table 3) patients with STS score >10 are randomized between surgical or percutaneous AV replacement (group A). Most of these patients have a high estimated surgical risk based on age, previous cardiac surgery, renal failure, cerebrovascular disease and pulmonary disease. On the other hand, patients with estimated surgical mortality of more than 15% that are deemed inoperable by two surgeons with experience in performing high risk AV replacement are randomized between percutaneous AV replacement or no AV replacement in Group B (Table 3). Many of these patients have co-morbidities including severe chronic obstructive pulmonary disease or anatomical challenges to surgery such as porcelain aorta, cardiac chambers or grafts adherent to the sternum. Careful selection and a thorough clinical evaluation for the assessment of the surgical risk are therefore essential in these patients.

Extensive calcifications and tortuosity of the femoral artery and aorta may hamper positioning of the AV prosthesis. In patients with limited vascular access, a transapical approach should

be considered (27). Careful screening of vascular access is therefore important in patients referred for percutaneous AV replacement.

Procedure-related issues

The majority of the technical issues are related to vascular access, transeptal puncture, device positioning and deployment.

Vascular access The vascular access for percutaneous valve procedures may be challenging since catheters are often large: mitral balloon valvuloplasty or implantation of a coronary sinus device typically requires a 12F venous sheath (external diameter ~5 mm) (11). In contrast, percutaneous AV implantation may require a sheath as large as 24F (external diameter ~9 mm) (26). Insertion of such a large sheath is associated with a significant potential for vascular injury including bleeding, dissection, occlusion and perforation. In 50 high-risk patients undergoing percutaneous AV replacement through the femoral artery, vascular injury occurred in 4 patients (8%) (26). However, vascular access techniques, equipment and pre-procedural screening may reduce this number.

Transeptal puncture Many percutaneous valve procedures, including mitral valvuloplasty, paravalvular leak closure and antegrade aortic valvuloplasty or valve implantation, require a transeptal puncture to access the left atrium. Puncture of the interatrial septum is associated with a risk of pericardial bleeding and tamponade and may result in residual interatrial shunts. By visualizing the interatrial septum and the transeptal puncture needle, intracardiac echocardiography is helpful in performing transeptal punctures safely and at precisely the desired locations (45).

Device positioning and deployment In general, a clear learning curve for performing percutaneous valve procedures is present (26,30). During the procedure, various problems can be encountered while positioning and deploying the device. For all procedures, passage of bulky therapeutic catheters through the cardiac chambers, particularly in compromised patients can result in cardiac perforation or provoke arrhythmias, ranging from atrial to ventricular fibrillation.

In percutaneous edge-to-edge leaflet repair, inappropriate device positioning may result in partial clip detachment (30) and should be monitored carefully. In case of unsuccessful percutaneous mitral edge-to-edge repair, surgical repair may be needed (30). During percutaneous mitral annuloplasty, acute ischemia due to left circumflex coronary artery impingement can be encountered (13). A paravalvular plug may interfere with mechanical valve leaflets or may become dislodged and embolize requiring a complex percutaneous snaring procedure or even unplanned surgery (7).

In percutaneous AV replacement, technical errors can result in a percutaneous AV being implanted within the ventricle or aorta (36). In addition, percutaneous aortic valvuloplasty or

AV replacement may cause injury to adjacent conducting tissue and transient or sustained atrioventricular heart block requiring ventricular pacing. Finally, coronary occlusion may occur if a bulky native leaflet is displaced over a coronary ostium (25).

Follow-up

With the exception of valvuloplasty, little is known on late implications of percutaneous valve procedures. A careful follow-up of patients after percutaneous valve procedures is mandatory to assess prosthesis function and the presence of residual regurgitation or paravalvular leakage.

Prosthesis function should be monitored since device fatigue may result in late stent fracture, as has been common with first-generation pulmonary valve implants (46). In the initial feasibility study using the coronary sinus annuloplasty for MR, separation of the nitinol bridge segment occurred without any adverse clinical events (11). Regular follow-up on prosthesis function is therefore mandatory.

Furthermore, residual regurgitation, paravalvular leakage or failure of the bioprosthetic valve may require additional interventions. In a large cohort of 86 patients treated with the CoreValve for AS, two patients required an implantation of a second prosthesis (valve-in-valve) due to severe residual regurgitation (29).

Finally, percutaneous implants may have unexpected implications, such as thromboembolism and infection. In addition, the durability of percutaneous valves is currently unknown. Therefore, close follow-up of patients after a percutaneous valve procedure is warranted. In the reported and the ongoing trials on percutaneous valves, an extensive echocardiogram is typically performed for the assessment of prosthesis function and presence of residual regurgitation or paravalvular leakage.

THE ROLE OF IMAGING IN PERCUTANEOUS VALVE PROCEDURES

Accurate visualization of the native valve, the prosthesis or device and their relationship is crucial before, during and after the percutaneous valve procedure. An overview on the role of various imaging modalities in percutaneous valve procedures is provided in Table 4. Several imaging modalities are available including echocardiography (transthoracic, transesophageal and intracardiac), multi-slice computed tomography (MSCT), magnetic resonance imaging (MRI) and fluoroscopy. Whereas transthoracic echocardiography, MSCT and MRI are valuable imaging techniques before and after the procedure, transesophageal and intracardiac echocardiography are mainly used during the percutaneous valve procedure.

Before percutaneous valve procedures

Selection of potential candidates and procedural risk assessment are crucial issues before percutaneous valve procedures. The various imaging modalities are important for the assessment

Table 4. The role of imaging modalities in percutaneous valve procedures

Imaging modality	Before percutaneous valve procedure	During percutaneous valve procedure	Follow-up	General comment
Echocardiography, transthoracic (TTE)	Assessment of valve morphology Quantification of severity of valve disease	---	Assessment of prosthesis function Detection of complications	
Echocardiography, transesophageal (TEE)	Assessment of valve morphology* Quantification of severity of valve disease*	Facilitating transseptal puncture Prosthesis sizing Prosthesis positioning Detection of complications	Assessment of prosthesis function* Detection of complications*	Mainly used peri-operatively
Echocardiography, intracardiac (ICE)	---	Facilitating transseptal puncture Prosthesis positioning Detection of complications	---	Only used peri-operatively
Fluoroscopy	Assessment of vascular access †	Prosthesis sizing Prosthesis positioning Detection of complications	---	Mainly used peri-operatively
Multi-slice Computed Tomography	Assessment of vascular access † Assessment of valve morphology Assessment of surrounding structures ‡	---	Assessment of prosthesis position/morphology	Mainly used pre-operatively
Magnetic Resonance Imaging	Assessment of vascular access † Assessment of valve morphology Assessment of surrounding structures ‡	---	---	Mainly used pre-operatively

* Recommended if TTE quality is not sufficient. † In particular for retrograde aortic valve implantation. ‡ For example, relation between coronary sinus and circumflex coronary artery/ mitral annulus in percutaneous mitral annuloplasty.

of valve morphology, quantification of the severity of valvular disease and assessment of vascular access and surrounding structures.

For the assessment of both mitral and aortic valve morphology and the quantification of the severity of valve disease, a routine transthoracic echocardiogram (Figure 10) is typically performed (1,2). However in case of suboptimal image quality of transthoracic echocardiography, transesophageal echocardiography may be needed. In addition, recent studies have demonstrated that MSCT and MRI can also provide detailed information on valve morphology and function. Good correlations between MSCT and echocardiography for the assessment of

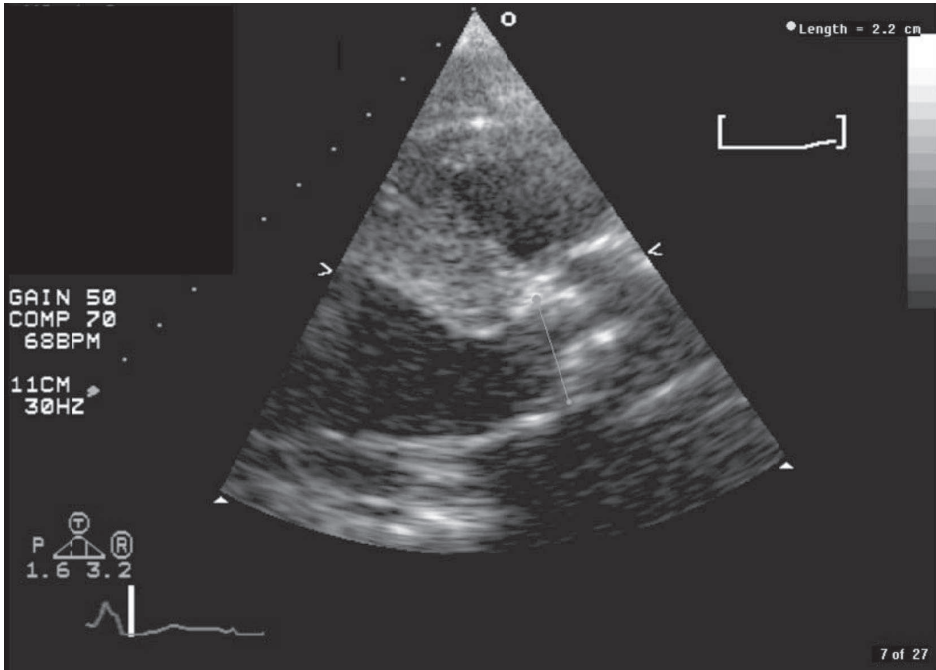


Figure 10. Transcatheter aortic valve implantation requires non-invasive estimation of the size of the annulus. One method is to estimate the diameter of the aortic annulus from a transthoracic long axis echocardiogram. Typically the measurement is made at the ventricular aspect of the leaflet insertion.

valve morphology and valve area have been reported (47). Finally, assessment of specific surrounding structures, such as coronary arteries, is important before percutaneous MV and AV procedures.

Percutaneous mitral valve procedures For coronary sinus annuloplasty in patients with MR, assessment of coronary sinus anatomy is of critical importance (Figure 11). Particularly, the relation with the MV annulus and the left circumflex coronary artery should be explored. The close relationship between the coronary sinus and the circumflex coronary artery (48) may explain the impingement of the coronary artery described in the first animal studies (13). With the use of MSCT, this relation can be assessed non-invasively before the mitral annuloplasty procedure (49,50). In a recent study, the relation between the coronary sinus and the circumflex coronary artery was assessed in 105 patients, including 34 patients with heart failure and/or severe MR. It was noted that the circumflex artery coursed between the coronary sinus and the MV annulus in almost 70% of the patients, with a minimal distance of 1.3 ± 1.0 mm between the two structures (49). In addition, a broad variation in minimal distance between the coronary sinus and the mitral annulus was noted (Figure 12). Performing a percutaneous mitral annuloplasty may not be feasible if the coronary sinus courses along the left atrial posterior wall rather than along

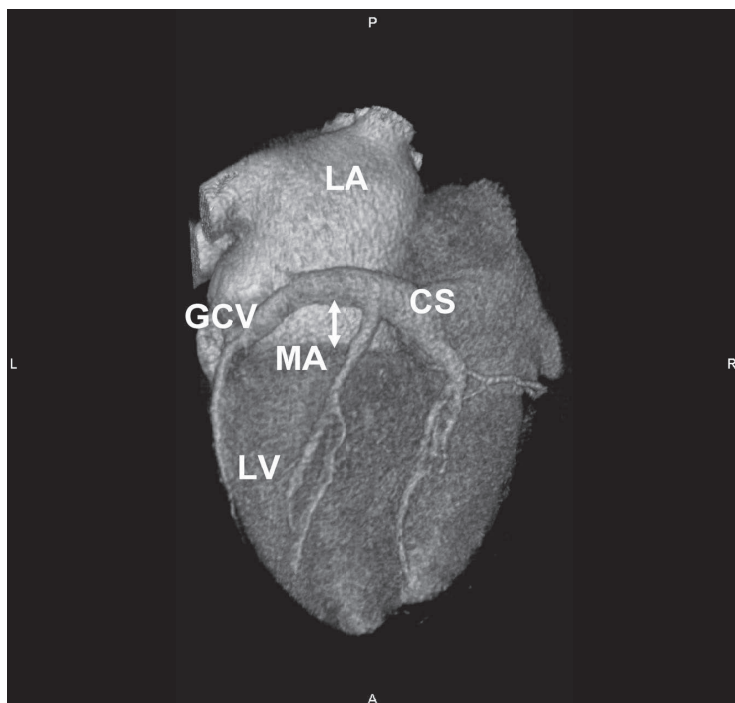


Figure 11. Three-dimensional volume-rendered reconstruction of a 64-slice MSCT scan demonstrating the relationship between the coronary sinus (CS) and the mitral annulus (MA). In this patient, the CS coursed along the left atrial (LA) posterior wall, rather than along the MA, as indicated by the white arrow. Percutaneous mitral valve annuloplasty via the coronary sinus may not be feasible in these patients. GCV = great cardiac vein; LV = left ventricle.

the mitral annulus. By visualizing the coronary sinus and other relevant structures, MSCT may help in the selection of patients for percutaneous mitral annuloplasty.

Percutaneous aortic valve procedures Before percutaneous AV procedures, vascular access should be screened. The calcifications and tortuosity of the aorta and femoral arteries should be evaluated, since this has important implications for the delivery of the prosthesis (transarterial vs. transapical). Conventional angiography, MSCT and MRI are available for the assessment of vascular access.

In addition, the extent and location of AV calcifications can be accurately assessed with MSCT. An example of a heavily calcified AV is shown in Figure 13. In addition, MSCT enables accurate assessment of the diameter of the aortic annulus, necessary for correct prosthesis sizing. Finally, the relation between the aortic annulus and the ostium of the left coronary leaflet can be visualized with MSCT (51). This may be important since occlusion of the coronary ostium has been reported as a serious complication of percutaneous AV replacement (25).

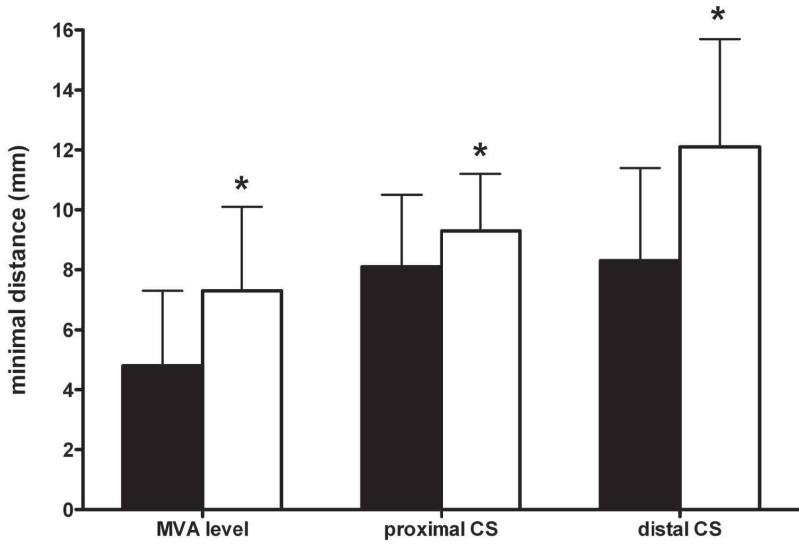


Figure 12. With the use of MSCT, the minimal distance between the coronary sinus (CS) and the mitral valve annulus (MVA) was assessed. In 90 patients without severe MR (black bars) and in 15 patients with severe MR (white bars), the distance was assessed at three different levels (MVA level, proximal CS, distal CS). In the patients with severe MR, the distance between the CS and the MVA was significantly greater compared to the patients without severe MR at all levels. The greater distance between the CS and MVA may hamper the use of percutaneous mitral annuloplasty. * = $p < 0.05$.

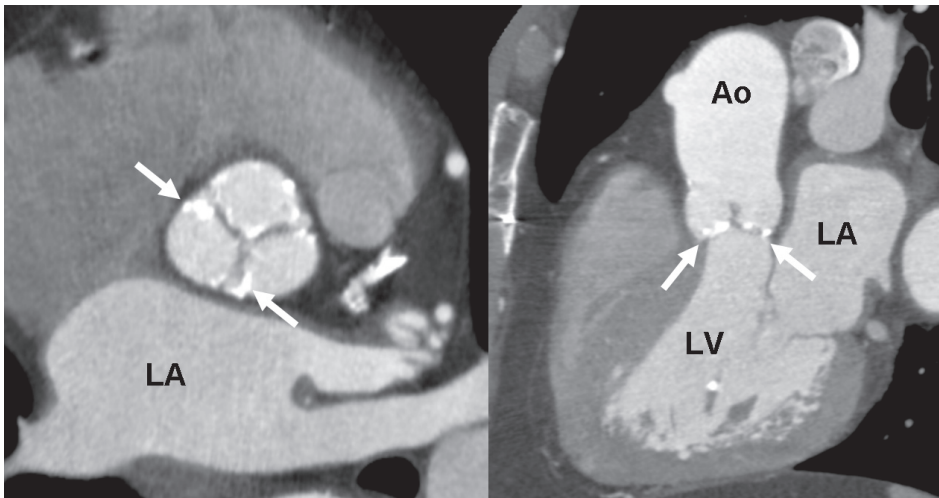


Figure 13. Multi-slice computed tomography images demonstrating a heavily calcified AV in a patient referred for percutaneous AV implantation. The left panel shows a short-axis reconstruction of the AV, indicating the calcifications on all leaflets (white arrows). In the right panel, the reconstructed sagittal view (similar to a parasternal long-axis view on transthoracic echocardiography) clearly demonstrates the extent and location of the calcifications. Ao = aorta; LA = left atrium; LV = left ventricle.

Procedure-related issues

During percutaneous valve procedures, performing a transseptal puncture, positioning and deployment of the device are all critical processes and can be guided by various imaging modalities. Fluoroscopy remains the technique of choice, although it does not permit visualization of cardiac soft-tissue structures and for patient and physician safety the radiation burden should be kept to a minimum. Therefore, both transesophageal and intracardiac echocardiography have been used during AV (25,26,28,37) and MV (17,18,33,35) procedures in addition to fluoroscopy.

Transesophageal and intracardiac echocardiography are valuable techniques for performing transseptal procedures (45). Accurate real-time visualization of the interatrial septum and the transseptal puncture needle may greatly facilitate safe and accurate transseptal punctures.

The positioning and deployment of the prosthesis are the most important processes during percutaneous valve procedures. Using fluoroscopy (and contrast agents if needed) the relationship between the native valve and the prosthesis can be well visualized. An example of coronary sinus assessment with the use of fluoroscopy during a percutaneous MV procedure is shown in Figure 14. In addition to fluoroscopy, transesophageal and intracardiac echocardiography can facilitate percutaneous valve procedures. In an animal model of percutaneous edge-to-edge repair, Naqvi et al. demonstrated that intracardiac echocardiography can accurately visualize

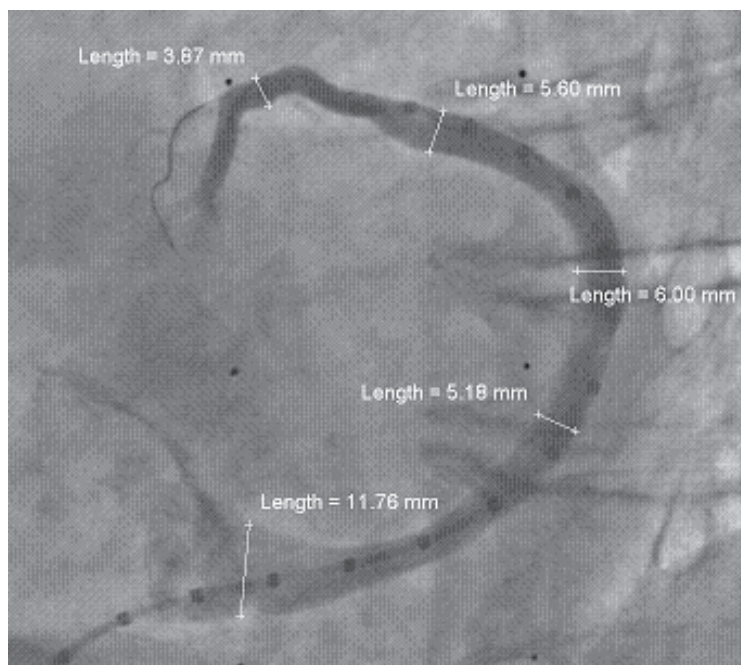


Figure 14. Assessment of the coronary sinus prior to MV annuloplasty in a patient with severe MR. The coronary sinus has been cannulated from the femoral vein with a calibrated angiographic catheter. Contrast injection allows visualization of the coronary sinus and calibration using the radiopaque 1 cm markers on the catheter allow estimation of diameter and length of the coronary veins.

the MV apparatus, guide the deployment of the leaflet suture and confirm a double orifice mitral valve (52).

Furthermore, transesophageal echocardiography is useful for the positioning of the percutaneous valve devices (Figure 2). In the EVEREST-I trial, a standardized protocol for transesophageal echocardiography was implemented during the course of the trial (53). It was noted that the use of a standardized imaging protocol reduced the median 'device time' (defined as the time from the initial insertion of the guiding catheter to the final removal of the clip delivery system) from 198 to 132 minutes. It was concluded that transesophageal echocardiography is essential for guiding percutaneous edge-to-edge repair (53). Recently, real-time three-dimensional transesophageal echocardiography has been introduced. The three-dimensional aspect of this technique may further facilitate percutaneous valve procedures. However, experience is currently limited and more studies are needed to assess the relative merit of this new technique.

Follow-up

After a percutaneous valve procedure careful follow-up of the patient is essential. In particular, assessment of prosthesis function and position, and the presence of residual regurgitation or paravalvular leakage are important during follow-up. Transthoracic echocardiography is the primary imaging modality for all these issues. An example of transthoracic echocardiography in a patient with severe MR undergoing percutaneous edge-to-edge repair with the use of MitraClip is shown in Figure 15. Transthoracic echocardiography allows serial and quantitative assessment of prosthesis function and the presence of residual regurgitation or paravalvular leakage (54). In the EVEREST-I trial it has been demonstrated that it is feasible to use quantitative parameters systematically for the follow-up of MR in patients undergoing percutaneous edge-to-edge repair using transthoracic echocardiography (55).

For exact assessment of the position of the prosthesis, and its relation with surrounding structures, MSCT may be preferred over transthoracic echocardiography. Due to the high spatial resolution, MSCT enables a detailed evaluation of the prosthesis position in relation to the native valve and surrounding structures (11). An example of a patient with a percutaneous

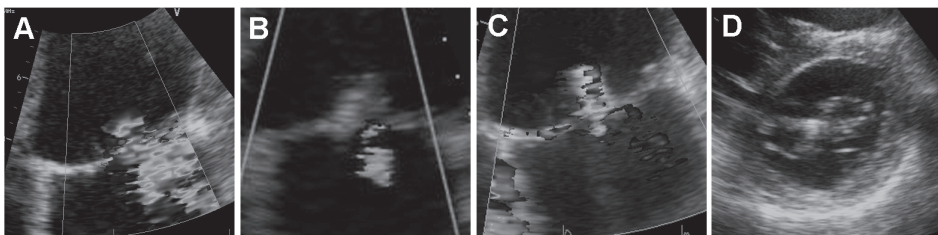


Figure 15. Transthoracic echocardiograms from a patient undergoing percutaneous edge-to-edge repair with the use of a MitraClip device. Severe MR is present at baseline (panel A). After placement of the MitraClip device there is immediate reduction in MR (panel B) with continued success on 2-year follow-up (panel C). Double barrel mitral orifice is seen on the short axis view (panel D).

AV, assessed with MSCT is shown in Figure 16. Although the radiation exposure of MSCT is significant and should always be considered, it may be the best imaging modality to visualize the exact prosthesis morphology and location.

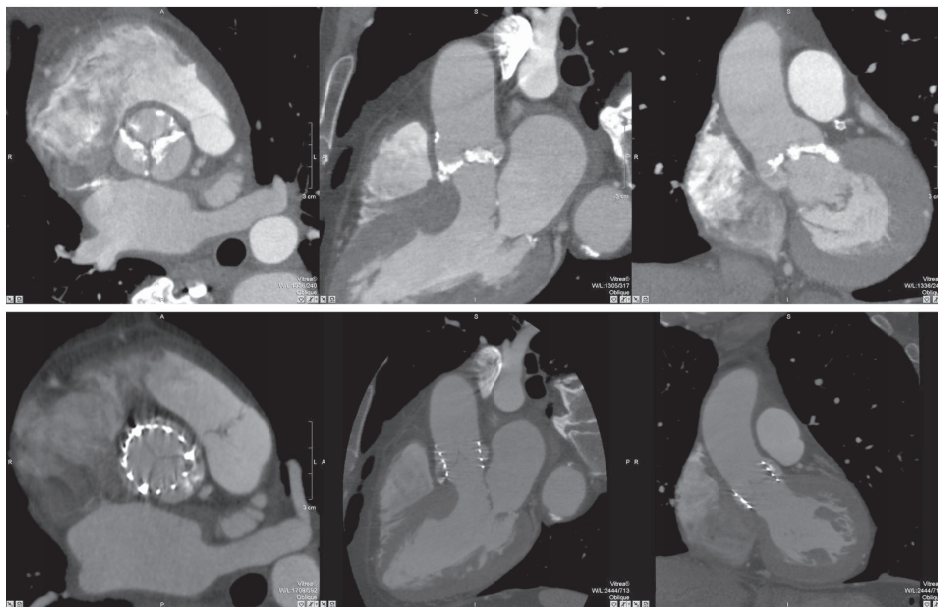


Figure 16. Multi-slice computed tomography of the aortic valve (AV) in a patient referred for percutaneous AV replacement, in an axial (left panel), sagittal (middle panel) and coronal view (right panel). In the upper panel the extensive calcifications of the native AV are well visualized. The lower panel clearly demonstrates the location of the AV prosthesis (Edwards SAPIEN valve).

CONCLUSIONS

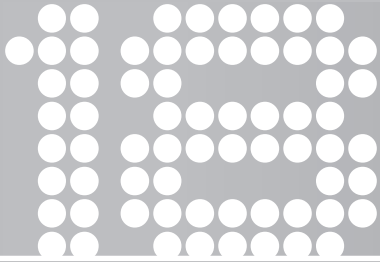
Percutaneous aortic and mitral valve procedures are promising strategies in the treatment of patients with valvular heart disease. Both for AS and MR, different procedures have demonstrated their feasibility and safety in animal and human studies. Several clinical trials, including randomized trials between surgical and percutaneous treatment, are currently performed. The results of these trials will demonstrate the precise value of percutaneous valve procedures in patients with severe valvular heart disease, unsuitable for surgical treatment. Careful selection and screening of patients is crucial for percutaneous valve procedures. Different imaging modalities are available for the selection of patients for percutaneous valve procedures. In addition, performing the actual procedure may be greatly facilitated by implementation of various imaging techniques. At present, only short-term results are available and therefore a careful follow-up of the patients after percutaneous valve procedures is mandatory.

REFERENCES

1. Vahanian A, Baumgartner H, Bax J et al. Guidelines on the management of valvular heart disease. *Eur Heart J* 2007;28:230-68.
2. Bonow RO, Carabello BA, Kanu C et al. ACC/AHA 2006 guidelines for the management of patients with valvular heart disease. *Circulation* 2006;114:e84-231.
3. Iung B, Baron G, Butchart EG et al. A prospective survey of patients with valvular heart disease in Europe: The Euro Heart Survey on Valvular Heart Disease. *Eur Heart J* 2003;24:1231-43.
4. Vassiliades TA, Jr., Block PC, Cohn LH et al. The clinical development of percutaneous heart valve technology. *J Am Coll Cardiol* 2005;45:1554-60.
5. Farhat MB, Ayari M, Maatouk F et al. Percutaneous balloon versus surgical closed and open mitral commissurotomy : seven-year follow-up results of a randomized trial. *Circulation* 1998;97:245-50.
6. Feldman T. Core curriculum for interventional cardiology: percutaneous valvuloplasty. *Catheter Cardiovasc Interv* 2003;60:48-56.
7. Pate GE, Al Zubaidi A, Chandavimol M, Thompson CR, Munt BI, Webb JG. Percutaneous closure of prosthetic paravalvular leaks: case series and review. *Catheter Cardiovasc Interv* 2006;68:528-33.
8. Alfieri O, De Bonis M, Lapenna E et al. "Edge-to-edge" repair for anterior mitral leaflet prolapse. *Semin Thorac Cardiovasc Surg* 2004;16:182-7.
9. St Goar FG, Fann JI, Komtebedde J et al. Endovascular edge-to-edge mitral valve repair: short-term results in a porcine model. *Circulation* 2003;108:1990-3.
10. Naqvi TZ, Buchbinder M, Zarbatany D et al. Beating-heart percutaneous mitral valve repair using a transcatheter endovascular suturing device in an animal model. *Catheter Cardiovasc Interv* 2007;69:525-31.
11. Webb JG, Harnek J, Munt BI et al. Percutaneous transvenous mitral annuloplasty: initial human experience with device implantation in the coronary sinus. *Circulation* 2006;113:851-5.
12. Liddicoat JR, Mac Neill BD, Gillinov AM et al. Percutaneous mitral valve repair: a feasibility study in an ovine model of acute ischemic mitral regurgitation. *Catheter Cardiovasc Interv* 2003;60:410-6.
13. Mani CV, Patel JB, Reuter DG et al. Acute and chronic reduction of functional mitral regurgitation in experimental heart failure by percutaneous mitral annuloplasty. *J Am Coll Cardiol* 2004;44:1652-61.
14. Fukamachi K, Inoue M, Popovic ZB et al. Off-pump mitral valve repair using the Coapsys device: a pilot study in a pacing-induced mitral regurgitation model. *Ann Thorac Surg* 2004;77:688-92.
15. Mishra YK, Mittal S, Jaguri P, Trehan N. Coapsys mitral annuloplasty for chronic functional ischemic mitral regurgitation: 1-year results. *Ann Thorac Surg* 2006;81:42-6.
16. Pedersen WR, Block P, Feldman T. The iCoapsys Repair System for the percutaneous treatment of functional mitral insufficiency. *EuroIntervention* 2007;1:A44-A48.
17. Rogers JH, Macoviak JA, Rahdert DA, Takeda PA, Palacios IF, Low RI. Percutaneous septal sinus shortening: a novel procedure for the treatment of functional mitral regurgitation. *Circulation* 2006;113:2329-34.
18. Palacios IF, Condado JA, Brandi S et al. Safety and feasibility of acute percutaneous septal sinus shortening: first-in-human experience. *Catheter Cardiovasc Interv* 2007;69:513-8.
19. Cribier A, Savin T, Saoudi N, Rocha P, Berland J, Letac B. Percutaneous transluminal valvuloplasty of acquired aortic stenosis in elderly patients: an alternative to valve replacement? *Lancet* 1986;1:63-7.
20. Otto CM, Mickel MC, Kennedy JW et al. Three-year outcome after balloon aortic valvuloplasty. Insights into prognosis of valvular aortic stenosis. *Circulation* 1994;89:642-50.
21. Andersen HR, Knudsen LL, Hasenkam JM. Transluminal implantation of artificial heart valves. Description of a new expandable aortic valve and initial results with implantation by catheter technique in closed chest pigs. *Eur Heart J* 1992;13:704-8.
22. Cribier A, Eltchaninoff H, Bash A et al. Percutaneous transcatheter implantation of an aortic valve prosthesis for calcific aortic stenosis: first human case description. *Circulation* 2002;106:3006-8.

23. Webb JG, Pasupati S, Achem L, Thompson CR. Rapid pacing to facilitate transcatheter prosthetic heart valve implantation. *Catheter Cardiovasc Interv* 2006;68:199-204.
24. Cribier A, Eltchaninoff H, Tron C et al. Early experience with percutaneous transcatheter implantation of heart valve prosthesis for the treatment of end-stage inoperable patients with calcific aortic stenosis. *J Am Coll Cardiol* 2004;43:698-703.
25. Webb JG, Chandavimol M, Thompson CR et al. Percutaneous aortic valve implantation retrograde from the femoral artery. *Circulation* 2006;113:842-50.
26. Webb JG, Pasupati S, Humphries K et al. Percutaneous transarterial aortic valve replacement in selected high-risk patients with aortic stenosis. *Circulation* 2007;116:755-63.
27. Lichtenstein SV, Cheung A, Ye J et al. Transapical transcatheter aortic valve implantation in humans: initial clinical experience. *Circulation* 2006;114:591-60.
28. Grube E, Laborde JC, Gerckens U et al. Percutaneous implantation of the CoreValve self-expanding valve prosthesis in high-risk patients with aortic valve disease: the Siegburg first-in-man study. *Circulation* 2006;114:1616-24.
29. Grube E, Schuler G, Buellesfeld L et al. Percutaneous aortic valve replacement for severe aortic stenosis in high-risk patients using the second- and current third-generation self-expanding CoreValve prosthesis: device success and 30-day clinical outcome. *J Am Coll Cardiol* 2007;50:69-76.
30. Feldman T, Wasserman HS, Herrmann HC et al. Percutaneous mitral valve repair using the edge-to-edge technique: six-month results of the EVEREST Phase I Clinical Trial. *J Am Coll Cardiol* 2005;46:2134-40.
31. Rinaldi M, Kar S, Hermiller J, Smalling RW, Gray W, Carroll J et al. Significant reverse remodeling of the left ventricle one year after percutaneous mitral repair with the MitraClip device. *Am J Cardiol* 2007;100:S56-S59.
32. Webb JG, Kuck KH, Stone G et al. Percutaneous mitral annuloplasty with the MONARC system: Preliminary results from the EVOLUTION trial. *American Journal of Cardiology* 2006;98:49M.
33. Dubreuil O, Basmadjian A, Ducharme A et al. Percutaneous mitral valve annuloplasty for ischemic mitral regurgitation: first in man experience with a temporary implant. *Catheter Cardiovasc Interv* 2007;69:1053-61.
34. Kaye DM, Byrne M, Alferness C, Power J. Feasibility and short-term efficacy of percutaneous mitral annular reduction for the therapy of heart failure-induced mitral regurgitation. *Circulation* 2003;108:1795-7.
35. Grossi EA, Saunders PC, Woo YJ et al. Intraoperative effects of the coapsys annuloplasty system in a randomized evaluation (RESTOR-MV) of functional ischemic mitral regurgitation. *Ann Thorac Surg* 2005;80:1706-11.
36. Cribier A, Eltchaninoff H, Tron C et al. Treatment of calcific aortic stenosis with the percutaneous heart valve: mid-term follow-up from the initial feasibility studies: the French experience. *J Am Coll Cardiol* 2006;47:1214-23.
37. Walther T, Simon P, Dewey T et al. Transapical minimally invasive aortic valve implantation: multicenter experience. *Circulation* 2007;116:1240-1245.
38. Kodali S, O'Neill W, Moses J, Kapadia S, Williams M, Hanzel G et al. Six month to one year clinical outcomes following retrograde percutaneous aortic valve replacement in high risk patients: A report from the REVIVAL-II trial. *Am J Cardiol* 2007;100:S56-S59.
39. Grube E, Laborde JC, Zickmann B et al. First report on a human percutaneous transluminal implantation of a self-expanding valve prosthesis for interventional treatment of aortic valve stenosis. *Catheter Cardiovasc Interv* 2005;66:465-9.
40. Walther T, Falk V, Dewey T et al. Valve-in-a-valve concept for transcatheter minimally invasive repeat xenograft implantation. *J Am Coll Cardiol* 2007;50:56-60.
41. Wenaweser P, Buellesfeld L, Gerckens U, Grube E. Percutaneous aortic valve replacement for severe aortic regurgitation in degenerated bioprosthesis: the first valve in valve procedure using the CoreValve Revalving system. *Catheter Cardiovasc Interv* 2007;70:760-4.

42. Astor BC, Kaczmarek RG, Hefflin B, Daley WR. Mortality after aortic valve replacement: results from a nationally representative database. *Ann Thorac Surg* 2000;70:1939-45.
43. Shemin RJ. Percutaneous valve intervention: a surgeon's perspective. *Circulation* 2006;113:774-5.
44. Casserly IP, Kapadia SR. Advances in percutaneous valvular intervention. *Expert Rev Cardiovasc Ther* 2005;3:143-58.
45. Jongbloed MR, Schaliij MJ, Zeppenfeld K, Oemrawsingh PV, van der Wall EE, Bax JJ. Clinical applications of intracardiac echocardiography in interventional procedures. *Heart* 2005;91:981-90.
46. Nordmeyer J, Khambadkone S, Coats L et al. Risk stratification, systematic classification, and anticipatory management strategies for stent fracture after percutaneous pulmonary valve implantation. *Circulation* 2007;115:1392-7.
47. Tops LF, Krishnan SC, Schuijff JD, Schaliij MJ, Bax JJ. Noncoronary Applications of Cardiac Multidetector Row Computed Tomography. *J Am Coll Cardiol Img* 2008;1:94-106.
48. Maselli D, Guarracino F, Chiaromonte F, Mangia F, Borelli G, Minzioni G. Percutaneous mitral annuloplasty: an anatomic study of human coronary sinus and its relation with mitral valve annulus and coronary arteries. *Circulation* 2006;114:377-80.
49. Tops LF, Van de Veire NR, Schuijff JD et al. Noninvasive evaluation of coronary sinus anatomy and its relation to the mitral valve annulus: implications for percutaneous mitral annuloplasty. *Circulation* 2007;115:1426-32.
50. Choure AJ, Garcia MJ, Hesse B et al. In vivo analysis of the anatomical relationship of coronary sinus to mitral annulus and left circumflex coronary artery using cardiac multidetector computed tomography: implications for percutaneous coronary sinus mitral annuloplasty. *J Am Coll Cardiol* 2006;48:1938-45.
51. Tops LF, Wood DA, Delgado V et al. Noninvasive evaluation of the aortic root with multislice computed tomography: Implications for transcatheter aortic valve replacement. *J Am Coll Cardiol Img* 2008;1:321-30.
52. Naqvi TZ, Zarbatany D, Molloy MD, Logan J, Buchbinder M. Intracardiac echocardiography for percutaneous mitral valve repair in a swine model. *J Am Soc Echocardiogr* 2006;19:147-53.
53. Silvestry FE, Rodriguez LL, Herrmann HC et al. Echocardiographic guidance and assessment of percutaneous repair for mitral regurgitation with the Evalve MitraClip: lessons learned from EVEREST I. *J Am Soc Echocardiogr* 2007;20:1131-40.
54. Gottdiener JS, Bednarz J, Devereux R et al. American Society of Echocardiography recommendations for use of echocardiography in clinical trials. *J Am Soc Echocardiogr* 2004;17:1086-119.
55. Foster E, Wasserman HS, Gray W et al. Quantitative assessment of severity of mitral regurgitation by serial echocardiography in a multicenter clinical trial of percutaneous mitral valve repair. *Am J Cardiol* 2007;100:1577-83.



Non-invasive evaluation of coronary sinus anatomy and its relation to the mitral valve annulus: implications for percutaneous mitral annuloplasty

Laurens F. Tops¹
Nico R. Van de Veire¹
Joanne D. Schuijf¹
Albert de Roos²
Ernst E. van der Wall¹
Martin J. Schalij¹
Jeroen J. Bax¹

¹*Department of Cardiology, Leiden University Medical Center, Leiden, the Netherlands*

²*Department of Radiology, Leiden University Medical Center, Leiden, the Netherlands*

Circulation 2007;115:1426-32

ABSTRACT

Background: Percutaneous mitral annuloplasty has been proposed as an alternative to surgical annuloplasty. In this respect, evaluation of the coronary sinus (CS) and its relation with the mitral valve annulus (MVA) and the coronary arteries is relevant. The feasibility of evaluating these issues non-invasively with Multi-slice Computed Tomography (MSCT) was determined.

Methods and Results: In 105 patients (72 men, age 59 ± 11 years), 64-slice MSCT was performed for non-invasive evaluation of coronary artery disease. Thirty-four patients with heart failure and/or severe mitral regurgitation were included. Three-dimensional reconstructions and standard orthogonal planes were used to assess CS anatomy, and its relation with the MVA and circumflex artery. In 71 patients (68%) the circumflex artery coursed between the CS and the MVA, with a minimal distance between the CS and the circumflex artery of 1.3 ± 1.0 mm. The CS was located along the left atrial wall, rather than along the MVA, in the majority of the patients (ranging from 90% at the level of the MVA to 14% at the level of the distal CS). The minimal distance between the CS and MVA was 5.1 ± 2.9 mm. In patients with severe mitral regurgitation, the minimal distance between the CS and the MVA was significantly greater as compared to patients without severe mitral regurgitation (mean 7.3 ± 3.9 mm vs. 4.8 ± 2.5 mm, $p < 0.05$).

Conclusion: In the majority of the patients, the CS courses superior to the MVA. In 68% of the patients, the circumflex artery courses between the CS and the mitral annulus. MSCT may provide useful information in the selection of potential candidates for percutaneous mitral annuloplasty.

INTRODUCTION

Mitral annuloplasty is the most commonly performed surgical procedure for ischemic mitral regurgitation (MR) (1). Recently, a percutaneous approach to mitral annuloplasty has been proposed. Validation studies in animals have shown the feasibility of the percutaneous transvenous mitral annuloplasty (2-5). In addition, preliminary results of the first human experience with percutaneous mitral annuloplasty have been described (6).

However, anatomical studies have demonstrated the variable relationship between the coronary sinus (CS) and the mitral valve annulus (MVA) (7-9). It was noted that the CS may course adjacent to the posterior wall of the left atrium rather than along the MVA. Furthermore, a close relation between the CS and the left circumflex coronary artery (LCX) was detected, potentially limiting the use of percutaneous mitral annuloplasty. However, these anatomical studies were performed in structural normal hearts.

Evaluation of the CS anatomy and its relation with the MVA and the coronary arteries may be of value in patients who are considered for percutaneous mitral annuloplasty. Multi-slice computed tomography (MSCT) can provide an accurate non-invasive evaluation of the anatomy of the CS (10). Recent preliminary data suggest a potential use of MSCT scanning in patients considered for percutaneous mitral annuloplasty (11).

Accordingly, the purpose of the present study was to evaluate the relation between the CS, the MVA and the coronary arteries using 64-slice MSCT in patients with structural normal hearts and in patients with severe MR.

METHODS

Study population

The study population comprised 105 consecutive patients referred for MSCT coronary angiography. The total study population was divided into 3 groups: group I (controls, n=35) included patients without coronary artery disease and without structural heart disease; group II (CAD, n=36) comprised patients with either a history of myocardial infarction / percutaneous transluminal coronary angioplasty / coronary artery bypass grafting, or a significant stenosis in ≥ 1 coronary artery on the MSCT scan; group III (heart failure, n=34) included patients with severe heart failure (left ventricular ejection fraction $\leq 35\%$).

Multi-slice Computed Tomography

MSCT was performed using a Toshiba Multi-slice Aquilion 64 system (Toshiba Medical Systems, Tokyo, Japan) with a collimation of 64 x 0.5 mm and a rotation time of 400 – 500 ms, depending on the heart rate. The tube current was 300 mA, at 120 kV. Non-ionic contrast material (Iomeron 400, Bracco, Altana Pharma, Konstanz, Germany) was administered in the antecubital vein, with

an amount of 80 to 110 ml depending on the total scan time, and a flow rate of 5.0 ml/sec. Automated peak enhancement detection in the descending aorta was used for timing of the contrast bolus. After the threshold level of +100 Hounsfield units was reached, data acquisition was automatically initiated. Data acquisition was performed during an inspiratory breathhold of approximately 8 to 10 seconds, while the ECG was recorded simultaneously to allow retrospective gating of the data. The data set was reconstructed at 75% of the RR interval, with a slice thickness of 0.5 mm and a reconstruction interval of 0.3 mm.

Data analysis

310

Data analysis was performed on a remote post-processing workstation (Vitrea 2, Vital Images, Plymouth, Minnesota). Three-dimensional volume rendered reconstructions and standard orthogonal planes were used to assess the anatomy and the course of the CS and its tributaries. Furthermore, the course of the coronary arteries and the coronary artery dominance (right, left, or balanced) was assessed. In particular, the course of the LCX in relation to the CS (inferior or superior) was determined (Figure 1). The axial slices were studied to assess the minimal distance between the LCX and the CS.

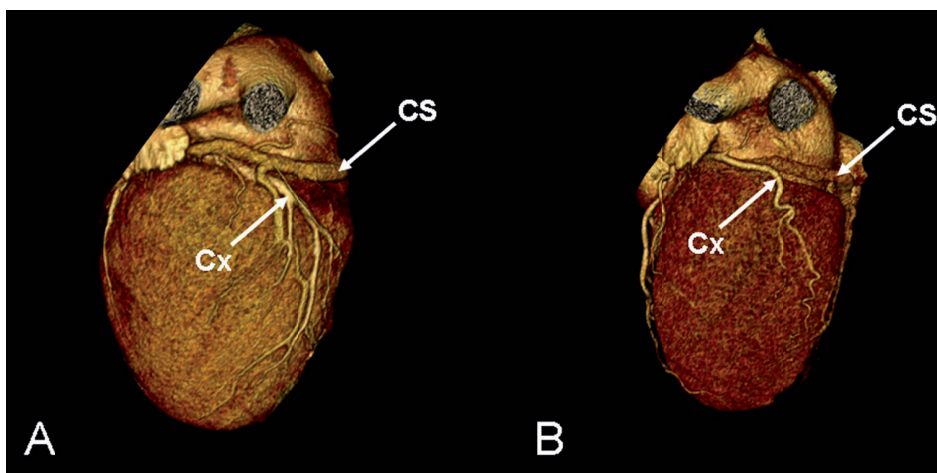


Figure 1. Volume-rendered reconstructions showing the relation between the coronary sinus (CS) and the left circumflex coronary artery (Cx). In panel A, the Cx courses deeper than the CS, and lies between the CS and the mitral valve annulus. In panel B, the Cx courses superior to the CS.

With the use of reconstructed long-axis two- and four-chamber views and volume-rendered three-dimensional reconstructions, the relation between the CS and the MVA was assessed (Figure 2). The position of the CS in relation to the MVA (superior/inferior/same level), and the minimal distance between the CS and the MVA was determined (Figure 3). The anatomical and quantitative data were assessed at three different levels: at the proximal CS, the distal CS, and at the level of the MVA. The proximal CS was defined as the site where the CS makes an angle with the right atrium. The distal CS was defined as the site where the CS makes a sharp angle

anteriorly and continues as the anterior interventricular vein (12). The level of the MVA was reconstructed using the long-axis two- and four-chamber views.

Furthermore, the diameter of the MVA was derived from the long-axis two- and four-chamber views (Figures 2A and 2B); the perimeter of the MVA was assessed on the reconstructed level of the MVA (Figure 2C). In addition, the anterior-posterior diameter and the superior-inferior diameter of the proximal and distal CS were determined, as previously described (10). The analyses of the anatomical relations and the quantitative data were performed by two independent observers, blinded to the clinical data of the patients.

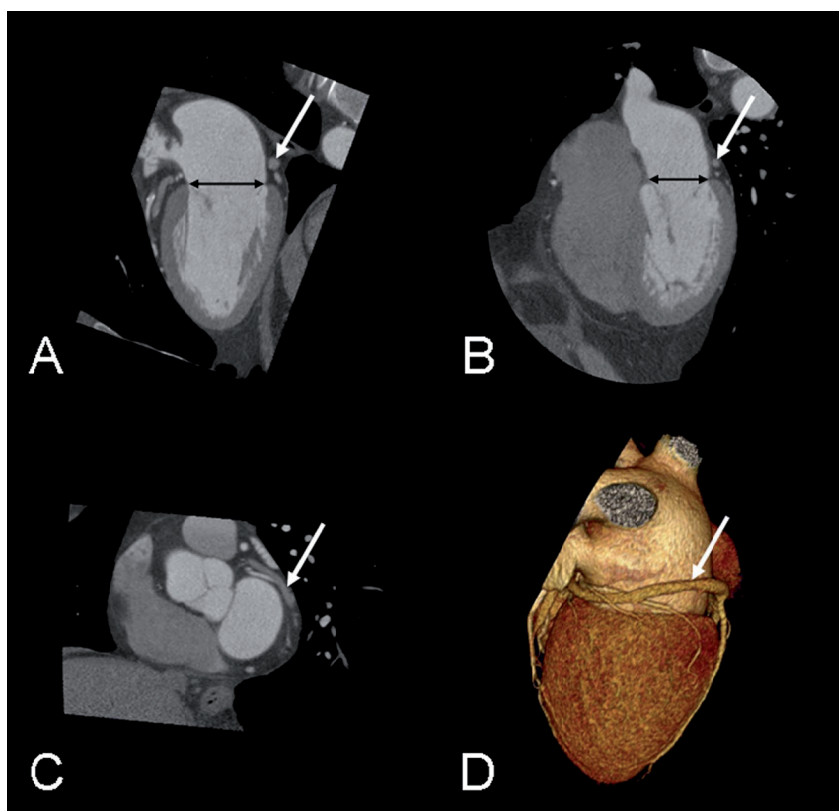


Figure 2. Long-axis 2-chamber (panel A) and 4-chamber (panel B) views were used to assess the course of the coronary sinus (CS) (white arrow) in relation to the mitral valve annulus (MVA), and the diameter of the MVA (black arrow). Furthermore, at the reconstructed level of the MVA (panel C), the CS location and the MVA perimeter were determined. Panel D shows a three-dimensional volume-rendered reconstruction demonstrating the course of the CS and its relation to the MVA and the left circumflex coronary artery.

Echocardiography

Standard two-dimensional echocardiograms were obtained with patients in the left lateral decubitus position using a commercially available system (Vingmed Vivid 7, General Electric-Vingmed, Milwaukee, Wisconsin, USA). Images were obtained using a 3.5-MHz transducer at a depth of 16 cm in the parasternal (long- and short-axis) and apical (two- and four-chamber)

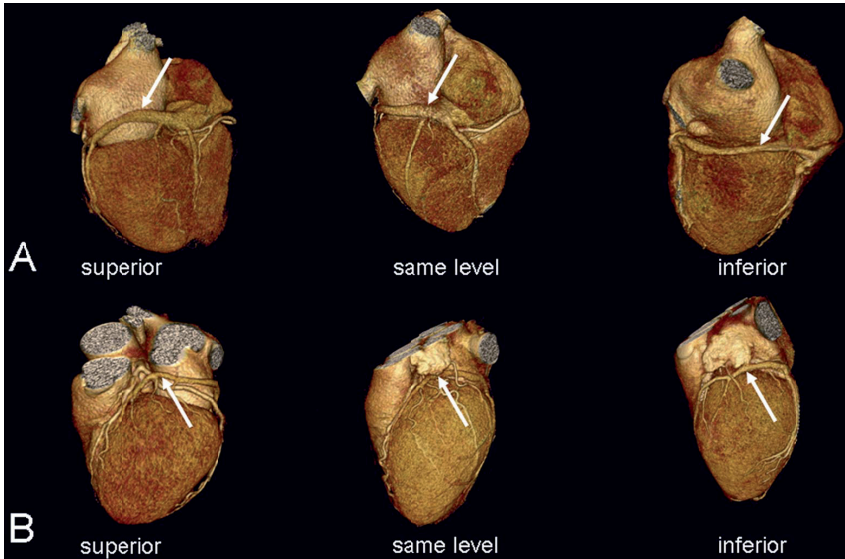


Figure 3. Three-dimensional volume-rendered reconstructions were used to assess the position of the coronary sinus (CS)(white arrow) in relation to the mitral valve annulus. At the proximal CS (panel A) and at the distal CS (panel B), the relative position (super / same level / inferior) of the CS was determined.

views. Standard two-dimensional images and color Doppler data triggered to the QRS complex were digitally stored in cine-loop format. Left ventricular ejection fraction was calculated from apical two- and four-chamber images using the biplane Simpson's rule (13). The severity of MR was graded semi-quantitatively using color-flow Doppler in the conventional parasternal long-axis and apical four-chamber images (14). MR was characterized as: minimal = 1+ (jet area/left atrial area <10%), moderate = 2+ (jet area/left atrial area 10-20%), moderate-severe = 3+ (jet area/left atrial area 20-45%), or severe = 4+ (jet area/left atrial area >45%) (14).

Statistical analysis

Continuous data are presented as mean values \pm standard deviation (SD); categorical data are presented as frequencies and percentages. Differences between the three groups were compared using one-way Analysis of Variance (ANOVA) with Scheffé post-hoc testing for continuous variables, and Chi-square tests for dichotomous variables. Differences between patients with and without severe MR were evaluated using Mann-Whitney U test (continuous variables), or Fisher's Exact tests (dichotomous variables). All statistical analyses were performed using SPSS software (version 12.0, SPSS Inc. Chicago, Illinois, USA). All statistical tests were two-sided, whereas a p-value <0.05 was considered statistically significant.

RESULTS

Study population

A total of 105 patients (age 59 ± 11 years, 72 men) were studied. The study population was divided in 3 groups: controls (n=35), patients with coronary artery disease (n=36), and patients with severe heart failure (n=34, 19 (56%) ischemic cardiomyopathy, 15 (44%) idiopathic cardiomyopathy). The baseline characteristics of the patients are listed in Table 1.

Table 1. Baseline characteristics of the three patient groups

	Controls (n=35)	CAD (n=36)	HF (n=34)
Age, years	54 ± 11	$61 \pm 10^*$	$63 \pm 11^*$
Gender, M/F	21 / 14	25 / 11	26 / 8
LVEF, %	62 ± 5	61 ± 9	$27 \pm 7 \dagger \ddagger$
Previous MI, n (%)	0	9 (25%)	19 (56%)
Risk factors, n (%)			
Diabetes mellitus	12 (34%)	14 (39%)	6 (18%)
Hypertension	15 (43%)	17 (47%)	14 (41%)
Hypercholesterolemia	14 (40%)	22 (61%)	17 (50%)
Smoking	5 (14%)	15 (42%)	17 (50%)
Positive family history	11 (31%)	10 (28%)	11 (32%)

* $p < 0.05$ vs. controls, † $p < 0.001$ vs. controls, ‡ $p < 0.001$ vs. CAD; CAD = coronary artery disease; HF = heart failure; LVEF = left ventricular ejection fraction; MI = myocardial infarction

Anatomical observations

Coronary arteries and relation with coronary sinus Right coronary artery dominance was observed in 91 patients (87%), left coronary dominance in 13 (12%) and balanced in 1 patient (1%). In 71 patients (68%) the LCX coursed inferior to the CS; thus between the CS and the mitral annulus. In 34 patients (32%) the LCX coursed superior to the CS (Figure 1). The minimal distance between the CS and the LCX was 1.3 ± 1.0 mm. The mean number of marginal branches was 1.2 ± 0.6 ; there were no differences in number of marginal branches between the three groups, or between the patients with right or left coronary dominance.

Anatomical relation between the coronary sinus and mitral valve annulus At the level of the MVA, the CS was located more superiorly in 95 patients (90%), more inferiorly in 1 patient (1%), and at the same level in 9 patients (9%). The minimal distance from the CS to the MVA was 5.1 ± 2.9 mm (range 1.4 to 16.8 mm). Also, the relation of the CS and the MVA was determined at the proximal and the distal CS. At the proximal CS, the CS was located more superior to the MVA in 57 patients (54%), more inferiorly in 7 patients (7%), and at the same level in 41 patients (39%). The minimal distance between the CS and the MVA at the proximal CS was 8.3 ± 2.3 mm (range 2.2 to 15.3 mm). At the distal CS, the CS was located more superiorly to the MVA in 15 patients (14%), more inferiorly in 31 patients (30%), and at the same level in 59 patients (56%).

The minimal distance between the CS and the MVA at the distal CS was 8.8 ± 3.4 mm (range 2.6 to 18.6 mm).

There were no statistical differences between the 3 groups, with regard to the location of the CS in relation to the MVA at any level. In contrast, the minimal distance between the CS and the MVA was significantly greater in the heart failure patients, compared with the control patients and the patients with coronary artery disease (Table 2).

Table 2. Quantitative analyses of the coronary sinus and the mitral valve annulus in the three patient groups

	Controls (n=35)	CAD (n=36)	HF (n=34)	p value *
Minimal distance between CS and MVA				
at MVA level	4.4 ± 2.2	4.9 ± 2.7	6.2 ± 3.4 †	0.019
at proximal CS	7.6 ± 1.6	7.9 ± 2.1	9.3 ± 2.8 †	0.006
at distal CS	7.3 ± 3.3	8.5 ± 3.2	10.7 ± 3.0 ‡ §	<0.001
CS diameter at proximal CS				
AP diameter	10.5 ± 2.7	9.7 ± 2.3	9.9 ± 3.3	0.5
SI diameter	15.0 ± 3.2	14.0 ± 3.0	14.2 ± 3.0	0.3
CS diameter at distal CS				
AP diameter	3.9 ± 0.7	3.9 ± 0.6	4.0 ± 0.7	0.7
SI diameter	4.1 ± 0.9	3.9 ± 0.7	4.0 ± 0.9	0.7
Total CS length	108 ± 12	106 ± 14	126 ± 19 ‡	<0.001

* Assessed by analysis of variance with Scheffé post-hoc testing. † $p < 0.05$ vs. controls; ‡ $p < 0.001$ vs. controls; § $p < 0.05$ vs. CAD; || $p < 0.001$ vs. CAD; AP = anterior-posterior; CAD = coronary artery disease; CS = coronary sinus; HF = heart failure; MVA = mitral valve annulus; SI = superior-inferior

Coronary sinus and mitral valve annulus: quantitative observations The mean diameter of the MVA at the two-chamber view was 40.8 ± 4.7 mm, the mean diameter at the four-chamber view was 36.4 ± 4.6 mm. The mean perimeter of the MVA was 119.4 ± 13.3 mm.

The mean diameter of the CS at the proximal part was 10.0 ± 2.8 mm in the anterior-posterior direction, and 14.4 ± 3.1 mm in the superior-inferior direction. The diameter of the CS at the distal part was 3.9 ± 0.7 mm in the anterior-posterior direction, and 4.0 ± 0.9 mm in the superior-inferior direction. No significant differences in diameter of the CS were observed between the 3 groups (Table 2). With the use of multi-planar reformatted images, the total length of the CS was calculated. The mean length was 113 ± 18 mm (range 76 to 170 mm). The mean CS length was significant larger in the heart failure patients, compared with the controls and the patients with coronary artery disease (Table 2).

Mitral regurgitation

In the total study population 50 patients (48%) had no MR, 30 (29%) patients had MR grade 1+ and 10 patients (9%) had MR grade 2+; whereas MR was characterized as 3+ in 13 patients (12%), and 4+ in 2 patients (2%). To detect differences in the anatomical and quantitative data between patients with and without severe MR, the study population was divided in two groups: patients with MR grade $\leq 2+$ ($n=90$) and patients with MR grade 3+ or 4+ ($n=15$).

There were no differences between the two groups in the anatomical relation between the CS and MVA at any level. Furthermore, no significant differences in diameters of the CS were

noted. However, the minimal distance between the CS and the MVA at all levels was significant greater in the patients with severe MR, compared to the patients without severe MR (Table 3). In addition, the diameters of the MVA and the total length of the CS were significantly larger in the patients with severe MR (Table 3).

Table 3. Quantitative analyses of the coronary sinus and the mitral valve annulus in patients with and without severe mitral regurgitation

	Patients without severe MR (n=90)	Patients with severe MR (n=15)	p value *
Minimal distance between CS and MVA			
at MVA level	4.8 ± 2.5	7.3 ± 3.9	0.005
at proximal CS	8.1 ± 2.4	9.3 ± 1.9	0.019
at distal CS	8.3 ± 3.1	12.1 ± 3.6	<0.001
MVA diameter (two-chamber view)	40.2 ± 4.7	44.3 ± 3.3	0.001
MVA diameter (four-chamber view)	35.8 ± 4.4	39.9 ± 4.4	0.002
MVA perimeter	118.1 ± 12.6	127.6 ± 14.7	0.020
Total CS length	110.1 ± 16.6	128.6 ± 14.6	<0.001

* As assessed with Mann-Whitney U test.

DISCUSSION

In the present study, the relation between the CS, the MVA and the coronary arteries was evaluated non-invasively using MSCT. The major findings of the study are as follows: In 68% of the patients, the LCX courses between the CS and the MVA. In the majority of the patients, the CS courses superior to the MVA. In addition, the minimal distance between the CS and the MVA is greater in patients with heart failure and severe MR. The findings of the present study have important implications for percutaneous mitral annuloplasty.

Anatomical observations

Coronary sinus and coronary arteries A close relation between the CS and the LCX may limit the use of a percutaneous mitral annuloplasty. Circumflex artery compression has been reported as a serious complication in one of the first animal studies on the percutaneous mitral annuloplasty (4). Previous anatomical studies have reported the relation between the CS, the coronary arteries and the MVA (8,9). Maselli et al (9) demonstrated that the LCX coursed between the CS and the MVA in 63.9% of the 61 studied human hearts. Of note, when the LCX coursed inferior to the CS, the number of marginal branches of the LCX was larger. However, no data on the minimal distance between the CS and the LCX were provided.

These anatomical observations have previously been confirmed with electron beam computed tomography (15,16). Mao et al (15) reported that in 80.8% of the studied patients, the LCX coursed inferiorly to the CS. Furthermore, it was demonstrated that the overlapping segment of the CS and the LCX was longer than 30 mm in 17.8% of the cases. However, again no data on the minimal distance between the CS and the LCX were provided.

In the present study, the LCX coursed inferiorly to the CS in 68% of the patients, with a minimal distance between the CS and the LCX of 1.3 ± 1.0 mm. The close relation between the CS and the LCX may limit the use of percutaneous mitral valve annuloplasty, in particular when the LCX courses inferior to the CS over a large distance (Figure 4).

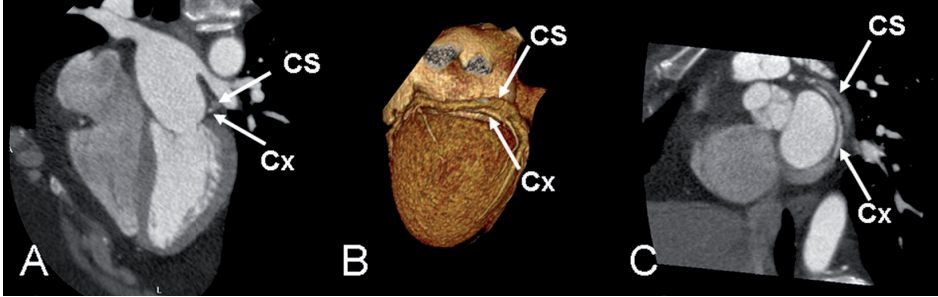


Figure 4. In this patient, the left circumflex coronary artery (Cx) courses between the coronary sinus (CS) and the mitral valve annulus (panel A, four-chamber view). The volume rendered reconstruction (panel B) and the reconstructed mitral valve annulus level (panel C) show that the Cx courses inferior to the CS over a large distance. Performing percutaneous mitral annuloplasty may result in compression of the Cx.

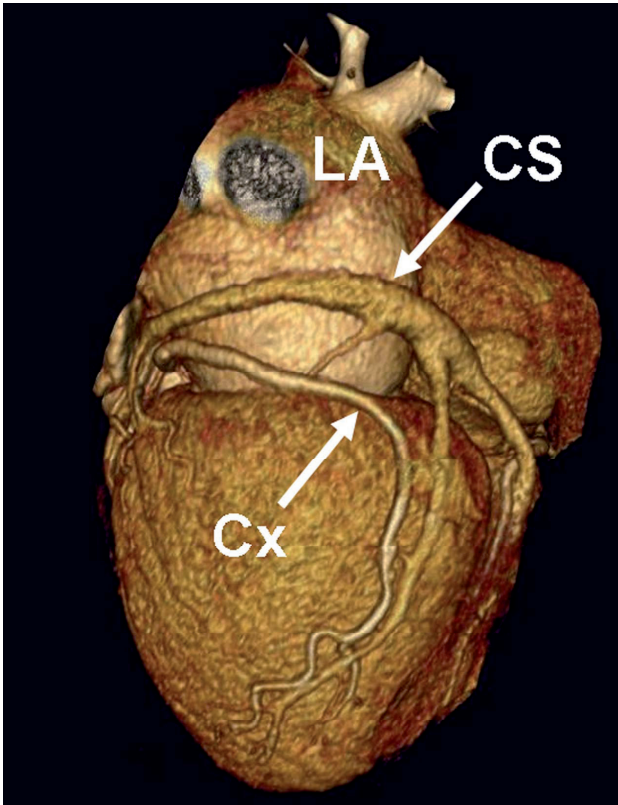


Figure 5. In this patient, the coronary sinus (CS) courses along the left atrial (LA) posterior wall, rather than along the mitral valve annulus. Cx = left circumflex coronary artery.

Coronary sinus and mitral valve annulus Several anatomical studies have addressed the relation between the CS and the MVA (7-9). Shinbane et al (7) studied 10 normal adult cadaver hearts, and reported variable distances between the CS and the MVA along the course of the CS. Mean distances between the CS and the MVA were 14.1 ± 3.1 mm, 10.2 ± 4.9 mm and 10.7 ± 3.5 mm, at 20, 40 and 60 mm distance from the ostium of the CS, respectively. El-Maasarany et al (8) studied the distances between the CS and the MVA in 32 normal cadaver hearts. Distances were assessed in 6 separate regions along the course of the CS. Mean distance was highly variable for the 6 regions; the shortest distance (5.8 mm) was observed at the anterolateral commissure of the MVA. Unfortunately, no data were provided regarding the position of the CS in relation to the MVA (superior/deeper/same level). In the largest anatomical study reported, Maselli et al (9) also noted variable distances between the CS and the MVA. At the level of the P2 and P3 scallops of the mitral valve, mean distances between the CS and the MVA of 5.7 ± 3.3 mm and 9.7 ± 3.2 mm were reported.

In the present study, the highly variable relation between the CS and the MVA was assessed non-invasively with MSCT. The CS was located more superior to the MVA in the majority of the patients (ranging from 90% at the level of the MVA to 14% at the level of the distal CS). Furthermore, minimal distances between the CS and the MVA were assessed at the proximal and the distal CS, and appeared to be highly variable (Table 2). Although this confirms the previous anatomical studies, the use of different reference points makes a direct comparison between the present study and previous *in vitro* studies difficult. Importantly, in patients with severe MR, the minimal distance between the CS and the MVA may increase significantly. In particular, in patients where the CS courses along the left atrial wall the use of percutaneous mitral annuloplasty may be not feasible (Figure 5).

It should be noted however, that in the present study images were routinely reconstructed at 75% of the RR interval. However, the diameter and the distance between the CS and the MVA may vary during the cardiac cycle. Nevertheless, the present study shows that MSCT can accurately depict CS anatomy and its relation with the MVA, thereby providing important information in patients who are considered for percutaneous mitral annuloplasty.

Implications for percutaneous mitral annuloplasty

The present study shows the feasibility of the non-invasive evaluation of the CS anatomy and its relation with the MVA and the coronary arteries. In previous *in vitro* (7-9) and *in vivo* (15,16) studies, the relation between the CS, the MVA and the coronary arteries has been investigated. However, in none of these studies, patients with severe MR were studied. The present study emphasizes the variability in the relation between the CS and MVA. More importantly, it demonstrates that in patients with severe MR, the minimal distance between the CS and the MVA is larger than in control patients (Table 3).

The close relation between the CS and the LCX, and the variable distance between the CS and the MVA may hamper the clinical use of the percutaneous mitral annuloplasty in selected

patients (4). MSCT may identify the patients in whom percutaneous transvenous mitral annuloplasty may not be feasible. In 68% of the patients, the LCX courses between the CS and the MVA (Figure 4), with a potential risk of compression of the LCX when applying percutaneous mitral annuloplasty. Furthermore, in a large number of patients, the CS courses along the left atrial posterior wall, rather than along the MVA (Figure 5). In addition, in patients with severe calcifications of the MVA (Figure 6), a surgical approach may be preferred over a percutaneous approach.

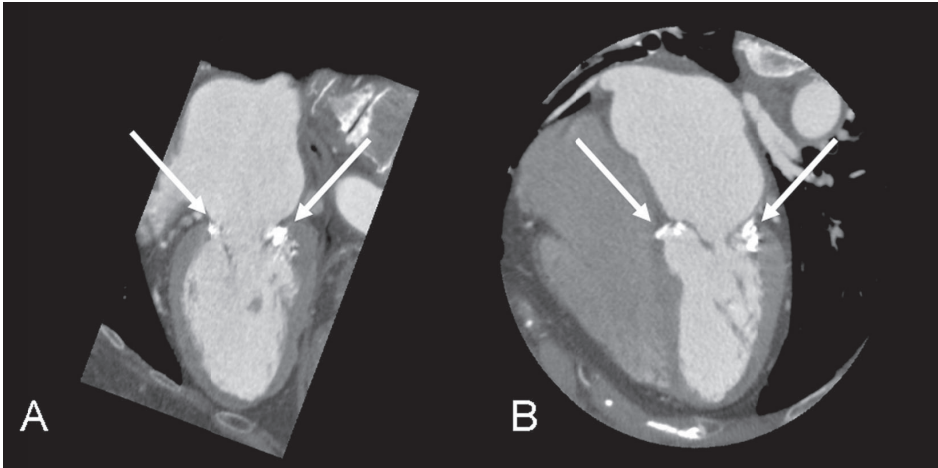


Figure 6. Long-axis two-chamber (panel A) and four-chamber (panel B) views demonstrating a patient with a heavily calcified mitral valve (white arrows).

Our findings are in good relation with recent data demonstrating the feasibility of non-invasive evaluation of the CS anatomy in relation to the MVA using MSCT (11). Similar to the present study, a large variability in the distance between the CS and the MVA was noted (11). Novelties of the present study include the use of a 64-slice MSCT scanner, whereas in the previous study a 16-slice CT scanner (with a collimation of 4 x 1 mm) was used. In addition, in the present study patients with heart failure and patients with severe LV dilatation and subsequent functional MR were included. Therefore, a substantial part of the present study population consisted of potential candidates for percutaneous mitral annuloplasty. Both studies show that MSCT can accurately depict CS anatomy and its relation with the MVA, thereby providing important information in patients who are considered for percutaneous mitral annuloplasty.

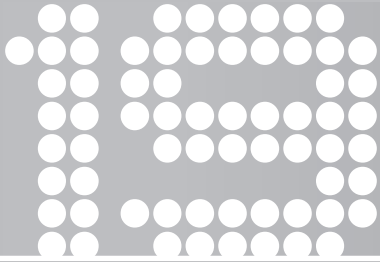
CONCLUSIONS

The relation between the CS, the MVA and the LCX can be evaluated non-invasively with MSCT. In 68% of the patients, the LCX coursed between the CS and the mitral annulus. Furthermore, at

the level of the MVA, the CS was located more superiorly in 90% of the patients. In the patients with severe MR, the minimal distance between the CS and the MVA was significantly greater at all levels, compared to the patients without severe MR. MSCT may provide useful information in the selection of potential candidates for percutaneous mitral annuloplasty.

REFERENCES

1. Borger MA, Alam A, Murphy PM, Doenst T, David TE. Chronic ischemic mitral regurgitation: repair, replace or rethink? *Ann Thorac Surg* 2006;81:1153-61.
2. Liddicoat JR, Mac Neill BD, Gillinov AM et al. Percutaneous mitral valve repair: a feasibility study in an ovine model of acute ischemic mitral regurgitation. *Catheter Cardiovasc Interv* 2003;60:410-6.
3. Kaye DM, Byrne M, Alferness C, Power J. Feasibility and short-term efficacy of percutaneous mitral annular reduction for the therapy of heart failure-induced mitral regurgitation. *Circulation* 2003;108:1795-7.
4. Maniu CV, Patel JB, Reuter DG et al. Acute and chronic reduction of functional mitral regurgitation in experimental heart failure by percutaneous mitral annuloplasty. *J Am Coll Cardiol* 2004;44:1652-61.
5. Daimon M, Shiota T, Gillinov AM et al. Percutaneous mitral valve repair for chronic ischemic mitral regurgitation: a real-time three-dimensional echocardiographic study in an ovine model. *Circulation* 2005;111:2183-9.
6. Webb JG, Harnek J, Munt BI et al. Percutaneous transvenous mitral annuloplasty: initial human experience with device implantation in the coronary sinus. *Circulation* 2006;113:851-5.
7. Shinbane JS, Lesh MD, Stevenson WG et al. Anatomic and electrophysiologic relation between the coronary sinus and mitral annulus: implications for ablation of left-sided accessory pathways. *Am Heart J* 1998;135:93-8.
8. El Maasarany S, Ferrett CG, Firth A, Sheppard M, Henein MY. The coronary sinus conduit function: anatomical study (relationship to adjacent structures). *Europace* 2005;7:475-81.
9. Maselli D, Guarracino F, Chiaramonti F, Mangia F, Borelli G, Minzioni G. Percutaneous mitral annuloplasty: an anatomic study of human coronary sinus and its relation with mitral valve annulus and coronary arteries. *Circulation* 2006;114:377-80.
10. Jongbloed MR, Lamb HJ, Bax JJ et al. Noninvasive visualization of the cardiac venous system using multislice computed tomography. *J Am Coll Cardiol* 2005;45:749-53.
11. Choure AJ, Garcia MJ, Hesse B et al. In vivo analysis of the anatomical relationship of coronary sinus to mitral annulus and left circumflex coronary artery using cardiac multidetector computed tomography: implications for percutaneous coronary sinus mitral annuloplasty. *J Am Coll Cardiol* 2006;48:1938-45.
12. von Lüdinghausen M. The venous drainage of the human myocardium. *Adv Anat Embryol Cell Biol* 2003;168:1-104.
13. Schiller NB, Shah PM, Crawford M et al. Recommendations for quantitation of the left ventricle by two-dimensional echocardiography. *J Am Soc Echocardiogr* 1989;2:358-67.
14. Thomas JD. How leaky is that mitral valve? Simplified Doppler methods to measure regurgitant orifice area. *Circulation* 1997;95:548-50.
15. Mao S, Shinbane JS, Girsky MJ et al. Coronary venous imaging with electron beam computed tomographic angiography: three-dimensional mapping and relationship with coronary arteries. *Am Heart J* 2005;150:315-22.
16. Gerber TC, Sheedy PF, Bell MR et al. Evaluation of the coronary venous system using electron beam computed tomography. *Int J Cardiovasc Imaging* 2001;17:65-75.



Assessment of mitral valve anatomy and geometry with 64-slice multi-slice computed tomography

Victoria Delgado¹
Laurens F. Tops¹
Joanne D. Schuijf¹
Albert de Roos²
Josep Brugada³
Martin J. Schalij¹
James D. Thomas⁴
Jeroen J. Bax¹

¹Department of Cardiology, Leiden University Medical Center, Leiden, the Netherlands

²Department of Radiology, Leiden University Medical Center, Leiden, the Netherlands

³Thorax Institute, Hospital Clinic, Barcelona, Spain

⁴Department of Cardiovascular Medicine, the Cleveland Clinic Foundation, Cleveland, USA

ABSTRACT

Background: By providing detailed anatomical information, MSCT may give more insight into the underlying mechanisms of functional mitral regurgitation (FMR).

Objectives: The purpose of the present study was to assess the anatomy and the geometry of the mitral valve by using 64-slice multi-slice computed tomography (MSCT).

Methods: In 151 patients, including 67 patients with heart failure (HF) and 29 patients with moderate to severe FMR, 64-slice MSCT coronary angiography was performed. The anatomy of the subvalvular apparatus of the mitral valve was assessed, and mitral valve geometry, comprising the mitral valve tenting height and leaflet tethering, was evaluated at the anterolateral, central and posteromedial levels.

Results: In the majority of patients, the anatomy of the subvalvular apparatus was highly variable due to multiple anatomic variations of the posterior papillary muscle: the anterior PM had a single insertion, whereas the posterior PM showed multiple heads and insertions (n=114, 83%). The assessment of mitral valve geometry demonstrated that HF patients with moderate to severe FMR had significantly increased posterior leaflet angle and mitral valve tenting height at the central ($44.4 \pm 11.9^\circ$ vs. $37.1 \pm 9.0^\circ$, $p=0.008$; 6.6 ± 1.4 mm/m² vs. 5.3 ± 1.3 mm/m², $p<0.0001$, respectively) and posteromedial levels ($35.9 \pm 10.6^\circ$ vs. $26.8 \pm 10.1^\circ$, $p=0.04$; 5.4 ± 1.6 mm/m² vs. 4.1 ± 1.2 mm/m², $p<0.0001$, respectively), as compared to HF patients without FMR. In addition, a more outward displacement of the PMs, reflected by a higher mitral valve sphericity index, was observed in HF patients with FMR (1.4 ± 0.3 vs. 1.2 ± 0.3 , $p=0.004$). Mitral valve tenting height at the central level and mitral valve sphericity index were the strongest determinants of FMR severity.

Conclusions: MSCT provides anatomical and geometric information on the mitral valve apparatus. In HF patients with moderate to severe FMR, a more pronounced tethering of the mitral leaflets at the central and posteromedial levels was demonstrated using MSCT.

INTRODUCTION

Functional mitral regurgitation (FMR) is associated with poor outcome in patients with coronary artery disease and left ventricular (LV) dysfunction (1-3). One of the characteristics of FMR, different from organic mitral regurgitation, is the preserved anatomy of the leaflets and tendinous cords. Accordingly, mitral valve repair is a suitable surgical procedure to treat FMR. However, the results still remain controversial (4-7). The complex pathophysiology of FMR makes this entity a challenge for surgery. Several underlying mechanisms may contribute to FMR: LV remodeling, wall motion abnormalities, displacement of the papillary muscles (PMs) or mitral annulus deformation (8). All these mechanisms result in tethering of the mitral valve with failure of anteroposterior leaflet coaptation.

Recent advances in 3-dimensional imaging techniques have allowed for a better understanding of the aforementioned changes in the mitral valve apparatus and LV geometry (9,10). Subsequently, new strategies for surgical mitral valve repair have been proposed (11,12). Multi-slice computed tomography (MSCT) may be a valuable technique to study both LV geometry and mitral valve anatomy and geometry. Therefore, the purpose of the present study was to assess the anatomy and geometry of the mitral valve and the LV with the use of 64-slice MSCT in a large cohort of patients, including patients with FMR.

METHODS

Study population

A total of 151 consecutive patients referred to Leiden University Medical Center (Leiden, The Netherlands) for MSCT coronary angiography were studied. The study population was divided into 2 groups: group I (control patients, $n = 84$) comprised patients without coronary artery disease or structural heart disease and group II (heart failure-patients [HF], $n = 67$) comprised patients with heart failure and documented LV systolic dysfunction. The anatomy and geometry of the mitral valve were examined, and differences among the two patient groups were assessed. In addition, differences in mitral valve geometry between HF patients with and without moderate to severe FMR were assessed.

Multi-slice computed tomography

All patients underwent scanning on a 64-slice MSCT scanner (Aquilion, Toshiba Medical Systems, Tokyo, Japan) using the following protocol: 120 kV, 300 mA, a rotation time of 400 to 500 ms (depending on the heart rate), and collimation of 64×0.5 mm. A total of 80 to 110 ml of nonionic contrast medium (Iomeron 400, Bracco, Altana Pharma, Konstanz, Germany) was administered in the antecubital vein at 5 mL/s. Automated peak enhancement detection in the descending aorta was used to time the contrast bolus. Data acquisition started automatically

after the threshold level of +100 Hounsfield units was reached, and it was performed during an inspiratory breath-hold of 8 to 10 seconds. The ECG was recorded simultaneously to allow retrospective gating and reconstruction of the data at desired phases of the cardiac cycle. Data acquisition was performed at a rotation time of 400 ms resulting in a temporal resolution of 200 ms in case of half reconstruction. In those patients with a heart rate > 70 beats/s, 3 cardiac beats were acquired resulting in segment reconstruction algorithm with slightly lower temporal reconstruction. All images were transferred to a dedicated workstation for data analysis (Vitrea 2, Vitral Images, Plymouth, Minnesota).

324

Data analysis

To study the anatomy and geometry of the mitral valve and the LV, the data set was reconstructed with a slice thickness of 0.5 mm and a reconstruction interval of 0.3 mm, at 30% and 75% of the RR interval for the systolic and diastolic phases, respectively. Standard orthogonal planes were used to assess the anatomy of the mitral valve apparatus. A reconstructed LV short-axis view was used to assess the mitral valve geometry. All parameters were corrected for body surface area.

Anatomy of the subvalvular apparatus Reconstructed long-axis 2- and 4-chamber views and the reconstructed LV short-axis view in the diastolic phase were used to study the anatomy of the subvalvular apparatus. The anatomy of the PMs was assessed focusing on the number of heads (ranging from I to III) and the type of insertion to the ventricular wall (type A-C), according to the classification of morphological variants of the PMs, as described by Berdajs et al. (13) (Figure 1). Furthermore, the attachment of the basal part of the PMs to the LV wall was studied, with special attention to the type of attachment (solid or trabecularized attachment, Figure 1).

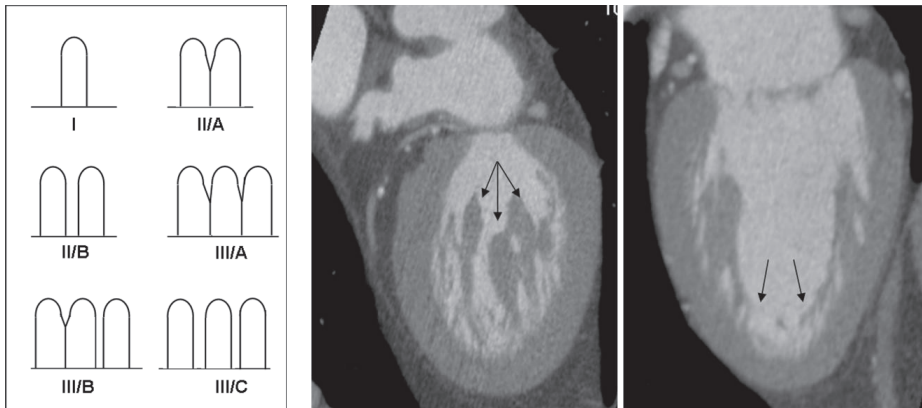


Figure 1. Assessment of subvalvular apparatus of the mitral valve. Left panel: the anatomical variations of the papillary muscles (PMs) were classified according to the number of heads and insertions (modified after Berdajs et al, reference #13). The number of PM heads could range from 1 to 3 (type I, II and III, respectively), and the insertions could be common (subtype A) or divided (subtype B or C). Middle panel: Example of a type III/B posterior PM, demonstrating 3 PM heads, with 2 insertions. Right panel: The attachment of 2 type I PM showed thin trabeculae upholstering the surface of the LV wall.

Left ventricular geometry To assess LV volumes and systolic function, the data set was reconstructed with a slice thickness of 5.0 mm in the short-axis view, starting at early systole (0% of cardiac cycle) to end-diastole (95% of cardiac cycle) in steps of 5%. Endocardial borders were traced manually on the short-axis cine images and the PMs were regarded as being part of the LV cavity. Table 1 summarizes the LV parameters that were evaluated. The LV end-diastolic volume (LVEDV) and end-systolic volume (LVESV) were obtained and the LV ejection fraction (LVEF) was calculated by the difference between LVESV and LVEDV divided by the LVEDV (Table 1). The sphericity index of the LV was calculated with the use of the following equation: LV sphericity index = $EDV / [(LAD^3 \times 3.14) / 6]$, where LAD is the long axis diameter of the LV (14).

Table 1. Summary of the left ventricular and mitral valve variables

Left ventricle
LV end-diastolic volume index
LV end-systolic volume index
LV ejection fraction
LV sphericity index
Mitral valve
Mitral annulus area
Intercommisural diameter (CC diameter)
Anteroposterior diameter (AP diameter)
Mitral valve sphericity index
Distance between heads of papillary muscles
Anterior leaflet angle (A α)
Posterior leaflet angle (P α)
Tenting height (MVTht)

LV = left ventricular.

Mitral valve geometry The mitral valve geometry was assessed in the reconstructed systolic phase. An overview of the measured variables is shown in Table 1. With the use of 2- and 4-chamber views and the reconstructed LV short-axis view, a plane parallel to the mitral valve was reconstructed (Figure 2). At the level of the mitral valve annulus, the mitral annulus area was calculated by planimetry and the anteroposterior diameter (AP diameter) and the intercommisural diameter (CC diameter) were measured (Figure 2).

Subsequently, a second plane parallel to the mitral valve was reconstructed, which clearly visualized both mitral commissures. Three anteroposterior planes perpendicular to this plane were defined to assess the geometry of the anterolateral, central and posteromedial parts of the mitral leaflets (Figure 3). In all 3 planes, the degree of leaflet tethering was assessed by measuring the angle at which each leaflet met the mitral annulus plane (anterior leaflet, A α ; posterior leaflet, P α ; Figure 3). Mitral valve tenting height, defined as the distance between the leaflet coaptation and the mitral annulus plane, was also measured in all 3 planes (Figure 3) (9). Finally, in the systolic phase, the distance between the heads of PMs was measured (Figure 4).

As an estimate of PMs displacement, the sphericity index of the mitral valve was calculated (9). The mitral valve sphericity index was defined as the ratio between the distance at the level of the basis of the PMs and the distance between this level and the mitral annulus plane (Figure 5).

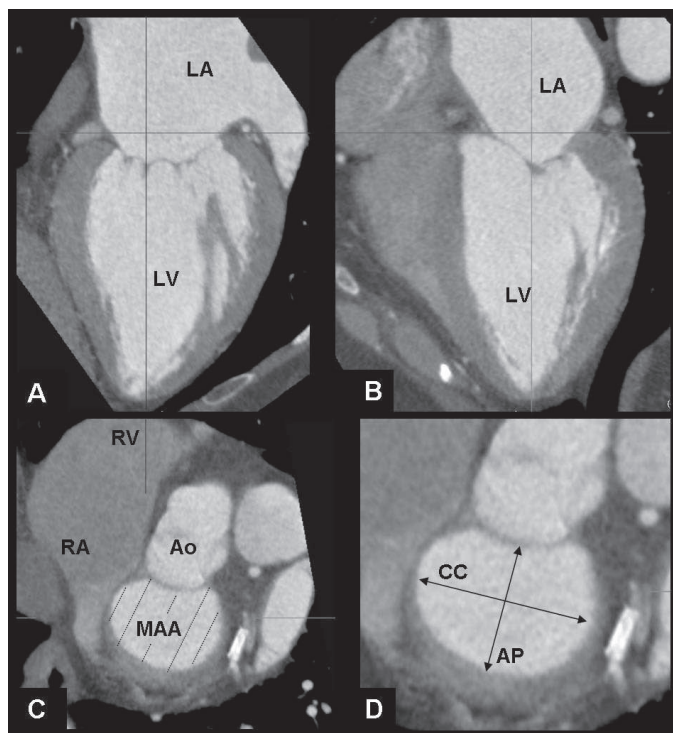


Figure 2. Assessment of the mitral valve annulus geometry. From the 2- and 4-chamber views (panel A and B), a short-axis view at the level of the mitral annulus was reconstructed (panel C). The area of the mitral annulus was quantified by planimetry. In addition, the intercommissural diameter (CC diameter) and the anteroposterior diameter (AP diameter) of the mitral annulus were assessed (panel D). Ao = aorta; LA = left atrium; LV = left ventricle; MAA = mitral annulus area; RA = right atrium; RV = right ventricle.

Echocardiography

Standard 2-dimensional echocardiograms were performed with patients in the left lateral decubitus position with a commercially available ultrasound system (Vingmed Vivid 7, General Electric-Vingmed, Milwaukee, Wisconsin). Images were obtained with a 3.5-MHz transducer at a depth of 16 cm in the parasternal (long- and short-axis) and apical (2- and 4-chamber) views. Standard 2-dimensional gray-scale images and color Doppler data were digitally stored in cine-loop format. LVEF was calculated from apical 2- and 4-chamber views with the biplane Simpson's rule (15). The severity of mitral regurgitation was graded quantitatively from color-flow Doppler in the conventional parasternal long-axis and apical 4-chamber views, using the proximal isovelocity surface area method. Effective regurgitant orifice area and regurgitant volume were calculated and mitral regurgitation was characterized according to the ACC/AHA guidelines: mild (regurgitant orifice area <0.2 cm² and regurgitant volume <30 ml/beat); moderate (regurgitant orifice area 0.2 - 0.39 cm² and regurgitant volume 30 - 59 ml/beat); severe (regurgitant orifice area ≥ 40 cm² and regurgitant volume ≥ 60 ml/beat) (16).

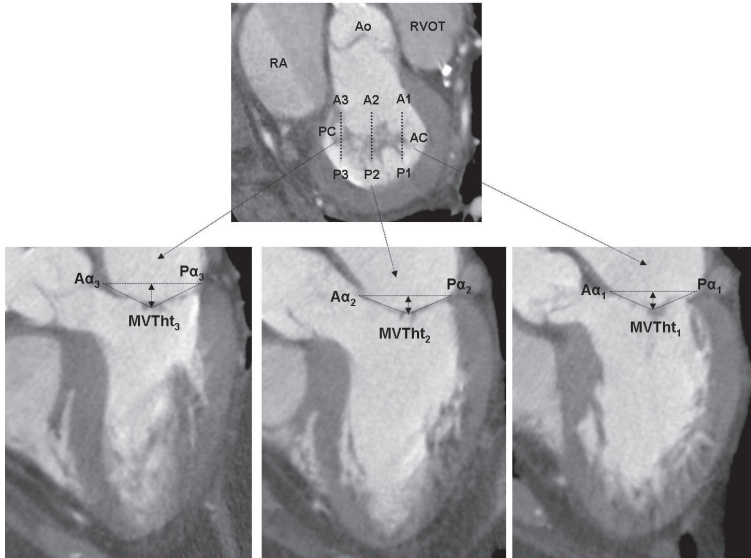


Figure 3. Assessment of the mitral valve geometry. Three anteroposterior planes perpendicular to the reconstructed LV short-axis view, at the level of the mitral commissures, were defined to assess the geometry of the anterolateral (A1-P1), central (A2-P2) and posteromedial (A3-P3) parts of the mitral leaflets. The leaflet angles ($A\alpha$ and Pa , as a reflection of tenting of the leaflets) and the mitral valve tenting height were measured in all 3 planes. AC = anterior commissure; $A\alpha$ = anterior leaflet angle; MVTh = mitral valve tenting height; PC = posterior commissure; Pa = posterior leaflet angle; RA = right atrium; RVOT = right ventricular outflow tract.



Figure 4. Displacement of papillary muscles. At the reconstructed systolic phase, the distance between the heads of the papillary muscles was measured, as indicated by the black arrow.

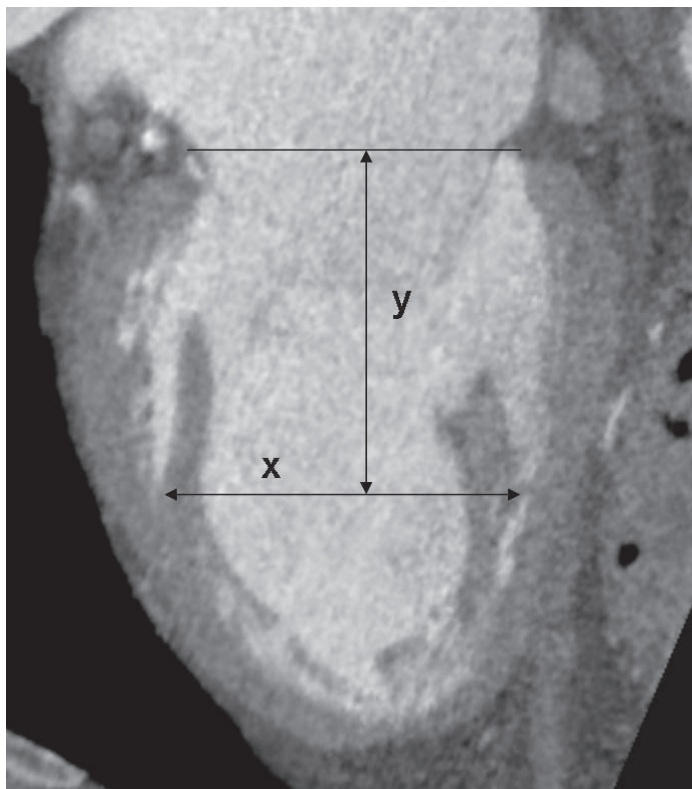


Figure 5. Sphericity index of the mitral valve. The sphericity index of the mitral valve was calculated as the ratio between the distance at the level of the papillary muscles basis (x) and the distance between this level and the mitral annulus plane (y).

Statistical analysis

Continuous variables are presented as mean values \pm SD; categorical variables are presented as frequencies and percentages. Differences between the two patient groups (controls vs. HF patients) were compared with the unpaired Student t-test for continuous variables and the chi-square tests for dichotomous variables. Differences between HF patients with moderate to severe FMR and HF patients without FMR were evaluated with the unpaired Student t-test. In addition, univariate linear regression analysis was performed to correlate various MSCT data on mitral valve geometry (mitral valve tenting height, anterior and posterior leaflet angles, mitral valve sphericity index) with the effective regurgitant orifice area obtained from echocardiography. Subsequently, major determinants of FMR severity were assessed among MSCT data on mitral valve geometry with a significant correlation in the univariate analysis ($p < 0.05$). For this purpose, multivariate linear regression analysis based on enter multiple regression analysis was performed. The dependent variable was the effective orifice regurgitant area and independent variables were anterior and posterior mitral leaflet angles and mitral tenting height at antero-lateral, central and posteromedial levels and the mitral valve sphericity index.

The reproducibility for the assessment of the tenting height, posterior and anterior leaflet angle at each level of the mitral valve was analyzed with repeated measurements by one experienced observer at two different time points and by a second experienced observer. Intra- and inter-observer agreements for these measurements were evaluated by Bland-Altman analysis. Furthermore, intra-class correlation coefficients were used as indicators of reproducibility.

All statistical analyses were performed with SPSS software (version 12.0, SPSS Inc., Chicago, Illinois). All statistical tests were two-sided, and a p-value <0.05 was considered statistically significant.

RESULTS

Study population

A total of 151 patients (mean age 60 ± 11 , 87 men) were studied. The overall population was divided into two groups: controls (n = 84) and HF patients (n = 67; 36 [54%] with ischemic cardiomyopathy and 31 [46%] with idiopathic cardiomyopathy). Baseline characteristics of the two groups are shown in Table 2.

Anatomic variations of subvalvular apparatus

In the majority of the patients, the anterior PM had a single insertion in the LV wall, either with 1 PM head (type I, n = 75 [50%]) or 2 PM heads (type IIA n = 49 [33%]). Other anatomical variations of the anterior PM are listed in Table 3. In contrast, the anatomy of the posterior PM was more variable, showing multiple PM heads or multiple PM insertions in the majority of the patients (Table 3).

Table 2. Baseline characteristics of the study population

	Controls (n = 84)	HF patients (n = 67)
Age (yrs)	57 ± 11	63 ± 11 *
Gender (M/F)	47/37	40/27
Body surface area (m ²)	1.9 ± 0.2	1.9 ± 0.2
Hypertension, n (%)	37 (44)	29 (43)
Hypercholesterolemia, n (%)	32 (38)	27 (40)
Diabetes mellitus, n (%)	29 (35)	15 (22)
Smoking, n (%)	24 (29)	27 (40)
Positive family history, n (%)	25 (30)	24 (36)
Previous myocardial infarction, n (%)	0	23 (34)
Anterior location, n(%)	0	14 (23)
Inferior location, n(%)	0	9 (14)
MR severity, n (%)		
Non-MR	54 (64)	4 (6)
Mild	30(36)	44(51)
Moderate	0	14 (21)
Severe	0	15 (22)

*p-value = 0.002; HF = heart failure; MR = mitral regurgitation.

Table 3. Anatomic variations of the papillary muscles (n=151)

Type	Anterior PM	Posterior PM
I	75 (50%)	31 (21%)
IIA	49 (33%)	43 (29%)
IIB	15 (10%)	48 (32%)
IIIA	8 (5%)	6 (4%)
IIIB	4 (3%)	14 (9%)
IIIC	0	9 (6%)

PM = papillary muscle.

In addition, the type of attachment of the PMs to the LV wall was assessed. In all patients the solid body of the PM connected to the solid portion of the LV wall through a network of trabeculae covering the surface of the LV cavity. This type of attachment was seen for both the anterior PM and the posterior PM in all patients.

Left ventricular and mitral valve geometry

The HF patients showed significantly larger LV volumes and lower LVEF as compared to controls (Table 4). In addition, the LV sphericity index was significantly increased in the HF patients (0.4 ± 0.1 vs. 0.3 ± 0.1 ; $p < 0.001$). The area of the mitral annulus was significantly higher in HF patients compared to controls (Table 4), indicating annular dilatation. In addition, both the AP diameter and the CC diameter of the mitral annulus were increased in the HF patients.

Table 4. Left ventricular and mitral valve geometry in the study population

	Controls (n=84)	HF patients (n=67)	p-value
LVEDV index (ml/m ²)	63 ± 15	95 ± 33	<0.0001
LVESV index (ml/m ²)	23 ± 9	66 ± 31	<0.0001
LVEF (%)	62 ± 13	33 ± 12	<0.001
LV Sphericity index	0.3 ± 0.1	0.4 ± 0.1	<0.001
Mitral annulus area index (cm ² /m ²)	4.8 ± 0.9	5.8 ± 1.4	<0.0001
CC-D index (mm/m ²)	21.6 ± 2.5	23.6 ± 2.9	<0.0001
AP-D index (mm/m ²)	12.5 ± 2.1	15.0 ± 2.7	<0.0001
Mitral valve sphericity index	1.2 ± 0.2	1.3 ± 0.3	0.02
D-PM index (mm/m ²)	11.3 ± 2.4	15.4 ± 2.8	<0.0001
Aα (°)			
Anterolateral	24.6 ± 8.1	29.8 ± 9.6	<0.001
Central	24.6 ± 7.0	32.2 ± 9.8	<0.001
Posteromedial	23.6 ± 7.6	28.6 ± 10.0	0.001
Pa (°)			
Anterolateral	27.1 ± 8.6	30.7 ± 10.3	0.02
Central	34.7 ± 9.6	40.3 ± 10.9	0.001
Posteromedial	28.4 ± 8.7	32.8 ± 10.5	0.006
MVTHt index (mm/m ²)			
Anterolateral	3.4 ± 0.9	4.5 ± 1.2	<0.0001
Central	4.2 ± 1.1	5.8 ± 1.5	<0.0001
Posteromedial	3.4 ± 0.9	4.6 ± 1.5	<0.0001

AP-D = mitral valve anteroposterior diameter; Aα = anterior leaflet angle; CC-D = mitral valve intercommissural diameter; D-PM = distance between the heads of the papillary muscles; HF = heart failure; LVEDV = left ventricular end-diastolic volume index; LVEF = left ventricular ejection fraction; LVESV = left ventricular end-systolic volume index; MVTHt = mitral valve tenting height; Pa = posterior leaflet angle.

The mitral valve sphericity index was defined as the ratio between the distance at the level of the basis of the PMs and the distance between this level and the mitral annulus plane (Figure 5). In the HF patients, a significantly greater distance between the bases of the PMs was observed ($15.4 \pm 1.8 \text{ mm/m}^2$ vs. $11.3 \pm 2.4 \text{ mm/m}^2$; $p < 0.001$). In addition, the distance between the mitral annulus level and the PM line was significantly different ($24.9 \pm 4.3 \text{ mm/m}^2$ vs. $22.3 \pm 3.6 \text{ mm/m}^2$; $p < 0.0001$). As a consequence, the mitral valve sphericity index was significantly larger in HF patients (Table 4). In addition, the distance between the heads of the PMs was also significantly larger in HF patients (Table 4). Finally, HF patients showed a significant increase in the leaflet angles with a significantly higher tenting height at all 3 levels of the mitral valve (Table 4).

Mitral valve geometry in patients with FMR

Among HF patients, 29 patients showed on echocardiography moderate to severe FMR (mean regurgitant volume $64.6 \pm 21.8 \text{ ml/beat}$ and mean effective regurgitant orifice area $0.4 \pm 0.1 \text{ cm}^2$). To detect changes in mitral valve geometry in FMR, HF patients with moderate to severe FMR ($n=29$) were compared with HF patients without FMR ($n=38$). Previous history of inferior myocardial infarction was present in 2 (7%) HF patients with moderate to severe FMR and in 7 (18%) HF patients without ($p = 0.11$). The patients with moderate to severe FMR had comparable LV volumes and LVEF to patients without FMR (Table 5). The mitral annulus area was significantly larger among patients with moderate to severe FMR, with also a significantly larger CC diameter (Table 5).

The distance between the basis of the PMs was larger in HF patients with moderate to severe FMR as compared to HF patients without FMR ($16.5 \pm 2.6 \text{ mm/m}^2$ vs. $14.7 \pm 2.7 \text{ mm/m}^2$, respectively; $p=0.006$). There were no differences in the distance between the PM line and the mitral annulus plane between both groups of patients ($25.1 \pm 3.5 \text{ mm/m}^2$ vs. $24.8 \pm 4.9 \text{ mm/m}^2$; $p=0.8$). Consequently, the sphericity index of the mitral valve was significantly higher in HF patients with moderate to severe FMR (Table 5). In addition, the distance between the heads of the PMs was significantly larger among HF patients with moderate to severe FMR (Table 5).

Compared to HF patients without FMR, HF patients with moderate to severe FMR showed an asymmetrical deformation of the mitral valve. Particularly, the angles of the posterior leaflet values at central and posteromedial levels were significantly higher, whereas no significant differences were observed either at the anterolateral level or the angles of the anterior leaflet (Table 5). As a consequence, the differences in mitral valve tenting height were more prominent at the central and the posteromedial levels (Table 5).

MSCT determinants of FMR severity

All MSCT derived parameters on mitral valve geometry (mitral valve tenting height, anterior and posterior leaflet angles and mitral valve sphericity index) showed a significant correlation with the effective regurgitant orifice area assessed by echocardiography in all 3 levels of the mitral valve (anterolateral, central and posteromedial) (Table 6). However, on multivariate

analysis, the mitral valve tenting height at the central level ($r = 0.58$; $p < 0.0001$) and the mitral valve sphericity index ($r = 0.36$; $p < 0.0001$) were the strongest determinants of FMR severity.

Table 5. Left ventricular and mitral valve geometry in HF patients with and without moderate to severe FMR

	HF patients with moderate to severe FMR (n=29)	HF patients without FMR (n=38)	p-value
EROA (cm ²)	0.4 ± 0.1	0.1 ± 0.02	<0.0001
Regurgitant volume (ml/beat)	64.6 ± 21.8	15.6 ± 12.3	<0.0001
LVEDV index (ml/m ²)	101 ± 37	91 ± 30	0.2
LVESV index (ml/m ²)	72 ± 37	62 ± 25	0.2
LVEF (%)	32 ± 14	33 ± 10	0.7
LV Sphericity index	0.4 ± 0.1	0.3 ± 0.1	0.1
Mitral annulus area index (cm ² /m ²)	6.3 ± 1.7	5.4 ± 0.9	0.02
CC-D index (mm/m ²)	24.8 ± 2.5	22.8 ± 2.9	0.006
AP-D index (mm/m ²)	15.6 ± 2.9	14.5 ± 2.4	0.1
Mitral valve sphericity index	1.4 ± 0.3	1.2 ± 0.3	0.004
D-PM index (mm/m ²)	16.5 ± 2.5	14.7 ± 2.7	0.006
Aα (°)			
Anterolateral	29.9 ± 8.3	29.9 ± 10.6	0.9
Central	33.2 ± 8.6	31.5 ± 10.7	0.5
Posteromedial	30.9 ± 9.7	26.8 ± 10.1	0.1
Pa (°)			
Anterolateral	32.3 ± 10.9	29.5 ± 9.7	0.3
Central	44.4 ± 11.9	37.1 ± 9.0	0.008
Posteromedial	35.9 ± 10.6	26.8 ± 10.1	0.04
MVTHt index (mm/m ²)			
Anterolateral	4.8 ± 1.2	4.2 ± 1.0	0.02
Central	6.6 ± 1.4	5.3 ± 1.3	<0.0001
Posteromedial	5.4 ± 1.6	4.1 ± 1.2	<0.0001

EROA = effective regurgitant orifice area; FMR = functional mitral regurgitation; other abbreviations as in Table 4.

Table 6. MSCT determinants of effective regurgitant orifice area: univariate and multivariate analysis.

	Univariate		Multivariate
	r	p-value	p-value
Aα (°)			
Anterolateral	0.19	0.02	0.7
Central	0.31	<0.0001	0.3
Posteromedial	0.26	0.001	...
Pa (°)			
Anterolateral	0.25	0.002	0.3
Central	0.32	<0.0001	0.9
Posteromedial	0.25	0.002	...
MVTHt index (mm/m ²)			
Anterolateral	0.36	<0.0001	0.5
Central	0.53	<0.0001	<0.0001
Posteromedial	0.43	<0.0001	...
Mitral valve sphericity index	0.36	<0.0001	<0.0001

R² of the model selected for multivariate analysis = 0.428. The anterior and posterior leaflet angle and the mitral valve tenting height at the posteromedial level were not included in the model because of the high inter-correlation of these variables (Pearson correlation coefficient >0.70). Aα = anterior leaflet angle; MVTHt = mitral valve tenting height; Pa = posterior leaflet angle.

Reproducibility data

In 15 randomly selected patients, reproducibility data was assessed. The intra-observer agreement for the tenting height and leaflet angle measurements was good. The average differences were: $0.9 \pm 1.4\%$ for the tenting height, $-3.3 \pm 5.7\%$ for the posterior leaflet angle, and $-0.8 \pm 4.9\%$ for the anterior leaflet angle. The intra-class correlation coefficients for each intra-observer comparison were: 0.92 for the tenting height, 0.86 for the posterior leaflet angle and 0.85 for the anterior leaflet angle.

Similarly, agreement of the measurements by two different observers was good. The average differences were: $0.1 \pm 1.2\%$ for the tenting height, $0.9 \pm 2.9\%$ for the posterior leaflet angle and $-0.4 \pm 4.4\%$ for the anterior leaflet angle. The intra-class correlation coefficients for each inter-observer comparison were: 0.84 for the tenting height, 0.83 for the posterior leaflet angle and 0.84 for the anterior leaflet angle.

DISCUSSION

The present study demonstrates that MSCT enables a comprehensive assessment of the mitral valve apparatus, by providing an exact characterization of the anatomy of the subvalvular apparatus and the geometry of the mitral valve. The main findings can be summarized as follows: the anatomy of the subvalvular apparatus is highly variable, with variations in both the number of heads and insertions of the anterior and posterior PMs. Furthermore, the attachment of the PMs to the LV wall is not solid, but trabecularized in all patients. With the use of MSCT, an asymmetric deformation of the mitral valve was observed in HF patients with moderate to severe FMR. The posterior leaflet angles and the mitral valve tenting height were significantly increased at the central and the posteromedial levels, as compared to HF patients without FMR. In addition, a more outward displacement of the PMs, reflected by a higher mitral valve sphericity index, was observed in this subgroup of patients. The findings of the present study may have important implications for surgical mitral valve repair in patients with severe FMR.

Anatomic variations of subvalvular apparatus

A large variability in the anatomy of the subvalvular apparatus was observed in the present study (Figure 1 and Table 3). The characterization of the subvalvular apparatus may be of great importance for various surgical mitral valve repair approaches that include translocation or reconstruction and relocation of the PMs (11,17). Previous anatomical studies have also reported variations in PM anatomy (13,18). Berdajs et al. (13) studied 100 structural normal hearts and classified the PMs according to the number of heads and insertions (Figure 1). The authors demonstrated that the anatomy of the posterior PM was more heterogeneous compared with the anterior PM (13). The results of the present study are in line with previous anatomical studies: in

the majority of the patients, the posterior PM consisted of multiple heads or multiple insertions, whereas the anatomy of the anterior PM was more homogeneous (Table 3).

In addition to PM anatomy, the characteristics of the PM attachments to the LV wall were assessed in the present study. Conventionally, the anchorage of the PM to the solid heart wall has been described as a direct connection with a broad base. However, recently, Axel noted that the attachment may rather be through a network of trabeculae (19). In the present study, similar attachments of the PMs were found. In all patients the bases of the PMs connected to the solid wall of the LV through a network of trabeculae instead of a solid attachment (Figure 1). The attachment of the PMs to the LV wall may have implications for surgical mitral valve repair. However, the exact clinical importance of this finding remains to be determined. Nonetheless, MSCT allows for a detailed analysis of the anatomy of the PMs and their attachment to the LV wall.

Geometric changes in FMR

The geometry of the mitral valve was studied in 29 HF patients with moderate to severe FMR, and compared to HF patients without FMR ($n = 38$). In HF patients with moderate to severe FMR, remodeling of the LV and the mitral valve was observed. Importantly, mitral valve deformation affected predominantly the central and posteromedial parts of the valve, and the increase in mitral valve tenting height at the central level was the strongest determinant of FMR severity. In addition, the higher sphericity index of the mitral valve indicates that the displacement of the PMs plays a role in the development of FMR. These results are in agreement with previous *in vitro* and *in vivo* studies (9,20). Nielsen et al. (20) used an *in vitro* LV model to study the impact of PM misalignment on mitral leaflet coaptation and its relation with the severity of mitral regurgitation. The asymmetrical displacement of the PMs towards a more posterior level resulted in preserved or excessive anterior leaflet motion (prolapse-like) at the anterolateral level (close to the anterior commissure), whereas at the posteromedial level (close to the posterior commissure), a failure of leaflet coaptation was observed (20). Kwan et al. (9), confirmed these results using 3-dimensional echocardiography in patients with ischemic cardiomyopathy. An asymmetrical deformation of the mitral valve, with a “funnel-shaped” deformity on the level close to the posterior commissure and a “prolapse-like” deformity on the anterolateral side, was noted in patients with ischemic cardiomyopathy, in contrast to patients with idiopathic cardiomyopathy (9). The present study confirms these results and demonstrates that MSCT may be of value for assessment of mitral valve remodeling in patients with FMR.

Determinants of FMR severity

The geometry parameters of the mitral valve assessed by 64-slice MSCT were related to the severity of FMR, particularly the mitral valve tenting height at the central level and the sphericity index of the mitral valve. These findings are in agreement with previous data based on 2- and 3-dimensional echocardiography (9). Kwan et al. demonstrated using 3-dimensional

echocardiography, that the medial mitral valve tenting area was the major determinant of the severity of mitral regurgitation in patients with dilated cardiomyopathy (9). In addition, the mitral valve sphericity index, as an indicator of the outward displacement of the PMs, suggests that FMR severity is also related to changes in LV cavity geometry, as previously described (21).

Clinical implications

Accurate assessment of the interaction of the LV and the mitral valve apparatus is crucial in surgical treatment of FMR (8). New surgical techniques that include restoration of LV geometry and relocation of the PMs have been proposed (11,17). For these procedures, an exact characterization of the LV geometry and the subvalvular apparatus is mandatory. Furthermore, assessment of the deformation of the mitral annulus is important for surgical procedures that attempt to restore the geometry of the mitral valve (12). Finally, the assessment of leaflet tethering is of critical importance and may even predict the outcome of surgical mitral valve repair (22).

Previously, it has been demonstrated that MSCT may be of value for assessment of mitral valve anatomy (23-25). However, in none of these studies, the geometry of the mitral valve and the interaction with the LV was studied. In the present study, 64-slice MSCT was used to assess mitral valve anatomy and geometry in a large cohort of patients, including patients with FMR. By providing detailed information on all components of the LV and mitral valve complex, MSCT may be of great value to guide surgical therapy for FMR.

Study limitations

There is little evidence on the assessment of regurgitant mitral valve with MSCT (26). In the present study, the regurgitant orifice area was not quantified with MSCT, which is a limitation. Furthermore, surgical data was not systematically available in all patients with FMR, precluding us to confirm prospectively the value of MSCT in the surgical treatment decision. Future studies, assessing both the anatomical and the functional aspects of the mitral valve with MSCT and with larger populations including patients with several grades of FMR, may provide more insight in this issue. Finally, radiation dose (currently 10-15 mSv) is one of the general disadvantages of MSCT and adjustments in imaging protocols are warranted to keep the radiation exposure within limits.

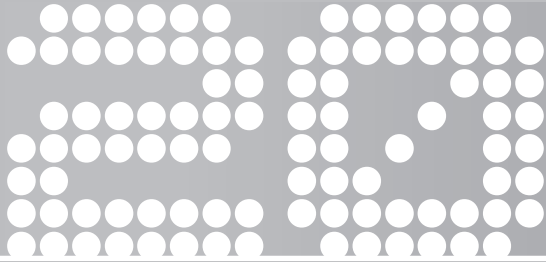
CONCLUSIONS

The present study shows that MSCT allows detailed assessment of mitral valve anatomy and geometry. In patients with moderate to severe FMR, an asymmetrical remodeling of the mitral valve was observed, with tethering of the mitral leaflets at the central and posteromedial levels of the mitral valve. MSCT provides the anatomical and geometric analysis of the mitral valve apparatus and may be of value to guide surgical treatment of FMR.

REFERENCES

1. Feinberg MS, Schwammenthal E, Shlizerman L et al. Prognostic significance of mild mitral regurgitation by color Doppler echocardiography in acute myocardial infarction. *Am J Cardiol* 2000;86:903-7.
2. Grigioni F, Enriquez-Sarano M, Zehr KJ, Bailey KR, Tajik AJ. Ischemic mitral regurgitation: long-term outcome and prognostic implications with quantitative Doppler assessment. *Circulation* 2001;103:1759-64.
3. Koelling TM, Aaronson KD, Cody RJ, Bach DS, Armstrong WF. Prognostic significance of mitral regurgitation and tricuspid regurgitation in patients with left ventricular systolic dysfunction. *Am Heart J* 2002;144:524-9.
4. Borger MA, Alam A, Murphy PM, Doenst T, David TE. Chronic ischemic mitral regurgitation: repair, replace or rethink? *Ann Thorac Surg* 2006;81:1153-61.
5. Calafiore AM, Gallina S, Di MM et al. Mitral valve procedure in dilated cardiomyopathy: repair or replacement? *Ann Thorac Surg* 2001;71:1146-52.
6. McGee EC, Gillinov AM, Blackstone EH et al. Recurrent mitral regurgitation after annuloplasty for functional ischemic mitral regurgitation. *J Thorac Cardiovasc Surg* 2004;128:916-24.
7. Mihaljevic T, Lam BK, Rajeswaran J et al. Impact of mitral valve annuloplasty combined with revascularization in patients with functional ischemic mitral regurgitation. *J Am Coll Cardiol* 2007;49:2191-201.
8. Levine RA, Schwammenthal E. Ischemic mitral regurgitation on the threshold of a solution: from paradoxes to unifying concepts. *Circulation* 2005;112:745-58.
9. Kwan J, Shiota T, Agler DA et al. Geometric differences of the mitral apparatus between ischemic and dilated cardiomyopathy with significant mitral regurgitation: real-time three-dimensional echocardiography study. *Circulation* 2003;107:1135-40.
10. Yu HY, Su MY, Liao TY, Peng HH, Lin FY, Tseng WY. Functional mitral regurgitation in chronic ischemic coronary artery disease: analysis of geometric alterations of mitral apparatus with magnetic resonance imaging. *J Thorac Cardiovasc Surg* 2004;128:543-51.
11. Liel-Cohen N, Guerrero JL, Otsuji Y et al. Design of a new surgical approach for ventricular remodeling to relieve ischemic mitral regurgitation: insights from 3-dimensional echocardiography. *Circulation* 2000;101:2756-63.
12. Gillinov AM, Cosgrove DM, III, Shiota T et al. Cosgrove-Edwards Annuloplasty System: midterm results. *Ann Thorac Surg* 2000;69:717-21.
13. Berdajs D, Lajos P, Turina MI. A new classification of the mitral papillary muscle. *Med Sci Monit* 2005;11:BR18-21.
14. Kono T, Sabbah HN, Stein PD, Brymer JF, Khaja F. Left ventricular shape as a determinant of functional mitral regurgitation in patients with severe heart failure secondary to either coronary artery disease or idiopathic dilated cardiomyopathy. *Am J Cardiol* 1991;68:355-9.
15. Schiller NB, Shah PM, Crawford M et al. Recommendations for quantitation of the left ventricle by two-dimensional echocardiography. *J Am Soc Echocardiogr* 1989;2:358-67.
16. Bonow RO, Carabello BA, Kanu C et al. ACC/AHA 2006 guidelines for the management of patients with valvular heart disease. *Circulation* 2006;114:e84-231.
17. Kron IL, Green GR, Cope JT. Surgical relocation of the posterior papillary muscle in chronic ischemic mitral regurgitation. *Ann Thorac Surg* 2002;74:600-1.
18. Victor S, Nayak VM. Variations in the papillary muscles of the normal mitral valve and their surgical relevance. *J Card Surg* 1995;10:597-607.
19. Axel L. Papillary muscles do not attach directly to the solid heart wall. *Circulation* 2004;109:3145-8.
20. Nielsen SL, Nygaard H, Fontaine AA et al. Papillary muscle misalignment causes multiple mitral regurgitant jets: an ambiguous mechanism for functional mitral regurgitation. *J Heart Valve Dis* 1999;8:551-64.

21. Yiu SF, Enriquez-Sarano M, Tribouilloy C, Seward JB, Tajik AJ. Determinants of the degree of functional mitral regurgitation in patients with systolic left ventricular dysfunction: A quantitative clinical study. *Circulation* 2000;102:1400-6.
22. Magne J, Pibarot P, Dagenais F, Hachicha Z, Dumesnil JG, Senechal M. Preoperative posterior leaflet angle accurately predicts outcome after restrictive mitral valve annuloplasty for ischemic mitral regurgitation. *Circulation* 2007;115:782-91.
23. Willmann JK, Kobza R, Roos JE et al. ECG-gated multi-detector row CT for assessment of mitral valve disease: initial experience. *Eur Radiol* 2002;12:2662-9.
24. Alkadhi H, Bettex D, Wildermuth S et al. Dynamic cine imaging of the mitral valve with 16-MDCT: a feasibility study. *AJR Am J Roentgenol* 2005;185:636-46.
25. Messika-Zeitoun D, Serfaty JM, Laissy JP et al. Assessment of the mitral valve area in patients with mitral stenosis by multislice computed tomography. *J Am Coll Cardiol* 2006;48:411-3.
26. Alkadhi H, Wildermuth S, Bettex DA et al. Mitral regurgitation: quantification with 16-detector row CT--initial experience. *Radiology* 2006;238:454-63.



Percutaneous aortic valve therapy: clinical experience and the role of multi-modality imaging

Laurens F. Tops
Victoria Delgado
Frank van der Kley
Jeroen J. Bax

Department of Cardiology, Leiden University Medical Center, Leiden, the Netherlands

Heart 2009;95:1538-46

INTRODUCTION

Degenerative aortic stenosis (AS) accounts for the majority of native valve disease (1). Surgical aortic valve (AV) replacement is a treatment option that provides good outcome in the majority of the patients, with good durability of the prosthetic valve (2). However, a large proportion of patients with severe AS are not referred for, or denied surgery. The Euro Heart Survey on valvular heart disease demonstrated that up to 33% of the patients with severe AS did not undergo surgery, although there was an indication (3). Patient's age and (multiple) co-morbidities were the main reasons for denial of surgery (4). Therefore, there is a need for a less invasive treatment option in older patients with severe AS.

In the past few years, new percutaneous AV implantation procedures have been introduced (5). Two different types of percutaneous AV prostheses now have CE mark approval in Europe. In addition, European (6) and American (7,8) recommendations on percutaneous AV implantation have been published. In the present manuscript, the clinical experience with the two different percutaneous AVs will be reviewed. In addition, the role of different imaging modalities in the selection of patients, guidance during percutaneous AV implantation and follow-up will be discussed.

PROSTHESES AND CLINICAL EXPERIENCE

Currently, two different types of percutaneous AV devices are commercially available. The balloon-expandable Edwards SAPIEN valve (Edwards Lifesciences Inc., Irvine, California, USA) and the self-expanding CoreValve Revalving prosthesis (CoreValve Inc., Irvine, California, USA). At present, more than 2500 patients worldwide have been treated with percutaneous AV implantation, and the number of studies reporting the clinical experience and results with percutaneous AV procedures is rapidly growing (Table 1). In the following paragraphs, technical aspects of the different prostheses and clinical experience with percutaneous AV implantations will be reviewed.

Balloon-expandable valve

Andersen et al. first tested the balloon-expandable percutaneous AV in an animal model in 1992 (9). Subsequently, Cribier et al. performed the first human implantation in 2002 (10). The first generation balloon-expandable valve was entitled Cribier-Edwards valve (Edwards Lifesciences Inc.), whereas at present the Edwards SAPIEN valve (Edwards Lifesciences Inc.) is commercially available (Figure 1). This prosthesis incorporates a balloon-expandable stainless steel stent, fabric sealing cuff and bovine pericardial leaflets. At present, available prosthesis sizes are 23 and 26 mm for aortic annulus diameters between 18 to 22 mm and 21 to 25 mm, respectively.

Table 1. Overview of published reports to date on the results of percutaneous AV implantation

Study (reference)	Year	Valve	Implantation	Number of patients	Logistic EuroSCORE (%)	Procedural success (%)	30 day mortality (%)	AVA pre (cm ²)	AVA post (cm ²)	Mean pressure gradient pre (mmHg)	Mean pressure gradient post (mmHg)
Cribier et al. (13)	2004	Cribier-Edwards	Antegrade	6	N/A	83.3	50	0.49 ± 0.08	1.66 ± 0.13	38 ± 11	5.6 ± 3.4
Webb et al. (11)	2006	Cribier-Edwards	Retrograde	18	26.2 ± 13.1	77.8	11.1	0.6 ± 0.2	1.6 ± 0.4	50 ± 12	13 ± 6
Cribier et al. (14)	2006	Cribier-Edwards	Antegrade (n=26) Retrograde (n=7)	36	N/A	75.0	16.7	0.60 ± 0.09	1.70 ± 0.11	37 ± 13	9 ± 2
Lichtenstein et al. (12)	2006	Cribier-Edwards	Transapical	7	35 ± 26	100	14	0.7 ± 0.1	1.8 ± 0.8	31 ± 10	9 ± 6
Grube et al. (21)	2006	CoreValve	Retrograde	25	Median 11.0 (9.2-19.9)	84.0	20	0.72 ± 0.13	N/A	44 ± 11	12 ± 3
Walther et al. (41)	2007	Cribier-Edwards	Transapical	30	27.1 ± 12.2	96.7	10	0.5 ± 0.2	N/A	43 ± 14	8 ± 5
Ye et al. (42)	2007	Cribier-Edwards	Transapical	7	31 ± 23	100	14	0.7 ± 0.3	1.6 ± 0.6	32 ± 8	10 ± 7
Grube et al. (18) *	2007	CoreValve	Retrograde	86	21.7 ± 12.6	74	12	0.60 ± 0.16	1.67 ± 0.41	44 ± 15	N/A
Webb et al. (15)	2007	Cribier-Edwards	Retrograde	50	28	86	12	0.6 ± 0.2	1.7 ± 0.4	46 ± 17	11 ± 5
Walther et al. (43) *	2007	Edwards SAPIEN	Transapical	59	26.8 ± 13.5	93.2	13.6	0.50 ± 0.15	N/A	N/A	9 ± 6
Marcheix et al. (44)	2007	CoreValve	Retrograde	10	Median 32 (21-40)	100	20	0.57 ± 0.19	1.20 ± 0.35	51 ± 19	11 ± 3

Table 1. continued

Study (reference)	Year	Valve	Implantation	Number of patients	Logistic EuroSCORE (%)	Procedural success (%)	30 day mortality (%)	AVA pre (cm ²)	AVA post (cm ²)	Mean pressure gradient pre (mmHg)	Mean pressure gradient post (mmHg)
Walther et al. (16)	2008	Edwards SAPIEN	Transapical	50	27.6 ± 12.2	100	8	N/A	N/A	N/A	7 ± 4
Descoutures et al. (45)	2008	Edwards SAPIEN	Retrograde	12	31.1 ± 14.4	83	25	0.5 ± 0.1	1.7 ± 0.5	50 ± 19	11 ± 3
Svensson et al. (46) *	2008	Edwards SAPIEN	Transapical	40	35.5 ± 15.3	90	17.5	0.62 ± 0.13	1.61 ± 0.37	40 ± 10	8 ± 3
Piazza et al. (22) *	2008	CoreValve	Retrograde	646	23.1 ± 13.8	97.2	8	0.6 ± 0.2	N/A	49 ± 14	3 ± 2
Zierer et al. (47)	2008	Cribier-Edwards	Transapical	26	36.5 ± 5.8	96	15	0.6 ± 0.1	N/A	N/A	6 ± 2
Rodes-Cabau et al. (48)	2008	Edwards SAPIEN	Retrograde (n=10) Transapical (n=12)	22	26 ± 16	91	8.7	0.63 ± 0.18	1.48 ± 0.31	34 ± 10	9 ± 3

* multi-center study; AV = aortic valve; AVA = aortic valve area.

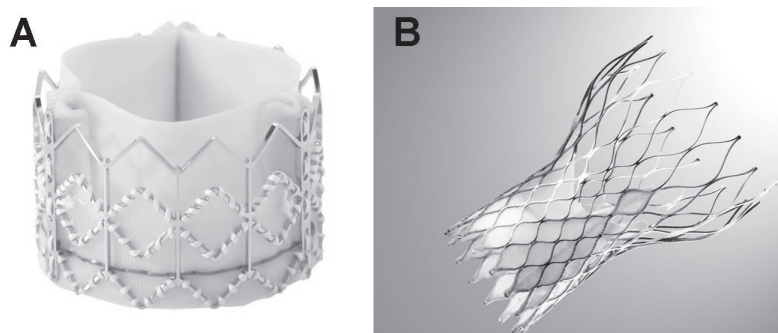


Figure 1. Currently commercially available prostheses for percutaneous AV implantation. Panel A shows the balloon-expandable Edwards-SAPIEN valve. Panel B shows the self-expanding CoreValve prosthesis.

In the first studies, an antegrade implantation of the valve was performed, using transeptal access to the left atrium and passage through the mitral valve to reach the AV (10). However, at present a retrograde approach through the femoral artery is used (11). During the procedure, a balloon valvuloplasty is first performed to facilitate passage of the native AV. During rapid right ventricular pacing, the prosthesis is positioned and deployed under fluoroscopy and echocardiographic guidance. Alternatively, in patients with difficult vascular access because of extensive calcifications or tortuosity of the femoral artery or aorta, a transapical approach can be used. After a partial thoracotomy, direct puncture of the apical portion of the left ventricular free wall is performed to gain catheter access to the left ventricle and AV. The prosthesis is subsequently positioned and deployed, similar to the antegrade approach (12).

Clinical experience: Cribier-Edwards and Edwards SAPIEN valve A single center Phase 1 project was started in 2003 for compassionate use of the Cribier-Edwards valve in patients with end-stage AS after the first successful animal and human studies. In the Initial Registry of Endovascular Implantation of Valves in Europe (I-REVIVE) trial, followed by the Registry of Endovascular Critical Aortic Stenosis Treatment (RECAST) trial, a total of 36 patients (mean EuroSCORE 12 ± 2) were included (13,14). Twenty seven patients underwent successful percutaneous AV implantation (23 antegrade, 4 retrograde). The 30-day mortality was 22% (6 of 27 patients), and mean aortic valve area (AVA) increased from $0.60 \pm 0.11 \text{ cm}^2$ to $1.70 \pm 0.10 \text{ cm}^2$ ($p < 0.001$). Importantly, this improvement in AVA was maintained up to 24 months follow-up (14).

After these first trials, the Cribier-Edwards prosthesis and the Edwards SAPIEN prosthesis have been used in numerous studies (Table 1). Overall, acute procedural success is achieved in 75 to 100% of the procedures, and 30-day mortality ranges between 8 and 50% in the published studies. In a large study using the retrograde approach, Webb et al. treated 50 AS patients (mean age 82 ± 7 years, 45 patients in New York Heart Association (NYHA) functional class III or IV) (15). A Cribier-Edwards valve was successfully implanted in 43 of the 50 patients (86%). Interestingly, a clear learning curve was observed when comparing the first 25 patients with the second 25 patients. Procedural success increased from 76% in the first 25 patients

to 96% in the second 25, and 30-day mortality fell from 16% to 8% (15). Recently, Walther et al. reported their initial single-center experience with the transapical implantation of the Edwards SAPIEN valve in 50 high-risk AS patients (16). Via an anterolateral minithoracotomy, the prosthesis was successfully implanted in 47 patients (94%); early conversion to conventional sternotomy had to be performed in 3 patients. Cardiopulmonary bypass was used in 16 patients (32%). After implantation, all prostheses showed good valvular function, with only mild aortic incompetence (mean aortic regurgitation grade 0.5 ± 0.5). During the first 30 days post-operative 4 patients died and during follow-up another 10 patients died (overall survival at 12 months 71.4%). A post-hoc analysis of the first 25 patients versus the second 25 patients did not show a difference in long-term survival after AV implantation (16).

Importantly, a randomized trial using the Edwards SAPIEN valve is currently comparing percutaneous AV implantation against surgical AV replacement (objective: demonstrating non-inferiority of the percutaneous prosthesis) and medical therapy (objective: demonstrating superiority of the prosthesis) (Figure 2). The primary endpoint in the two arms is mortality at 12 months follow-up, with secondary endpoints that focus on long-term adverse cardiovascular events composite, valve performance and quality-of-life indicators (17). The results of this first randomized trial with percutaneous AV implantations are eagerly awaited.

Self-expanding valve

The CoreValve Revalving system™ (CoreValve Inc.) consists of a tri-leaflet bioprosthetic porcine pericardial tissue valve, mounted and sutured in a self-expanding nitinol alloy stent (Figure 1).

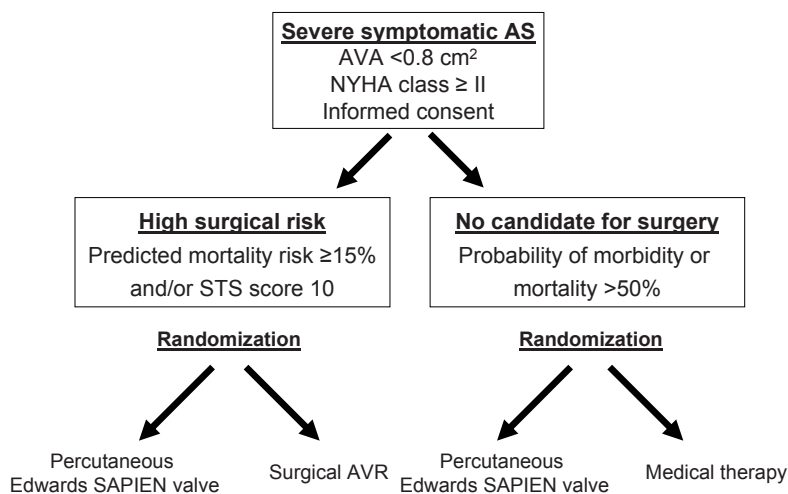


Figure 2. Flowchart of the randomized Placement of AoRTic traNscathetER valves (PARTNER) trial. In the first treatment arm (surgical) the Edwards SAPIEN prosthesis is compared against standard surgical AV replacement in 350 patients. The second arm (medical management) compares the Edwards SAPIEN valve against medical therapy and/or balloon valvuloplasty in 250 patients. The primary endpoint in the two arms is mortality at 12 months follow-up. Secondary endpoints include an adverse cardiovascular events composite, valve performance and quality-of-life indicators.

The device is constrained within a delivery sheath, and expands to its predetermined shape when the sheath is withdrawn. It has a specific design consisting of three distinct parts: The lower portion of the prosthesis has high radial force to expand and avoid recoil. The middle portion includes the pericardial tissue valve and is constrained to avoid coronary occlusion. The upper part is flared to center and fix the prosthesis in the ascending aorta. At present, the third generation CoreValve Revalving system is commercially available. The size of the delivery system has gradually declined from a 25F and 21F system (first- and second-generation, respectively) to the currently available third-generation 18F system. Two different sizes are currently available: a 26 mm prosthesis (aortic annulus diameter 20 – 24 mm) and a 29 mm prosthesis (aortic annulus diameter 24 – 27 mm). The CoreValve prosthesis is implanted retrograde through the femoral artery. While in the first series the prosthesis was implanted under general anesthesia with a cardiac assist device, extracorporeal membrane oxygenation or a full-bypass support (18), at present local anesthesia combined with mild systemic sedative/analgesic medication is used without cardiac assist or full-bypass support (19). After balloon valvuloplasty, the device is positioned under fluoroscopy guidance. Retraction of the outer sheath allows deployment of the self-expanding prosthesis. Postdilatation of the prosthesis can be performed if deemed necessary, depending on the position of the prosthesis and the presence of aortic regurgitation (19).

Clinical experience: CoreValve Revalving system. After the first implantation of the CoreValve prosthesis in a patient in 2005 (20), a large number of patients have been treated with this device to date (Table 1). In the first pilot study, Grube et al. treated 25 patients with severe AS deemed unsuitable for open-heart surgery using first- and second-generation prostheses (21). Acute procedural success was achieved in 21 of 25 patients (84%). Major in-hospital cardiovascular and cerebral events occurred in 8 patients (32%) whereas major bleeding occurred in 5 of 10 patients (50%) treated with the first-generation device and in 1 of 15 patients (7%) treated with the second-generation prosthesis. At 30-days follow-up, mean AV gradient decreased from 44.2 ± 10.8 mmHg to 11.8 ± 3.4 mmHg ($p < 0.001$), and NYHA class improved from 2.9 ± 0.2 to 1.7 ± 0.5 ($p < 0.001$) (21).

Recently, Grube et al have reported the results with the three different generations CoreValve Revalving system (19). In this nonrandomized, prospective study, a total of 136 patients were included. Ten patients were treated with first-generation devices, 24 patients with second-generation and 102 patients with third-generation devices. At baseline, mean AVA was 0.67 ± 0.9 cm² and mean logistic EuroSCORE was 23.1 ± 15.0 % in the overall study population. Overall procedural success rate increased significantly with the new generation devices from 70.0% and 70.8% to 91.2% for first-, second- and third-generation prostheses, respectively ($p = 0.003$). Interestingly, periprocedural mortality decreased using newer devices from 10% (first-generation) to 8.3% (second-generation) to 0% (third-generation). Overall 30-day mortality for the three generations was 40%, 8.3% and 10.8%, respectively. Pooled data demonstrated a significant improvement in NYHA functional class (from 3.3 ± 0.5 to 1.7 ± 0.7 , $p < 0.001$),

without a difference between the 3 generations. Importantly, NYHA functional class and mean pressure gradient remained stable up to 12 months follow-up in all 3 generations. This largest single-center experience with three generations CoreValve prostheses demonstrates that the use of the latest generation prosthesis is associated with an improved procedural and mid-term outcome (19).

In addition, the results of a multi-center registry with the third-generation CoreValve Revalving system have recently been reported (22). A total of 646 patients from 51 centers were included in the registry. It was a high risk elderly population (mean age 81 ± 7 years) with a poor functional class (85% of the patients in NYHA class III or IV), and a high logistic EuroSCORE (mean $23.1 \pm 13.8\%$). Procedural success was achieved in 628 of the 646 patients (97.2%). All-cause 30-day mortality was 8%, and the combined end-point of procedural-related death, stroke or myocardial infarction was reached in 60 patients (9.3%). After successful implantation, mean pressure gradient decreased from 49 ± 14 mmHg to 3 ± 2 mmHg (22). This large registry confirms the results of earlier studies, and demonstrates the safety, feasibility and efficacy of the CoreValve Revalving system.

Valve-in-valve procedure

The concept of a percutaneous AV implantation in an existing AV prosthesis ('valve-in-valve') has recently been introduced. The feasibility was demonstrated in an animal model by Walther et al. (23). Afterwards, the valve-in-valve concept has been successfully applied in patients with degenerated aortic bioprostheses (24,25). It may be of great value in these patients, since re-operation for degenerated xenografts is challenging, and is associated with an increased mortality risk as compared with first isolated AV replacement (26).

Furthermore, the valve-in-valve concept can be used during first percutaneous CoreValve prosthesis implantation, in case of suboptimal implantation of the prosthesis (19). Good function of the prostheses and durability of the valve-in-valve has been demonstrated up to three years follow-up (27). Recently, a multi-center study demonstrated that in up to 2.6% of first CoreValve prosthesis implantation procedures, a valve-in-valve procedure is performed (22). However, it should be performed with caution because future access to the coronary ostia may be limited by the two overlying nitinol frames of the prostheses.

SELECTION OF PATIENTS

The selection of patients for percutaneous AV implantation involves several critical steps. In general, a multi-disciplinary team, including cardiologists, surgeons, anesthesiologists and imaging specialists, should decide if patients are eligible for percutaneous AV implantation. Recently, two position statements on the use of percutaneous AV procedures have been published, that provide important information on the patient selection procedure (6,8). A summary

of the European statement (endorsed by the European Association of Cardio-Thoracic Surgery and the European Society of Cardiology) is provided in Table 2.

One of the first steps in the selection procedure is the assessment of AS severity. At present, percutaneous AV implantation is only recommended in symptomatic patients with severe AS. The surgical risk, life expectancy, and quality of life should also be assessed. Preferably, the surgical risk is determined using a combination of clinical judgement and multiple risk scores, such as the logistic EuroSCORE, the STS Predicted Risk of Mortality score, or Ambler score (6). When patients are deemed inoperable due to a high surgical risk, a percutaneous procedure can be considered.

Finally, the feasibility of a percutaneous procedure and contraindications should be assessed in the potential candidates (Table 2). Typically, coronary anatomy, the aortic annulus and the peripheral vessels are evaluated. For this purpose, various imaging modalities are available. These modalities and their relative merits will be reviewed in the following paragraphs.

Table 2. Recommendations on patient selection for percutaneous AV implantation (adapted from Vahanian et al. ref # (6))

Patient selection steps	Recommendation on patient selection	Comment
1. Confirmation of AS severity 2. Clinical evaluation	Only in severe AS	Echocardiography is preferred tool
3A. Evaluation of surgical risk	Only in patients with severe symptoms related to AS Only in high-risk patients or patients with contra-indications for surgery	Clinical judgement and the use of a combination of risk scores (EuroSCORE, STS Predicted Risk of Mortality score, Ambler score) is preferred
3B. Evaluation of life expectancy / quality of life 4A. Assessment of feasibility of procedure	Not in patients with life expectancy < 1 year (conservative treatment) Evaluation should include: Coronary anatomy assessment Aortic annulus assessment Peripheral arteries assessment	Coronary angiography or MSCT should be used to assess: Coronary artery disease Position of coronary arteries relative to aortic cusps Echocardiography/ MSCT/ MRI/ Aortography should be used to assess aortic annulus size Angiography/ MSCT/ MRI should be used to assess size, tortuosity, calcifications.
4B. Assessment of contraindications	Contraindications are: Aortic annulus <18 or >25 mm (Edwards-SAPIEN) and <20 or >27 mm (CoreValve) Bicuspid AV Asymmetric heavy valvular calcification Aortic root dimension >45 mm Presence of LV apical thrombus	

AS = aortic stenosis; AV = aortic valve; MRI = magnetic resonance imaging; MSCT = multi-slice computed tomography

IMAGING IN PERCUTANEOUS AORTIC VALVE IMPLANTATION

Various imaging modalities are available for the selection of patients, performing percutaneous AV implantation, and for follow-up after the procedure. An overview on the role of various imaging modalities in percutaneous AV implantation procedures is provided in Table 3. Whereas transthoracic echocardiography (TTE), multi-slice computed tomography (MSCT), and magnetic resonance imaging (MRI) are valuable imaging techniques before and after the procedure, transesophageal echocardiography (TEE) is mainly used during the actual implantation procedure. The various processes and imaging modalities will be reviewed in the following paragraphs

Patient selection

The selection of candidates for percutaneous AV implantation involves a number of critical steps. The different imaging modalities can assist in the selection process by providing important information on the AV, coronary arteries and vascular structures. First, the severity of AS should be assessed. Both TTE and TEE are the preferred tools to assess the severity of AS (1). However, recent reports have suggested a good correlation between echocardiography and both MSCT (28) and MRI (29) to assess AVA with planimetry.

In addition, the exact anatomy of the AV should be assessed. Echocardiography, MSCT and MRI all can help to distinguish between a bicuspid and a tricuspid AV. It has been suggested that a bicuspid AV may result in a higher incidence of stent misdeployment and peri-stent leakage

Table 3. The role of imaging in percutaneous AV implantation procedures

Process	Preferred imaging modality
Patient selection	
AS severity	TTE or TEE
AV anatomy	TTE or TEE
AV calcifications (severity, location)	MSCT
Coronary anatomy (CAD, relation with annulus)	Angiography or MSCT
Aortic annulus diameter	All modalities can be used
Aortic arch (angulation, atheroma)	MSCT
Peripheral arteries (calcifications, tortuosity)	Angiography or MSCT
Atrial or ventricular thrombus	TTE or TEE
LV ejection fraction	All modalities can be used
AV implantation	
Vascular access	Fluoroscopy and/or TEE
Prosthesis sizing	Fluoroscopy and/or TEE
Prosthesis positioning and deployment	Fluoroscopy and/or TEE
Assessment of valve competence	Fluoroscopy and/or TEE
Assessment of coronary patency	Fluoroscopy and/or TEE
Detection of complications	Fluoroscopy and/or TEE
Follow-up	
Assessment of prosthesis function	TTE or TEE
Assessment of prosthesis position	TTE, TEE or MSCT
Detection of complications	All modalities can be used

AS = aortic stenosis; AV = aortic valve; CAD = coronary artery disease; LV = left ventricular; MSCT = multi-slice computed tomography; TEE = transesophageal echocardiography; TTE = transthoracic echocardiography.

(30). Therefore, at present it is not recommended to perform percutaneous AV implantation in bicuspid AV (6). Furthermore, the exact location and severity of AV calcifications and the presence of bulky AV leaflets should be assessed. Before the implantation procedure, MSCT may be the preferred tool to identify AV calcifications (19). A severely calcified AV may result in the inability to cross the native valve with the catheter. Bulky leaflets and calcifications on the free edge of the leaflets may increase the risk of occlusion of the coronary ostia during AV implantation (15). Therefore, the extent and exact location of calcifications should be carefully assessed before the implantation procedure (Figure 3).

The assessment of coronary anatomy is also important in the selection process. Conventional coronary angiography should be performed to exclude the presence of significant coronary artery disease (6). Although conventional angiography remains the 'gold standard', non-invasive evaluation of coronary artery disease may be performed with MSCT as well. This technique also allows detailed, three-dimensional evaluation of the relation between the coronary ostia and the AV leaflets. This may be important to avoid coronary occlusion during AV implantation. It has been demonstrated that the relation between the aortic annulus, the coronary ostia and leaflets is highly variable. In a cohort of 169 patients undergoing MSCT scanning,

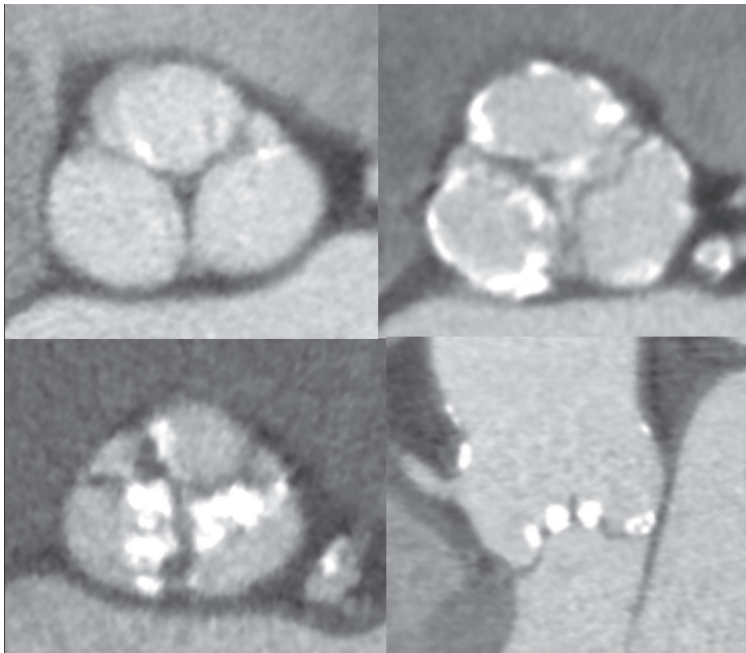


Figure 3. Before the percutaneous valve procedure, MSCT can depict the extent and exact location of calcifications. During percutaneous AV replacement, extensive calcifications may hamper the ability to cross the native valve. On transverse reconstructions through the plane of the AV, the calcifications can be quantified. Panel A shows small isolated spots (mildly calcified AV). In contrast, panel B shows multiple larger spots, predominantly at the base of the leaflets (moderately calcified AV). Panel C shows a heavily calcified AV, mainly located at the tips of the leaflets. In panel D, a sagittal view through the AV is shown, demonstrating bulky calcifications at the tip of the AV leaflets.

it was noted that the distance between the aortic annulus and the coronary ostia was smaller than the length of the AV leaflets in up to 49% of the patients (31). In these patients, the risk of coronary occlusion during percutaneous AV implantation may be increased. Therefore, both invasive and non-invasive evaluation of coronary anatomy can provide important information for the selection of candidates for percutaneous AV implantation.

The assessment of aortic annulus diameters is of utmost importance for correct prosthesis sizing. Various prosthesis sizes for the balloon-expandable and self-expanding prostheses are available for a wide range of annulus diameters. However, at present no gold-standard is available for the exact measurement of the aortic annulus diameter. Typically, TTE is used to assess the aortic annulus diameter (Figure 4, panel A). However, it may underestimate the diameter when compared with TEE (32). Importantly, with both techniques the basal attachments of the leaflets are used as landmark points, potentially underestimating the true/ full aortic annulus diameter (33). In contrast, three-dimensional echocardiography, MRI and MSCT allow a three-dimensional, multi-planar reconstruction of the aortic annulus (Figure 4, panels B and C). This may result in a more accurate measurement of the aortic annulus diameter.

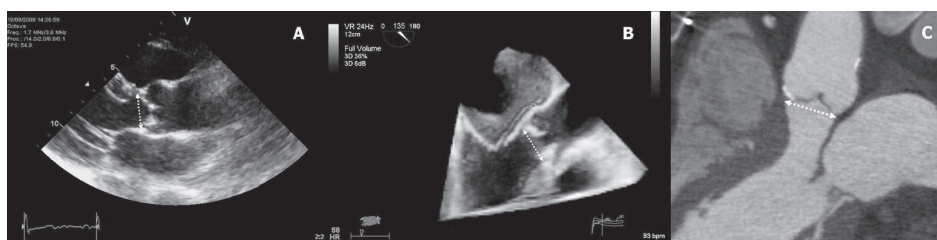


Figure 4. Before percutaneous AV implantation, the aortic annulus diameter should be assessed. For this purpose, different imaging modalities are available. Panel A demonstrates conventional TTE, where the annulus diameter is assessed at the ventricular aspect of the leaflet insertion. In panel B, three-dimensional TEE is shown. Panel C demonstrates a sagittal reconstruction through the AV. The dotted arrow indicates the measurement of the aortic annulus.

Furthermore, the anatomy of the aorta and peripheral vasculature should be assessed. Conventional angiography is the preferred imaging modality. However, MSCT and MRI may also provide the necessary information. A transapical approach is preferred over the transfemoral approach in patients with a severe angulation of the aortic arch, or the presence of atheroma in the aorta. In patients with severe calcifications and/or tortuosity of the femoral vessels, or small vessel diameters (typically < 6 to 9 mm), a transfemoral approach is contraindicated, because of the high risk of vascular complications. Finally, contraindications such as the presence of atrial or ventricular thrombi, and a very poor left ventricular ejection fraction should be assessed.

Aortic valve implantation

During the AV implantation procedure, a combination of fluoroscopy/ angiography and TEE is typically used (8). Rather than replacing each other, these techniques are complimentary during the AV implantation. Contrast aortography can be used for final assessment of the aortic

annulus diameter and prosthesis sizing. However, similar to echocardiography, it is limited by its two-dimensional nature.

Positioning and final deployment of the prosthesis is performed under fluoroscopy and/or TEE guidance (Figure 5, panel A and B). In patients with severely calcified AS, fluoroscopy allows easy localization of the prosthesis in relation to the aortic annulus and leaflets. Conversely, in patients without severe calcifications, TEE may be more helpful for exact prosthesis positioning. Typically, a long-axis (130°) transesophageal view is used (32). Critical assessment of the exact location of the undeployed prosthesis, in relation to the native AV is important. When the correct positioning is confirmed with fluoroscopy and/or echocardiography, the prosthesis is deployed under rapid right ventricular pacing.

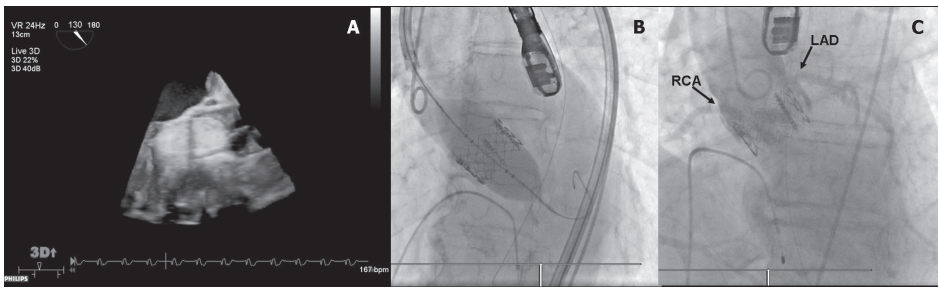


Figure 5. Imaging during a percutaneous implantation procedure of a balloon-expandable valve. Panel A demonstrates a long-axis 3D TEE view during balloon inflation. Panel B demonstrates the final deployment of the prosthesis. After the implantation, coronary angiography should be performed to confirm coronary patency (Panel C). LAD = left anterior descending artery; RCA = right coronary artery

Immediately after the stent deployment, valve competence should be assessed. A transesophageal short-axis view is the best view to differentiate between valvular and paravalvular aortic regurgitation. The severity of paravalvular aortic regurgitation can be used as an indicator of procedural success, and can help to decide if balloon (re-)dilatation is necessary. In 32 patients undergoing TEE guided balloon-expandable AV implantation, Moss et al. noted some degree of aortic regurgitation in 88% of the patients (32). In the majority of the patients (84%) paravalvular aortic regurgitation was present. Thirteen patients underwent subsequent redilatation of the prosthesis, with an improvement in aortic regurgitation of more than 1 grade in 7 of the 13 patients. Mild valvular regurgitation typically resolves during the first days after implantation (32).

For the assessment of coronary patency, coronary angiography should be performed after prosthesis implantation (Figure 5, panel C). Acute coronary occlusion is a serious, but rare complication. Interestingly, it has been demonstrated that correct positioning of the prosthesis even allows coronary intervention after percutaneous AV implantation (34).

Various complications have been reported after percutaneous AV implantation, mainly related to vascular access and thromboembolic complications. In addition, new atrioventricular block may occur in up to 6% of the patients (35). In addition to fluoroscopy, TEE may help in the

recognition of complications during percutaneous AV implantation. In a study of 11 patients (median logistic EuroScore 36%) undergoing self-expanding CoreValve implantation, it was noted that routine TEE enabled the early detection of complications (a thrombus in the left ventricular outflow tract and pericardial effusion) (36).

Finally, intracardiac echocardiography and novel three-dimensional TEE may be helpful in guidance of percutaneous AV implantation. Three-dimensional TEE may allow a more precise evaluation of the AV, and may improve spatial orientation and prosthesis positioning (37). However, more studies are needed to fully understand the exact value of these techniques in percutaneous AV implantations.

Follow-up

In addition to complications and conventional outcome parameters (such as mortality, stroke, major cardiac events), prosthesis function and position should be assessed during follow-up (38). For this purpose, TTE is the most commonly used technique (39). In most studies, the AVA and mean pressure gradient are used to quantify AV function (Table 1). In addition, aortic regurgitation should be assessed.

The exact position of the prosthesis and the relation between the stent and the coronary arteries can be assessed with MSCT. This technique may be preferred over TTE because it is less hampered by artifacts, and has a high spatial resolution. In addition, it allows a more precise evaluation of prosthesis deployment and diameters (40). Examples of MSCT images after percutaneous AV implantation are shown in Figure 6.

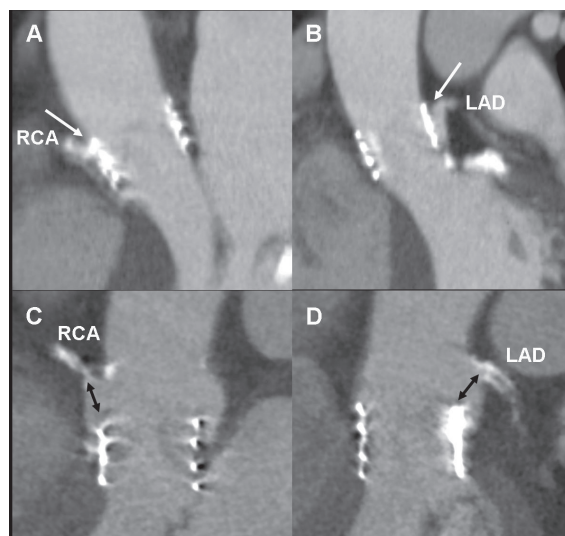


Figure 6. With the use of MSCT, the exact location of the prosthesis can be assessed, and the relation with the coronary ostia. In panels A and B, an example is demonstrated where the prosthesis extends beyond the coronary ostia (white arrows). During the implantation procedure, good patency of the coronary arteries was demonstrated. In panels C and D, an example is demonstrated where the prosthesis is positioned below the coronary ostia (black arrows).

CONCLUSIONS

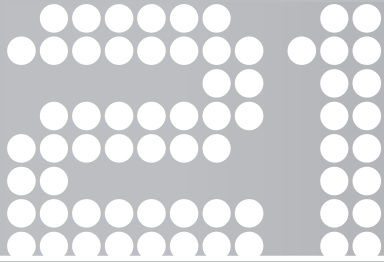
Percutaneous AV implantation is a promising technique for highly symptomatic patients with severe AS. Several studies have demonstrated good results for both the balloon-expandable and self-expanding valves. A critical selection of potential candidates, including clinical evaluation, assessment of surgical risk and feasibility of the procedure is needed. Several imaging modalities are available for patient selection, procedural assistance and follow-up.

REFERENCES

1. Vahanian A, Baumgartner H, Bax J et al. Guidelines on the management of valvular heart disease. *Eur Heart J* 2007;28:230-68.
2. Puvimanasinghe JP, Takkenberg JJ, Eijkemans MJ et al. Comparison of Carpentier-Edwards pericardial and supraannular bioprostheses in aortic valve replacement. *Eur J Cardiothorac Surg* 2006;29:374-9.
3. Iung B, Baron G, Butchart EG et al. A prospective survey of patients with valvular heart disease in Europe: The Euro Heart Survey on Valvular Heart Disease. *Eur Heart J* 2003;24:1231-43.
4. Iung B, Cachier A, Baron G et al. Decision-making in elderly patients with severe aortic stenosis: why are so many denied surgery? *Eur Heart J* 2005;26:2714-20.
5. Tops LF, Kapadia SR, Tuzcu EM et al. Percutaneous valve procedures: an update. *Curr Probl Cardiol* 2008;33:417-57.
6. Vahanian A, Alfieri O, Al Attar N et al. Transcatheter valve implantation for patients with aortic stenosis. *Eur Heart J* 2008;29:1463-70.
7. Vassiliades TA, Jr., Block PC, Cohn LH et al. The clinical development of percutaneous heart valve technology. *J Am Coll Cardiol* 2005;45:1554-60.
8. Rosengart TK, Feldman T, Borger MA et al. Percutaneous and minimally invasive valve procedures. *Circulation* 2008;117:1750-67.
9. Andersen HR, Knudsen LL, Hasenkam JM. Transluminal implantation of artificial heart valves. Description of a new expandable aortic valve and initial results with implantation by catheter technique in closed chest pigs. *Eur Heart J* 1992;13:704-8.
10. Cribier A, Eltchaninoff H, Bash A et al. Percutaneous transcatheter implantation of an aortic valve prosthesis for calcific aortic stenosis: first human case description. *Circulation* 2002;106:3006-8.
11. Webb JG, Chandavimol M, Thompson CR et al. Percutaneous aortic valve implantation retrograde from the femoral artery. *Circulation* 2006;113:842-50.
12. Lichtenstein SV, Cheung A, Ye J et al. Transapical transcatheter aortic valve implantation in humans: initial clinical experience. *Circulation* 2006;114:591-6.
13. Cribier A, Eltchaninoff H, Tron C et al. Early experience with percutaneous transcatheter implantation of heart valve prosthesis for the treatment of end-stage inoperable patients with calcific aortic stenosis. *J Am Coll Cardiol* 2004;43:698-703.
14. Cribier A, Eltchaninoff H, Tron C et al. Treatment of calcific aortic stenosis with the percutaneous heart valve: mid-term follow-up from the initial feasibility studies: the French experience. *J Am Coll Cardiol* 2006;47:1214-23.
15. Webb JG, Pasupati S, Humphries K et al. Percutaneous transarterial aortic valve replacement in selected high-risk patients with aortic stenosis. *Circulation* 2007;116:755-63.
16. Walther T, Falk V, Kempfert J et al. Transapical minimally invasive aortic valve implantation; the initial 50 patients. *Eur J Cardiothorac Surg* 2008;33:983-8.
17. The Placement of AoRTic TraNscathetER Valve Trial. www.clinicaltrials.gov, NCT00530894.
18. Grube E, Schuler G, Buellesfeld L et al. Percutaneous aortic valve replacement for severe aortic stenosis in high-risk patients using the second- and current third-generation self-expanding CoreValve prosthesis: device success and 30-day clinical outcome. *J Am Coll Cardiol* 2007;50:69-76.
19. Grube E, Buellesfeld L, Mueller R et al. Progress and current status of percutaneous aortic valve replacement: results of three device generations of the CoreValve Revalving System. *Circ Cardiovasc Intervent* 2008;1:167-75.
20. Grube E, Laborde JC, Zickmann B et al. First report on a human percutaneous transluminal implantation of a self-expanding valve prosthesis for interventional treatment of aortic valve stenosis. *Catheter Cardiovasc Interv* 2005;66:465-9.
21. Grube E, Laborde JC, Gerckens U et al. Percutaneous implantation of the CoreValve self-expanding valve prosthesis in high-risk patients with aortic valve disease: the Siegburg first-in-man study. *Circulation* 2006;114:1616-24.

22. Piazza N, Grube E, Gerckens U et al. Procedural and 30-day outcomes following transcatheter aortic valve implantation using the third generation (18 Fr) corevalve revalving system: results from the multicentre, expanded evaluation registry 1-year following CE mark approval. *EuroIntervention* 2008;4:242-9.
23. Walther T, Falk V, Dewey T et al. Valve-in-a-valve concept for transcatheter minimally invasive repeat xenograft implantation. *J Am Coll Cardiol* 2007;50:56-60.
24. Wenaweser P, Buellesfeld L, Gerckens U, Grube E. Percutaneous aortic valve replacement for severe aortic regurgitation in degenerated bioprosthesis: the first valve in valve procedure using the Corevalve Revalving system. *Catheter Cardiovasc Interv* 2007;70:760-4.
25. Walther T, Kempfert J, Borger MA et al. Human minimally invasive off-pump valve-in-a-valve implantation. *Ann Thorac Surg* 2008;85:1072-3.
26. Astor BC, Kaczmarek RG, Hefflin B, Daley WR. Mortality after aortic valve replacement: results from a nationally representative database. *Ann Thorac Surg* 2000;70:1939-45.
27. Ruiz CE, Laborde JC, Condado JF, Chiam PT, Condado JA. First percutaneous transcatheter aortic valve-in-valve implant with three year follow-up. *Catheter Cardiovasc Interv* 2008;72:143-8.
28. Tops LF, Krishnan SC, Schuijff JD, Schalij MJ, Bax JJ. Noncoronary applications of cardiac multidetector row computed tomography. *J Am Coll Cardiol Img* 2008;1:94-106.
29. Pouleur AC, le Polain de Waroux JB, Pasquet A, Vancraeynest D, Vanoverschelde JL, Gerber BL. Planimetric and continuity equation assessment of aortic valve area: Head to head comparison between cardiac magnetic resonance and echocardiography. *J Magn Reson Imaging* 2007;26:1436-43.
30. Zegdi R, Ciobotaru V, Noghin M et al. Is it reasonable to treat all calcified stenotic aortic valves with a valved stent? Results from a human anatomic study in adults. *J Am Coll Cardiol* 2008;51:579-84.
31. Tops LF, Wood DA, Delgado V et al. Noninvasive evaluation of the aortic root with multislice computed tomography: Implications for transcatheter aortic valve replacement. *J Am Coll Cardiol Img* 2008;1:321-30.
32. Moss R, Ivens E, Pasupati S et al. Role of echocardiography in percutaneous aortic valve implantation. *J Am Coll Cardiol Img* 2008;1:15-24.
33. Piazza N, de Jaegere P, Schultz C, Becker AE, Serruys PW, Anderson RH. Anatomy of the aortic valvar complex and its implications for transcatheter implantation of the aortic valve. *Circ Cardiovasc Intervent* 2008;1:74-81.
34. Geist V, Sherif MA, Khattab AA. Successful percutaneous coronary intervention after implantation of a CoreValve percutaneous aortic valve. *Catheter Cardiovasc Interv* 2009;73:61-7.
35. Sinhal A, Altwegg L, Pasupati S et al. Atrioventricular block after transcatheter balloon expandable aortic valve implantation. *J Am Coll Cardiol Intv* 2008;1:305-9.
36. Berry C, Oukerraj L, Asgar A et al. Role of transesophageal echocardiography in percutaneous aortic valve replacement with the CoreValve Revalving system. *Echocardiography* 2008;25:840-8.
37. Balzer J, Kuhl H, Rassaf T et al. Real-time transesophageal three-dimensional echocardiography for guidance of percutaneous cardiac interventions: first experience. *Clin Res Cardiol* 2008;97:565-74.
38. Chiam PTL, Ruiz CE. Percutaneous transcatheter aortic valve implantation: assessing results, judging outcomes, and planning trials: the interventionalist perspective. *J Am Coll Cardiol Intv* 2008;1:341-50.
39. Gottdiener JS, Bednarz J, Devereux R et al. American Society of Echocardiography recommendations for use of echocardiography in clinical trials. *J Am Soc Echocardiogr* 2004;17:1086-119.
40. Wood DA, Tops LF, Mayo JR et al. Role of multislice computed tomography in transcatheter aortic valve replacement. *Am J Cardiol* 2009.
41. Walther T, Falk V, Borger MA et al. Minimally invasive transapical beating heart aortic valve implantation--proof of concept. *Eur J Cardiothorac Surg* 2007;31:9-15.
42. Ye J, Cheung A, Lichtenstein SV et al. Six-month outcome of transapical transcatheter aortic valve implantation in the initial seven patients. *Eur J Cardiothorac Surg* 2007;31:16-21.
43. Walther T, Simon P, Dewey T et al. Transapical minimally invasive aortic valve implantation: multi-center experience. *Circulation* 2007;116:1240-1245.

44. Marcheix B, Lamarche Y, Berry C et al. Surgical aspects of endovascular retrograde implantation of the aortic CoreValve bioprosthesis in high-risk older patients with severe symptomatic aortic stenosis. *J Thorac Cardiovasc Surg* 2007;134:1150-6.
45. Descoutures F, Himbert D, Lepage L et al. Contemporary surgical or percutaneous management of severe aortic stenosis in the elderly. *Eur Heart J* 2008;29:1410-7.
46. Svensson LG, Dewey T, Kapadia S et al. United States feasibility study of transcatheter insertion of a stented aortic valve by the left ventricular apex. *Ann Thorac Surg* 2008;86:46-54.
47. Zierer A, Wimmer-Greinecker G, Martens S, Moritz A, Doss M. The transapical approach for aortic valve implantation. *J Thorac Cardiovasc Surg* 2008;136:948-53.
48. Rodes-Cabau J, Dumont E, De LaRochelliere R et al. Feasibility and initial results of percutaneous aortic valve implantation including selection of the transfemoral or transapical approach in patients with severe aortic stenosis. *Am J Cardiol* 2008;102:1240-6.



Noninvasive evaluation of the aortic root with multislice computed tomography: implications for transcatheter aortic valve replacement

Laurens F. Tops¹
David A. Wood²
Victoria Delgado¹
Joanne D. Schuijf¹
John R. Mayo²
Sanjeevan Pasupati²
Frouke P.L. Lamers¹
Ernst E. van der Wall¹
Martin J. Schalij¹
John G. Webb²
Jeroen J. Bax¹

¹Department of Cardiology, Leiden University Medical Center, Leiden, the Netherlands

²Division of Cardiology, St. Paul's Hospital, University of British Columbia, Vancouver, Canada

J Am Coll Cardiol Img 2008;1:321-30

ABSTRACT

Background: Transcatheter aortic valve replacement has been proposed as an alternative to surgery in high-risk patients with severe aortic stenosis (AS). For this procedure, detailed knowledge on aortic annulus diameters and the relation between the annulus and the coronary arteries is needed.

Objectives: In the present study, the anatomy of the aortic root was assessed non-invasively with Multislice Computed Tomography (MSCT).

Methods: In 169 patients (111 men, age 54 ± 11 years) a 64-slice MSCT scan was performed for evaluation of coronary artery disease. Nineteen patients with moderate-severe AS were included. Reconstructed coronal and sagittal views were used for assessment of the aortic annulus diameter in two directions. In addition, the distance between the annulus and the ostium of the right and left coronary artery and the length of the coronary leaflets were assessed.

Results: The diameter of the aortic annulus was 26.3 ± 2.8 mm on the coronal view, and 23.5 ± 2.7 mm on the sagittal view. Mean difference between the two diameters was 2.9 ± 1.8 mm, indicating an oval shape of the aortic annulus. Mean distance between the aortic annulus and the ostium of the right coronary artery was 17.2 ± 3.3 mm, and mean distance between the annulus and the ostium of the left coronary artery was 14.4 ± 2.9 mm. In 82 patients (49%) the length of the left coronary leaflet exceeded the distance between the annulus and the ostium of the left coronary artery.

Conclusions: MSCT can provide detailed information on the shape of the aortic annulus, and the relation between the annulus and the ostia of the coronary arteries. Thereby, MSCT may be helpful for avoiding paravalvular leakage and coronary occlusion and may facilitate the selection of candidates for transcatheter aortic valve replacement.

INTRODUCTION

Degenerative aortic stenosis (AS) is the most common native valve disease (1). Although surgical aortic valve replacement provides good long-term results and symptom relief, it is complex in high-risk patients with extensive co-morbidity (2). In patients with severe, symptomatic AS and a very high risk of morbidity or mortality with conventional surgery, a percutaneous transcatheter aortic valve replacement may be preferred.

Several studies have shown the feasibility of transcatheter aortic valve replacement (3-5). Difficulties with accurate positioning of the prosthesis in the aortic annulus, prosthesis sizing, the covering of the coronary ostia by the upper part of the prosthesis (5) and even occlusion of the left coronary artery (4) are important issues in transcatheter aortic valve replacement. Therefore, detailed information on the anatomy of the aortic annulus and the relation of the annulus with the coronary arteries is important for performing these procedures. Fluoroscopy and transesophageal echocardiography are helpful imaging modalities during percutaneous valve replacement procedures (3-5). However, these modalities are limited by their two-dimensional character. Multislice computed tomography (MSCT) can provide three-dimensional images with a high spatial resolution, and may therefore be of great value for percutaneous valve replacement procedures.

The purpose of the present study was to assess the anatomy of the aortic root non-invasively with 64-slice MSCT. We sought to determine standardized measurements on the aortic annulus and the relation with the left coronary artery in a large cohort of patients, including patients with moderate-severe AS.

METHODS

The study population comprised 169 patients referred for MSCT coronary angiography in the period from February 2005 until January 2007 at the Leiden University Medical Center. In all patients, the aortic root could be analyzed on the acquired MSCT scan. To detect differences in aortic root anatomy between patients with and without AS, the study population was divided into 2 groups: patients with no or mild AS (n=150) and patients with moderate to severe AS (n=19).

Multislice Computed Tomography

The MSCT examinations were performed with a Toshiba Multislice Aquilion 64 system (Toshiba Medical Systems, Tokyo, Japan). Before MSCT angiography, a prospective coronary calcium scan was performed (collimation 4×3.0 mm, rotation time 500 ms, tube voltage 120 kV, and tube current 200 mA). The temporal window was set at 75% after the R wave for electrocardiographically triggered prospective reconstruction.

For the MSCT coronary angiogram, a collimation of 64 x 0.5 mm and a rotation time of 400 ms were used. A multi-segment reconstruction algorithm was used, resulting in a temporal resolution of < 200 ms depending on heart rate and pitch. The tube current was 300 mA, at 120 kV. Non-ionic contrast material (Iomeron 400, Bracco, Altana Pharma, Konstanz, Germany) was administered in the antecubital vein, in an amount of 80 to 110 ml depending on the total scan time, and a flow rate of 5.0 ml/sec.

Automated peak enhancement detection in the descending aorta was used for timing of the scan. After the threshold level of +100 Hounsfield units was reached, data acquisition was automatically initiated. Data acquisition was performed during an inspiratory breathhold of approximately 8 to 10 seconds, while the ECG was recorded simultaneously to allow retrospective gating of the data.

The data set of the contrast enhanced scan was reconstructed at 30% and 75% of the RR interval for the systolic and diastolic phases, respectively. All images were reconstructed with a slice thickness of 0.5 mm and a reconstruction interval of 0.3 mm. Axial data sets were then transferred to a remote workstation (Vitrea 2, Vital Images, Plymouth, Minn) for post-processing and subsequent image analysis.

Image analysis

All images were analyzed by two experienced observers blinded to the clinical and echocardiographic information. An overview of the measured variables is shown in Table 1.

Table 1. Anatomical analysis of the aortic root

Variable	MSCT view
Aortic valve	
Aspect (bicuspid/tricuspid)	Double oblique transverse *
Calcification (grade 1-4)	Double oblique transverse
Agatston calcium score	Prospective calcium scan
Calcium volume	Prospective calcium scan
Aortic annulus	
Diameter (diastole / systole)	Coronal † Single oblique sagittal ‡
Sinus of Valsalva	
Diameter	Coronal
Distance between annulus and sinus of Valsalva	Coronal
Relation Aortic annulus, coronary leaflet, ostium coronary artery	
Distance between annulus and ostium coronary artery (left and right)	Coronal
Length of coronary leaflet (left and right)	Coronal
Distance between tip of left coronary leaflet and ostium left coronary artery (diastole / systole)	Coronal
Sinotubular junction	
Diameter	Coronal
Distance between annulus and sinotubular junction	Coronal

* The double oblique transverse view is perpendicular to the aortic axis; † The coronal view has the same orientation as the anterior posterior view on aortic root angiography; ‡ The single oblique sagittal view has the same orientation as the parasternal long axis view on transthoracic echocardiography and the midesophageal long axis view on transesophageal echocardiography.

Aortic valve anatomy and calcification The aspect of the aortic valve (tricuspid or bicuspid) and the presence of aortic valve calcifications were assessed on double oblique transverse reconstructions of the MSCT coronary angiogram. Aortic valve calcifications were then graded subjectively as previously described (6,7). The degree of aortic valve calcification was graded as follows: grade 1: no calcification; grade 2: mildly calcified (small isolated spots); grade 3: moderately calcified (multiple larger spots); grade 4: heavily calcified (extensive calcification of all cusps). Examples of the different calcification grades are shown in Figure 1. In addition, an Agatston calcium score (8) and the calcium volume for the aortic valve was obtained from the prospective calcium scan using dedicated Calcium scoring software (Vitrea 2, Vital Images, Plymouth, Minn).

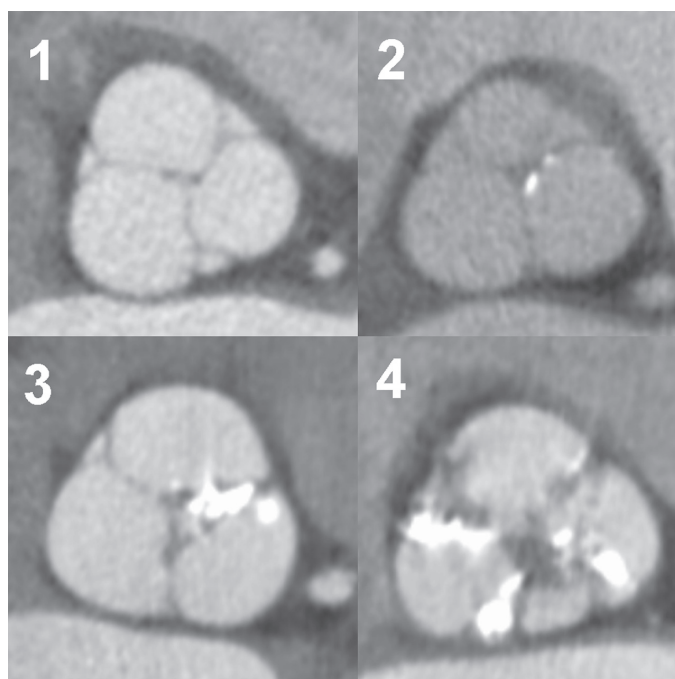


Figure 1. The degree of aortic valve calcification was graded as follows: grade 1: no calcification; grade 2: mildly calcified (small isolated spots); grade 3: moderately calcified (multiple larger spots); grade 4: heavily calcified (extensive calcification of all cusps).

Anatomical analysis of the aortic root Standard orthogonal axial and sagittal views were used for initial orientation on the aortic valve. Since the aortic valve is oriented oblique to the standard axial view, a coronal and a single oblique sagittal view through the aortic valve were reconstructed. The anatomy of the aortic root and the relationship of the aortic annulus, the coronary leaflets and the ostia of the coronary arteries was assessed on the coronal view and the reconstructed single oblique sagittal view, both in the systolic and diastolic phases. The coronal view is similar to the anterior-posterior view on aortic root angiography. The reconstructed single oblique sagittal view has the same orientation as the parasternal long-axis view

on transthoracic echocardiogram and the mid oesophageal long-axis view on transesophageal echocardiogram. Care was taken for correct orientation of both views by reviewing the reconstructed double oblique transverse view at the level of the aortic valve. Examples of the coronal, single oblique sagittal and double oblique transversal views are shown in Figure 2.

The diameter of the annulus was assessed in the systolic and diastolic phases. The orientation of the views was similar to those used for percutaneous aortic valve replacement procedures (4). In addition, the maximal diameter of the sinus of Valsalva and the sinotubular junction, and their respective distance to the level of the aortic annulus was assessed (Figure 3). These variables are important to assess, since they may have implications for prosthesis sizing during transcatheter aortic valve replacement and paravalvular leakage after the procedure. Furthermore, the distance between the annulus and the ostium of the left and the right coronary artery, and the coronary leaflet length were assessed. An example of these measurements

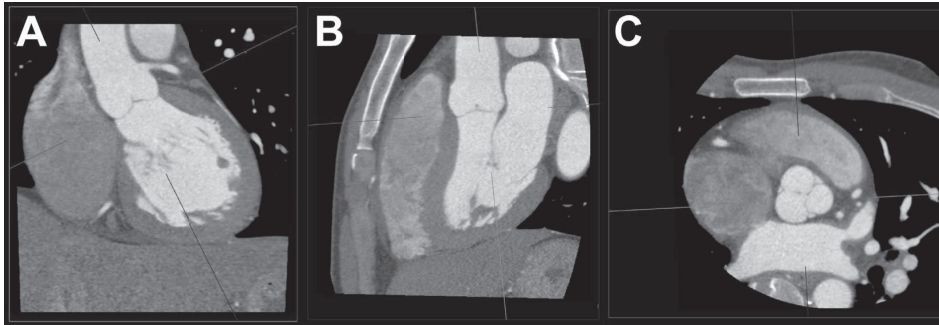


Figure 2. The anatomy of the aortic root was assessed on three reconstructed views. The coronal view (A) is similar to the anterior-posterior view on aortic root angiography. The reconstructed single oblique sagittal (B) view has the same orientation as the parasternal long-axis view on transthoracic echocardiogram and the mid oesophageal long-axis view on transesophageal echocardiogram. The reconstructed double oblique transverse view (C) is parallel to the plane of the aortic root. See Table 1 for detailed description of the variables.

for the left coronary artery is shown in Figure 4. In addition, the distance between the tip of the left coronary leaflet and the ostium of the left coronary artery was assessed in diastole and systole (Figure 5). These variables may have implications for transcatheter aortic valve replacement, since they may determine the risk of coronary artery occlusion during the procedure, as previously described (4).

Finally, the left ventricular outflow tract and the interventricular septum were analyzed on the single oblique sagittal view at end-diastole. The diameter of the left ventricular outflow tract was assessed, parallel to the aortic valve annulus plane. The largest diameter of the interventricular septum was assessed, and the aspect of the interventricular septum was subjectively graded as normal or sigmoid. An example of a sigmoid septum is shown in Figure 6.

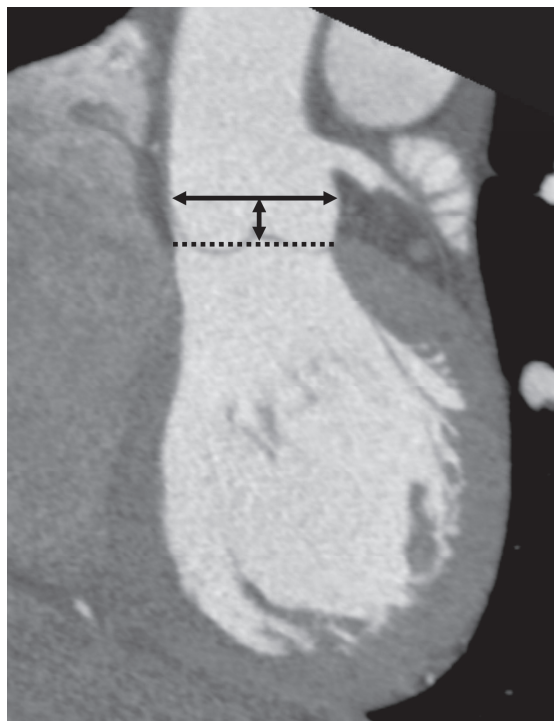


Figure 3. On the coronal view, the maximal diameter of the sinus of Valsalva was assessed (indicated by the double arrow). In addition, the distance between the aortic annulus (indicated by the dotted line) and the level of the maximal diameter of the sinus was assessed on the coronal view.

Echocardiography

Two-dimensional echocardiograms were obtained with patients in the left lateral decubitus position using a commercially available system (Vingmed Vivid 7, General Electric-Vingmed, Milwaukee, Wisconsin, USA). Images were obtained using a 3.5-MHz transducer at a depth of 16 cm in the parasternal (long- and short-axis) and apical (two-chamber and four-chamber) views. Standard two-dimensional images and color Doppler data were digitally stored in cine-loop format. Left ventricular ejection fraction was calculated from apical two-chamber and four-chamber images using the biplane Simpson's rule (9). The diameter of the aortic annulus was assessed from the parasternal long-axis view. Aortic stenosis was graded according to the ACC/AHA guidelines (2): 'Mild': area 1.5 cm^2 , mean gradient less than 25 mm Hg, or jet velocity less than 3.0 m per second; 'Moderate': area 1.0 to 1.5 cm^2 , mean gradient 25 to 40 mm Hg, or jet velocity 3.0 to 4.0 m per second; 'Severe': area less than 1.0 cm^2 , mean gradient greater than 40 mm Hg, or jet velocity greater than 4.0 m per second. To detect differences in anatomical variables between patients with and without AS, the study population was divided into 2 groups: patients with no or mild AS ($n=150$) and patients with moderate to severe AS ($n=19$).

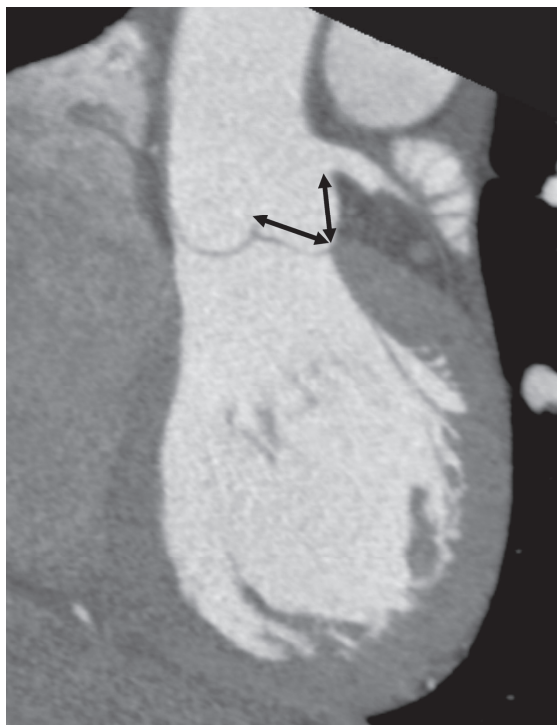


Figure 4. With the use of a coronal view, the distance between the annulus and the ostia of the coronary arteries, and the length of the coronary leaflets were assessed. This figure demonstrates the measurements of the distance between the annulus and the ostium of the left coronary artery, and the measurement of the left coronary leaflet length.

Statistical analysis

All continuous variables had normal distribution (as evaluated by Kolmogorov-Smirnov tests). Summary statistics for these variables are therefore presented as mean values \pm one standard deviation (SD). Categorical data are summarized as frequencies and percentages. Differences in aortic annulus diameter in the different views were evaluated with paired Student t-tests. The agreement between echocardiography and MSCT for the aortic annulus measurement was assessed with Bland-Altman analysis. Differences in anatomical variables between patients with and without AS are evaluated using unpaired Student t-tests (continuous variables) or Chi-square tests (dichotomous variables), as appropriate. All analyses were performed using SPSS software (version 12.0, SPSS Inc. Chicago, Illinois, USA). All statistical tests were two-sided, and a p-value <0.05 was considered significant.

RESULTS

A total of 169 patients were studied. Baseline characteristics of the study population are listed in Table 2. In all patients, adequate images for evaluation of the aortic root were available.

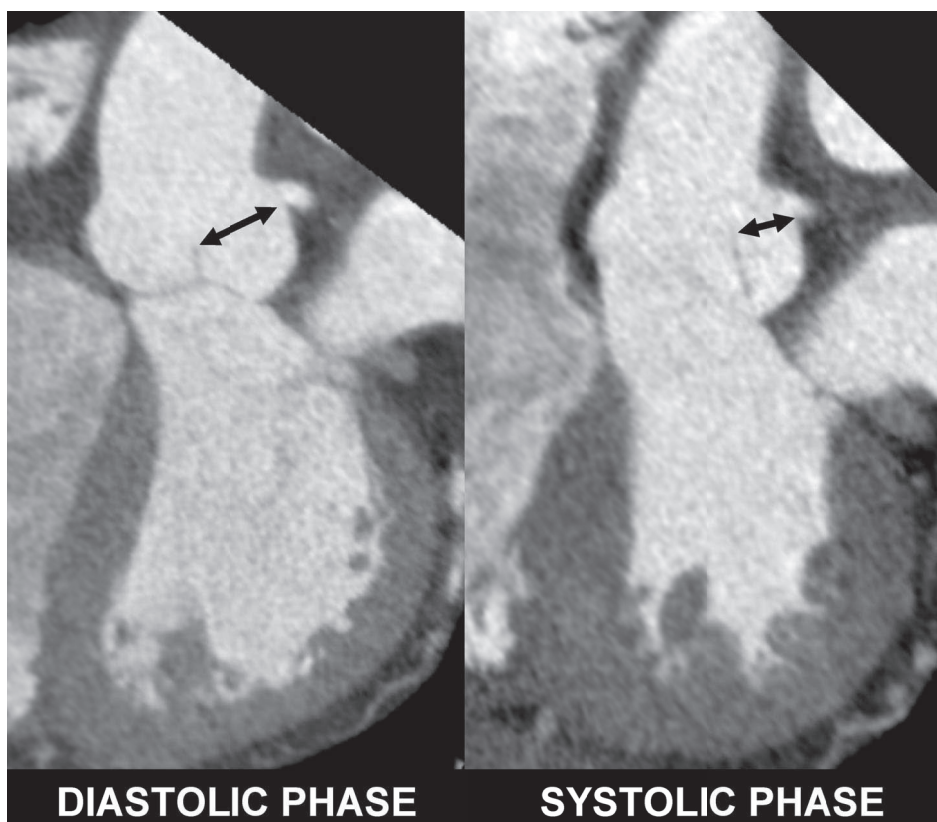


Figure 5. On the coronal view, the distance between the tip of the left coronary leaflet and the ostium of the left coronary artery was assessed in diastole and systole.

Aortic valve anatomy and calcification

In 167 patients a tricuspid aortic valve was present, whereas 2 patients had a bicuspid aortic valve. The 2 patients with a bicuspid aortic valve were excluded from the anatomical analysis. Calcifications of the aortic valve were graded subjectively as previously described (6,7). In 123 patients (73%), no calcifications were present (grade 1). In 29 patients (17%) calcifications were characterized as grade 2; whereas 11 patients (6%) had calcifications grade 3, and 6 patients (4%) had calcifications grade 4. Calcifications were present on the left coronary cusp in 36 of the 46 patients (78%) with aortic valve calcifications, and on the right coronary cusp in 30 of the 46 patients (65%). Mean Agatston score was 819 ± 1245 and mean calcium volume of the aortic valve calcifications was $663 \pm 960 \text{ mm}^3$.

Aortic root diameter and geometry

In the diastolic phase, mean diameter of the aortic annulus on the coronal view was 26.3 ± 2.8 mm; whereas the mean diameter on the reconstructed single oblique sagittal view was 23.5 ± 2.7 mm. The mean difference between the coronal and the sagittal diameter was 2.9 ± 1.8 mm.

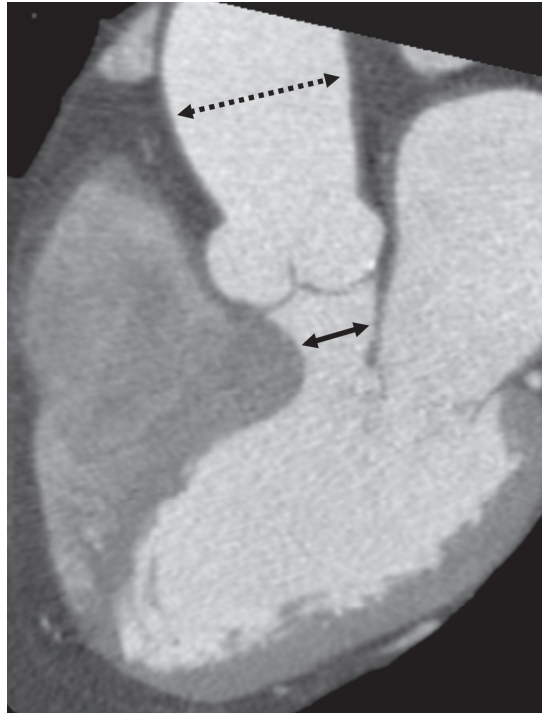


Figure 6. A single oblique sagittal view was used to assess the largest diameter of the interventricular septum, and to grade the aspect of the interventricular septum as normal or sigmoid. In this patient, accurate positioning of the percutaneous aortic valve may be hampered by the small diameter of the left ventricular outflow tract (indicated by the double arrow). Also note the post-stenotic dilatation of the ascending aorta, indicated by the dotted arrow in this patient.

Table 2. Baseline characteristics of the study population

	Study population (n=169)
Age, years	54 ± 11
Gender, M/F	111 / 58
Previous myocardial infarction, n (%)	40 (24)
Previous CABG, n (%)	12 (7)
LVEF, %	57 ± 17
Risk factors, n (%)	
Diabetes mellitus	51 (30)
Hypertension	81 (48)
Hypercholesterolemia	71 (42)
Smoking	50 (30)
Positive family history	59 (35)

CABG = Coronary artery bypass grafting; LVEF = left ventricular ejection fraction.

In 78 patients (47%), the difference between the two diameters was ≥ 3 mm, indicating an oval shape of the aortic annulus. In the systolic phase, the diameter of the aortic annulus on the coronal view was 26.5 ± 2.9 mm and the diameter on the single oblique sagittal view was 24.2 ± 2.6 mm. The mean difference between the coronal and the sagittal diameter in the systolic phase was 2.4 ± 1.9 mm. The mean diameter of the aortic annulus assessed with echocardiog-

raphy was 21.6 ± 2.6 mm. There was a good agreement between MSCT and echocardiography, as assessed with Bland-Altman analysis (Figure 7).

The maximal diameter of the sinus of Valsalva in diastole on the coronal view was 32.4 ± 4.0 mm. The mean distance between the level of the annulus and the maximal diameter of the sinus of Valsalva was 17.2 ± 2.9 mm. The maximal diameter of the sinotubular junction was 28.2

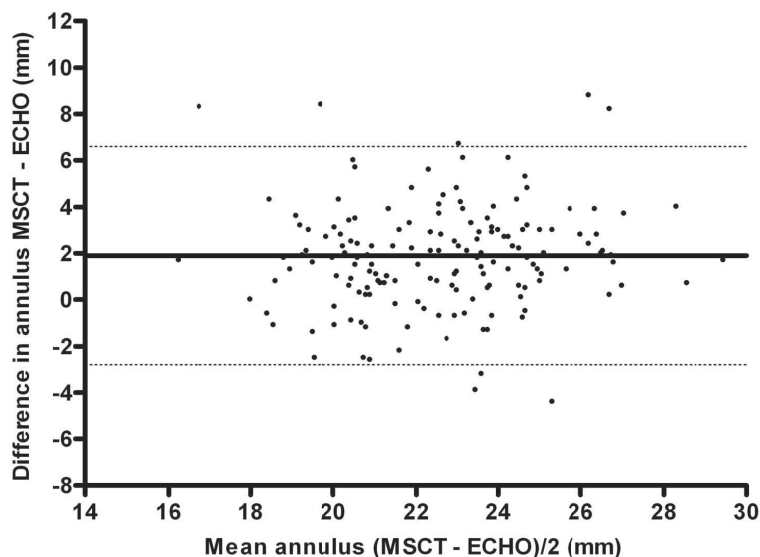


Figure 7. Bland-Altman analysis revealed a good agreement between MSCT and echocardiography for the assessment of aortic annulus diameter. The difference between each pair (Y axis) is plotted against the average value of the same pair (X axis). Mean difference was 1.9 mm (solid line), 95% confidence interval -2.8 – 6.6 mm (dotted lines).

± 3.2 mm. The mean distance between the level of the annulus and the sinotubular junction was 20.3 ± 3.3 mm.

Relation aortic annulus, leaflet and coronary artery

The relation of the aortic annulus, the coronary leaflets and the ostia of the coronary arteries was assessed on the coronal view. The mean distance between the aortic annulus and the ostium of the left coronary artery was 14.4 ± 2.9 mm, with a range of 7.1 to 22.7 mm. The length of the left coronary leaflet was 14.2 ± 1.8 mm (range 10.0 – 21.3 mm). In 82 patients (49%) the left coronary leaflet was longer than the distance between the annulus and the ostium of the left coronary artery (mean difference 2.1 ± 1.7 mm). In the remaining 85 patients (51%), the length of the left coronary leaflet was shorter than the distance between the annulus and the ostium of the left coronary artery (mean difference 2.4 ± 1.5 mm). Similar, the mean distance between the aortic annulus and the ostium of the right coronary artery was 17.2 ± 3.3 mm, with a range of 9.2 to 26.3 mm. The length of the right coronary leaflet was 13.2 ± 1.9 mm (range 9.0 – 19.6 mm). In 17 patients (10%) the length of the coronary leaflet was longer than

the distance between the annulus and the ostium of the right coronary artery (mean difference 1.5 ± 1.2 mm). In the remaining 150 patients (90%) the length of the right coronary leaflet was shorter than the distance between the annulus and the ostium of the right coronary artery (mean difference 4.7 ± 2.7 mm).

The minimal distance from the tip of the left coronary leaflet to the left coronary ostium was measured in the diastolic and systolic phases. In diastole the distance between the leaflet tip and the coronary ostium was 17.6 ± 2.7 mm, whereas in systole this distance was 12.1 ± 3.4 mm ($p < 0.001$).

Left ventricular outflow tract and interventricular septum

The left ventricular outflow tract and the interventricular septum were analyzed on the single oblique sagittal view at end-diastole. Mean diameter of the left ventricular outflow tract was 21.2 ± 2.6 mm. Mean end-diastolic diameter of the interventricular septum was 12.4 ± 2.6 mm (range 7.9 – 20.9 mm). In 12 patients (7%), a sigmoid aspect of the interventricular septum was observed (Figure 6). End-diastolic diameter in these 12 patients was 16.2 ± 1.8 mm.

Anatomic observations in aortic stenosis

Of the 169 patients, 19 patients had moderate-severe AS. In these patients, mean pressure gradient was 50 ± 21 mmHg and mean aortic valve area was 0.8 ± 0.2 cm². In the 19 patients with AS, aortic valve calcification was characterized as grade 2 in 3 patients, as grade 3 in 10 patients and 6 patients had calcifications grade 4. The severity of calcification was significantly different between the patients with and the patients without AS ($p < 0.001$). To detect possible differences in aortic root anatomy between patients with and patients without AS, the patients with a bicuspid aortic valve were excluded and subsequently, the study population was divided in two groups: patients with no or mild AS ($n=150$) and patients with moderate to severe AS ($n=17$). There were no significant differences in the diameter of the annulus, the diameter of the sinus of Valsalva, or the distance between the annulus and the sinus of Valsalva between the patients with and the patients without AS (Table 3). In addition, no differences in the distance between the annulus, the left coronary leaflet and the ostium of the left coronary artery were detected between the two groups (Table 3).

In 13 of the 17 patients with AS (76%), the left coronary leaflet was longer than the distance between the annulus and the ostium of the left coronary artery (mean difference 2.5 ± 2.2 mm). Of interest, the percentage of patients in which the left coronary leaflet was longer than the distance between the annulus and the ostium of the left coronary artery was significantly greater in the AS group than in the control group (76% vs. 46%, $p < 0.05$).

Table 3. Anatomical analysis of the aortic root in patients with and without AS

Variable	Patients without AS (n=150)	Patients with AS (n=17)*	P value
Aortic annulus diameter			
Coronal view, diastole, mm	26.3 ± 2.6	26.7 ± 3.9	0.6
Sagittal view, diastole, mm	23.4 ± 2.7	24.2 ± 3.0	0.2
Coronal view, systole, mm	26.4 ± 2.8	27.3 ± 3.7	0.3
Sagittal view, systole, mm	24.0 ± 2.6	24.7 ± 3.0	0.4
Sinus of Valsalva			
Diameter, mm	32.3 ± 3.9	33.4 ± 4.6	0.2
Distance between annulus and sinus of Valsalva, mm	17.2 ± 2.7	17.3 ± 3.9	0.9
Relation Aortic annulus, coronary leaflet, ostium coronary artery			
Distance between annulus and ostium left coronary artery, mm	14.4 ± 2.8	14.0 ± 3.3	0.6
Length of left coronary leaflet, mm	14.1 ± 1.7	14.7 ± 2.4	0.3
Distance between annulus and ostium right coronary artery, mm	17.2 ± 3.3	17.2 ± 3.6	0.9
Length of right coronary leaflet, mm	13.1 ± 1.7	14.1 ± 2.9	0.2
Distance between tip of left coronary leaflet and ostium left coronary artery, diastole, mm	17.6 ± 2.7	17.1 ± 2.9	0.4
Distance between tip of left coronary leaflet and ostium left coronary artery, systole, mm	11.9 ± 3.1	12.1 ± 2.4	0.9
Sinotubular junction			
Diameter, mm	28.1 ± 3.1	28.9 ± 4.2	0.3
Distance between annulus and sinotubular junction, mm	20.3 ± 3.1	20.7 ± 4.6	0.8

* 2 patients with a bicuspid aortic valve were excluded from the anatomical analysis; AS = aortic stenosis.

DISCUSSION

In the present study, the anatomy of the aortic root was assessed with the use of 64-slice MSCT in 169 patients, including 19 patients with AS. It was noted that the annulus of the aorta has an oval shape, with a larger diameter on the coronal view than on the sagittal view. In addition, a wide variability in the distance between the annulus and the ostium of the left coronary artery and a wide variability in the leaflet length was observed. MSCT of the aortic root may be helpful in planning and performing transcatheter aortic valve replacement procedures, and in the selection of potential candidates for these procedures.

Aortic root diameter and geometry

In the present study, the diameter of the aortic annulus was assessed on a coronal and a sagittal view (similar to the anterior-posterior and the parasternal long-axis view, respectively). The diameter of the annulus on the coronal view was consistently larger than on the sagittal view, indicating an oval shape of the aortic annulus. From previous anatomical studies, it has become apparent that the annulus of the aorta is not a circular structure, but rather a three-pronged coronet (10). In addition, at the base of the right and left coronary sinuses, a

crescent of ventricular musculature is incorporated, in contrast to the non-coronary sinus that is exclusively fibrous (11). These anatomical observations may explain the variations in aortic annulus diameter as found in the present study.

Detailed, non-invasive information on the aortic annulus diameter, as provided by MSCT, may be of great value in transcatheter aortic valve replacement. Kazui et al (12) studied the anatomy of the aortic root in 25 patients without significant valvular disease using 16-slice CT. The reported diameter of the aortic annulus in the diastolic phase was 22.1 ± 2.2 mm (12). Similar to the results of the present study, no differences in annulus diameter were found between diastole and systole. Unfortunately, no patients with AS were studied in the study by Kazui et al (12).

Recently, Willmann et al (7) studied 25 patients with severe AS prior to surgical aortic valve replacement. With the use of 4-slice CT, the smallest diameter of the annulus was assessed on a reconstructed double oblique view. The mean diameter was 2.4 ± 0.2 cm, and a good agreement between non-invasive assessment of the aortic annulus with CT and the measurement during aortic valve replacement was noted (mean difference 0.7 mm) (7). In the present study, similar results for the annulus diameter were observed (mean diameters were 26.3 ± 2.8 mm and 23.5 ± 2.7 mm on the coronal and the sagittal view, respectively). The use of a 64-slice scanner in the current study, and the use of different reconstructions may explain the subtle differences between the previously reported results (7) and the present study. By providing detailed information on variations in aortic annulus diameter, MSCT may be of great value for prosthesis sizing and avoidance of paravalvular leakage in percutaneous aortic valve replacement.

Relation aortic annulus, leaflet and left coronary artery

In the present study, a large variability in the relation between the aortic annulus and the left coronary artery was found, with important implications for transcatheter aortic valve replacement. Jatene et al (13) evaluated the anatomy of the aortic root in an autopsy study of 100 structural normal hearts. The mean distance between the ostium of the left coronary artery and the base of the sinus of Valsalva was 13.3 mm (13). Unfortunately, no range in distances was reported in that study. In another anatomical study, McAlpine et al (14) studied 100 human hearts. The mean distance between the annulus and the right and left coronary orifices was 18.5 ± 2.5 mm (14). Abedin et al (15) studied 54 patients undergoing coronary angiography. Average distance from the base of the left coronary sinus to the origin of the left main coronary artery was 19.4 ± 2.7 mm (15). Of interest, this distance showed a large variability, and was independent of the patient's height. In the present study, mean distance between the ostium and the annulus was 14.4 ± 2.9 mm. Importantly, a wide variation in distance was found, ranging from 7.1 to 22.7 mm. In 49% of the patients, the distance between the ostium and the annulus was smaller than the left coronary leaflet length. This may increase the risk of coronary occlusion when a transcatheter aortic valve replacement is performed (4). Of note, the percentage of patients in which the left coronary leaflet was longer than the distance between the annulus

and the ostium of the left coronary artery was significantly greater in the patients with AS than in the remaining patients.

Implications for transcatheter aortic valve replacement

The present study demonstrates that there is a wide variability in the anatomy of the aortic root. These findings have important implications for percutaneous aortic valve replacement procedures (Figure 8). From the first human experience with the self-expanding aortic valve prosthesis (CoreValve, Paris, France), it has become apparent that difficulties with positioning of the device in the aortic annulus were responsible for failure of half of the procedures (5). In addition, correct prosthesis sizing is of great importance in percutaneous valve procedures. At present, prosthesis diameters range between 21 and 26 mm (3-5). Annulus-prosthesis mismatch as a consequence of inaccurate sizing of the prosthesis may result in severe paravalvular leakage. MSCT provides detailed non-invasive information on the aortic annulus diameter before the procedure, and may thereby be helpful in planning and performing of percutaneous aortic valve replacement.

Furthermore, in the present study, a variable distance between the level of the aortic annulus and the ostium of the left coronary artery was observed, ranging from 7.1 to 22.7 mm. At present, the height of the aortic valve prostheses ranges between 14.5 mm (Edwards, Irvine, California) and 50 mm (CoreValve, Paris, France). To avoid interference of the coronary ostia by the prosthesis stent struts, the Edwards prosthesis is preferably positioned under the level of the coronary ostia. However, occlusion of the coronary ostia with this prosthesis may still occur (4). The larger CoreValve has a design feature with a waist in the middle part to protect the coronary ostia. Cribier and co-workers did not observe problems accessing the coronary ostia after percutaneous aortic valve replacement (16). However, if the distance between the annulus

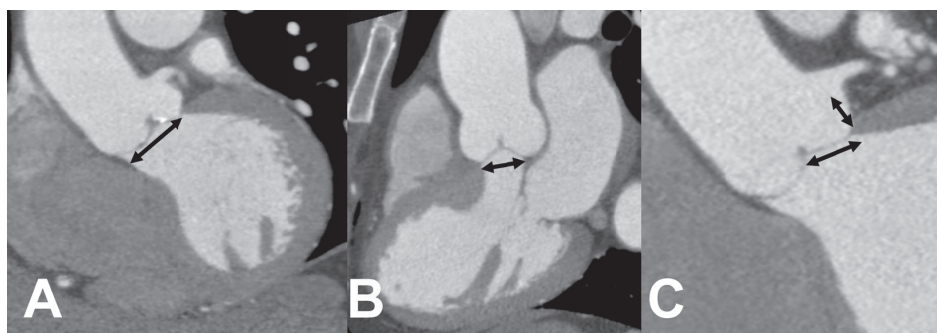


Figure 8. Representative examples of patients in which difficulties with transcatheter aortic valve replacement may be encountered. Panel A and B demonstrate an example of a patient with an oval shape of the aortic annulus. The diameter of the aortic annulus on the coronal view (panel A) was 27.3 mm, whereas the annulus diameter on the sagittal view (panel B) was 20.3 mm. A significant oval shape of the aortic annulus may increase the risk of paravalvular leakage after percutaneous aortic valve replacement. Panel C demonstrates a patient in which the length of the coronary leaflet exceeded the distance between the aortic annulus and the ostium of the left coronary leaflet (distances were 13.4 and 11.6 mm, respectively). There is an increased risk of coronary occlusion by the coronary leaflet or the prosthesis sealing annular cuff in these patients.

and the left coronary ostium is small, it may be difficult to access the coronary ostia after transcatheter aortic valve replacement. Furthermore, the lower part of the currently available aortic prostheses incorporates a sealing annular cuff. If the distance between the annulus and the coronary ostium is smaller than the lower two-third of the prosthesis, coronary occlusion may occur. With the use of MSCT, the distance between the aortic annulus and the ostium of the left coronary artery can accurately be assessed.

In addition, MSCT can provide accurate quantification of the severity and the exact location of aortic valve calcification. Heavily calcified aortic valves may hamper the ability of the prosthesis to cross the native valve in percutaneous valve replacement (5). In contrast to transthoracic and transesophageal echo and magnetic resonance imaging, MSCT allows for an accurate, non-invasive evaluation of aortic valve calcification. Finally, MSCT can also provide detailed, non-invasive information on the tortuosity, diameter and calcification of the descending aorta and femoral arteries, which is of great importance for the advancement of the sheath during transcatheter aortic valve replacement procedures (4). Therefore, MSCT may help in the selection of potential candidates for transcatheter aortic valve replacement.

Study limitations

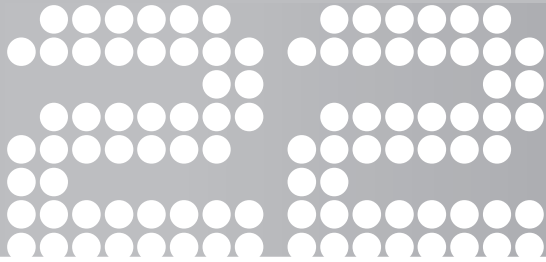
Some limitations of the present study need to be addressed. First, the study population of the present study does not comprise AS patients referred for percutaneous aortic valve replacement. Future studies are needed to assess the value of noninvasive evaluation of the aortic root with MSCT in these patients. Second, the use of MSCT before percutaneous aortic valve replacement may be optimized by recent technical advances and newer generation MSCT scanners. The use of dual-source technology allows for a significant improvement in temporal resolution. Furthermore, radiation exposure may be significantly reduced by the use of dose modulation during scanning.

CONCLUSIONS

The anatomy of the aortic root can be assessed non-invasively with MSCT. A large variability in the aortic annulus diameter and the relation between the annulus, the left coronary leaflet and left coronary artery exists. MSCT may provide useful information for the selection of potential candidates for transcatheter aortic valve replacement.

REFERENCES

1. Iung B, Baron G, Butchart EG et al. A prospective survey of patients with valvular heart disease in Europe: The Euro Heart Survey on Valvular Heart Disease. *Eur Heart J* 2003;24:1231-43.
2. Bonow RO, Carabello BA, Kanu C et al. ACC/AHA 2006 guidelines for the management of patients with valvular heart disease. *Circulation* 2006;114:e84-231.
3. Cribier A, Eltchaninoff H, Tron C et al. Treatment of calcific aortic stenosis with the percutaneous heart valve: mid-term follow-up from the initial feasibility studies: the French experience. *J Am Coll Cardiol* 2006;47:1214-23.
4. Webb JG, Chandavimol M, Thompson CR et al. Percutaneous aortic valve implantation retrograde from the femoral artery. *Circulation* 2006;113:842-50.
5. Grube E, Laborde JC, Gerckens U et al. Percutaneous implantation of the CoreValve self-expanding valve prosthesis in high-risk patients with aortic valve disease: the Siegburg first-in-man study. *Circulation* 2006;114:1616-24.
6. Rosenhek R, Binder T, Porenta G et al. Predictors of outcome in severe, asymptomatic aortic stenosis. *N Engl J Med* 2000;343:611-7.
7. Willmann JK, Weishaupt D, Lachat M et al. Electrocardiographically gated multi-detector row CT for assessment of valvular morphology and calcification in aortic stenosis. *Radiology* 2002;225:120-8.
8. Agatston AS, Janowitz WR, Hildner FJ, Zusmer NR, Viamonte M, Jr., Detrano R. Quantification of coronary artery calcium using ultrafast computed tomography. *J Am Coll Cardiol* 1990;15:827-32.
9. Schiller NB, Shah PM, Crawford M et al. Recommendations for quantitation of the left ventricle by two-dimensional echocardiography. *J Am Soc Echocardiogr* 1989;2:358-67.
10. Anderson RH, Lal M, Ho SY. Anatomy of the aortic root with particular emphasis on options for its surgical enlargement. *J Heart Valve Dis* 1996;5 Suppl 3:S249-S257.
11. Anderson RH. Clinical anatomy of the aortic root. *Heart* 2000;84:670-3.
12. Kazui T, Izumoto H, Yoshioka K, Kawazoe K. Dynamic morphologic changes in the normal aortic annulus during systole and diastole. *J Heart Valve Dis* 2006;15:617-21.
13. Jatene MB, Monteiro R, Guimaraes MH et al. Aortic valve assessment. Anatomical study of 100 healthy human hearts. *Arq Bras Cardiol* 1999;73:75-86.
14. McAlpine WA. An introduction to the aorto-ventricular unit. In: McAlpine WA, editor. *Heart and coronary arteries. An anatomical atlas for clinical diagnosis, radiological investigation, and surgical treatment.* Berlin: Springer-Verlag, 1975: 9-27.
15. Abedin Z, Goldberg J. Origin and length of left main coronary artery: its relation to height, weight, sex, age, pattern of coronary distribution, and presence or absence of coronary artery disease. *Cathet Cardiovasc Diagn* 1978;4:335-40.
16. Zajarias A, Eltchaninoff H, Cribier A. Successful coronary intervention after percutaneous aortic valve replacement. *Catheter Cardiovasc Interv* 2007;69:522-4.



Role of multislice computed tomography in transcatheter aortic valve replacement

David A. Wood¹
Laurens F. Tops²
John R. Mayo³
Sanjeevan Pasupati¹
Martin J. Schalij²
Karin Humphries¹
May Lee¹
Abdullah Al Ali¹
Brad Munt¹
Rob Moss¹
Christopher R. Thompson¹
Jeroen J. Bax²
John G. Webb¹

¹*Division of Cardiology, St. Paul's Hospital, University of British Columbia, Vancouver, Canada*

²*Department of Cardiology, Leiden University Medical Center, Leiden, the Netherlands*

³*Department of Radiology, Vancouver General Hospital, University of British Columbia, Vancouver, Canada*

ABSTRACT

378

Transcatheter aortic valve replacement (TAVR) requires precise knowledge of the anatomic dimensions and physical characteristics of the aortic valve, annulus and aortic root. Most groups currently utilize angiography, transthoracic echocardiography (TTE) or transesophageal echocardiography (TEE) to assess aortic annulus dimensions and anatomy. However, multislice computed tomography (MSCT) may allow more detailed 3-dimensional assessment of the aortic root. Twenty-six patients referred for TAVR underwent MSCT. Scans were also performed in 18 patients following TAVR. All patients underwent pre- and post-procedural aortic root angiograms, TTE and TEE. Mean differences in measured aortic annular diameters were 1.1 mm (95% CI 0.5, 1.8 mm) for calibrated angiography and TTE, 0.9 mm (95% CI -1.7, -0.1 mm) for TTE and TEE, 0.3 mm (95% CI -1.1, 0.6 mm) for MSCT (sagittal) and TTE, 1.2 mm (95% CI -2.2, -0.2 mm) for MSCT (sagittal) and TEE. The coronal systolic measurements on MSCT, which correspond to the angiographic orientation, were 3.2 mm (1st and 3rd quartiles 2.6, 3.9) larger than the sagittal systolic measurements, which are in the same anatomic plane as standard TTE and TEE views. There was no significant association between either the shape of the aortic annulus or the amount of AV calcium and the development of perivalvular aortic regurgitation. Following TAVR the prosthesis extended to or beyond the inferior border of the left main ostium in 9 of 18 patients (50%) and in 11 patients (61%) valvular calcium was <5mm from the left main ostium. In conclusion, MSCT identified that the aortic annulus is commonly eccentric and often oval. This may, in part, explain the small but clinically insignificant differences in measured aortic annular diameters with other imaging modalities. MSCT following TAVR demonstrated the close proximity of both the prosthesis and displaced valvular calcium to the left main ostium in most patients. Neither eccentricity nor calcific deposits appeared to contribute significantly to the severity of paravalvular regurgitation following TAVR.

INTRODUCTION

Transcatheter aortic valve replacement (TAVR) shows promise as an alternative to conventional open heart surgery for selected patients with severe symptomatic aortic stenosis (AS) (1-7). Transthoracic echocardiography (TTE), transesophageal echocardiography (TEE) and calibrated aortic angiography are commonly used to determine aortic annular size to assist in prosthesis selection (8). Recent work with multislice computed tomography (MSCT) provided detailed information on the shape of the aortic annulus and the relation between the annulus and the ostia of the coronary arteries (9). MSCT identified that the aortic annulus is oval, rather than circular, which might help explain the differences in measured aortic annular diameters with TTE, TEE, and calibrated angiography. We sought to determine if MSCT could provide clinically useful information beyond that available from angiographic and echocardiographic assessment that might influence patient selection and procedural issues during TAVR.

METHODS

Patients with severe symptomatic AS were referred to St. Paul's Hospital, University of British Columbia, Vancouver, Canada for TAVR due to a high risk of morbidity or mortality with conventional valve surgery. As part of their assessment 26 patients underwent screening MSCT in Vancouver between June 2005 and January 2007. These patients represent the study population. It was the consensus of a group of senior cardiac surgeons and cardiologists that the patients were unsuitable for conventional AVR due to excessive surgical risk. Of the initial 26 patients screened with MSCT, 23 subsequently underwent TAVR, 2 were determined not to be candidates for TAVR for technical reasons, and 1 patient was subsequently accepted for conventional surgery (Table 1). Of the 23 patients who underwent TAVR, 18 subsequently underwent evaluation with MSCT at a median of 4 (1st and 3rd quartiles 3, 6) months after TAVR. During this period an additional 52 patients underwent TAVR but did not undergo MSCT assessment due to renal dysfunction, poorly controlled arrhythmias or logistical issues.

All MSCT scans were obtained using a cardiac gated Siemens Sensation 64 slice scanner (Siemens Medical Solutions, Erlangen, Germany) during suspended full inspiration. An initial non contrast enhanced coronary calcium scoring scan was performed using the following specifications: 120kVp, 123 effective mAs, ECG modulation on, pitch 0.2, rotation time 164 msec, detector aperture 0.6 mm, 180 degree B25f cardiac gated reconstruction algorithm at 75% R-R, 3 mm slice thickness, 3 mm spacing. A contrast enhanced bolus timing scan was performed at the level of the carina using a scan delay of 10 seconds. Twenty ml of Isovue 370 (Bracco Diagnostics, Mississauga, Ontario) contrast media was followed by 50 ml of normal saline delivered at 5 ml per second through an 18 gauge catheter in the antecubital fossa. Time-to-peak enhancement in the ascending aorta was used to determine the scan delay for

Table 1. Summary of TTE, TEE, MSCT and angiographic annular measurements

Age	MSCT Sagittal Diastole (mm)	MSCT Sagittal Systole (mm)	MSCT Coronal Diastole (mm)	MSCT Coronal Systole (mm)	Angiography (mm)	TTE (mm)	TEE (mm)	AVA (cm ²)	MPG (mmHg)	EF (%)	MSCT post-TAVR (mo follow-up)	Stent (mm)	MSCT Mid-stent Sagittal Systole (mm)	MSCT Mid-stent Coronal Systole (mm)
63	26	-	29	-	26	24	24	1.0	20	60	Died (before TAVR)	-	-	-
66	24	-	28	-	26	23	23	0.7	50	65	12	26	20	21
70	21	21	26	25	22	20	21	0.3	65	40	9	23	20	22
74	21	22	23	24	21	21	25	0.7	54	65	3	26	20	19
74	23	23	27	26	25	23	-	0.9	47	65	Accepted for surgery	-	-	-
77	20	-	20	-	23	22	21	0.6	43	65	3	26	20	21
77	24	24	30	29	25	24	28	0.6	40	20	8	26	23	23
79	20	24	30	27	27	26	25	0.7	37	50	6	26	24	25
80	23	-	27	-	26	22	-	0.8	41	65	Died	26	-	-
81	22	22	29	27	24	24	25	0.6	22	10	4	26	22	24
83	24	24	27	27	23	22	23	0.5	88	65	4	26	21	25
84	18	20	24	26	21	23	24	0.7	29	55	Declined follow-up	26	-	-
85	21	22	26	25	24	23	-	0.7	57	60	Declined procedure	-	-	-
85	23	23	25	25	23	21	-	0.5	74	65	Metastatic Cancer	-	-	-
86	23	25	26	27	23	24	24	0.5	42	55	4	26	21	24
86	19	22	24	25	25	23	23	0.7	64	65	3	26	20	25
87	23	23	27	27	25	24	21	0.3	46	45	3	23	23	24
88	18	20	24	23	22	21	21	0.6	41	65	6	23	19	20
89	21	22	25	26	25	24	24	0.6	55	60	Died	26	-	-
89	20	23	25	26	25	22	24	0.6	35	35	6	26	22	24
89	24	22	26	25	20	20	24	0.5	54	50	4	26	20	23
89	22	23	24	25	26	23	25	0.7	40	60	2	26	22	24
92	21	22	23	23	21	22	21	0.6	74	60	2	23	20	19
93	19	-	22	-	22	19	23	0.5	62	65	13	23	19	20
93	19	-	23	-	21	20	22	0.5	32	65	12	23	21	20
95	21	-	23	-	22	22	22	0.6	53	70	Died (before TAVR)	-	-	-

AVA = aortic valve area; EF = ejection fraction; MPG = mean pressure gradient (transaortic).

the subsequent diagnostic cardiac CT scan. This scan of the entire heart was acquired during the injection of 100 ml of 370 Isovue contrast media followed by 50 ml of normal saline at 5 ml per second. The scan acquisition used the following parameters: 120 kVp, 830-870 effective mAs, EKG modulation off, pitch 0.2, rotation time 330 msec, detector aperture 0.6 mm. Image reconstruction parameters included: 180 degree cardiac gated B30f reconstruction algorithm, 165 msec temporal resolution, timed to 30% and 70% of the R-R interval, 0.75 mm slice thickness, 0.4 mm spacing.

Non-contrast and contrast-enhanced images were transferred over the hospital's imaging network to the Multi Modality Workplace workstation (Version VE22A, Siemens Medical Solutions, Erlangen, Germany). Agatston method (10) aortic valve calcium scoring was performed using the Calcium Scoring software package (Syngo 2007C VE27B, Siemens Medical Solutions, Erlangen, Germany). Aortic valve measurements were made using electronic calipers within the Circulation software package (Syngo 2007C VE27B, Siemens Medical Solutions, Erlangen, Germany). Pre-implantation images were evaluated using window width of 1000 Hounsfield units (HU) and level of 150 HU. Due to artifact arising from the struts of the aortic valve prosthesis, post implantation images were evaluated using window width of 2500 HU and level of 1000 HU.

Images were analyzed using the workstation by consensus of two observers. The largest transverse diameter of the aortic annulus was measured in coronal and single oblique sagittal projections using the 30% (systole, or R-R with maximum leaflet excursion) and 70% (diastole) images. These proved to be the longest and shortest annular measurements in all patients. The correct orientation of these two orthogonal images was confirmed by inspection of the double oblique transverse (DOT) images of the aortic valve, which allowed confirmation of the level of insertion of the aortic valve leaflets (Figure 1). The single oblique sagittal view has the same orientation as both the parasternal long axis view on TTE and the midesophageal long axis view on TEE (11) (Figure 2). The coronal view has the same orientation as the anterior posterior view on aortic root angiography (Figure 3). The coronal view in diastole was used to measure the diameter of the sinus of Valsalva, the distance from the annulus to the inferior border of the left main coronary artery, and the length of the left coronary cusp leaflet (9). The coronal view in systole was used to measure the above leaflet length as well as the distance from the leaflet tip to the inferior border of the left main coronary artery (Figure 4). The DOT view was used to measure the maximum diameter of the sinus of Valsalva at the level of the inferior border of the left main coronary artery.

We subjectively graded the AV calcium using the scoring system of Willmann et al (12), which was adapted from Rosenhek et al. (13). Agatston method (10) calcium scores were obtained from the aortic valve leaflets using the Calcium Scoring program on the Siemens workstation from the non contrast enhanced images. Areas of AV calcium were highlighted and surrounding areas of calcium were excluded to generate a composite score for each valve.

MSCT scans performed post TAVR were analyzed using the same orthogonal viewing planes. Stent diameter was measured in systole in the single oblique sagittal and coronal planes at the

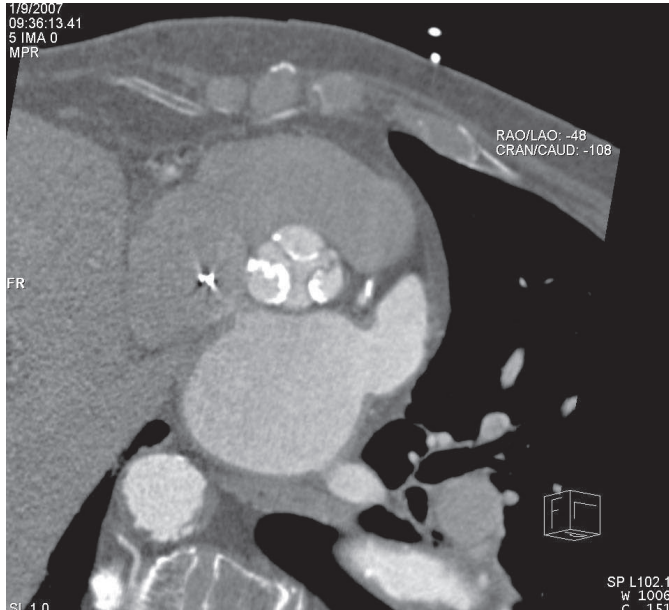


Figure 1. Double oblique transverse (DOT) view is used to derive the other standard orthogonal planes (single oblique sagittal and coronal projections). It is critical that the DOT view is parallel to the true valve plane. Calcium appears white in this projection.

level of the aortic annulus (Figure 5). The coronal view was used to measure the distance from the inferior border of the left main coronary artery to both the native valve calcification and the stent wall (Figure 6A). The distance from the superior edge of the stent to the inferior edge of the left main coronary artery was measured on an oblique coronal image that was rotated to pass through the origin of the left main artery and the centre of the stent (Figure 6A).

Standard 2 dimensional TTE was performed as part of our screening assessment. Images were obtained with patients in the left lateral decubitus position with a commercially available system (Sonos 5500, Philips Medical Systems) interfaced with an S3 compound probe and stored on a digital archive system. The diameter of the aortic annulus was measured by an independent viewer in systole in the parasternal long axis view at the site of leaflet attachment (Figure 2B).

TEE was performed immediately before and after TAVR. Images were obtained with patients intubated and sedated in the supine position with the same system interfaced with a T6210 omniplane probe. The diameter of the aortic annulus was measured by an independent viewer in systole in the midesophageal long axis view at the site of leaflet attachment (Figure 2C). Aortic regurgitation (AR) severity immediately post implantation and at hospital discharge was the consensus grade of two senior echocardiographers using the ratio of regurgitation jet to left ventricular outflow tract height and regurgitation pressure half-time determination (8,14,15). The site of AR was judged to be either valvular (through the valve) or perivalvular (around the valve).

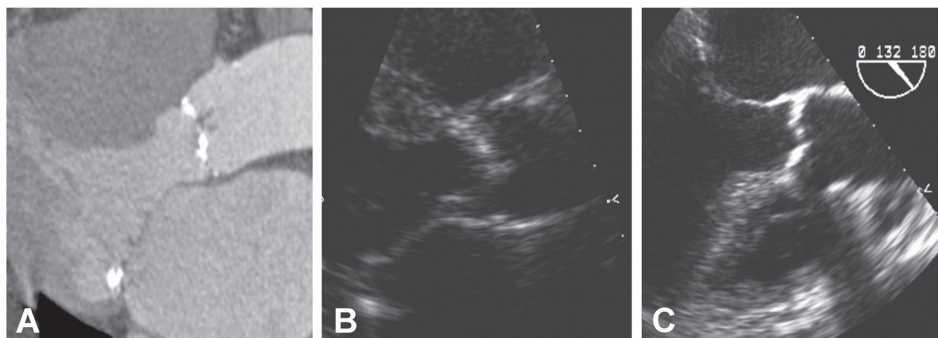


Figure 2. The (A) single oblique sagittal view on MSCT is equivalent to the (B) parasternal long axis-view on TTE and the (C) midesophageal long-axis view on TEE. The aortic annular measurements for this patient were 23, 23, and 24 mm respectively.

Calibrated angiographic annular measurements were performed by two independent viewers as part of the screening assessment. The diameter at the leaflet hinge point at the presumed level of the aortic annulus was measured in systole in the anterior posterior view (Figure 3B).

Continuous data are presented as mean values \pm standard deviation (SD) or median values with 1st and 3rd quartiles, as appropriate. Categorical data are presented as percentages. Bland-Altman plots were used to compare annular measurements obtained using different techniques (angiographic, echocardiographic and MSCT) (16). All statistical analyses were performed with SPSS TM software (version 13.0, SPSS Inc., Chicago, Illinois). All statistical tests were 2 sided. A p value of < 0.05 was considered statistically significant.

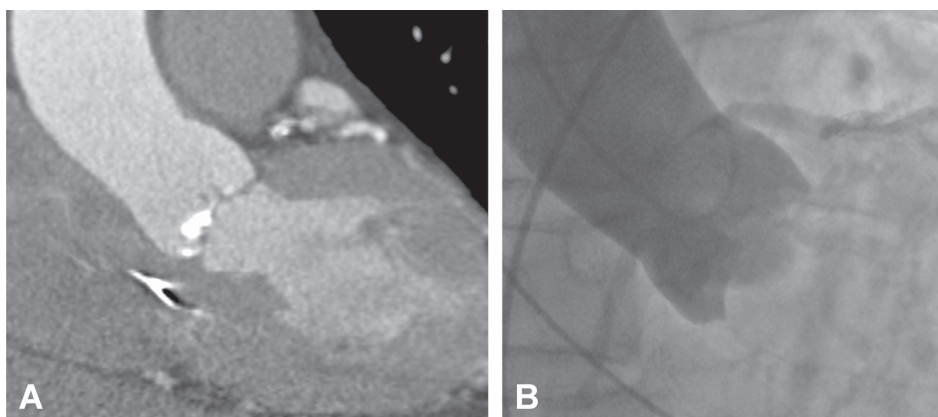


Figure 3. The (A) coronal view on MSCT has the same orientation as the (B) anterior posterior view on aortic root angiogram. Images from the same patient as Figure 2 are displayed with aortic annular measurements of 25 and 26 mm respectively.

RESULTS

Mean age of the 26 patients was 82 ± 9 years. A balloon expandable valve was implanted in 23 patients, utilizing the femoral approach in 21 and the apical approach in 2 due to the presence of femoral artery disease. Coronary artery disease was present in 83%, with 30% having

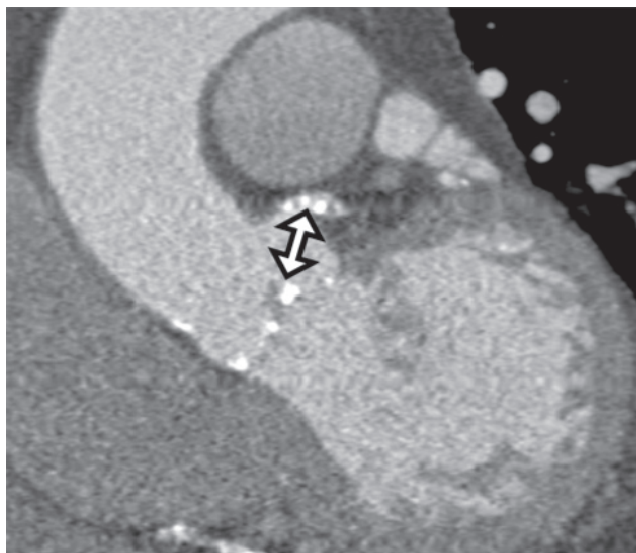


Figure 4. The coronal view in systole on MSCT was used to measure the distance from the left coronary cusp leaflet tip to the inferior border of the left main coronary artery.

undergone prior percutaneous intervention and 39% having had prior coronary artery bypass graft surgery. The logistic EuroSCORE (17,18) estimate of operative mortality was $31.5 \pm 19.7\%$.

Screening MSCT measurements were applied to our 26 patients with severe AS. The average left coronary cusp leaflet length in systole, from leaflet insertion to leaflet tip, was 14.8 ± 1.3 mm. The mean distance from the aortic annulus to the inferior border of the left main coronary artery was 15 ± 3.0 mm. The maximum diameter of the sinus of Valsalva in the DOT view was 32.5 ± 3.0 mm.

The differences in aortic annular dimensions for calibrated angiography, TTE, TEE, and MSCT are listed in Table 1 and selected Bland-Altman plots are shown in Figure 7. The mean differences in measured aortic annular diameters were 1.1 mm (95% CI 0.5, 1.8 mm) for calibrated angiography and TTE, 0.9 mm (95% CI -1.7, -0.1 mm) for TTE and TEE, 0.3 mm (95% CI -1.1, 0.6 mm) for MSCT (sagittal) and TTE, 1.2 mm (95% CI -2.2, -0.2 mm) for MSCT (sagittal) and TEE (Figure 7). In the systolic phase, the mean diameter of the aortic annulus on the coronal view was 25.7 ± 1.5 mm and 22.4 ± 1.3 mm in the sagittal view. The mean difference between the coronal and sagittal diameters was 3.2 mm (95% CI 2.6, 3.9). In the diastolic phase, the mean diameter of the aortic annulus on the coronal view was 25.5 ± 2.5 mm and 21.5 ± 2.1 mm in the sagittal view. The mean difference between the coronal and sagittal diameters was 4.0 mm (95% CI 3.1, 4.8).

Patients were considered to have an oval annulus if the difference between their coronal and sagittal annular measurements was ≥ 3 mm (9). Twenty patients (77%) had an oval annulus. Eight patients had \geq moderate perivalvular AR on TEE immediately post implantation. There was no significant association between the shape of the aortic annulus and the proportion of

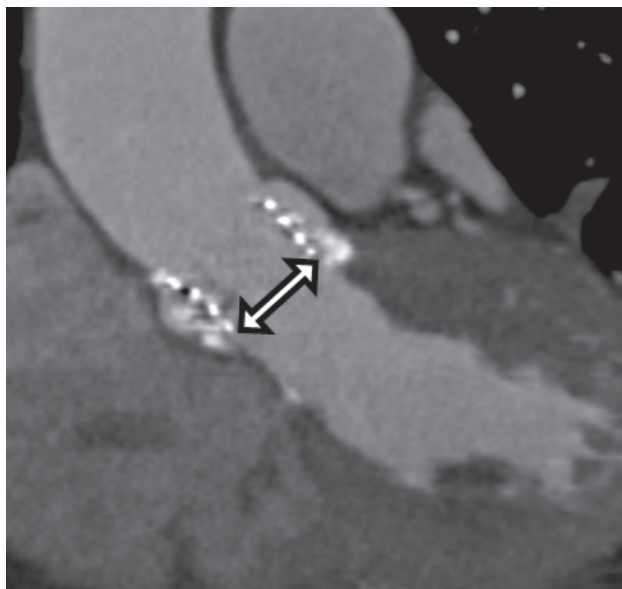


Figure 5. The coronal view in systole on MSCT was used to measure the stent diameter at the level of the aortic annulus.

patients that developed moderate perivalvular AR (Fisher's exact test, $p=1.0$). Seven of these patients went on to have successful re-dilation of their balloon expandable aortic valve immediately following implantation with a reduction in perivalvular leak.

Seventeen patients had grade 4, 6 grade 3, and none grade 1 or 2 AV calcific deposits. There was no significant association between the grade of calcium and the proportion of patients that developed moderate perivalvular AR (Fisher's exact test, $p=0.35$). AV calcium scores were also stratified above and below 3500, corresponding to subjective AV calcium scores of 3 or 4. There was no significant association between the stratified objective calcium scores and the proportion of patients that developed moderate perivalvular AR (Fisher's exact test, $p=0.37$).

Post TAVR the prosthesis was observed to extend above the inferior border of the left main coronary artery in 50% of patients ($n=9$) (Figure 6A); extending a median of 0.5 mm (1st and 3rd quartiles 0, 8) above the left main ostium. The median distance from the left main coronary artery to the displaced native valve calcium was 4 mm (1st and 3rd quartiles 3, 5). Eleven patients (61%) had displaced calcium that was <5mm from the left main ostium (Figure 6A).

The stent diameter was measured at the level of the aortic annulus (Figure 5). The implanted stent was considered circular if the difference between the coronal and sagittal annular measurements was <3 mm. By this definition, 14 patients (78%) had a circular annulus post implantation and 4 (22%) had a non-circular annulus. Of those with a non-circular annulus, 3 of the 4 patients had an oval annulus prior to TAVR.

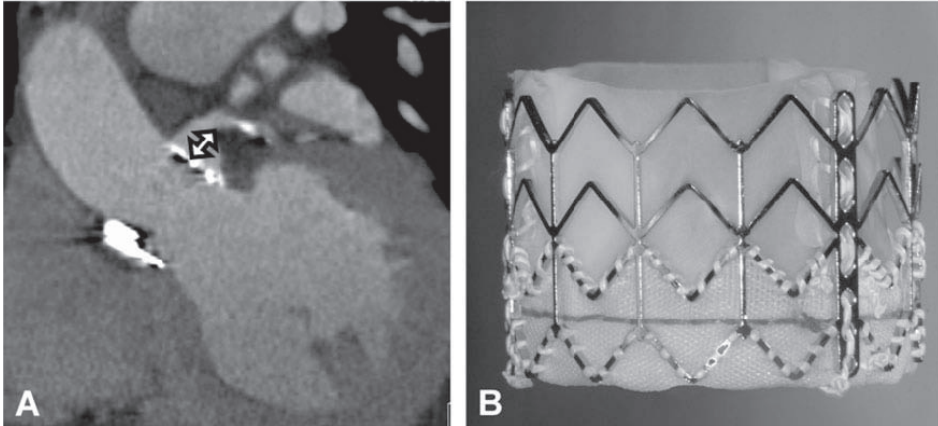


Figure 6. The (A) coronal view in systole on MSCT was used to measure the distance from the inferior border of the left main coronary artery to both the native valve calcium and the stent wall. The distance the stent was placed above or below the inferior border of the left main coronary artery was also recorded. Panel B: A digital picture of a 23 mm balloon expandable prosthesis (Cribier-Edwards™, Edwards Lifesciences Inc., Irvine, CA) demonstrates the fabric cuff that covers the bottom third of the stent.

DISCUSSION

Anderson et al. first noted that the site of attachment of the three aortic valvar leaflets is not circular, as the term “annulus” implies (19). Recently, studies using both MSCT and magnetic resonance imaging have supported these observations (9,20). The word “annulus” is actually a misnomer as the aortic valvar complex consists of several small rings within the aortic root that do not all correspond to discrete anatomic structures. We have used the term “annulus” for simplicity. The mean difference between the coronal and sagittal annular diameters was 3.2 mm (95% CI 2.6, 3.9) during the systolic phase and 4.0 mm (95% CI 3.1, 4.8) during the diastolic phase and is similar to the results we obtained with a larger cohort (169 patients) with and without AS (9). There was no significant difference between the systolic and diastolic measurements in either study. An oval aortic annulus helps explain the differences in annular measurements seen with imaging modalities that are restricted to a single plane or a limited field of view (Table 1). The current practice of routinely oversizing the prosthesis by 10 to 20% makes the small

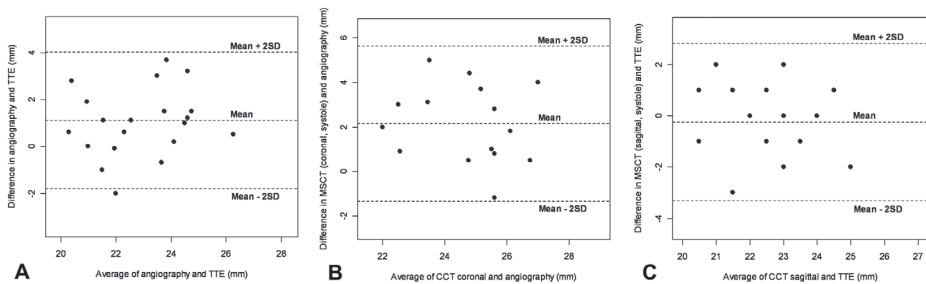


Figure 7. Bland-Altman plots comparing (A) annular measurements using angiography and TTE, (B) the coronal view obtained in systole on MSCT and angiography, and (C) the sagittal view obtained in systole on MSCT and TTE.

differences in measured aortic annular diameters with TTE, TEE, and calibrated angiography clinically insignificant. An oval annulus also has important implications for echocardiography as the parasternal short axis view assumes a circular annulus as a point of reference. Physicians should be aware of this potential limitation.

There was no significant association between the shape of the aortic annulus and the proportion of patients that developed moderate perivalvular AR. It is possible that an association may become apparent with a larger cohort over a longer time period although this has not been observed (7). Our routine practice of oversizing the prosthesis by 10 to 20% may have also obscured any potential association (4,8).

There was no significant association between either the calcium grade or the AV calcium score and the proportion of patients that developed moderate perivalvular AR. It is possible that an association may become apparent with a larger cohort although this does not appear to be a major concern in the majority of patients. This is consistent with the clinical impression that severe native AV calcium is not a major contraindication to TAVR (3).

In one half of the current cohort (n=9) the prosthesis was observed to extend to or beyond the level of the ostium of the left main coronary artery (Figure 6A). Currently available balloon expandable transcatheter valves incorporate a sealing cuff in the portion of the prosthesis that lies within the annulus. The portion of the valve extending to or beyond the left main typically consists of an open mesh that does not interfere with coronary perfusion (Figure 6B). Cell size is sufficiently large to permit catheter access to the coronaries although a leaflet support strut may be problematic. However, obstruction of the left main ostium due to a displaced bulky native valve leaflet has been an infrequent occurrence (3,4). Our finding of native calcified tissue in relatively close proximity to the left main ostium argues for careful screening and surveillance.

CONCLUSIONS

MSCT prior to TAVR may be useful to assess aortic valve morphology, annular dimensions, assist in prosthesis selection and assess the potential for coronary compromise. That the annulus is commonly oval rather than circular has implications with regards to the interpretation of other imaging modalities. MSCT following TAVR may be useful to assess prosthesis positioning and adequacy of deployment.

REFERENCES

1. Cribier A, Eltchaninoff H, Bash A et al. Percutaneous transcatheter implantation of an aortic valve prosthesis for calcific aortic stenosis: first human case description. *Circulation* 2002;106:3006-8.
2. Cribier A, Eltchaninoff H, Tron C et al. Early experience with percutaneous transcatheter implantation of heart valve prosthesis for the treatment of end-stage inoperable patients with calcific aortic stenosis. *J Am Coll Cardiol* 2004;43:698-703.
3. Webb JG, Pasupati S, Humphries K et al. Percutaneous transarterial aortic valve replacement in selected high-risk patients with aortic stenosis. *Circulation* 2007;116:755-63.
4. Webb JG, Chandavimol M, Thompson CR et al. Percutaneous aortic valve implantation retrograde from the femoral artery. *Circulation* 2006;113:842-50.
5. Lichtenstein SV, Cheung A, Ye J et al. Transapical transcatheter aortic valve implantation in humans: initial clinical experience. *Circulation* 2006;114:591-6.
6. Ye J, Cheung A, Lichtenstein SV et al. Six-month outcome of transapical transcatheter aortic valve implantation in the initial seven patients. *Eur J Cardiothorac Surg* 2007;31:16-21.
7. Webb JG. Percutaneous aortic valve replacement will become a common treatment for aortic valve disease. *J Am Coll Cardiol Int* 2008;1:122-6.
8. Moss R, Ivens E, Pasupati S et al. Role of echocardiography in percutaneous aortic valve implantation. *J Am Coll Cardiol Img* 2008;1:15-24.
9. Tops LF, Wood DA, Delgado V et al. Noninvasive evaluation of the aortic root with multislice computed tomography: Implications for transcatheter aortic valve replacement. *J Am Coll Cardiol Img* 2008;1:321-30.
10. Agatston AS, Janowitz WR, Hildner FJ, Zusmer NR, Viamonte M, Jr., Detrano R. Quantification of coronary artery calcium using ultrafast computed tomography. *J Am Coll Cardiol* 1990;15:827-32.
11. Shanewise JS, Cheung AT, Aronson S et al. ASE/SCA guidelines for performing a comprehensive intraoperative multiplane transesophageal echocardiography examination. *J Am Soc Echocardiogr* 1999;12:884-900.
12. Willmann JK, Weishaupt D, Lachat M et al. Electrocardiographically gated multi-detector row CT for assessment of valvular morphology and calcification in aortic stenosis. *Radiology* 2002;225:120-8.
13. Rosenhek R, Binder T, Porenta G et al. Predictors of outcome in severe, asymptomatic aortic stenosis. *N Engl J Med* 2000;343:611-7.
14. Perry GJ, Helmcke F, Nanda NC, Byard C, Soto B. Evaluation of aortic insufficiency by Doppler color flow mapping. *J Am Coll Cardiol* 1987;9:952-9.
15. Teague SM, Heinsimer JA, Anderson JL et al. Quantification of aortic regurgitation utilizing continuous wave Doppler ultrasound. *J Am Coll Cardiol* 1986;8:592-9.
16. Bland JM, Altman DG. Statistical methods for assessing agreement between two methods of clinical measurement. *Lancet* 1986;1:307-10.
17. Nashef SA, Roques F, Hammill BG et al. Validation of European System for Cardiac Operative Risk Evaluation (EuroSCORE) in North American cardiac surgery. *Eur J Cardiothorac Surg* 2002;22:101-5.
18. Roques F, Nashef SA, Michel P. Risk factors for early mortality after valve surgery in Europe in the 1990s: lessons from the EuroSCORE pilot program. *J Heart Valve Dis* 2001;10:572-7.
19. Anderson RH, Lal M, Ho SY. Anatomy of the aortic root with particular emphasis on options for its surgical enlargement. *J Heart Valve Dis* 1996;5: S249-S257.
20. Burgstahler C, Kunze M, Loffler C, Gawaz MP, Hombach V, Merkle N. Assessment of left ventricular out-flow tract geometry in non-stenotic and stenotic aortic valves by cardiovascular magnetic resonance. *J Cardiovasc Magn Reson* 2006;8:825-9.

Summary, conclusions and future perspectives

SUMMARY

In recent years, a number of new cardiac interventional procedures have been introduced. For atrial fibrillation (AF), catheter ablation procedures have been refined and are now considered a good treatment option in patients with drug-refractory AF. In cardiac pacing, cardiac resynchronization therapy (CRT) is now standard of care in patients with drug-refractory heart failure. At the same time, CRT may also be beneficial in patients with heart failure after long-term RV apical pacing. Finally, new percutaneous procedures for valvular heart disease have been introduced for patients that are deemed inoperable. At the same time, various imaging modalities have been further developed and important advances have been made in the integration of different imaging modalities.

The aim of the present thesis was to explore the role of multimodality imaging in cardiac interventional procedures. In **Part I**, the integration of different imaging modalities during catheter ablation procedures for AF was studied. In addition, the effects of these procedures on left atrial (LA) and left ventricular (LV) size and function were investigated. **Part II** studied the effects of right ventricular (RV) apical pacing on LV dyssynchrony and mechanics, and the effect of upgrade to CRT. Finally, in **Part III** the role of imaging in new percutaneous procedures for valvular heart disease was explored.

PART I: Catheter ablation for atrial fibrillation

The first part of the thesis focused on catheter ablation procedures for AF. These procedures are performed in an increasing number of patients worldwide. For these procedures, accurate visualization of the LA and pulmonary veins (PVs) is of critical importance. **Chapter 2** reviews the different imaging modalities that are available for the assessment of LA and PV anatomy. In daily clinical practice, conventional transthoracic echocardiography is most frequently used to assess LA size and volumes. Three-dimensional imaging techniques such as magnetic resonance imaging and multi-slice computed tomography (MSCT) are mainly used to assess PV anatomy before catheter ablation of AF. In addition, intracardiac echocardiography may be a valuable tool during these procedures. Finally, the integration of MSCT and electroanatomic mapping during catheter ablation procedures is discussed.

Chapter 3 is a clinically oriented review on the use of imaging in the work-up of patients with AF, and provides an overview on the role of imaging in catheter ablation procedures. In the evaluation of patients with AF, associated conditions such as coronary artery disease, valvular heart disease and heart failure should carefully be analyzed. The various imaging modalities that are available for this are reviewed in this chapter. In addition, relevant issues before catheter ablation (detection of thrombi, assessment of LA and PV anatomy) and available imaging techniques are discussed. Finally, an overview of the different imaging modalities that can be integrated to guide catheter ablation procedures is provided.

In **Chapter 4**, the feasibility of the integration of MSCT images and electroanatomic mapping was tested in 16 patients undergoing catheter ablation for drug-refractory AF. The fusion of pre-procedural acquired MSCT images and electroanatomic maps may facilitate catheter ablation procedures by improved visualization of critical structures such as the PVs. A new image integration module (CartoMerge™) was used to merge the two imaging modalities using dedicated registration algorithms. After fusion of the two images, the mean distance between all mapping points and the MSCT image was 2.1 ± 0.2 mm (range 1.7 – 2.8). The integrated image was subsequently used to guide the catheter ablation. This study demonstrates that it is feasible to integrate MSCT images and electroanatomic maps. Image integration can facilitate catheter ablation procedures by improved visualization of important anatomical structures.

The findings of the previous study were extended in **Chapter 5**. In this study, the feasibility of the integration of intracardiac echocardiography, electroanatomic mapping and MSCT was tested. For this purpose, a newly developed intracardiac echocardiography probe, with an incorporated Carto™ navigation sensor located at its tip, was used. After positioning of the catheter in the right atrium, electroanatomic maps were created by drawing endocardial contours on the real-time intracardiac echocardiography images. Seventeen patients (13 men, mean age 56 ± 8 years) referred for catheter ablation for AF were studied.

A mean of 31.1 ± 8.5 contours were used to create the 3D maps of the LA and PVs, and the mean distance between the contours and the MSCT image (registration accuracy) was 2.2 ± 0.3 mm. Furthermore, a good agreement between intracardiac echocardiography and MSCT for the assessment of PV anatomy and PV diameters was noted. In conclusion, the feasibility of the integration of intracardiac echocardiography, electroanatomic mapping and MSCT was clearly demonstrated in this study.

Chapter 6 focused on PV anatomy assessment with MSCT before catheter ablation, and its impact on the outcome of the ablation procedures. A total of 100 patients undergoing catheter ablation for AF were evaluated with MSCT. Pulmonary vein anatomy was classified as 'normal' or 'complex' based on the absence or presence of additional PVs or common ostia (single insertion of PVs). Furthermore, LA dimensions were assessed in three directions. Complex PV anatomy of the left-sided and right-sided PVs was present in 26% and 22% of patients, respectively. Mean LA diameter in the anterior-posterior direction was 41 ± 7 mm. Interestingly, the presence of right-sided complex PV anatomy was associated with an improved outcome of the catheter ablation procedure (OR = 0.149 [0.038-0.576], $p=0.006$), whereas LA dilatation was associated with a worse outcome (OR = 1.083 [1.009-1.162], $p=0.027$). This study underlines the importance of pre-procedural PV and LA anatomy assessment. Favorable anatomy may have impact on the outcome of catheter ablation procedures.

In the following studies, the effect of catheter ablation procedures on LA and LV size and function were investigated. We hypothesized that successful elimination of AF results in reverse remodeling of the LA. The study described in **Chapter 7** included 57 patients treated with catheter ablation for AF. At baseline and after three months follow-up LA size and volumes were assessed with conventional 2D echocardiography. In patients who maintained sinus rhythm during follow-up (n=39), LA size significantly decreased, whereas in patients with recurrence of AF (n=18) LA size increased. In addition, a decrease in LA end-diastolic volume (from 37 ± 9 ml to 31 ± 7 ml, $p < 0.01$) and LA end-systolic volume (from 59 ± 12 ml to 50 ± 11 ml, $p < 0.01$) was noted in patients who maintained sinus rhythm during follow-up. These findings were confirmed in **Chapter 8**. In this study, real-time 3D echocardiography was used to assess LA size and volumes. This technique may be more accurate and reproducible than conventional 2D echocardiography for assessment of LA volumes. In addition to LA size and volumes, LA function was assessed at baseline and follow-up (mean 7.9 ± 2.7 months). Based on minimum and maximum LA volume, and LA volume just before atrial active contraction, LA function (total emptying fraction, active emptying fraction and passive emptying fraction) was assessed. Significant improvements in LA active function (from $22 \pm 8\%$ to $33 \pm 9\%$, $p < 0.01$) and LA reservoir function (from $116 \pm 45\%$ to $152 \pm 54\%$, $p < 0.01$) were noted in patients who maintained sinus rhythm. In contrast, LA function showed a trend towards deterioration in patients who had recurrence of AF.

From the abovementioned studies, it appears that LA reverse remodeling may occur after catheter ablation for AF. The following study aimed to elucidate the clinical and echocardiographic determinants of LA reverse remodeling (**Chapter 9**). Reverse remodeling was defined as $\geq 15\%$ reduction in maximum LA volume at follow-up. Tissue Doppler imaging was used to assess LA systolic and end-diastolic strain, representing LA expansion function and LA active contraction function, respectively. The study population (n=148) was divided according to the presence or absence of LA reverse remodeling at follow-up ('responders' [n=93] or 'non-responders' [n=55]). In the responders, a significant increase in LA systolic strain was noted from baseline to follow-up (from $19 \pm 8\%$ to $22 \pm 9\%$, $p < 0.05$), whereas no change was noted in the non-responders (from $14 \pm 6\%$ to $15 \pm 8\%$, $p = \text{NS}$). Interestingly, LA systolic strain at baseline was the strongest predictor of LA reverse remodeling (OR 1.089; 95% CI 1.014-1.169, $p = 0.019$). This study suggests a close association between LA reverse remodeling after catheter ablation and LA strain.

Finally, in **Chapter 10** the long-term effects of catheter ablation on LV function were studied. In this study, speckle-tracking echocardiography was used to assess LV strain in 3 directions (radial, circumferential and longitudinal). This technique may detect more subtle abnormalities in LV systolic function, as compared with conventional parameters such as LV ejection fraction. A total of 78 patients (mean LV ejection fraction $60 \pm 7\%$) were included in the study. After 13.8 ± 4.7 months follow-up, 54 patients maintained sinus rhythm, whereas 24 patients had

recurrence of AF. In the patients who maintained sinus rhythm, LV circumferential strain and LV longitudinal strain significantly improved from baseline to follow-up (from $-18.3 \pm 3.2\%$ to $-20.4 \pm 3.8\%$, $p < 0.001$ and from $-18.8 \pm 2.7\%$ to $-19.6 \pm 2.6\%$, $p < 0.001$, respectively). In contrast, LV circumferential strain remained unchanged and LV longitudinal strain significantly deteriorated in patients with recurrence of AF. This study demonstrates that LV strain improves in patients with preserved LV ejection fraction that are successfully treated with catheter ablation for AF.

PART II: Ventricular pacing and dyssynchrony

The second part of this thesis focused on cardiac pacing and mechanical dyssynchrony. In **Chapter 11**, an extensive review of the available evidence on the effects of RV apical pacing on LV function and dyssynchrony is provided. Large randomized trials on the selection of pacing mode have demonstrated an association between long-term RV pacing and deterioration of LV systolic function and heart failure. These negative effects may be related to the presence of LV dyssynchrony. Several studies have demonstrated that the upgrade from RV apical pacing to biventricular pacing results in (partly) reversal of the detrimental effects of RV pacing. In addition, there is increasing evidence that 'de novo' CRT may be preferred over RV apical pacing in patients requiring high amounts of ventricular pacing.

The long-term effects of RV apical pacing on LV function, LV dyssynchrony and heart failure symptoms were studied in **Chapter 12**. For this purpose, 55 patients were studied 3.8 ± 1.7 years after atrio-ventricular node ablation and pacemaker implantation. Left ventricular dyssynchrony was assessed with conventional 2D echocardiography: with the use of M-mode echocardiography the septal-to-posterior wall motion delay was assessed as a measure of intra-ventricular dyssynchrony. A delay ≥ 130 ms was used to define significant LV dyssynchrony. In addition, tissue Doppler imaging was used to assess the septal-to-lateral delay at follow-up. At baseline, none of the patients exhibited ventricular dyssynchrony. However, in 27 patients (49%) LV dyssynchrony was present at long-term follow-up. Importantly, LV ejection fraction significantly decreased in patients with LV dyssynchrony (from $48 \pm 7\%$ to $43 \pm 7\%$, $p < 0.05$), whereas it remained unchanged in patients without LV dyssynchrony (from $49 \pm 6\%$ to $49 \pm 8\%$, $p = \text{NS}$). In addition, NYHA functional class deteriorated in patients with LV dyssynchrony (from 1.8 ± 0.6 to 2.2 ± 0.7 , $p < 0.05$), whereas it improved in patients without LV dyssynchrony (from 1.7 ± 0.7 to 1.4 ± 0.5 , $p < 0.01$). This study demonstrates that patients may develop significant LV dyssynchrony after long-term permanent RV apical pacing. Importantly, the development of LV dyssynchrony is associated with a deterioration of LV function and functional class.

After these findings, a subsequent study was conducted to investigate if LV dyssynchrony is induced acutely (**Chapter 13**). For this purpose, 25 patients undergoing electrophysiological testing for supraventricular arrhythmias, and 25 control subjects were studied. At baseline and after at least 5 minutes of RV apical pacing, LV function and dyssynchrony were assessed.

Speckle-tracking echocardiography was used to assess global LV longitudinal strain, LV dyssynchrony and LV twist. At baseline, the 25 patients and 25 control subjects were comparable with regard to LV function and LV synchrony (median 21 ms vs. 20 ms, $p=NS$). However, during RV apical pacing, a significant decrease in LV ejection fraction was noted (from $56 \pm 8\%$ to $48 \pm 9\%$, $p=0.001$). In addition, the time difference between the earliest and the latest activated segments (representing LV dyssynchrony) significantly increased in the study population (from 21 ms [10, 53] to 91 ms [40, 204], $p<0.001$). In 36% of the patients significant LV dyssynchrony (≥ 130 ms) was present. In addition, deterioration in LV global longitudinal strain and LV twist was noted after onset of RV apical pacing. Thus, the detrimental effects of RV apical pacing may (partly) occur immediately after onset of pacing.

In patients with significant LV dyssynchrony immediately after onset of pacing or at long-term follow-up, ventricular synchrony may be restored with biventricular pacing (or CRT). For optimal benefit of CRT, the site of latest activation (maximum dyssynchrony) should be identified. Speckle-tracking echocardiography was used in 58 patients with permanent RV apical pacing to detect the site of latest activation in the study described in **Chapter 14**. Furthermore, the effect of upgrade from RV apical pacing to CRT was studied in a subset of patients. Before RV pacing, similar time-to-peak strain was noted among six LV segments (mean 371 ± 114 ms). However, after long-term RV apical pacing, heterogeneity in time-to-peak strain was noted. Most frequently, the lateral and posterior segments of the LV wall were the site of latest activation (31% and 25%, respectively). This delay resulted in significant LV dyssynchrony in 57% of the patients. Unfortunately, no clinical parameters at baseline could predict LV dyssynchrony. Importantly, 11 patients underwent an upgrade from RV apical pacing to biventricular pacing. In these patients, LV dyssynchrony disappeared and LV ejection fraction significantly improved from $30 \pm 8\%$ to $39 \pm 7\%$ ($p<0.001$) after upgrade to CRT. Thus, the detrimental effects of RV apical pacing may (partly) be reversed by CRT.

In **Chapter 15** the effect of RV pacing on myocardial oxidative metabolism and efficiency was studied. A total of 10 pacemaker patients (mean age 62 ± 17 years) were studied with the use of echocardiography and positron emission tomography during pacing-OFF (sinus rhythm or atrial pacing) and pacing-ON (RV pacing). Left ventricular dyssynchrony was studied with tissue Doppler imaging and speckle-tracking echocardiography. Myocardial blood flow, oxidative metabolism and myocardial efficiency were derived from the positron emission tomography images. During RV pacing, global myocardial blood flow and oxidative metabolism did not change significantly in the overall study population. However, different effects on cardiac metabolism and efficiency were observed according to the presence or absence of LV dyssynchrony during RV pacing. In patients with LV dyssynchrony during pacing-ON ($n=6$) a significant decrease in myocardial efficiency was noted (from 78.11 ± 25.35 mmHg-l/g to 60.40 ± 13.93 mmHg-l/g, $p<0.05$), whereas in patients without LV dyssynchrony ($n=4$) no significant

change was noted (from 73.55 ± 24.78 mmHg-l/g to 75.32 ± 31.33 mmHg-l/g, $p=NS$). The presence of LV dyssynchrony during RV pacing appears to be associated with a worsening of LV oxidative metabolism and efficiency. From the abovementioned studies, it becomes clear that assessment of ventricular dyssynchrony in patients with RV pacing has important clinical implications. The presence of LV dyssynchrony is associated with deterioration of LV function, impaired oxidative metabolism and functional status.

Finally, in **Chapter 16** the prevalence of ventricular dyssynchrony in patients with arrhythmogenic right ventricular dysplasia (ARVD) was studied. Arrhythmogenic right ventricular dysplasia is an inherited disease characterized by fibrofatty infiltration of the myocardium. This infiltration may result in electrical conduction delay and mechanical dyssynchrony. However, the prevalence of mechanical dyssynchrony in ARVD has not been studied yet. A total of 52 patients (mean age 41 ± 12 years, 22 men) with ARVD and 25 healthy controls were studied. Transthoracic echocardiography was used to assess ventricular volumes and tissue Doppler imaging was used to determine the extent of mechanical dyssynchrony using time-to-peak systolic velocity (T_{SV}) of the RV free wall, the interventricular septum and the LV lateral wall. Significant RV dyssynchrony was defined as a difference between the RV free wall and interventricular septum, >2 SD above the mean value for control subjects. Mean difference in T_{SV} between the septum and RV free wall was 26 ± 15 ms in the controls (resulting in a cut-off value of ≥ 56 ms for RV dyssynchrony) and 55 ± 34 ms in the ARVD patients ($p<0.001$). In 26 ARVD patients (50%) significant RV dyssynchrony was present. Interestingly, no differences in QRS duration, prevalence in T-wave inversion or right bundle branch block were noted between ARVD patients with and without significant RV dyssynchrony. However, RV fractional area change was significantly lower ($29 \pm 8\%$ vs. $34 \pm 8\%$, $p<0.05$) and RV peak systolic strain was significantly lower ($-16 \pm 6\%$ vs. $-22 \pm 7\%$, $p<0.01$) in ARVD patients with RV dyssynchrony compared with ARVD patients without RV dyssynchrony. The present study demonstrates that significant RV dyssynchrony may be present in up to 50% of ARVD patients. The presence of RV dyssynchrony is associated with RV remodeling rather than electrocardiographic abnormalities.

PART III: Percutaneous valve procedures

The third part of this thesis focused on percutaneous valve procedures. In recent years, a number of new transcatheter procedures have been introduced to treat severe mitral regurgitation (MR) and aortic stenosis (AS). Various imaging modalities may be of great value for these procedures, in particular in the selection of patients. The various percutaneous valve procedures, the available evidence and the role of imaging in these procedures are reviewed in **Chapter 17**.

In **Chapter 18**, MSCT was used in 105 patients to assess coronary sinus anatomy. The relation between the coronary sinus, the mitral valve annulus and the coronary arteries is of critical importance for percutaneous mitral valve procedures that use the coronary sinus to remodel

the mitral valve annulus. Unfavorable anatomy may result in inefficient remodeling and may impair coronary blood flow. In the present study, a highly variable relation between the coronary sinus and the mitral valve annulus was noted. The coronary sinus was located along the LA wall in the majority of the patients (mean distance 5.1 ± 2.9 mm). Importantly, the circumflex artery coursed between the coronary sinus and the mitral valve annulus in 68% of the patients. In addition, it was noted that the minimal distance between the coronary sinus and the mitral valve annulus was significantly larger in patients with MR as compared with patients without MR (mean 7.3 ± 3.9 mm vs. 4.8 ± 2.5 mm, $p < 0.05$). In patients with large distance between the coronary sinus and mitral valve annulus, or in patients where the circumflex artery courses between the two structures, percutaneous mitral valve procedures may not be feasible. Therefore, MSCT provides important information for the selection of patients for these procedures.

The evaluation of the mitral valve with MSCT was further explored in **Chapter 19**. The subvalvular apparatus and mitral valve geometry (mitral valve tenting height and leaflet tethering) was evaluated in 151 patients, including 29 patients with moderate to severe MR. An asymmetric deformation of the mitral valve was observed in patients with MR. In these patients, an increased posterior leaflet angle was noted at the central ($44.4 \pm 11.9^\circ$) and the posteromedial ($35.9 \pm 10.6^\circ$) levels. In addition, mitral valve tenting height was significantly increased in patients with MR, compared with patients without MR at these levels (central level: 6.6 ± 1.4 mm/m² vs. 5.3 ± 1.3 mm/m², $p < 0.001$; posteromedial level: 5.4 ± 1.6 mm/m² vs. 4.1 ± 1.2 mm/m², $p < 0.001$). This study demonstrates the value of MSCT in the evaluation of anatomical and geometric characteristics of the mitral valve.

The remaining of the studies focused on percutaneous aortic valve procedures. In **Chapter 20**, an extensive review of the available studies on percutaneous aortic valve procedures is provided. The majority of these studies clearly demonstrate high procedural success rates, low 30-day mortality and good prosthesis function during follow-up. In addition, the recommendations on selection of patients for percutaneous aortic valve procedures are reviewed in this chapter. At present, these procedures are only recommended in patients with symptomatic, severe AS that are deemed inoperable. Finally, the use of various imaging modalities in the selection of patients, performing aortic valve procedures and follow-up is reviewed.

Multi-slice computed tomography is one of the imaging modalities that may provide important information on aortic valve anatomy before percutaneous valve procedures. Therefore, the anatomy of the aortic root was assessed with MSCT in 169 patients referred for non-invasive coronary angiography (including 19 patients with moderate to severe AS) in **Chapter 21**. In addition to the extent and location of valvular calcifications, standardized measurements of the aortic root were performed. Reconstructed MSCT images were used to assess the aortic annulus diameter in two directions. The orientation of the reconstructions was similar to the image orientation that is used during the actual percutaneous valve implantation. Furthermore,

the distance between the aortic annulus and the ostia of the coronary arteries was measured. These parameters may have great impact on prosthesis sizing and on the feasibility of the procedure. Interestingly, an oval shape of the aortic annulus was noted, with a mean diameter of 26.3 ± 2.8 mm on the coronal view, and 23.5 ± 2.7 mm on the sagittal view. Large variation in the distance between the aortic annulus and the left coronary ostium (mean 14.4 ± 2.9 mm, range 7.1 to 22.7 mm) and the right coronary ostium (mean 17.2 ± 3.3 mm, range 9.2 to 26.3 mm) was noted. Importantly, the length of the coronary leaflet exceeded this distance in up to 49% of the patients. This may increase the risk of coronary occlusion during percutaneous valve procedures. Thus, MSCT may provide important information for the selection of patients for percutaneous aortic valve replacement.

These findings were confirmed in a group of 26 patients with severe AS referred for percutaneous aortic valve replacement (**Chapter 22**). Before the percutaneous valve implantation and after 4 months follow-up, MSCT images were analyzed using the same measurements as in the previous study. Measurements of aortic annulus diameters with MSCT, echocardiography and fluoroscopy were compared. In addition, the stent diameter and the distance between the left coronary artery and the stent wall were assessed. Mean distance between the aortic annulus and the left coronary ostium was 15.0 ± 3.0 mm. Comparable results for aortic annulus diameters were noted with different imaging modalities: mean difference between MSCT and transthoracic echocardiography was -0.3 mm (95% confidence interval -1.1 to 0.6 mm). After percutaneous aortic valve replacement, the prosthesis extended above the coronary ostia in 50% of the patients. In addition, in 78% of the patients a circular deployment of the prosthesis was noted. Importantly, no association was found between the aortic annulus shape and the proportion of patients who developed perivalvular aortic regurgitation. This study clearly demonstrates the value of MSCT in the pre-procedural assessment and follow-up of patients with severe AS referred for percutaneous aortic valve replacement.

CONCLUSIONS AND FUTURE PERSPECTIVES

The studies described in the present thesis explore the role of multimodality imaging in cardiac interventional procedures. In recent years, exciting advances have been made in the invasive treatment of AF, cardiac pacing and the percutaneous treatment of valvular heart disease. The selection of patients for these procedures, the procedures themselves and the follow-up of patients may be greatly facilitated by the use of imaging modalities. Importantly, the integration of different imaging techniques may enhance visualization of critical anatomic structures during the interventional procedures.

Catheter ablation for atrial fibrillation

Careful identification of LA and PV anatomy is of critical importance for successful catheter ablation of AF. Importantly, the anatomy of the PVs and LA has impact on the outcome of the catheter ablation procedure. Different imaging modalities are available for assessment of LA and PV anatomy. Unfortunately, each imaging modality also has its drawbacks. Image integration may overcome the limitations of each separate imaging modality by combining the different techniques. The studies in the present thesis demonstrate that the integration of different imaging modalities is feasible, and provides additional information during the catheter ablation procedure. Future studies are needed to further explore image integration in the electrophysiology laboratory. Large randomized trials are needed to assess the impact of image integration on the outcome of AF ablation procedures. In addition, in the near future new imaging techniques such as rotational angiography (providing real-time 3D fluoroscopic images comparable to MSCT) and real-time magnetic resonance imaging (in a hybrid suite) may have great impact on AF ablation procedures.

Furthermore, the present studies demonstrate that successful catheter ablation of AF results in reverse remodeling of the LA and improvement of LA and LV function. Unfortunately, the exact pathophysiologic mechanism remains to be determined. Furthermore, it remains unclear whether the maintenance of sinus rhythm results in reverse remodeling, or vice versa ('chicken or egg'). Additional studies are therefore needed to find predictors of reverse remodeling, and pre-clinical studies may contribute to a better understanding of this phenomenon. It may well be that the amount of fibrosis in the LA plays an important role in the outcome of catheter ablation procedures. Pre-procedural evaluation of LA scar with dedicated imaging techniques may then be of great value. Finally, assessment of LA scar and ablation lesions using magnetic resonance imaging after the procedure may provide important information on the effect of catheter ablation procedures on LA and LV function.

Ventricular pacing and dyssynchrony

The detrimental effects of long-term RV apical pacing as demonstrated in large pacing mode trials and smaller observational studies may be related to the induction of LV dyssynchrony. The present studies demonstrate that about half of the patients with long-term RV apical pacing develop significant LV dyssynchrony and exhibit deterioration of LV function. The presence of LV dyssynchrony during RV pacing is also associated with worsening of cardiac oxidative metabolism and efficiency. By restoration of synchronous contraction, CRT may (partly) reverse the detrimental effects of long-term permanent RV apical pacing. Importantly, LV dyssynchrony may be present immediately after onset of RV apical pacing. Finally, from the present studies it has become apparent that significant ventricular dyssynchrony is also present in up to 50% of patients with ARVD. More studies are needed to clarify the underlying mechanism, and the clinical implications of these findings.

With regard to RV pacing and ventricular dyssynchrony, a number of important questions remain unanswered, and need to be addressed in future studies. For example, why do some patients develop significant LV dyssynchrony with RV pacing, while others do not? Both patient- and pacemaker-related parameters that may predict the development of mechanical dyssynchrony and deterioration of cardiac function need to be identified. Is acutely induced LV dyssynchrony associated with deterioration of LV function during follow-up? Should future studies confirm that there is a relation between acutely induced LV dyssynchrony and worsening of LV function and functional class at long-term follow-up, assessment of LV dyssynchrony at pacemaker implantation may have important implications. Biventricular pacing may then be considered in patients with significant LV dyssynchrony immediately after onset of pacing. Furthermore, screening for LV dyssynchrony on a regular basis in patients with conventional RV pacing may identify patients that may benefit from upgrade to CRT.

Percutaneous valve procedures

In recent years, a number of exciting procedures and prostheses have been introduced for the percutaneous treatment of severe valvular heart disease. The present studies demonstrate that cardiac imaging provides critical information for percutaneous valve procedures. In particular, MSCT plays an important role in the selection of patients referred for these procedures. This 3D imaging technique clearly visualizes the relation between the coronary arteries, coronary veins and affected valves. Both for percutaneous mitral valve procedures using coronary sinus annuloplasty and transcatheter aortic valve replacement, this relation is of utmost importance. Furthermore, MSCT allows visualization of the prosthesis, and the relation with surrounding structures, after implantation.

Future studies will need to address a number of important issues. The long-term durability of the prostheses and favorable long-term clinical outcome needs to be demonstrated. At the same time, more studies comparing percutaneous and surgical treatment of valvular heart disease are warranted. The results of the PARTNER trial (The Placement of AoRTic TraNscathetER Valve Trial) comparing percutaneous and surgical aortic valve replacement in 350 patients are eagerly awaited. This trial may add important evidence on the role of percutaneous valve procedures in the treatment of patients with severe AS. Should future studies demonstrate equal or superior efficacy and long-term durability, it may well be that the indication for percutaneous valve procedures is expanded. This is of particular interest when considering the percutaneous 'valve-in-valve' concept in patients with degenerated aortic bioprostheses. Finally, more studies are needed to examine the ability of different imaging modalities to improve the safety of percutaneous valve procedures. In particular, the feasibility of image integration during percutaneous valve procedures needs to be studied.

Samenvatting, conclusies en toekomstperspectieven

SAMENVATTING

Dit proefschrift behandelt twee belangrijke deelgebieden van de klinische cardiologie: Cardiale beeldvorming ('multimodality imaging') en cardiale interventies ('interventional procedures'). In de afgelopen jaren heeft een aantal belangrijke ontwikkelingen plaatsvonden op het gebied van cardiale beeldvorming en cardiale interventie procedures. Een aantal nieuwe beeldvormende technieken zoals multi-slice computer tomografie (MSCT) scan is geïntroduceerd. Daarnaast zijn andere beeldvormende technieken (zoals echocardiografie) verfijnd zodat nu een meer gedetailleerde analyse van cardiale anatomie en functie mogelijk is. Verder is er grote vooruitgang geboekt op het gebied van integratie van verschillende beeldvormende technieken.

Tegelijkertijd is een aantal nieuwe interventie procedures beschikbaar gekomen voor de behandeling van hartritmestoornissen en hartkleplijden. Catheter ablatie procedures worden tegenwoordig beschouwd als een goede behandeloptie voor patiënten met therapieresistent atriumfibrilleren (AF). Bij deze procedures wordt via de liesader en de grote aders een catheter in het linker atrium (LA) van het hart gebracht. Hiermee worden vervolgens de pulmonaalvenen (PV) elektrisch geïsoleerd met behulp van radiofrequente energie (Figuur 2 in Hoofdstuk 1). Zodoende wordt de hartritmestoornis verholpen. Op het gebied van pacemakers is de laatste jaren duidelijk geworden dat conventioneel rechter ventrikel (RV) stimulatie (of 'pacen') negatieve effecten heeft op de functie van het linker ventrikel (LV) van het hart. Een deel van de patiënten die een pacemaker krijgt, bijvoorbeeld vanwege een traag hartritme, ontwikkelt op de lange termijn hartfalen. Dit hangt mogelijk samen met het abnormale activatie patroon van de ventrikels tijdens het pacen. Het abnormale activatie patroon resulteert in een niet-synchroon samentrekken van de verschillende delen van de ventrikels van het hart (ofwel: 'dyssynchronie', Figuur 6 in Hoofdstuk 1). Cardiale resynchronisatie therapie (CRT) is een speciale vorm van pacen die zorgt voor het herstel van het synchroon samentrekken van de ventrikels. Wellicht dat CRT ook een goede optie is voor patiënten met een gewone pacemaker en dyssynchronie. Ten slotte zijn er nieuwe procedures en protheses geïntroduceerd voor de behandeling van patiënten met ernstig hartkleplijden die niet in aanmerking komen voor een open-hart operatie. Bij deze procedures wordt via de lies en de grote (slag)aders een catheter in het hart gebracht, waarmee een nieuwe hartklep of een andere prothese wordt geplaatst (Figuur 8 in Hoofdstuk 1).

In dit proefschrift wordt de rol van verschillende beeldvormende technieken bij cardiale interventie procedures bestudeerd. In **Deel I** werd gekeken naar catheter ablatie procedures voor AF. Het doel van het onderzoek was te kijken of het mogelijk is om deze procedures te verbeteren door verschillende beeldvormende technieken te integreren. Daarnaast werd het effect van deze procedures op de functie van het LA en LV bestudeerd. Het doel van de studies in **Deel II** was om de effecten van RV pacen op LV dyssynchronie en LV functie te bekijken. Daarnaast werd het effect van CRT bij patiënten met dyssynchronie na lange termijn RV pacen

onderzocht. **Deel III** behandelt de rol van beeldvormende technieken bij nieuwe percutane procedures voor ernstige hartklepafwijkingen.

Deel I: Catheter ablatie voor atriumfibrilleren

Het eerste deel van dit proefschrift gaat over catheter ablatie procedures voor AF. Steeds meer patiënten met therapieresistent AF ondergaan dergelijke procedures. Het is belangrijk om voorafgaand en tijdens de procedure het LA en de PV goed in beeld te brengen. **Hoofdstuk 2** geeft een uitgebreide beschrijving van de verschillende beeldvormende technieken die hiervoor gebruikt kunnen worden. In de dagelijkse praktijk is transthoracale echocardiografie de meest gebruikte techniek om het LA in beeld te brengen. Driedimensionale technieken zoals MSCT en magnetic resonance imaging (MRI) worden vaak gebruikt om voorafgaand aan een catheter ablatie procedure de PV te visualiseren. Tijdens de ablatie procedure kan intracardiale echocardiografie gebruikt worden. Ten slotte wordt de integratie van de verschillende technieken in dit hoofdstuk besproken.

Hoofdstuk 3 is een klinisch georiënteerd overzichtsartikel waarin de rol van beeldvormende technieken bij de evaluatie van patiënten met AF, en de rol van deze technieken bij catheter ablatie procedures wordt behandeld. Wanneer een patiënt met AF voor de eerste maal wordt beoordeeld, moet een aantal geassocieerde ziektebeelden (zoals kransslaglijden, hartkleplijden en hartfalen) zorgvuldig worden bestudeerd. De diverse beeldvormende technieken die hiervoor beschikbaar zijn, worden in dit hoofdstuk beschreven. Verder wordt een overzicht gegeven van de aandachtspunten die belangrijk zijn voorafgaand en tijdens catheter ablatie procedures en wordt beschreven hoe de verschillende beeldvormende technieken hiervoor gebruikt kunnen worden.

Tijdens catheter ablatie procedures wordt veelvuldig gebruik gemaakt van 'elektroanatomische maps'. Dit zijn reconstructies van het LA die zowel informatie over anatomie als over elektrische geleiding bevatten. Deze maps worden gemaakt met behulp van de ablatie catheters. In **Hoofdstuk 4** werd de integratie van MSCT en deze elektroanatomische maps bestudeerd bij 16 patiënten die een catheter ablatie procedure voor AF ondergingen. Hiervoor werd gebruik gemaakt van een nieuwe 'image integration module' (CartoMerge™), uitgerust met speciale algoritmes. Na de integratie van de MSCT beelden en de elektroanatomische maps was de gemiddelde afstand tussen deze twee beelden 2.1 ± 0.2 mm (range 1.7 – 2.8). Het geïntegreerde beeld werd vervolgens gebruikt om de catheter ablatie procedure te sturen (Figuur 3 in Hoofdstuk 4). Deze studie laat zien dat het mogelijk is om MSCT beelden en elektroanatomische maps te integreren en vervolgens te gebruiken voor catheter ablatie procedures.

Deze bevindingen worden verder uitgewerkt in **Hoofdstuk 5**. In deze studie werd de integratie van intracardiale echocardiografie, elektroanatomische maps en MSCT beelden bestudeerd.

Hiervoor werd gebruik gemaakt van een nieuwe intracardiale echocardiografie 'camera' (probe) die uitgerust is met een speciale sensor van het Carto™ elektroanatomische mapping systeem. Hiermee kunnen vanuit het rechter atrium elektroanatomische maps van het LA worden gemaakt door contouren te trekken op de echocardiografische beelden (Figuur 1 in Hoofdstuk 5). Zeventien patiënten (13 mannen, gemiddelde leeftijd 56 ± 8 jaar) werden bestudeerd. Gemiddeld waren 31.1 ± 8.5 contouren nodig om een driedimensionale reconstructie van het LA en de PV te maken. De gemiddelde afstand tussen de contouren en de MSCT beelden (als maat voor de nauwkeurigheid van de integratie) was 2.2 ± 0.3 mm. Verder werd een goede overeenkomst gevonden tussen intracardiale echocardiografie en MSCT voor het vaststellen van de anatomie en diameters van de PV.

Het in beeld brengen van de anatomie van de PV met behulp van MSCT, en het effect van PV anatomie op de uitkomst van catheter ablatie procedures waren de doelen van **Hoofdstuk 6**. Bij 100 patiënten met AF die een catheter ablatie procedure ondergingen werd een MSCT scan gemaakt. Gebaseerd op de aan- of afwezigheid van additionele PV of 'common ostia' (één enkele PV uitmonding aan een zijde van het LA, zie ook Figuur 3 in Hoofdstuk 6), werd de anatomie van de PV gedeut als 'normaal' of 'complex'. Verder werd de diameter van het LA in drie verschillende richtingen gemeten. Complexe PV anatomie aan de linker zijde was aanwezig bij 26% van de patiënten, en aan de rechter zijde bij 22%. De gemiddelde voorachterwaartse diameter van het LA was 41 ± 7 mm. Complexe PV anatomie aan de rechter zijde was geassocieerd met een verbeterde uitkomst van de catheter ablatie procedure (OR = 0.149 [0.038-0.576], $p=0.006$), terwijl LA dilatatie was geassocieerd met een slechtere uitkomst (OR = 1.083 [1.009-1.162], $p=0.027$). Deze studie benadrukt de relevantie van het beoordelen van LA en PV anatomie voorafgaand aan catheter ablatie procedures.

In de volgende studies werd gekeken naar het effect van catheter ablatie procedures op de grootte en functie van het LA en LV. Onze hypothese was dat een geslaagde ablatie procedure een gunstig effect heeft op zowel de grootte als de functie van het LA en LV. De studie in **Hoofdstuk 7** bevatte 57 patiënten die werden behandeld met catheter ablatie voor AF. Voorafgaand aan, en drie maanden na de ablatie procedure werden de volumes van het LA berekend met tweedimensionale echocardiografie. Bij patiënten die normaal sinusritme behielden (geslaagde procedure, $n=39$) werd het LA significant kleiner, terwijl bij patiënten die opnieuw AF kregen (niet geslaagde procedure, $n=18$) het LA groter werd. Daarnaast werd zowel het LA einddiastolisch volume kleiner (van 37 ± 9 ml naar 31 ± 7 ml, $p<0.01$), als het LA eindsystolisch volume (van 59 ± 12 ml naar 50 ± 11 ml, $p<0.01$) bij patiënten die sinusritme behielden. Deze bevindingen worden bevestigd in **Hoofdstuk 8**. In deze studie werd gebruik gemaakt van driedimensionale echocardiografie (Figuur 1 in Hoofdstuk 8). Deze nieuwe techniek is mogelijk nauwkeuriger voor het bepalen van LA grootte en volumes en beter reproduceerbaar dan tweedimensionale echocardiografie. In deze studie werd naast de grootte en volumes ook

gekeken naar de functie van het LA. De functie van het LA kan ingedeeld worden in drie fases: de expansie functie, de reservoir functie en de actieve contractie functie. Bij patiënten die sinusritme behielden na de catheter ablatie procedure werden significante verbeteringen in de actieve functie van het LA (van $22 \pm 8\%$ naar $33 \pm 9\%$, $p < 0.01$) en de reservoir functie van het LA (van $116 \pm 45\%$ naar $152 \pm 54\%$, $p < 0.01$) gevonden. Deze verbeteringen werden echter niet gezien bij patiënten die opnieuw AF kregen gedurende follow-up.

De voorafgaande studies laten zien dat er sprake is van 'LA reverse remodeling' na een succesvolle ablatie procedure voor AF, waarbij er sprake is van een afname van de LA grootte en een verbetering van LA functie. In **Hoofdstuk 9** werd gezocht naar de klinische en echocardiografische determinanten van LA reverse remodeling. Reverse remodeling werd gedefinieerd als een afname van $\geq 15\%$ in het maximale LA volume. Tissue Doppler echocardiografie werd gebruikt om LA systolische strain (als een maat voor LA expansie functie) en LA diastolische strain (als een maat voor LA actieve contractie functie) te berekenen (Figuur 1 in Hoofdstuk 9). Aan de hand van de aan- of afwezigheid van reverse remodeling tijdens follow-up werd de studie populatie verdeeld in 'responders' ($n=93$) of 'non-responders' ($n=55$). De responders lieten een significante toename van LA systolische strain gezien (van $19 \pm 8\%$ naar $22 \pm 9\%$, $p < 0.05$), terwijl er geen significante verandering was bij de non-responders (van $14 \pm 6\%$ naar $15 \pm 8\%$, $p = \text{NS}$). De belangrijkste voorspeller van LA reverse remodeling was LA systolische strain op baseline (OR 1.089; 95% CI 1.014-1.169, $p = 0.019$). Deze studie laat een sterke relatie zien tussen LA reverse remodeling en LA strain.

In **Hoofdstuk 10** wordt het effect van catheter ablatie procedures op de LV functie onderzocht. Hiervoor werd gebruik gemaakt van 'speckle-tracking' echocardiografie, dat akoestische markers die aanwezig zijn op standaard echocardiografische beelden analyseert. Hiermee werd LV strain in drie richtingen (radiaal, circumferentieel en longitudinaal, zie ook Figuur 1 in Hoofdstuk 10) berekend op baseline en gedurende follow-up bij 78 patiënten (gemiddelde LV ejectie fractie $60 \pm 7\%$). Na 13.8 ± 4.7 maanden hadden 54 patiënten sinusritme behouden, terwijl 25 patiënten opnieuw AF kregen. Bij de patiënten met behoud van sinusritme was er sprake van een significante toename in LV strain in de circumferentiële richting (van $-18.3 \pm 3.2\%$ naar $-20.4 \pm 3.8\%$, $p < 0.001$) en LV strain in de longitudinale richting (van $-18.8 \pm 2.7\%$ naar $-19.6 \pm 2.6\%$, $p < 0.001$). Deze verbeteringen werden niet gezien bij patiënten die opnieuw AF kregen gedurende follow-up. Deze studie laat zien dat LV functie alleen verbetert na een succesvolle catheter ablatie procedure voor AF.

Deel II: Ventriculair pacen en dyssynchronie

In het tweede deel van het proefschrift staan pacemakers en mechanische dyssynchronie centraal. In **Hoofdstuk 11** wordt een overzicht gegeven van de effecten van RV pacen op LV functie en LV dyssynchronie. Grote gerandomiseerde studies die de optimale pacemaker

modus onderzochten, lieten een associatie zien tussen langdurig RV pacen en verslechtering van LV functie en hartfalen. De negatieve effecten op lange termijn zijn mogelijk gerelateerd aan het induceren van LV dyssynchronie door RV pacen, als gevolg van het abnormale activatie patroon. Meerdere studies hebben laten zien dat de upgrade van RV pacen naar CRT een gunstig effect heeft op LV functie. Wellicht dat CRT ook van betekenis kan zijn voor patiënten die een normale pacemaker nodig hebben, maar waarvan verwacht wordt dat ze langdurig pacen nodig hebben.

De effecten van RV pacen op LV functie, LV dyssynchronie en symptomen van hartfalen staan centraal in **Hoofdstuk 12**. Bij 55 patiënten werd een pacemaker geïmplantieerd na ablatie van de atrioventriculaire knoop (elektrische verbinding tussen de atria en de ventrikels). Voorafgaand aan de pacemaker implantatie, en na gemiddeld 3.8 ± 1.7 jaar werd een echocardiogram verricht. Linker ventrikel dyssynchronie werd onderzocht met tweedimensionale echocardiografie. Een verschil van ≥ 130 ms tussen de systolische beweging van het septum en de achterwand van het LV werd gebruikt voor de definitie van LV dyssynchronie. Voorafgaand aan de pacemaker implantatie had geen van de patiënten LV dyssynchronie. Echter na langdurig RV pacen was er sprake van significante LV dyssynchronie bij 27 patiënten (49%). Bij die patiënten was er sprake van een significante verslechtering van de LV ejectie fractie (van $48 \pm 7\%$ naar $43 \pm 7\%$, $p < 0.05$), terwijl deze gelijk bleef bij patiënten zonder LV dyssynchronie (van $49 \pm 6\%$ naar $49 \pm 8\%$, $p = \text{NS}$). Daarnaast was er een verslechtering in hartfalen symptomen bij patiënten met LV dyssynchronie (NYHA klasse van 1.8 ± 0.6 naar 2.2 ± 0.7 , $p < 0.05$), terwijl de symptomen verbeterden bij patiënten zonder LV dyssynchronie (NYHA klasse van 1.7 ± 0.7 naar 1.4 ± 0.5 , $p < 0.01$). Deze studie laat zien dat patiënten significante LV dyssynchronie kunnen ontwikkelen na langdurig RV pacen. Het ontwikkelen van LV dyssynchronie is geassocieerd met verslechtering van de LV functie en hartfalen symptomen.

Na deze bevindingen werd een studie opgezet om te onderzoeken of LV dyssynchronie direct na het starten van RV pacen optreedt (**Hoofdstuk 13**). Hiervoor werden 25 patiënten die een elektrofysiologisch onderzoek ondergingen vanwege hartritme stoornissen, en 25 controle patiënten bestudeerd. Op baseline en na ten minste 5 minuten RV pacen werden LV functie en dyssynchronie gekwantificeerd. Speckle-tracking echocardiografie werd gebruikt om LV strain in longitudinale richting, LV dyssynchronie en LV twist (berekend met behulp van de rotatie van de LV tijdens systole) te berekenen. Op baseline waren er geen verschillen tussen de 25 studie patiënten en de 25 controle patiënten wat LV functie en LV dyssynchronie (mediaan 21 ms vs. 20 ms, $p = \text{NS}$) betreft. Echter, na het starten van RV pacen verslechterde de LV ejectie fractie bij de 25 studie patiënten (van $56 \pm 8\%$ naar $48 \pm 9\%$, $p = 0.001$). Tegelijkertijd was er sprake van een toename van LV dyssynchronie (van 21 ms [10, 53] naar 91 ms [40, 204], $p < 0.001$). Bij 36% van de patiënten was er sprake van significante LV dyssynchronie (≥ 130 ms). Daarnaast werd

er een verslechtering van LV strain en LV twist geconstateerd na het starten van RV pacen. Dus, de negatieve effecten van RV pacen ontstaan (gedeeltelijk) direct na aanvang van RV pacen.

Bij patiënten met significante LV dyssynchronie direct na aanvang of na langdurig RV pacen, kan een synchroon contractie patroon van de LV hersteld worden met behulp van biventriculair pacen (CRT). Voor een optimaal resultaat van CRT moet dat deel van de LV dat het laatste wordt geactiveerd (langste 'time-to-peak' strain), en waar dus maximale LV dyssynchronie is, worden bepaald. Hiervoor werd in **Hoofdstuk 14** speckle-tracking echocardiografie gebruikt bij 58 patiënten met een pacemaker. Daarnaast werd het effect van de upgrade van RV pacen naar CRT bestudeerd bij een deel van deze patiënten. Voor aanvang van RV pacen waren er vergelijkbare waarden voor time-to-peak strain in 6 mid-ventriculaire LV segmenten (gemiddeld 371 ± 114 ms). Echter na langdurig RV pacen was er sprake van heterogeniteit in time-to-peak strain van de 6 segmenten. De laterale en de achterwand segmenten waren meestal de delen van de LV met de laatste activatie (Figuur 1 in Hoofdstuk 14). Dit resulteerde in significante LV dyssynchronie bij 57% van de patiënten. Bij 11 patiënten werd een upgrade van RV pacen naar CRT verricht. Bij deze patiënten verdween de LV dyssynchronie, en de LV ejectie fractie verbeterde van $30 \pm 8\%$ naar $39 \pm 7\%$ ($p < 0.001$). De negatieve effecten van RV pacen kunnen dus (gedeeltelijk) worden verbeterd met CRT.

Hoofdstuk 15 gaat in op het effect van RV pacen op het oxidatieve metabolisme van het myocard. Tien patiënten met een pacemaker (gemiddelde leeftijd 62 ± 17 jaar) ondergingen echocardiografie en een 'positron emission tomography' scan tijdens pacing-OFF (normaal sinusritme of atriaal pacen) en pacing-ON (RV pacen). Linker ventrikel dyssynchronie werd bestudeerd met tissue Doppler en speckle-tracking echocardiografie. Verschillende parameters werden onderzocht middels de positron emission tomography scan, zoals de bloedstroom van het myocard, het oxidatieve metabolisme en de efficiëntie van het myocard. Tijdens RV pacen vond er geen verandering plaats in globale bloedstroom van het myocard en het oxidatieve metabolisme in de studie populatie als geheel. Echter, bij patiënten met significante LV dyssynchronie tijdens RV pacing-ON ($n=6$) werd een verslechtering in efficiëntie van het myocard gezien (van 78.11 ± 25.35 mmHg-l/g naar 60.40 ± 13.93 mmHg-l/g, $p < 0.05$), terwijl bij patiënten zonder LV dyssynchrony ($n=4$) geen verandering werd gezien (van 73.55 ± 24.78 mmHg-l/g naar 75.32 ± 31.33 mmHg-l/g, $p=NS$). Er is dus een associatie tussen LV dyssynchronie tijdens RV pacen, en een verslechtering van het oxidatieve metabolisme en de efficiëntie van het LV. De bovenstaande studies laten het belang van het bestuderen van LV dyssynchronie bij patiënten met een pacemaker zien. De aanwezigheid van LV dyssynchronie tijdens RV pacen is geassocieerd met een verslechtering van LV functie, het oxidatieve metabolisme en de functionele status van de patiënt.

Ten slotte werd in **Hoofdstuk 16** de prevalentie van dyssynchronie bij patiënten met aritmogene rechterventrikeldysplasie (ARVD) bestudeerd. ARVD is een erfelijke cardiomyopathie, en wordt gekenmerkt door vervanging van normaal myocardweefsel door vetweefsel (voornamelijk in het RV). Dit resulteert in ritme- en geleidingsstoornissen en mogelijk mechanische dyssynchronie. De prevalentie van dyssynchronie is echter nooit onderzocht bij deze patiënten populatie. Bij 52 ARVD patiënten (gemiddelde leeftijd 41 ± 12 jaar, 22 mannen) en 25 gezonde controles (vrijwilligers) werd de mate van mechanische dyssynchronie bestudeerd met behulp van tissue Doppler echocardiografie. De time-to-peak systolische snelheid (T_{SV}) van de RV vrije wand, het interventriculaire septum en de LV laterale wand werden gemeten, en zo werd ventriculaire dyssynchronie berekend (Figuur 1 in Hoofdstuk 16). Significante RV dyssynchronie werd gedefinieerd als het verschil tussen T_{SV} van de RV vrije wand en het interventriculaire septum, >2 standaard deviaties boven het gemiddelde van de controle groep. Het gemiddelde verschil tussen T_{SV} van het septum en de RV vrije wand was 26 ± 15 ms in de controle groep (resulterend in een cut-off waarde van ≥ 56 ms voor significante RV dyssynchronie), en 55 ± 34 ms bij de ARVD patiënten ($p < 0.001$). Bij 26 ARVD patiënten (50%) was er sprake van significante RV dyssynchronie. Er werden geen verschillen gevonden in QRS duur, mate van T golf inversie of rechter bundeltakblok tussen ARVD patiënten met en zonder RV dyssynchronie. Echter, RV 'fractional area change' (als maat voor RV functie) was significant lager ($29 \pm 8\%$ vs. $34 \pm 8\%$, $p < 0.05$) en RV systolische strain was significant lager ($-16 \pm 6\%$ vs. $-22 \pm 7\%$, $p < 0.01$) bij ARVD patiënten met RV dyssynchronie, vergeleken met ARVD patiënten zonder RV dyssynchronie. Samenvattend werd in deze studie aangetoond dat tot wel 50% van de ARVD patiënten significante RV dyssynchronie kan hebben. De aanwezigheid van RV dyssynchronie is geassocieerd met verslechtering van RV functie.

DEEL III: Percutane hartklep procedures

Het derde deel van dit proefschrift gaat over percutane procedures voor hartklepafwijkingen. In de afgelopen jaren zijn er nieuwe (percutane) procedures ontwikkeld om met behulp van catheters via de lies ernstige mitralisklepinsufficiëntie (MI) en aortaklepstenose (AS) te behandelen bij patiënten die geen open-hart operatie kunnen ondergaan. Verschillende beeldvormende technieken spelen een grote rol bij dergelijke procedures, voornamelijk in de selectie van patiënten. De verschillende percutane hartklep procedures en de rol van de diverse beeldvormende technieken wordt uitgebreid besproken in **Hoofdstuk 17**.

In **Hoofdstuk 18** werden MSCT scans gemaakt bij 105 patiënten om de anatomie van de sinus coronarius (een ader van het hart) te evalueren. De relatie tussen de sinus coronarius, de annulus (klepring) van de mitralisklep, en de kransslagvaten is van belang voor percutane mitralisklep procedures. Deze maken namelijk gebruik van protheses die in de sinus coronarius worden geplaatst om MI te behandelen. Een ongunstige relatie tussen de voornoemde structuren kan resulteren in een niet efficiënte procedure en zelfs afsluiting van de kransslagvaten. In deze

studie werd een grote variatie in de relatie tussen de sinus coronarius en de annulus van de mitralisklep geconstateerd (Figuur 3 in Hoofdstuk 18). In het merendeel van de patiënten was de sinus coronarius gelokaliseerd langs het LA, in plaats van langs de annulus van de mitralisklep. Bij 68% van de patiënten liep de circumflex coronair arterie tussen de sinus coronarius en de annulus; dit vergroot de kans op afsluiting van dit kransslagvat tijdens percutane behandeling van MI. Daarnaast werd gezien dat de minimale afstand tussen de sinus coronarius en de annulus van de mitralisklep significant groter was bij patiënten met ernstige MI, in vergelijking met patiënten zonder ernstige MI (gemiddelde afstand 7.3 ± 3.9 mm vs. 4.8 ± 2.5 mm, $p < 0.05$). Patiënten met een grote afstand tussen deze twee structuren hebben mogelijk geen baat bij de percutane behandeling van MI. Dus, MSCT kan belangrijke informatie geven bij de selectie van patiënten voor deze procedures.

De evaluatie van de mitralisklep met behulp van MSCT werd verder uitgediept in **Hoofdstuk 19**. Het subvalvulaire apparaat en de geometrie van de mitralisklep (mitralisklep 'tenting height' en 'leaflet tethering', Figuur 3 in Hoofdstuk 19) werden bestudeerd bij 151 patiënten, inclusief 29 patiënten met matig tot ernstige MI. Er werd geconstateerd dat patiënten met MI een asymmetrische geometrie van de mitralisklep hebben. Bij deze patiënten werd een vergrote hoek van het achterste mitralisklepblad gevonden op het centrale ($44.4 \pm 11.9^\circ$) en het posteromediale ($35.9 \pm 10.6^\circ$) niveau. Daarnaast was de mitralisklep 'tenting height' significant vergroot in deze patiënten, in vergelijking met patiënten zonder MI (centrale niveau: 6.6 ± 1.4 mm/m² vs. 5.3 ± 1.3 mm/m², $p < 0.001$; posteromediale niveau: 5.4 ± 1.6 mm/m² vs. 4.1 ± 1.2 mm/m², $p < 0.001$). Deze studie laat zien dat MSCT belangrijke informatie kan geven over de anatomie en geometrie van de mitralisklep, en dat er sprake is van asymmetrische geometrie bij patiënten met matig tot ernstige MI.

De rest van de studies betrof percutane procedures voor ernstige AS. In **Hoofdstuk 20** wordt een uitgebreid overzicht gegeven van de tot nu toe verrichte studies naar percutane behandeling van AS. Het merendeel van deze studies laten een hoog slagingspercentage van de procedure zien, een lage mortaliteit na 30 dagen, en een goede functie van de prothese gedurende follow-up. Daarnaast worden in dit hoofdstuk de recente aanbevelingen voor de percutane behandeling van AS besproken. Op dit moment worden deze procedures alleen aanbevolen voor patiënten met ernstige, symptomatische AS die in een te slechte conditie zijn voor een open-hart operatie. Verder wordt stilgestaan bij de verschillende beeldvormende technieken die gebruikt worden voor de selectie van patiënten, het begeleiden van de procedure, en de follow-up van patiënten.

MSCT is één van de technieken die belangrijke informatie voor de selectie van patiënten verschaft. Deze techniek werd dan ook gebruikt om de anatomie van de aortaklep te bestuderen bij 169 patiënten (inclusief 19 patiënten met matig ernstige AS) in **Hoofdstuk 21**. De hoeveelheid

en exacte locatie van aortaklep calcificaties werden beoordeeld, naast gestandaardiseerde metingen van de aortawortel (Figuur 1 t/m 5 in Hoofdstuk 21). De oriëntatie van de gereconstrueerde MSCT beelden is gelijk aan de oriëntatie van de echocardiografie en doorlichting beelden die normaliter tijdens percutane aortaklep procedures worden gebruikt. De diameter van de annulus van de aortaklep werd in twee richtingen gemeten. Daarnaast werd de afstand tussen de annulus en de kransslagvaten gemeten. Deze metingen zijn belangrijk voor het beoordelen van de diameter van de te plaatsen prothese, en het beoordelen van het risico op afsluiting van de kransslagvaten tijdens de implantatie procedure. In deze studie werd een ovale vorm van de annulus van de aortaklep gevonden; de gemiddelde diameter van de annulus was 26.3 ± 2.8 mm op de coronale beelden, en 23.5 ± 2.7 mm op de sagittale beelden. Daarnaast werd een grote variatie in de afstand tussen de annulus en het linker kransslagvat (gemiddeld 14.4 ± 2.9 mm, van 7.1 tot 22.7 mm) en tussen de annulus en het rechter kransslagvat (gemiddeld 17.2 ± 3.3 mm, van 9.2 tot 26.3 mm) gevonden. Belangrijk hierbij is dat de lengte van het aortaklepblad groter was dan deze afstand in 49% van de patiënten. Dit vergroot de kans op afsluiting van het kransslagvat tijdens de percutane aortaklep implantatie. Dus, MSCT verschaft belangrijke informatie voor de selectie van patiënten voor deze procedures.

Deze bevindingen werden bevestigd bij 26 patiënten met ernstige AS die werden verwezen voor percutane aortaklep implantatie (**Hoofdstuk 22**). Voorafgaand aan de procedure en na 4 maanden follow-up werd een MSCT scan gemaakt, en geanalyseerd zoals eerder beschreven. De metingen op de MSCT beelden werden vergeleken met echocardiografie en doorlichting. Op de follow-up scans werd de stent diameter en de afstand tussen de stent en het linker kransslagvat bepaald. De gemiddelde afstand tussen de annulus van de aortaklep en het linker kransslagvat was 15.0 ± 3.0 mm. Een goede overeenkomst werd gevonden tussen MSCT, echocardiografie en doorlichting voor de bepaling van de annulus van de aortaklep. Na de percutane implantatie van de aortaklep was bij 50% van de patiënten de prothese gelegen boven het linker kransslagvat. Bij 78% van de patiënten was er sprake van een goede circulaire ontplooiing van de prothese. Deze studie laat de waarde zien van MSCT voor de selectie en de follow-up van patiënten die worden verwezen voor percutane aortaklep implantatie.

CONCLUSIES EN TOEKOMSTPERSPECTIEVEN

De studies in dit proefschrift bestuderen de rol van beeldvormende technieken bij cardiale interventie procedures. In de afgelopen jaren zijn er belangrijke stappen gezet in de invasieve behandeling van AF, pacemakers en de percutane behandeling van ernstig hartkleplijden. De selectie van patiënten voor deze procedures, de procedures zelf en de follow-up van patiënten kunnen geoptimaliseerd worden met behulp van diverse beeldvormende technieken.

Daarnaast kan de integratie van diverse technieken het in beeld brengen van de belangrijkste anatomische structuren tijdens de procedures aanzienlijk vergemakkelijken.

Catheter ablatie voor atriumfibrilleren

Het nauwkeurig in beeld brengen van het LA en de PV is van groot belang voor het slagen van catheter ablatie procedures voor AF. Daarnaast is uit één van de huidige studies gebleken dat PV anatomie ook een prognostische waarde heeft. Verschillende beeldvormende technieken zijn beschikbaar voor het visualiseren van het LA en de PV. Echter, elke techniek heeft ook beperkingen. Integratie van verschillende technieken overwint de beperkingen van de individuele technieken door ze te combineren. De studies in dit proefschrift laten zien dat het mogelijk is om verschillende beeldvormende technieken te integreren, en dat dit meerwaarde heeft voor catheter ablatie procedures voor AF. Meer studies zijn nu nodig om verdere integratie van verschillende technieken tijdens elektrofysiologische procedures te exploreren. Daarnaast zijn grote gerandomiseerde studies nodig om te onderzoeken of het integreren van de verschillende technieken ook effect heeft op het resultaat van de ablatie procedure. Verder moet bekeken worden wat de rol is van recent geïntroduceerde beeldvormende technieken zoals 'rotational angiography' (waarbij doorlichting CT-achtige beelden geeft), en 'real-time MRI' (in een hybride catheterisatie kamer).

Verder lieten de studies in dit proefschrift zien dat de functie van het LA en LV kan verbeteren na succesvolle catheter ablatie voor AF. Helaas kan uit deze studies het onderliggende pathofysiologische proces niet duidelijk worden gemaakt. Verder blijft het onduidelijk of het behoud van sinusritme resulteert in 'reverse remodeling', of vice versa ('de kip of het ei'...). Daarom zijn meer studies nodig om de doorslaggevende factoren voor reverse remodeling te vinden, en preklinische studies kunnen wellicht het onderliggende proces ophelderen. Het kan goed zijn dat de hoeveelheid littekenweefsel in het LA een belangrijke rol speelt in het slagen van catheter ablatie procedures, en reverse remodeling erna. Het in beeld brengen van de hoeveelheid littekenweefsel in het LA met behulp van beeldvormende technieken voorafgaand aan de ablatie procedure kan dan van grote waarde zijn. Ten slotte kan het kwantificeren van de hoeveelheid littekenweefsel na de ablatie procedure met behulp van MRI meer duidelijkheid geven over de effecten van dergelijke procedures op de grootte en de functie van het LA.

Ventriculair pacen en dyssynchronie

De negatieve effecten van RV pacen, zoals aangetoond in grote gerandomiseerde studies, is mogelijk gerelateerd aan de aanwezigheid van LV dyssynchronie. In dit proefschrift wordt aangetoond dat ongeveer de helft van de patiënten die langdurig RV pacen ondergaan, significante LV dyssynchronie ontwikkelen en verslechtering van LV functie laten zien. De aanwezigheid van LV dyssynchronie tijdens RV pacen is ook geassocieerd met een verslechtering van het oxidatieve metabolisme en efficiëntie van het myocard. Door het corrigeren van het asynchrone contractie patroon kan CRT deze negatieve effecten gedeeltelijk herstellen. Verder

werd aangetoond dat LV dyssynchronie vrijwel direct na het starten van RV pacen aanwezig kan zijn. Ten slotte liet een studie in dit proefschrift zien dat significante RV dyssynchronie aanwezig is in ongeveer 50% van de patiënten met ARVD. Meer studies zijn nodig om het onderliggende mechanisme te verhelderen, en om de klinische relevantie van deze bevinding te verduidelijken.

Met betrekking tot RV pacen en ventriculaire dyssynchronie blijft een aantal belangrijke vragen onbeantwoord, en moeten dus worden behandeld in toekomstige studies. Waarom ontwikkelen sommige patiënten significante LV dyssynchronie en zelfs hartfalen tijdens RV pacen, en andere patiënten niet? Zowel patiënt- als pacemakergerelateerde factoren die het ontwikkelen van dyssynchronie en verslechtering van LV functie zouden kunnen voorspellen, moeten onderzocht worden. Is het ontstaan van LV dyssynchronie in de acute fase geassocieerd met een verslechtering van LV functie tijdens follow-up? Als toekomstige studies deze relatie laten zien, dan moet ten tijde van de pacemaker implantatie de aanwezigheid van LV dyssynchronie worden onderzocht. Dan kan vervolgens CRT worden overwogen bij patiënten met significante LV dyssynchronie bij pacemaker implantatie. Verder kan een regelmatige screening op LV dyssynchronie bij patiënten met een gewone pacemaker, de patiënten die baat hebben bij een CRT pacemaker identificeren.

Percutane hartklep procedures

In de afgelopen jaren is een aantal interessante, nieuwe percutane procedures geïntroduceerd voor de behandeling van patiënten met ernstige hartklepafwijkingen. Dit proefschrift laat zien dat beeldvormende technieken (en in het bijzonder MSCT scans) belangrijke informatie kunnen verschaffen voor de selectie van patiënten voor dergelijke procedures. MSCT is een driedimensionale beeldvormende techniek die uitstekend de relatie tussen de kransslagvaten, de sinus coronarius en de betreffende hartklep in beeld kan brengen. Deze relatie is van belang voor zowel percutane procedures voor ernstige MI die gebruik maken van de sinus coronarius, als voor percutane implantatie van een aortaklep. Verder kan MSCT de prothese en de relatie met omgevende structuren in beeld brengen na de percutane procedure. Voor percutane hartklep procedures moet nog een aantal belangrijke zaken onderzocht worden in toekomstige studies, zoals de lange termijn veiligheid en effectiviteit van de prothesen. Tegelijkertijd moeten meer studies de percutane benadering vergelijken met de chirurgische benadering. Er wordt momenteel uitgekeken naar de resultaten van de PARTNER trial (The Placement of AoRTic TraNscathetER Valve Trial) die bij 350 patiënten deze vergelijking onderzoekt. Als toekomstige studies vergelijkbare of betere resultaten van de percutane benadering laten zien, dan worden de indicaties voor een percutane procedure waarschijnlijk uitgebreid. Dit is voornamelijk interessant voor patiënten die eerder een aortakunstklep kregen, die nu aan vervanging toe is. Dit zou dan niet een nieuwe operatie betekenen, maar een percutane ingreep ('valve-in-valve'). Ten slotte, meer studies zijn nodig om te onderzoeken of beeldvormende technieken de veiligheid en effectiviteit van de procedures kunnen verbeteren. In het bijzonder moet worden gekeken naar de integratie van de verschillende technieken tijdens de implantatie procedure.

List of publications

Fusion of multislice computed tomography imaging with three-dimensional electroanatomic mapping to guide radiofrequency catheter ablation procedures.

Tops LF, Bax JJ, Zeppenfeld K, Jongbloed MR, Lamb HJ, van der Wall EE, Schalij MJ.
Heart Rhythm 2005;2:1076-81.

Intraatrial repair of transposition of the great arteries: use of MR imaging after exercise to evaluate regional systemic right ventricular function.

Tops LF, Roest AA, Lamb HJ, Vliegen HW, Helbing WA, van der Wall EE, de Roos A.
Radiology 2005;237:861-7.

Endoscopic fiberoptic balloon catheter: a new step in imaging-guided anatomically based catheter ablation for atrial fibrillation?

Tops LF, Schalij MJ, Bax JJ.
Heart Rhythm 2006;3:50-1.

Effect of radiofrequency catheter ablation for atrial fibrillation on left atrial cavity size.

Tops LF, Bax JJ, Zeppenfeld K, Jongbloed MR, van der Wall EE, Schalij MJ.
Am J Cardiol 2006;97:1220-2.

Fusion of electroanatomical activation maps and multislice computed tomography to guide ablation of a focal atrial tachycardia in a fontan patient.

Tops LF, de Groot NM, Bax JJ, Schalij MJ.
J Cardiovasc Electrophysiol 2006;17:431-4.

Right ventricular pacing can induce ventricular dyssynchrony in patients with atrial fibrillation after atrio-ventricular node ablation.

Tops LF, Schalij MJ, Holman ER, van Erven L, van der Wall EE, Bax JJ.
J Am Coll Cardiol 2006;48:1642-8.

Noninvasive evaluation of coronary sinus anatomy and its relation to the mitral valve annulus: implications for percutaneous mitral annuloplasty.

Tops LF, Van de Veire NR, Schuijf JD, de Roos A, van der Wall EE, Schalij MJ, Bax JJ.
Circulation 2007;115:1426-32.

Speckle-tracking radial strain reveals left ventricular dyssynchrony in patients with permanent right ventricular pacing.

Tops LF, Suffoletto MS, Bleeker GB, Boersma E, van der Wall EE, Gorcsan J 3rd, Schalij MJ, Bax JJ.
J Am Coll Cardiol 2007;50:1180-8.

Multi-modality imaging to assess left atrial size, anatomy and function.

Tops LF, van der Wall EE, Schalij MJ, Bax JJ.
Heart 2007;93:1461-70.

Noncoronary applications of cardiac multidetector row computed tomography.

Tops LF, Krishnan SC, Schuijf JD, Schalij MJ, Bax JJ.
J Am Coll Cardiol Img 2008;1:94-106.

Percutaneous valve procedures: an update.

Tops LF, Kapadia SR, Tuzcu EM, Vahanian A, Alfieri O, Webb JG, Bax JJ.
Curr Probl Cardiol 2008;33:417-57.

Multislice CT: is it essential before atrial fibrillation ablation?

Tops LF, Schalij MJ.

Heart 2008;94:973-5.

Applications of cardiac CT in electrophysiology interventions.

Tops LF, Schuijff JD, Bax JJ.

Cardiovascular Imaging & Therapeutics 2008;1:10-16.

Image integration in catheter ablation of atrial fibrillation.

Tops LF, Schalij MJ, den Uijl DW, Abraham TP, Calkins H, Bax JJ.

Europace 2008;10:iii48-56.

The role of speckle tracking strain imaging in cardiac pacing.

Tops LF, Delgado V, Bax JJ.

Echocardiography 2009;26:315-23.

Noninvasive evaluation of the aortic root with multislice computed tomography: implications for transcatheter aortic valve replacement.

Tops LF, Wood DA, Delgado V, Schuijff JD, Mayo JR, Pasupati S, Lamers FP, van der Wall EE, Schalij MJ, Webb JG, Bax JJ.

J Am Coll Cardiol Img 2008;1:321-30.

The year in imaging related to electrophysiology.

Tops LF, Bax JJ.

J Am Coll Cardiol Img 2009;2:498-510.

Prevalence and pathophysiologic attributes of ventricular dyssynchrony in arrhythmogenic right ventricular dysplasia/cardiomyopathy.

Tops LF, Prakasa K, Tandri H, Dalal D, Jain R, Dimaano VL, Dombroski D, James C, Tichnell C, Daly A, Marcus F, Schalij MJ, Bax JJ, Bluemke D, Calkins H, Abraham TP.

J Am Coll Cardiol 2009;54:445-51.

The effects of right ventricular apical pacing on ventricular function and dyssynchrony implications for therapy.

Tops LF, Schalij MJ, Bax JJ.

J Am Coll Cardiol 2009;54:764-76.

Percutaneous aortic valve therapy: clinical experience and the role of multi-modality imaging.

Tops LF, Delgado V, van der Kley F, Bax JJ.

Heart 2009;95:1538-46.

Long-term improvement in left ventricular strain after successful catheter ablation for atrial fibrillation in patients with preserved left ventricular systolic function.

Tops LF, den Uijl DW, Delgado V, Marsan NA, Zeppenfeld K, Holman E, van der Wall EE, Schalij MJ, Bax JJ.

Circ Arrhythmia Electrophysiol 2009;2:249-57.

Imaging and atrial fibrillation: the role of multimodality imaging in patient evaluation and management of atrial fibrillation.

Tops LF, Schalij MJ, Bax JJ.

Eur Heart J 2010, in press.

Left atrial strain predicts reverse remodeling after catheter ablation for atrial fibrillation.

Tops LF, Delgado V, Bertini M, Marsan NA, den Uijl DW, Trines SA, Zeppenfeld K, Holman E, Schalij MJ, Bax JJ.
Submitted.

Magnetic resonance cardiac vein imaging: relation to mitral valve annulus and left circumflex coronary artery.

Chiribiri A, Kelle S, Köhler U, **Tops LF**, Schnackenburg B, Bonamini R, Bax JJ, Fleck E, Nagel E.
J Am Coll Cardiol Img 2008;1:729-38.

Assessment of left ventricular dyssynchrony by speckle tracking strain imaging comparison between longitudinal, circumferential, and radial strain in cardiac resynchronization therapy.

Delgado V, Ypenburg C, van Bommel RJ, **Tops LF**, Mollema SA, Marsan NA, Bleecker GB, Schalij MJ, Bax JJ.
J Am Coll Cardiol 2008;51:1944-52.

Relation between global left ventricular longitudinal strain assessed with novel automated function imaging and biplane left ventricular ejection fraction in patients with coronary artery disease.

Delgado V, Mollema SA, Ypenburg C, **Tops LF**, van der Wall EE, Schalij MJ, Bax JJ.
J Am Soc Echocardiogr 2008;21:1244-50.

Assessment of mitral valve anatomy and geometry with multislice computed tomography.

Delgado V, **Tops LF**, Schuijff JD, de Roos A, Brugada J, Schalij MJ, Thomas JD, Bax JJ.
J Am Coll Cardiol Img 2009;2:556-65.

Acute effects of right ventricular apical pacing on left ventricular synchrony and mechanics.

Delgado V, **Tops LF**, Trines SA, Zeppenfeld K, Marsan NA, Bertini M, Holman ER, Schalij MJ, Bax JJ.
Circ Arrhythmia Electrophysiol 2009;2:135-45.

Successful deployment of a transcatheter aortic valve in bicuspid aortic stenosis: role of imaging with multislice computed tomography.

Delgado V, **Tops LF**, Schuijff JD, van der Kley F, Van de Veire NR, Schalij MJ, Bax JJ.
Circ Cardiovasc Imaging 2009;2:e12-3.

Strain analysis in patients with severe aortic stenosis and preserved left ventricular ejection fraction undergoing surgical valve replacement.

Delgado V, **Tops LF**, van Bommel RJ, van der Kley F, Marsan NA, Klautz RJ, Versteegh MI, Holman ER, Schalij MJ, Bax JJ.
Eur Heart J 2009;30:3037-47.

Transcatheter aortic valve implantation: role of multi-slice computed tomography to evaluate prosthesis positioning and deployment in relation to valve function.

Delgado V, Ng AC, Van de Veire NR, van der Kley F, Schuijff JD, **Tops LF**, de Weger A, Tavilla G, de Roos A, Kroft LJ, Schalij MJ, Bax JJ.
Eur Heart J 2010, in press.

Automatic assessment of the aortic root dimensions with multi-detector row computed tomography: implications for transcatheter aortic valve implantation.

Delgado V, Ng AC, Schuijff JD, van der Kley F, Shanks M, **Tops LF**, Van de Veire NR, de Roos A, Kroft LJ, Schalij MJ, Bax JJ.
Submitted.

Combined longitudinal and radial dyssynchrony predicts ventricular response after resynchronization therapy.

Gorcsan J 3rd, Tanabe M, Bleeker GB, Suffoletto MS, Thomas NC, Saba S, **Tops LF**, Schalij MJ, Bax JJ. *J Am Coll Cardiol* 2007;50:1476-83.

Cardiac resynchronization therapy devices guided by imaging technology.

Krishnan SC, **Tops LF**, Bax JJ. *J Am Coll Cardiol Img* 2009;2:226-30.

Comparison of left atrial volumes and function by real-time three-dimensional echocardiography in patients having catheter ablation for atrial fibrillation with persistence of sinus rhythm versus recurrent atrial fibrillation three months later.

Marsan NA, **Tops LF**, Holman ER, Van de Veire NR, Zeppenfeld K, Boersma E, van der Wall EE, Schalij MJ, Bax JJ. *Am J Cardiol* 2008;102:847-53.

Predicting response to CRT. The value of two- and three-dimensional echocardiography.

Marsan NA, Breithardt OA, Delgado V, Bertini M, **Tops LF**. *Europace* 2008;10:iii73-9.

Comparison between tissue Doppler imaging and velocity-encoded magnetic resonance imaging for measurement of myocardial velocities, assessment of left ventricular dyssynchrony, and estimation of left ventricular filling pressures in patients with ischemic cardiomyopathy.

Marsan NA, Westenberg JJ, **Tops LF**, Ypenburg C, Holman ER, Reiber JH, de Roos A, van der Wall EE, Schalij MJ, Roelandt JR, Bax JJ. *Am J Cardiol* 2008;102:1366-72.

Magnetic resonance imaging and response to cardiac resynchronization therapy: relative merits of left ventricular dyssynchrony and scar tissue.

Marsan NA, Westenberg JJ, Ypenburg C, van Bommel RJ, Roes S, Delgado V, **Tops LF**, van der Geest RJ, Boersma E, de Roos A, Schalij MJ, Bax JJ. *Eur Heart J* 2009;30:2360-7.

Usefulness of multimodality imaging for detecting differences in temporal occurrence of left ventricular systolic mechanical events in healthy young adults.

Marsan NA, **Tops LF**, Westenberg JJ, Delgado V, de Roos A, van der Wall EE, Schalij MJ, Bax JJ. *Am J Cardiol* 2009;104:440-6.

Real-time three dimensional echocardiography: current and future clinical applications.

Marsan NA, **Tops LF**, Nihoyannopoulos P, Holman ER, Bax JJ. *Heart* 2009;95:1881-90.

Comparison of aortic root dimensions and geometries pre- and post-transcatheter aortic valve implantation by 2- and 3-dimensional transesophageal echocardiography and multislice computed tomography.

Ng AC, Delgado V, van der Kley F, Shanks M, Van de Veire NR, Bertini M, Nucifora G, van Bommel RJ, **Tops LF**, de Weger A, Tavilla G, de Roos A, Kroft LJ, Leung DY, Schuijf JD, Schalij MJ, Bax JJ. *Circ Cardiovasc Imaging* 2010;3:94-102.

Prevalence of coronary artery disease assessed by multislice computed tomography coronary angiography in patients with paroxysmal or persistent atrial fibrillation.

Nucifora G, Schuijf JD, **Tops LF**, van Werkhoven JM, Kajander S, Jukema JW, Schreur JH, Heijnenbroek MW, Trines SA, Gaemperli O, Turta O, Kaufmann PA, Knuuti J, Schalij MJ, Bax JJ.

Circ Cardiovasc Imaging 2009;2:100-6.

Cardiac computed tomography: indications, applications, limitations, and training requirements: report of a Writing Group deployed by the Working Group Nuclear Cardiology and Cardiac CT of the European Society of Cardiology and the European Council of Nuclear Cardiology.

Schroeder S, Achenbach S, Bengel F, Burgstahler C, Cademartiri F, de Feyter P, George R, Kaufmann P, Kopp AF, Knuuti J, Ropers D, Schuijf J, **Tops LF**, Bax JJ.

Eur Heart J 2008;29:531-56.

Prolonged RV endocardial activation duration: a novel marker of arrhythmogenic right ventricular dysplasia/cardiomyopathy.

Tandri H, Asimaki A, Abraham TP, Dalal D, **Tops LF**, Jain R, Saffitz JE, Judge DP, Russell SD, Halushka M, Bluemke DA, Kass DA, Calkins H.

Heart Rhythm 2009;6:769-75.

Clinical efficacy of surgical heart failure therapy by ventricular restoration and restrictive mitral annuloplasty.

Tulner SA, Steendijk P, Klautz RJ, **Tops LF**, Bax JJ, Versteegh MI, Verwey HF, Schalij MJ, van der Wall EE, Dion RA.

J Card Fail 2007;13:178-83.

Real-time integration of intracardiac echocardiography and multislice computed tomography to guide radiofrequency catheter ablation for atrial fibrillation.

den Uijl DW, **Tops LF**, Tolosana JM, Schuijf JD, Trines SA, Zeppenfeld K, Bax JJ, Schalij MJ.

Heart Rhythm 2008;5:1403-10.

Impact of pulmonary vein anatomy and left atrial dimensions on the outcome of circumferential radiofrequency catheter ablation for atrial fibrillation.

den Uijl DW, **Tops LF**, Delgado V, Schuijf JD, Kroft LJ, de Roos A, Boersma E, Trines SA, Zeppenfeld K, Schalij MJ, Bax JJ.

Submitted.

Impact of left atrial fibrosis and left atrial size on the outcome of catheter ablation for atrial fibrillation.

den Uijl DW, Delgado V, Bertini M, **Tops LF**, Trines SA, Van de Veire NR, Zeppenfeld K, Schalij MJ, Bax JJ.

Submitted.

The effect of right ventricular pacing on myocardial oxidative metabolism and efficiency: relation with left ventricular dyssynchrony.

Ukkonen H, **Tops LF**, Saraste A, Naum A, Koistinen J, Bax JJ, Knuuti J.

Eur J Nucl Med Mol Imaging 2009;36:2042-8.

Ventricular response to stress predicts outcome in adult patients with a systemic right ventricle: a cardiovascular magnetic resonance imaging study.

Winter MM, Scherptong RW, Kumar S, Bouma BJ, Tulevski II, **Tops LF**, Roest AA, Vliegen HW, de Roos A, Groenink M, Mulder BJ.

Submitted.

Role of multislice computed tomography in transcatheter aortic valve replacement.

Wood DA, **Tops LF**, Mayo JR, Pasupati S, Schalij MJ, Humphries K, Lee M, Al Ali A, Munt B, Moss R, Thompson CR, Bax JJ, Webb JG.

Am J Cardiol 2009;103:1295-301.

Acute effects of initiation and withdrawal of cardiac resynchronization therapy on papillary muscle dyssynchrony and mitral regurgitation.

Ypenburg C, Lancellotti P, **Tops LF**, Bleeker GB, Holman ER, Piérard LA, Schalij MJ, Bax JJ.

J Am Coll Cardiol 2007;50:2071-7.

Mechanism of improvement in mitral regurgitation after cardiac resynchronization therapy.

Ypenburg C, Lancellotti P, **Tops LF**, Boersma E, Bleeker GB, Holman ER, Thomas JD, Schalij MJ, Piérard LA, Bax JJ.

Eur Heart J 2008;29:757-65.

Epicardial radiofrequency catheter ablation of ventricular tachycardia in the vicinity of coronary arteries is facilitated by fusion of 3-dimensional electroanatomical mapping with multislice computed tomography.

Zeppenfeld K, **Tops LF**, Bax JJ, Schalij MJ.

Circulation 2006;114:e51-2.

Book chapters

Effect of right ventricular apical pacing and cardiac resynchronization therapy on left ventricular dyssynchrony and function.

Tops LF, Schalij MJ, Bax JJ.

In: Cardiac resynchronization therapy in heart failure. Abraham WT, Baliga RR (ed). Lippincott, Williams and Wilkins, Philadelphia, 2009, pp 97-113.

Multislice computed tomography: role in cardiac electrophysiology.

Bax JJ, **Tops LF**, Saremi F, Krishnan SC.

In: Atlas of cardiovascular computed tomography. Budoff MJ, Achenbach S, Narula J, Braunwald E (ed). Springer, Philadelphia, 2007, pp 203-24.

Imaging: how can it help before transcatheter aortic valve implantation?

Delgado V, **Tops LF**, van der Kley F, Schuijf JD, Schalij MJ, Bax JJ.

In: Percutaneous implantation of the aortic valve: tips and tricks to avoid failure. Serruys PW, de Jaegere P, Piazza N, Cribier A, Webb JG, Laborde J (ed). Informa Healthcare, New York, 2010, *in press*.

Computed Tomography.

Schuijf JD, **Tops LF**, Bax JJ

In: Oxford textbook of heart failure. McDonagh T, Gardner R, Clark A, Dargie H (ed). Oxford University Press, Oxford, 2010, *in press*.

Intracardiac Echocardiography.

den Uijl DW, **Tops LF**, Van de Veire NR, Bax JJ.

In: Cardiovascular catheterization and intervention: a textbook of coronary, peripheral and structural heart disease. Mukherjee D, Bates ER, Roffi M, Moliterno DJ (ed). Informa Healthcare, London, 2010, *in press*.

Acknowledgements

Dit proefschrift was er niet geweest zonder de hulp en steun van velen. Graag wil ik iedereen bedanken die in de afgelopen jaren betrokken is geweest bij mijn promotieonderzoek. Zonder anderen tekort te doen wil ik een aantal personen in het bijzonder noemen.

Voor de secretariële ondersteuning wil ik graag het secretariaat van het stafcentrum, en in het bijzonder Cora, Monique en Talitha bedanken. Alle medewerkers van de hartfunctie en de poli (en in het bijzonder Carine, Edith en Anneke), en de verpleging van de afdeling Cardiologie wil ik bedanken voor hun hulp bij de verschillende onderzoeken.

Alle dames en de heer van het cathlab, en vooral diegene met wie ik samenwerkte tijdens de ablatie procedures, wil ik bedanken voor hun hulp en gezelligheid. Bea, veel dank voor de planning van de catheter ablatie procedures en de verschillende onderzoeken en poliafspraken er omheen.

Alle laboranten van de afdeling Radiologie: dank voor jullie hulp bij het scannen. Iedereen van de computer groep en in het bijzonder Enno, Tom en Hylke wil ik bedanken voor de technische ondersteuning in de afgelopen jaren.

Graag wil ik alle collega's van de afgelopen jaren bedanken. Te beginnen met alle (oud)collega's uit 'de tuin'. Wat heb ik een fantastische tijd met jullie gehad! Alle tuin-uitjes, congressen, borrels en etentjes waren stuk voor stuk fantastisch. Veel dank daarvoor. Een aantal collega's wil ik in het bijzonder noemen. Monique, dank voor het inwijden in het MAZE project. Joanne, dank voor je hulp bij het verkrijgen en analyseren van de CT data, en in de 'afrondende fase'. Claudia, overbuuv, dank voor de gezellige congressen. Victoria, ook jou wil ik bedanken voor de fijne samenwerking (you see, it's not that hard...). Pijnappels, ik bewonder je kritische houding, je kennis en doorzettingsvermogen. Niagara Falls was fantastisch, snel weer eens overdoen! Sjoerd, dank je wel dat je mijn paranimf wilt zijn. Veel succes met het afronden van jouw eigen onderzoek en veel succes en plezier op de twee mooiste dagen van dit najaar!

Na drie jaar onderzoek heb ik het Leidsche tijdelijk verruild voor een fellowship in Baltimore. I would like to thank all my colleagues from Johns Hopkins University for a wonderful time. Dear Ted, thank you very much for the opportunity to work in your lab. Dear Aurelio, Jacob, Lea, Denise, Irene, Daniel, the ARVD group and the Sedelaars, thank you all for the most amazing time!

Ten slotte mijn huidige collega's in het HagaZiekenhuis: veel dank voor jullie support en flexibiliteit.

Buiten het werk was er gelukkig (af en toe) tijd voor biertjes en gezelligheid met vrienden, oud-huisgenoten, clubgenoten en aanhang. Veel dank voor de afleiding en 'moral support'. Willem en Laura, dank voor jullie vriendschap.

Mijn familie en schoonfamilie, jullie staan altijd voor mij klaar. Dank daarvoor. Hein en Annelies, dank voor jullie oprechte interesse en steun.

Michiel en Carolyn, veel dank voor jullie support, ondanks de grote afstand. Ik kan niet wachten om mijn kleine neefje te zien.

Merijn, ik ben trots op jou als grote broer. Bedankt dat je mijn paranimf wilt zijn.

426

Papa en mama, jullie hebben de basis gelegd voor dit proefschrift. Dank voor jullie onvoorwaardelijke steun en liefde.

Lieve Eline, mijn dank voor jouw eindeloze geduld, adviezen, maar vooral liefde is moeilijk te omschrijven. Zonder jou was dit proefschrift er niet geweest. Op naar de volgende vijf nòg mooiere jaren! Lieve Marilène, jouw stralende lach maakt van elke dag een klein feestje. Now it's party time!

Laurens

Curriculum Vitae

The author of this thesis was born on April 17, 1979 in Oss, the Netherlands. After graduating from Titus Brandsma Lyceum in 1997, he studied Medicine at the Leiden University. During the doctoral phase, he completed a research project entitled 'Exercise-MRI of global and regional systemic right ventricular function after intra-atrial repair for transposition of the great arteries' under the supervision of Prof. dr. A. de Roos (Department of Radiology). As a result, he was awarded the 'LUMC Student Research Award 2002' by the board of managing directors of the Leiden University Medical Center. After finishing his internships, he received his medical degree in 2004. In January 2005, he started a research fellowship on the role of imaging in cardiac interventional procedures at the Department of Cardiology of the Leiden University Medical Center (supervisors: Prof. dr. J.J. Bax and Prof. dr. M.J. Schalij). In January 2008, he continued this research with a fellowship at the Division of Cardiology, Johns Hopkins Medical Institutions, Baltimore, USA (supervisor: Prof. dr. T.P. Abraham). The results of these studies are described in the present thesis. In August 2008, he started his clinical training in Cardiology, and is at present working at the Department of Internal medicine of the HagaZiekenhuis in The Hague (educational head: Dr. M.O. van Aken). His traineeship will continue at the Department of Cardiology of the HagaZiekenhuis (educational head: Dr. B.J.M. Delemarre) and the Department of Cardiology of the Leiden University Medical Center (educational head: Prof. dr. E.E. van der Wall).